

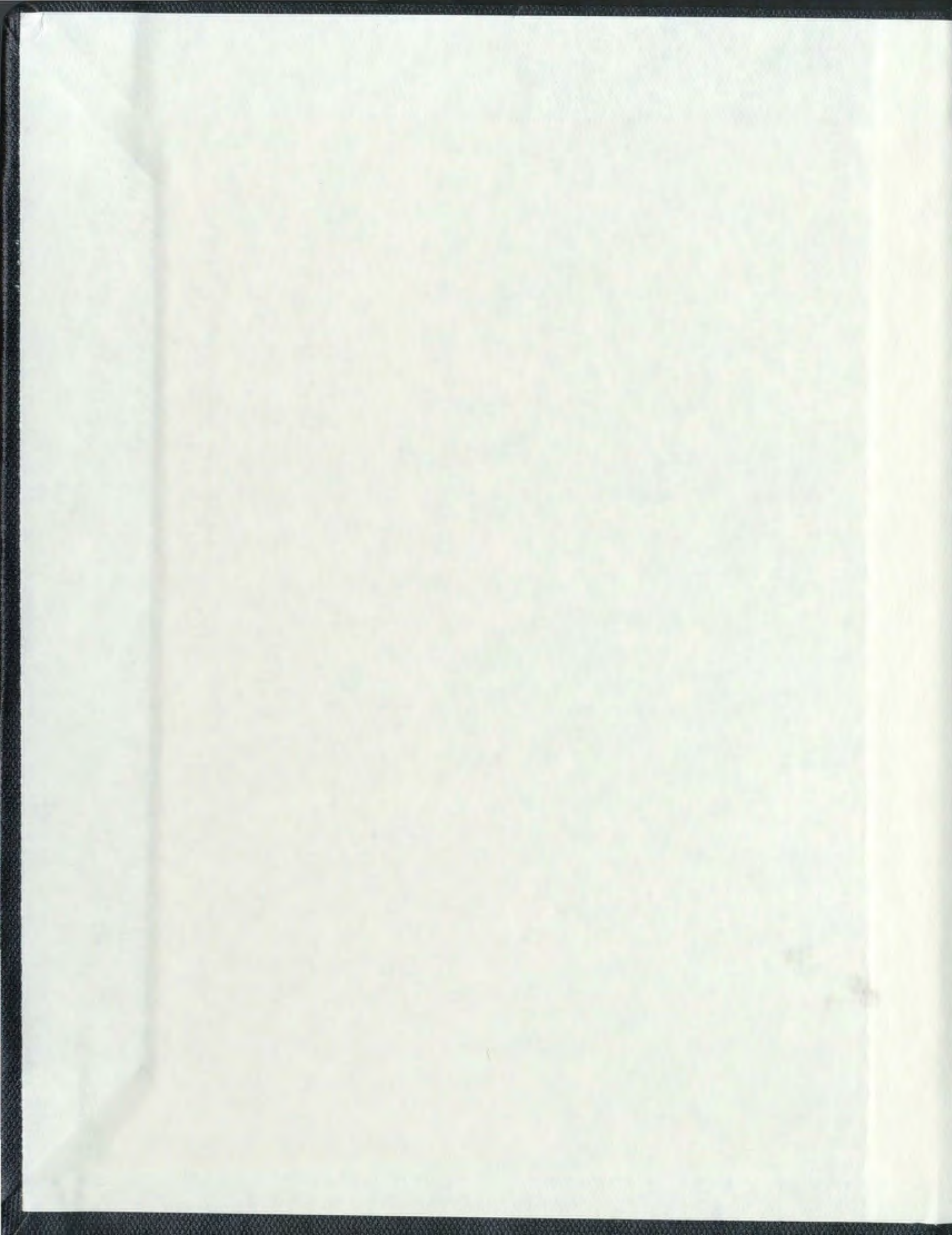
THE GEOLOGY, GEOCHEMISTRY AND METALLOGENY
OF THE TATI GREENSTONE BELT,
NORTHEASTERN BOTSWANA

CENTRE FOR NEWFOUNDLAND STUDIES

**TOTAL OF 10 PAGES ONLY
MAY BE XEROXED**

(Without Author's Permission)

AKOLANG RUSSIA TOMBALE





National Library
of Canada

Acquisitions and
Bibliographic Services Branch

395 Wellington Street
Ottawa, Ontario
K1A 0N4

Bibliothèque nationale
du Canada

Direction des acquisitions et
des services bibliographiques

395, rue Wellington
Ottawa (Ontario)
K1A 0N4

Your file *Votre référence*

Our file *Notre référence*

NOTICE

The quality of this microform is heavily dependent upon the quality of the original thesis submitted for microfilming. Every effort has been made to ensure the highest quality of reproduction possible.

If pages are missing, contact the university which granted the degree.

Some pages may have indistinct print especially if the original pages were typed with a poor typewriter ribbon or if the university sent us an inferior photocopy.

Reproduction in full or in part of this microform is governed by the Canadian Copyright Act, R.S.C. 1970, c. C-30, and subsequent amendments.

AVIS

La qualité de cette microforme dépend grandement de la qualité de la thèse soumise au microfilmage. Nous avons tout fait pour assurer une qualité supérieure de reproduction.

S'il manque des pages, veuillez communiquer avec l'université qui a conféré le grade.

La qualité d'impression de certaines pages peut laisser à désirer, surtout si les pages originales ont été dactylographiées à l'aide d'un ruban usé ou si l'université nous a fait parvenir une photocopie de qualité inférieure.

La reproduction, même partielle, de cette microforme est soumise à la Loi canadienne sur le droit d'auteur, SRC 1970, c. C-30, et ses amendements subséquents.

**THE GEOLOGY, GEOCHEMISTRY AND METALLOGENY OF THE TATI
GREENSTONE BELT, NORTHEASTERN BOTSWANA.**

by

• **Akolang Russia Tombale, BSc., MSc.**

**A thesis submitted to the School of Graduate Studies
in partial fulfilment of the**

requirements for the degree of

Doctor of Philosophy

Department of Earth Sciences

Memorial University of Newfoundland

October, 1992

St. John's

Newfoundland



National Library
of Canada

Acquisitions and
Bibliographic Services Branch

395 Wellington Street
Ottawa, Ontario
K1A 0N4

Bibliothèque nationale
du Canada

Direction des acquisitions et
des services bibliographiques

395, rue Wellington
Ottawa (Ontario)
K1A 0N4

Your file: Votre référence

Our file: Notre référence

The author has granted an irrevocable non-exclusive licence allowing the National Library of Canada to reproduce, loan, distribute or sell copies of his/her thesis by any means and in any form or format, making this thesis available to interested persons.

L'auteur a accordé une licence irrévocable et non exclusive permettant à la Bibliothèque nationale du Canada de reproduire, prêter, distribuer ou vendre des copies de sa thèse de quelque manière et sous quelque forme que ce soit pour mettre des exemplaires de cette thèse à la disposition des personnes intéressées.

The author retains ownership of the copyright in his/her thesis. Neither the thesis nor substantial extracts from it may be printed or otherwise reproduced without his/her permission.

L'auteur conserve la propriété du droit d'auteur qui protège sa thèse. Ni la thèse ni des extraits substantiels de celle-ci ne doivent être imprimés ou autrement reproduits sans son autorisation.

ISBN 0-315-91656-7

Canada

FRONTISPIECE:

The Tati Greenstone Belt has a long, mining history dating from the prehistoric stone age to the present. The two photographs in the frontispiece illustrate part of this long mining tradition.

Upper Photograph:

A stone carving which formed the mortar part of an ancient (pre-1866) mortar and pedestal gold processing plant. Such outcrops are scattered all over the Tati Greenstone Belt, especially near river beds. The grinding stones (mortars) are very difficult to find as they were made from loose stones.

Lower Photograph:

The ruins of an old gold milling plant used during the post-1866 mining period. The photograph was taken at the abandoned Vermaak Mine, about 23 km east of Francistown.



ABSTRACT

The Tati Greenstone Belt of Botswana occurs along the southern margin of the Archean Zimbabwe Craton in the northern contact zone of the Limpopo Belt. Detailed mapping and structural analysis indicates that the Tati Greenstone Belt consists of three fault-bounded volcano-plutonic sequences intruded by granitoids. The data further suggest that the belt formed from the accretion of the volcano-plutonic sequences to the Zimbabwe Craton in a manner resembling modern orogenic belts.

Geochemical data suggest that the Tati Greenstone Belt consists of a komatiite-tholeiite sequence representing a back-arc basin and calc-alkaline volcanic and feldspathic sedimentary rock sequences which overall indicate the existence of an arc environment. The geochemical data further indicate the presence of three different magmatic suites within the Lady Mary Group of the Tati Greenstone Belt and these suites have geochemical signatures similar to those of found in modern tectonic environments. The three magmatic suites include LREE-depleted rocks, LREE-enriched rocks and komatiites. The LREE-enriched rocks form the margins of a basinal structure with LREE-depleted and komatiites at the core. The komatiites are postulated to have formed from plume-type magmas generated in deep portions of the Archean mantle.

Gold mineralization in the Tati Greenstone Belt, northeastern Botswana, formed as an integral component of the tectonic evolution of the belt. Three main stages of gold mineralization are recognized. The first mineralization stage is related

to the late stages of volcanism which formed the volcanic sequences in the belt. During this stage hydrothermal fluids circulated through the volcanic structure along fissures, fractures and lithological boundaries, leaching metals and creating extensive carbonate alteration zones. The contact zones between basaltic rocks and synvolcanic gabbroic sills, and inter-pillow areas were the most extensively altered. Metal-bearing fluids, in which the metals were derived during the alteration of the basaltic crust, were discharged along the tops of the volcanic sequences depositing banded iron formations with siliceous, carbonate, oxide and sulphide facies. In particular, sulphide facies banded iron formations in the Tati Greenstone Belt are discontinuous units located at the top of major volcanic sequences, which are either covered by sedimentary rocks including carbonates and minor clastic rocks, or lie directly on the basaltic crust. In the waning stages of the hydrothermal activity, lower temperature phases of the hydrothermal fluids precipitated Au, Ag, Sb, As and other related metals in pockets at localized sites.

The second stage of gold mineralization coincided with the deformation of the belt and the creation of favourable structural sites. During this stage, related to NE to N directed compression and thrusting (D_1), NE to N verging recumbent and overturned folds were formed. Volcanic sequences were thrust onto each other along lithological boundary-parallel faults, which are demarked by banded iron formations and related sedimentary rocks. The second deformation, D_2 , was the main foliation-forming deformation event. Metamorphic de-watering during this event resulted in large scale foliation-parallel carbonate and quartz-carbonate veining. Carbonate

alteration formed during the first stage was extensively replaced by silica during this second stage, creating the silicified alteration zones which accommodated brittle deformation during subsequent deformation events.

The third stage of gold mineralization was related to D_3 shearing of the volcanic rocks in the belt and major granitoid magmatism. Shearing and faulting created cross stratigraphy faults/shear zones. Banded iron formations and silicified zones formed during the D_2 deformational event accommodated brittle failure during this D_3 shearing event. Secondary fluids penetrated through the lithologies along numerous structures and were heated by granitoid magmas. These fluids remobilized metals from banded iron formations and massive sulphide horizons, redepositing them into brittle fractures. The brittle structures were localised to areas of lithological heterogeneity, such as at contacts between gabbroic sills and basaltic host rocks and in relatively structurally competent rocks such as banded iron formations. The mineral occurrences formed during this stage were low temperature Au-only deposits.

Gold was produced from at least 70 small mines scattered across the Tati Greenstone Belt. Pre-1800 gold production by local tribesmen was also substantial. The various gold occurrences and their characteristics are summarized in a metallogenic map of the belt. Data presented on the metallogenic map include the main commodity produced, metallic associations, the form in which gold occurs, host rock type, and the nature of the structural control.

ACKNOWLEDGEMENTS

There are too many people who contributed to the successful completion of this research project, to be all mentioned here. I wish however, to express my sincere thanks and gratitude to all those who have in any way helped during this work. In particular I wish to express my gratitude to my supervisor, Dr. Derek Wilton. His counselling, guidance and constructive criticisms improved this manuscript. I also thank Drs. Malpas and Fryer very much for reviewing, and offering suggestions that led to the improvement of this thesis. Dr. Hank Willams, and the Department of Forestry, Faculty of Applied Sciences, allowed me to use map compilation facilities. I thank them very much. I also wish to extend my gratitude to the management and staff of Phelps Dodge Mining Company, at the Shashe Mine, for the help during underground mine tours and sampling. My deep appreciation also goes to the staff of the Mineral Dressing Laboratory of the Botswana Geological Survey, for helping with the preparation some of the samples. I also wish to thank Mr. G. Veinott and Mr. W. Gosse, who helped me with the preparation of most of the geochemical samples. I also thank Miss E. Hearn for helping with some of the logistics of this work.

I also wish to extend my gratitude to Dr. A.J. Sinclair, of the University of British Columbia. Dr. Sinclair has been my academic councillor, teacher and friend ever since completing the Master of Science degree at that University, under his supervision. I hope very much that the results of this research will live up to his high

standards and expectations. I also wish to thank my colleagues and friends, Dr. V. Sibiya, Messrs R. Chaoka, M. Chiepe, B. Mosigi and Modisi for the fruitful discussions on the subject. Mr. Chiepe shared his most valuable knowledge about the mineralization at the Shashe and Signal Hill Deposits. He worked as an exploration geologist for Phelps Dodge at the Shashe Mine, between 1985 and 1989. He subsequently joined Sedge Botswana, when they were evaluating the Signal Hill Deposit. Mr. M. Chiepe also made available members of his staff at Signal Hill, to help with core sampling. Mr. B. Mosigi brought in his experience on the other greenstone belts of northeast Botswana, Vumba and Matsitama. Mr. Mosigi worked in these belts, for both the Botswana Geological Survey and Falconbridge. Dr. V. Sibiya and Mr. T. Chaoka worked on the Gaborone Granite complex in the Archean Kaapvaal Craton. They therefore, brought to the discussion their most valuable observations on that craton for comparison. Mr. M. Modisi is carrying out a Ph.D research, on the tectonism of the Transvaal Basin in Botswana, at McMaster University. I also wish to thank my student colleagues, Mr. and Mrs. Aydin, for the fruitful discussions during this study. Mr. Aydin's knowledge of perspective drawing helped in shaping some of the diagrammatic illustrations in this thesis. General geological discussions with Mrs. Aydin contributed immensely in clarifying my thoughts on the subject.

I also wish to extend my acknowledgement to the Canadian International Development Agency (CIDA) for sponsoring this project. I wish to thank, in particular Dr. J. Wright, the manager of the Botswana-CIDA project. Dr. Wright

offered me the scholarship. I also thank Mr. B. Hoffe, the assistant manager of the Botswana-CIDA project. Mr. Hoffe also helped in providing some of the geophysical data.

I must also thank Mrs. S. Wilton and family for making my stay here a memorable one. Having left my family back in Botswana it was the most difficult time for me, especially during the holidays. They have always timely come to my rescue during these bad times. Lastly, I must express my sincere and heartfelt thanks to my wife Faith. She played the role of mother and father, to our three children Tebogo, Lesedi and Madome, during my absence. I must also extend my gratitude to the children for having endured my absence during this study period.

TABLE OF CONTENTS

	Page
TITLE	i
FRONTISPIECE CAPTION	ii
FRONTISPIECE	iii
ABSTRACT	iv
ACKNOWLEDGEMENTS	vii
TABLE OF CONTENTS	x
LIST OF TABLES	xvi
LIST OF FIGURES	xvii
LIST OF PLATES	xxiv

CHAPTER ONE

1. INTRODUCTION

1.1	Outline of the Project	1
1.2	Objectives and Aims of the Study	5
1.3	Location and Access	6
1.4	Physiography	9
1.5	Previous Studies	11
	1.5.1 Exploration	11
	1.5.2 Previous Geological Research	12
1.6	Methods of Research	14
	1.6.1 Laboratory and Desktop Studies	14
	1.5.2 Field Work	15

CHAPTER TWO

2. REGIONAL GEOLOGICAL FRAMEWORK

2.1	Introduction	16
2.2	Zimbabwe Craton	19
	2.2.1 Basement Complex	20
	2.2.2 Greenstone Belts of the Zimbabwe Craton	21
	2.2.2.1 Sebakwian Group	25
	2.2.2.2 Bulawayan Group	26
	2.2.2.3 Shamvaian Group	28
	2.2.3 Internal Granitoids	29
	2.2.4 Geotectonic Setting of Archean Greenstone Belts	31
	2.2.5 The Great Dyke	34

2.3	Limpopo Belt	34
	2.3.1 Northern Marginal Zone of the Limpopo Belt	38
2.4	Relationship between the Zimbabwe Craton and Limpopo Belt	42

CHAPTER THREE

3. GEOLOGY OF THE TATI GREENSTONE BELT

3.1	The State of Geological Knowledge on the Tati Greenstone Belt	47
3.2	Stratigraphy of the Tati Greenstone Belt	56
	3.2.1 Lady Mary Group	61
	3.2.1.1 Old Tati Formation	62
	3.2.1.2 Map-Nora Formation	66
	3.2.1.3 Golden Eagle Formation	69
	3.2.1.4 Matsiloje Formation	70
	3.2.2 Phenalonga Group	71
	3.2.2.1 Dinuku Formation	76
	3.2.3 Selkirk Group	76
	3.2.4 Last Hope Group	80
3.3	Plutonic Rocks of the Tati Greenstone Belt	84
	3.3.1 Tati Batholith	84
	3.3.2 Trondhjemite Plutons	85
	3.3.3 New Zealand Pluton	85
	3.3.4 Matsiloje Batholith	85
	3.3.5 Selkirk Igneous Complex	86
	3.3.6 Granitoids of the Northern Margin of the Tati Belt	87
	3.3.6.1 Undifferentiated Granitoids	87
	3.3.6.2 Ramokgwebana Batholith	87
	3.3.6.3 Mphoeng Plutonic Complex	88
3.4	Rocks outside the Tati Greenstone Belt	88
	3.4.1 Kgarimacheng Formation	88
	3.4.2 Northern Margin Zone of the Limpopo Belt	89
3.5	Phanerozoic Rocks	89

CHAPTER FOUR

4. THE STRUCTURE OF THE TATI GREENSTONE BELT

4.1	Introduction	90
-----	--------------	----

4.2	Regional Structural Framework of the Tati Greenstone Belt	92
4.2.1	Structure of Supracrustal Rocks of the Western Structural Zone	93
4.2.1.1	The D ₁ Structures	93
4.2.1.2	The D ₂ Structures	97
4.2.1.3	The D ₃ Structures	102
4.2.1.4	The D ₄ Structures	103
4.2.2	Structure of Supracrustal Rocks in the Last Hope Basin	106
4.2.2.1	The D ₁ Structures	113
4.2.2.2	The D ₂ Structures	113
4.2.2.3	The D ₃ Structures	114
4.2.2.4	The D ₄ Structures	114
4.2.3	Structure of Supracrustal Rocks of the Eastern Structural Zone	115
4.2.3.1	The D ₁ Structures	115
4.2.3.2	The D ₂ Structures	115
4.2.3.3	The D ₃ Structures	116
4.2.3.4	The D ₄ Structures	116
4.2.4	Major Lineaments in the Tati Greenstone Belt	119
4.2.5	Granitoid Intrusives	126
4.3	Structural Evolution of the Tati Greenstone Belt	133
4.4	Metamorphism	137

CHAPTER FIVE

5.GEOCHEMISTRY

5.1	Introduction	138
5.2	Alteration Effects on Rock Chemistry	139
5.3	Geochemistry of Ultramafic-mafic Rocks	140
5.3.1	Introduction	140
5.3.2	Major Element Geochemistry	147
5.3.3	Trace Element Geochemistry	155
5.3.4	Rare Earth Element Geochemistry	163
5.3.5	Discussion	170
5.4	Geochemistry of Granitoid Rocks of the Tati Greenstone Belt	174
5.4.1	Introduction	174
5.4.2	Sampling	176
5.4.3	Major Element Geochemistry	176
5.4.4	Trace Element Geochemistry	184

5.4.5	Rare Earth Element Geochemistry	189
5.4.6	Primitive Mantle-normalized Extended Trace	
Element Diagrams		192
5.4.7	Discussion	194

CHAPTER SIX

6. GEOLOGICAL SYNTHESIS OF THE TATI GREENSTONE BELT

6.1	Summary of the Stratigraphy of the Tati Greenstone Belt	201
6.2	Geochronology	201
6.3	Tectonic Evolution of the Tati Greenstone Belt	204
6.3.1	Paleotectonic Setting	204
6.3.2	Tectonics and Geodynamics	210

CHAPTER SEVEN

7. METALLOGENY OF THE TATI GREENSTONE BELT

7.1	Introduction	219
7.2	Regional Distribution of Mineral Deposits of the Tati Greenstone Belt	222
7.2.1	Historical Background	222
7.2.2	Elements of Metallogenic Mapping	222
7.2.3	Descriptions of Mineral Deposit Groups	224
7.2.3.1	Shashe Group	225
7.2.3.2	Golden Eagle Group	225
7.2.3.3	Charlie Group	228
7.2.3.4	New Zealand Group	228
7.2.3.5	Blue Jacket Group	229
7.2.3.6	Flora Group	229
7.2.3.7	Monarch Group	230
7.2.3.8	Francistown Group	231
7.2.3.9	Bonanza Group	231
7.2.3.10	Cherished Hope Group	231
7.2.3.11	Phenalonga Group	232
7.2.3.12	Vermaark Group	232
7.2.3.13	Signal Hill Group	233
7.2.3.14	Rainbow Group	233
7.2.3.15	Massive Sulphide Deposits	235
7.2.4	Regional Distribution of Mineral Deposits	237
7.3	Metallogenic Analysis	241
7.3.1	Introduction	241

7.3.2	Signal Hill Deposit	242
7.3.2.1	Local Geology	242
7.3.2.2	Method of Study	245
7.3.2.3	Structure of the Signal Hill Area	245
7.3.2.4	Alteration at Signal Hill Deposit	255
7.3.2.5	Nature of Mineralization	258
7.3.3	Shashe Deposit	259
7.3.3.1	Introduction	259
7.3.3.2	Local Geology	260
7.3.3.3	Method of Study	260
7.3.3.4	Structure and Alteration at the Shashe Deposit	261
7.3.3.5	Nature of Mineralization	267
7.4	Geochemistry of the Mineral Deposits	272
7.4.1	Introduction	272
7.4.2.	Geochemistry of Alteration Zones	272
7.4.2.1	Signal Hill Deposit	272
7.4.2.2	Shashe Deposit	277
7.4.4	Geochemistry of Banded Iron Formations	289
7.4.5	Fluid Inclusion Studies	294
7.4.5.1	Introduction	294
7.4.5.2	Method of Study	296
7.4.5.3	Nature and Occurrence of Fluid inclusions	298
7.4.5.4	Microthermometric Analysis	304
7.4.6	Oxygen and Carbon Isotope Geochemistry	308
7.4.6.1	Introduction	308
7.4.6.2	Oxygen Isotopes	309
7.4.6.3	Carbon Isotopes	313
7.4.6.4	Summary on Oxygen and Carbon Isotopic Composition	313
7.5	Occurrences of Banded Iron Formations and Gold Mineralization	315
7.6	Discussion	316
7.6.1	Summary of Geochemical Data of Mineral Deposits	317
7.6.2	Relationship of Banded Iron Formations to Gold Mineralization	321

CHAPTER EIGHT

8. METALLOGENIC MODEL FOR THE TATI GREENSTONE BELT GOLD DEPOSITS

8.1	Introduction	323
8.2	Gold Deposits in Archean Greenstone Belts of Zimbabwe	324
8.3	Characteristics of Gold Deposits of the Tati Greenstone Belt	329
	8.3.1 Summary of metallogenic features of gold mineralization in the Tati Greenstone Belt	329
8.4	Metallogenic Model	331

CHAPTER NINE

9. SUMMARY AND CONCLUSIONS

9.1	Summary of Geological Characteristics	337
9.2	Summary of Characteristics of Mineral Deposits	340
9.3	Recommendations for Future Studies	341

REFERENCES	343
------------	-----

APPENDIX (Geochemical Methods)	376
--------------------------------	-----

MAPS IN POCKET	
----------------	--

LIST OF TABLES

Table 5.1	Geochemical data of samples of mafic rocks of the Lady Mary Group of the Tati Greenstone Belt	148
Table 5.2	Element ratios of the mafic rocks of the Lady Mary Group	150
Table 5.3	Geochemical data of samples of granitoid rocks of the Tati Greenstone Belt	178
Table 5.4	Geochemical characteristics of granitoids of Tati Greenstone Belt (High-alumina-type)	195
Table 5.4	Geochemical characteristics of granitoids of Tati Greenstone Belt (Low-alumina-type)	196
Table 7.1	Geochemical data of samples from boreholes SGH 63 and 71 at the Signal Hill Deposit	274
Table 7.2a	Geochemical data of samples from the N9 reef zone of the Shashe Deposit	278
Table 7.2b	Geochemical data of samples from borehole UKD 31 at the Shashe Deposit	279
Table 7.3	Fluid inclusion geochemical data	297
Table 7.4	Carbon and Oxygen isotopic data	310
Table 7.5a	Metallic associations in mineral deposits of the Tati Greenstone Belt	319
Table 7.5b	Gangue minerals in the mineral deposits of the Tati Greenstone Belt	320

LIST OF FIGURES

	Page	
Figure 1.1	Map of Botswana showing location of the Tati Greenstone Belt	7
Figure 1.2	Map of northeastern Botswana showing the location of the Tati Greenstone Belt	8
Figure 1.3	Map showing geographic location names in the Tati Greenstone Belt	10
Figure 2.1	Geological map showing Archean granite-greenstone belts of the Kaapvaal and Zimbabwe Cratons	17
Figure 2.2	Map of Africa showing the locations of the Kalahari Shield	18
Figure 2.3	Map of Zimbabwe Craton showing the relationship of greenstone belts and granitoids	22
Figure 2.4	Map of the Zimbabwe Craton showing the distribution of the 3.0-2.9 Ga and 2.8-2.6 Ga greenstone belts	30
Figure 2.5	Map showing the tectonic subdivisions of the Limpopo Belt (after Mason, 1973)	36
Figure 2.6	Watkey's (1983) subdivision of the Limpopo Belt	39
Figure 3.1		IN POCKET
Caption to Figure 3.2		49
Figure 3.2	Geological Map of the Tati Greenstone Belt (adapted from Key, 1976)	50
Figure 3.3	Structural map of the Tati Greenstone Belt (adapted from Coward and James, 1974)	54
Figure 3.4	Map of the Tati Greenstone Belt showing its subdivision into Western, Southeastern and Eastern Zones	57
Figure 3.5		IN POCKET
Figure 3.6	Geological map of the Western Zone of the Tati Greenstone Belt subdivided into a northern granitoid terrane and a southern main volcano-sedimentary terrane by the Matsiloje-Francistown tectonic discontinuity	59
Figure 3.7		IN POCKET
Figure 3.8	Geological Map of the Tati Greenstone Belt	64
Figure 3.9	Stratigraphic column of the Lady Mary Group	72
Figure 3.10	Geological map of the Phenalonga Group	74
Figure 3.11	Stratigraphic column of the Phenalonga Group	77

Figure 3.12	Geological map of the Selkirk Group	78
Figure 3.13	Stratigraphic column of the Selkirk Group	81
Figure 3.14	Stratigraphic column of the Last Hope Group	83
Figure 4.1	Map showing the two structural zones of the Tati Greenstone Belt	91
Figure 4.2		IN POCKET
Figure 4.3	Simplified structural map of the Tati Greenstone Belt showing major lineaments/faults and folds	98
Figure 4.4	Major lineaments of the Western Structural Zone of the Tati Greenstone Belt	105
Figure 4.5	Geological Map of the area west of Francistown	108
Figure 4.6	Major lineaments/faults of the Tati Greenstone Belt	110
Figure 4.7	Map showing extensional faults that control the Last Hope Basin structure	112
Figure 4.8	Schematic cross-section of the Mphoeng area of the Tati Greenstone Belt	117
Figure 4.9	Geological map of the area between Matsiloje and Signal Hill ridges	118
Figure 4.10	Rose diagram of major lineaments of the Tati Greenstone Belt	120
Figure 4.11	Geological map showing the distribution of the komatiite-tholeiite sequence from calc-alkaline volcano-plutonic and feldspathic sedimentary rock sequences	125
Figure 4.12	Geological map of the area around the Southern Tati Pluton	130
Figure 5.1a	Log (CaO/K ₂ O) versus Log (Al ₂ O ₃ /K ₂ O) for mafic rocks of the Tati Greenstone Belt	141
Figure 5.1b	Nb versus Ba scatter diagram for mafic rocks of the Tati Greenstone Belt	141
Figure 5.2	Primitive-mantle-normalized element diagram for modern oceanic rocks	143
Figure 5.3	Jensen cation plot for mafic rocks of the Lady Mary Group	149
Figure 5.4	FeO*/MgO ratio versus TiO ₂ for mafic rocks	151
Figure 5.5a	Al ₂ O ₃ /TiO ₂ versus TiO ₂ for mafic rocks	153
Figure 5.5b	CaO/TiO ₂ versus TiO ₂ for mafic rocks	154
Figure 5.6a	Zr/Nb-Zr/Y-Y/Nb diagram for mafic rocks of the Tati Greenstone Belt	157
Figure 5.6b	Zr/Nb-Zr/Y-Y/Nb diagram for mafic rocks of the Barberton Mountain Land Greenstone Belt	158

Figure 5.7a	Nb-normalized diagram comparing mafic rocks of the Lady Mary Group (samples AR 47, and 204) with modern oceanic rocks	160
Figure 5.7b	Nb-normalized diagram for mafic rocks of the Lady Mary Group (samples AR 151 and 152)	160
Figure 5.7c	Nb-normalized diagram comparing mafic rocks of the Lady Mary Group (samples AR 47, 50, 98, 193 and 204) with modern oceanic rocks	161
Figure 5.7d	Nb-normalized diagram of mafic rocks of the Lady Mary Group (samples AR 45 and 207)	161
Figure 5.8	(La/Ce) _n -(La/Sm) _n -(La/Yb) _n diagram for mafic rocks of the Lady Mary Group	165
Figure 5.9a	Chondrite-normalized REE diagram for the LREE-enriched mafic rocks of the Lady Mary Group (samples AR 151 and 152)	167
Figure 5.9b	Chondrite-normalized REE diagram for MORB-likemafic rocks of the Lady Mary Group (samples AR 204, 193 and 47)	167
Figure 5.9c	Chondrite-normalized REE diagram for the komatiitic-affinity rocks of the Lady Mary Group (samples AR 45 and 207)	168
Figure 5.9d	Chondrite-normalized REE diagram comparing MORB-like Tati Greenstone Belt mafic rocks with modern MORB subtypes	168
Figure 5.9e	Chondrite-normalized REE diagram comparing the LREE-enriched mafic rocks of the Tati Greenstone Belt with modern P-MORB	169
Figure 5.9f	Chondrite-normalized REE diagram comparing the different magmatic suites of mafic rocks of the Lady Mary Group	169
Figure 5.10a	Primitive-mantle-normalized diagram comparing MORB-like Tati Greenstone Belt mafic rocks with modern MORB subtypes	171
Figure 5.10b	Primitive-mantle-normalized diagram for mafic rocks of the Tati Greenstone Belt	171
Figure 5.10c	Primitive-mantle-normalized diagram for LREE-enriched mafic rocks of Tati Greenstone Belt	172
Figure 5.10d	Primitive-mantle-normalized diagram for komatiitic-affinity rocks of the Lady Mary Group	172
Figure 5.11	Geological map of the Tati Greenstone Belt	

	showing the distribution of the granitoids	177
Figure 5.12	QAP mesonorm diagram of the Tati Greenstone granitoid rocks	180
Figure 5.13	O'Conner's (1965), Ab-Or-An diagram of Tati Greenstone Belt granitoids	181
Figure 5.14	K-Na-Ca ternary plot of Tati Greenstone Belt granitoids	182
Figure 5.15	The Al_2O_3 -Yb diagram of the Tati Greenstone Belt granitoids	185
Figure 5.16a	K-Rb binary plot of Tati Greenstone Belt granitoids	186
Figure 5.16b	Ba-Rb binary plot of Tati Greenstone Belt granitoids	186
Figure 5.16c	Rb-Sr binary plot of Tati Greenstone Belt granitoids	187
Figure 5.16d	Ba-Sr binary plot of Tati Greenstone Belt granitoids	187
Figure 5.17a	Chondrite-normalized REE diagram for the high alumina-type granitoids	190
Figure 5.17b	Chondrite-normalized REE diagram for the low alumina-type granitoids of Tati Greenstone Belt	190
Figure 5.18	Chondrite-normalized REE diagram for the Tati Batholith granitoids	191
Figure 5.19a	Primitive-mantle-normalized element diagram for the high alumina-type granitoids of the Tati Greenstone Belt	193
Figure 5.19b	Primitive-mantle-normalized diagram for the low alumina-type granitoids of Tati Greenstone Belt	193
Figure 5.20	Rb versus Nb+ Y diagram of the Tati Greenstone Belt granitoids	200
Figure 6.1	Stratigraphic column of supracrustal rocks of the Tati Greenstone Belt	205
Figure 6.2	Diagrammatic representation of the Archean Tati Greenstone Belt back-arc basin magmatic suites	208
Figure 6.3	Schematic diagram showing the tectonic setting of high-mg granitoids of the Tati Greenstone Belt relative ultramafic-mafic rocks	211
Figure 6.4	Relationship of structures in the Shashe Belt with those of the Tati Greenstone Belt	213
Figure 6.5	Tectonic evolution of the Tati Greenstone Belt	215

Figure 6.6	Schematic diagram showing the amalgamation of tectonostratigraphic terranes of the Tati Greenstone Belt	217
Figure 7.1	Geological map of the Shashe Group of Deposits	226
Figure 7.2	Alteration map at the Shashe Mine	227
Figure 7.3	Geological map of Signal Hill Deposit	234
Figure 7.4	Geological map showing structural domes related to massive sulphide deposits	236
Figure 7.5	Map of the Tati Greenstone Belt showing the relationship of mineral deposits with major lineaments	239
Figure 7.6	Map of the Tati Greenstone Belt showing the relationship of mineral deposits with banded iron formations	240
Figure 7.7	Borehole log of BH 63 in the Signal Hill Deposit	244
Figure 7.8	Schematic cross-section showing the Relationship of the Last Hope Fault Zone (LHFZ) and the Last Hope Basin	247
Figure 7.9	Schematic diagram showing the distribution of microfractures and quartz veins in the main shear zone at the Signal Hill Deposit	249
Figure 7.10	Schematic diagram illustrating the relationship of microfractures and microfolds during simple shear deformation at Signal Hill Deposit	252
Figure 7.11	Relationship of C-S and C'-S' shears at the Signal Hill Deposit	252
Figure 7.12	Borehole log for BH TMP 23 at the Shashe Deposit	262
Figure 7.13	Schematic diagram showing progressive development of the alteration zone at the Shashe Deposit	263
Figure 7.14a	K-Rb Log-Log diagram for mineralized sedimentary rocks from boreholes SGH 63 and SGH 71 at the Signal Hill Deposit	275
Figure 7.14b	K-Ba Log-Log diagram for mineralized sedimentary rocks from boreholes SGH 63 and SGH 71 at the Signal Hill Deposit	275
Figure 7.14c	The K-Sr Log-Log diagram for mineralized sedimentary rocks from boreholes SGH 63 and SGH 71 at the Signal Hill Deposit	276
Figure 7.15	Na ₂ O-CaO-K ₂ O diagram of the mineralization	

	and alteration zones at the Shashe Deposit	282
Figure 7.16	The Pb-Cu-Zn ternary diagram for altered rocks from N9 reef zone at the Shashe Mine	282
Figure 7.17a	K-Rb Log-Log diagram for rock samples from borehole UKD 31 at the Shashe Mine	284
Figure 7.17b	K-Ba Log-Log diagram for rock samples from borehole UKD 31 at the Shashe Mine	284
Figure 7.17c	Ba-Rb Log-Log diagram for rock samples from borehole UKD 31 at the Shashe Mine	285
Figure 7.17d	K-Sr Log-Log diagram for rock samples from borehole UKD 31 at the Shashe Mine	285
Figure 7.18a	Chondrite-normalized REE diagram for carbonate alteration zone samples from borehole UKD 31 at the Shashe Mine	287
Figure 7.18b	Chondrite-normalized REE diagram for silicified alteration zone samples from borehole UKD 31 at the Shashe Mine	287
Figure 7.19	Comparison of stratigraphic column of banded iron formations from Matsiloje ridge and gossans from Mphoeng area in Zimbabwe	291
Figure 7.20a	REE chondrite-normalized diagram of banded iron formation samples from Tati Greenstone Belt	292
Figure 7.20b	REE diagram of banded iron formation samples normalized to LREE-enriched of the Lady Mary Group of the Tati Greenstone Belt	292
Figure 7.20c	REE diagram of banded iron formation samples from Tati Greenstone Belt normalized to host basaltic rocks at the Shashe Mine	292
Figure 7.21	Chondrite-normalized REE diagram of banded iron formations from other parts of Southern Africa	295
Figure 7.22	Type A fluid inclusions shape-diagrams	301
Figure 7.23	Type B fluid inclusions shape-diagrams	302
Figure 7.24	Type C fluid inclusions shape-diagrams	303
Figure 7.25a	Homogenization temperature variation of the type C fluid inclusions	306
Figure 7.25b	Melting temperatures of clathrate solid	306
Figure 7.25c	Homogenization temperatures for CO ₂ -gas	306
Figure 7.26a	Homogenization temperatures for type A fluid inclusions	307
Figure 7.26b	Freezing temperatures for type A fluid inclusions	307
Figure 7.27	Variation diagram of oxygen isotopes	312

Figure 7.28	Variation diagram of carbon isotopes	314
Figure 8.1a	Lead isotopic signatures for gold Archean deposits in Zimbabwe from Robertson (1973)	325
Figure 8.1b	Lead isotopic signatures for gold Archean deposits in Zimbabwe from Kramers and Foster (1984)	325
Figure 8.2	Diagrammatic representation of the metallogenic model gold deposits of the Tati Greenstone Belt	333

LIST OF PLATES

	Page
Plate 4.1	94
Plate 4.2	100
Plate 4.3	100
Plate 4.4	101
Plate 4.5	104
Plate 4.6	107
Plate 4.7	109
Plate 4.8	109
Plate 4.9	122
Plate 4.10	123
Plate 4.11	127
Plate 4.12	127
Plate 4.13	128
Plate 4.14	128
Plate 7.1	251
Plate 7.2	254
Plate 7.3	254
Plate 7.4	256
Plate 7.5	256
Plate 7.6	257
Plate 7.7	265
Plate 7.8	265

Plate 7.9	Interconnected micro-fractures at the boundaries of carbonate mineral crystals	266
Plate 7.10	Silicification of carbonate alteration	266
Plate 7.11	Common brown biotite alteration zone found enveloping mineralized veins at the shashe Deposit	268
Plate 7.12	Late silicification quartz veins at the Shashe Deposit	268
Plate 7.13	Boundinaged quartz veins in mineralized shear zones at the Shashe Deposit	269
Plate 7.14	Mica-fish structures at the Shashe Deposit	269

CHAPTER ONE

1. INTRODUCTION

1.1 Outline of the Project

Although tremendous progress has been made in research on mesothermal gold mineralization in Archean greenstone belts, problems with respect to the sources of both metals and mineralizing fluids still remain largely unresolved. Structural studies during the past decade have revealed that mesothermal gold mineralization is structurally controlled at both deposit and district scales (e.g. Roberts, 1987; Colvine et al., 1984; Sibson, 1989; Hodgson, 1989; Poulsen and Roberts, 1989; Harris, 1987; Eisenlohr, 1989; Muller and Harris, 1987; Cox et al., 1986). Mineralization is localized in ductile-brittle environments within cross-stratigraphy, secondary shear zones in greenstone belts (e.g. Sibson, 1989). Such shear zones are generally associated with large terrane boundary faults, which themselves are not mineralized.

Studies on the chemical characteristics of gold mineralization have also contributed greatly to the understanding of Archean mesothermal gold deposits (Kerrick and Fryer, 1979; Colvine et al., 1984; Kerrich, 1989; Golding and Wilson, 1987; Perring et al., 1987). Such studies have indicated that the ore fluids were generally low salinity, high pH, CO₂-rich and with low base metal contents.

In spite of these determinations, disagreements still exist on what role host rock lithology plays in mineralization. For instance, most structural geologists contend that structure plays the dominant role in Archean mesothermal gold mineralization, with

the host rock playing little or no role. In general, they suggest that mesothermal gold deposits are deposited in low strain areas; at structural jogs, bends and other related dilatant zones in strike-slip fault/shear zones. In such models, mineralizing fluids and metals are derived from the lower crust, and were transported to mineralized areas along terrane boundary faults. Hutchison and Burlington (1984), however, wondered why gold mineralization would be restricted to greenstone belts, if lithology and stratigraphy do not play any role during the deposition of these deposits.

Geologists with a geochemical background, on the other hand, argue that the host rock lithology is a very important factor in localizing gold mineralization, in terms of providing both a chemical control for the deposition of metals from hydrothermal fluids, Fe-rich rocks being more favourable (cf. Phillips and Groves, 1984), and a mechanical control as competent rocks fracture easily (e.g. Eisenlor et al., 1989). In the Zimbabwe Craton greenstone belts, Foster (1985) showed that gold mineralization is most common in banded iron formations, especially those related to tholeiitic ultramafic-mafic volcano-plutonic rocks. Roberts et al. (1990) suggested that gold mineralization in Archean greenstone belts is more prominent in tholeiitic rocks than calc-alkaline rocks. Madu et al. (1990) observed that Sb-Au deposits in greenstone belts are most common in turbidites or feldspathic sedimentary rocks. Pirc and Rose (1990), on the other hand, indicated that red-bed sedimentary rocks generally contain high background levels of antimony. Stone (1990) concluded that there is a restriction of gold orebodies to specific rock types, suggesting a stratigraphic control to gold mineralization.

In general, however, the geochemical and structural characteristics of Archean mesothermal gold mineral deposits are similar whatever the host lithology within and between greenstone belts. Differences in the metallic associations of deposits may be a function of the interaction of mineralizing fluids with different host lithologies. The extent to which lithology and stratigraphy control gold mineralization is, however, poorly understood as research is generally undertaken on the scale of individual deposits or mines. Results from such small scale studies are usually extrapolated to suggest belt, or province, -wide characteristics. In such situations, similarities are usually overemphasized at the expense of distinct differences.

To reconcile these polarized views, an integrated approach to research is required. Such an integrated study should combine structural, stratigraphical and geochemical data at both deposit and regional scales. In a study of this nature, it should be possible to (i) assess the role of structure in the distribution and localization of mineral deposits, (ii) identify the relative influences of lithology on mineralization, (iii) define the interrelation of the rock succession (e.g. petrogenetic suites) with the tectonic evolution of the belt, and (iv) identify both the mode of assembly (or accretion) of disparate terranes that constitute the belt, and the structures that are related to that accretion such as faults, shear zones, folds and thrust slices. If all of the relevant data are available, it would then be possible to develop a comprehensive metallogenic model.

This then is the approach taken in this metallogenic study of gold mineralization in the Tati Greenstone Belt of northeastern Botswana. Unfortunately

the geology of the Tati Greenstone Belt is poorly defined. This means that much of the required data had to be generated during the limited time span of this Ph.D research project, and therefore, some aspects of the metallogenic study were not subjected to the same degree of scrutiny. The relative value of specific components in the study depended on the author's perception of its relation to the understanding of gold mineralization. Nevertheless, a regional study of this magnitude, that integrates the stratigraphy, structure and tectonic history is essential to assess the distribution and localization of gold mineralization.

Metallogeny is defined as the study of factors that control the distribution of mineral deposits in space and time (Strong, 1987; Laznicka, 1985). In other words, the tectonic settings of ore-bearing lithologies control the distribution and nature of mineral deposits that develop in a particular environment. The metallogenic characterization of a tectonic environment and the understanding of lithological associations in that environment, require high quality stratigraphical, structural and geochemical data.

The main focus of this study is the relationship of gold mineralization to the evolution of the Tati Greenstone Belt. Although organized mining in Tati Greenstone Belt lasted for just under a century from 1866 to 1964, all mining activities were centred around ancient (ie. pre-1866) mining excavations and most modern mineral exploration has been concentrated around these ancient workings. Rainbow is the only gold deposit discovered by conventional mineral exploration techniques. There has been very little primary exploration in the unexamined areas of the belt. Key

(1976) suggested that for a belt of its size, very little gold has been produced from the Tati Greenstone Belt. Much greater gold production has been achieved from greenstone belts of similar size in adjacent Zimbabwe, and also in other parts of the world. As such, it was concluded that the Tati Greenstone Belt has a great, if unexamined, potential for further mineral discovery. Successful exploration, however, will depend on understanding the nature and distribution of the mineralization, and the relationship of mineralization to the tectonostratigraphic evolution of the belt. Essentially, the controls on the mineralization need to be evaluated.

1.2 Objectives and Aims of the Study

The aims and objectives of this study are as follows:

1. To constrain and evaluate the geotectonic setting of Tati Greenstone Belt rocks through the use of geochemical and structural data. Such geochemical studies will also contribute to the understanding of the geological evolution of Archean greenstone belts in general.
2. To constrain the stratigraphy of problem areas within the belt through the use of geochemical data.
3. To investigate the relationships between gold mineralization and the tectonic evolution of the Tati Greenstone Belt.
4. To compare mineralizing fluids from different types of gold deposits in the belt through comparative geochemical analysis of alteration zones at the Shashe and Signal Hill Deposits.

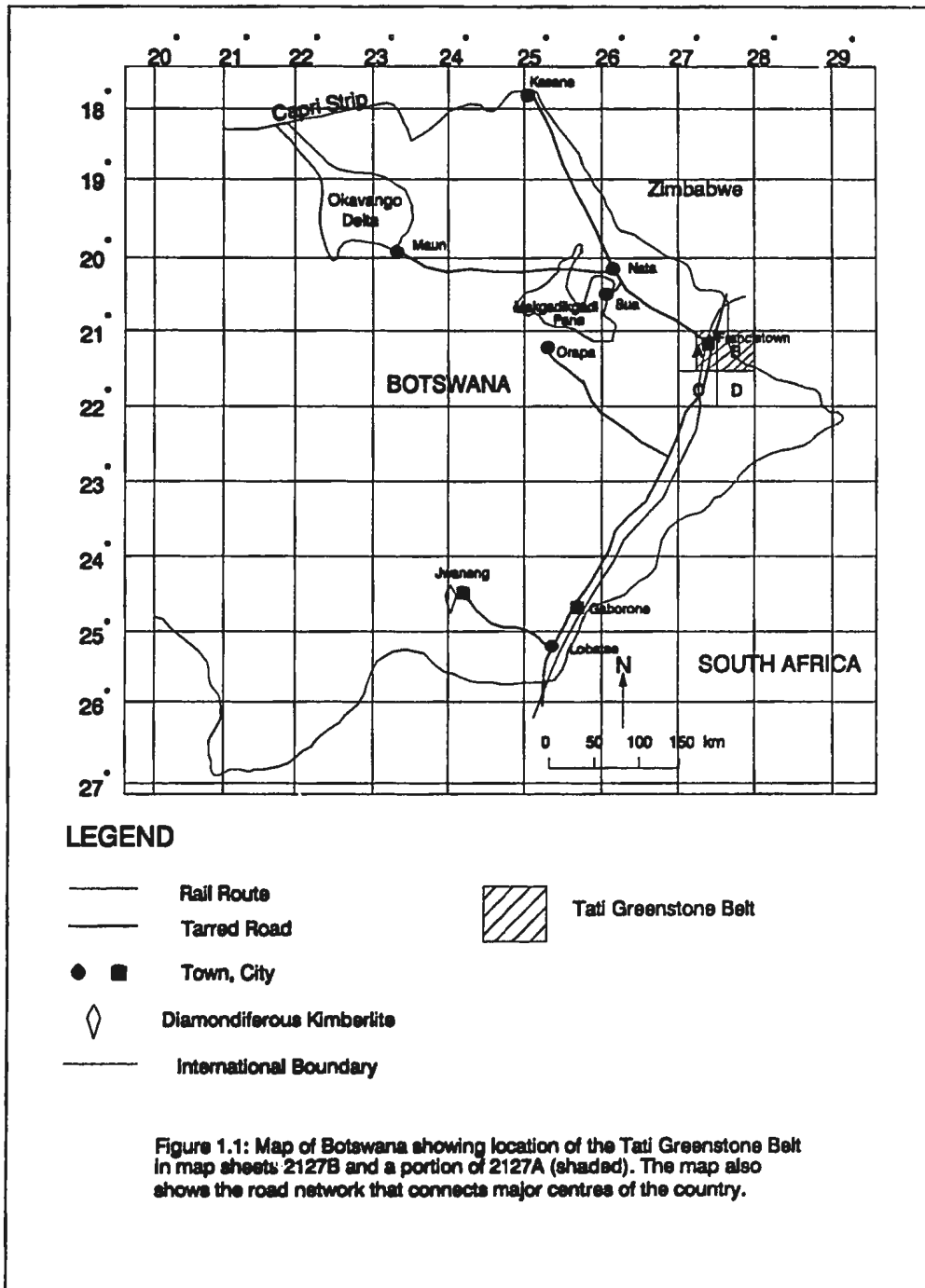
5. To produce a metallogenic map and model for the Tati Greenstone Belt.

This study was also aimed at utilising the abundant data accumulated during mining and mineral exploration periods (albeit incomplete) to produce a metallogenic map. It is hoped that this study will provide a basis for future mineral assessment of the Tati Greenstone Belt and similar belts elsewhere in Botswana.

1.3 Location and Access

The study area is located in northeastern Botswana, between latitudes 21°00' and 21°30' south and longitudes 27°25' and 27°45' east and is covered by Botswana quarter degree map sheet 2127B and a portion of 2127A (Figure 1.1). The Tati Greenstone Belt extends from Francistown, eastward for about 60 kilometres to Matsiloje village. The Ramokgwebana River, which flows through Matsiloje, forms both the international boundary between Botswana and Zimbabwe and the eastern limit of the Tati Greenstone Belt (Figure 1.2). The belt extends to the south from Francistown to the Shashe River. This river lies in the Tuli-Sabi shear zone system of the Limpopo Belt.

Francistown, with a population of about 70,000, is the second largest town in Botswana. A road network connects Francistown to the southern part of the country and to western Zimbabwe. Other roads link Francistown to the western part of the country and a gravel road runs westwards for 200 kilometres from Francistown to the Orapa Mine, the largest diamond mine in Botswana (Figure 1.1). A north-south railway line runs the entire length of eastern Botswana, connecting Botswana,



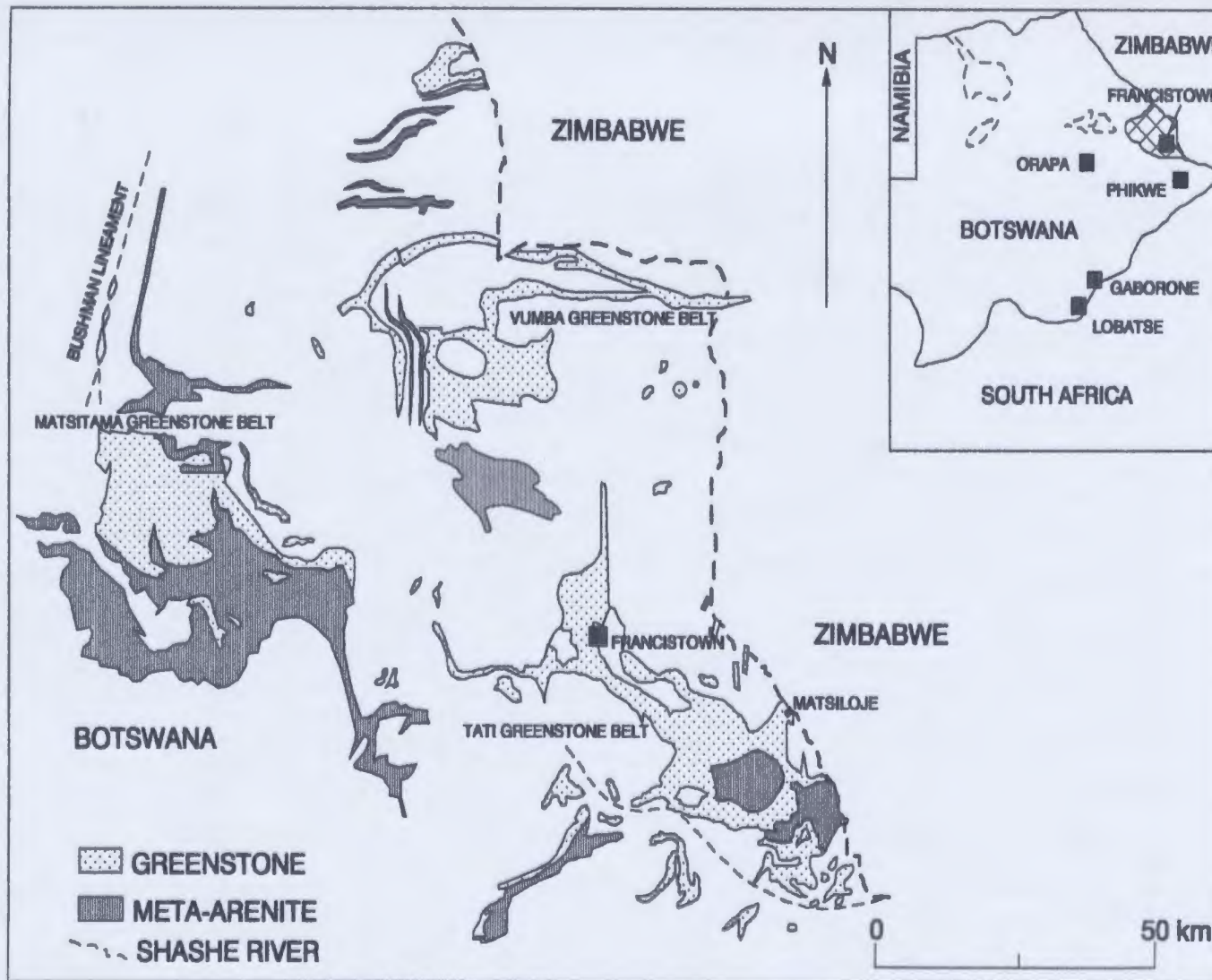


Figure 1.2: Map of northeastern Botswana showing the location of the Tati Greenstone Belt and other Archean greenstone belts. These belts form the western margin of the Zimbabwe Craton (after Crockett et al., 1974).

Zimbabwe and South Africa. A second railway line runs northwestwards from Francistown to the mining town of Sua in the Makgakgadi salt pans (Figure 1.1).

Good tracks and mineral prospecting cutlines traverse the study area. These tracks were developed during past and current mineral prospecting endeavours. A gravel road runs eastward through farms and mining camps connecting Matsiloje to Francistown. Farm roads and fence cutlines also provide important access routes through much of the Tati belt. Two major rivers, the Tati and the Sekukwe, also traverse the Tati Belt from the northwest and north to the southeast and provide good cross sections of the geology within the belt. The area between Francistown and Matsiloje is a very important cattle farming area. Disused mines on these farms are commonly used as watering points for cattle.

1.4 Physiography

The area is flat, with low lying hills throughout the entire exposure of the belt. Granitoid hills are prominent in the south and hills underlain by banded iron formations dot the area to the east. The highest hills in the area are the Matsiloje Ridges and Signal Hill with elevations of 1187m (3957 ft) and 1136m (3786 ft) above sea level, respectively (Figure 1.3). Nyambabwe Hill, in Francistown, is 1081m (3604 ft) above sea level.

The Matsiloje Ridges and Signal Hill are underlain by banded iron formations. Nyambabwe Hill in Francistown is composed of tonalite. Valleys and low land areas are underlain by mafic rocks and gneisses. Geological control of the topography is

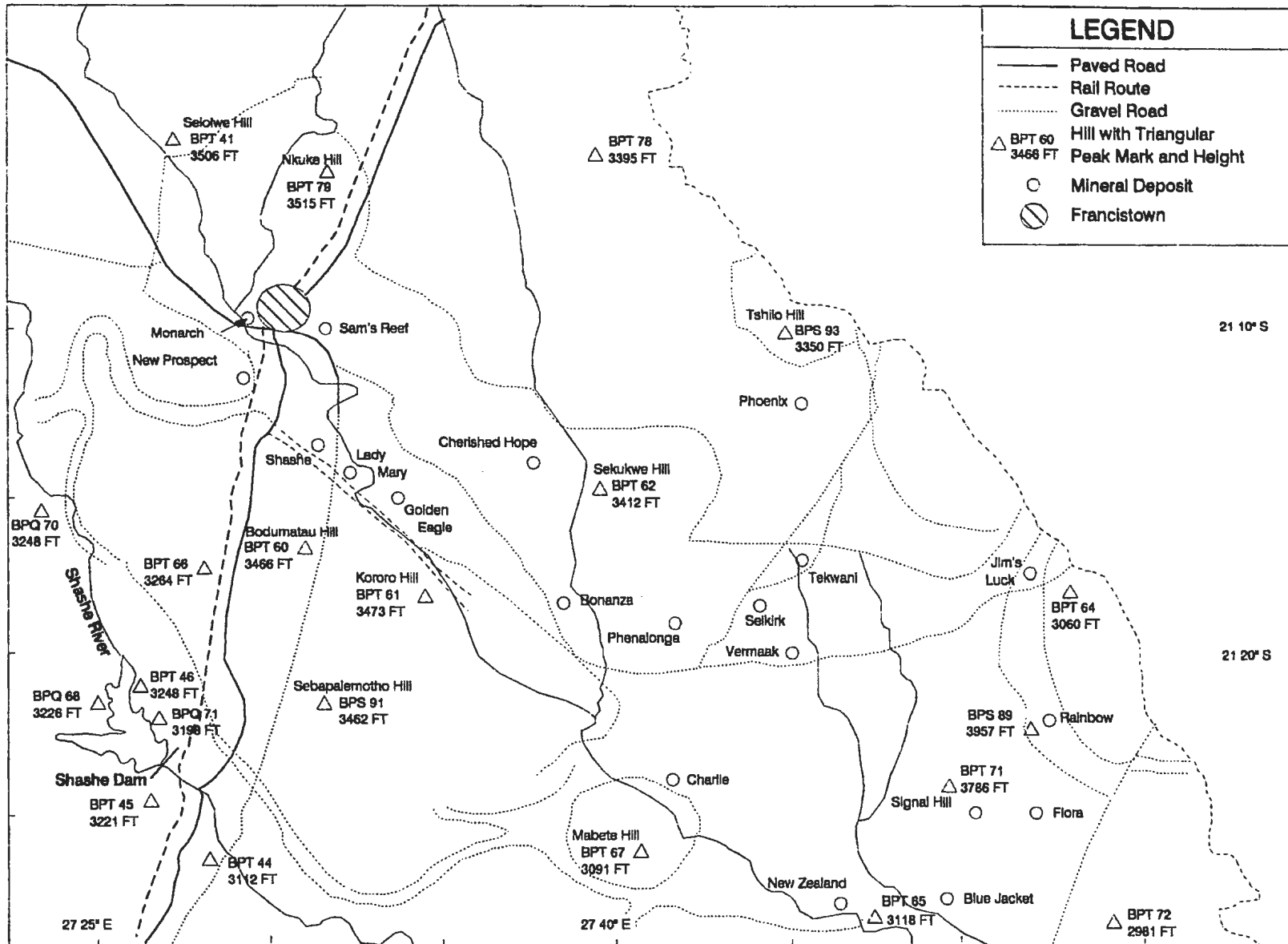


Figure 1.3: Map showing geographic location names in the Tati Greenstone Belt area.

also reflected in the distribution of soils and vegetation. The mafic rock-bearing areas are covered by black cotton soils, grey earthy soils, and small thorny, scrub bushes with long grass. The granitoid and pink gneiss areas are overlain by pink sandy soils with tall savanna-type trees and short grasses.

1.5 Previous Studies

1.5.1 Exploration

The first discovery of gold in Southern Africa was made by Carl Mauch in 1864 in the Tati Greenstone Belt. Following this discovery, mining started in 1866 and carried on for almost a century until 1964 when the last operation ceased production. Although mining went on for almost a century, mining and exploration records from this period were poorly kept. The Tati Company, formed in 1871, acquired exclusive mining rights in the area in the early 1960's. The company undertook several exploration programmes throughout this period, and the most comprehensive of these programmes was carried out in 1960. The 1960 program included an evaluation of abandoned gold mines, and belt-wide geochemical sampling with limited geophysical surveys. Anomalies were further investigated by wagon and diamond drilling. Between 1969 and 1971 Sedge Botswana, a subsidiary of Anglo American Corporation, undertook an extensive exploration programme in Tati Greenstone Belt, which included geochemical sampling and drilling, to estimate mineral potential of abandoned small gold mines. Geophysical surveys and wagon drilling were used to further evaluate geochemical anomalies. Two small mines, Map-Nora and Bonanza

(Figure 1.3), were reported to have mineral potential (Molyneux, 1971). Prussag Botswana also explored the Tati area between 1978 and 1979.

The increase in gold price during the early 1980's led to renewed interest in the Tati Greenstone Belt. This interest centred mainly on secondary recovery from mine dumps. Grassroots exploration was carried out by Falconbridge Ltd. (Johnston and Griffiths, 1982) and Goldfields (Sheeran, 1986). Morex Botswana concentrated on the evaluation of massive sulphide deposits at Selkirk and Phoenix. They also evaluated abandoned gold mines in the Tekwani and Rainbow areas and brought the Rainbow Mine into production in 1986. Map-Nora (now called the Shashe Mine) was operated between 1988 and 1990 by Phelps Dodge, Botswana. The Bonanza deposit is now being worked on a small scale. Joint venture partners Falconbridge and Seltrust evaluated the Signal Hill Au-Sb prospect for three years, until 1989, when Seltrust withdrew from the venture. Falconbridge is continuing with its exploration programme at Signal Hill. Morex and BCL are mining the Selkirk massive sulphide deposit. Mining and Development Botswana is currently evaluating the Monarch mine west of Francistown.

1.5.2 Previous Geological Research

The first geological map of the Tati area was produced by Tulloch in 1929. Several members of the then Bechuanaland Geological Survey (now the Botswana Geological Survey) reviewed different aspects of the geology and mineral deposits of the Tati Greenstone Belt. Boocck (1951) mapped part of the southern

arm of the belt. Kyanite and gold occurrences in the belt were reviewed by Lamont (1950a; 1950b) and Poldervaart (1950). Gerrard (1960) produced petrographic descriptions of some rocks from the belt. Chemical analyses of metalliferous samples were carried out by Van Stratzen (1954). Gravel resources of the area were assessed by Jones (1962). Mason mapped the Tati Greenstone Belt, and the adjacent area of Limpopo Belt, for his Ph.D. thesis between 1967 and 1969 (Mason, 1970). Key (1976) carried out further geological mapping in the area covered by Mason. A photogeological interpretation of the Archean geology of NE Botswana was undertaken by Key and Hutton (1976). Baldock et al. (1976) commented on the geology of the area while reviewing the mineral deposits of Botswana. Crockett et al. (1974) produced a map of the Precambrian geology of northeast Botswana, and Bennett (1971) produced a tectono-metamorphic map of the same area. Structural studies on portions of the belt were carried out by the Leeds University structural geology group between 1973 and 1976 (Coward et al., 1973,1976; Coward and James, 1974; Coward, 1980,1984). These studies concentrated on the relationship between the Limpopo Belt and greenstone belts of the Zimbabwe Craton. Mineralogical and fluid inclusion studies were carried out by Harwood (1986), for Falconbridge Exploration Botswana, on samples from the Signal Hill Au-Sb prospect.

Regional geophysical survey coverage of Botswana has been completed. Gravity surveys were carried out between 1970 and 1971 (Reeves and Hutchins, 1976). Aeromagnetic surveys were completed between 1976 and 1977 in western Botswana (Reeves, 1978); and in 1986 in eastern Botswana.

1.6 Method of Research

1.6.1 Laboratory and Desktop Studies

There are a considerable amount of data on mineral deposits within the Tati Greenstone Belt on file with the Botswana Geological Survey, and thus considerable time was spent synthesizing and collating these data to compile a metallogenic map. It was initially planned to compile the geological information available from all existing geological maps as a geological base for the metallogenic map. It was soon realized that most of the geological information and interpretations in these maps could not be reconciled. An extensive photogeological interpretation was therefore undertaken using aerial photographs of the area, at a working scale of 1:50,000, and satellite imagery. The combination of aerial photogeological interpretation, systematic field checks and the incorporation of the recently acquired aeromagnetic data for eastern Botswana, made it possible to adapt and re-interpret geological data contained on old geological maps. The data were also used to produce the current version of the geological map, on which the metallogenic map was based.

Rock sample preparations were carried out (see Appendix for details) at both the Botswana Geological Survey and the Centre for Earth Resources Research (CERR)/Department of Earth Sciences, Memorial University of Newfoundland. Analyses were completed at the CERR laboratories. Major elements were determined by atomic absorption spectroscopy (AAS), while trace element (Nb, Zr, Y, Ga, Rb, Pb, Th, U, Sr, Cr, Zn, Cu, Ni, and V) contents were determined on pressed powder pellets by X-Ray Fluorescence spectroscopy. A suite of samples was

analyzed for trace elements, including rare earth elements (REE), by Inductively Coupled Plasma-Mass Spectrometry (ICP-MS). C and O isotope data for carbonate mineral separates were determined with a gas source mass spectrometer. Fluid inclusions in doubly polished sample wafers were analyzed using a Leitz petrographic microscope with a Fluid Inc. heating/freezing stage.

1.6.2 Field Work

Field work was carried out during two field seasons; the first covered the period from July to October 1988, and the second was from June to September 1989. The field work involved general field mapping, field checking of the photogeological map, and investigation of lithological, stratigraphic and regional structural relations. Rock samples for geochemical studies were collected from both the regional mapping and selected cored boreholes at the Shashe and Signal Hill Deposits. Field traverses were carried out along major rivers and streams that provide cross sections of the geology of the area.

CHAPTER TWO

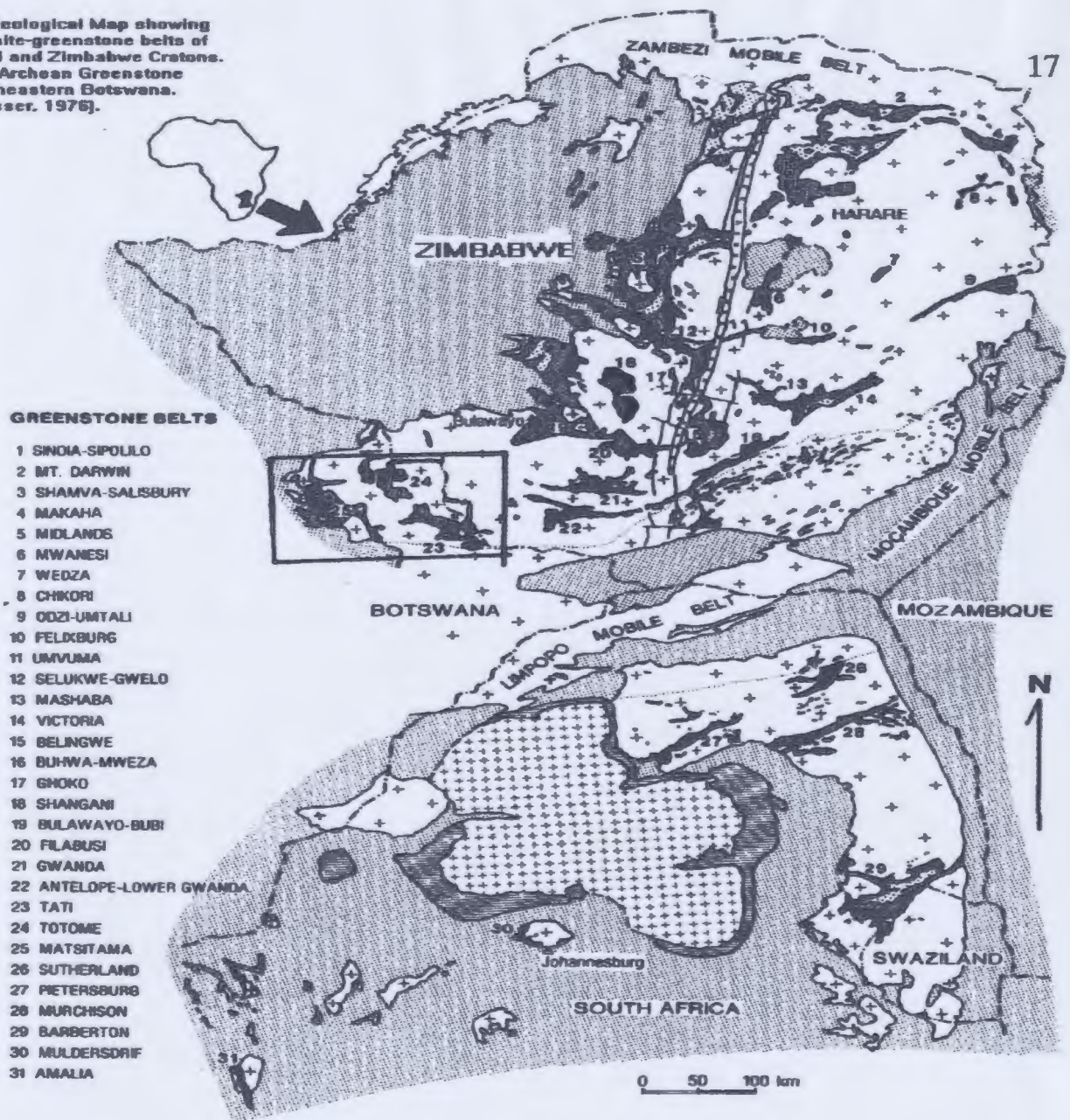
2. REGIONAL GEOLOGICAL FRAMEWORK

2.1 Introduction

The Archean Tati Greenstone Belt is one of the greenstone belt enclaves of the Zimbabwe Craton (Figure 2.1). The Zimbabwe Craton is separated from the Kaapval Craton by linear, polydeformed, high metamorphic grade rocks of the Limpopo Belt. These two Archean cratons and the Limpopo Belt constitute the oldest Precambrian shield in the southern African Subcontinent (Kalahari Shield; Figure 2.2). Isotopic ages of rocks from this shield suggest the presence of crust older than 3.64 Ga (Hunter, 1991) or even as old as 3.8 Ga (Barton, 1981).

This chapter briefly reviews the geology of the Zimbabwe Craton, with the aim of introducing the broad regional stratigraphic and tectonic relations of the Archean supracrustal rocks that constitute this craton. Furthermore, this review will attempt to summarize the stratigraphy of supracrustal rocks from the Zimbabwe Craton in light of recent research on Archean greenstone belts elsewhere in the world, most especially in Canada and Australia (Ayres and Thurston, 1985; Thurston and Chivers, 1990; Barley and Groves, 1990). The geological and stratigraphic relations of rocks within the Limpopo Belt, especially along the northern margin, will also be summarized. The northern margin of the Limpopo Belt constitutes a unique geological terrane, the Northern Marginal Zone, that has different structures and stratigraphy than the other terranes within the Limpopo Belt. The Tati Greenstone

Figure 2.1: Geological Map showing Archean granite-greenstone belts of the Kaapvaal and Zimbabwe Cratons. Inset shows Archean Greenstone belts of Northeastern Botswana. (After Ahacusser, 1976).



GREENSTONE BELTS

- 1 SINOA-SIPOLO
- 2 MT. DARWIN
- 3 SHAMVA-SALISBURY
- 4 MAKAHA
- 5 MIDLANDS
- 6 MWANESI
- 7 WEDZA
- 8 CHIKORI
- 9 ODZI-UMTALI
- 10 FELDBURG
- 11 UMVUMA
- 12 SELUKWE-GWELO
- 13 MASHABA
- 14 VICTORIA
- 15 BELINGWE
- 16 BUHWA-MWEZA
- 17 GNOKO
- 18 SHANGANI
- 19 BULAWAYO-BUBI
- 20 FILABUSI
- 21 GWANDA
- 22 ANTELOPE-LOWER GWANDA
- 23 TATI
- 24 TOTOME
- 25 MATSITAMA
- 26 SUTHERLAND
- 27 PIETERSBURG
- 28 MURCHISON
- 29 BARBERTON
- 30 MULDESDRIF
- 31 AMALIA

LEGEND

- Younger cover
- Great Dyke
- Felsic phase
- Mafic phase
- Archean granites, gneisses, migmatites
- Bushveld Igneous Complex

GREENSTONE BELT LITHOLOGICAL UNITS

	ZIMBABWE	BOTSWANA	SOUTH AFRICA/SWAZILAND
	Shamvalan	Lasthope	Figtree, Moodles
	Bulawayan	Phenalonga	
	Sebakwian	Ladymary	Onverwacht

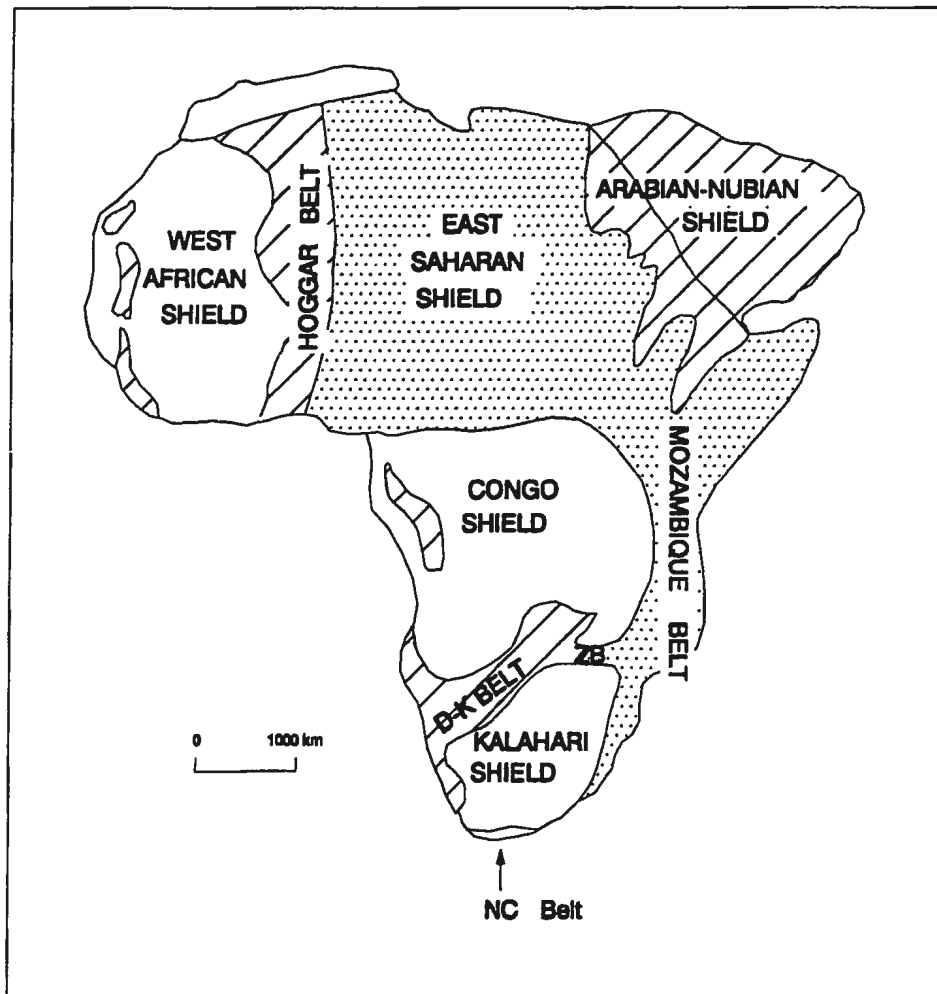


Figure 2.2: Map of Africa showing the location of the Kalahari Shield, which is separated from Congo Shield by the polydeformed late Proterozoic-Paleozoic Damara- Katangan Belt (D-K). To the north, east and south, the Kalahari Shield is bounded by the Zambezi Belt (ZB), Mozambique Belt and the North Cape Belt (NC) respectively. The Kalahari Shield contains the Archean Cratons of Zimbabwe and Kaapvaal (modified after Clifford, 1968).

Belt shares a boundary with the northern margin of the Limpopo Belt.

2.2 Zimbabwe Craton

The Archean Zimbabwe Craton underlies most of the areal surface of Zimbabwe and a portion of northeastern Botswana (Figure 2.1). Proterozoic to younger cover rocks obscure the western margin of the craton. The Mozambique and Limpopo belts form the eastern and the southern margins of the craton, respectively. As in Precambrian shields elsewhere in world, two tectonostratigraphic terranes have been described in the Zimbabwe Craton; (i) polydeformed, high metamorphic grade (granulite facies) gneiss-granulite terranes, and (ii) lower metamorphic grade (greenschist facies) granite-greenstone belts (Stagman, 1978; Wilson, 1979; Orpen and Wilson, 1981).

It is generally suggested that the gneiss-granulite terranes are older than the granite-greenstone belts. For example, high grade gneisses in the Minnesota River Valley, Superior Province, have isotopic ages of up to 3.5 Ga, compared to the 2.7 Ga average age of greenstone belts in the province (Card and Ciesielski, 1985). The Ancient Gneiss Complex of Swaziland and South Africa contains rocks with isotopic ages up to 3.64 Ga compared with the 3.5 or 3.46 Ga ages of granite-greenstone belts (Kröner and Compston, 1988; Hunter, 1991). In western Australia, the Western Gneiss Terrane contains rocks with isotopic ages of around 3.4 Ga compared with 2.7 Ga for old granite-greenstone belts of the Yilgarn Block and the > 3.0 Ga old greenstone belts of the Pilbara Block (Einsenhohr et al., 1989; Barley, 1992).

Structural and stratigraphic relations suggest that contacts between gneiss-granulite terranes and granite-greenstone belts, although disrupted by granitoid plutonism, were tectonic (e.g. Card, 1990; Drugova et al., 1990; Hunter, 1991).

In some Precambrian shields, high grade gneisses similar to those in gneiss-granulite terranes have been suggested to form basement upon which the volcano-plutonic sequences of granite-greenstone belts were emplaced (Hunter, 1991; Drugova et al., 1990; Eisenlohr et al., 1989). For example, in western Australia, the Western Gneiss Terrane has been interpreted as exhumed deep crustal material that formed basement upon which the greenstone belt sequences were deposited (Myers, 1990). In Zimbabwe, it has also been suggested that some greenstone belt rocks may have been emplaced in a continental environment on a basement consisting of high grade gneisses (Hawkesworth and O'Nions, 1977).

2.2.1 Basement Complex

There is no hard evidence in the Zimbabwe Craton for the existence of basement gneisses. Furthermore, it has proven very difficult to differentiate between basement gneisses and diapiric granitoids within greenstone belts, because the Archean terranes are highly tectonized and deformed. Contacts between lithological units are highly sheared and faulted, making it very difficult to differentiate initially conformable contacts from unconformable and faulted contacts. Several claims have, however, been made as to the existence of basement gneisses in the Zimbabwe Craton (e.g., Wilson et al., 1978; Coward and James, 1974; Coward et al., 1976).

Coward et al. (1976) argued on structural grounds that there is "indisputable evidence" which indicates the existence of basement gneisses in the Zimbabwe Craton. They pointed out that sedimentary rocks near Shabani, in Zimbabwe, were deposited unconformably on a migmatite basement (Figure 2.3). They further argued that the gneisses on which these sedimentary rocks were deposited have a dominant NE-SW structural trend which is different from the dominant SW-NE structural trend developed within most of the greenstone belts.

In Botswana, NNW-trending high grade gneisses cropping out west of Francistown have been described as basement gneisses (Key, 1976; Key et al., 1976; Key and Hutton, 1976; Tankard et al., 1982). These rocks constitute Key's (1976) Shashe Gneiss Formation and also form Crockett's (1968) Shashe Mobile Belt, suggested to be an offshoot of the Limpopo Belt. The tectonic affinity of the Shashe Gneiss Formation in Botswana is, however, uncertain and only serves to underscore the difficulties in distinguishing basement gneisses from other types of granitoids. It has proven extremely difficult to recognise indisputable basement to Archean supracrustal rocks within the Zimbabwe Craton.

2.2.2 Greenstone Belts of the Archean Zimbabwe Craton

The supracrustal stratigraphies within Archean greenstone belts throughout the world, including those in the Zimbabwe Craton, are similar from belt to belt and as such the belts can be described by the same stratigraphic and/or tectonic model (Anhaeusser, 1973; Windley, 1973; Tarney et al., 1976; Jahn and Sun, 1979; Goodwin,

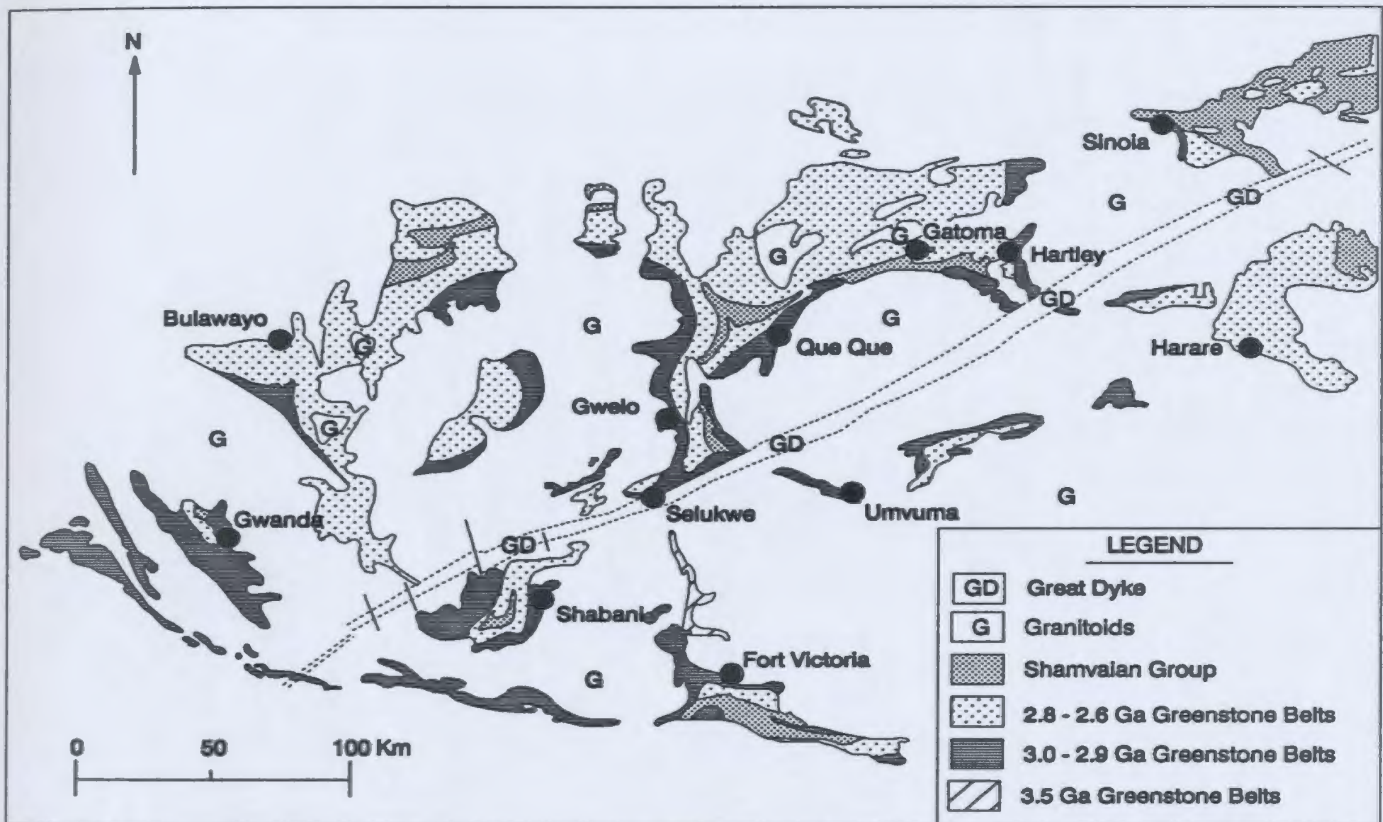


Figure 2.3: Map of part of the Zimbabwe Craton, showing distribution of different generations of supracrustal rocks (modified after Anhaeusser, 1976).

1981; Sun, 1984). The classic stratigraphic models for Archean greenstone belts were based on the stratigraphy of the Barberton Mountain Land Greenstone Belt of South Africa and Swaziland. The Barberton stratigraphy consists of two main units; a lower unit of volcano-plutonic rocks (Onverwacht Group) and overlying, younger, clastic sedimentary rocks (Fig Tree and Moodies groups). The Onverwacht Group is generally subdivided into two main subgroups, the lower Tjakstad and upper Geluk. The two subgroups are separated from each other by a thin persistent unit, the Middle Marker, which consists mainly of cherts and carbonate sediments.

The Tjakstad Subgroup is comprised mainly of ultramafic-mafic volcano-plutonic rocks, especially in the lower Sandspruit and the topmost Komati Formations (Viljoen et al., 1983). The middle unit, the Theespruit Formation, consists mainly of siliceous sedimentary and volcanic rocks with minor intercalations of ultramafic-mafic rocks (Viljoen et al., 1983; de Wit, 1991). The upper Geluk Subgroup, consists of mainly basalts, andesites, and other intermediate and siliceous volcanic rocks with interrelated sedimentary rocks. The proportions of intermediate and siliceous volcanic rocks increase towards the top of the Geluk Subgroup. The main feature emphasized by the Barberton stratigraphic model is the cyclic nature of the Archean volcanism (Viljoen et al., 1983). Viljoen and Viljoen (1969) and Anhaeusser and Ryan (1979) extended the Barberton stratigraphic model to the greenstone belts of the Zimbabwe Craton.

There are at least 24 greenstone belts (or greenstone belt enclaves; Litherland, 1973) within the Zimbabwe Craton, including the Tati, Matsitama and Vumba

Greenstone Belts, which occur in northeastern Botswana (Figure 2.1). Supracrustal rocks within the greenstone belts of the Zimbabwe Craton can be grouped into three main lithostratigraphic units (Stagman, 1978; Wilson et al., 1978). These are, from oldest to youngest; the Sebakwian, Bulawayan and Shamvaian Groups (sic). Although the lithostratigraphic term "group" is used for these rocks; they are in fact chronostratigraphic units. Their names are derived from the use of adjectival extensions (an and ian) in the geographic name component of the stratigraphic unit (ISSC, 1976). Although the distribution and nature of the Sebakwian Group is poorly known (Stagman, 1978; Wilson, 1979), it has been compared to and correlated with the Onverwacht Group, whereas the Bulawayan and Shamvaian Groups were considered to be post-Onverwacht (Viljoen and Viljoen, 1969).

Later work, including the acquisition of geochronological data (mainly Rb/Sr) (Wilson, 1979; Orpen and Wilson, 1981), suggested that the Bulawayan Group contains two generations of volcano-sedimentary rocks. These were called the Lower and Upper Greenstones (Martin, 1978). The Lower Greenstones consist of mainly tholeiitic volcanic rocks with minor sedimentary rocks. The Upper Greenstones are made up of calc-alkaline volcanic rocks.

Wilson (1979) suggested a three-fold subdivision for igneous rocks within the greenstone belt rocks of the Zimbabwe Craton, based on isotopic age. These subdivisions are: 3.5 Ga, 3.0-2.9 Ga, and 2.8-2.6 Ga (Figure 2.3) which crudely coincide with the previously defined Sebakwian, Lower and Upper Greenstones, respectively. The Lower and Upper Greenstones (collectively known as Bulawayan

Group) constitute the main volcanic rocks of the Zimbabwe Craton.

2.2.2.1 Sebakwian Group

The Sebakwian Group has been described as consisting of ultramafic-mafic volcano-plutonic rocks intercalated with banded iron formations that are both underlain and overlain by sedimentary units (Stagman, 1978; Wilson, 1979; Foster, 1985). The base of the Sebakwian Group is defined by shallow water quartzites, sandstones and conglomerates which constitute the Mont d'Or Formation (Wilson, 1979). These sedimentary rocks are overlain by a sequence of interlayered basaltic and komatiitic rocks with intercalated banded iron formations and ultramafic intrusive complexes (Wilson, 1979). Grits, conglomerates, banded iron formations, minor carbonates, and volcanic rocks of the Wanderer Formation occur towards the top of the group (Stagman, 1978; Wilson et al., 1978). These rocks are considered to underlie the Bulawayan Group with a marked unconformity, and in some instances they exhibit high grades of metamorphism and deformation. The 3.5 Ga Sebakwian Group rocks constitute a very minor component in the Archean greenstone stratigraphy of the Zimbabwe Craton, and are best developed in the vicinity of Selukwe, Mashaba and Fort Victoria (Figure 2.3). The Sebakwian Group has been correlated with the Onverwacht Group (e.g. Viljoen et al., 1983) despite the fact that it lacks the thick volcanic piles which are characteristic of some sections of the Onverwacht Group such as the Komati Formation.

2.2.2.2 Bulawayan Group

The Bulawayan Group consists mainly of an association of ultramafic-mafic volcanic-plutonic rocks and intermediate volcanic rocks together with feldspathic sedimentary rock units (Stagman, 1978; Wilson, 1979). The Bulawayan Group greenstone belt rocks crop out over a much larger area within the Zimbabwe Craton than the Sebakwian Group rocks and have been divided into two major lithotectonic units; 3.0-2.9 Ga and 2.8-2.6 Ga (Figure 2.3). The 3.0-2.9 Ga rocks are equivalent to the Lower Greenstones, whereas the 2.8-2.6 Ga are equivalent to the Upper Greenstones (Wilson, 1979). The Lower and Upper Greenstones are separated from each other by the Manjeri Formation which consists of sedimentary rocks dominated by shallow water quartzites, greywackes, sulphide-facies banded iron formations, cherts and minor limestones.

The 3.0-2.9 Ga Lower Greenstone supracrustal rocks in western successions were divided into two main lithostratigraphic units (Wilson, 1979; Haynes, 1982; Foster, 1985); (i) the lower Hokonui Formation and (ii) the upper Bend Formation. The Hokonui Formation consists mainly of andesites, felsic volcanic and pyroclastic rocks with minor mafic pillow lavas and ultramafic flows towards the base (Wilson, 1979; Haynes, 1982; Foster, 1985). A polymictic conglomerate overlies the whole succession. In the southeastern part of the Selukwe Greenstone Belt, the 3.0-2.9 Ga volcano-sedimentary rocks constitute the Brooklands Formation which consists of lower quartzites, grits, and rare conglomerates, passing upwards into high-magnesian pillow basalts with intercalations of banded iron formations and phyllites (Wilson,

1979).

The Bend Formation consists of cyclic sequences of pillow basalts, overlain by spinifex-textured high-magnesian basalts (komatiites) and ultramafic schists. Ultramafic-mafic volcanic rocks of the Bend Formation are commonly intercalated with both oxide and sulphide facies banded iron formations which form prominent ridges. An assemblage of banded iron formations and phyllites cap this unit (Stagman, 1978; Wilson, 1979; Haynes, 1982). The whole succession is underlain by an amphibolite unit which is infolded with the 2.9 Ga Chengezi gneiss.

Supracrustal rocks overlying the Manjeri Formation constitute the 2.8-2.6 Ga greenstone belt rocks of the Zimbabwe Craton. In areas around the Selukwe and Belingwe Greenstone Belts, the 2.8-2.6 Ga Upper Greenstones supracrustal rocks have been subdivided into the western and eastern successions (Wilson, 1979; Foster, 1985) which consist of a succession of ultramafic and mafic tholeiitic pillow lavas, high-magnesian basaltic sills, and minor sedimentary rocks. The 2.8-2.6 Ga old supracrustal rocks have been subdivided into two main formations; the basal Reliance Formation and the upper Zeederbergs Formation (Martin, 1978; Stagman, 1978; Wilson, 1979).

The Reliance Formation consists of spinifex-textured peridotite flows, tholeiitic pillow basalts and layered ultramafic intrusions. The Zeederbergs Formation consists of a thick pile of tholeiitic basaltic rocks, that pass upwards into a cyclic, bimodal volcanic rock association (Foster, 1985). The Zeederbergs Formation also contains, in some places, spinifex-textured basaltic and peridotitic flows alternating with felsic

and pyroclastic rocks (Stagman, 1978; Wilson, 1979). The 2.8-2.6 Ga old greenstone belt volcanic rocks are capped by a shallow water clastic sedimentary rock unit, the Cheshire Formation, which contains local developments of banded iron formations and limestones.

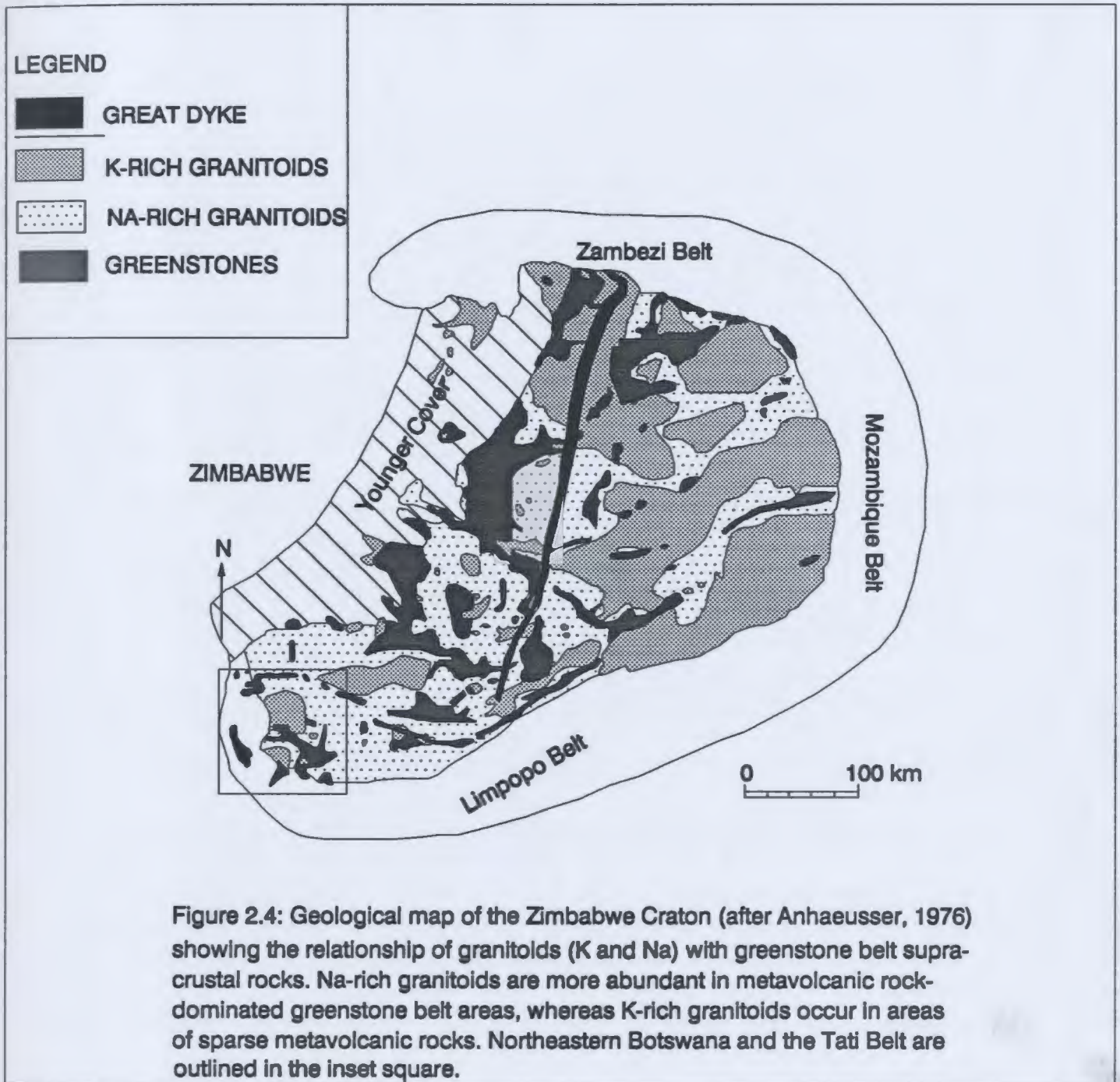
2.2.2.3 Shamvaian Group

The youngest unit in the Zimbabwe Craton is the Shamvaian Group which consists mainly of sedimentary rocks with minor igneous rocks. Rocks of the Shamvaian Group have been described as unconformably overlying the 2.8-2.6 Ga old greenstone belt sequence (Stagman, 1978; Wilson, 1979). Stagman (1978), however, points out that Shamvaian Group rocks are commonly infolded with the underlying, dominantly volcanic, rock units described above. Deformation has obliterated marker unconformities, making it difficult to distinguish between sedimentary rocks of the Shamvaian Group and those interlayered with the underlying volcanic rocks (Stagman, 1978). The Shamvaian Group contains a basal polymictic conglomerate with granite pebbles. This unit is overlain by poorly sorted arkosic and subgreywacke sedimentary rocks which were deposited in a shallow water environment. The Shamvaian Group, however, varies from place to place. In the southeast, near Fort Victoria, felsic volcanic rocks are part of the sequence, whereas elsewhere in the craton, the unit solely contains sedimentary rocks. These rocks are intruded by the 2.6 Ga Chilimanzi and Sesombi granitoids.

2.2.3 Internal Granitoids

Internal granitoids (cf. Martin et al., 1983) as described here, refer to granitoids intruded into the volcano-sedimentary sequences of greenstone belts. They are, therefore, similar to Hunter's (1974) diapiric granitoids. Anhaeusser (1976) argued that two main types of granitoids can be recognised in the Archean Zimbabwe Craton. These are (i) Na-rich granitoids, consisting of tonalites and trondhjemites which occur mainly within mafic greenstone rocks (Hunter, 1991), and (ii) K-rich granitoids made up of granodiorites, adamellites and granites (Figure 2.4). The K-rich granitoids mainly intrude sialic crust, such as grey gneisses and other granitoids. K-rich granitoids occur predominantly east of the Great Dyke (Figure 2.4), the area where supracrustal volcanic rocks are minor. Na-rich granitoids, on the other hand, are more common west of the Great Dyke where supracrustal volcanic rocks are also concentrated.

Conversely, Wilson et al. (1978) subdivided granitoids of the Zimbabwe Craton on the basis of isotopic age, and suggested that the three periods of greenstone belt volcanism were each terminated by granitoid plutonism. The oldest granitoids in this subdivision are the 3.35 Ga Mount d'Or granitoid gneisses which consist mainly of tonalites and granodiorites. The second group comprises 2.9 Ga granitoids which are characterised by the Mashaba and Chengezi-type tonalite gneisses. The 2.7 Ga Sesombi-type tonalites constitute the third group. The final group comprises the 2.6 Ga Chilimanzi-type granitoids which consist of adamellites and granites. It was further argued that the first three granitoid groups, the Mount d'Or, Mashaba-Chengezi, and



Sesombi types, are characterized by low initial strontium ($^{87}\text{Sr}/^{86}\text{Sr}$) ratios, whereas, initial strontium ratios of the Chilimanzi type granitoids are comparatively high (Wilson, 1979).

2.2.4 Geotectonic Setting of Archean Greenstone Belts

Research on Archean greenstone belts in the last ten years has shown that these belts are made up of accreted terranes from variable tectonic settings (De Wit, 1991; Hunter, 1991; Barley and Groves, 1990; Kusky, 1990; Thurston and Chivers, 1990). The recognition of these terranes is based on lithological associations (Thurston and Chivers, 1990; Barley and Groves, 1990) and the recognition of major lineaments (e.g. linear magnetic anomalies) that separate lithotectonic units. For example, the Keith-Kilkenny tectonic zone in the Norseman-Wiluna Greenstone Belt of the Yilgarn Craton in western Australian separates a komatiite-tholeiite sequence from the calc-alkaline volcano-plutonic and feldspathic sedimentary rock sequences (Barley and Groves, 1990). In the Slave Province of the Canadian Shield, major tectonic zones separate dissimilar terranes from each other (Kusky, 1990). In the Barberton Mountain Land Greenstone Belt of South Africa and Swaziland, supracrustal rocks have been interpreted as consisting of an arc sequence (Theespruit Formation) and an ophiolite sequence (rest of Onverwacht Group) separated by internal shear/fault zones (De Wit, 1991). The second major development in research on Archean greenstone belts is recognition of the geochemical characteristics of the supracrustal rock sequences. Jahn et al. (1982) noted that there are three

geochemical groups of Archean komatiite rocks; Group I with flat heavy rare earth element (HREE) patterns and Gd/Yb ratios ≈ 1.0 , Group II with HREE-depleted patterns and Gd/Yb ratios of >1.0 , and Group III with HREE-enriched patterns and Gd/Yb ratios of <1.0 . Groups I and II komatiites are dominant in Archean greenstone belt sequences, but each is more important in a particular Archean period (Jahn et al., 1982). Group II were considered to have been prevalent in older greenstone belts (> 3.5 Ga; e.g. Barberton) whereas Group I are more important in younger greenstone belts (≈ 2.7 Ga; e.g. Upper Greenstones of Zimbabwe; greenstones of the Yilgarn Craton, western Australia and most greenstone belts of the Superior Province, Canada). Cattell and Arndt (1987) and Cattell and Taylor (1990) suggested that the two komatiite types can occur in any one greenstone belt, even though their geochemical evidence is not conclusive.

Based on field and geochemical characteristics, Viljoen et al. (1983) suggested that the tectonic settings of the two groups of Archean komatiites may not have been different. By comparing the 2.7 Ga Pyke's Hill flow of Munro Township, Ontario, and the 3.5 Ga Richard's flow of Komati Formation, Barberton, South Africa, they showed that lithologically, individual komatiitic flows of both age groups are similar.

Even though major lineaments have been described and were shown to transect the Zimbabwe Craton (Stowe, 1980; Wilson, 1990; Treloar et al., 1992), their relationships to greenstone belt stratigraphy have not been recognised due to the lack of a wide geophysical data base. In Botswana, however, where the geophysical coverage is much more substantial, there is much better control on the relationships

between stratigraphy and internal greenstone belt shear/fault zones.

The geotectonic settings of greenstone belts in the Zimbabwe Craton have not been defined based on these formulations for greenstone belts elsewhere. The older Sebakwian Group, which consists of arenaceous basal sediments overlain by komatiite-tholeiitic volcano-plutonic rocks, may approximate Thurston and Chivers' (1990) supracrustal platformal sequences.

Although it cannot be directly demonstrated that the Upper and Lower Greenstones of the Bulawayan Group are separated by a major discontinuity, it is probable that the unconformity which separates these two units (Foster, 1985) is a deformed and disrupted tectonic break. Furthermore, the Brooklands Formation sedimentary rocks and equivalent intermediate to siliceous volcanic and minor basaltic rocks of the Hokonui Formation, all of which constitute the Lower Greenstones, have lithological associations similar to those of the arc-terrane Theespruit Formation of the Onverwacht Group as defined by De Wit (1991). While the Reliance-Zeederbergs Formations of the Upper Greenstones have been described as continental rift volcanics (Hawkesworth and O'Nions, 1977; Foster, 1985), Kusky and Kidd (1992) have suggested that the Reliance-Zeederbergs Formations constitute an assemblage analogous to Mesozoic ophiolites and oceanic plateaus, and as such the rocks may be comparable to De Wit's (1991) oceanic volcanic rocks of the Onverwacht Group.

2.2.5 The Great Dyke

The Great Dyke, with an age of approximately 2.5 Ga, has until recently been regarded as the last major Archean igneous event in the Zimbabwe Craton (Stagman, 1978; Wilson, 1979); 2500 Ma is regarded as the age which marks the end of the Archean era (Plumb and James, 1986). A re-evaluation of the age data by Wilson (1990) indicated that the Great Dyke's age may be 2416 ± 16 Ma instead of 2500 Ma and therefore the Great Dyke was a Proterozoic igneous event. Nesbit (1982) had argued that the Great Dyke should be regarded as a magmatic manifestation marking the transition from the Archean to the Proterozoic.

The Great Dyke consists of a major layered ultramafic-mafic igneous body (the Great Dyke proper) and associated dykes with a NNE trend (Wilson, 1982). These dykes are controlled by the "Great Dyke Fracture System" (Stowe, 1980) that has a NNE trend.

2.3 Limpopo Belt

The Limpopo Belt is commonly described as a linear, highly deformed, and high metamorphic grade terrane separating the Kaapvaal Craton from the Zimbabwe Craton (e.g., Watkeys, 1983; McCourt and Vearncombe, 1987; Van Reenen et al., 1987). A survey of the literature on the Limpopo Belt shows considerable disagreement as to what actually constitutes the Limpopo Belt (Mason, 1973; Coward et al., 1976; Key and Hutton, 1976; Kröner, 1977b; Ermanovics, 1977; Light, 1982; Tankard et al., 1982; Van Reenen et al., 1987). The debates are most intense with

respect to the boundaries between the Limpopo Belt and the surrounding cratons (McCourt and Vearncombe, 1987;1992; Tankard et al., 1982). Early models, summarised by Mason (1973), defined the Limpopo Belt as a parallel-sided metamorphic and structural terrane, divisible into three zones (Figure 2.5) viz.; the Central Zone (CZ), and two marginal zones, the Northern Marginal Zone (NMZ), and the Southern Marginal Zone (SMZ). The Central Zone was defined as being separated from the Northern Marginal Zone by the Tuli-Sabi dextral shear zone system; and from the Southern Marginal Zone by the sinistral Soutpansberg Fault Zone (Mason, 1973). In the most recent geological maps of Botswana, the boundary between the CZ and the SMZ has been renamed the Zoetfontein Fault System (Reeves, 1978). The Zoetfontein Fault forms part of McCourt and Vearncombe's (1987, 1992) Palala Shear Zone System which has been interpreted from aeromagnetic data to extend westwards into Botswana, where it is truncated by the Kalahari tectonic line. The term Soutpansberg Fault Zone, on the other hand, is confined to the graben boundaries of the 1.8 Ga Soutpansberg Group Basin in Eastern Transvaal (Reeves, 1978) which covers part of the SMZ.

As more detailed information on the Limpopo Belt was derived, it was realised that the parallel-sided nature of the belt was more apparent than real (Treloar et al., 1992). Tankard et al. (1982) suggest that the NMZ should be defined as a granulite-facies metamorphic zone confined to southern Zimbabwe which tapers off southwestwards into Botswana. On the basis of this definition, the CZ in Botswana is believed to be in contact with the Zimbabwe Craton (Tankard et al., 1982). Key

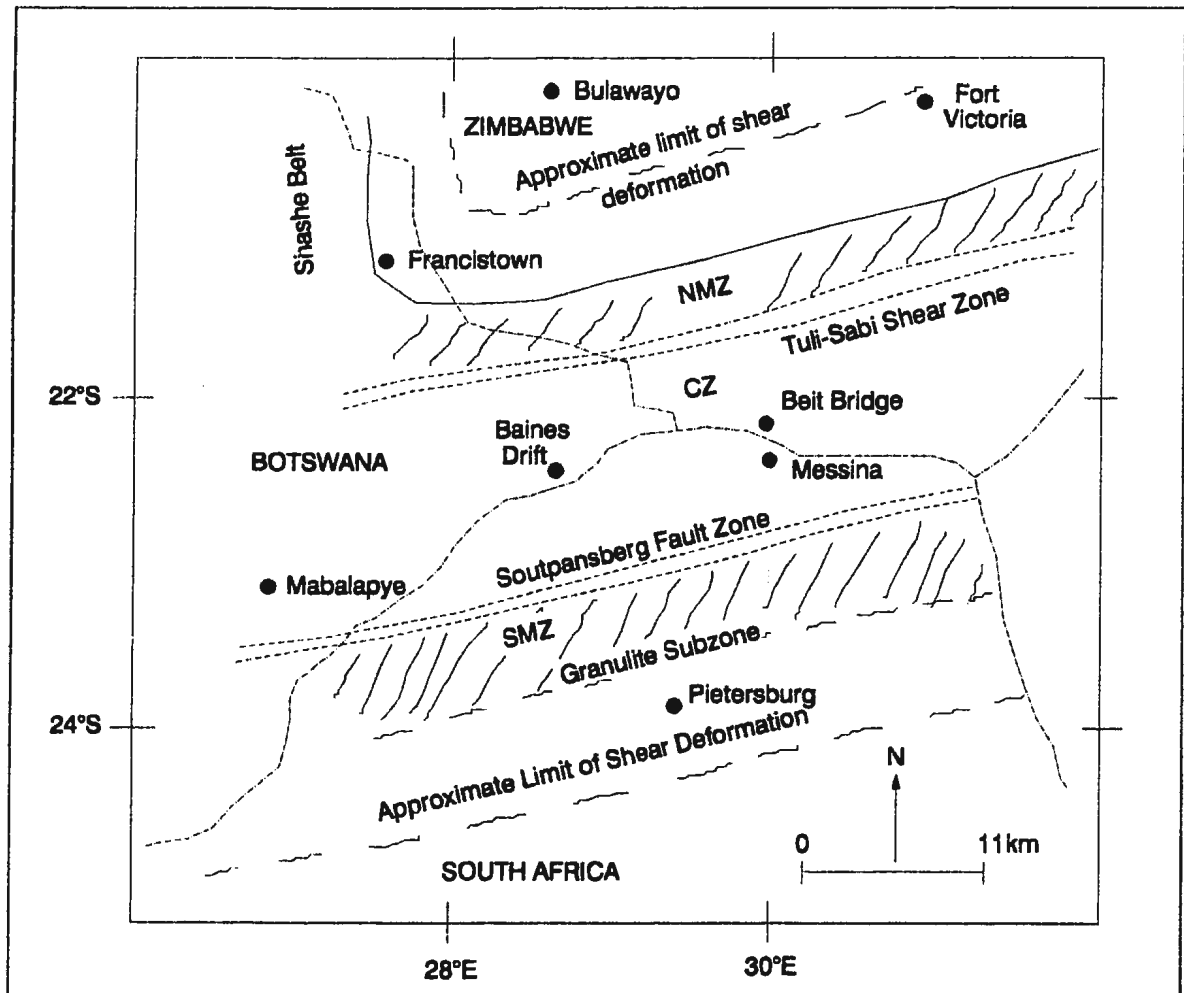


Figure 2.5: Map of the Limpopo Belt and its three constituent structural zones as defined by Mason (1973). NMZ, SMZ, and CZ, are the Northern Marginal Zone, Southern Marginal Zone, and Central Zone, respectively.

and Hutton (1976) suggested that the Monatshane Formation supracrustal rocks and Shashe gneisses which occur between the Tuli-Sabi shear zone and the Tati Greenstone Belt, form part of the basement to the greenstone belts.

Ermanovics (1977) provided an alternative definition of the Limpopo Belt as "a structural province with polyphase folding that occurs as an east-west zone, approximately 100 kilometres wide and 400 kilometres long." He suggested that the marginal zones are remobilized equivalents of the cratons and that they should not, therefore, be included as part of the Limpopo Belt.

Ermanovics' (1977) definition is supported by some geochronological data which suggest that the CZ contains some of the oldest rocks in the Southern Africa subcontinent (≈ 3.8 Ga Sand River Gneisses; Barton, 1981). In accommodating the geochronological data, Barton (1981) defined the CZ as "a graben or aulacogen in a protocraton" with the remnants of the protocraton are preserved as the Sand River Gneiss. The marginal zones in this case were said to have formed by the clockwise rotation of the Zimbabwe Craton (ZC) relative to the Kaapvaal Craton (KC), leading to the thrusting of a portion of the CZ over the ZC, and the KC over the CZ. Defined on the basis of Ermanovics (1977) and Barton (1981), the central zone of the Limpopo Belt, therefore, constitutes the Limpopo Belt (LB) proper and as such is a protocraton that is stratigraphically and structurally distinct from the surrounding Zimbabwe and Kaapvaal Cratons. The marginal zones would have formed through the interaction of the Limpopo Belt with the surrounding cratons.

The most comprehensive definition of the Limpopo Belt was that provided

by Watkeys (1983) who suggested that the belt can be subdivided, on both structural and stratigraphic grounds, into several subzones or domains (Figure 2.6). According to this definition, the CZ is characterized by north-trending structures, whereas the marginal zones consist of ENE-trending structures. These subzones were described as having internally consistent stratigraphies different from those of adjacent subzones. The structures within each subzone would also be characteristic of the particular zone. As such, the tectonic subzones of the Limpopo Belt consist of tectonostratigraphic terranes separated from each other by faults/shear zones (Watkeys, 1983). The metamorphism is consistently high grade, whereas structures are generally oblique to those in the adjoining cratons. The cratons are made up mainly of low grade metamorphic rocks. Defined this way, the Limpopo Belt consists of both the Central Zone and the two marginal zones.

Barton's (1981) age for of the Sand River Gneisses has, however, recently been questioned by some researchers (e.g. McCourt and Vearncombe, 1992; Harris et al., 1987). These workers suggest, on the basis of U/Pb and Sm/Nd isotopic ages, that the Sand River Gneisses are ca. 3.2 Ga.

2.3.1 Northern Marginal Zone of the Limpopo Belt

The boundary between the Central Zone (CZ) and the Northern Marginal Zone (NMZ) of the Limpopo Belt is the Triangle-Tuli-Sabi Shear Zone (Mason, 1973; Key and Hutton, 1976; Tankard et al., 1982; Watkeys, 1983). Although there are some similarities in structures within the area north of the Tuli Sabi Shear Zone

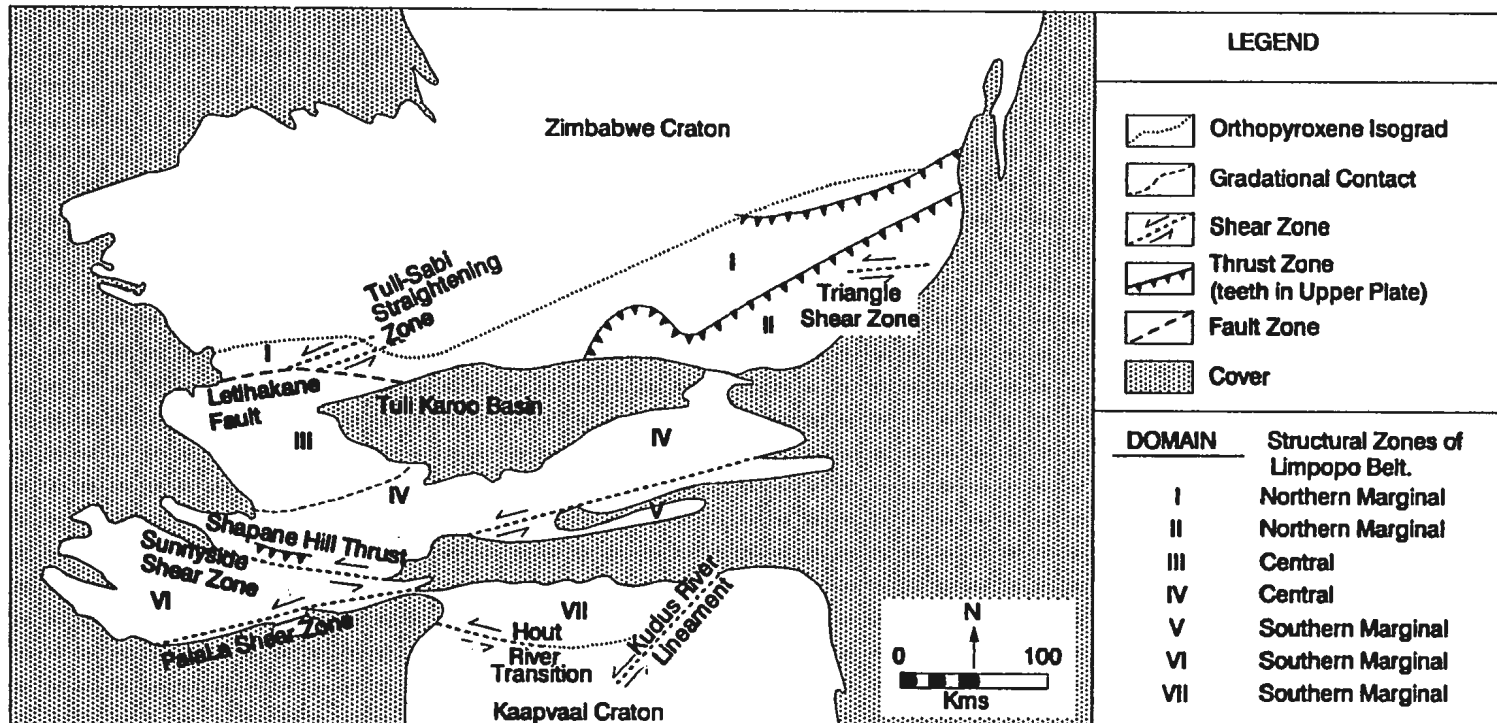


Figure 2.6: Tectonostratigraphic domains of the Limpopo Belt(after Watkeys, 1983).

(NMZ) and those further north in the Zimbabwe Craton, Coward et al. (1976) suggested that the northern limit of granulite facies metamorphism defines the boundary between the craton and NMZ. This granulite metamorphism was supposed to have resulted from the reworking of Zimbabwe Craton greenstone belt rocks. Key and Hutton (1976), on the other hand, suggested that the area between Shashe and the Tuli-Sabi Shear Zone (NMZ) shares a common structural history with the CZ south of the shear zone. They also suggested, however, that the rocks within this area, comprising the Monatshane and Shashe Gneiss Formations, are different from the main lithologies in the CZ, the Beitbridge sequence, and those in the Tati Greenstone Belt. Rocks of the Shashe Gneiss and Monatshane terranes were interpreted as being older than rocks of the Tati Greenstone Belt (Key and Hutton, 1976).

Shashe Gneiss and Monatshane terranes consist of a series of layered gneisses and migmatites, metaquartzites, marbles, porphyroblastic gneisses, mafic gneisses and amphibolites. Graphitic schists, biotite schists, calc-silicates and banded iron formations are also present, and marbles and banded iron formations are locally associated with layered amphibolites (Key, 1976). These rocks were metamorphosed from amphibolite to granulite metamorphic facies.

The contact between these gneissic terranes and the Tati Greenstone Belt is defined by a linear zone of porphyritic granites. This contact is also a region of high strain and high grade metamorphism. The metamorphism and deformation in this contact increases from the cratonic area of the Tati Greenstone Belt southwards to the Tuli Sabi Shear Zone (Key, 1976). This change is marked by an increase in the

occurrence of migmatites; it was, therefore, defined as a "migmatite front" (Key, 1976).

The contact between the Monatshane terrane and the CZ consists of a major NE trending ductile dextral shear zone and the Lethakane Fault Zone. The shear zone deviates from the Lethakane Fault Zone in Botswana and widens to several kilometres eastward into Zimbabwe, where it is also called the Triangle shear zone. The Lethakane Fault Zone was interpreted as marking the southern limit of cataclastic deformation (Key, 1976).

Tankard et al. (1982) defined the NMZ as a wedge-shaped terrane in southeastern Zimbabwe which tapers out westwards before reaching Botswana. This model was based on the perceived difference in structural timing between the Shashe area in Botswana and the NMZ in southeastern Zimbabwe. The structures in Botswana were regarded as having formed from a later shear deformation than those in southeastern Zimbabwe (Tankard et al., 1982). There is very little information on the two zones of NMZ (Terranes I and II; Figure 2.6) delineated by Watkeys (1983) in southeastern Zimbabwe. It has been argued by several workers (e.g., Robertson, 1977; Coward et al., 1976; Tankard et al., 1982) that rocks of this area, although metamorphosed to granulite facies, are equivalent to the cratonic supracrustal rocks. They have, therefore, been interpreted as reworked Zimbabwe Craton greenstone belt rocks (Coward et al., 1976).

2.4 Relationship between the Zimbabwe Craton and Limpopo Belt

The approximate upper age limit on the Limpopo deformation has been suggested to be 2700 Ma (Van Reenen et al., 1987). Kröner (1977a), however, points out that the 2.7 Ga tectonothermal event may not have been confined to the Limpopo Belt and its environs. This deformational episode may have been a much more widespread crustal forming event affecting most of the African continent. Kröner named this event the Limpopo-Liberian tectogenetic cycle and suggested that it was accompanied by extensive and widespread granite intrusion in shield areas. Much of the deformation within the Central Zone of the Limpopo Belt is suggested to have been pre-2.7 Ga (Barton, 1981). Barton also suggested that the 2700 Ma deformation event was accompanied by extensive granitic magmatism.

Early models for the evolution of the Limpopo Belt suggested that the belt formed from the reworking of the surrounding Zimbabwe and Kaapvaal cratons (e.g. Mason, 1973; Kröner, 1977b). The two cratons are not, however, stratigraphic mirror images of each other. The Zimbabwe Craton consists mainly of volcanic supracrustal rocks (Wilson, 1979; Wilson et al., 1978) of two age generations (3.0-2.9 and 2.8-2.6 Ga), and each generation defines a different tectonostratigraphic terrane. The Kaapvaal Craton, on the other hand, consists mainly of 3.5 Ga supracrustal volcanic rocks (De Wit, 1991; Hunter, 1991). The 3.1-2.4 Ga interval in the Kaapvaal Craton is dominated by the formation of large sedimentary basins such as the Pongola, Witwatersrand, Ventersdorp and Transvaal.

The other element in this complicated tectonic jigsaw puzzle is the presence

of kimberlites with Archean eclogitic xenoliths (Kinny et al., 1989; Kirkley et al., 1992) in the Kaapvaal Craton. This observation prompted Helmstaedt and Schulze (1989) to suggest that part of the Limpopo Belt evolutionary history included subduction of the so-called "Limpopo Oceanic Basin" southward under the Kaapvaal Craton. Such a supposition was based on Light's (1982) advocacy of a north to south collision process between the Zimbabwe and Kaapvaal Cratons. Helmstaedt and Schulze (1989) suggested that the eclogitic xenoliths indicate the presence of Archean subcontinental mantle beneath the Kaapvaal Craton. There are no reported eclogite xenoliths in kimberlites from the Zimbabwe Craton.

Although early definitions of the Limpopo Belt suggested that it consisted of parallel-sided linear belts (e.g. Mason, 1973), subsequent studies have clearly shown that the Limpopo Belt and its marginal zones can be subdivided into different domains with internally consistent structures and stratigraphies (Figure 2.6). These domains are separated from each other by shear/fault zones (Watkeys, 1983; Ermanovics, 1977).

In general, the CZ contains rocks older than those of the marginal zones, but the suggested boundaries between marginal zones and the surrounding cratons have been poorly defined. Most researchers believe that the boundary between the NMZ and the ZC is gradational and should be defined as the orthopyroxene isograd confined to the southeastern Zimbabwe (Coward et al., 1976; Tankard et al., 1982). According to Ridley (1992), the orthopyroxene isograd is defined by charnockites that are stratigraphically equivalent to highly deformed, porphyritic (or megacrystic

feldspar) granites that form the southern margin of the Tati Greenstone Belt. The increase in metamorphism and deformation from the Tati Greenstone Belt to the NMZ (Key, 1976) suggests that the boundary between the ZC and NMZ as defined by these granitoid intrusions may be a major discontinuity. The NMZ, itself can also be subdivided into subzones which are also stratigraphically and structurally different from each other (Figure 2.6).

Therefore, in this study, it is suggested that the Limpopo Belt be defined as consisting of tectonostratigraphic terranes which were probably accreted together along shear/fault zones. The Central Zone consists of two distinct subzones with distinct stratigraphies. These are herein termed the Mmadinare Subzone (terrane III; Figure 2.6) and the Bietbridge-Messina Subzone (terrane IV; Figure 2.6) which includes the area covered by the Mesozoic Tuli Karoo Basin rocks. The Mmadinare Subzone consists mainly of granitoid gneisses which are grouped under the Bains Drift Formation (Ermanovics, 1974) and are lateral equivalents of the Sand River gneisses of South Africa. In contrast, the Bietbridge-Messina Subzone contains metasedimentary rocks described in early Limpopo Belt models as constituting cover to the Sand River Gneisses. These two terranes are separated from each other by shear/fault zones (Figure 2.6).

The Central Zone microcontinent is separated from the Northern Marginal Zone by the major dextral Tuli-Sabi-Triangle shear zone, and from the Southern Marginal Zone by a linear trough filled with the late Proterozoic red beds of the Soutpansburg-Palapye Group. The southwestern margin of this trough is defined by

the Sunnyside shear zone. Ermanovics (1977) defined two subzones in the Southern Marginal Zone of Botswana; the Machaneng subzone and the Mahalapye Plutonic Block, separated from each other and from the Central Zone by shear zones. These Southern Marginal Zones are characterised by distinct structures and stratigraphies. The Machaneng Subzone is characterised by granulite facies paragneisses and contains a east-west structure that is truncated in the north by northwest-trending Sunnyside shear zone which separates it from the Moeng Subzone. The Mahalapye Plutonic Block, on the other hand, consists of massive migmatites and plutonism (Ermanovics, 1977) separated from the Central Zone by the linear trough filled with late-Proterozoic Soutpansburg-Palapye Group sedimentary rocks.

The Northern Marginal Zone (NMZ) also consists of distinct terranes accreted along shear/fault zones. The boundary between the NMZ and the Zimbabwe Craton, as already pointed out, is defined by a zone of charnockite-porphyratic granites. In this respect, this boundary is a major discontinuity, although the deformation which accompanied cratonic suturing and the Limpopo Belt tapers well into the craton.

In Botswana, the NMZ area southeast of the Tati Greenstone Belt was covered by greywackes and argillites which are now metamorphosed to at least amphibolite facies. Structures in this area generally trend NE-SW to E-W. Further southwest, granitoid gneisses of the Shashe Gneiss Formation predominate and are characterised by N-S to NNW-SSE structural trend.

The Limpopo Belt displays structural characteristics analogous to the Churchill Province of the Canadian Shield. The Churchill Province (Hoffman, 1988) is a

Proterozoic mobile belt which contains a central zone consisting of two accreted Archean cratons, the Hearne and Nain. The central zone of the Churchill Province is surrounded by the New Quebec Orogen to the west and the Torngat Orogen to the east. These two orogens formed when the central zones accreted to the Superior Province shield craton. These two orogens are themselves made up of accreted terranes. The structural characteristics of the Limpopo Belt and Churchill Province are strikingly similar and they may have formed under similar tectonic regimes.

CHAPTER THREE

3. GEOLOGY OF THE TATI GREENSTONE BELT

3.1 The State of Geological Knowledge on the Tati Greenstone Belt

The Tati Greenstone Belt is approximately 30 km wide and 60 km long. It extends from Francistown in the west, to the border village of Matsiloje in the east (Figure 1.2 and 1.3) and is bounded to the north and south by granitoids. Further to the south, the granite-greenstone rocks of Tati Greenstone Belt are bounded by high grade metamorphic rocks of the Northern Marginal Zone of the Limpopo Belt (Figure 1.2). The Tati Greenstone Belt is a typical Archean greenstone belt consisting mainly of polydeformed volcano-sedimentary rocks intruded, especially at the margins, by syn-tectonic and post-tectonic granitoids. The rocks are of low metamorphic grade (greenschist facies), although pockets of higher grade metamorphism (lower amphibolite facies) are present in high strain areas, especially in the highly sheared/faulted contacts with granitoids. Primary igneous structures including pillows, vesicles, brecciated volcanic tops, and sedimentary structures such as bedding, graded bedding, and cross bedding are commonly preserved.

The first comprehensive interpretation of the structure and stratigraphy of the Tati Greenstone Belt was carried out between 1963 and 1968 by Mason (1970). During this work, Mason (1970) produced an unpublished geological map (Figure 3.1) in which he subdivided supracrustal rocks of the Tati Greenstone Belt into six formations. From oldest to youngest these are the Old Tati, Matsiloje

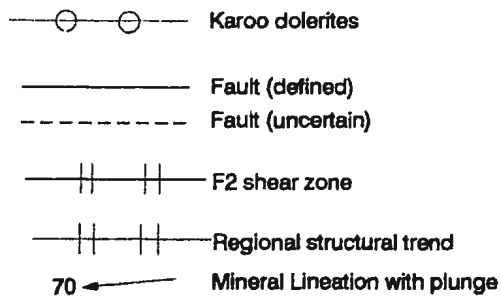
Metasedimentary, Lady Mary, Penhalonga (sic), Selkirk and Last Hope formations. Lithologies present within these lithostratigraphic units are as shown on the map Figure 3.1 (in pocket).

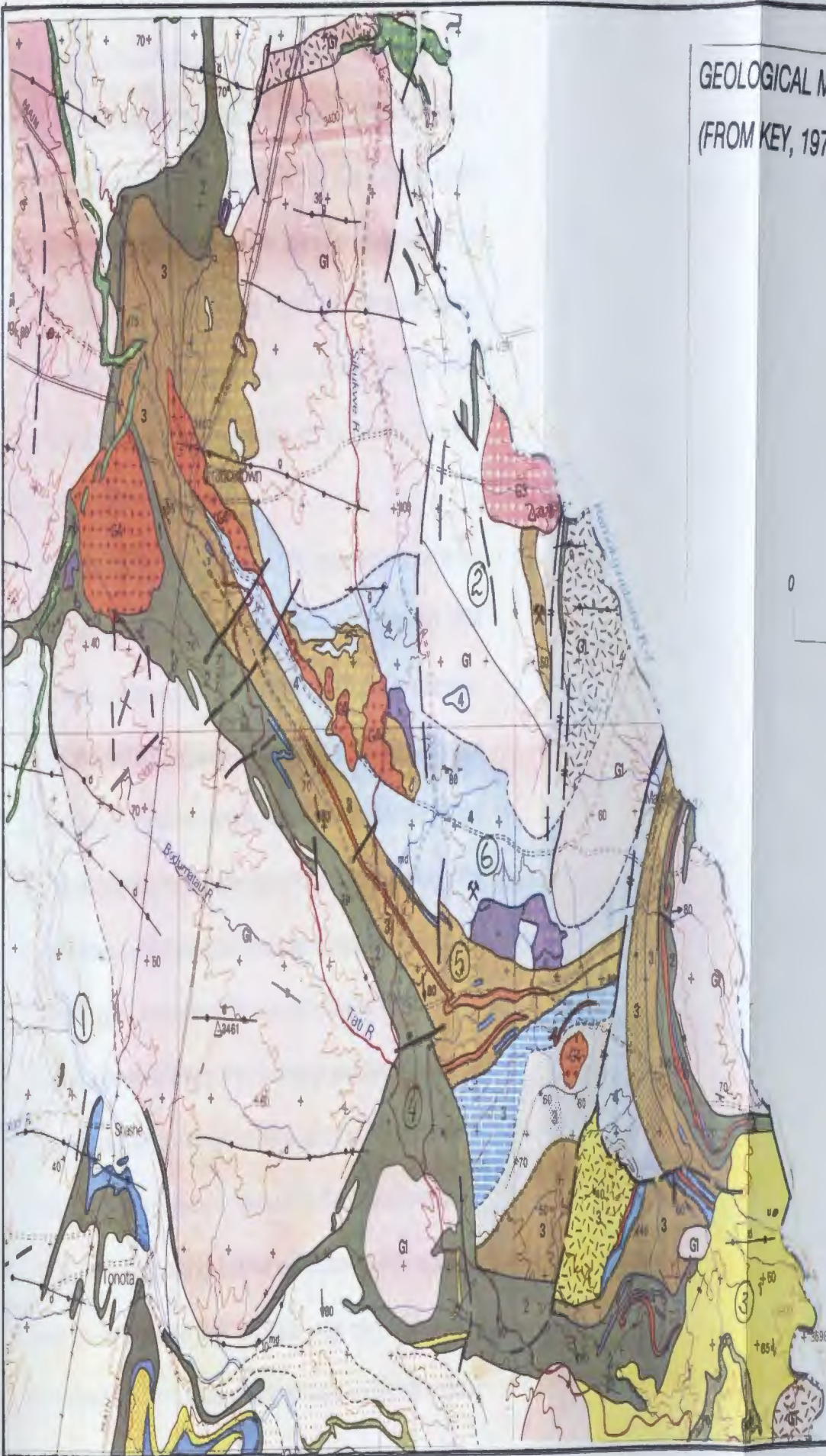
Mason (1970) interpreted the Tati Greenstone Belt to be a synform with major granitoids intruded at the core of the structure. Mason (1970) recognised NNE-SSW trending faults around the Selkirk-Phoenix massive sulphide prospects as the only major lineaments (or fault/shear zones) present within the Tati Greenstone Belt. The significance of these lineaments and their relationships to the stratigraphy and tectonic evolution of the belt were not discussed. In addition, although granitoids within the Tati Greenstone Belt were recognised to have petrographical characteristics similar to granitoids in Archean greenstone belts elsewhere (i.e. consisting of tonalite-granodiorite-trondhjemite-adamellite/granite suites), their relationships to the overall stratigraphy of the belt and tectonic significance were not fully investigated.

Mason's (1970) area was re-mapped by Key between 1973 and 1974 leading to the production of the Botswana Geological Survey District Memoir Number 3 (Key, 1976); Figure 3.2 is the geological map of the Tati Greenstone Belt produced from this work. Apart from a reduction in the number of lithostratigraphic units from Mason's (1970) six formations to three main formations, Key's (1976) work did not differ very much from that of Mason. Key (op cit.) derived three lithostratigraphic units: (i) combining Mason's Old Tati, Lady Mary and Matsiloje Metasedimentary Formations into one formation, the Lady Mary Formation; (ii) by combining Mason's

CAPTION FOR FIGURE 3.2

6	Meta-rhyolites/dacites	Selkirk Formation
5	Meta-andesites/rhyolites/dacites arkoses/limestones/aluminous schists/banded iron formations	Phenalonga Formation
4	Meta-basalts/ultramafic schists/ serpentinites/argillites/quartzites /banded iron formations	Lady Mary Formation
3	Ultramafic schists/arkoses/ banded iron formations	Kgarimacheng Formation
2	Paragneisses	
1	High grade metamorphic of the Limpopo and Shashe Belts	
G4	Undeformed tonalites	
G3	Anatectites (adamellites and granites)	
G2	Gneisses (adamellites/granites biotite/k-feldspar porphyritic granites and tonalites)	
G1	Monzonites and tonalites	





GEOLOGICAL MAP OF THE TATI GREENSTONE BELT
(FROM KEY, 1976). LEGEND ON PAGE 53.



N

0 15km

FIGURE 3.2.

Penhalonga and Last Hope Formations into the Penhalonga Mixed Formation; and (iii) leaving the Selkirk Formation as proposed by Mason (1970). The Selkirk Igneous Complex was considered by both Mason (1970) and Key (1976) to be a synvolcanic plutonic complex. Key (1976) classified granitoids of the Tati Greenstone Belt into chronologically distinct units G1 to G4 (Figure 3.2); G3 granitoids were considered to have formed from anatexis of metasedimentary rocks. Although Key (op cit.) fully described major fabric orientations and relationships, very few lineaments/faults were recognised (Figure 3.2).

Johnston and Griffiths (1982) and Sheeran (1986) mapped portions of the belt during mineral exploration programs. These mapping programs used Mason's (1970) stratigraphic interpretations, instead of Key's (1976), with some slight differences. Johnston and Griffiths (1982) suggested that the Selkirk Igneous Complex was a younger intrusive complex whose stratigraphic position was equivalent to that of the Last Hope Formation, the youngest sedimentary unit in the belt. Sheeran (1986) agreed with Johnston and Griffiths (1982) about the stratigraphic position of the Selkirk Igneous Complex, but, considered Mason's (1970) Matsiloje Metasedimentary Formation to be equivalent to the top of the Penhalonga (sic) Formation. These two studies concentrated only on lithological relations and did not recognize any more lineaments/faults than those recognised by Mason (1970). The re-adoption of Mason's (1970) stratigraphic nomenclature by Johnston and Griffiths (1982) and Sheeran (1986), along with the existence of Key's (1976) map as the only published map of the Tati Greenstone Belt with a different stratigraphic nomenclature from that of

Mason (1970), meant that two different stratigraphic nomenclatures were in use. Generally in all these studies, supracrustal rocks of the Tati Greenstone Belt were interpreted as ranging from a basal mafic-ultramafic unit (Old Tati-Lady Mary Formations of Mason (1970) or Lady Mary Formation of Key (1976)), to intermediate volcano-plutonic rock sequences (Penhalonga and Selkirk Formations, Key, 1976; Masoñ, 1970), and a feldspathic sedimentary unit (Last Hope Formation, Mason (1970)).

Structural interpretations in the Tati Greenstone Belt are even more problematic. The first comprehensive structural interpretation of the belt was carried out by Morel (1968) who suggested that all structures were the products of a single major deformational event; an Alpine-type nappe tectonism. Morel also noted that the boundary between the Tati Greenstone Belt and the Northern Marginal Zone of the Limpopo Belt was a major discontinuity which had been disrupted by granitoid intrusions. He concluded that this boundary was not gradational as previously interpreted, but was a sharp major discontinuity.

Anhaeusser and Ryan (1979) examined the extension of the Tati Greenstone Belt into Zimbabwe and commented on the relationship of granitoids to the structure of the belt. Their work indicated that the Tati Greenstone Belt has a synclinal form cored by granitoids and that structures were the products of vertical tectonism due to gravitational instabilities triggered by major granitoid plutonism. These granitoids were considered to underplate supracrustal rocks.

Coward and James (1974) carried out strain measurements in parts of the Tati

and Matsitama Greenstone Belts, Botswana. Their structural interpretations are summarised on the geological map (Figure 3.3), most notable on this map are the regional shear/fault zones within the Tati Greenstone Belt. These include a major NW-trending shear zone that traverses the volcano-plutonic stratigraphy in the northwestern part of the belt, and NE-trending shear zones, some of which are similar to those defined by Mason (1970).

Coward and James (1974) also recognised a major shear zone bounding the eastern part of the belt. These shear zones were suggested to have formed through "billiard ball-type" tectonism that resulted from the interaction of competent granitoids with less competent supracrustal rocks. The relationship of these shear zones to the stratigraphy was, however, not discussed. The 1986 aeromagnetic survey of eastern Botswana indicated the presence of major regional lineaments within the Tati Greenstone Belt that had not been previously recognised.

Both Key (1976) and Coward and James (1974) recognised three major deformation events within the Tati Greenstone Belt. The first deformational event (D_1) produced the synformal structure of the belt, whereas the second deformation (D_2) was the main foliation-forming event which also produced regional isoclinal folds. The third deformation (D_3) was described as a shearing event which resulted in the formation of major shear zones and minor upright folds (Key, 1976; Coward and James, 1974). Coward (1984) summarised the structural developments and suggested that deformation within the Tati Greenstone Belt was related to deformations within the Limpopo Belt.

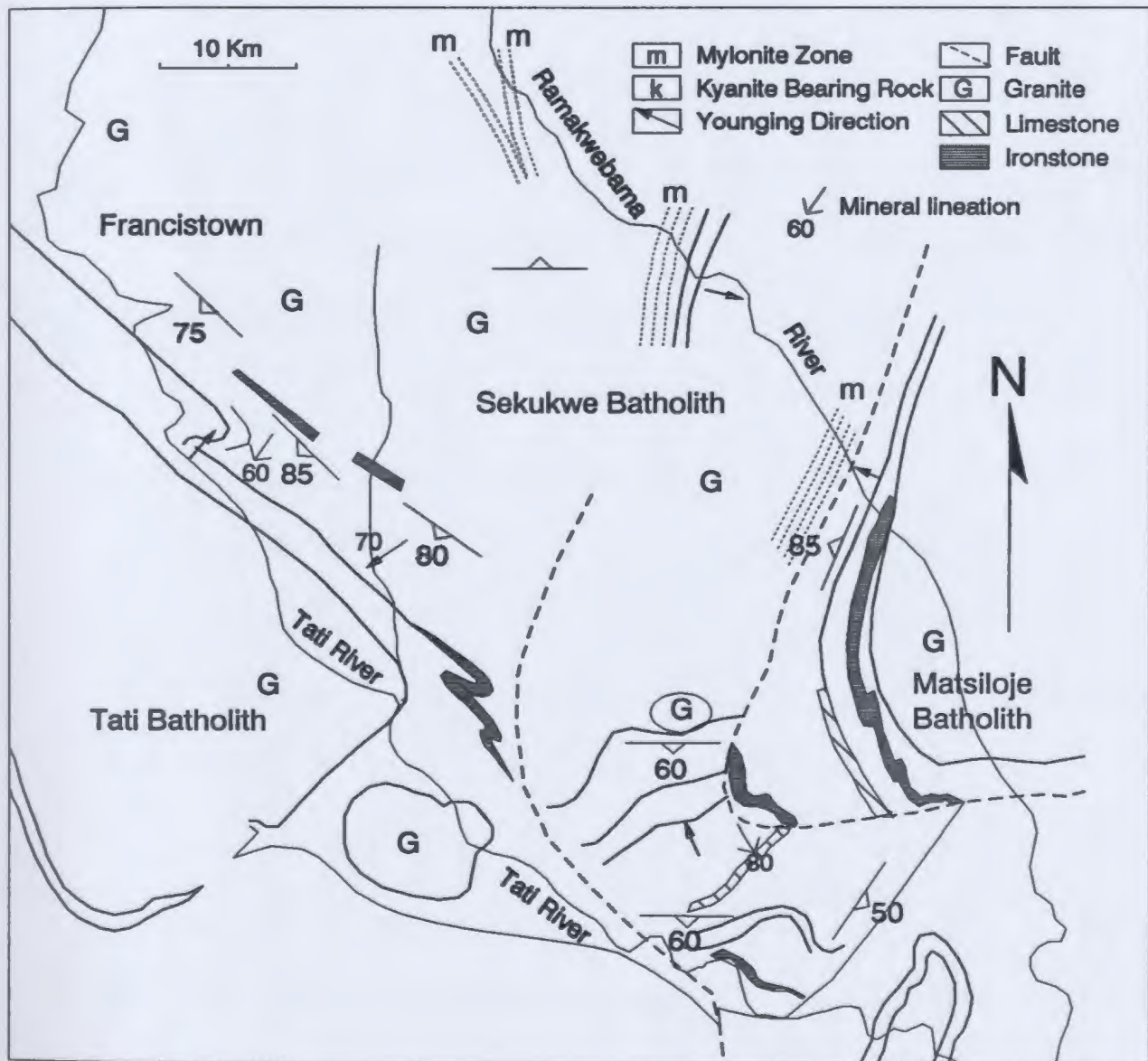


Figure 3.3: Geological and structural map of Tati Greenstone Belt (modified after Coward and James, 1974). The eastern arm of the belt was regarded as having been rotated from the south, through the southward movement of the Matsiloje Batholith relative to the batholiths in the western part of the belt, creating NNE-trending mylonites (m).

Geological work carried up to the time of this study on the Tati Greenstone Belt was based mainly on structural and lithological descriptions with only minimal geochemical and geochronological research. The previous state of the geological knowledge on the belt can be summarised as follows:

1. Two separate stratigraphic nomenclatures were in use.
2. Few lineaments and faults were recognised, and even in those that were, relationships to the stratigraphy and mineralization were not fully investigated.
3. Structural models, except that of Morel (1968), interpreted the structural evolution of the belt to be related to the evolution of the Limpopo Belt, despite the fact that deformational events and related structures within the belt are similar to those in Archean greenstone belts elsewhere in the world. Such structures are also similar to those in other greenstone belts within the Zimbabwe Craton that are located both near and further inland from the Limpopo Belt.
4. Although Foster (1985) noted the association of major gold deposits with banded iron formations (BIF) within the Zimbabwe Craton, the relationships of BIF to the whole supracrustal rock stratigraphy of the belt were hardly noticed.
5. There were virtually no geochemical data for rocks within the belt, except for a few major element analysis from isolated areas.
6. The role of plutonic rocks, especially granitoids, in the evolution of the belt, including their tectonic and stratigraphic significance, were unexplained.

7. The tectonic significance of komatiite-tholeiite sequences and calc-alkaline-feldspathic sedimentary lithological associations were also not discussed.

8. The relationship of mineralization to the stratigraphy, regional structure and tectonic evolution of the belt was not considered, let alone understood.

3.2 Stratigraphy of the Tati Greenstone Belt

Fault/shear zones subdivide the Tati Greenstone Belt into three zones (Figure 3.4); the Western Zone (area west, southeast of, and near Francistown), the Southeastern Zone (Old Tati Area), and the Eastern Zone (Matsiloje area). The Old Tati area occurs at the southeastern edge of the belt, which is where the two main structural trends of the Tati Greenstone Belt intersect; the NW trend of the Western Zone and NNE trend of the Eastern Zone. Although the structure of the Old Tati area is complex compared to the Western Zone due to its location near the Northern Marginal Zone of the Limpopo Belt, the ultramafic-mafic volcano-plutonic rocks in this area are generally continuous with those of the Western Zone. They form the base of a major ultramafic-mafic unit stretching just west of Francistown, southeastwards to the Old Tati area.

The Western Zone (Figure 3.5 - in pocket) forms the major part of the Tati Greenstone Belt and contains the greatest development of volcano-plutonic rocks in the Tati Greenstone Belt. This zone, therefore, constitutes the type area for stratigraphic units described in this work. The combination of aeromagnetic data, photogeological and satellite imagery interpretations indicate the presence of a major

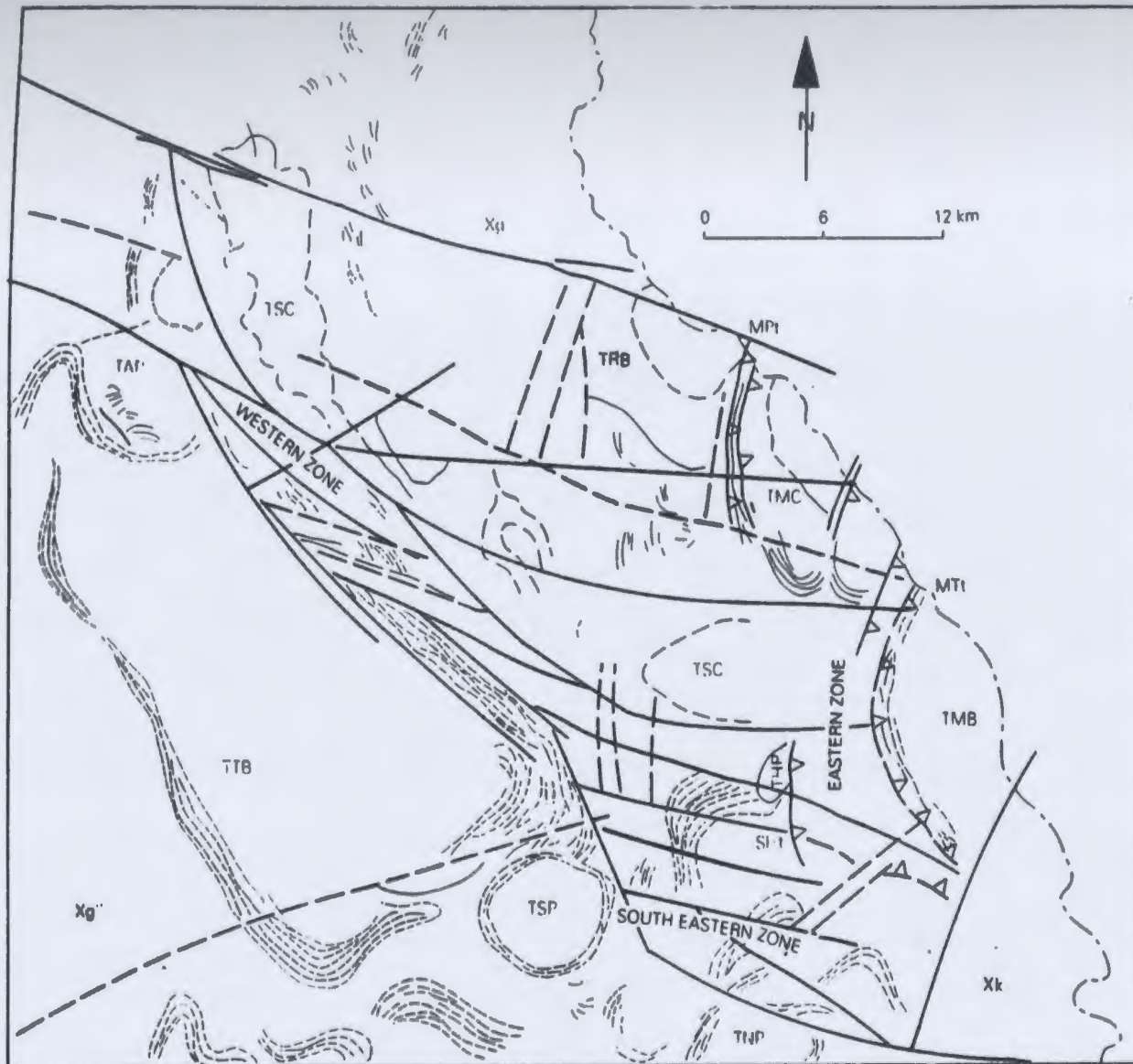


Figure 3.4: Geological map of the Tati Greenstone Belt showing the Western, Southeastern and Eastern Zones of the belt.

- MAP LEGEND:**
- Volcano-Sedimentary rocks
 - TSC Selkirk Igneous Complex
 - TRB Ramokgwebana Batholith
 - TMC Mphoeng Plutonic Complex
 - THP Hillview Pluton
 - TSP Southern Tati Pluton
 - TMP Airport Pluton
 - TNP New Zealand Pluton
 - TMB Matsiloje Batholith
 - TTB Tati Batholith
 - Xk Kgarimacheng Formation
 - Xg Granitoid Gneisses
 - Xg* Granitoid & Amphibolite Gneisses
 - Structural trend
 - Major Fault/lineament
 - Fault/lineament
 - SHt** Signal Hill Thrust
 - MTt** Matsiloje Thrust
 - MPt** Mphoeng Thrust
 - Thrust

lineament, the MFL or Matsiloje-Francistown Lineament, that separates the Western Zone of the Tati Greenstone Belt into two main terranes (Figure 3.6). The southern terrane consists of the main volcano-sedimentary rocks of the Tati Greenstone Belt, and the northern terrane is made up of granitoid plutons and fragments of paragneisses within the granitoid intrusions. The second major observation is the recognition of major shear/fault zones within the volcano-plutonic sequences of the Western Zone of the belt (Figure 3.5). These shear zones are parallel to lithological boundaries within volcano-plutonic sequences and, therefore, subdivide the volcano-plutonic rocks of the Western Zone into fault-bounded rock sequences with distinct lithological associations.

In their discussion on the relationship of fault-bound rock sequences to lithostratigraphy, Johnson and Rust (1988) suggested that the term "tectonostratigraphy" should only be used in the context of tectonostratigraphic terranes that are fault-bounded crustal blocks with distinct geological evolution, in terms of structure, stratigraphy and tectonism. They also suggested that these tectonostratigraphic terranes should be regarded as legitimate stratigraphic units with formalised nomenclature. Johnson and Rust (1988) further pointed out that "the special tectonic character of such units need not, however, preclude the recognition of various conventional lithostratigraphic units (formations, groups, etc.) within them". Each of the fault-bounded volcano-plutonic rock sequences within the Tati Greenstone Belt can be subdivided into distinct mappable lithostratigraphic units (formations), that can be classified as groups in accordance with rules of the

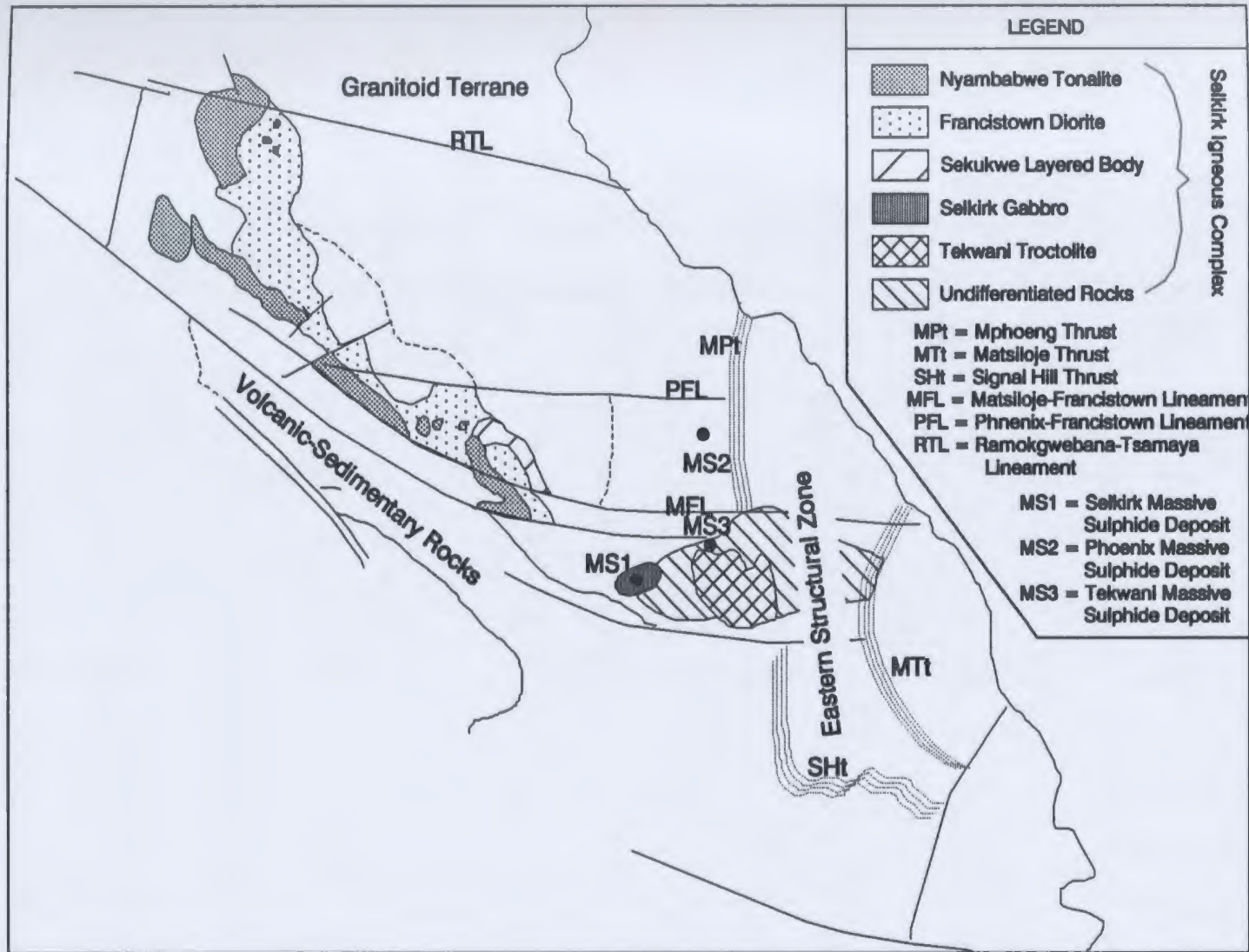


Figure 3.6: Geological map of part of the Tati Greenstone Belt showing the separation into terranes consisting of the main volcano-sedimentary rocks of the belt and a mainly granitoid terrane to the north. The granitoid terrane is a tectonic zone bounded by the MFL and RTL. The SE end of the MFZ is intruded by plutonic rocks the most prominent being the Selkirk Igneous Complex whose orientation is controlled by the direction of the MFL.

International Subcommittee on Stratigraphic Classification (ISSC, 1976). Each fault-bounded volcano-plutonic rock sequence of the Tati Greenstone Belt is equivalent to the lithostratigraphic unit "Group". In accordance with the same rules (ISSC, 1976), however, these groups cannot be classified into a single "Supergroup", as stratigraphic units bounded by regional unconformities cannot be unified into one lithostratigraphic unit (ISSC, 1976).

The Eastern Zone of the Tati Greenstone Belt (Figure 3.4) consists mainly of prominent banded iron formations along the Matsiloje Ridge. Other lithologies along this ridge are similar to those that form the upper portions of the ultramafic-mafic unit in the Western Zone and, therefore, can be correlated. Although correlation is possible on lithological grounds, the western margin of the Eastern Zone is truncated by a major regional NNE-trending shear zone, the Matsiloje thrust zone (MT₁ on Figure 3.4). The eastern margin of the Eastern Zone has been obliterated by intrusion of the Matsiloje Batholith.

Southwest of Matsiloje Ridge is the Last Hope Basin, a major sedimentary basin. The margins of this basin are defined, from the east to the north, by the prominent banded iron formation ridges underlying Signal Hill and Mapanipani Ridge, respectively. The southeastern margin is defined by a thrust fault of the Last Hope Fault Zone (LHFZ). Sedimentary rocks in the Last Hope Basin consist mainly of immature sandstones and greywackes with conglomeratic horizons, shales, grits and calcareous sediments.

Stratigraphic relations described in this study are based on lithologies exposed

in the Western Zone of the Tati Greenstone Belt (Figure 3.5). Since ultramafic-mafic rocks of the Old Tati area are continuous with those of the Western Zone, these two zones are described together. Rocks of the Tati Greenstone Belt, are subdivided into three fault-bound volcano-plutonic sequences, each with minor interflow sediments and an upper dominantly sedimentary unit. The volcano-plutonic sequences are separated from each other by thin sedimentary units consisting of banded iron formations, carbonates and minor clastic sediments. These volcano-plutonic sequences, as classified in the Western Zone type area, are, from south to north, the Lady Mary, Phenalonga and Selkirk groups. The younger sedimentary unit is classified as the Last Hope Group.

3.2.1 Lady Mary Group

The Lady Mary Group is the best exposed unit in the Tati Greenstone Belt and includes all ultramafic-mafic volcano-plutonic rocks in the Old Tati and Western Zones with a sedimentary cap. A sedimentary clastic wedge, consisting of sericitic schists, arkoses with minor conglomeratic interbeds, banded iron formations and cherts, defines the base of the Lady Mary Group, especially in the western part of the Old Tati area. Further east, relatively mature quartzite horizons become prominent. The sedimentary clastic wedge is overlain by a succession of mainly ultramafic-mafic volcano-plutonic rocks with minor interlayered sedimentary rocks that form a continuous unit, stretching from just west of Francistown southeastwards to the Old Tati Area. These volcano-plutonic rocks were previously classified as the Lady Mary

Formation (Key, 1976), or separated into two formations, the Old Tati and Lady Mary formations (Mason, 1970). Geochemical data (Chapter 5), especially of mafic lithologies from both the Old Tati and Western Zone, have shown that these rocks are remarkably similar. These geochemical similarities, when combined with field data, suggest that these rocks had a common origin and supports the grouping of these rocks into a single lithostratigraphic unit. Stratigraphically overlying ultramafic-mafic volcano-plutonic rocks, especially in the Western Zone, is a thin discontinuous sedimentary rock unit consisting feldspathic clastic sediments, calcareous sediments and banded iron formations. The relatively well exposed nature and strong photogeological expression provide good control for mapping the geological distribution of this unit. The Lady Mary Group can be further subdivided into three subunits which, from the base to top, are; the Old Tati, Map-Nora and Golden Eagle formations.

3.2.1.1 Old Tati Formation

Within the Old Tati area (Figure 3.7 - in pocket) are the best exposures of ultramafic rocks in the Tati Greenstone Belt, however, rocks in this area are comparatively more deformed than similar lithologies elsewhere in the belt. The higher degree of deformation, together with the effects of fragmentation due to faulting/shearing, have created some uncertainties as to the true stratigraphic position of the ultramafic rocks in the Old Tati area. They have been considered to be part of a different unit than the ultramafic-mafic rocks of the Western Zone (Mason,

1970; Sheeran, 1986; Johnston and Griffiths, 1982). Key (1976), on the hand, suggested that these rocks form part of the same ultramafic-mafic sequence that occurs in the Francistown area. Field mapping, photogeological and satellite imagery interpretations, including geochemical studies carried out for this study, all suggest that the dominantly ultramafic volcano-plutonic rocks in the Old Tati area are part of a continuous komatiite-tholeiite sequence stretching from west of Francistown (Figure 3.8). The name "Old Tati Formation" is, therefore, re-introduced (after Mason, 1970) to classify the dominantly ultramafic-mafic volcano-plutonic rocks with a basal clastic sedimentary wedge; the type area being around Old Tati.

The Old Tati Formation constitutes the base of the Lady Mary Group. A clastic wedge consisting of quartz-mica schists, quartzites, minor quartz-pebble conglomerates and gritty sandstone interbedded with banded iron formations and cherts, found only in the Old Tati area, constitutes the base of the Old Tati Formation. Pebbles in the conglomerate were derived mainly from granite-gneisses and consist of quartz and rock fragments. The clastic sediments are generally feldspathic as evidenced by a dominant pink colouration and the banded iron formation is finely laminated, consisting of creamy-white cherty layers alternating with brown to black hematite/magnetite layers.

In some locations, especially south of the Tati River, chert bands in banded iron formations are typically boudinaged with the long axes of boudins parallel to the main trend of the banded iron formation ridge (NW-SE). The banded iron formation in this area rests directly on pink granite gneiss that contains numerous quartz veins;

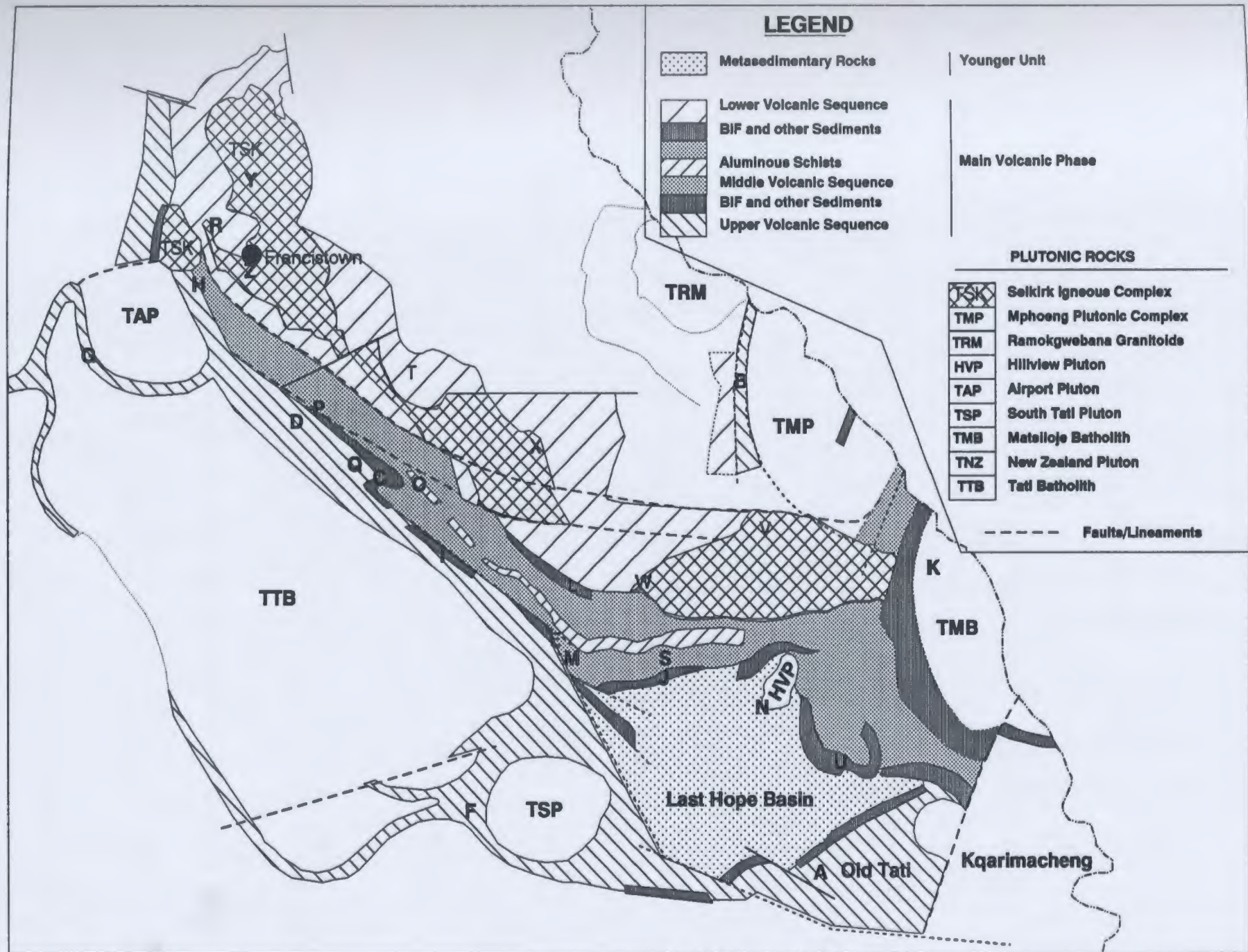


Figure 3.8: Geological map of the Tati Greenstone Belt. Areas marked by letters (A-X) are discussed in the text.

the veins also follow the main iron formations and are highly metamorphosed and have a metallic lustre due to the presence of granular specularite.

Although exposures are very poor, a succession of komatiites, dark green high-Mg basalts with stubby pyroxene phenocrysts, talc schists, ultramafic and mafic schists, gabbroic sills, and serpentinites conformably overlie the basal clastic sedimentary wedge. The volcano-plutonic sequence of the Old Tati Formation is, however, poorly exposed and, therefore, very difficult to classify. As a result there have been claims and counter claims made with respect to the presence of komatiites in the area (e.g. Sheeran, 1986). The problem has been clarified somewhat by the results of a geochemical and mineralogical study of borehole core samples from the area (Mosigi, 1991). This study indicated the presence of both peridotitic and basaltic komatiites and pointed out that komatiite-bearing ultramafic sequences in the Old Tati area are cyclic in character (Mosigi, 1991). A typical cycle consists of basal peridotite followed by komatiite and basaltic lavas. The stubby pyroxene-bearing, high-Mg basalts form the tops of the cycles and are capped by bedded cherts and banded iron formations.

Komatiites are poorly exposed and are relatively rare at the surface. A black, very fine-grained and finely layered and reddish-brown weathering rock that crops out in the area around the Blue Jacket Mine (A on Figure 3.8) has been shown, on the basis of geochemistry (Chapter 5), to be of komatiitic affinity. Elsewhere in the area, this rock is associated with other ultramafic schists and thus, probably represents a chilled komatiitic lava.

In the Francistown area, ultramafic rocks are not very common. A dark green,

fine to medium-grained ultramafic volcanic rock, however, occurs towards the base of a sequence of predominantly mafic rocks. In outcrop, the rock has a spotty appearance resulting from the presence of small mafic mineral clots made up of stubby pyroxene crystals in a relatively fine grained matrix. The rock crops out as thin sills interlayered with basaltic rocks.

The top of the Old Tati Formation is defined by a purplish to reddish brown pillowed ferrous basaltic unit which is underlain by whitish-grey relatively fine-grained, pyroclastic sedimentary rocks. The pyroclastic rocks contain rounded boom-clasts of the ferrous basalt.

Peridotites in these ultramafic-mafic sequences are commonly highly altered to a mineral assemblage of magnetite, carbonate, chlorite and talc. Komatiites, on the other hand, contain amphibolitized, spinifex pyroxene in a fine-grained matrix of chlorite, sericite and minor amphibole.

3.2.1.2 Map-Nora Formation

The name Map-Nora Formation, derived from the old gold mine workings of the Map and Nora Mines (now Shashe Mine, Figure 1.3), is used to define these dominantly mafic volcano-plutonic rocks of the Lady Mary Group. The rationale is that the gold deposits at these old mines are hosted by basaltic rocks belonging to this formation. The main outcrop areas are around the Shashe Mine (Map-Nora), near the Lady Mary Mine along the Tati River, and at the Sekukwe bridge along the Francistown-Matsiloje road. Pillow basalts, amygdaloidal basalts, gabbroic sills and

basaltic lavas with interflow sedimentary rock units constitute the Map-Nora Formation. On aerial photographs, the Map-Nora Formation has strong linear features resulting from the interlayering of basalts and gabbroic sills and dykes.

The best exposures occur in a belt which extends for about 30 km from the west of Francistown to the Old Tati area (Western Zone; Figure 3.5). South of the Mphoeng area, and north of Matsiloje Ridge (B on Figure 3.8), a thin linear belt of mafic rocks with the same characteristics as those in the Western Zone crops out. East of Matsiloje Ridge, basalts and interlayered gabbroic sills similar to those in the Western Zone also occur.

The base of the Map-Nora Formation is defined by the dark-green pyroxene-bearing ultramafic schist that is interlayered with komatiitic lavas, other ultramafic lavas and plutonic rocks. The basal unit is overlain by interlayered pillow basalts and gabbroic sills. Pillow basalts become more amygdaloidal towards the top of the formation.

The top of this formation, especially in the Western Zone, consists of discontinuous serpentinite bodies and ultramafic actinolite-tremolite-chlorite schist. Near the abandoned Golden Eagle mine (C on Figure 3.8), the ultramafic actinolite-chlorite schists crop out as prominent linear ridges towards the top of the volcano-plutonic sequence immediately below the sedimentary cover. These schists consist of felted masses of randomly oriented tremolite-actinolite crystals, together with chlorite \pm clinozoisite \pm epidote.

Two types of mafic rocks can be recognized, a dark green very fine-grained

variety, and a relatively massive feldspathic gabbro. These two units are generally separated by interflow black pyritic shales, such as in the N9 reef at the Shashe Mine. The dark green basalts are recognizable lavas with brownish stained weathering surfaces and are most frequently interlayered with coarse gabbroic sills. Where fresh, the dark green, fine-grained basaltic rock contain subhedral crystals of hornblende and laths of actinolite \pm tremolite. Where altered, the basaltic rocks are grey to pale-green chlorite schists consisting of fibrous chlorite laths and acicular tremolite crystals in matrices of fine grained chlorite, magnetite, and hematite. Quartz and carbonate veinlets which parallel the main rock fabric are typical.

The chlorite schists are more common in high strain areas (shear zones), with whitish-grey to bluish-grey talc-chlorite schist consisting of talc and chlorite \pm prehnite, and highly altered minor plagioclase and tremolite. The fine-grained basalts generally occur as pillows and are locally amygdaloidal, especially in the area around the Dunham Mine (D on Figure 3.8). East of the Sekukwe River bridge (E on Figure 3.8), the basalts interlayered with gabbroic sills are finely banded and are yellowish-green due to hydrothermal alteration. In an area south of Mphoeng, the mafic rocks are also intruded by numerous trondhjemitic dykes of various sizes.

The gabbroic rock is black to dark-grey and ranges from fine to coarse-grained. The rock consists mainly of hornblende and acicular crystals of tremolite and plagioclase in a matrix of chlorite, epidote, sericitized plagioclase, and clinozoisite. Alternating layers of amphibole and plagioclase crystals impart a banded texture to this rock.

Interflow sedimentary rocks are minor and are represented by garnetiferous siliceous rocks and banded iron formations found at contacts between the coarse-grained gabbroic sill-rocks and the fine-grained pillow basalts. Other occurrences of interflow sedimentary rocks have been noted in the area near the Southern Tati Pluton, where a greenish-grey (with yellowish tints), highly foliated, and steeply dipping fine-grained arkosic sedimentary rock crops out (F on Figure 3.8) at the contact between gabbroic sills and fine-grained pillow basalts. Ferruginous and manganiferous concretions give this rock a spotty surface appearance.

Serpentinite bodies occur towards the top of the Map-Nora Formation near major boundary faults throughout the Western Zone of the Tati Greenstone Belt. They vary widely in size and form from area to area. West of the Airport Pluton (G on Figure 3.8), a bluish-grey, crudely layered serpentinite body crops out on a low-lying hillock. Just north of the Airport Pluton (H on Figure 3.8), a black to grey, very fine-grained rock crops out on comparatively hilly ground. The rock contains numerous carbonate veinlets, where these carbonate veins have been weathered out, only empty grooves remain, giving the rock a crudely banded appearance. Serpentinites also occur near contacts between supracrustal rocks and granitoids, together with other ultramafic rocks.

3.2.1.3 Golden Eagle Formation

Rocks of this unit host the ancient gold mine workings of the Golden Eagle Mine, hence, they are named the Golden Eagle Formation. Rocks of this formation

constitute the sedimentary cap to the volcano-plutonic rocks of the Lady Mary Group and consist of interbedded, laminated limestones, pink massive marbles, banded iron formations, greywackes and arkosic sandstones. These rocks crop out in a northerly facing, overturned anticlinal fold in the vicinity of the mine. A similar suite of sedimentary rocks crop out at Long Gossan (I on Figure 3.8), and further east at Mapanipani and Matsiloje Ridges (J and K on Figure 3.8). Banded iron formations of the Mapanipani Ridge and Long Gossan areas are brownish red to black and gossaniferous, indicating that they are sulphide facies banded iron formations. In these two areas (Mapanipani and Long Gossan), the base of the succession is marked by greenish grey phyllites and minor clastic sediments.

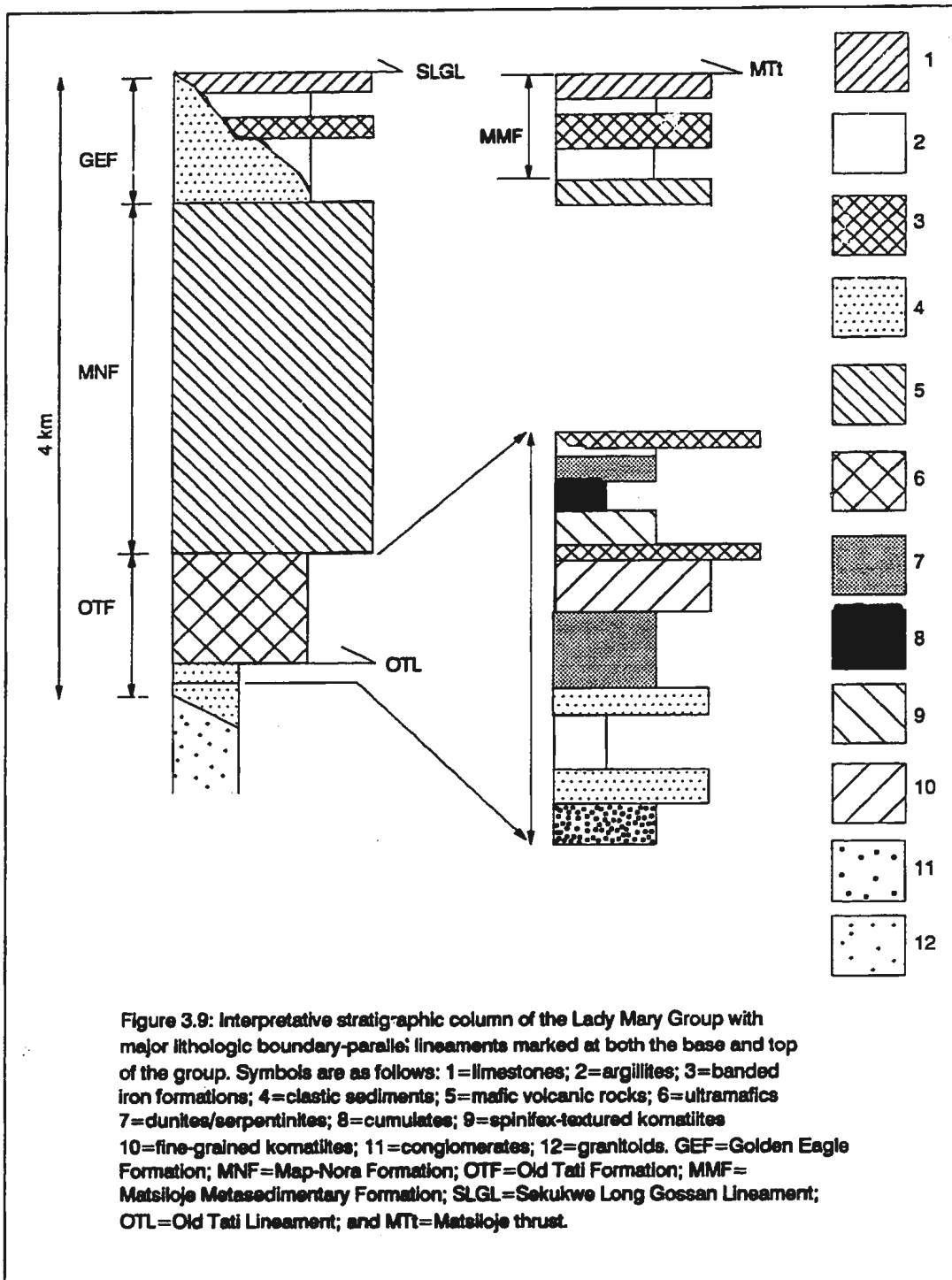
3.2.1.4 Matsiloje Formation

The sedimentary package that constitutes the Matsiloje Ridge is quite similar to that of the Golden Eagle Formation at the top of the Lady Mary Group in the Western Zone. This similarity suggests that rocks at Matsiloje Ridge may be correlated with the Golden Eagle Formation as originally suggested by Key (1976). Structural data (Chapter 4), however, indicate that these rocks are allochthonous. The Matsiloje rocks are, therefore, classified here as a separate lithostratigraphic unit because they are bounded by fault/shear zones which cannot at this stage be correlated with fault/shear zones that bound the Lady Mary Group in the Western Zone. The name Matsiloje Formation is re-introduced, following Mason's (1970) previous application, for banded iron formation-bearing metasedimentary rocks of

Matsiloje Ridge. Towards the base of Matsiloje Ridge, sedimentary rocks consist of greenish-grey phyllites and whitish-grey sandstones. Various types of banded iron formations follow directly above the phyllites. These banded iron formations consist of thin, alternating, dark-brown to red-hematite and creamy-white cherty bands. Pink to purplish-brown and yellowish-brown, sulphide-bearing banded iron formation varieties occur locally. Brecciated reddish-brown jaspelitic varieties also occur towards the top of the banded iron formation assemblage. Dull white, calcareous sediments (dolomites and limestones) constitute the top of the Matsiloje Formation. The north-south trend of the Matsiloje banded iron formation ridge is orthogonal to the northwest-southeast trend of the main part of the Tati Greenstone Belt. To the east of the Matsiloje Ridge, basalts occur that are similar to those of the Lady Mary Group in the Western Zone. The lithostratigraphy of the Lady Mary Group is summarized on Figure 3.9.

3.2.2 Phenalonga Group

The name Phenalonga is re-introduced after Mason (1970) and re-defined as a lithostratigraphic unit "Group" which includes all rocks that crop out in the area between the Long Gossan-Mapanipani (I and J on Figure 3.8) and Phenalonga (L on Figure 3.8) banded iron formation-bearing linear ridges. These rocks are similar to those of the Golden Eagle Formation. Banded iron formation and associated sedimentary rocks that crop out along the Long Gossan-Mapanipani Ridges of the Golden Eagle Formation, Lady Mary Group, form the southern boundary of the



Phenalonga Group (Figure 3.10). The northern boundary between the Phenalonga Group, and the structurally underlying volcano-plutonic rock unit to the north, is defined by banded iron formation and associated sedimentary rocks that crop out at Phenalonga Hill (L on Figure 3.8).

The base of the Phenalonga Group is defined by a pale green agglomerate that consists of elongated and angular clasts of andesitic rocks in a fine-grained andesitic matrix. This agglomerate crops out about five hundred metres northwest of Mapanipani Ridge (M on Figure 3.8). Reddish-brown weathering feldspathic shales are immediately above the agglomerates, but generally crop out at the base of a prominent linear ridge of aluminous schists that extends from Hillview Ridge (N on Figure 3.8) to the abandoned Halfway-kop kyanite mine (O on Figure 3.8). This linear ridge consists of whitish-grey to pink aluminous schists (Figure 3.10). Key (1976) subdivided the aluminous schist unit into three main lithotypes; chloritoid schists, kyanite schists and pyrophyllite schists. The most widely distributed aluminous schist rocks are reddish-brown pyrophyllite and chloritoid schists which consist mainly of chloritoid or pyrophyllite crystals in quartz, sericite and white mica matrices (Key, 1976).

The kyanite schists crop out mainly at the Halfway-kop Hill (O on Figure 3.8) where the only kyanite mine in Botswana is located; kyanite was mined here in the early 1950's. The kyanite schist contains bluish green radiating blades of kyanite crystals in a matrix of quartz and white mica; sericite with minor quartz, and locally with hematite also occur. Kyanite replaces pyrophyllite laths.

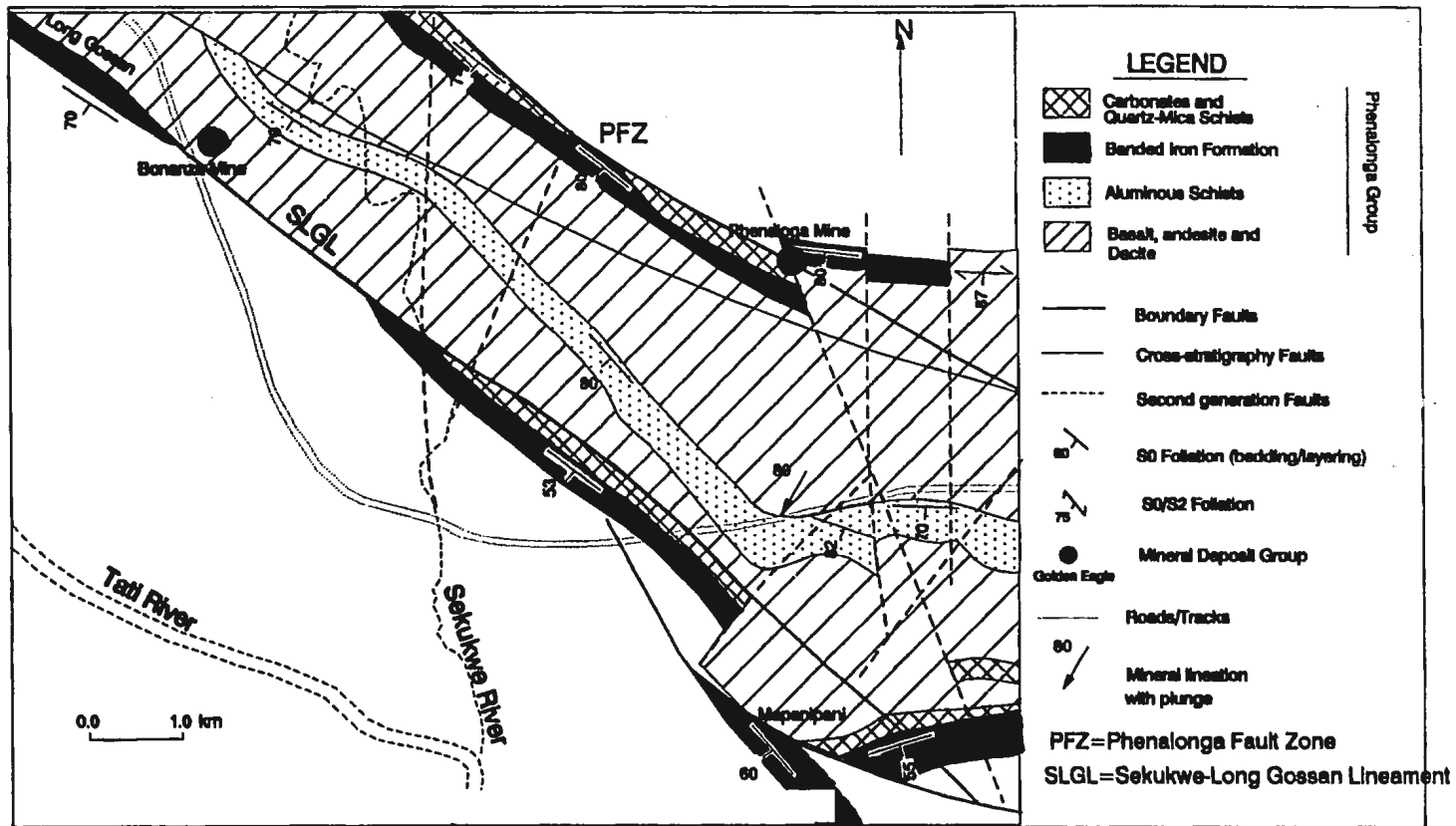


Figure 3.10: Geological map of part of the Western Zone of the Tati Greenstone Belt showing the distribution of the Phenalonga Group.

The volcano-plutonic rocks of the Phenalonga Group consist of a succession of basalts, gabbroic sills, basaltic andesites, andesites, dacites, diorites and rhyolites. The most common rock type is greenish-grey, fine to medium-grained andesite. South of the Tati River around Francistown and along the river, andesites are interlayered with rhyolites. In the area north of Mapanipani Ridge, the andesitic rock contains quartz-filled vesicles. The andesite consists mainly of elongated hornblende and plagioclase crystals, which give the rock a characteristic banded appearance. Minor biotite and chlorite are locally present. Interlayered rhyolite is fine-grained and crops out as massive units; locally the rock displays a parting lineation where muscovite and/or sericite are present. Elsewhere in the belt, dioritic and gabbroic sills and a greenish-grey fine-grained basaltic rock, similar to those found in the Lady Mary Group, are associated with the andesite. These sills occur in the Tati River near Menard's farm (P on Figure 3.8) and further southeast towards the Lady Mary Mine (Q on Figure 3.8).

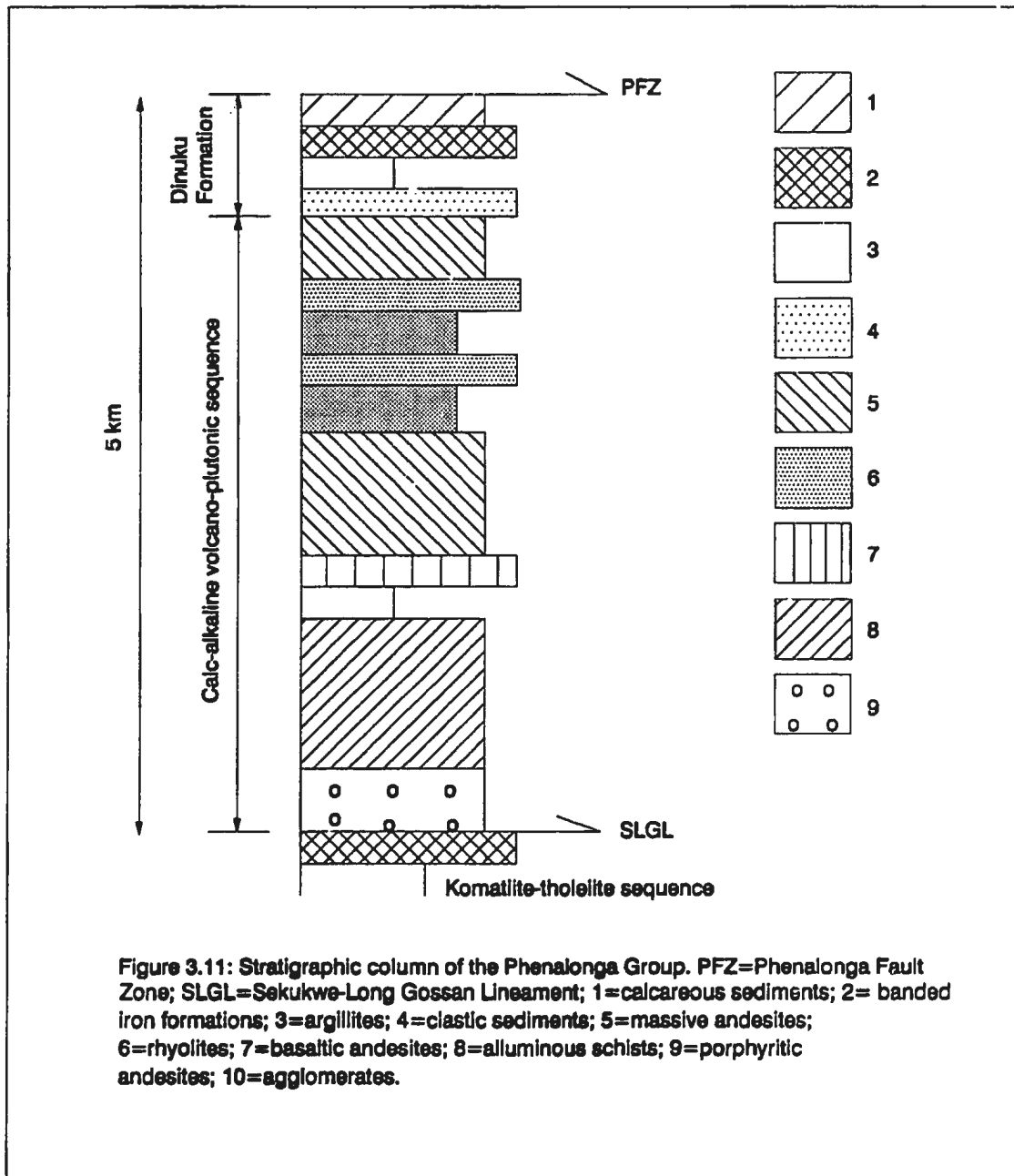
Although the spatial distribution of the Phenalonga Group lithologies is well constrained both stratigraphically and by major fault/shear zones that occur both at the base and top of the group, the rocks themselves are poorly exposed. The current state of knowledge on their distribution does not provide sufficient control for subdividing the group into constituent formations, except for the sedimentary assemblage, the Dinuku Formation, that caps the unit.

3.2.2.1 Dinuku Formation

The top of the Phenalonga Group is marked by a sedimentary succession at Phenalonga Hill (L on Figure 3.8) that consists mainly of dark-brown banded iron formations that are locally gossaniferous (i.e. sulphide-bearing). In addition to banded iron formations, laminated manganese-rich carbonaceous sedimentary rocks are also common, interbedded with brown pebble conglomerates. This entire sedimentary package is grouped under the Dinuku Formation. Lithologies of this formation are similar to those within the Golden Eagle Formation which separates the Lady Mary Group from the Phenalonga Group. These similarities have prompted some geologists (e.g. Jackson, 1981) to suggest that the two units may actually represent the limbs of a single synclinal structure. Stratigraphic and structural relations (Chapter 4) indicate, however, that although these two units are lithologically similar, they are stratigraphically different. The lithostratigraphy of the Phenalonga Group is summarized on Figure 3.11.

3.2.3 Selkirk Group

The Selkirk Group encompasses all volcano-sedimentary rocks that overlie the Dinuku Formation, Phenalonga Group (Figure 3.12). The top of the Dinuku Formation coincides with a tectonic discontinuity, the Phenalonga Fault Zone, that separates the Phenalonga Group volcano-sedimentary rocks from those of the Selkirk Group. It is difficult to develop a coherent picture from the outcrop distribution of this unit, as only fragments remain due to numerous plutonic intrusions. The base of



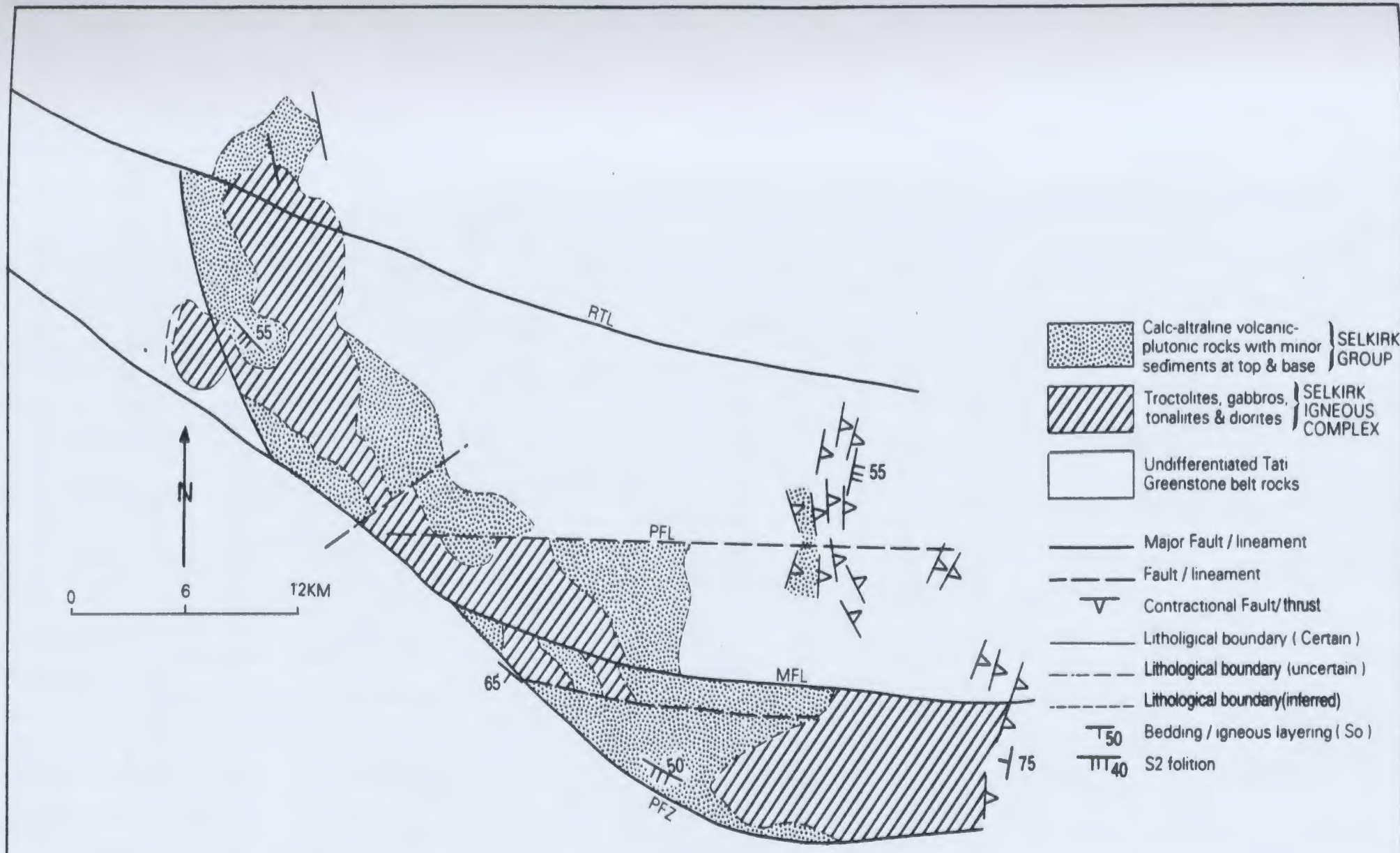


Figure 3.12: Simplified Geological map showing the distribution of the Selkirk Group and its relationship with the Selkirk Igneous Complex.

Selkirk Group rocks is defined by a black to greenish-grey biotite schist that crops out few kilometres north of Monarch Mine (R on Figure 3.8). Minor greenish-grey pebble conglomerates, which are generally interbedded with quartz-mica schists, follow the biotite schist, especially southeast of the Selkirk Mine and near the abandoned Vermaak gold mine (S on Figure 3.8).

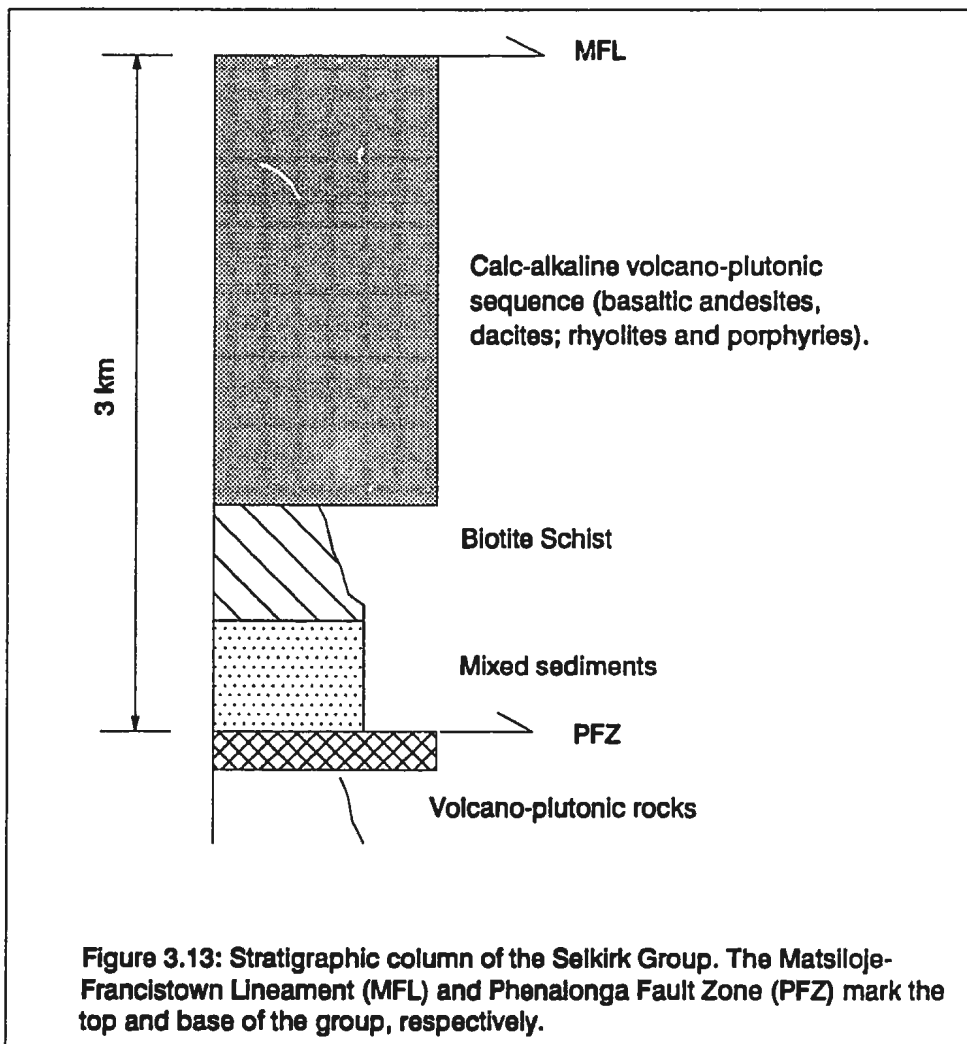
Johnston and Griffiths (1982) included these rocks and volcano-plutonic counterparts in their Phenalonga Formation. They suggested that the Selkirk Formation should only refer to the intrusive complex, which Key (1976) and Mason (1970) had regarded as a synvolcanic plutonic complex. Geological relations and structural interpretations (Chapter 4) indicate that these rocks are separated from the Phenalonga Group by a tectonic discontinuity, the Phenalonga Fault Zone, and hence, constitute a distinct fault-bounded unit. More detailed geological and structural investigations, including exploration drilling at the Selkirk Mine, confirm Johnston and Griffiths's (1982) interpretation that the plutonic complex, which occurs towards the top the dominantly siliceous volcano-plutonic rocks, is intrusive into the volcano-plutonic rocks.

Rocks of this unit are dominated by a greenish grey feldspar-porphyry that occurs with dacitic and andesitic rocks around the Selkirk Massive Sulphide Mine. In a north-south section along the Sekukwe River (T on Figure 3.8), the unit is exposed as rafts of andesitic volcanic rocks within granodiorite and diorite intrusions. The Selkirk Group cannot at this stage be subdivided into constituent formations because of outcrop fragmentation resulting from the emplacement of the Selkirk Igneous

Complex and granitoid intrusions. Although poorly exposed, rocks of this group resemble those of the Phenalonga Group, in that they consist of basaltic andesites, andesites, dacites and rhyolites, with dioritic sills. No geochemical work has been carried out on these rocks. A summary of rock descriptions and distributions in the Selkirk Group is shown on Figure 3.13.

3.2.4 Last Hope Group

Perhaps one of the most intractable problems in understanding the geology of Tati Greenstone Belt is the stratigraphic position of the Last Hope Group sedimentary rocks. Mason (1970) suggested that these rocks were deposited in a discrete sedimentary basin south of the Mapanipani Ridge banded iron formation. Key (1976), on the other hand, suggested that they formed part of the base of the Penhalonga (sic) Formation. Much of the confusion results from the structural relationships between these sedimentary rocks and the rest of the belt. Geological and structural relations (Chapter 4) suggest that these sedimentary rocks crop out in an oval shaped structural basin, here named the Last Hope Basin, which is bounded to the north by Mapanipani Ridge banded iron formation and to the east by Signal Hill (U on Figure 3.8). The name Last Hope is, therefore, re-introduced after Mason (1970) and the sequence is re-defined as a lithostratigraphic group comprising all sedimentary rocks within the Last Hope Basin. Exposure of the Last Hope Group is poor, with discontinuous and isolated outcrops scattered throughout the entire basin. Lithologies within the Last Hope Basin can be subdivided into northern and southern



zones. The northern zone constitutes the area just south of the Mapanipani Ridge banded iron formation. In this region, and areas further south towards the basin centre, are isolated outcrops of dirty grey to pale green calcareous argillites, limestones, shales and greywackes. Photogeological interpretations indicate that these rocks are folded into NW-trending folds.

The southern zone consists of the Signal Hill area which is the portion of the basin that has received the greatest attention from mineral exploration companies searching for sedimentary hosted gold-antimony mineralization. In this area, sedimentary rocks consist of meta-arkosic sandstones transitional to siltstones and conglomerates. The reddish brown arkosic sandstone is commonly interbedded with pale grey, relatively mature, gritty quartzitic sandstone. These rocks crop out on ENE-trending low-lying hills and dip at steep to moderate angles to the south. Diamond drilling during mineral exploration indicated that the area is underlain by interbedded, matrix-supported, conglomerates and arkosic sandstones. Banded iron formation-bearing outcrops, of which Signal Hill (U on Figure 3.8) is the most prominent, are considered to be SW-directed thrust slices emplaced onto the sedimentary basin. Because of poor exposure, the Last Hope Group rocks are not divided into constituent formations. Figure 3.14 summarizes lithological characteristics and stratigraphy of the Last Hope Group.

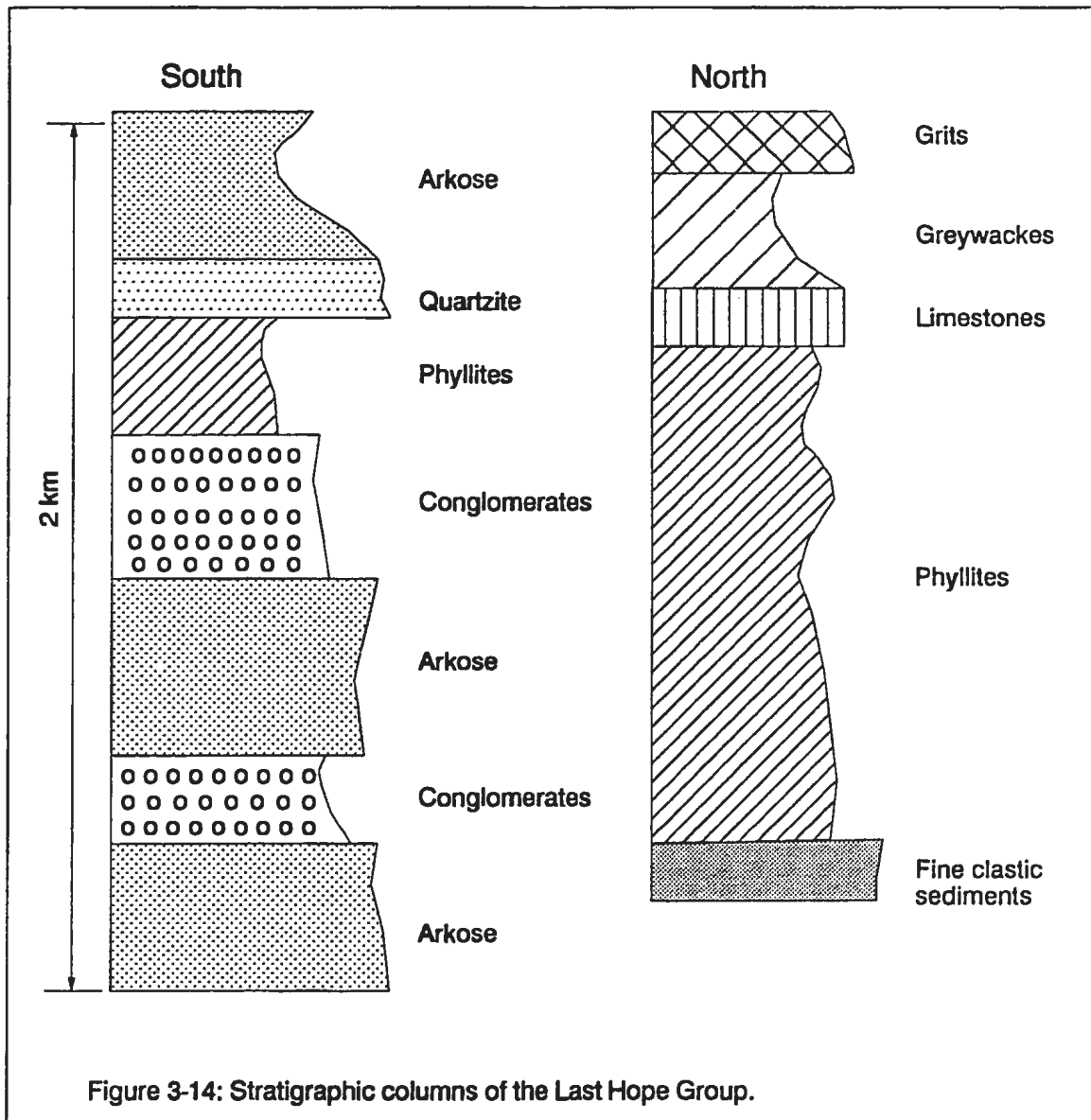


Figure 3-14: Stratigraphic columns of the Last Hope Group.

3.3 Plutonic Rocks of Tati Greenstone Belt

3.3.1 Tati Batholith

The Tati Batholith is a composite, elliptically shaped, plutonic igneous body which intruded along the southern margin of the Lady Mary Group (Figure 3.8). The batholith consists of granitoids ranging from tonalites, granodiorites, feldspar megacrystic granites, to equigranular granites. The granitoids vary in composition and degree of metamorphism from north to south. In the north, at contacts between granitoids and supracrustal rocks, medium to coarse-grained pinkish-white granodiorites crop out. The granodiorites contain plagioclase, biotite and minor quartz, and are foliated. The foliation is marked by relatively large, orientated feldspar crystals within a deformed groundmass of biotite and quartz. This foliation is concordant with the foliation in the host supracrustal rocks.

In the south, towards the Northern Marginal Zone of the Limpopo Belt, foliated feldspar megacrystic granites occur. These rocks are pink to grey and are coarse-grained to porphyritic. They consist of large potassic feldspar ovoids in a coarse-grained matrix of biotite, hornblende, and quartz. The degrees of metamorphism and deformation increase in these rocks towards the Northern Marginal Zone of the Limpopo Belt and satellite plutons of this rock type are present in the Northern Marginal Zone. Undeformed, whitish-grey to pink, equigranular granites form the rugged hilly terrain at the core of the batholith. These rocks intrude coarse-grained grey tonalites. The intrusive relationship is marked by numerous deformed aplites, dykes and small scale shear zones at the margins of the tonalites.

3.3.2 Trondhjemite Plutons

Three small, whitish-grey to pink, equigranular trondhjemite plutons intrude ultramafic-mafic rocks in the southern, southwestern and southeastern parts of the Tati Greenstone Belt (Figure 3.8). These are the Airport Pluton, cropping out southwest of Francistown, the Southern Tati Pluton, near the NE margin of Tati Batholith, and the Hillview Pluton which intrudes sedimentary rocks of the Last Hope Basin. These plutons are relatively uniform in composition compared to large complex bodies such as the Tati Batholith.

3.3.3 New Zealand Pluton

A grey to pink, coarse-grained granodiorite intrudes the base of the ultramafic-mafic rocks in the Old Tati area (Figure 3.8). The rock is compositionally similar to some of the Tati Batholith rocks and the body is also highly sheared and foliated.

3.3.4 Matsiloje Batholith

An elliptical granitoid body, with its long axis trending N-S, is present as flat lying outcrops at the extreme eastern end of the Tati Greenstone Belt (Figure 3.8). The batholith is a homogenous, coarse-grained grey tonalite body, containing hornblende, biotite, plagioclase and quartz.

3.3.5 Selkirk Igneous Complex

The top of the northernmost volcano-plutonic unit of the Tati Greenstone Belt, the Selkirk Group, is highly dissected by plutonic rocks. The most significant of these plutonic rocks constitute the Selkirk Igneous Complex which ranges in composition from troctolite to tonalite. The complex forms a linear belt of plutonic bodies extending from Tekwani in the east, to Francistown in the west (Figure 3.12). Coarse-grained troctolites, the Tekwani Troctolite, intrude siliceous volcanic rocks of the Selkirk Group in the area around Tekwani (V on Figure 3.8). Further west, a grey, medium to coarse-grained gabbroic body, the Selkirk Gabbro, is covered by sulphide gossans at the Selkirk massive sulphide mine (W on Figure 3.8). Scattered outcrops of feldspar porphyry occur in the vicinity of the gabbroic body.

West of the Selkirk Gabbro, near the Sekukwe River (X on Figure 3.8), a layered ultramafic body occurs on the same trend as the other two bodies. This body, called the Sekukwe Kop Layered Plutonic Body, consists of a cap of serpentinites underlain by a crudely layered anorthositic gabbro and minor peridotites. Minor chromite seams occur in this layered body. A series of coarse-grained dioritic bodies, best exposed around Francistown (Y on Figure 3.8), extend from the area around the Sekukwe Kop Layered Plutonic Body westwards to Francistown. The diorite was named the Francistown Diorite by Key (1976) and this name is retained here. These rocks follow the same structural trend as the three plutonic bodies described above. The dioritic bodies enclose or surround small outcrops of coarse-grained tonalite which has its greatest area of outcrop on the Nyambabwe Hill (Z on Figure 3.8) in

Francistown. The tonalite is here named the Nyambabwe Hill Tonalite.

These five plutonic bodies have been variously interpreted as synvolcanic plutonic units (Key, 1976; Mason, 1970), or as separate plutonic bodies intrusive into the main volcanic component of the Tati Greenstone Belt (Johnston and Griffiths, 1982; Sheeran, 1986). Field mapping carried out during this study indicates that the five bodies are genetically and tectonically related. Although intrusive relationships among members of these plutonic bodies cannot be demonstrated in the field, they all occur at the same stratigraphic and structural positions. These rocks may either be derived from the same magmatic source, or have been emplaced during the same tectonic event.

3.3.6 Granitoids of the North Margin of the Tati Belt

3.3.6.1 Undifferentiated Granitoids

Granitoids intrude much of the Tati Greenstone Belt volcanic rocks in the north. These are generally trondhjemites, granodiorites and granites. Granitoid gneisses are exposed along road cuttings as rafts and xenoliths in the younger granitoids. Little work was completed in this part of the belt and therefore these rocks are collectively referred to as undifferentiated granitoids. These rocks include part of Key's (1976) Selukwe Batholith.

3.3.6.2 Ramokgwebana Batholith

A pink to whitish-grey, coarse-grained to porphyritic feldspar granite crops out

at the northern edge of the Tati Belt. This granite contains large ovoidal potassic feldspar crystals in a coarse-grained matrix of feldspar, biotite, hornblende and quartz. Because of the coarse-grained nature of the matrix, the rocks are friable. The megacrystic granite intrudes pale-grey coarse-grained granodiorites. These two granitoids comprise the Ramokgwebana Batholith which is intrusive into the undifferentiated granitoids discussed above.

3.3.6.3 Mphoeng Plutonic Complex

A plutonic complex with north-south trend intrudes the northeastern part of the Tati Greenstone Belt (Figure 3.9). The complex extends from north of Matsiloje to Mphoeng in southern Zimbabwe. The plutonic complex consists of coarse-grained to porphyritic gabbros, tonalites and granodiorites. The gabbros crop out in the southernmost part of the complex where they intrude pale green andesites of the middle volcanic sequence. The gabbro consists of large milky white plagioclase ovoids in a dark green coarse-grained matrix of pyroxene, plagioclase, minor hornblende and biotite.

3.4 Rocks outside the Tati Greenstone Belt

3.4.1 Kgarimacheng Formation

An assemblage of ultramafic-mafic volcanic and plutonic rocks with minor sedimentary intercalations occurs southeast of the main Tati Greenstone Belt in the Old Tati-Matsiloje area (Figure 3.2). These rocks were considered by Key (1976) and

Mason (1970) to be remnants of an Archean greenstone belt older than the Tati Belt.

3.4.2 Northern Margin Zone of the Limpopo Belt

In Botswana, two areas are classified as being part of the Northern Marginal Zone of the Limpopo Belt. These are the Madinare-Monatshane Tuli-Sabi shear zone and the Shashe areas. Lithologically these areas are underlain by supracrustal rock successions of banded gneisses, marbles and magnetite-quartzites, interlayered with thin amphibolite sheets. These rocks were metamorphosed to amphibolite and granulite facies and intruded by megacrystic feldspar granites.

3.5 Phanerozoic Rocks

Mesozoic (Karoo) to Cenozoic dolerite dykes intrude rocks of the Tati Greenstone Belt. These northwest-trending dykes are the mostly widely distributed dykes in the area. They consist of dull grey, coarse-grained rocks composed of plagioclase and pyroxene. The distribution of the Karoo dykes is related to the presence of the Mesozoic Karoo Basin that covers most of the central part of eastern Botswana. In northeastern Botswana, Karoo basalts overlie the Central Zone of the Limpopo Belt. The dolerite dykes both pre- and post-date Karoo basaltic volcanism.

Tertiary dolerite dykes crop out as a narrow belt, termed the Tertiary Dyke Swarm. These rocks were interpreted by Reeves and Hutchins (1978) as the failed rift arm of a triple point junction localized somewhere in Zimbabwe.

CHAPTER FOUR

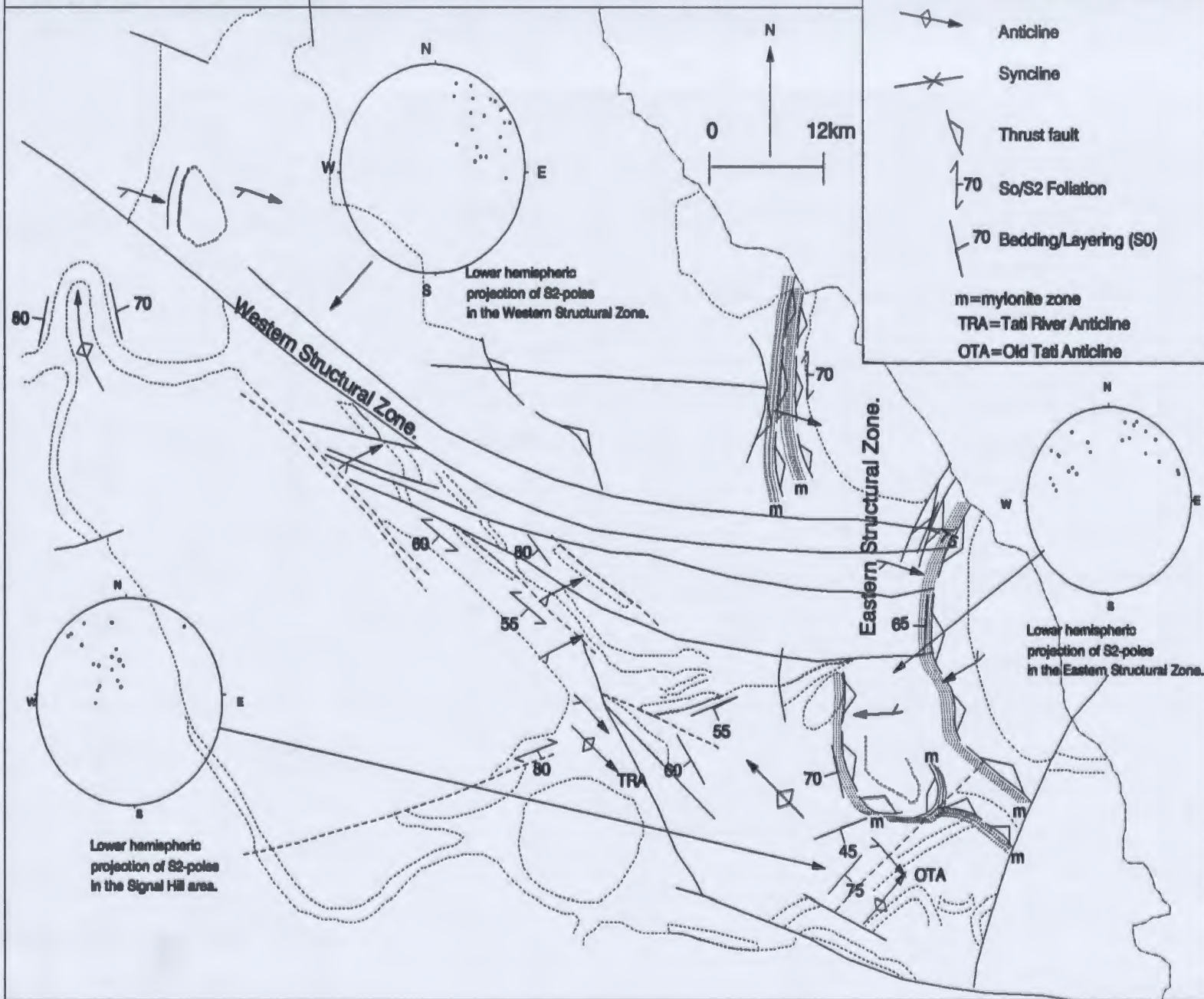
4. THE STRUCTURE OF THE TATI GREENSTONE BELT

4.1 Introduction

The Tati Greenstone Belt can be subdivided into two main structural zones based on two dominant structural trends (Figure 4.1); the Western and Eastern Structural Zones (Mason, 1970; Key, 1976; Coward and James, 1974). The area west of Francistown consists mainly of volcano-plutonic rocks and intrusive granitoids. These rocks have a dominant N-S structural trend, with moderate to steep dips to the west. Further south and east of Francistown, the trend of the belt swings southeastwards producing a NW-trending belt, that extends from Francistown for 35 kilometres to the Old Tati area. This part of the Tati Greenstone belt is generally referred to as the Western Structural Zone (Key, 1976; Sheeran, 1986; Johnston and Griffiths, 1982). The Western Structural Zone (Figure 3.5) contains the largest development of volcano-plutonic rocks in the Tati Greenstone Belt.

The structural trend of the Eastern Structural Zone is almost at right angles to the trend of the Western Structural Zone (Figure 4.1). The Tati Greenstone Belt rocks in the Matsiloje Ridge, Signal Hill areas and around Ramokgwebana (i.e. south of Mphoeng) have a dominant NNE structural trend, with steep dips to the west and southwest (Figure 4.2 - in pocket). The fault-bounded Last Hope Sedimentary Basin, containing a feldspathic sedimentary rock succession younger than the main volcano-sedimentary rocks of the belt, occurs at the eastern end of the Western Structural

Figure 4.1: Simplified Structural Map of the Tati Greenstone Belt showing the two structural zones of the belt.



Zone, near the intersection of the two structural trends (Figure 3.7).

Mason (1968) suggested that the Last Hope Group constitute a discrete basin of "rightway up" sediments. This was disputed by Key (1976), who showed that the stratigraphic and structural trends of these sedimentary rocks are generally NW-SE, similar to the trends of the main supracrustal rocks in the Western Structural Zone. Key (op cit.) suggested that these sedimentary rocks are a continuation of the supracrustal rocks in the Western Structural Zone and, therefore, are part of the same sequence. It has also been shown that Last Hope Group conglomerates contain rock fragments derived from volcano-sedimentary rocks and gneisses of the Tati Greenstone Belt (Molyneux, 1971). In this study it is suggested that the Last Hope Group rocks (see section 4.2.2) were deposited in a basin controlled by S to SW steeply dipping, E-W to NW-SE trending normal faults that formed at the restraining bend between two major shear zones (see section 4.2.3). The structures of the Last Hope Group sedimentary rocks will therefore, be discussed separately.

4.2 Regional Structural Framework of the Tati Greenstone Belt

Rocks of the Tati Greenstone Belt have been subjected to at least five deformational events (D_1 to D_5). The use of D_1 ... D_n to designate deformation events does not necessarily mean that these structural events are not related, the subdivisions simply indicate the relative chronology of overprinting structural events. Although five overprinting deformation events are recognised, primary structures in the polydeformed igneous and sedimentary rocks of the belt are well preserved.

These primary structures constitute the primary planar foliation fabric (S_0) which consists of features such as sedimentary stratification and igneous layering.

4.2.1 Structure of Supracrustal Rocks in the Western Structural Zone

Tati Greenstone Belt rocks in the Western Structural Zone dip steeply to the SW and S, but young to the N and NE. Primary structures, such as pillows (Plate 4.1), graded bedding and flow tops, indicate that the succession is inverted and overturned to the N and NE (Morel, 1968; Mason, 1970; Key, 1976; Key et al., 1976). Key et al. (1976) suggested that rocks in the Western Structural Zone form the southern limb of a major anticline whose northern limb is located somewhere in the Vumba Greenstone Belt (Figure 1.2), north of the Tati Greenstone Belt. No stratigraphic or structural evidence exists, however, to unequivocally indicate that rocks of the Vumba Greenstone Belt form the overturned northern limb of such a major fold. In this study, rocks of the Western Structural Zone are interpreted to form steeply inclined and overturned homoclinal panels of fault-bounded sequences. Similar structures and stratigraphy have been described in the Abitibi Greenstone Belt of the Superior Province by Hubert and Marquis (1989).

4.2.1.1 The D_1 Structures

The nature of the first deformational event (D_1) in the Tati Greenstone Belt has been the subject of much speculation. Coward and James (1974) suggested that a synclinal structure must exist to the northeast of the belt (Figure 3.5) because rocks



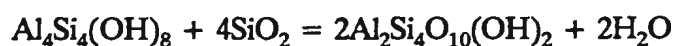
Plate 4.1: Pillow structures in basaltic rocks of the Lady Mary Group. Note the curved surface to the top right of the photograph indicating that these rocks are inverted. The picture was taken facing north along a stream near the Blue Jacket Mine in the Old Tati area (45 cm long hammer for scale).

of the Western Structural Zone young to the north and northeast, whereas those of the Eastern Structural Zone young to the west and southwest. They pointed out that since the main foliation is constant throughout the Western Structural Zone, the syncline formation preceded development of the main foliation. Hence, D_1 was defined as a folding event which led to the formation of this syncline (Coward and James, 1974).

The consistency of foliation attitudes in all rocks from the Western Structural Zone and the concordance of this foliation with the primary foliation S_0 (bedding/layering) were used by Key (1976) as evidence that the main foliation formed on tilted and vertically inclined rocks; i.e. indicating these rocks were inverted and overturned prior to formation of the main foliation. Hence, the overturning and tilting of these rocks occurred during an earlier deformational event (D_1). Key (1976) also suggested that remnants of an earlier tectonic foliation (S_1), which predated the main foliation, could be found in isolated outcrops scattered around the belt. Planar fabrics interpreted by Key (1976) as S_1 foliation were not confirmed during the field mapping for this study. Therefore, apart from the fabric described by (Key, 1976) which could not be confirmed during this study, D_1 has no visible foliation.

A thin aluminous schist unit, the Halfway Kop Member of the Phenalonga Group, occurs in the centre of the Western Structural Zone. It has variously been interpreted as a paleo-aquifer (Johnston and Griffiths, 1982), a metamorphosed laterite deposit (Key, 1976), or a hydrothermal alteration product of andesitic rocks (Blaine, 1986a; Sheeran, 1986). Based on observations of similar Precambrian

aluminous schists in other parts of the world, Serdyuchenko (1968) suggested that they may have formed by the metamorphism of kaolinite-bauxite weathering crusts. The aluminous schists of the Tati Greenstone Belt contain both pyrophyllite and kyanite. According to Turner (1980), pyrophyllite is widely distributed in those slates and phyllites that form in the early stages of the metamorphism of aluminium-rich (kaolinite-bearing) shales and clays through reactions such as;



kaolinite + quartz = pyrophyllite + water

At low temperature and high pressure greenschist facies metamorphic conditions, pyrophyllite would be eliminated and replaced by either kyanite or andalusite.

The transformation reaction may be as follows:



pyrophyllite + kyanite = quartz + water

The aluminous schists contain boudinaged quartz veins which parallel banding. Formation of these boudins and the well developed S_2 foliation post-dates the transformation of the aluminous schists. Formation of these rocks pre-dates the main foliation-forming deformation event (D_2), and so they must have formed in an earlier deformation/ metamorphic event (D_1). The formation of fault-bounded homoclinal panels, the metamorphism of the aluminous schists, and inversion of the stratigraphy in the Western Structural Zone of the Tati Greenstone Belt occurred during the D_1 deformational event prior to formation of the main regional, D_2 , foliation.

4.2.1.2 The D₂ Structures

The most important feature of the second deformation is the presence of a regional penetrative fabric that is common throughout the belt. The second deformation (D₂) is, therefore, the main foliation-forming event. The D₂ regional penetrative fabric in these rocks is called S₂ because it formed during D₂ deformation, although no older foliation has been observed. The planar fabric, S₂, consists of small slip planes, pressure solution surfaces, and oriented platy and tabular minerals such as talc, chlorite, biotite and amphibole in metavolcanic rocks. In metasedimentary rocks, micas, elongated quartz grains, quartz lenses and other phyllosilicates define the S₂ foliation. The S₂ foliation has a general NW trend, and steep dips between 55° and 80° to the south and southwest.

Two major F₂ folds are recognised in the ultramafic-mafic volcano-plutonic sequences of the Lady Mary Group in the Western Structural Zone (Figure 4.3; the Tati River Anticline) and around the Old Tati area (Figure 4.3; Old Tati Anticline). Photogeological and satellite imagery interpretations indicate that ultramafic-mafic rocks of the Lady Mary Group envelop the Tati batholith and are very thin at the southern margin of the batholith compared to the northern margin. At both the northern and southern margins of the batholith, the volcano-plutonic rocks all dip to the south. Mapping indicates that the batholith was emplaced at the core of the NE-verging, F₂, Tati River Anticline (TRA). Supracrustal rocks at both the northern and southern margins of the batholith, therefore, form the northern and southern limbs of an overturned anticline. In the Old Tati area, Lady Mary Group rocks have been

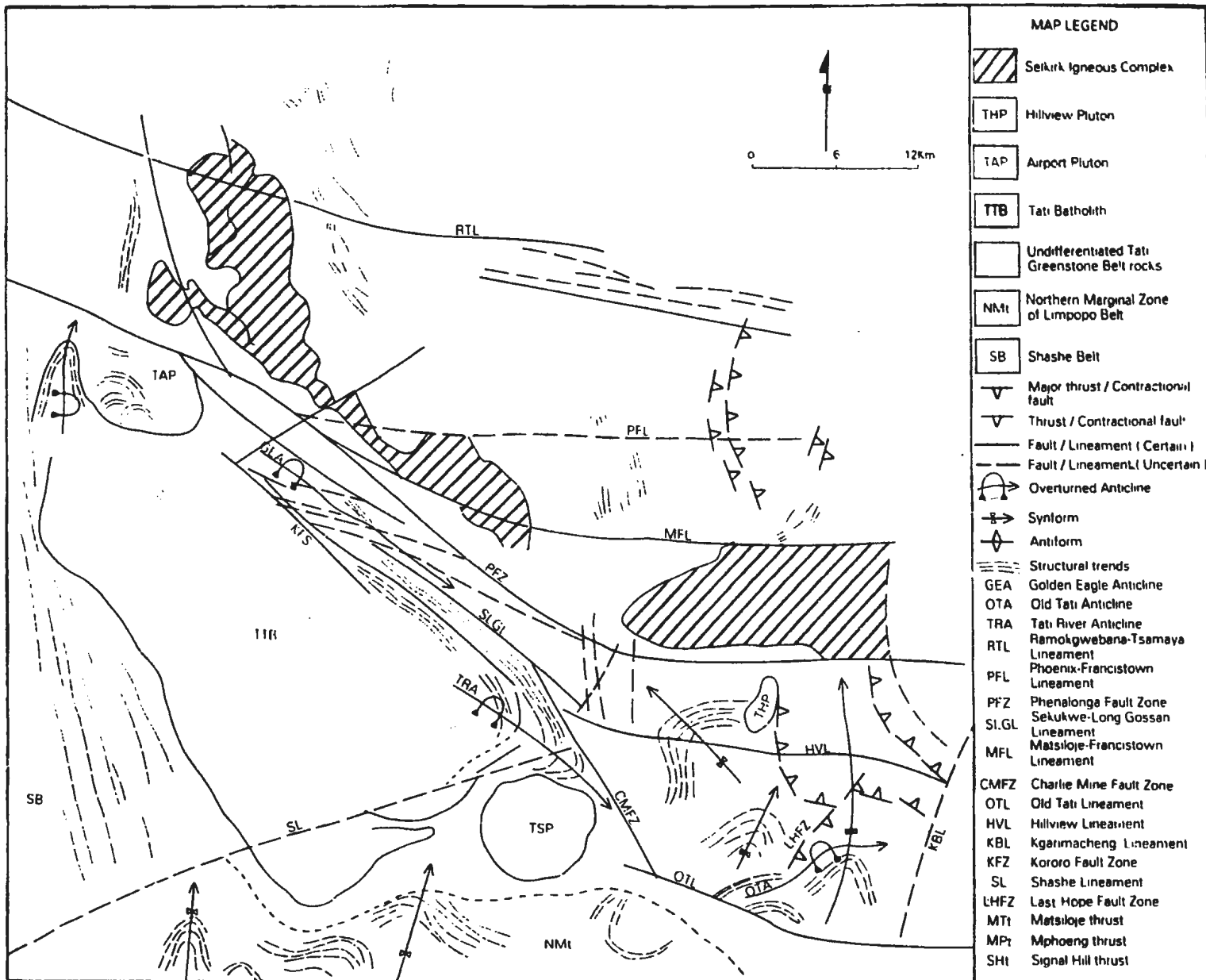


Figure 4.3: Simplified geological map of the Tati Greenstone Belt showing fold trends and major Lineament

folded into a disrupted anticline, the Old Tati Anticline (OTA), which has been refolded by later deformations producing curved axial surfaces. Small, rare asymmetrical, isoclinal F_2 folds, cut by the main foliation, are also present. Axes of these microfolds are steep and are parallel to the stretching lineation. Small cylindrical folds also occur at the boundaries of major volcano-plutonic sequences, especially in banded iron formations and related sediments that form the tops of these major volcano-plutonic sequences (Plate 4.2).

The boundaries of these volcano-plutonic sequences, marked by banded iron formation ridges, are generally linear and coincide with mylonite zones (Plate 4.3). These areas, therefore, mark the locations of large lineaments or lithological boundary-parallel shear zones. In places, these shear zones contain rare down dip mineral stretching lineations indicating dip-slip movements. Shear sense movement indicators, including drag folds (Plate 4.4), C-S surfaces, asymmetric pressure shadows, spaced cleavage (or shear bands) and small slip surfaces, all suggest that these shear zones are thrust planes with south on north thrust movement. N-vergent folds at the top of the Lady Mary Group have their northern limbs disrupted by shear zones. These shear zones were formed during later stages of the D_2 deformational event since minor folds in banded iron formations and related sediments deform the S_0/S_2 foliation surfaces.

Because of poor outcrop exposure and the subparallel relationship of the main foliation (S_2) with the primary igneous layering and bedding (S_0), the relationship of S_2 to folding is poorly understood. Isolated outcrops near fold noses indicate that S_2



Plate 4.2: (Top) Cylindrical folds in argillaceous sediments marking the top of the Lady Mary Group in a river bed, Old Tati area, about two hundred metres southwest of the Blue Jacket mine (45 cm long hammer for scale).

Plate 4.3: (Bottom) Mylonite zone marking the location of lithological boundary parallel lineament between Phenalonga and Selkirk groups. The photograph was taken along the Tati River near Marang Hotel in Francistown about 500 metres east of the bridge (45 cm long hammer for scale).



Plate 4.4: Parasitic microfolds in veined metabasalts of the Lady Mary Group near the margin with granitoids (a 6 cm diameter lens cap for scale). The photograph was taken along the Tati River near Kororo Hill (see Figure 1.3 for location).

may be axial planar to both major and minor folds. In the limbs of these folds, S_0 and S_2 are subparallel. The S_2 foliation, therefore, forms the axial planar cleavage to these folds. The S_2 foliation (schistosity) also carries a well developed mineral stretching lineation (LS_2), that commonly plunges to the NW on SW-dipping foliation surfaces. This stretching lineation commonly consists of stretched and elongated minerals such as actinolite and chlorite, and locally hornblende, in metabasalts and andesites, whereas in granitoids biotite and hornblende form this lineation.

4.2.1.3 The D_3 Structures

The S-shaped axial surface trace of the Old Tati Anticline (OTA; Figure 4.1) illustrates the extensive deformation of D_2 structures by subsequent deformations. F_3 folds range in size from millimetres to tens of metres and include tight, asymmetrical isoclinal flexures of primary lithological contacts (S_0) and the main foliation (S_2). These folds generally are north-verging asymmetrical drag folds or crenulation folding. Examples of F_3 folds are found a few metres north of the Sekukwe bridge across the Matsiloje-Francistown road, northward along the Sekukwe River, and a few metres from the confluence of the Tati River and Wolf Creek, south of the abandoned Lady Mary mine. A crenulation cleavage (S_3) parallels F_3 axial planes. A weak crenulation lineation and a poorly defined lineation marked by the intersection of S_2/S_3 foliations can be seen in some outcrops, especially in the hinges of F_3 folds. The progressive rotation of F_3 fold axes resulted in the re-orientation of this lineation parallel to the D_2 stretching lineation. F_2 and F_3 folds may, therefore,

be co-axial, and generally oriented NW-SE to the main structural trend of the volcano-plutonic rocks in the Western Structural Zone. In some places, varioles and empty groves (Plate 4.5) in basalts and pillow structures in the Lady Mary Group are flattened into pancake-type structures. Along the south-dipping surfaces (stretching direction), the varioles are stretched suggesting up-dip movement. In the Old Tati area, an F_3 synform occurs in the area around New Zealand Mine where the Old Tati Anticline (F_2 fold) has been re-folded into a NE-vergent synform (Figure 4.1).

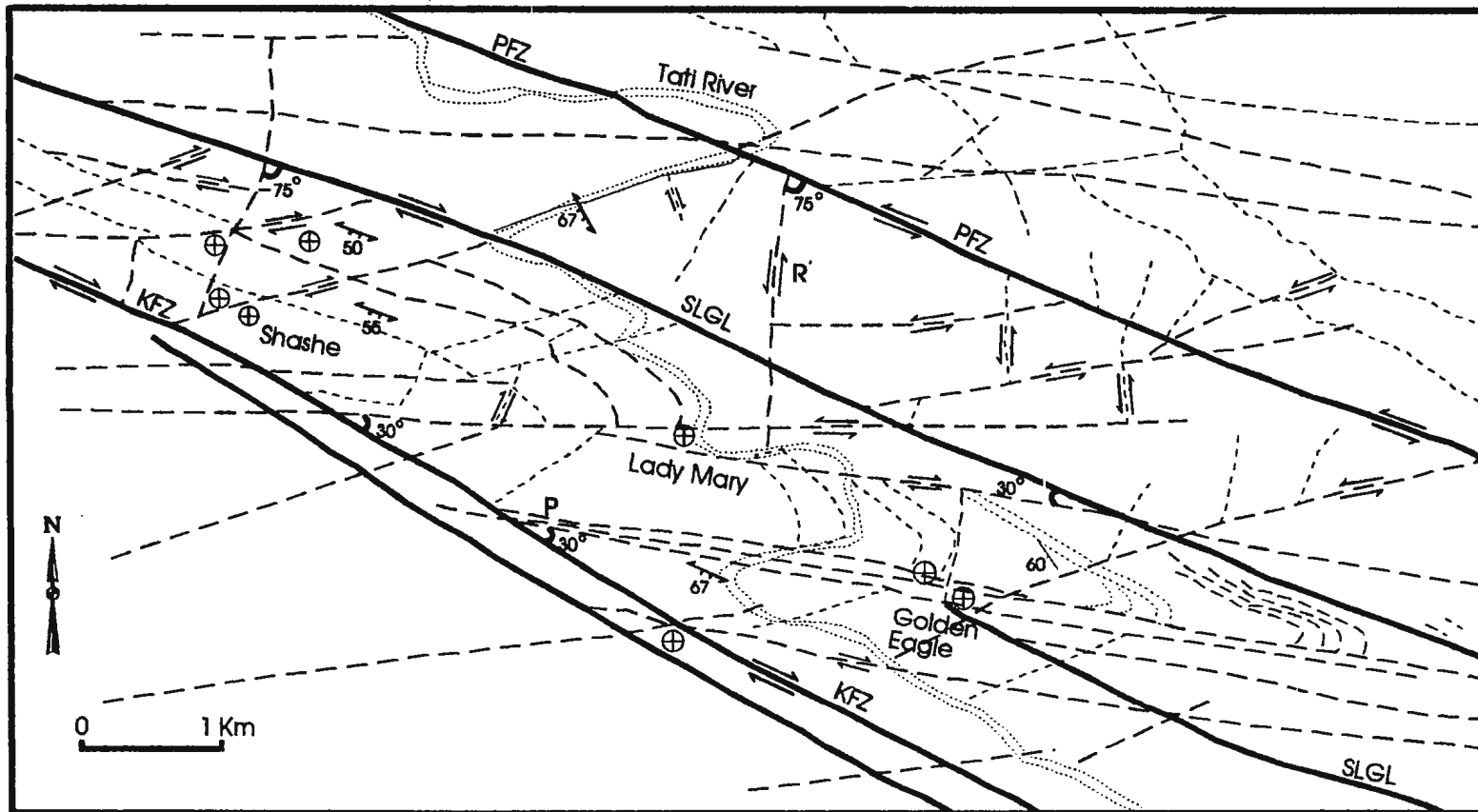
4.2.1.4 The D_4 Structures

A period of dominantly strike-slip movement became prominent during subsequent deformation resulting in the flattening, shearing, re-activation and re-orientation of earlier structures. During D_4 deformation, pre-existing faults/thrusts were re-activated with strike-slip movements, although in some cases dip-slip movements are still observed in some of these major faults.

A large fold, < 1 km across, deforms steeply inclined south-dipping sedimentary rocks of the Golden Eagle Formation into the NE-vergent Golden Eagle Anticline (GEA) (Figure 4.3). Similar but smaller folds are also observed in basaltic rocks northeast of the Bonanza mine. The axial planes of these folds are generally parallel to the dextral Sekukwe-Long Gossan Lineament (SLGL). Progressive deformation between two major strike-slip fault/shear zones, the KFS and SLGL (Figure 4.4), resulted in the formation of secondary shear structures such as riedel shears (R and R'), principal shears (P), tension veins (T) and asymmetrical folds such



Plate 4.5: Strained amygdaloidal structures that mark the surface expression of mineralized shear zones in the Shashe Group of deposits (6 cm diameter camera lens for scale).



Legend

- | | |
|---|--|
| KFZ - Kororo Fault Zone. |  S2 - foliation |
| PKZ - Phenalonga Fault Zone. |  Mine |
| SLGL - Sekukwe-Long Gossan Lineament. |  Bedding/layering (So - foliation) |
|  Major strike-slip fault/shear zone |  Angle between secondary fault/shear zones and the main shear zone boundary. |
|  Secondary strike-slip fault/shear zone. | |
|  Geological boundary | |

Figure 4.4: Lineament map of the area around Shashe, Lady Mary and Golden Eagle mines in the western structural zone, showing the relationship of large lithological boundary-parallel faults/shear zones (SLGL; PFZ and KFZ), with secondary shear zones (P= low angle shears with opposite sense of movement to the main shear zone. (eg. SLGL)), and R' = high angle riedel shears with opposite sense of movement to the main shear zone.

as the GEA. Along the Sekukwe River within the SLGL shear zone, D_3 crenulation folds with subhorizontal axial planes were rotated into steeply inclined axial planes (Plate 4.6) during dextral movements. This rotation was accompanied by down-dip slip between igneous layers resulting in the formation of fault striations and mineral stretching lineations.

In the western part of the belt (Figure 4.5), interaction of the N-S trending high metamorphic grade Shashe Belt and the NW-SE trending Western Structural Zone resulted in NW-SE compression in the Tati supracrustal rocks. This compression, especially near the margins of the Airport Pluton, resulted in constrictional strains and formation of cigar-shaped fold trains (Plate 4.7). Elsewhere in the area, and away from the margins of this pluton, rare asymmetrical folds (Plate 4.8) are observed. The interaction of the Tati Greenstone Belt with the Limpopo protocraton resulted in the formation of the high grade metamorphic core rocks in the Shashe Belt during the D_4 deformation event.

4.2.2 Structure of Supracrustal Rocks in the Last Hope Basin

East of the Charlie Mine Fault Zone (CMFZ; Figure 4.6), the sedimentary rocks of the Last Hope Basin change from feldspathic sandstone and grits interbedded with pebble conglomerates in the E and SE to black shales, calcareous argillites, limestones and phyllites in the N and NW. This suggests that the basin depth increased in the same direction. The basin structure or outline is controlled by a series of E-W trending normal faults with throws to the N (Figure 4.6). These faults



Plate 4.6: Mineral stretching lineation (arrow) on metabasalts of the Lady Mary Group associated with lithological boundary parallel faults/shear zone. The photograph was taken near the Sekukwe bridge at the Francistown-Matsiloje road crossing (6 cm diameter camera lens cover for scale).

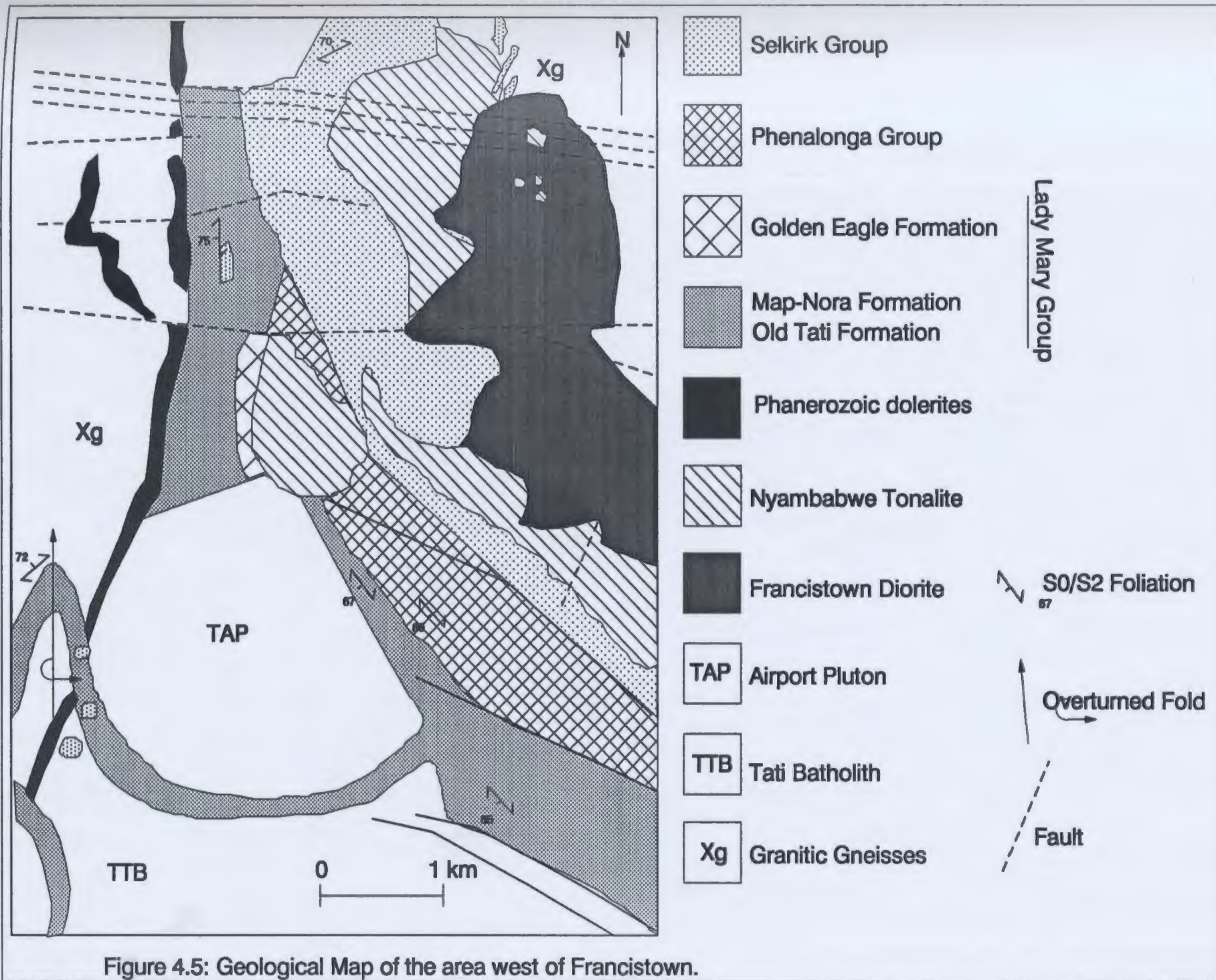




Plate 4.7: NNW-trending upright folds in metabasalts of the Lady Mary Group at the western margin of the Airport Pluton. These folds occur near the boundary of the Tati Greenstone Belt and the Shashe Belt (45 cm long hammer for scale).

Plate 4.8: E to NE vergent asymmetrical folds in talc-chlorite schists of the Lady Mary Group at the southern margin of the intrusive Airport Pluton (6 cm diameter camera lens cover for scale).



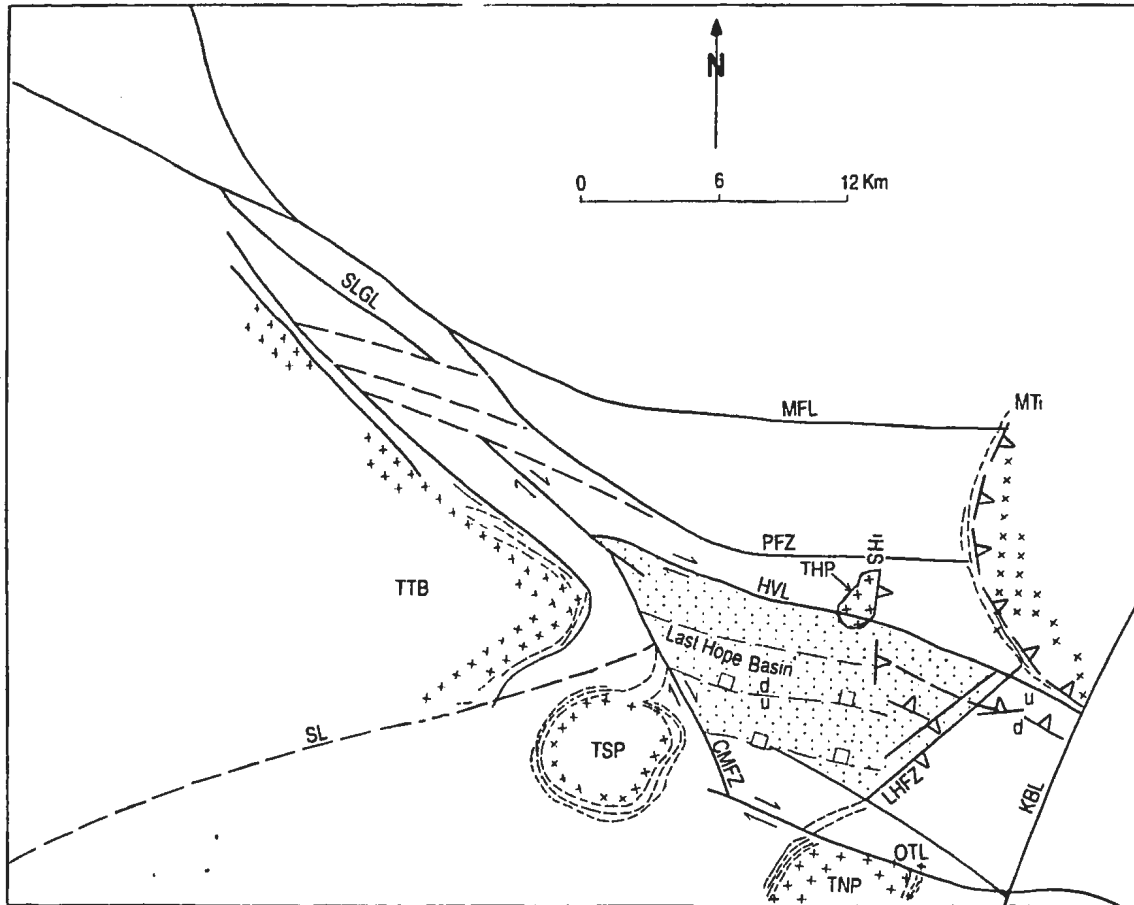
Figure 4.6 Simplified structural map of the Tati Greenstone Belt showing major Lineaments

MAP LEGEND

- RTL Ramokgwebana-Tsamaya Lineament
- PFL Phoenix-Francistown Lineament
- MFL Matsiwe-Francistown Lineament
- SLGL Sekake-Long Gossan Lineament
- PFZ Phetatonga Fault Zone
- CMFZ Charlie Mine Fault Zone
- KFZ Kororo Fault Zone
- KBL Kgaramacheng boundary lineament
- HVL Hillview Lineament
- LHFZ Last Hope Fault Zone
- OTL Old Tati Lineament
- SL Shashe Lineament
- OTA Old Tati Anticline
- TRA Tati River Anticline
- GEA Golden Eagle Anticline
- MTt Matsiwe Thrust
- MPt Mphoeng thrust
- SHt Signal Hill thrust
- ▽ Major thrust
- ▽ Thrust /contractional fault
- Extensional fault
- ≡≡≡ Lithological boundary Fault/ shear Zone
- Major Fault / Lineament
- - - Fault /Lineament
- ↔ Synform
- ⊕ Antiform
- ⊕ Overturned Anticline

splay from the strike-slip couple represented by the CMFZ and Hillview Lineament (HVL). The simple shear couple suggests that the splay faults became active sequentially in a SE direction (Figure 4.6). HVL coincides with silicified banded iron formations of the Mapanipani Ridge. This basin was therefore, formed by movements of strike-slip faults past a restraining bend. The restraining bend was created by the change in strike and displacement from the NW-SE trending SLGL to the SSE-NNW trending CMFZ. Since these two strike-slip faults have dextral senses of displacement, the area to the north of these faults was uplifted, whereas past the bend, the basin progressively widened to the south (Figure 4.7). This basin progressively died out in the same direction with increasing distance from the restraining bend (Figure 4.7). The margins of the Last Hope Basin are marked by thin, steeply south-dipping, banded iron formation (BIF) and associated sedimentary successions (Figure 3.14). To the east, the N-S trending Signal Hill ridge, BIF and associated sedimentary rocks form the eastern margin of the basin. Rocks in this ridge dip at steep angles to the west (i.e. towards the basin centre). Signal Hill ridge rocks have strikes which are at right angles to the trends of the sedimentary rocks in the Last Hope Basin.

A small hill, consisting of highly brecciated BIF overlaying pale grey, calcareous, argillaceous sedimentary rocks, occurs at the eastern end of Signal Hill. These argillaceous rocks trend 032° and contain crenulation cleavages (20° to 090°) on a shallowly dipping foliation. To the north, the south dipping BIF and associated sedimentary rocks of the Mapanipani Ridge constitute the northern margin of the



MAP LEGEND

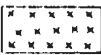
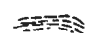
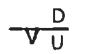
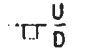
	Last Hope Group Sediments	TTB	Tati Batholith
	Volcano-plutonic rocks	TMB	Matsiloje Batholith
	Granitoids	TNP	New Zealand Pluton
	Shear zone	THP	Hillview Pluton
	Contractional/ thrust fault (U= up plate D= down plate)	TSP	Southern Tati Pluton
	Extensional fault	MFL	Matsiloje- Francistown Lineament
	Major fault/ lineament	PFZ	Phenatonga Fault Zone
	Fault / Lineament	SLGL	Sekukwe-Long Gossan Lineament
	Strike- slip fault	KFZ	Kororo Fault Zone
HVL	Hillview Lineament	CMFZ	Charlie Mine Fault Zone
MTt	Matsiloje thrust	KBL	Kgarimacheng Boundary Lineament
SHt	Signal Hill thrust	OTL	Old Tati Lineament
		LHFZ	Last Hope Fault Zone

Figure 4.7: Geological Map of Southeastern part of the Tati Greenstone Belt showing the location of the Last Hope Basin between two strike-slip faults.

basin (Figure 3.7). These BIF and associated rocks dip steeply towards the basin centre. The southern margin of the basin is marked by D_4 thrusts.

4.2.2.1 The D_1 Structures

The dips in Last Hope Group rocks are variable across the entire basin. They are steep at the northern margin and centre of the basin, but progressively shallow southeastwards towards Signal Hill. The structural trends of these sediments also varies from WSW-ENE to NW-SE. These trends and dips are controlled by D_2 basement faults which dip steeply to the south and southeast (Figure 4.7). The Last Hope Basin is, therefore, interpreted to have formed during D_1 and, hence, no D_1 structures are recognised.

4.2.2.2 The D_2 Structures

The main penetrative fabric in the sedimentary rocks of the Last Hope Basin formed on steeply dipping S_0 foliation surfaces (stratification/bedding). The S_2 foliation consists mainly of elongated phyllosilicate (micas, sericite and aluminosilicates) crystals. Linear fabrics are defined by bedding parallel quartz veins, stretched minerals and rock fragments. The foliation in these sedimentary rocks, although affected by extensive faulting within the basin, is generally subparallel to primary stratification/bedding (S_0). No F_2 folds were observed.

4.2.2.3 The D_3 Structures

Most of the structural data available on the Last Hope Basin mainly come from the area around Signal Hill, however, this area is located at the northern edge of the basin where shearing and thrusting are very intense. Because of poor outcrop exposure, NE-vergent F_3 folds that parallel similar folds in the Old Tati area can only be interpreted from satellite imagery and aerial photogeological interpretations. On the southern limb of the Signal Hill syncline, drag folds or crenulation folds with steeply inclined south dipping axial planes are exposed. A strong crenulation lineation and a lineation marking the intersection of S_2/S_3 foliations are more common in hinges of F_3 folds within argillite outcrops. Stretching lineations, defined by the long axes of vein quartz boudins and stretched rock fragments, parallel the S_0/S_2 foliation. The direction of maximum boudin separation, or the direction of maximum finite extension (cf. Williams et al., 1989), is parallel to the S_0/S_2 foliation and limbs of the F_3 folds. Thin quartz and quartz-carbonate veins connect adjacent boudins.

4.2.2.4 The D_4 Structures

NW-directed D_4 thrusting in the Eastern Structural Zone (section 4.2.3) affected most of the Last Hope Group rocks, especially at the eastern end of the basin. The D_4 deformational event in the Last Hope Basin was also responsible for the duplication of BIF outcrops in the Mapanipani area (Figure 3.7). The quartz vein-filled, dextral, Charlie Mine Fault Zone (CMFZ) accommodated D_4 strike slip movements that fragmented the Mapanipani BIF Ridges. NNW-trending F_4 folds also

occur south of Mapanipani Ridge and north of Signal Hill within the Last Hope Group (Figure 4.6). These folds deform bedding-parallel D_2 foliation and are related to the D_4 , NW-directed, thrust movement.

4.2.3 Structure of Supracrustal Rocks of the Eastern Structural Zone

4.2.3.1 The D_1 Structures

The main foliation (S_2) in the Eastern Structural Zone is subparallel to, and concordant with, the primary igneous layering and sedimentary stratification (S_0) and hence is similar to the main foliation in the Western Structural Zone. The general structural trends in this zone, with NNE strikes and steep W and SW dips, are consistent throughout. The difference in main foliation orientation between the Eastern Structural Zone and the rest of the belt was suggested to result from the horizontal southward movement of the Matsiloje Batholith relative to the rest of the belt (Coward and James, 1974). Strain measurements by these authors also suggested that the main foliation in both the Western and Eastern Structural Zones may have formed under the same strain regime. Such foliation would have formed on vertically inclined igneous layering and sedimentary bedding surfaces. Therefore, as in the Western Structural Zone, the tilting of the strata into vertically inclined surfaces on which the foliation formed, occurred during the D_1 deformation event.

4.2.3.2 The D_2 Structures

The most prominent rock bodies in the Eastern Structural Zone are SW-NE

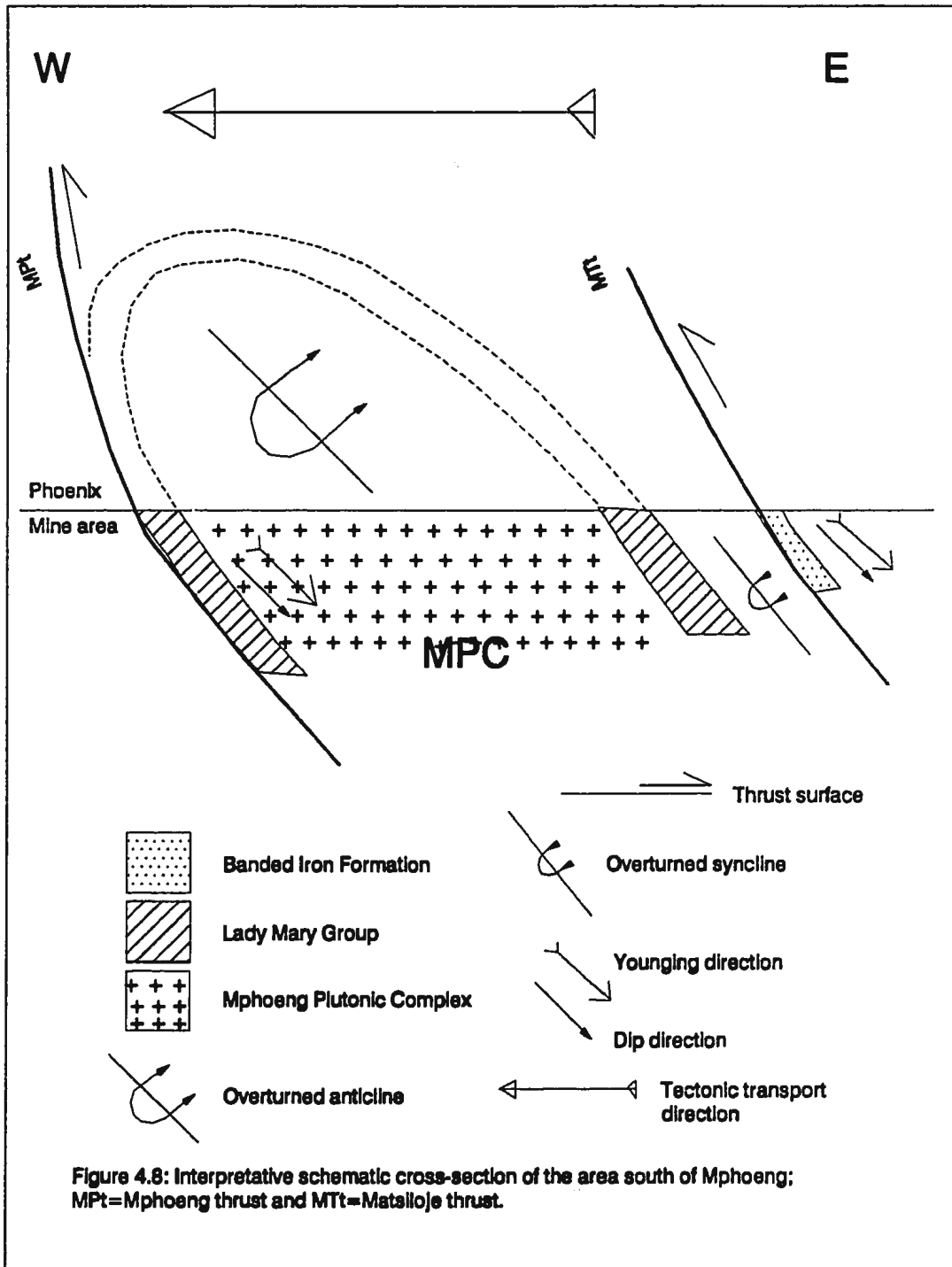
trending BIF at Matsiloje Ridge and Signal Hill. The BIF ranges from cherty through thinly bedded to brecciated varieties. Limestones, or calcareous sediments, and talc-chlorite-actinolite schist constitute the top and base of these ridges, respectively. A well developed planar fabric subparallel to the bedding constitutes the S_2 foliation. In most cases, siliceous bands and quartz veins within BIFs are boudinaged with the long axes of the boudins parallel to the foliation. Because of the high competency of BIF units, microfractures filled by quartz-carbonate veins develop between boudins.

4.2.3.3 The D_3 Structures

A major F_3 syncline occurs between Signal Hill and Matsiloje Ridge, but, because of poor outcrop exposure, this syncline is defined mainly from satellite imagery and photogeological interpretations. The formation of the syncline may have been related to NW-directed thrust movements.

4.2.3.4 The D_4 Structures

The trends of rocks in Signal Hill and Matsiloje Ridge and a klippen of ultramafic-mafic rocks south of Mphoeng area (NE-SW; Figure 4.2) are generally orthogonal to the trends of the rest of the belt. West of the ultramafic-mafic klippen, the Selkirk Group rocks that host the Phoenix massive sulphide deposit dip eastwards at shallow angles below the steeply dipping ultramafic rocks (Figure 4.8). Further SE from the Phoenix Mine, just north of Matsiloje Ridge, Selkirk Group rocks also dip at steep angles to the east.



The contact between the ultramafic-mafic klippen and the Selkirk Group rocks is marked by highly sheared lithologies (talc-chlorite schists) dipping at relatively high angles to the east. These schists contain mineral stretching lineations and other linear structures (LS_4) which plunge 59° towards 100° on steeply east-dipping, SW-NE trending S_2 foliation surfaces. Further south, the contacts between Signal Hill rocks and the sedimentary rocks of the Last Hope Basin, and between Matsiloje Ridge rocks and rocks west of this ridge, are marked by pink to reddish-brown, relatively fissile carbonates dipping at low angles to the east. These highly schistose rocks underlie brecciated BIFs and, although lineation and other kinematic indicators are poorly defined due to poor outcrop exposure, these schistose carbonate rocks have mineral stretching lineations and other linear structures (LS_4) that plunge at 70° towards 190° . These carbonated schists constitute the soles of east-dipping thrust surfaces.

In all these areas, the contacts are defined by WSW-ENE trending fault/shear zones. These boundary fault/shear zones (Figure 4.3) are interpreted as having formed from a NW-directed thrust movement and the thrust slices actually make up the Eastern Structural Zone of the Tati Greenstone Belt (Figure 4.2). The elliptically-shaped Mphoeng Flutonic Complex has its long axis oriented SSW-NNE following the main trend of the Eastern Structural Zone, indicating NW-SE compression during D_4 deformation event. The curvature of the D_3 syncline between Matsiloje Ridge and Signal Hill (Figure 4.9 - in pocket) also suggests the existence of such a compressional deformation.

4.2.4 Major Lineaments in the Tati Greenstone Belt

Figure 4.10 delineates all lineaments and fractures compiled from photogeological and satellite imagery interpretations. In general, two lineament and fracture trends can be recognised in the Tati Greenstone Belt. The first group trends between 100-280° and 110-290°, and the second group trends between 180-360° and 220-040°. A third fracture set is subordinate to these two main directions in terms of the number of fractures; this third group has a general trend between 140-320° and 150-330° and coincides with the trend of the Western Structural Zone. The third fracture system is part of the Sekukwe-Long Gossan Lineament System (SLGL; Figure 4.6). The SLGL lineaments are concordant with bedding/layering, especially at the tops of major volcano-plutonic sequences, and because they separate major volcano-plutonic sequences, they are referred to as boundary faults.

The largest group of lineaments are those with the 100-280° to 110-290° structural trends. Two of these lineaments coincide with narrow, linear, magnetic anomalies which extend beyond the limit of the Tati Belt and which have been interpreted to be fault/shear zones. Current work has confirmed that these large anomalies coincide with shear zones on the ground. Tertiary tectonism in northeastern Botswana, as represented by NW-SE trending dyke swarms, coincides with the trend of these ancient lineaments, suggesting that they represent weak crustal zones along which the Tertiary tectonism was localised. These lineaments are collectively referred to as the Matsiloje-Francistown Lineament system.

The majority of fractures and lineaments with 220° to 040° structural trends

Number of fractures plotted = 135

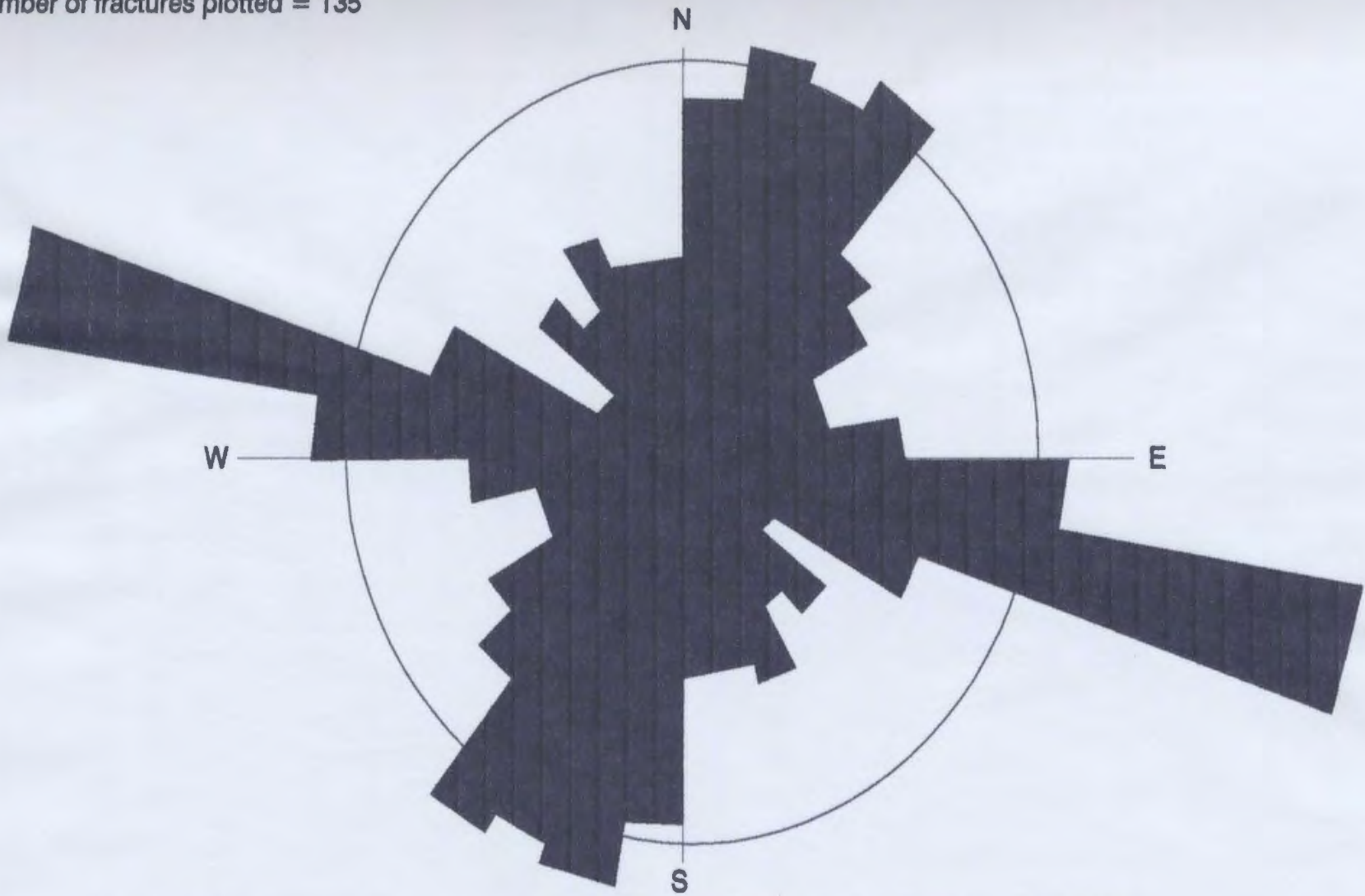


Figure 4.10: Rose Diagram of fractures and lineaments in the Tati Greenstone Belt. The data are derived from both field mapping and photogeological interpretations.

occur around the Eastern Structural Zone. On the ground, these shear/fracture zones are found where they intersect river courses. These major lithological boundary-parallel shear zones are generally ductile to ductile-brittle zones (Plate 4.9), whereas secondary shear zones (Figure 4.5) are mainly brittle structures (Plate 4.10).

Figure 3.6 showed that the Tati Greenstone Belt is a composite terrane separated from the continental margin to the north by a 8 km wide tectonic zone. This tectonic zone is bounded to the south by the Matsiloje-Francistown Lineament (MFL) and to the north by the Tsamaya-Ramokgwebana Lineament (RTL). The zone is intruded by major plutonic complexes; the Selkirk Igneous Complex (SIC) to the south, the Mphoeng Plutonic Complex to the east, and the Ramokgwebana Batholith to the northeast. These plutonic complexes contain remnants of paragneisses and volcano-plutonic rocks. To the north of this tectonic zone (i.e. north of RTL), Key (1976) suggested that the granitoids were derived from granitization of old rocks. Such granitoids, although not studied in this thesis, are believed to have been derived from the partial melting of upper crustal rocks.

The composite terrane south of the MFL comprises the main volcano-plutonic rocks the Tati Greenstone Belt. The boundary of this terrane with the Northern Marginal Zone (NMZ) of the Limpopo Belt (i.e. its southern margin) is marked by a metamorphic and structural transition from lower grade (greenschist facies) in the Tati Greenstone Belt to higher grade (amphibolite-granulite facies) in the NMZ. Structures south of the transition zone are dominated by north-trending isoclinal to tight parallel folds in gneisses. This structure contrasts with the dominant NW-SE



Plate 4.9: Mafic rocks of the Lady Mary Group, generally contain foliation-parallel quartz-feldspar veins near contacts with granitoids. (a) Photograph shows that these veins parallel the S_0/S_2 foliation. A large late quartz vein cut the later. (b) Quartz-feldspar veins indicate that deformation was mainly ductile.

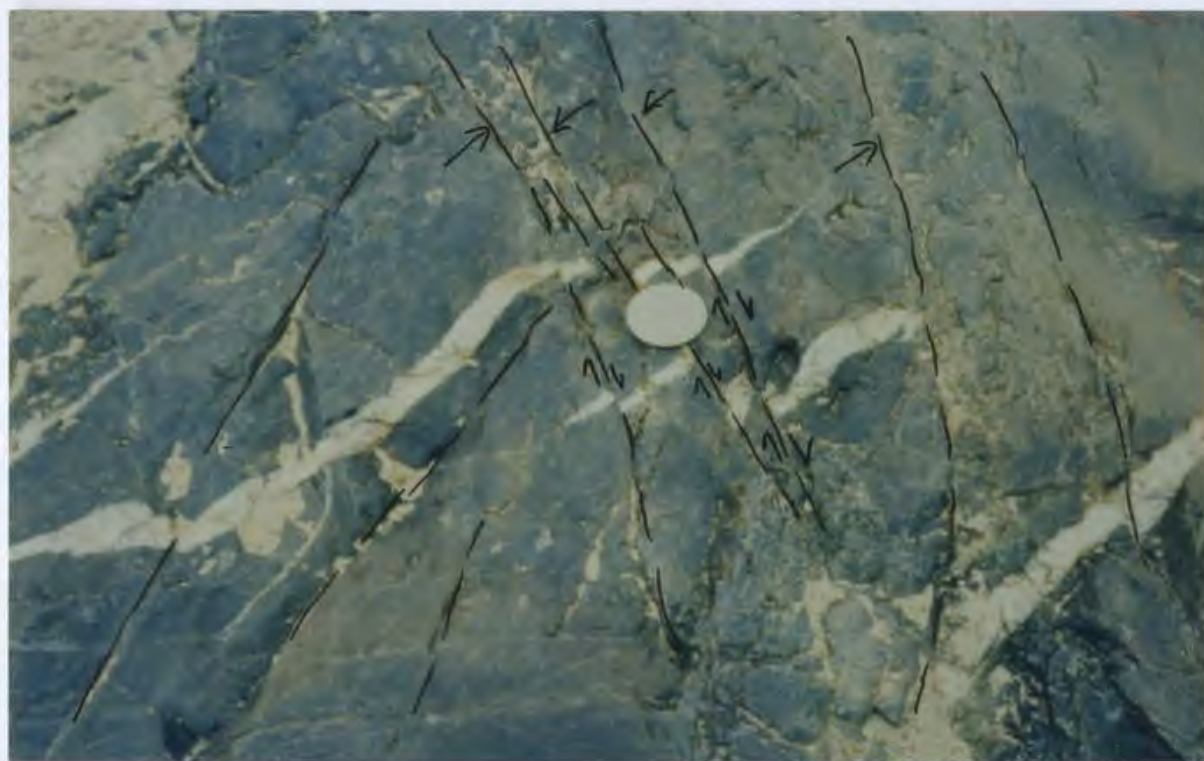


Plate 4.10 (a): Brittle fractures (arrows) in basaltic andesites of the Phenalonga Group along the Tati River near Francistown. Quartz-filled zones are more common in areas further away from granitoid contacts than quartz-feldspar veins. (b) Brittle secondary fractures localized to early quartz veins emplaced in highly fractured basaltic rocks of the Lady Mary Group (45 cm long hammer for scale).

structural trend in the Western Structural Zone of the Tati Greenstone Belt (i.e. north of this transition zone). The width of the composite terrane that makes up the Western Structural Zone of the Tati Greenstone Belt, measured from its boundary with the NMZ to the MFL, is about 40 km.

The Sekukwe-Long Gossan Lineament (SLGL) and the Charlie Mine Fault Zone (CMFZ) form major fault/shear zone boundaries that separate komatiite-tholeiitic volcano-plutonic rocks of the Lady Mary Group from the calc-alkaline volcano-plutonic and feldspathic sedimentary rock sequences (Figure 4.11). These two dextral shear zones may actually be components of the same shear zone that was fragmented by subsequent deformations. On the other hand, the CMFZ may be a secondary shear zone joining two right-stepping major strike-slip fault/shear zones, the SLGL and the Old Tati Lineament (OTL). The dextral OTL separates the base of the Lady Mary Group from rocks of the NMZ (Limpopo Belt). In the Western Structural Zone, the sinistral Kororo Fault System (KFS) marks the boundary between the northern margin of the Tati Batholith and the volcano-plutonic rocks of the Lady Mary Group. The KFS is restricted to the northern margin of the Tati Batholith.

The Phenalonga Group, a calc-alkaline volcano-plutonic sequence with minor sedimentary rocks in the Western Structural Zone, lies between the SLGL to the south and the Phenalonga Fault Zone (PFZ) to the north. These two lineaments coincide with the locations of silicified banded iron formations. Williams et al. (1989) described similar "silica-rich chert-hematite b.i.f. horizons as discordant mylonite

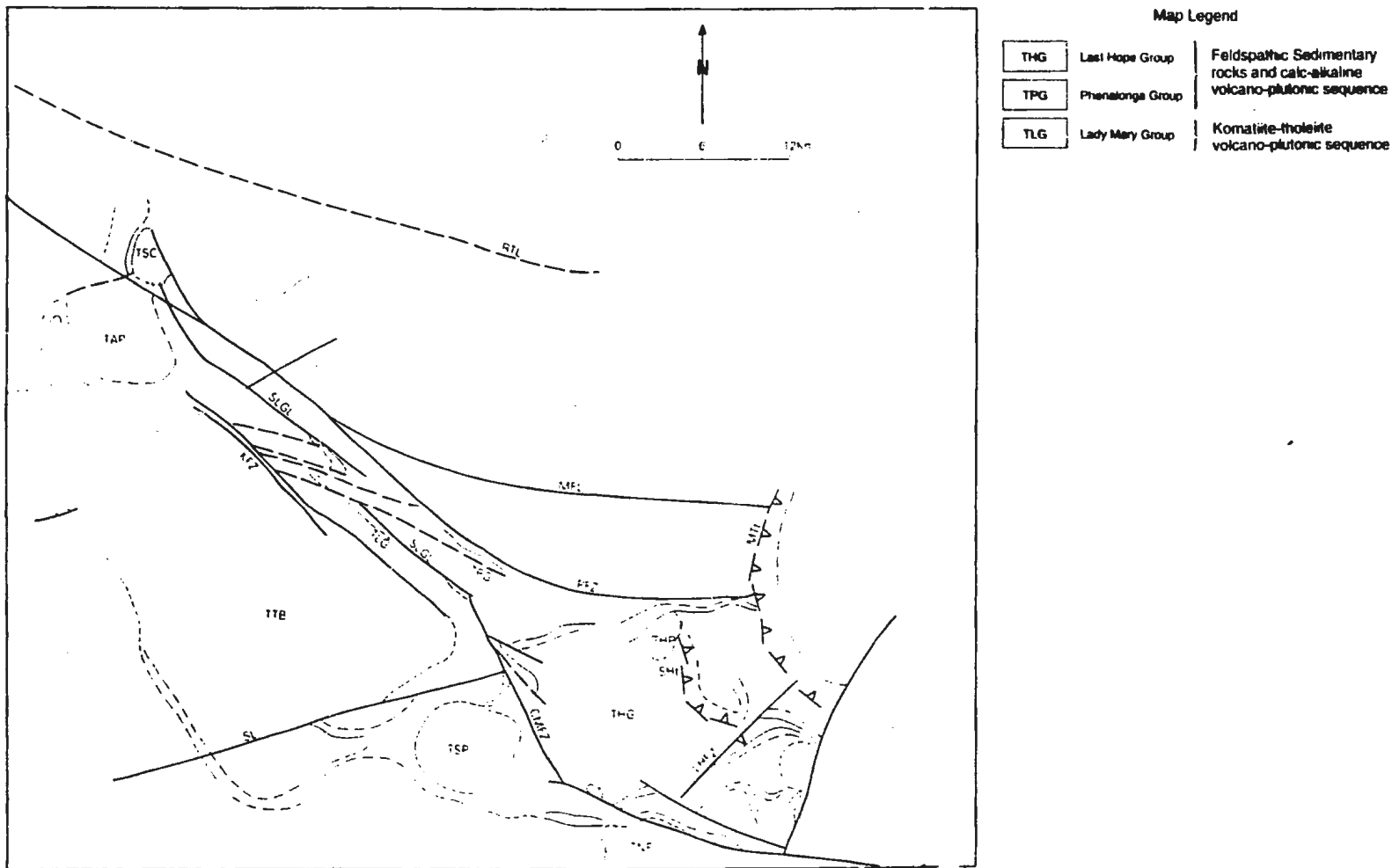


Figure 4.11: Simplified geological map of the Tati Greenstone Belt showing the separation of the Lady Mary Group komatiite-tholeiite sequence from the calcalkaline Phenalonga Group volcano-plutonic sequence and the feldspathic sedimentary rocks of the Last Hope Group by lithological boundary-parallel linemaments (SLGL, CMFT & OTL). Other letter and character symbols as in Figures 4.1 to 4.6.

zones" in the Leonora District of the Eastern Goldfields Province, Western Australia.

Calc-alkaline volcano-plutonic rocks, with minor sedimentary intercalations north of the PFZ, constitute the third volcano-plutonic sequence, the Selkirk Group, of the Tati Greenstone Belt. The northern margin of the Selkirk Group is disrupted by plutonic rocks within the MFL-RTL tectonic zone.

SLGL, CMFZ, OTL and PFZ are lithological boundary-parallel shear zones of regional extent. They traverse the whole of the Western Structural Zone and are generally cut by E-W trending shear/fault zones, some of which (e.g. MFL and RTL) extend beyond the limit of the Tati Greenstone Belt (Figure 4.3). The Last Hope Fault Zone (LHFZ) marks the boundary between the Last Hope Basin to the north (Figure 4.9) and the Old Tati area to the south. The southern edge of this fault zone is marked steeply south-dipping brecciated banded iron formations and pinkish-brown carbonaceous sediments. Microstructural data, such as shear bands (Plate 4.11), spaced fracture cleavage (Plate 4.12), asymmetrically folded quartz veins (Plate 4.13), pressure solution and pressure shadows (Plate 4.14), all indicate reverse dip-slip movement on the LHFZ of south over north.

4.2.5 Granitoid Intrusives

Granitoids form an integral component of Archean granite-greenstone geology and there are several granitoid bodies of different shapes and sizes within the Tati Greenstone Belt. The roles that such granitoids play in the structural evolution of Archean greenstone belts remains an unresolved aspect of Archean geology. Early

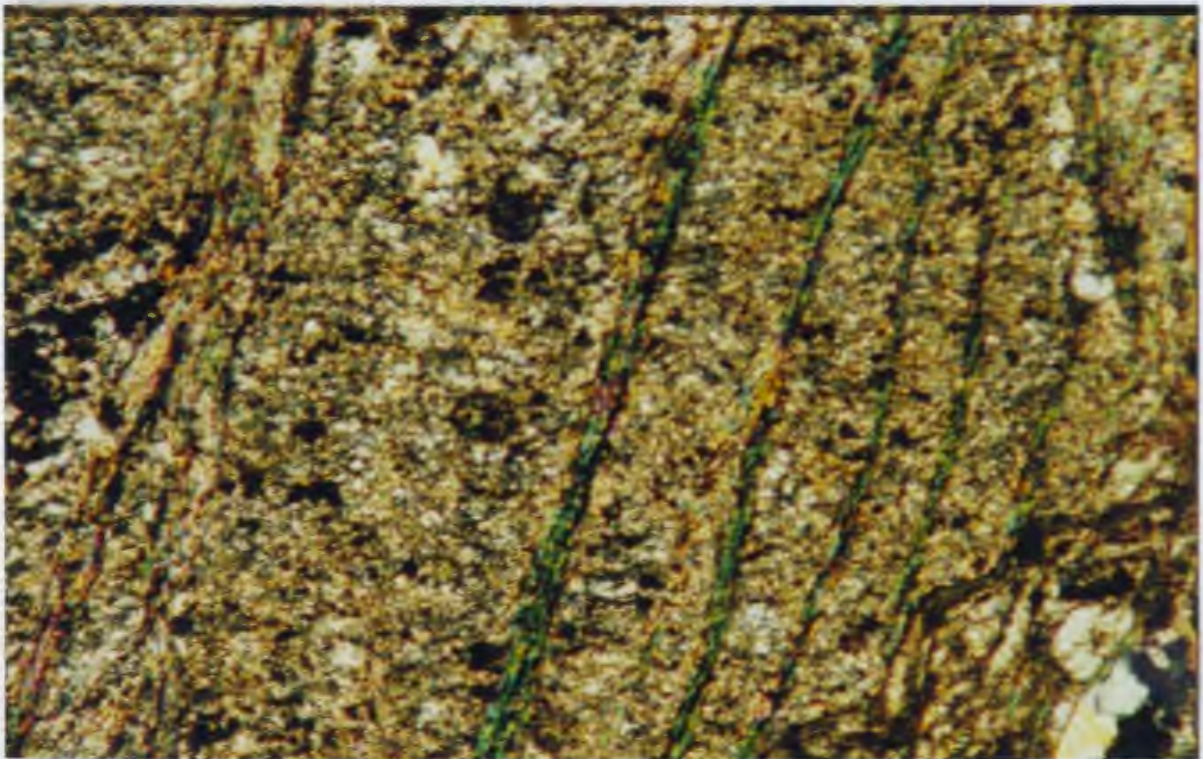
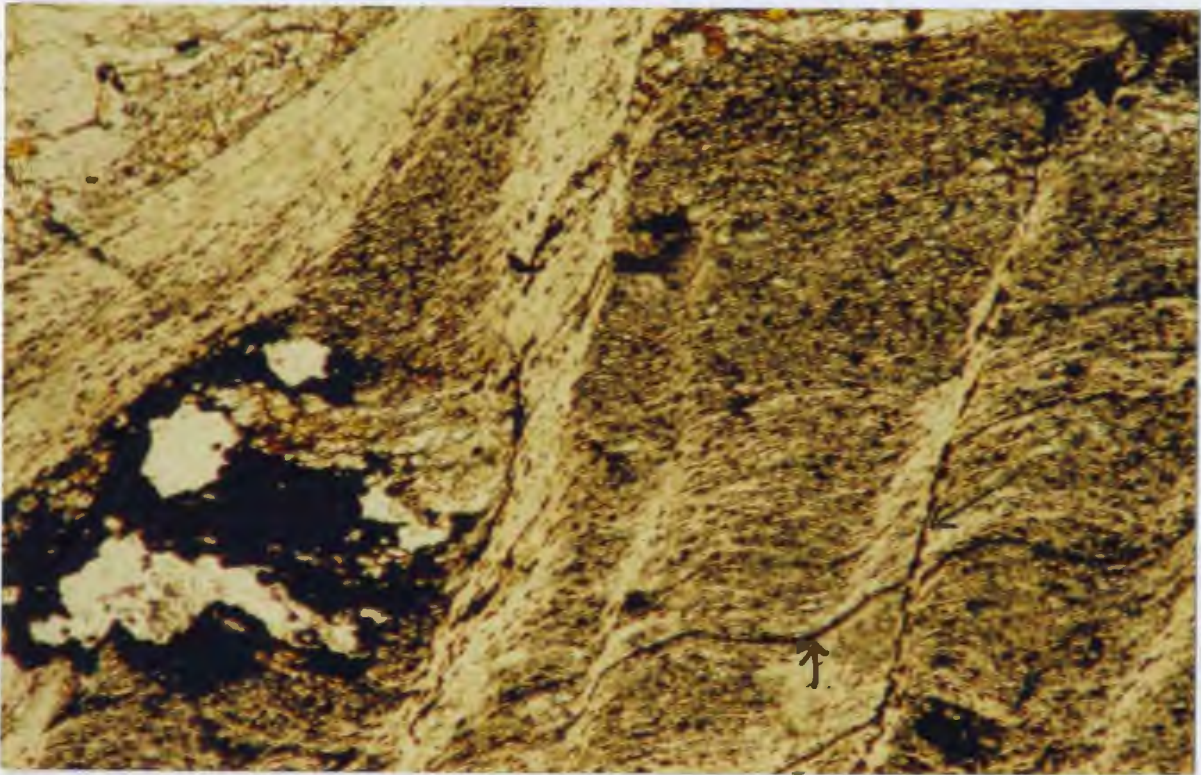


Plate 4.11: Photomicrograph showing microshear bands in metasedimentary rocks of the Last Hope Group (scale 0.5mm PL).

Plate 4.12: Photomicrograph showing spaced fracture cleavage within metasedimentary rocks of the Last Hope Group, in which phyllosilicates were deposited as bands (scale 0.5mm PL).

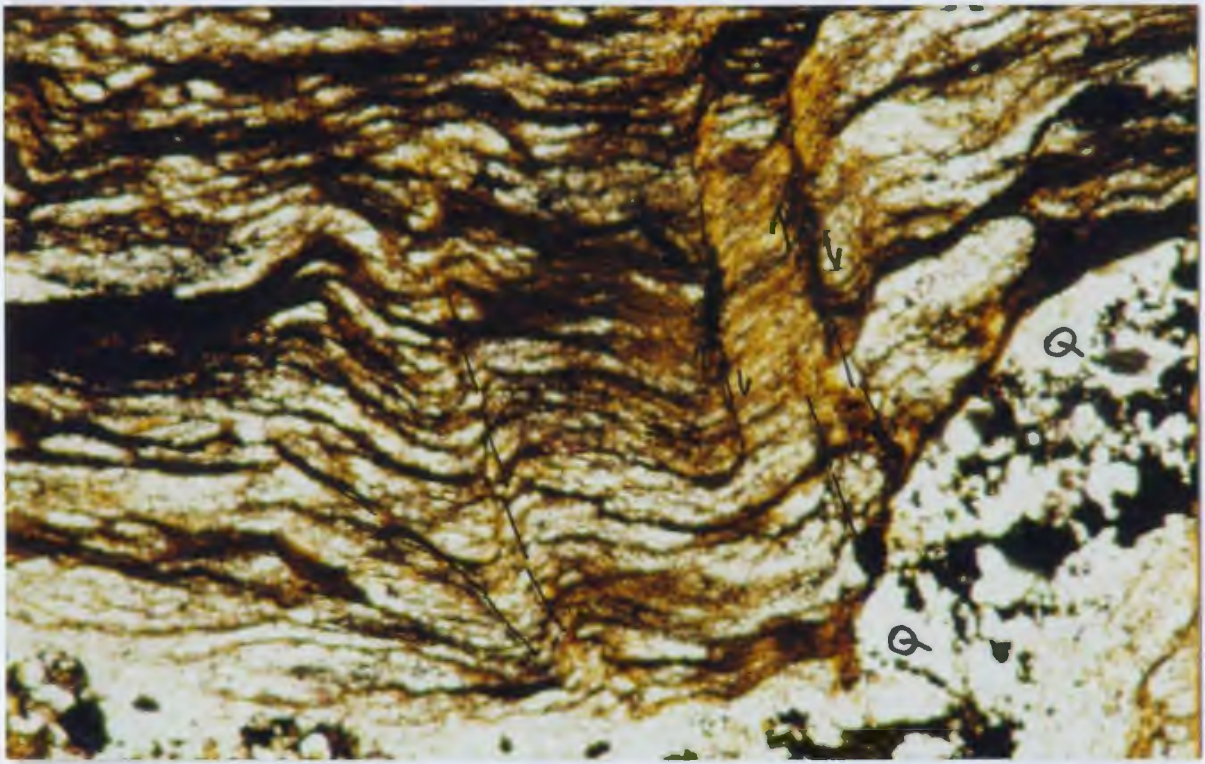


Plate 4.13: Photomicrograph showing the relationship of microfractures to folded quartz veins (Q) lying in the plane of the main shear zone. The microfractures form oblique to the shear zone boundary varying from high angle reverse microfaults near fold noses to low angle thrust microfaults away from these areas (scale = 0.5 mm PL).

Plate 4.14: Photomicrograph of a large detrital quartz grain (D) which exhibits growth features or pressure shadows. Microfractures resulting from the pile up crenulation folds crests and accumulation strains between detrital quartz clasts are also visible (scale = 0.4 mm PL).

structural and tectonic models for Archean granite-greenstone belt evolution depicted granitoid diapirism as the driving force for the vertical tectonics that were interpreted to have been responsible for most of the structures seen in these belts (e.g. Gorman et al., 1978). Other models interpreted granitoids as part of an overall orogenic cycle dominated by horizontal movements (e.g. Burke et al., 1976). More recently, Collins (1989) argued that "the typical domal structure of granite batholiths within granite-greenstone terranes suggests that diapirism was involved in their genesis." He further pointed out that greenstone belts were initially subjected to subhorizontal tectonics involving thrusting and recumbent folding, which were later modified by upright structures probably related to diapirism.

The main focus of this section is to review the role of granitoids in the structural and tectonic evolution of the Tati Greenstone Belt. In the belt, granitoid bodies range from large composite bodies to small homogeneous plutons (Figure 3.8). The largest of these, the Tati Batholith, is an elliptically-shaped composite body which forms part of the southern boundary of the belt. Medium-sized bodies, such as the Matsiloje and Ramokgwebana batholiths, are also irregular in shape, but less variable compositionally. Small plutons, such the Southern Tati, Airport, New Zealand and Hillview, are sub-circular in shape and compositionally more homogenous.

Structures in supracrustal rocks near the margin of the granitoids have clearly been modified by the emplacement of granitoids. For example, foliated supracrustal rocks at the margins of the Southern Tati Pluton (Figure 4.12) wrap around this granitoid body. This "wrapping" foliation contrasts with the planar structural trends

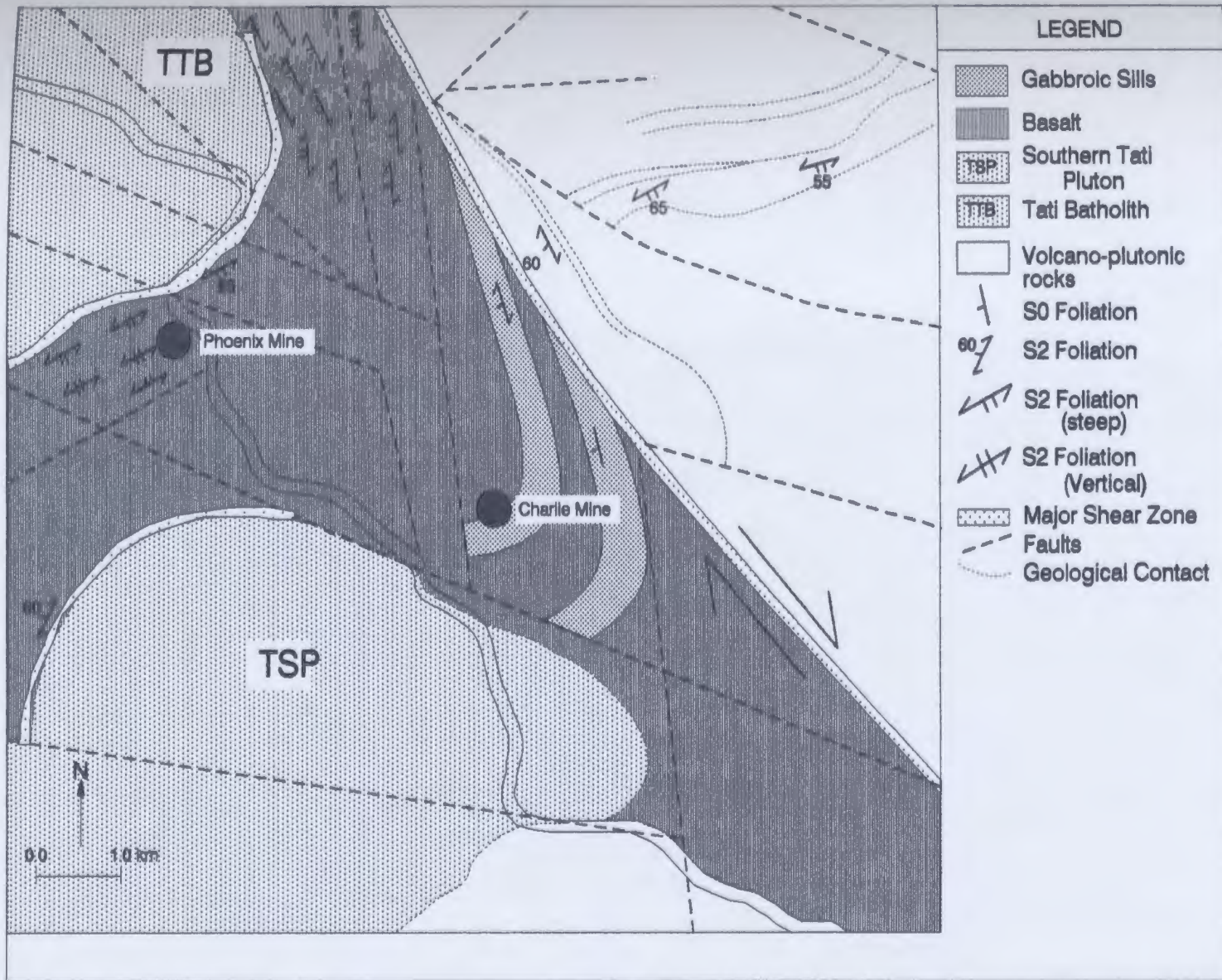


Figure 4.12: Geological map of the southeastern part of the Tati River Subzone showing the relationship of supracrustal rocks to intrusive granitoids; TSP=Southern Tati Pluton and TTB=Tati Batholith.

common in most parts of the Tati Belt; eg. the regularity of the NW structural trends in most of the Western Structural Zone. In other words, granitoid emplacement apparently disrupted the main trends of regional structures. Dips of the foliation around granitoid margins are inwards towards the batholith, and the intensity and complexity of the deformation increases towards the granitoid contacts.

Asymmetrical microfolds in veined supracrustal rocks are commonly found near the northern contact of the Tati Batholith. The importance of these microfolds is that they deform the S_0/S_2 foliation surfaces of supracrustal rocks. The microfolds contain subvertical axial planes on the steeply south-dipping foliation of supracrustal rocks. Axial planes of these microfolds, although inclined at high angles towards the batholith, dip to the south, the same direction as the foliation in supracrustal rocks. The geometry of these microfolds suggests batholithic up-movement; i.e. that they were formed by the uplift of supracrustal rocks during emplacement of the batholith. Since this uplift post-dated S_2 foliation, the emplacement of the Tati Batholith must have been post- D_2 deformation. These microfolds could also have been formed by northward-directed tectonic transport with respect to the Tati Batholith. The restriction of these structures to the margins of granitoids and the presence of wrap-around foliations suggests diapirical emplacement of the batholith.

Composite granitoid bodies, such as the Tati Batholith, consist of multiple intrusions emplaced at various ages. Structures between the various members of these bodies, indicate that the younger plutonic members at the cores of the batholiths were emplaced in already deformed outer gneissic varieties. For instance

in the Tati Batholith, granitoid units at the northern margin consist of whitish-grey to pale pink even-grained granodiorite gneisses which have well developed foliation or gneissosity defined by elongated biotite and hornblende crystals around deformed feldspar crystals. This foliation parallels the S_0/S_2 foliation of supracrustal rocks.

Southeast of the northern margin, are grey gneisses (biotite gneiss) which have well developed foliations defined by the preferred orientation of biotite crystals and feldspar. The contacts between the grey gneisses and the undeformed batholith core rocks are defined by highly deformed rocks. Small scale dextral shear zones are localized in deformed biotite gneisses, parallel to the gneissic foliation. Folded aplitic dykes curve into these shear zones, suggesting that they were being progressively rotated into parallelism within these minor shear zones. Dimroth et al. (1986) pointed out that contact-parallel mylonitic fabrics at the margins of granitoids occur in both pre and syn-kinematic granitoids, indicating, in the case of syn-kinematic granitoids, that deformation outlasted crystallization. In the Tati Batholith, core granitoids are relatively undeformed and the shear zones are localised to within the host biotite gneisses rather than in the younger granitoids. The folding of aplitic and granitic dykes occurred during the shearing event which accompanied emplacement of the undeformed granitoids.

Along the southern margin, megacrystic granitoids form elliptical plutonic bodies within the Tati Batholith. These rocks are progressively deformed southward towards the Northern Marginal Zone of the Limpopo Belt. These rocks consist of large feldspar crystals, biotite, hornblende and quartz. The feldspar crystals have

preferred orientations at 286°-316° and they generally contain microfractures, which together with wisps of biotite, indicate the presence of S-C shear bands. In these areas, deformation was superimposed on magmatic textures.

Further south, megacrystic granitoids are progressively deformed into grey porphyroblastic gneisses. In these areas, folded aplitic dykes and pegmatites are rotated into parallelism with minor shear zones. Buckled and sheared aplite dykes are common. The contact of these granitoids with supracrustal rocks in this area is not exposed. However, structures within these granitoids suggest that they were emplaced syn-tectonically (cf. Paterson et al., 1989; Dimroth et al., 1986; Windley, 1991). Granitoids in the Tati Greenstone Belt post-date the D_2 deformational event which was the main foliation-forming event in the supracrustal rocks. Since these granitoids modified and deformed regional foliation in host supracrustal rocks, they were probably emplaced sometime between the D_2 and D_3 deformational events.

4.3 Structural Evolution of the Tati Greenstone Belt

Morel (1968) argued that the Tati Greenstone Belt underwent only one period of deformation, an Alpine-type nappe folding event. This deformational event resulted in the formation of an inverted synclinal structure. Mason (1970) and Anhaeusser and Ryan (1979) suggested that the Tati Greenstone Belt is a synclinal keel, in which the core was intruded by large granitoids. All structures according to this model are related to the interaction of the greenstone belt rocks with the intrusive diapiric granitoids. Coward and James (1974), Coward et al. (1976), Coward

(1980; 1984) and Key (1976) proposed, on the other hand, that the Tati Greenstone Belt structures were related to deformational events in the Limpopo Belt, and most especially in the Northern Marginal Zone.

Coward and James (1974) also interpreted the structure of the Tati Greenstone Belt as a synclinal structure, the core of which was intruded by granitoid diapirs. They, however, suggested that the Eastern Structural Zone (Eastern limb of the syncline) could not be explained by a simple infolded syncline model. They postulated that the Eastern Structural Zone was rotated from a southern position to its present position and used the existence of NNE-trending shear zones within this area of belt (Figure 3.5) as evidence for this rotational movement. More recently, models for greenstone belts of the Zimbabwe Craton in Zimbabwe have explained the deformational histories in terms of the interaction between small crustal blocks or microplates (Wilson, 1990; Treloar et al., 1992). These crustal blocks, according to Wilson (1990), were cored by large granitoid bodies that acted as rigid bodies during deformation. Relative movements between these blocks were interpreted to have resulted in the formation of the widespread shear zones present in the craton.

To the south, in the Kaapvaal Craton in South Africa, structures within the Pietersburg and Sutherland Greenstone Belts are believed to have been generated by horizontal crustal movements (De Wit et al., 1992; McCourt and van Reenen, 1992). These two greenstone belts have similar spatial relations to the Limpopo Belt, as the Tati Greenstone Belt. In both the Pietersburg and Sutherland Greenstone Belts, structures indicate north to south directed thrust movements (De Wit et al.,

1992; McCourt and van Reenen, 1992). According to Roering et al. (1992), this south-directed thrusting is related to the uplift of the Central Zone of the Limpopo Belt, as a "pop up" type deformation, resulting in similar structures at both the northern and south margins of the Limpopo Belt. Treloar et al. (1992) suggested, however, that there is evidence for NW-SE shortening, thrusting, folding and flattening from the Witwatersrand Basin on the Kaapvaal Craton to the Shamva district of northern Zimbabwe. Similarly, there is evidence for an apparently equally dominant SW or WSW movement direction accommodated by WSW-ENE or SW-NE striking shear zones. They suggested that the different movement directions may either represent different collisional events, or a single collisional event that was accompanied by lateral extrusion between crustal blocks.

In general, fold trends change from N-S in the Shashe Belt, to NNE-SSW in the Tonata area of the Northern Marginal Zone (NMZ) of the Limpopo Belt. ENE-SWS directions are recorded in the NMZ, southeast of Old Tati. Fold trends in the different subzones of the Tati Greenstone Belt mirror those of the high metamorphic grade areas outlined above. In the Francistown Subzone, fold trends are N-S, similar to those of the Shashe Belt. In the Tati River Subzone, they are at right angles to those of the Tonata area. The Old Tati Subzone fold trends follow the ENE trend of the Northern Marginal Zone of the Limpopo Belt.

The contact between the Shashe Belt and the Tati Greenstone Belt is a sharp tectonic discontinuity. Mason (1973) noted that metamorphism and deformation increase quite sharply from the greenstone areas to the Shashe gneissic belt.

Structures in the Shashe Belt west of Francistown, and in the NMZ, south of the Tati Greenstone Belt, record SW-directed movements of the Zimbabwe Craton. This collisional deformation led to thrusting in the Shashe Belt and probably block tilting and buckling in the NMZ. This SW-directed movement postdates the main foliation-forming deformation event (D_2). D_2/D_4 SW-NE or WSW-ENE trending shear zones (Figure 4.6) formed at this time.

The Eastern Structural Zone has a N-S trending S_2 foliation and NNE boundary shear zones. Similar shear zones in Zimbabwe were interpreted to have been derived from NW-SE compression, which resulted in thrusting, folding and flattening (Treloar et al., 1992). Emplacement of the Eastern Structural Belt of the Tati Greenstone Belt is consequently manifested by folding in the Last Hope Basin related to the thrusting of the Signal Hill block onto the Last Hope Basin. These structures have the same general trend as those at the western margin between the Tati Greenstone Belt and the Shashe Belt and may therefore have formed by the same WSW-directed movement.

A major tectonic zone, bounded by the major MFL and RTL lineaments (Figure 3.7), separates the Tati Greenstone Belt rocks in the south from a dominantly granitoid terrain in the north. Plutonic rocks of the Selkirk Igneous Complex (SIC) are intruded into this zone of major crustal weakness. The MFL-RTL structures and SIC plutonic bodies form a tectonic marker zone/break that probably represents a collisional suture zone. Igneous bodies similar to the Selkirk Igneous Complex in the Trans-Himalayan batholith are related to modern suture zones (Searle et al., 1987).

4.4 Metamorphism

All rocks of the Tati Greenstone Belt are generally metamorphosed to greenschist facies with the most common mineral assemblage being chlorite + zoisite/clinozoisite + actinolite/tremolite \pm quartz. However, pockets of higher grade metamorphism are present, especially in high strain areas (shear zones) and near the margins of granitoid intrusive where pyroxene hornfels are recorded. Key (1976) and Key et al. (1976) suggested that in isolated areas, greenschist facies chlorite-talc-sericite assemblages constitute the S₁ fabric. This was not confirmed during this study, although the assemblage is more common in highly altered rocks in some shear zones. Because of the low grade of metamorphism, and dry climatic conditions, some Tati Greenstone Belt rocks are remarkably fresh where exposed (cf. Kusky and Kidd's (1992) remarks on Belingwe Greenstone Belt rocks). Because of the low grade of metamorphism, the prefix meta- is generally dropped and igneous rock names such as basalts are maintained.

CHAPTER FIVE

5. GEOCHEMISTRY

5.1 Introduction

There is very little stratigraphic continuity between units within the Tati Greenstone Belt due to the complex regional structure. The fragmented nature of the exposed sections has contributed immensely to problems of stratigraphic subdivision. The great dependence of by previous workers on equivocal field relations for defining the stratigraphy of the belt, in the absence of fossil evidence and isotopic dating, has further compounded the problem. Furthermore, there have only been minimal geochemical data available to constrain stratigraphic problems.

During geological mapping of the Tati Greenstone Belt for this work, rock sampling was carried out in traverses across individual units and groups of lithological units. The main aim of the sampling was to assess compositional variations within and across geological units. The sampling was also designed to provide geochemical control for the stratigraphic classification of rock units within the Tati Greenstone Belt. Furthermore, geochemical data were also used to develop petrogenetic interpretations for the volcanic and plutonic rocks. The main thrust of this work is metallogenic analysis of the gold deposits of the Tati Greenstone Belt, and since the majority of gold deposits in the belt are either hosted by ultramafic-mafic rocks or occur at contacts between granitoids and supracrustal rocks, this Chapter will summarize the geochemical features of the ultramafic-mafic rocks and granitoid rocks in the belt.

The ubiquitous presence of granitoids in Archean greenstone belts and the broad geochemical resemblance of these Archean granitoids to the North American Cordilleran batholiths (Tarney, 1976; Tarney and Saunders, 1979), suggests the possibility of a similar tectonic setting for granitoids in both Archean greenstone and North American Cordilleran belts. The role played by granitoids in the geological evolution of Archean greenstone belts and associated gold mineralization has remained an enigma to geologists working in the Archean. Because of this, the second part of this Chapter concentrates on the general chemistry of Tati Greenstone Belt granitoids. The term granitoid is used in this thesis as a collective term for diorites, granodiorites, and granites, among other rock types. The reason for this usage is that most Archean granitoid rocks occur as composite bodies that range in composition from gabbro to granodiorite and/or trondhjemite. Units in such composite bodies may be related genetically by petrogenetic processes such as crystal fractionation or partial melting of a common source.

5.2 Alteration Effects on Rock Chemistry

Most rocks in the Tati Greenstone Belt are metamorphosed to at least greenschist or lower amphibolite facies grade. Therefore, the effects of metamorphism and hydrothermal alteration must be evaluated if chemical data from these rocks are to be applied correctly in the identification of magma source(s) and differentiation trends. For example, Beswick and Soucie (1978), Rollinson and Roberts (1987) and Hughes and Hussey (1979) have addressed the problems inherent

when examining volcanic rocks that have undergone alteration. A combination of chemical and petrographic tests were applied in selecting "fresh" rocks to be used in this study. All rocks with a loss of ignition (LOI) greater than 2.5 wt% (cf. Hughes and Hussey, 1979) were rejected as being significantly altered. Beswick and Soucie's (1978) igneous trend diagrams indicate that the remaining Tati Belt rock samples were not significantly altered (e.g. Figure 5.1a).

Plots of relatively immobile elements, such as Zr, against mobile alkali elements, such as Rb or K, were also studied (e.g. Figure 5.1b). The scatter on such plots increases as alteration increases. Using all these different methods, six ultramafic-mafic volcanic rock samples out of a total of thirty-five were rejected as being significantly altered. Some of these six rock samples were, however, analyzed for rare earth elements (REE). Such samples show coherent chondrite-normalised REE patterns. Samples with very high LOI produced erratic REE patterns, especially in the light rare earth elements (LREE) (cf. Bienvenu et al., 1990). The "rejected" samples with coherent REE patterns indicate that alteration in such rocks was minor and did not significantly affect REE.

5.3 Geochemistry of the Ultramafic-mafic Rocks

5.3.1 Introduction

Elemental distributions within modern volcanic rocks have been used with some degree of success to characterize geotectonic settings (e.g. Pearce and Cann, 1973; Pearce and Norry, 1979; Pearce, 1982; Pearce et al., 1984; Wood et al., 1979;

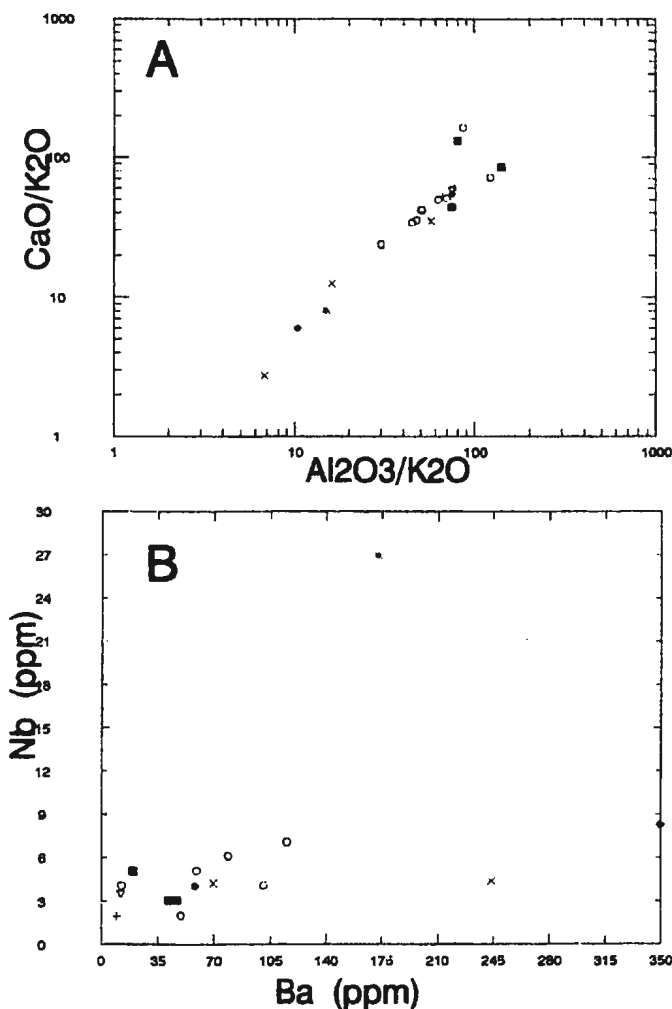


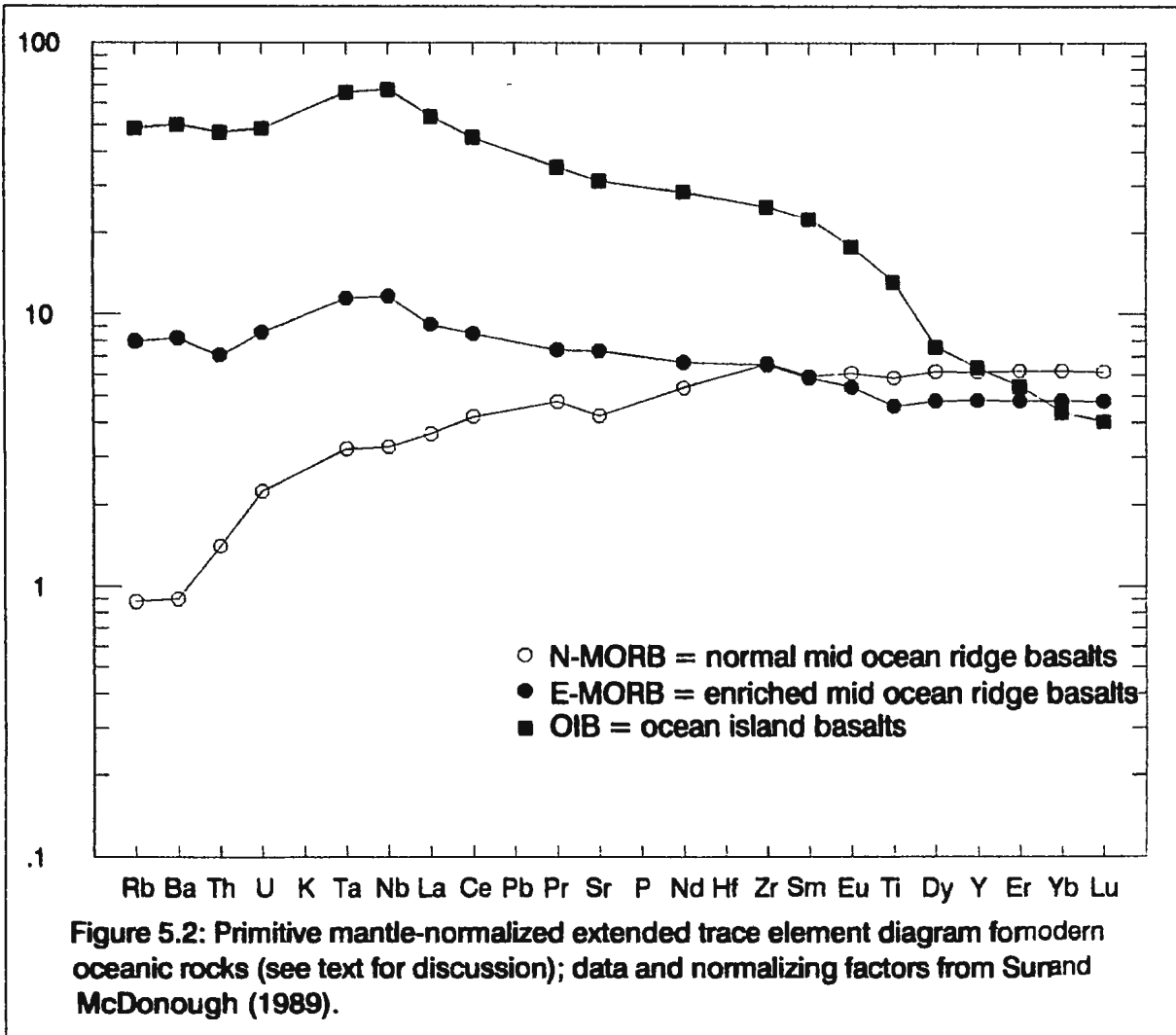
Figure 5.1a: CaO/K₂O vs. Al₂O₃ diagram (after Beswick et al., 1978) for rocks from the Tati Greenstone Belt. The samples define a tight curve from mafic (top right) to intermediate compositions (bottom left) CaO metasomatism would cause displacement parallel to the CaO/K₂O axis, Al₂O₃ metasomatism would cause displacement parallel to the Al₂O₃/K₂O axis, whereas K₂O displacement will be at an angle of 45° to the two axes. Compositional differences would lead to the departure of samples from the main trend; eg. the two samples above the main trend are low Al-komatites.

Figure 5.1b: Nb vs. Ba diagram for Tati Greenstone Belt samples. Since both Nb and Ba are both incompatible elements in feldspar-poor mafic rocks, they should show positive correlation in related rocks. Ba metasomatism would cause scatter as Nb is relatively immobile. The wide variability of Nb, however, especially in basaltic rocks from different environments, could also lead to the scatter of samples on this diagram.

Winchester and Floyd, 1977; Kay, 1984; Sun, 1980; Le Roex et al., 1983, 1985, 1987, 1989; Fodor and Vetter, 1984). Early geotectonic models related discrete magmatic suites to specific environments. These simplistic models failed to adequately discriminate complicated geodynamic systems. For example, differences in magmatic chemistry have been observed between rocks emplaced at midocean ridge spreading axes (normal mid-oceanic ridge basalts; N-MORB) and those at flanks of such ridges (incompatible element-enriched mid-oceanic ridge basalts; E-MORB) (Figure 5.2). During rifting and seafloor spreading, hot refractory mantle regions well up, migrating to areas of lower pressure. This displaces geotherms upwards, resulting in zones of partial melting beneath ridge axes (Natland, 1989). N-MORB rocks are produced in such environments. Away from refractory (depleted) areas of the mantle, relatively undepleted areas of the mantle melt to produce E-MORB magmas.

Similar differences have been observed in the Lau Basin where incompatible element-enriched back arc basin basalts (BABB of Price et al., 1990) border N-MORB-like rocks at the centre of the basin (Hawkins and Mekhior, 1985). These back arc basin basalts were related to the initial stages of crustal extension (Tarney et al., 1977). Overlaps in magma chemistry exist between E-MORB and low potassium arc magmas in some back arc basins (Ikeda and Yuasa, 1989). Mixed signatures have also been documented in some continental flood basalts, such as the Karoo and those at the southeastern Brazilian continental margin (Duncan, 1987; Fodor and Vetter, 1984).

The complexity of modern geotectonic environments makes the application of



similar models to older rocks, such as those of the Archean, very difficult. The problem of defining Archean tectonic environments is compounded by complicating factors such as deformation, metamorphism, and hydrothermal alteration.

The possibility that a different planetary thermal structure existed during the Archean compared to the present, makes matters even worse. Heat production during the Archean is widely believed to have been higher than today because radioactive elements, such as K, U and Th, were more abundant. Calculated metamorphic pressure and temperature regimes for Archean granulites, however, suggest that the Archean crust may not have been significantly thicker than it is today (Bickle, 1986; Wells, 1979).

The combination of only a partial understanding of modern tectonic environments (Abbott and Hoffmann, 1984), a poor understanding of the thermal evolution of the Earth through time, and the transposition of Archean rocks from their primary tectonic environments, have resulted in a diversity of geotectonic models being proposed for Archean greenstone belts. These models range from island-arc settings (Goodwin, 1981; Condie, 1976,1982,1989; Sun, 1982), through back arc settings (Tarney et al., 1977) to oceanic rifting (Helmstaedt et al., 1986; Rivalenti, 1976) including sagtectonics (Anhaeusser, 1975; Gorman et al., 1978). In recent studies, however, it has been realised that Archean volcanic suites in greenstone belts may represent different tectono-magmatic environments brought together by deformational events (Ludden and Hubert, 1984; Barley et al., 1989). Thurston and Chivers (1990) describe greenstone belts as tectonic collages. Recognition of bedding-

parallel shear/fault zones in greenstone complexes enhances this view (Colvine et al., 1984; Colvine, 1989).

Because of the possibility of secular geochemical changes, Arculus (1987) warned against the assumption that trace element discrimination diagrams employed for tectonic study of modern volcanic rocks can be unambiguously applied to substantially older rocks, such as those of the Archean. Chemical differences between Phanerozoic and Precambrian shales have been interpreted as possible evidence for secular crustal growth and evolution of the continental lithosphere (Taylor and McLennan, 1985). Secular chemical change in the composition of the Earth is still, however, a very controversial subject. For instance, studies such as those of Sun (1982;1987), Nesbitt and Sun (1976) and Jahn and Sun (1979) have been unable to confirm secular chemical change.

Phanerozoic MORB compositions suggest that basaltic rock compositions are dependent on the source composition, the degree of partial melting, and the physical and chemical conditions under which melting occurred. Perhaps one of most important characteristics of these rocks is the uniformity in their overall geochemical composition, despite their age. This uniformity makes the possibility of secular chemical change in the derived partial melts difficult to conceive. If the chemical composition of the Earth has changed through time (Taylor and McLennan, 1985) in response to crustal growth and continental lithospheric evolution, it should be possible to establish an optimum length of the period required for chemical change to occur. This could be done by examining the geochemistry of basaltic rocks

emplaced throughout geological time. Because secular change cannot be observed in basaltic rocks spanning the Phanerozoic era, this optimum period of secular change is unknown. The lack of secular chemical variation in Phanerozoic basaltic rocks suggests, therefore, that basaltic rock compositions over time have varied only as function of the degree of melting, depth, and physio-chemical conditions under which they were derived. Older rocks that formed under similar conditions as modern rocks would show the same chemical characteristics. Similar views have been expressed by Abbott and Hoffman (1984).

Christensen (1984) also suggested that heat flow during the Archean may not have been different from modern day heat flow, which implies that temperature-dependent geodynamic processes were the same in the Archean as they are today. Since mantle sources from which different basaltic rocks were derived, are chemically heterogeneous (Joron and Treuil, 1989), differing enrichment and/or depletion of these sources may have existed at different locations of the mantle at any given time. Thus, it is concluded that with appropriate modifications, modern tectonic element discrimination diagrams can be used in studying the chemical characteristics of Precambrian rocks. The main application of these diagrams is to distinguish between different magmatic suites within any group of rocks that were derived under different physical and chemical conditions, and/or from different sources. Appropriate element discrimination diagrams, similar to those used for modern magmatic suites, will be employed in this study to investigate geochemical characteristics of mafic and granitoid rocks within the Tati Greenstone Belt.

5.3.2 Major Element Geochemistry

Major and trace element data for selected ultramafic-mafic rock samples from the Lady Mary Group of the Tati Greenstone Belt are summarised in Table 5.1. The data show that the majority of these samples have SiO_2 contents ranging from 48 to 54 wt%, $\text{Al}_2\text{O}_3 > 12$ wt% and $\text{MgO} + \text{CaO}$ between 12 and 20 wt%. When plotted on Jensen's (1976) cation plot, these rocks range in composition from high magnesian to high iron tholeiitic basalts (Figure 5.3). The compositional range is, however, restricted, suggesting limited magmatic differentiation. Two samples (AR 45 and 207 on Table 5.1) fall outside the common trend and plot in the basaltic komatiite field (Figure 5.3). These two samples have low alumina contents (<7 wt%) and high $\text{CaO}/\text{Na}_2\text{O}$ and $\text{CaO}/\text{Al}_2\text{O}_3$ ratios (>22 and >1, respectively) (Table 5.2). They also have the highest Cr and Ni contents, and low Sr contents (Table 5.1). Overall, the two samples are similar to komatiites from the Barberton Mountain Land Greenstone Belt (Jahn et al., 1982).

During the early stages of tholeiitic magmatic differentiation, Fe and Ti preferentially concentrate into the melt because the first crystallizing phases such as olivine, are Fe and Ti-poor. Thus in the early stages of crystallization of a tholeiitic magma, both the FeO^*/MgO ratio and TiO_2 contents will increase in the residual melts. Diagrams defining the distribution of these ratios can be used to assess the degree of magmatic differentiation (Le Roex et al., 1985). Figure 5.4, although showing some scatter, clearly demonstrates the covariation of the two parameters in mafic rocks from the Lady Mary Group. The samples with the lowest Mg# have high

Table 5.1: Geochemical data for mafic rocks of the Lady Mary Group.

	AR 45	AR 47	AR 50	AR 98	AR 104	AR 114	AR 123	AR 151	AR 152	AR 153	AR 154	AR 193	AR 204	AR 207	AR 225	AR 226	AR 228	AR 217	P-MORB	N1-MORB	N2-MORB	MORB
SiO2	50.70	48.00	51.10	49.20	51.10	49.10	54.40	57.70	52.90	49.50	48.50	50.30	53.80	52.80	51.90	48.10	48.30	50.80	49.08	50.26	50.42	50.42
TiO2	0.88	0.92	1.12	1.24	1.04	0.80	0.80	0.84	0.56	0.60	1.20	1.04	0.52	0.72	0.60	0.80	0.88	1.04	2.04	1.10	1.10	1.50
Al2O3	8.04	17.10	14.70	13.70	15.00	15.10	14.10	11.60	14.40	14.30	14.10	14.00	12.70	6.47	13.40	13.90	14.20	14.20	16.06	15.80	14.83	14.83
Fe2O3*	13.44	11.00	11.84	14.14	11.86	12.00	9.91	8.72	9.52	10.39	14.32	11.83	7.49	14.83	11.53	11.45	12.42	12.30	11.31	10.45	11.57	11.57
MnO	0.20	0.14	0.16	0.20	0.16	0.18	0.14	0.13	0.18	0.18	0.20	0.18	0.14	0.21	0.21	0.18	0.17	0.22	0.22	0.17	0.18	0.18
MgO	15.88	9.82	5.80	5.96	5.80	8.02	5.12	8.58	6.65	8.04	5.74	6.82	9.52	11.39	3.06	4.87	7.14	5.34	8.13	7.84	7.48	7.48
CaO	11.42	10.08	10.70	11.24	10.90	11.92	8.12	8.82	11.46	11.46	11.84	8.62	7.56	10.66	5.40	10.88	8.72	10.70	8.66	12.48	11.48	11.48
Na2O	0.53	2.28	2.51	1.97	2.55	2.34	2.56	3.25	1.87	2.23	1.40	3.24	4.09	0.48	3.23	2.28	2.66	2.71	3.24	2.13	2.43	2.43
K2O	0.07	0.14	0.21	0.27	0.20	0.20	1.38	0.26	0.48	0.23	0.28	0.10	0.17	0.08	1.88	0.87	0.25	0.30	1.08	0.24	0.20	0.20
P2O5	0.04	0.07	0.09	0.13	0.15	0.08	0.10	0.18	0.09	0.08	0.13	0.09	0.01	0.08	0.11	0.07	0.07	0.09	0.44	0.09	0.14	0.14
LOI	0.73	0.85	1.03	1.01	0.92	0.44	1.52	0.52	0.85	0.74	0.80	3.31	2.02	1.69	3.14	2.94	4.16	2.43	1.43	0.00	0.00	0.00
TOTAL	99.83	100.3	99.26	99.06	99.78	100.18	98.13	99.8	99.04	98.73	98.51	99.43	98.02	99.41	94.78	96.42	98.97	100.13	101.69	100.56	100.32	100.32
Mg #	70	83	49	45	49	57	51	57	58	63	44	52	72	80	35	48	53	48	59	60	56	56
Cr	1923	471	401	381	388	442	249	241	241	448	297	418	157	1403	304	221	257	292	---	---	---	---
Ni	638	252	88	83	87	149	81	91	88	161	102	118	75	285	101	96	128	131	---	---	---	---
Sc	21	20	39	22	41	---	28	33	32	---	---	---	---	33	42	---	38	---	27	40	40	40
V	181	173	313	316	309	247	218	178	182	177	313	304	289	177	355	250	297	281	190	---	---	---
Cu	49	71	45	101	47	59	86	21	55	31	93	88	8	129	273	170	87	133	53	---	---	---
Pb	4	1	2	2	---	---	7	7	5	---	1	---	---	---	6	13	---	2	---	---	---	---
Zn	104	75	78	113	79	90	74	95	81	81	112	75	43	138	122	132	118	91	89	78	88	88
Rb	1	2	4	6	5	2	67	3	14	6	6	1	3	1	75	38	8	10	11	2	2	2
Cs	---	0.43	0.83	0.24	0.82	---	6.30	0.18	0.42	---	---	---	---	---	17.84	---	0.67	---	---	---	---	---
Ba	12	50	80	80	59	---	353	116	102	---	---	42	47	20	247	---	71	---	175	8	12	12
Sr	12	218	113	182	115	105	181	257	148	148	140	170	75	8	81	83	77	78	567	86	104	104
Tl	---	---	0.04	0.04	0.06	---	0.37	0.03	0.12	---	---	0.01	0.01	---	2.03	---	0.09	---	---	---	---	---
Ga	10	17	18	17	17	18	17	15	14	14	18	17	15	11	19	19	18	15	---	---	---	---
Li	4.14	31.99	10.58	22.38	11.53	---	87.51	4.75	8.35	---	---	11.08	8.48	7.84	35.18	---	25.58	---	---	---	---	---
Ta	0.28	0.19	0.21	0.29	0.19	---	0.55	0.37	0.24	---	---	0.34	0.25	0.46	0.18	---	0.22	---	---	0.10	0.20	0.20
Nb	4.1	2.0	5.2	6.2	4.1	4.1	8.4	7.1	4.1	4.1	6.2	3.2	3.1	5.2	4.4	4.3	4.3	4.1	27.2	2.0	3.5	3.5
Hf	1.05	0.48	0.58	0.54	0.87	---	3.44	1.22	0.51	---	---	0.62	0.55	0.82	0.78	---	1.37	---	---	1.53	2.28	2.28
Zr	53	80	81	90	82	58	134	116	74	83	89	71	49	75	64	86	77	62	171	63	90	90
Y	12	15	23	25	27	20	19	30	17	20	29	22	21	14	20	21	22	23	24	25	35	35
Th	1.08	0.30	0.82	1.24	0.57	---	8.92	3.40	2.52	---	---	0.46	1.30	2.38	0.51	2.17	1.07	---	---	0.09	0.19	0.19
U	0.39	0.09	0.15	0.32	0.12	---	6.28	1.03	0.74	---	---	0.14	0.38	0.69	---	---	---	---	---	---	---	---
La	4.75	3.10	5.98	8.77	5.97	---	19.88	20.08	9.65	---	---	3.73	2.89	3.85	3.33	---	7.04	---	20.96	1.81	2.86	2.86
Ce	8.62	8.20	14.63	22.74	14.70	---	41.75	32.73	19.27	---	---	9.80	7.73	7.88	8.24	---	15.63	---	48.81	8.04	9.38	9.38
Pr	1.57	1.22	2.18	3.09	2.18	---	4.87	4.50	2.31	---	---	1.54	1.15	1.36	1.23	---	2.07	---	---	---	---	---
Nd	8.04	8.08	10.58	14.28	10.55	---	19.00	17.84	9.54	---	---	8.14	5.57	8.76	6.09	---	9.38	---	23.00	5.83	6.77	6.77
Sm	2.33	1.85	3.13	3.75	3.11	---	4.12	4.01	2.25	---	---	2.61	1.88	2.12	2.01	---	2.69	---	5.30	2.23	3.20	3.20
Eu	0.79	0.78	1.01	1.27	1.01	---	1.05	1.14	0.72	---	---	1.03	0.77	0.77	0.78	---	0.80	---	1.79	0.90	1.21	1.21
Gd	2.66	2.44	3.77	4.48	3.79	---	4.31	4.46	2.67	---	---	3.63	2.47	2.58	2.67	---	3.33	---	---	---	---	---
Tb	0.40	0.42	0.85	0.71	0.64	---	0.68	0.69	0.42	---	---	0.64	0.44	0.43	0.45	---	0.58	---	0.82	0.61	0.88	0.88
Dy	2.28	2.87	4.20	4.64	4.22	---	4.10	4.37	2.77	---	---	4.12	3.25	2.87	2.97	---	3.83	---	---	---	---	---
Ho	0.45	0.56	0.87	0.95	0.87	---	0.82	0.91	0.59	---	---	0.84	0.72	0.51	0.63	---	0.80	---	---	---	---	---
Er	1.24	1.87	2.52	2.78	2.45	---	2.38	2.88	1.74	---	---	2.50	2.12	1.42	1.81	---	2.33	---	---	---	---	---
Tm	0.17	0.24	0.37	0.40	0.36	---	0.32	0.39	0.25	---	---	0.36	0.33	0.19	0.26	---	0.33	---	---	---	---	---
Yb	1.07	1.52	2.31	2.64	2.29	---	2.18	2.51	1.64	---	---	2.05	2.03	1.20	1.77	---	2.09	---	2.09	2.62	3.54	3.54
Lu	0.14	0.23	0.34	0.38	0.32	---	0.31	0.37	0.25	---	---	0.31	0.30	0.15	0.25	---	0.31	---	0.30	0.47	0.85	0.85

--- denotes not analysed for. P-MORB and N-MORB data taken from Le Roex et al. (1985) and Viereck et al. (1989) respectively.

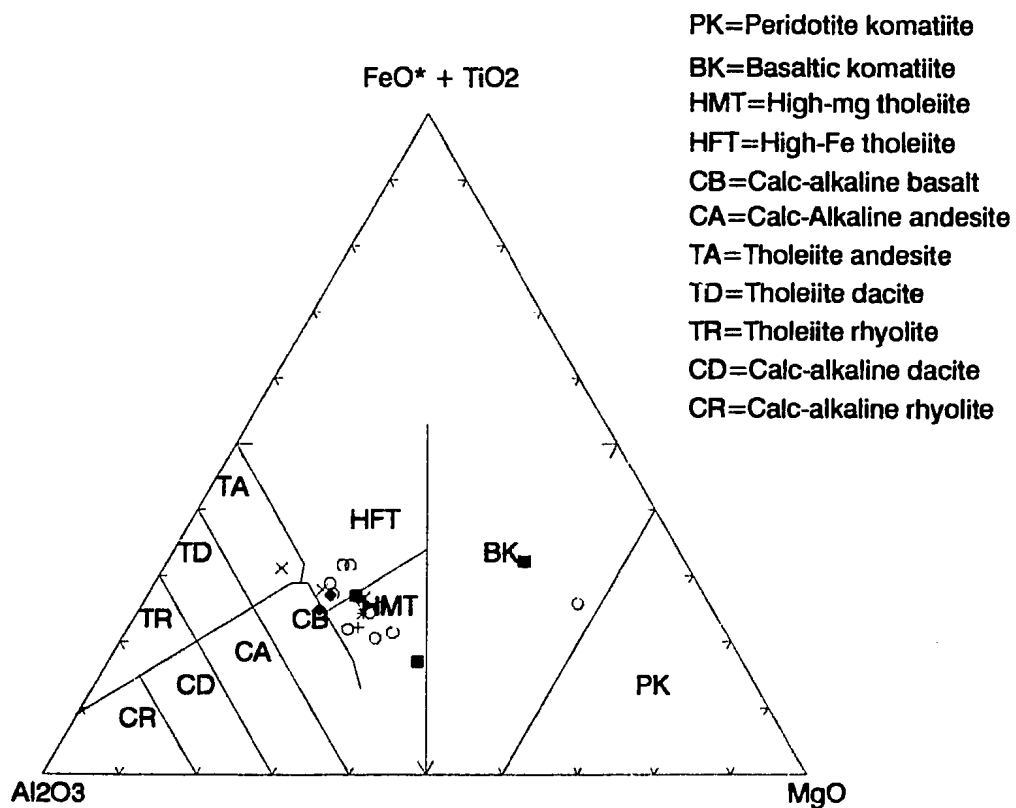


Figure 5.3: Jensen (1976) cation plot of mafic rocks from the Lady Mary Group, Tati Greenstone Belt. Solid squares are samples from the Old Tati area, open circles are samples from the Tati River Subzone of the Tati Belt near Francistown, crosses are samples from the Matsiloje area, solid diamonds are mafic dykes. Other symbols are samples from modern oceanic environments after Le Roex et al. (1985) and Viereck et al. (1989).

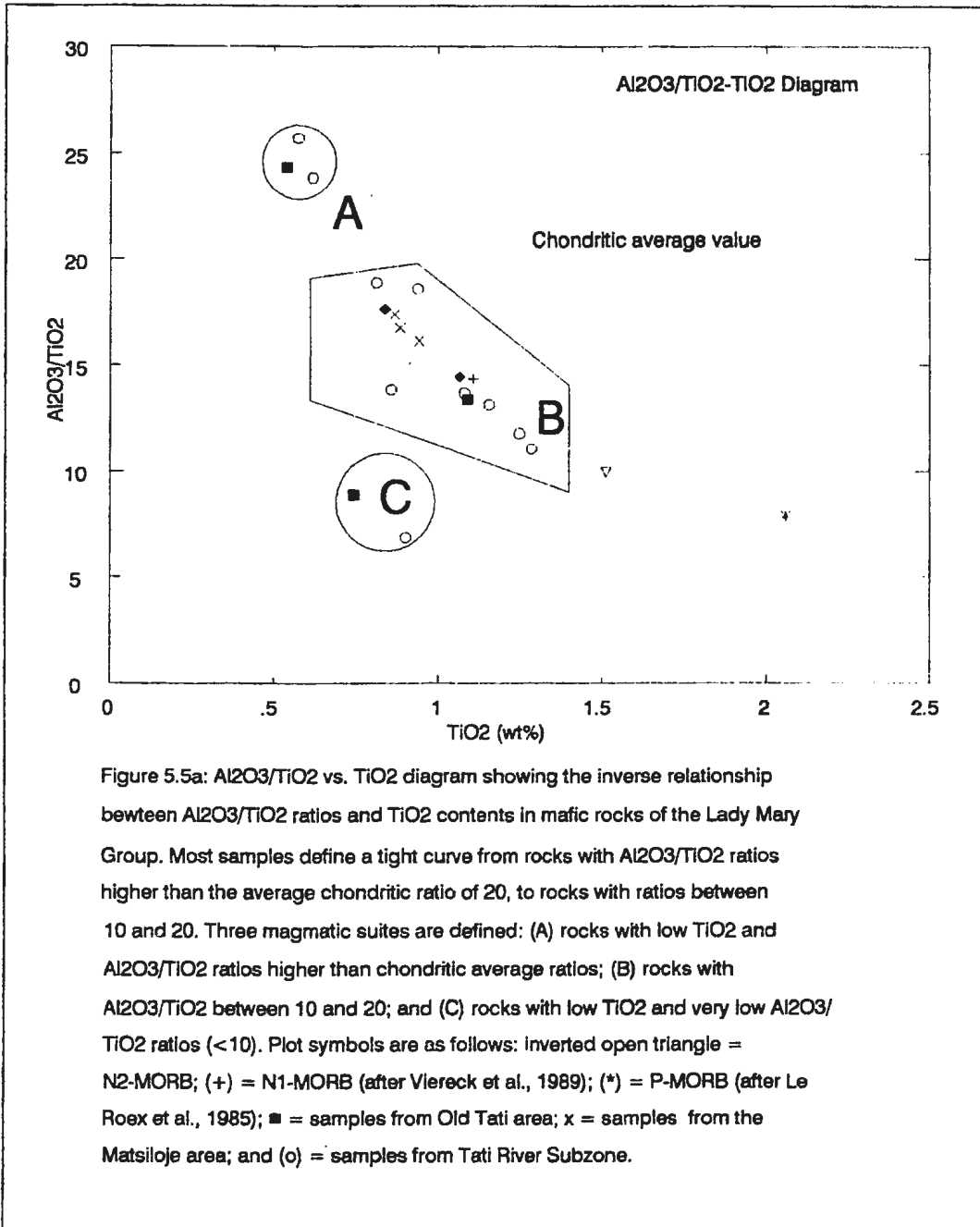
Table 5.2: Element ratios of mafic rocks of the Lady Mary Group.

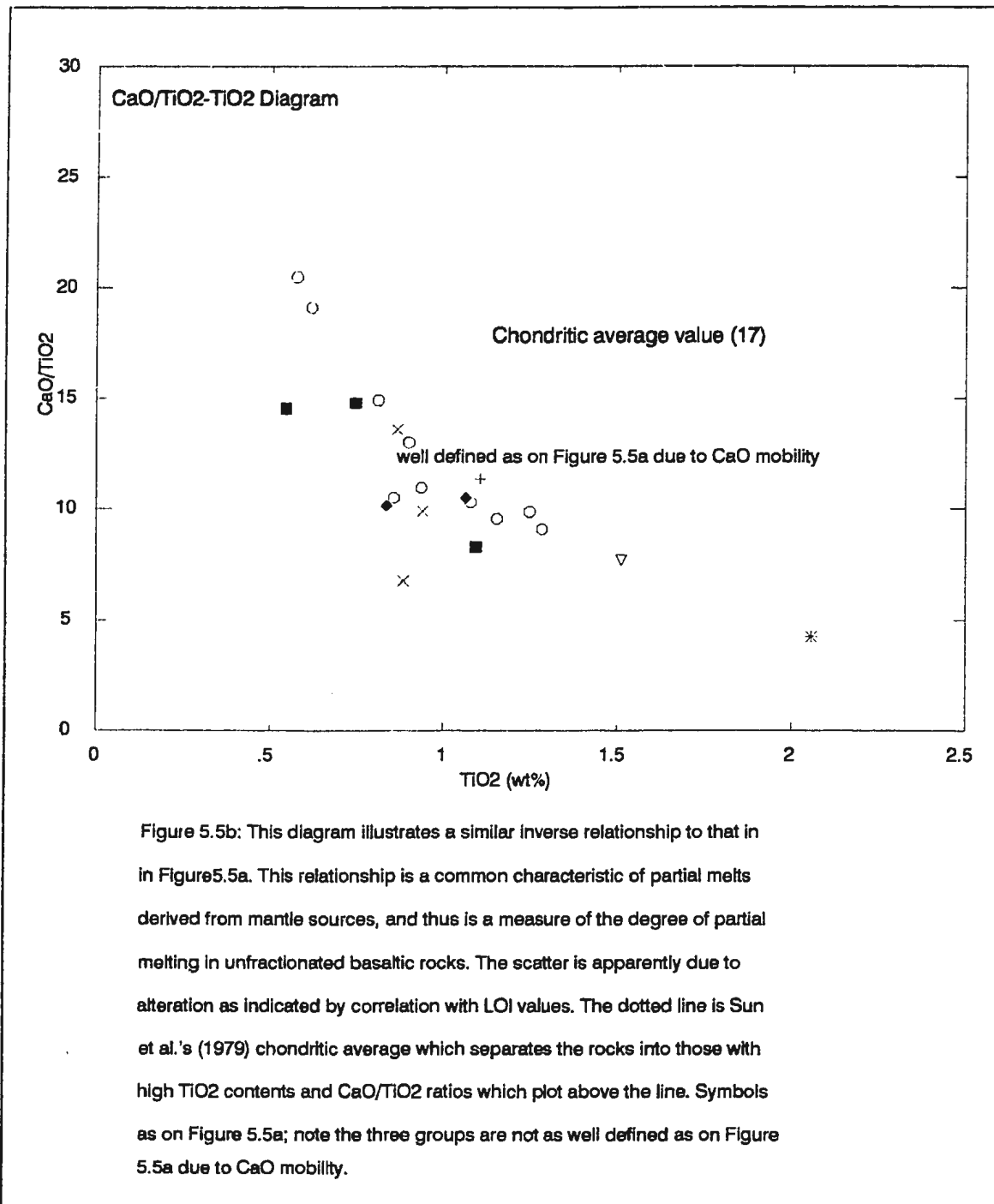
	AR 45	AR 47	AR 50	AR 98	AR 104	AR 114	AR 123	AR 151	AR 152	AR 153	AR 154	AR 193	AR 204	AR 207	AR 225	AR 226	AR 228	AR 217	P-MORB	N1-MORB	N2-MORB	MORB
Al ₂ O ₃ /TiO ₂	7	19	13	11	14	19	18	14	28	24	12	13	24	9	17	17	16	14	8	14	10	
CaO/Al ₂ O ₃	1.89	0.59	0.73	0.82	0.73	0.78	0.58	0.76	0.80	0.80	0.84	0.62	0.60	1.65	0.40	0.78	0.61	0.75	0.54	0.79	0.77	
CaO/Na ₂ O	22	4	4	6	4	5	3	3	6	5	8	3	2	22	2	5	3	4	3	6	5	
CaO/TiO ₂	13	11	10	9	11	15	10	10	20	19	10	8	14	15	7	14	10	10	4	11	8	
K/Rb	581	581	436	374	332	830	176	718	285	318	387	966	470	664	242	206	346	249	854	1311	630	
Rb/Cs	---	4.76	6.56	26.09	8.20	---	10.63	18.75	34.14	---	---	---	---	---	4.21	---	9.52	---	---	---	---	
Ce/Pb	2.40	8.06	7.10	10.98	---	---	5.70	4.59	3.75	---	---	---	---	---	1.49	---	---	---	---	---	---	
Rb/Sr	0.08	0.01	0.04	0.03	0.04	0.02	0.37	0.01	0.10	0.04	0.04	---	0.04	0.12	1.24	0.45	0.08	---	0.02	0.02	0.02	
Th/U	2.8	3.2	4.0	3.9	4.7	---	1.1	3.3	3.4	---	---	3.4	3.4	3.5	---	---	---	---	---	---	---	
Sm/Nd	0.29	0.31	0.30	0.26	0.29	---	0.22	0.22	0.24	---	---	0.35	0.33	0.31	0.33	---	0.29	---	0.23	0.38	0.38	
La/Nb	1.2	1.5	1.2	1.6	1.5	---	2.4	2.8	2.3	---	---	1.2	0.9	0.8	0.8	---	1.6	---	0.8	1.0	0.8	
La/Ta	18.8	18.1	29.0	33.7	30.7	---	35.9	54.7	40.8	---	---	10.8	11.5	8.7	20.9	---	31.5	---	---	19.0	14.7	
Nb/Ta	16	11	25	21	21	---	15	19	17	---	---	9	12	11	28	---	19	---	---	20	17	
Nb/U	10.53	22.22	33.33	19.35	33.33	---	1.33	6.93	5.56	---	---	23.07	8.33	7.58	0.00	---	---	---	---	---	---	
Ti/Eu	6852	7162	6851	6044	6311	---	4772	4496	4786	---	---	6382	4241	5832	6961	---	6281	---	6910	7328	7494	
Ti/V	30	32	22	24	21	20	23	29	19	21	24	22	11	25	15	21	19	23	65	---	---	
Ti/Y	440	398	305	310	240	240	266	174	197	189	257	297	156	332	266	252	251	283	510	264	257	
Ti/Zr	101	93	85	85	78	87	37	44	47	59	84	88	66	60	83	61	73	104	72	105	101	
Y/Nb	3.0	7.5	4.4	4.0	6.5	5.0	2.3	4.1	4.2	4.7	4.7	7.0	6.7	2.6	4.5	4.7	5.2	5.5	0.9	12.6	10.0	
Zr/Nb	13	29	18	15	20	14	16	16	18	15	14	22	16	14	15	20	18	15	8	32	25	
Zr/Y	4.3	3.9	3.8	3.6	3.1	2.7	7.1	3.9	4.2	3.2	3.1	3.2	2.3	5.5	3.2	4.2	3.4	2.7	7.1	2.5	2.5	
(La/Ce) _n	1.27	0.99	1.77	1.13	1.07	---	1.25	1.61	1.32	---	---	1.00	0.98	1.32	1.06	---	1.17	---	1.18	0.83	0.83	
(La/Sm) _n	1.26	1.03	1.18	1.61	1.19	---	2.98	3.09	2.64	---	---	0.82	0.96	1.15	1.02	---	1.61	---	2.44	0.53	0.57	
(La/Yb) _n	2.96	1.37	1.73	2.48	1.74	---	6.14	5.35	3.94	---	---	1.21	0.85	2.19	1.28	---	2.25	---	6.72	0.49	0.58	

TiO₂ contents suggesting that such samples are indeed evolved. The covariation of these two parameters is also consistent with transition metal abundances.

Sun et al. (1979) used diagrams of Al₂O₃/TiO₂ and CaO/TiO₂ vs. TiO₂ to assess the degree of mantle partial melting involved in the formation of relatively unfractionated MORB rocks. At lower degrees of partial melting, Ti will act as an incompatible element and will preferentially concentrate in the melt. Ca and Al will be buffered by residual phases pyroxene, garnet, plagioclase and spinel, leading to lower CaO/TiO₂ and Al₂O₃/TiO₂ ratios in the melt. Higher degrees of melting would lead to higher ratios, approaching the chondritic values of 17 and 20 respectively, as more calcium and aluminum enter the melt. Figures 5.5a and 5.5b show that the Lady Mary Group mafic rocks range from very high CaO/TiO₂ and Al₂O₃/TiO₂ ratios and low TiO₂, to lower ratios and high TiO₂. These diagrams also suggest that the rocks can be divided into three subgroups. The subgroups are; (1) rocks with low TiO₂ contents and Al₂O₃/TiO₂ and CaO/TiO₂ ratios greater than chondritic values; (2) rocks with Al₂O₃/TiO₂ and CaO/TiO₂ ratios that are lower than chondritic averages; and 3) rocks of komatiitic affinity with Al₂O₃/TiO₂ ratios <7 and CaO/Al₂O₃ ratios >1.5.

Le Roex et al.'s (1985) P-MORB value (Figure 5.5a) and Viereck et al.'s (1989) average N-MORB compositions (Figure 5.5a) are also plotted on the same diagram. These MORB subtypes fall in the same trend defined by the Lady Mary Group mafic volcanic rocks. P-MORB, as used by Le Roex et al. (1985), refers to plume-type mid oceanic ridge basalts similar to E-MORB.





5.3.3 Trace Element Geochemistry

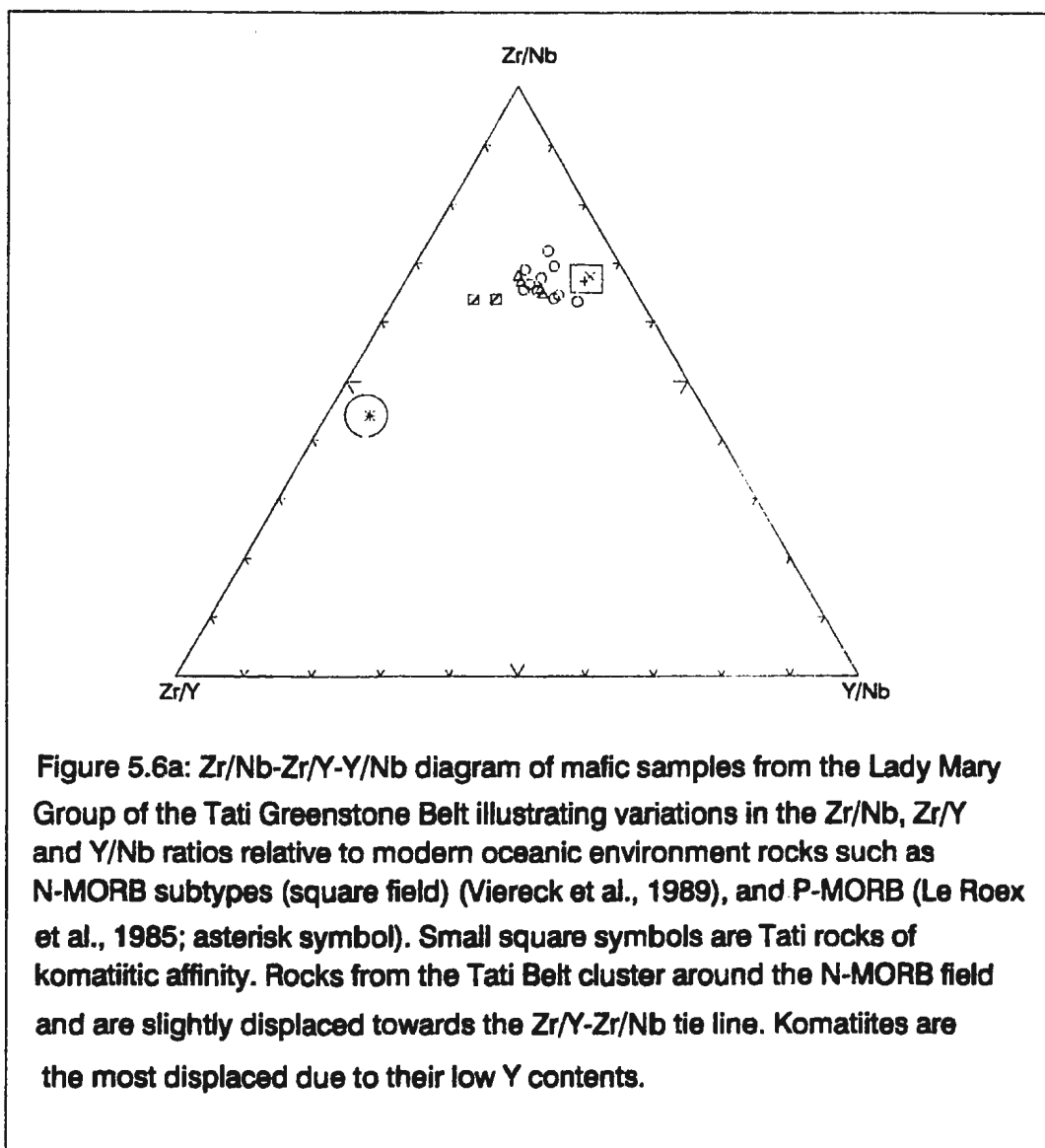
The discussions that follow are based mainly on the relative distributions of trace elements as illustrated on element normalized diagrams. These diagrams include Sun and McDonough's (1989) mantle normalized diagrams, Thompson et al.'s (1984) spidergrams, and Hoffman et al.'s (1986) Masuda-Coryell diagrams.

On element normalized diagrams (e.g. Figure 5.2), elements are plotted on the basis of their decreasing incompatibility (i.e. Rb to Lu) relative to mantle mineralogy (Wood et al., 1979). Although different types of normalized diagrams can be designed using different combinations of elements, the elements most commonly plotted are those whose bulk partition coefficients (D) between modal mantle mineralogy and basaltic magma are generally less than one. Such elements are preferentially partitioned into melts during both partial melting and crystal fractionation. They are therefore referred to as hygromagmaphile (HYG) elements by Wood et al. (1979).

Elements range from more-HYG, on the left side of the diagrams, to less-HYG on the right (Briqueu et al., 1983; Joron and Treuil, 1989). Figure 5.2 illustrates that the relative hygromagmaphile character for elements such as Nb, Zr and Y increases from Y through Zr to Nb. Ratios of Y/Nb, Zr/Nb and Zr/Y define ratios between less-HYG and more-HYG elements, between mid-HYG and more-HYG elements, and between mid-HYG and less-HYG elements, respectively. These ratios were presented on ternary diagrams by Le Roex et al. (1983,1985,1989) and Foder and Vetter (1984). On the basis of these ternary diagrams, basalts from the southwestern Indian Ridge (Le Roex et al., 1983) and the southern Brazil margin

(Foder and Vetter, 1984) were subdivided into three MORB subtypes. N-MORB (normal mid oceanic ridge basalts) have Zr/Nb and Y/Nb ratios greater than the chondritic averages of 16 and 6.5, respectively: E-MORB (enriched mid oceanic ridge basalts) have lower ratios, and T-MORB (transitional mid oceanic ridge basalts) have characteristics intermediate between the other two.

Mafic volcanic rocks of the Lady Mary Formation have Zr/Nb ratios averaging 17, which approximate Le Roex et al.'s (1985) average chondritic value of 16. The average Y/Nb ratio of 4.8 is, however, lower than the chondritic value of 6.5. The Zr/Y average ratio of 3.6 is greater than the chondritic value of 2.5 (Tables 5.2). Figure 5.6a (a Zr/Nb - Zr/Y - Y/Nb ternary diagram) shows element distribution patterns for Tati Greenstone Belt ultramafic-mafic volcanic rocks and their plutonic equivalents. These rocks plot between the fields of modern P-MORB and N-MORB. The trend is displaced towards higher Zr/Nb and lower Y/Nb ratios. Based on this diagram, the Tati Greenstone Belt mafic volcanic rocks appear to have geochemical features similar to N-MORB, since they cluster near the N-MORB field. Figure 5.6b illustrates element distribution patterns for komatiites and tholeiitic rocks from the Barberton Mountain Land Greenstone Belt (data from Jahn et al., 1982). The Tati Greenstone Belt data field is defined by a circle. The diagram indicates that the majority of the Barberton rocks also fall in the field of Tati rocks. The Barberton rocks, however, also spread from the Tati field towards the Zr/Y corner (Figure 5.6b). This is similar to modern oceanic rocks which extend from the field of N-MORB to that of P-MORB (Le Roex et al., 1985).



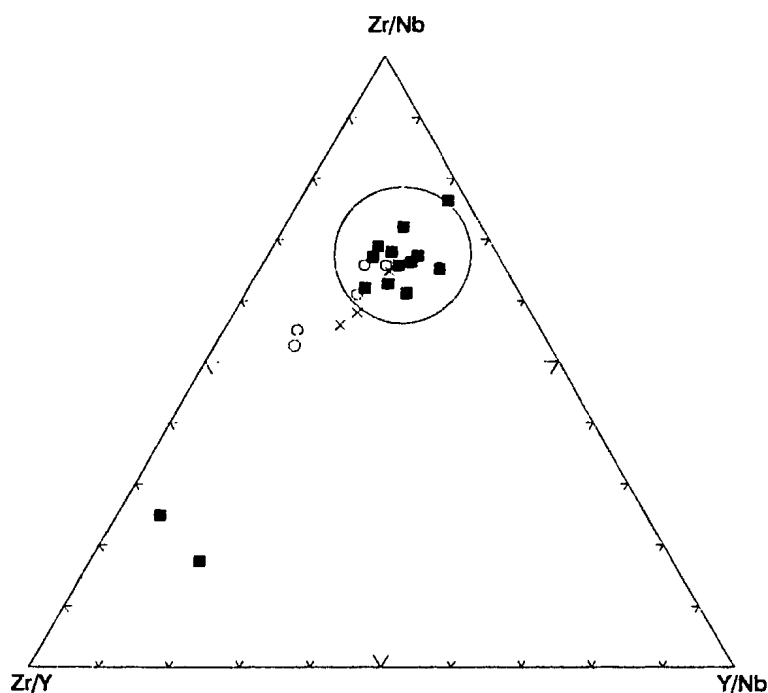


Figure 5.6b: Tati Greenstone belt field (large circle) overlaps the field of Barberton Mountainland Greenstone Belt komatiites and tholeiites. The square symbols are basaltic komatiites diamonds are peridotitic komatiites, open circles are tholeiitic rocks; data from Jahn et al. (1982). Samples with x symbol outside the circle are rocks of komatiitic-affinity and the x-sample inside circle is AR 204; all of the Tati Belt.

The significance of the Zr, Y and Nb ratio diagrams was evaluated by Myers and Breitkopf (1989). They showed that, although these diagrams could distinguish between enriched and normal MORB subtypes, they were unable to separate rocks from the southwestern Indian Ridge (an oceanic environment) from those from the southern Brazil margin (continental environment). They, therefore, suggested that a multi-element Nb-normalized diagram, using elements Nb, La, Ce, P, Zr, Ti and Y, would produce better discrimination between different magma types. On such a diagram, elements are doubly normalized to both element concentrations in the reference material (e.g. Primitive mantle) and to the Nb content in the rock sample being studied. This facilitates the recognition of subtle differences between rocks which may not otherwise be apparent on the Le Roex et al.'s (1985) ternary ratio diagram.

On a Nb-normalized diagram (Figure 5.7), rocks derived from an enriched mantle source which contains high Nb will plot below the reference line of one, whereas, those from a depleted source will plot above the reference line. Rocks with decoupled Nb contents, relative to such elements as the LREE, or more specifically samples with negative Nb anomalies, may show high positive deviation in the more-HYG elements relative to Nb. The slope between La and Ce on these diagrams is diagnostic, being positive for LREE-depleted and negative for LREE-enriched rocks. The slope between Ti and Y is also diagnostic, positive for depleted and negative for enriched rocks.

Figure 5.7 illustrates the variation of Tati Greenstone Belt ultramafic-mafic

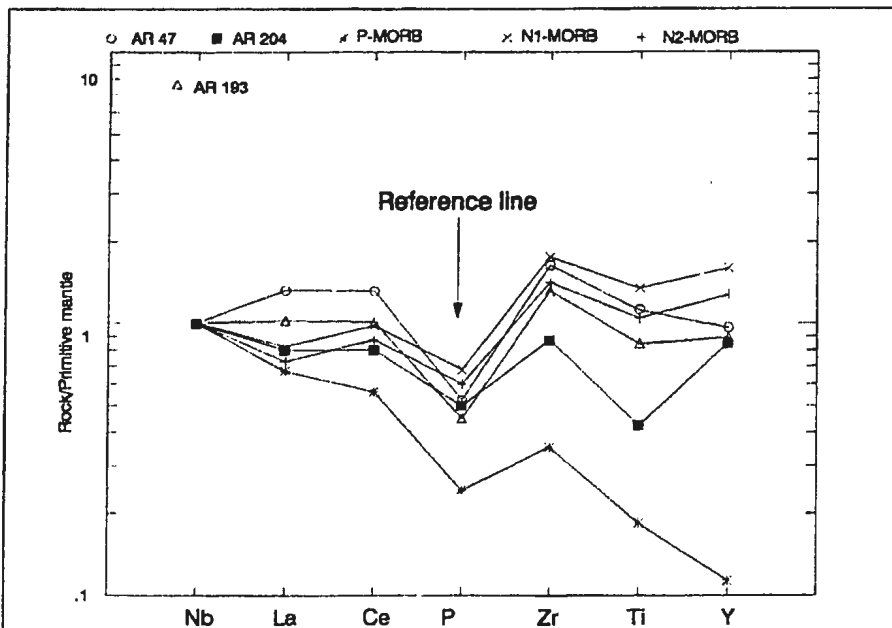


Figure 5.7a: Nb-primitive mantle-normalized diagram comparing some mafic rocks from the Lady Mary Group with modern oceanic rocks (P-MORB from Le Roex et al., 1985, and N-MORB subtypes from Viereck et al., 1989 - normalizing factors from Wood et al. (1989)).

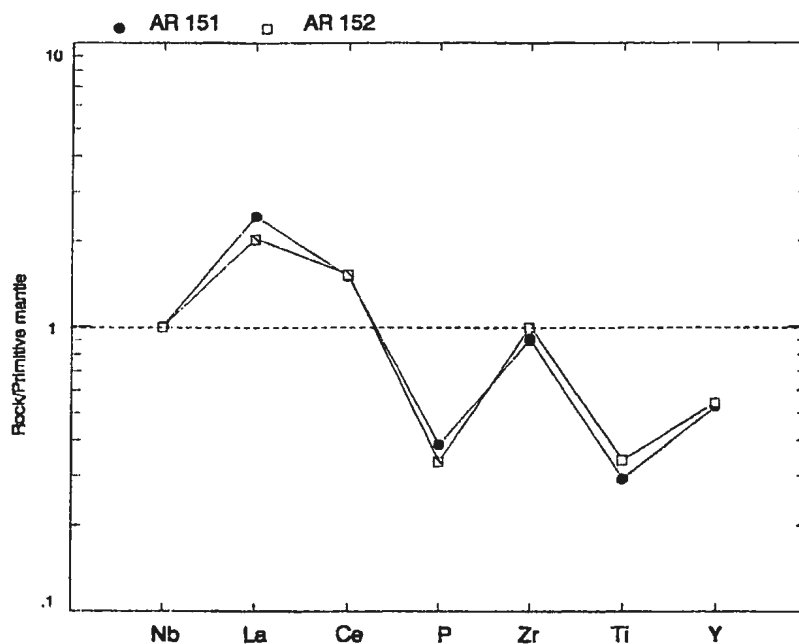


Figure 5.7b: Nb-primitive mantle-normalized diagram showing samples with strong LREE-enrichment. Normalizing factors from Wood et al. (1979).

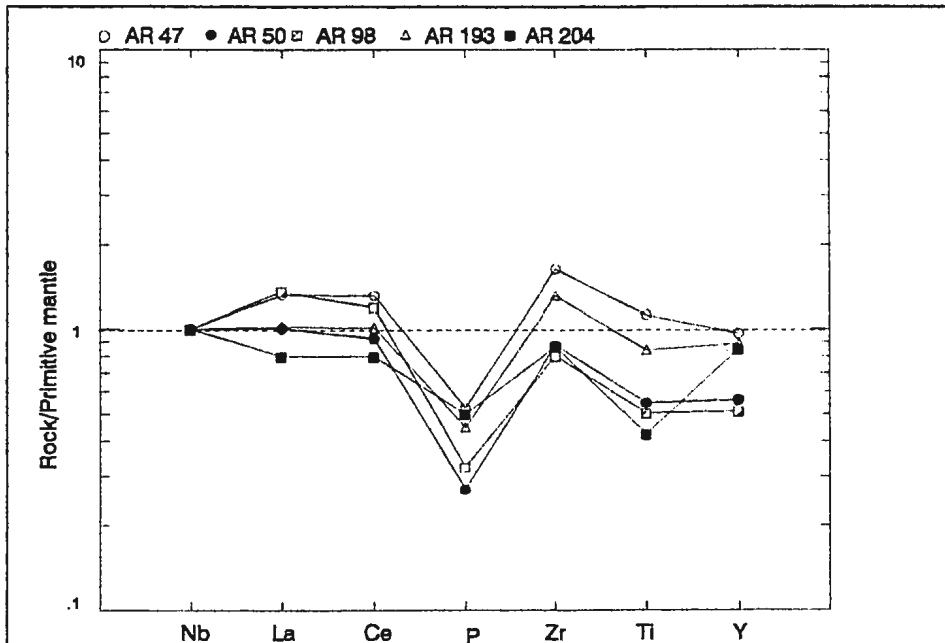


Figure 5.7c: Nb-primitive mantle-normalized diagram for some mafic rocks from the Lady Mary Group of the Tati Greenstone Belt. Normalizing factors from Wood et al. (1979).

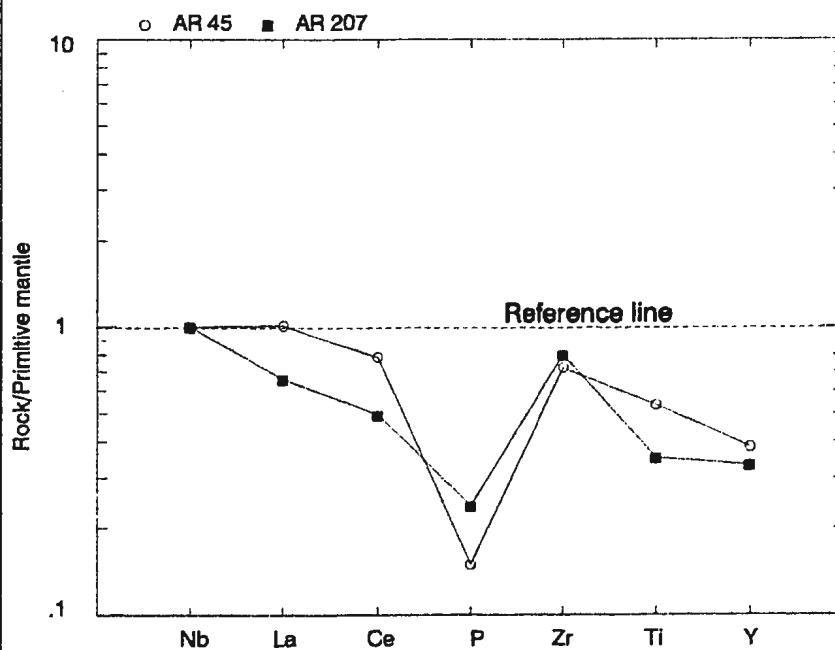


Figure 5.7d: Nb-primitive mantle-normalized diagram for samples with komatiitic affinity. Normalizing factors from Wood et al. (1989).

rocks on Nb-normalized diagrams. P-MORB values (Le Roex et al., 1985) and N-MORB subtypes from Viereck et al.(1989) are also plotted. On this diagram the relatively high Nb contents of modern P-MORB is indicated by all the other elements plotting below the reference line. N-MORB subtypes plot above the reference line (Figure 5.7a). The Nb-normalized diagrams define some interesting broad characteristics for the Lady Mary Group rocks, indicating:

1. Rock samples with Nb depletion relative to LREE (samples AR 151 and AR 152). These samples also have negative slopes between La and Ce and positive slopes between Ti and Y (Figure 5.7b). Negative slopes between La and Ce suggest LREE enrichment and, when taken together with Nb depletion relative to the LREE, indicate characteristics similar to modern island arcs. On the other hand, positive slopes between Ti and Y would indicate, in simple cases, enrichment in less-HYG elements (compatible) relative to the more-HYG elements (incompatible). This will result in a convex upward normalized element pattern (MORB in Figure 5.2). The positive slopes between Ti and Y result from the fact that Ti is more incompatible than Y. The two patterns taken together would therefore suggest that these rocks were derived from a previously depleted source that was subsequently enriched before renewed partial melting.

2. Samples whose Nb contents are not very much different from N-MORB and have LREE-depleted abundances (samples AR 204, and AR 193). These samples also contain positive to flat slopes between La and Ce, and between Ti and Y (Figure 5.7c). The combination of these two positive slopes and the normal to slightly

depleted Nb contents relative to LREE is indicative of depletion in the more-HYG (incompatible elements) relative to the less-HYG (compatible elements). Normalized element diagrams of such patterns (Figure 5.2) are characteristic of modern MORB. Samples AR 47 and AR 50 have flat slopes between La and Ce and between Ti and Y (Figure 5.7a). These samples also show high Zr/Nb, Y/Nb and low Zr/Y ratios (Table 5.2) and may belong to this subgroup.

3. Samples AR 207 and AR 45 have Nb-enrichment relative to all the other elements. These samples have a small negative slope between La and Ce and a flat to negative slope between Ti and Y (Figure 5.7d), and also high CaO/Na₂O and low Al₂O₃ ratios. These samples have characteristics typical of alumina-depleted komatiites. The chemistry of these samples, such as depletion of Y, Al and the HREE, suggests derivation from the partial melting of a very deep source in which garnet was residual (Ohtani, 1990). The three groups defined in this section are similar to those suggested by major element geochemistry (Figures 5.5a and 5.5b).

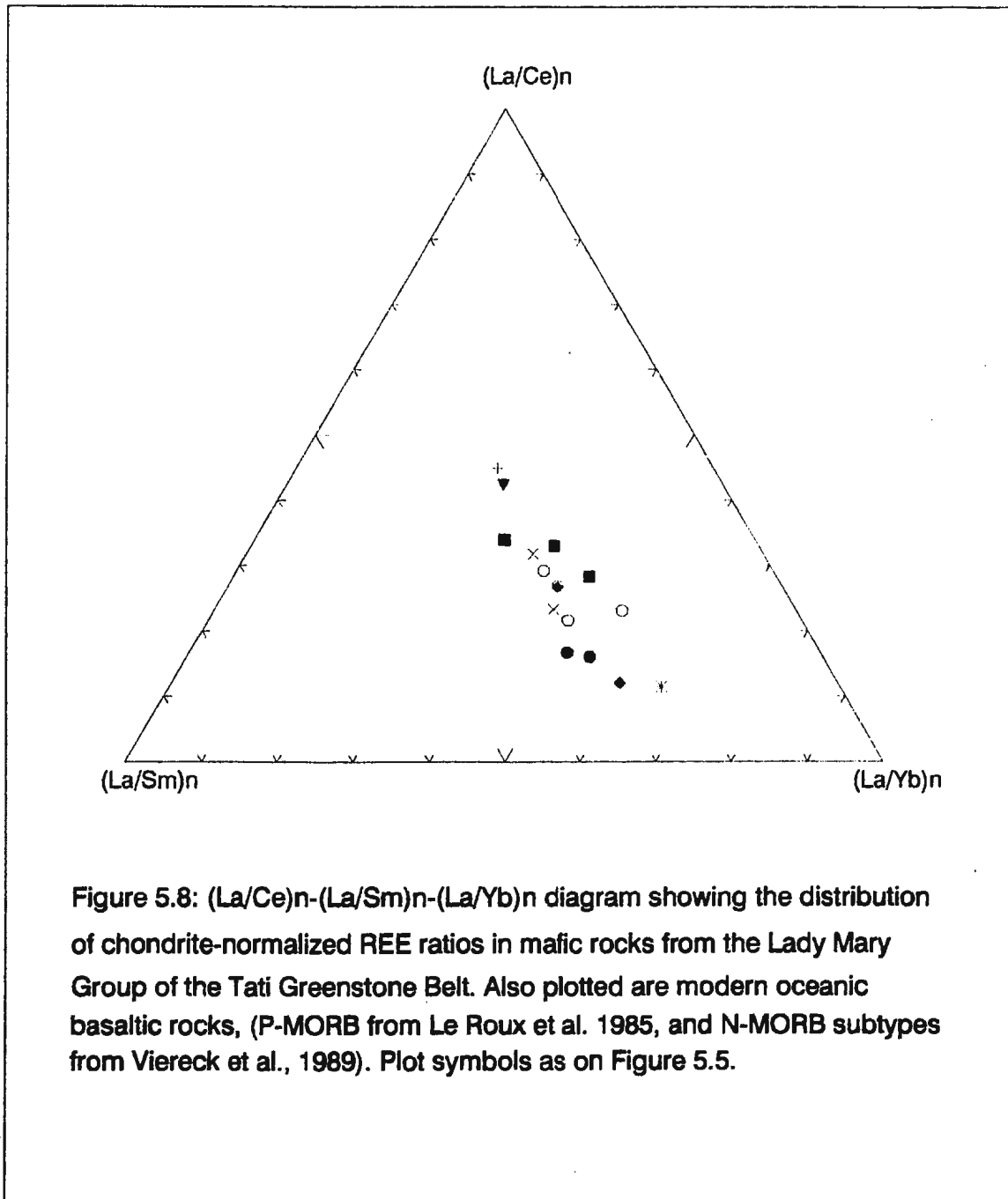
5.3.4 Rare Earth Element Geochemistry

Major and trace element distributions consistently suggest the presence of at least three magmatic suites within Lady Mary Group ultramafic-mafic rocks, viz.; (1) low-Ti, high-CaO tholeiitic rocks, (2) basaltic komatiites and (3) rocks with characteristics similar to modern MORB. Consideration of each individual normalized REE diagram for a considerable number of samples can be overwhelming and confusing at times. Even where representative samples are chosen for consideration

on these diagrams, as is done in most studies, it is still necessary to go over all the samples in order to pick the most representative. Normalized ratios of REE such as LREE/LREE (La/Ce), LREE/MREE (La/Sm) and LREE/HREE (La/Yb) are, however, commonly quoted when summarizing REE variation patterns, and are usually presented in table form. Searching through these tables for representative samples can be as overwhelming as the diagrams themselves.

These ratios can, however, be presented in a simple ternary diagram (Figure 5.8). On such a diagram REE patterns can be shown for a large number of rocks on the same diagram without masking an individual rock REE pattern. It is therefore possible to use this diagram to select representative rocks, such as those most depleted or enriched in HYG elements, from any suite of rocks for petrogenetic modelling. Because of the positive slopes between La and Ce in normalised diagram (e.g. Figure 5.2), the $(La/Ce)_n$ ratio is less than one for rocks derived from HYG element depleted sources, and more than one in rocks derived from enriched sources (Figure 5.8). The $(La/Yb)_n$ ratio, on the other hand, is comparatively low for rocks derived from enriched sources (less than one), and vice versa for rocks derived from depleted sources. $(La/Sm)_n$ ratios vary very little between rocks from depleted and enriched sources by virtue of the mid-REE character of Sm. Basaltic rocks, such as those from oceanic environments, plot along a curve extending from the $(La/Yb)_n$ ratio corner to the $(La/Ce)_n$ ratio corner, convex towards the $(La/Sm)_n$ ratio side.

Tati Greenstone Belt ultramafic-mafic volcanic rocks and their plutonic equivalents plot between the fields of modern N-MORB subtypes and P-MORB.



Thus the source for these rocks has characteristics intermediate between depleted and enriched end members. Traditional chondrite-normalized REE diagrams (Figure 5.9) indicate variations from REE-enriched patterns in the low-Ti and evolved basalts (Figure 5.9a) to flat/slightly depleted (LREE) patterns in komatiites, and relatively unfractionated normal basalts (Figures 5.9b and 5.9c) in the Tati Greenstone Belt rock samples. REE contents of Tati Greenstone Belt ultramafic-mafic volcanic rocks vary from about 10 to 100x chondritic abundances.

Rocks with komatiitic affinities (samples AR 45 and AR 207) are relatively depleted in HREE (Figure 5.9c), which is also consistent with their Ti/Y ratios (Table 5.2). The slight enrichments in the LREE (Figure 5.9c), in addition to the depletion in Y, Al_2O_3 and HREE, are consistent with the presence of garnet in the residuum (Ohtani, 1990). Figure 5.9d compares those Tati Greenstone Belt rocks with flat to slightly LREE depleted patterns, to modern N-MORB subtypes. Although the Tati rocks have flat REE patterns, they overlap with modern MORB REE patterns. A similar comparison can be made between the P-MORB from the southwestern Indian Ridge of Le Roex et al. (1985) and LREE-enriched rocks of Tati Greenstone Belt (Figure 5.9e). Although the decrease in abundances from LREE to HREE is similar, the Tati rocks are slightly concave upwards in their REE patterns.

Figure 5.9f compares all the geochemical subgroups within the Lady Mary Group ultramafic-mafic rocks. Further differences between the three main geochemical groups of the Tati rocks are illustrated by elemental patterns on primitive mantle normalized diagrams (Figure 5.10a-d). Figure 5.10a compares the

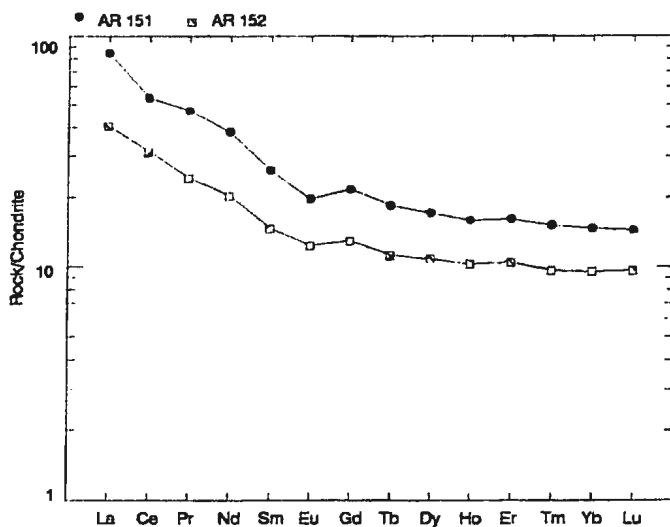


Figure 5.9a: Chondrite normalized REE patterns for LREE-enriched rocks from the Tati River Subzone of the belt, about 15 kilometres south of Francistown. Normalizing factors are from Sun and McDonough (1989).

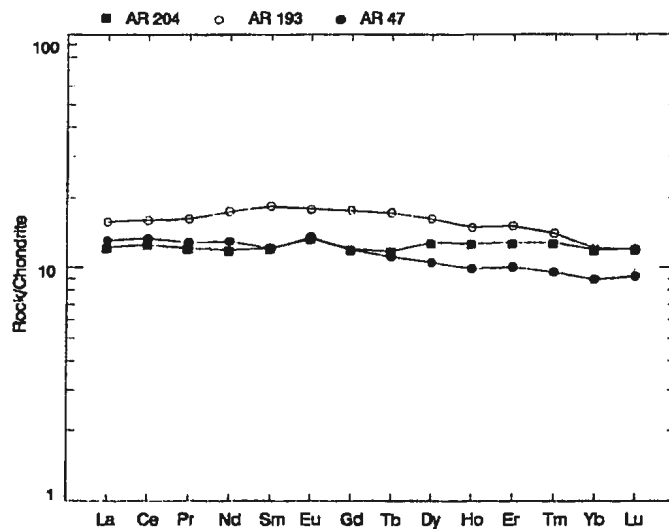


Figure 5.9b: Chondrite normalized REE diagram for some mafic rocks from Lady Mary Group. These three samples (two are from the Old Tati area, samples AR 193 and AR 204, and one is from near Francistown, sample AR 47) are part of a suite that shows flat to slight LREE depletion. Normalizing factors are from Sun and McDonough (1989).

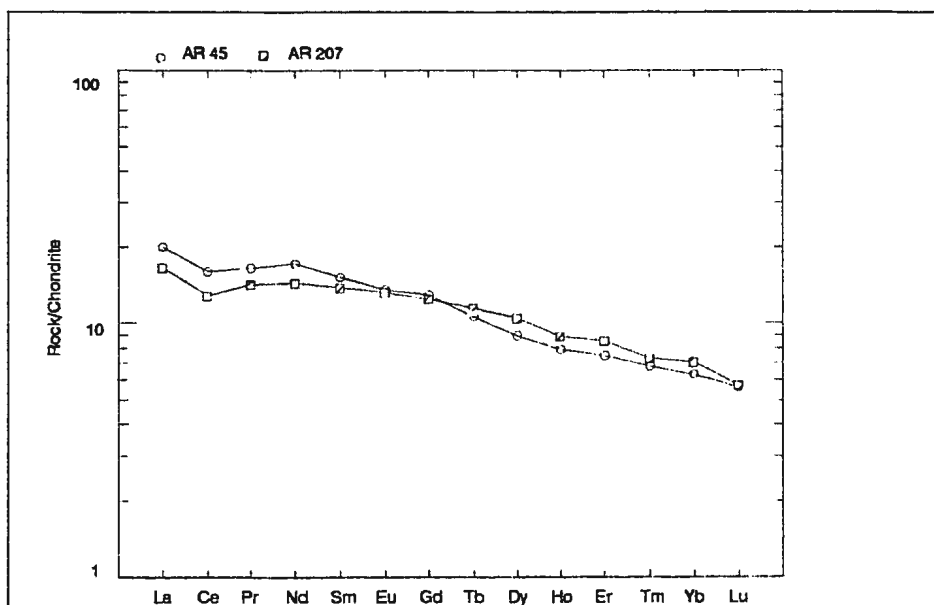


Figure 5.9c: HREE-depleted rocks of komatiitic affinity from both the Old Tati area and the Western Zone of the belt. Normalizing factors from Sun and McDonough (1989).

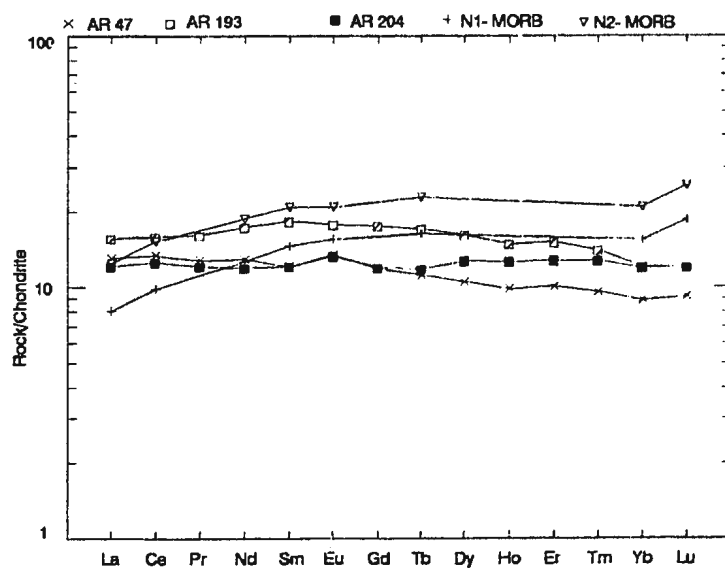


Figure 5.9d: Comparison of chondrite-normalized REE patterns of the mafic rocks from the Lady Mary Group, Tati Greenstone Belt that have flat to depleted LREE patterns with average compositions of N-MORB subtypes from Viereck et al. (1989). Normalizing factors from Sun and McDonough (1989).

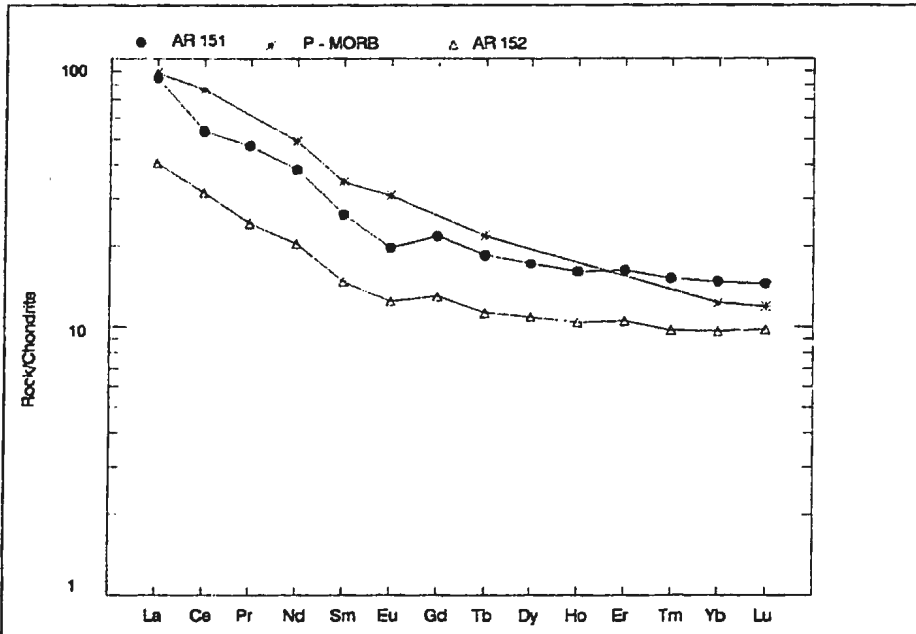


Figure 5.9e: Comparisons of the chondrite-normalized REE patterns for LREE-enriched mafic rocks of Tati Greenstone Belt and P-MORB from Le Roux et al. (1985). Normalizing factors as before.

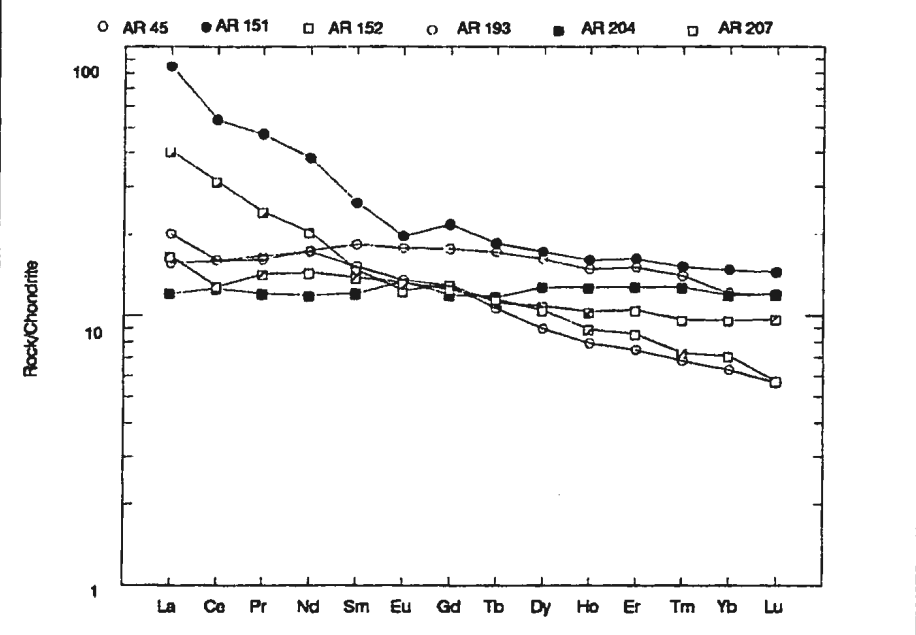


Figure 5.9f: Comparisons of chondrite-normalized REE patterns from the different groups shown in Figures 5.9a to 5.9c. Normalizing factors as before.

flat to depleted Tati rocks with the average compositions of Viereck et al.'s (1989) N-MORB subtypes. The patterns are similar except for higher contents of Ba and Sr in the Tati rocks. Figure 5.10b shows rocks with flat to depleted LREE patterns. Figure 5.10c shows the normalized elemental patterns of the LREE-enriched Lady Mary Group rocks. These rocks contain negative anomalies in the TNT elements (Ta, Nb and Ti), a feature common in modern island arc rocks. Figure 5.10d shows normalized elemental patterns for the komatiitic rocks of Tati Greenstone Belt. These rocks, apart from showing depletion in Sr, also have a negative sloping pattern from Ba to Lu. High values of Th and U in element normalized patterns of the Tati komatiites are illustrated on Figure 5.10d. The elevated concentrations of these elements is as yet unexplained.

5.3.5 Discussion

In Chapter 4, structural analysis indicated that the stratigraphy in the Tati Greenstone Belt can be summarised as three fault-bound volcano-plutonic sequences. One of these sequences, the Lady Mary Group, consists dominantly of ultramafic-mafic volcano-plutonic rocks in which three main magmatic suites can be recognised: (1) basaltic-komatiites, (2) modern MORB-like rocks and (3) LREE-enriched rocks. The spatial distributions of these rock suites suggests that MORB-like and komatiite rocks are surrounded by LREE-enriched rocks. A second observation is that the tholeiites and komatiites in the Old Tati are geochemically indistinguishable from similar rocks in the Tati River area, therefore, they all constitute the Old Tati

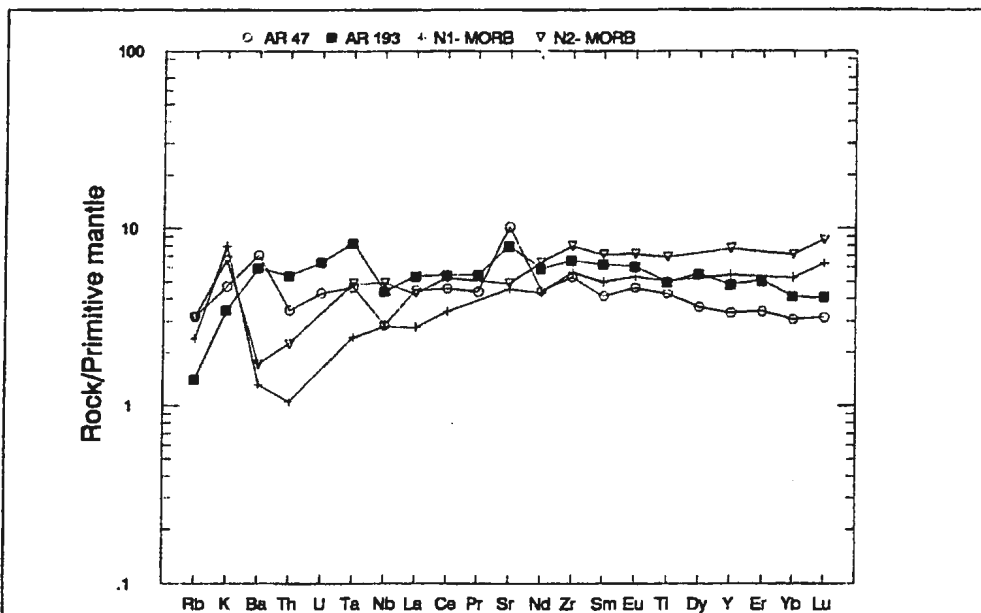


Figure 5.10a: Primitive-mantle normalized extended trace element diagram comparing rocks of the Lady Mary Group with flat to depleted REE patterns and average modern N-MORB subtypes from Viereck et al. (1989). Normalizing factors are from Sun and McDonough (1989).

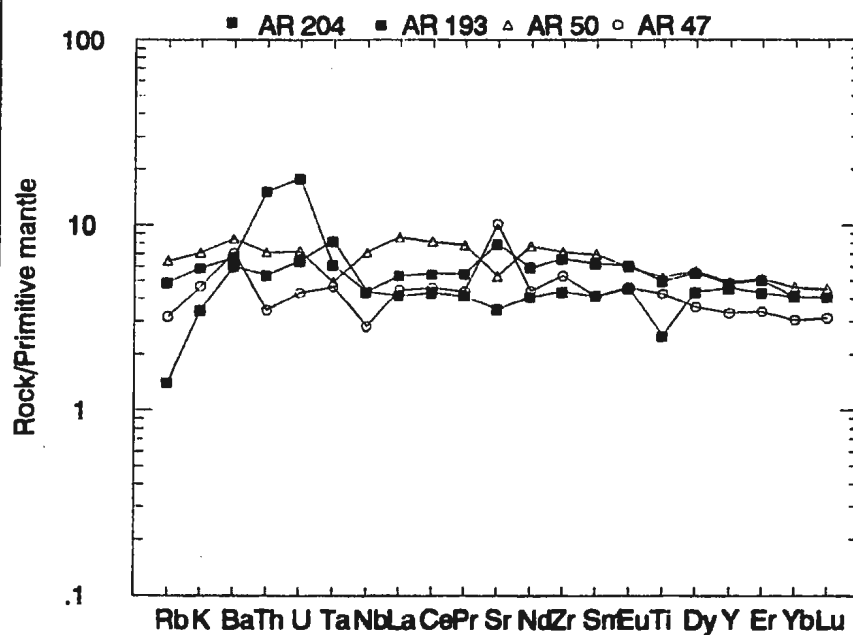


Figure 5.10b: Primitive-mantle normalized extended trace element diagram for mafic rocks from the Lady Mary Group with flat to depleted REE patterns. These rocks show flat patterns, although sample AR 204 has high Th and U, and they lack the Nb-Ta negative anomaly of the LREE-enriched rocks (Figure 5.10c). Normalizing factors as before.

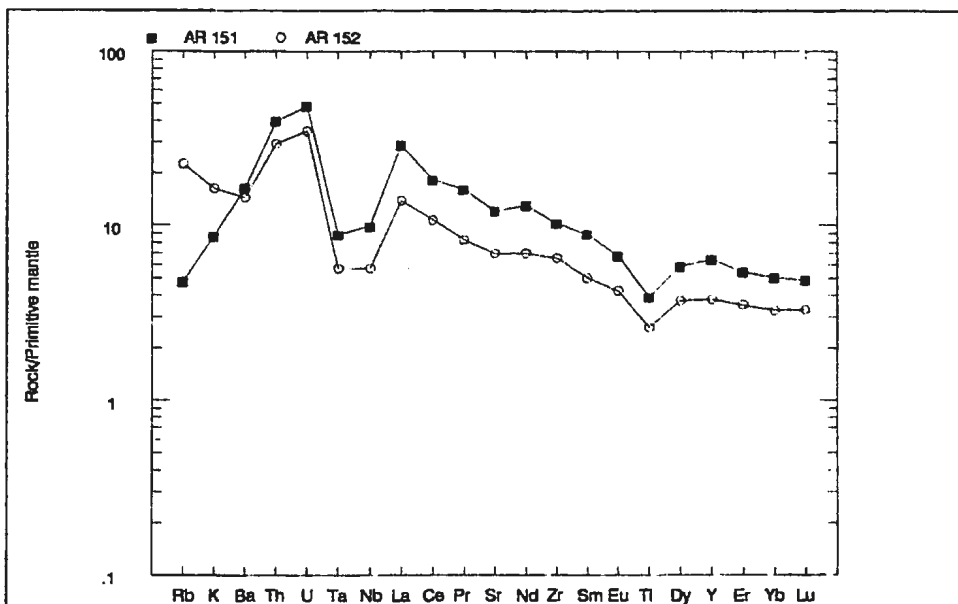


Figure 5.10c: Primitive-mantle normalized extended trace element diagram of the LREE-enriched Belt mafic rocks from the Lady Mary Group that show depletions in TNT elements (Ta, Nb and Ti), relative to other incompatible elements (eg. Th, U and LREE), a common feature of low-K basalts of modern island arcs. Normalizing factors as in Figure 5.10a.

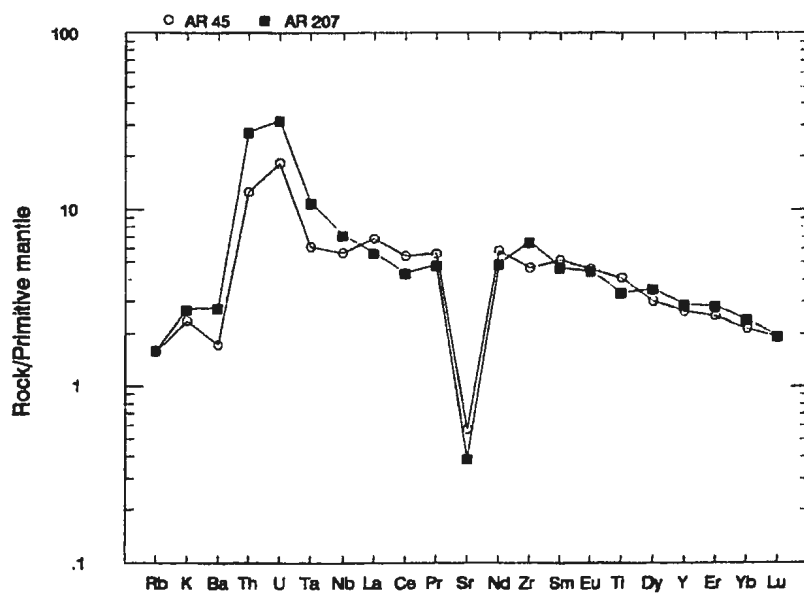


Figure 5.10d: Primitive-mantle normalized extended trace element diagram for komatiitic rocks from the Lady Mary Group. These rocks are depleted in the HREE and Sr; features common to Al-depleted komatiites. Normalizing factors as in Figure 5.10a.

Formation of the Lady Mary Group.

Geochemical features of the basaltic rocks in the Lady Mary Group can be summarised as follows:

(1) Ce/Pb, Rb/Cs and Nb/U ratios average 9, 25 and 33, respectively (Table 5.2). These values are very low compared to those in modern oceanic environments (MORB and OIB) which are fairly constant at 25, 80 and 47 respectively (Newsom et al., 1986; Hoffmann et al., 1986). Ratios for Tati rocks are, however, similar to primitive mantle or Bulk Silicate Earth values (9, 20 and 30 respectively; Hoffmann et al., 1986).

(2) Some Lady Mary Group ultramafic-mafic volcanic rocks have generally elevated concentrations of incompatible elements. High-Mg basalts in Archean greenstone belts generally have elevated contents of incompatible elements (Barley, 1986; Condie, 1985). Condie (1985) suggested that high Th and Zr contents in Archean basaltic rocks, compared to modern island arc basalts, may be related to differences in the degree of partial melting of the source. As such, melting in the Archean would result in the enrichment of these elements in the magma. Barley (1986), however, suggested that elevated contents of incompatible elements in high Mg Archean basalts may be due to secondary processes as Archean high Mg-basalts would be more susceptible to secondary processes (hydrothermal alteration and contamination).

The mafic volcanic rocks in the Archean Tati Greenstone Belt had previously been described as members of the same magmatic suite. The most interesting and

important observation from the geochemical data derived in this study is that different magmatic suites can be identified in the Lady Mary Group. These magmatic suites have geochemical signatures that are similar to those of modern tectonic environments.

The main emphasis of models which suggest that different geodynamic processes occurred in the Archean, as compared to the Phanerozoic, centre around the problem of heat dissipation. Higher heat flow in the Archean is believed to have caused the restriction of komatiites to the Archean. Basaltic komatiites, however, have modern analogues in boninites (Cameron et al., 1979), and, data emerging from recent research on Archean greenstone belts (e.g. Ludden et al., 1984), suggest that komatiite-bearing magmatic suites may not be the oldest rocks in these terranes, but may have been emplaced sometime later in the tectonic cycle. A similar model was suggested for lunar komatiite-like rocks by Ringwood et al. (1986).

A further observation from this study is that geochemical differences between Archean ultramafic-mafic igneous rocks and those of the Phanerozoic tectonic environments may result from an oversimplification of the complex Archean greenstone belt lithostratigraphy, through the averaging of rock compositions from different tectono-magmatic terranes.

5.4 Geochemistry of Granitoids of the Tati Greenstone Belt

5.4.1 Introduction

There are two widely used granitoid classification schemes. The first, proposed

by Chappell and White (1974), subdivides granitoids into genetic subgroups. In this classification, granitoids are commonly subdivided into S-type derived from partial melting of a sedimentary rock protolith, and I-type derived from partial melting of an igneous protolith. Subgroups of the I-type granitoids are M-type, derived from differentiation of juvenile mantle-derived magmas, and A-type, derived from the partial melting of dehydrated re-cycled continental crustal materials (Whalen et al., 1987). Castro et al (1990) further subdivided I and S-types granitoids on the basis of the degree of hybridization between mantle and crustal derived magmas. In this model, granitoids are classified by the type of the dominant component in the hybrid magma. Whalen et al. (1987) pointed out that I and S-type granitoid compositions are dependent on the geochemical signature of the protolith. They further pointed out that in felsic granites ($\text{SiO}_2 > 74 \text{ wt\%}$), the restite component is minimal and mineralogical/ chemical compositions of the different types of the granitoid converge, making classification into I and S subgroups difficult.

The second most widely used granitoid classification is that proposed by Pearce et al. (1984) based on a statistical analysis of compiled chemical data on granitoids from different tectonic settings. In this classification granitoids are subdivided into Within-plate granitoids (WPG), Volcanic-arc granitoids (VAG), Syn-collision granitoids and Oceanic granitoids. The classification of granitoids into these tectonic groups is based on the use of a series of discriminant diagrams.

Both the mineralogical/chemical classification scheme (Chappell and White, 1974) and the chemical tectonic discriminant diagrams (Pearce et al., 1984) are

utilized to describe Tati Greenstone Belt granitoids. Following Mason (1970), Key (1976) classified granitoids of the Tati Greenstone Belt into four groups (G1-G4) on the basis of mineralogical composition, metamorphic characteristics and field relations (Figure 3.2). G1 and G2 granitoids are mainly tonalite plutons and gneisses and were described as the oldest units in the belt. These generally intrude the margins of the Tati Greenstone Belt. G3 granitoids, on the other hand, consist of granites and adamellites, described as having been derived from granitization of the old crustal rocks. G4 granitoids intrude volcano-sedimentary rocks of the belt.

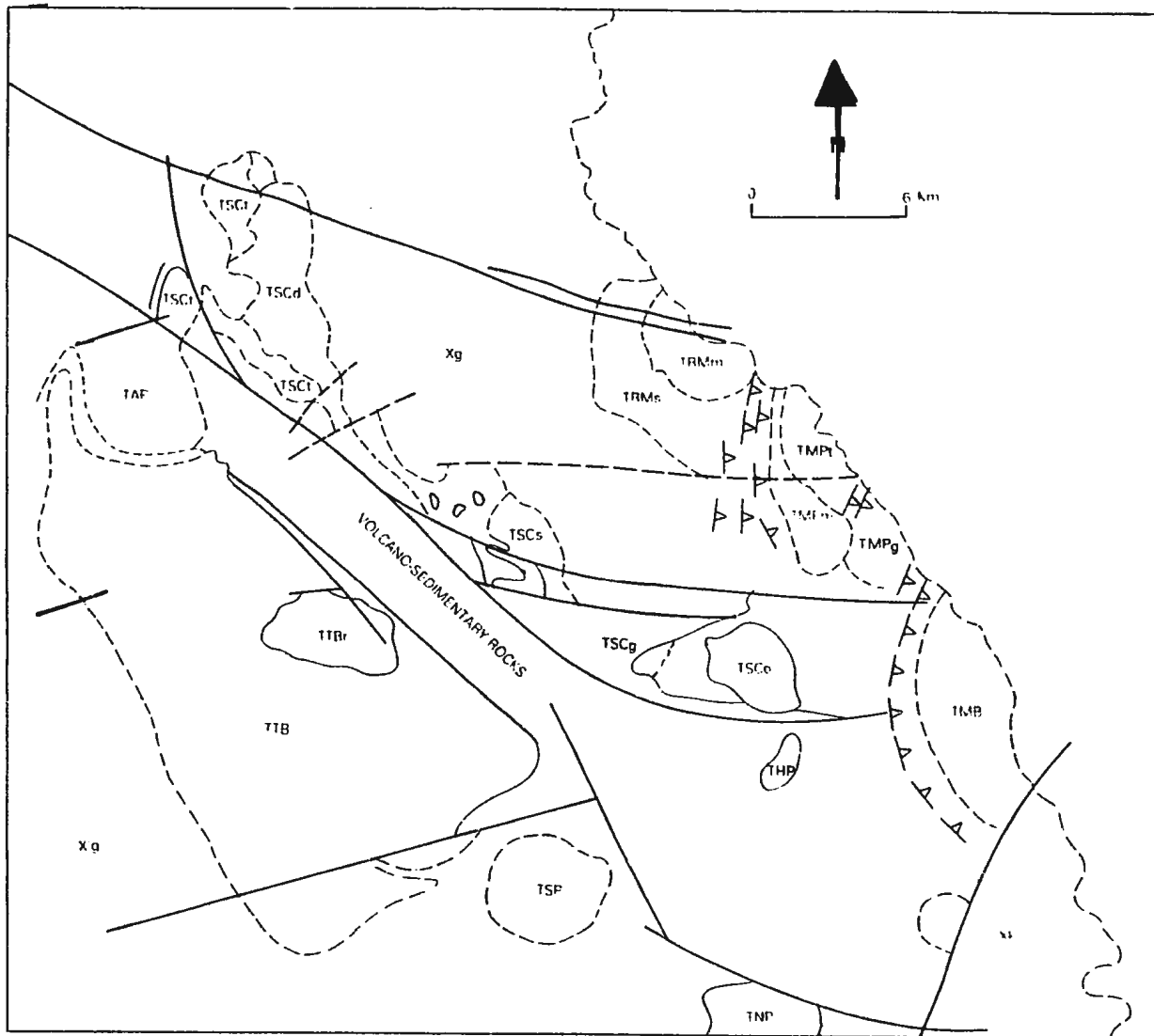
Key's (1976) classification further suggested that granitoids in the Tati Greenstone Belt are homogenous plutons. Based on mapping during this study, this is clearly not the case. Some batholiths, such as the Tati Batholith, are composite bodies consisting of a number of intrusive plutons.

5.4.2 Sampling

This study encompasses the majority of granitoids in the Tati Greenstone Belt (Figure 5.11), including a total of about 10 individual bodies as described in Chapter 3. A total of 35 samples were collected from 9 of the 10 granitoid bodies; the majority of the samples (14) were taken from the Tati batholith.

5.4.3 Major Element Geochemistry

Tati Greenstone Belt granitoids have a wide range of silica contents, from 48.0 wt% to about 77 wt% (Table 5.3). When plotted on Le Maitres' (1989) QAP diagram



Map Legend

TSCt	Nyambabwe Tonalite	Selkirk Igneous Complex
TSCd	Francistown Diorite	
TSCa	Sekukwe Layered body	
TSCg	Selkirk Gabbro	
TSCo	Tekwane Troctolite	
TSC	Undivided plutonic rocks	Mphoeng Plutonic Complex
TMPT	High-mg tonalites	
TMPTm	Coarse-grained granodiorites	
TMPTg	Porphyritic gabbros and pyroxenites	Ramokgwebana Batholith
TRMm	Megacrystic feldspar granite	
TRMe	Undivided plutonic rocks	Hillview Pluton
TNP	Coarse-grained trondhjemite	
TSP	Medium-grained trondhjemites	Southern Tati Pluton
TAP	High-mg granodiorites and granites	Airport Pluton
TNP	Coarse-grained tonalites	New Zealand Pluton
TMB	Grey coarse-grained tonalites	Matsikoje Batholith
TTB	Tonalites, diorites, granodiorites, megacrystic feldspar granites and undeformed alkali granites at the core	Tati Batholith
Xg Xg' Xlc	Gneisses	

Figure 5.11: Geological map of the Tati Greenstone Belt showing the distribution of granitoids.

Table 5.3 Geochemical data for granitoid rocks.

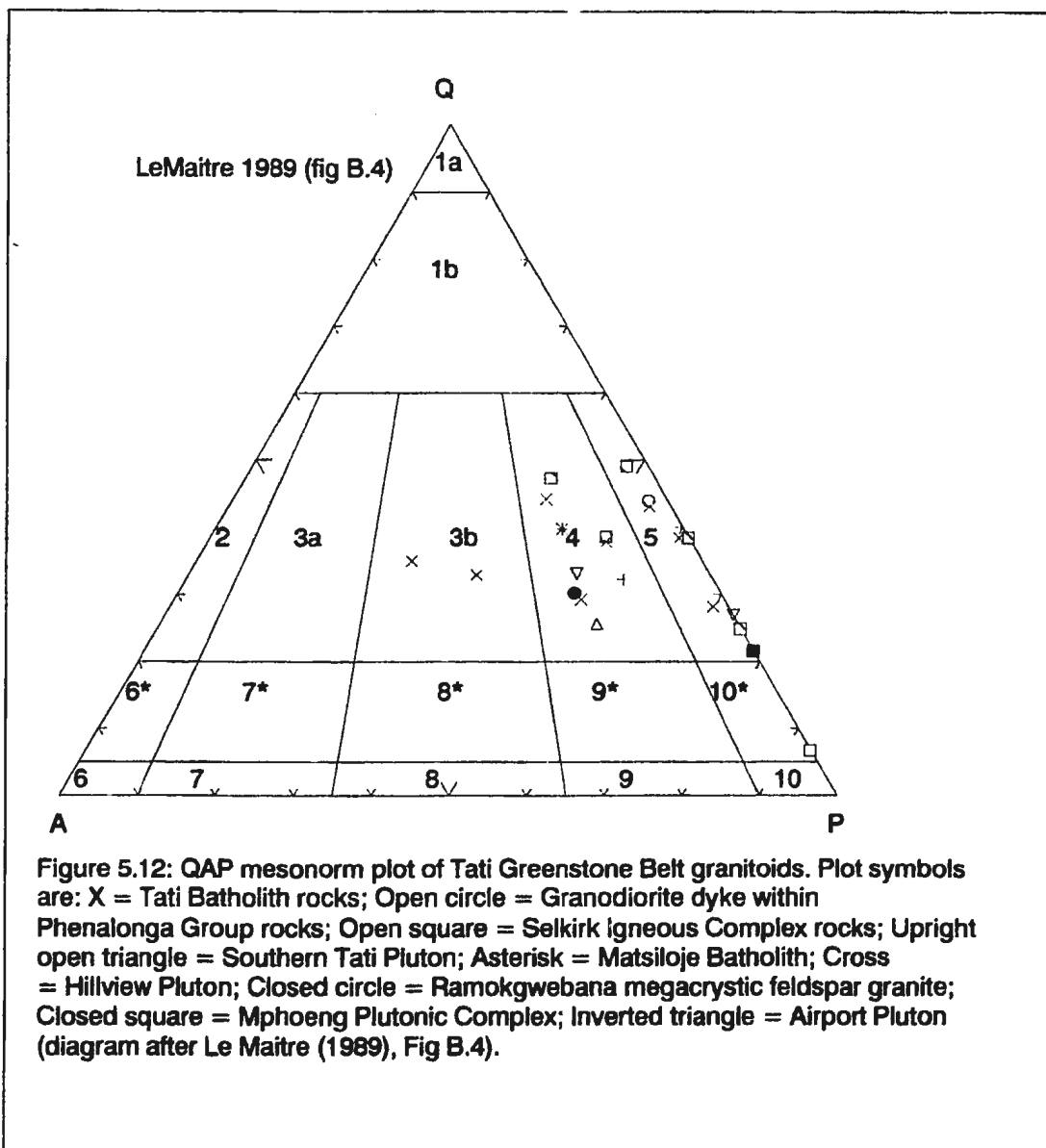
	AR 55	AR 60	AR 65	AR 78	AR 81	AR 86	AR 108	AR 126	AR 128	AR 142	AR 143	AR 145	AR 150	AR 155	AR 181	AR 188	AR 232	AR 234	AR 245	AR 246	AR 71	AR 73	AR 217	AR 227	AR 63	AR 77
Mg#	22.50	42.11	31.84	34.25	29.16	45.51	14.82	31.12	59.89	19.51	31.79	31.22	39.87	31.31	37.81	47.82	44.20	72.21	72.72	44.05	69.86	72.79	72.60	57.82	46.46	39.98
SiO2	72.60	68.80	74.00	51.10	78.50	72.90	75.20	74.80	82.40	72.60	69.90	71.40	69.30	71.30	72.90	71.10	70.30	53.10	55.50	71.00	53.40	51.60	55.10	48.00	60.20	48.90
TiO2	0.24	0.72	0.32	1.24	0.20	0.32	0.32	0.28	0.52	0.40	0.40	0.56	0.40	0.36	0.16	0.24	0.32	0.36	0.36	0.28	0.28	0.24	0.36	0.50	0.88	1.83
Al2O3	13.10	14.10	12.80	14.10	11.50	13.40	10.80	12.70	14.30	12.60	15.40	12.30	16.00	14.40	13.00	15.30	14.10	17.30	17.20	14.10	16.20	15.90	17.10	21.70	15.20	14.00
Fe2O3	0.19	0.45	0.25	1.59	0.26	0.25	0.47	0.21	0.88	0.29	0.26	0.40	0.22	0.28	0.14	0.12	0.24	0.59	0.58	0.24	0.65	0.69	0.57	0.71	0.69	1.34
FeO	1.55	3.68	2.02	12.87	2.07	2.02	3.84	1.87	7.90	2.32	2.07	3.22	1.79	2.25	1.12	0.89	1.90	4.78	4.68	1.94	5.28	5.59	4.65	5.71	5.58	10.81
MnO	0.03	0.06	0.03	0.19	0.06	0.05	0.05	0.03	0.17	0.06	0.05	0.05	0.03	0.04	0.04	0.03	0.04	0.08	0.08	0.04	0.11	0.13	0.08	0.11	0.12	0.17
MgO	0.28	1.68	0.69	4.18	0.53	1.05	0.41	0.47	7.39	0.35	0.60	0.81	0.74	0.64	0.42	0.56	0.94	7.74	7.74	0.95	7.63	8.32	7.68	4.88	3.27	4.49
CaO	1.20	3.68	2.48	8.10	2.04	2.18	2.56	2.38	7.76	0.94	2.10	2.38	2.20	2.70	1.24	2.32	2.22	6.70	6.68	2.16	12.94	12.92	8.78	13.08	5.06	10.60
Na2O	3.46	4.08	4.28	2.83	3.21	4.17	4.11	4.55	3.82	2.48	4.41	2.85	4.86	3.89	4.04	4.84	4.44	2.44	2.42	4.11	1.80	1.41	2.43	1.85	3.82	2.90
K2O	5.09	1.49	1.14	0.38	2.66	2.53	0.81	1.03	0.20	6.49	3.60	3.43	3.58	2.48	2.86	2.28	3.47	2.45	2.31	3.46	0.13	0.18	2.40	0.14	1.95	0.36
P2O5	0.05	0.17	0.05	1.83	0.07	0.09	0.16	0.06	0.08	0.08	0.12	0.29	0.19	0.10	0.02	0.13	0.29	0.12	0.14	0.15	0.04	0.01	0.14	0.03	0.18	2.15
LOI	0.45	0.53	1.50	0.76	0.70	1.22	0.50	0.86	1.78	0.73	0.25	0.36	0.48	0.56	2.83	1.02	0.75	2.27	2.33	0.64	1.06	1.31	2.28	1.94	0.86	0.47
TOTAL	98.24	99.50	99.44	99.37	99.79	100.18	99.23	99.01	97.28	99.31	99.15	98.14	99.75	99.03	98.87	98.83	99.01	97.93	99.97	99.06	99.52	99.30	99.57	98.64	97.83	97.82
Cr	35.00	62.00	35.00	74.00	39.00	30.00	64.00	33.00	234.00	21.00	29.00	50.00	21.00	28.00	14.00	18.00	29.00	188.00	194.00	28.00	---	---	---	---	---	---
Ni	4.00	17.00	7.00	2.00	6.00	11.00	3.00	7.00	81.00	4.00	6.00	8.00	8.00	4.00	8.00	11.00	12.00	340.00	339.00	13.00	---	---	---	---	---	---
Sc	2.00	8.00	5.30	---	3.50	---	---	---	40.86	---	---	6.60	2.87	---	3.00	1.45	4.00	11.00	10.59	---	44.86	---	---	---	14.64	37.33
V	10.00	70.00	24.00	148.00	22.00	33.00	5.00	19.00	248.00	6.00	21.00	47.00	30.00	23.00	8.00	13.00	35.00	76.00	73.00	30.00	---	---	---	---	---	---
Cu	17.00	11.00	11.00	8.00	12.00	15.00	10.00	15.00	18.00	15.00	18.00	14.00	19.00	46.00	34.00	15.00	26.00	53.00	53.00	27.00	---	---	---	---	---	---
Pb	40.00	8.00	2.00	1.00	17.00	16.00	3.00	3.00	---	36.00	26.00	23.00	22.00	12.00	16.00	19.00	30.00	16.00	16.00	30.00	1.55	---	---	0.49	---	---
Zn	50.00	60.00	30.00	80.00	45.00	47.00	29.00	23.00	51.00	68.00	69.00	57.00	63.00	52.00	39.00	49.00	56.00	56.00	56.00	52.00	---	---	---	---	---	---
B	0.12	0.13	0.02	---	0.04	---	---	---	0.02	---	---	0.10	0.09	---	0.03	0.08	---	0.31	0.33	---	---	---	---	---	---	---
Mn	1.42	0.89	0.82	---	1.06	---	---	---	0.15	---	---	1.34	0.72	---	0.62	0.73	---	3.32	3.81	---	0.50	---	---	0.16	0.65	0.84
Rb	259	86	35	12	65	79	24	32	2	193	173	125	102	91	144	75	163	115	116	162	2	---	---	3	---	10
Ca	3.28	4.67	0.36	---	1.38	---	---	---	0.05	---	---	1.73	1.52	---	1.73	3.49	---	5.46	5.66	---	0.10	---	---	0.31	5.73	0.28
Ba	759.86	444.80	400.68	---	483.80	---	---	---	26.80	---	---	917.00	1007.00	---	543.00	1232.00	---	490.00	504.00	---	60.88	---	---	34.72	338.90	135.81
Sr	106.00	257.00	181.00	218.00	82.00	262.00	104.00	184.00	151.00	68.00	159.00	218.00	493.00	225.00	101.00	430.00	314.00	251.00	252.00	317.00	176.76	---	---	143.32	288.35	228.87
Ga	16.00	18.00	13.00	17.00	13.00	15.00	15.00	14.00	17.00	23.00	19.00	22.00	18.00	15.00	18.00	20.00	20.00	14.00	15.00	20.00	---	---	---	---	---	---
L	51.35	108.53	5.84	---	37.25	---	---	---	6.08	---	---	20.18	24.39	---	3.55	54.40	---	29.23	32.15	---	7.61	---	---	11.60	185.22	8.70
Ta	1.37	0.65	0.84	---	1.82	---	---	---	0.10	---	---	1.99	0.33	---	1.23	0.31	---	0.76	0.75	---	0.08	---	---	1.11	0.53	0.26
Nb	17.00	9.00	9.00	5.00	11.00	4.00	15.00	8.00	3.00	15.00	19.00	19.00	4.00	9.00	9.00	3.00	6.00	4.00	5.00	6.00	0.99	---	---	0.97	6.08	3.29
Zr	248.00	200.00	188.00	81.00	179.00	103.00	382.00	178.00	450.00	361.00	160.00	450.00	163.00	223.00	91.00	116.00	158.00	108.00	111.00	155.00	16.19	---	---	7.91	62.78	33.54
Y	26.0	17.0	22.0	29.0	23.0	4.0	36.0	21.0	19.0	34.0	10.0	26.0	2.0	5.0	18.0	1.0	4.0	7.0	6.0	4.0	6.7	---	---	8.0	20.8	28.8
Th	75.0	12.0	16.0	1.0	26.0	6.0	15.0	18.0	1.0	86.0	19.0	55.0	---	21.0	11.0	2.0	18.0	20.0	18.0	17.0	0.8	---	---	0.2	3.1	2.2
U	11.0	1.0	2.0	---	3.0	2.0	2.0	2.0	0.3	2.0	2.0	5.0	4.0	1.0	3.0	0.8	4.0	6.0	5.0	5.0	0.2	---	---	---	2.0	0.7
La	75.01	50.84	26.78	---	35.41	---	---	---	3.30	---	---	127.63	26.57	---	14.24	10.66	---	24.13	23.84	---	3.99	---	---	1.61	25.34	21.10
Ce	147.66	77.46	52.90	---	60.51	---	---	---	7.89	---	---	232.48	49.43	---	27.21	20.02	---	48.66	44.77	---	8.07	---	---	4.00	40.21	45.81
Pr	15.83	8.89	5.56	---	5.99	---	---	---	1.09	---	---	23.45	5.30	---	2.94	2.42	---	5.28	5.07	---	1.00	---	---	0.60	5.67	8.13
Nd	51.91	30.54	19.13	---	20.06	---	---	---	5.04	---	---	76.20	18.46	---	10.68	8.40	---	19.03	18.48	---	4.14	---	---	2.67	22.37	27.57
Sm	8.38	5.04	3.43	---	3.84	---	---	---	1.56	---	---	11.06	2.95	---	2.46	1.57	---	3.41	3.37	---	0.88	---	---	1.00	4.45	8.18
Eu	0.59	1.35	0.89	---	0.57	---	---	---	0.50	---	---	1.59	0.81	---	0.47	0.41	---	0.74	0.77	---	0.41	---	---	0.47	1.44	2.10
Gd	6.32	4.43	3.47	---	4.24	---	---	---	2.14	---	---	9.01	2.48	---	2.86	1.27	---	2.91	3.13	---	1.19	---	---	1.28	4.26	6.94
Tb	0.79	0.59	0.51	---	3.58	---	---	---	0.38	---	---	0.96	0.21	---	0.43	0.11	---	0.33	0.30	---	0.18	---	---	0.22	0.63	0.89
Dy	4.29	3.34	3.29	---	3.64	---	---	---	2.59	---	---	5.22	0.97	---	2.68	0.60	---	1.67	1.78	---	1.16	---	---	1.47	3.74	5.23
Hf	0.80	0.65	0.67	---	0.76	---	---	---	0.58	---	---	0.99	0.15	---	0.54	0.10	---	0.32	0.31	---	0.25	---	---	0.31	0.75	1.00
Er	2.22	1.75	1.99	---	2.38	---	---	---	1.69	---	---	2.88	0.41	---	1.70	0.21	---	0.81	0.80	---	0.78	---	---	0.85	2.08	2.83
Tm	0.32	0.24	0.29	---	0.36	---	---	---	0.25	---	---	0.42	0.06	---	0.26	0.04	---	0.13	0.13	---	0.11	---	---	0.13	0.30	0.37
Yb	2.02	1.57	1.85	---	2.47	---	---	---	1.68	---	---	2.70	0.33	---	1.80	0.21	---	0.75	0.78	---	0.88	---	---	0.88	1.93	2.25
Lu	0.30	0.25	0.28	---	0.38	---	---	---	0.24	---	---	0.39	0.05	---	0.27	0.03	---	0.12	0.12	---	0.11	---	---	0.13	0.28	0.36

--- denotes not analysed for.

(Figure 5.12), Tati Greenstone Belt granitoids fall in the tonalite-granodiorite-monzogranite fields. O'Conner (1965) modified the Ab-Or-An ternary diagram in order to classify granitoids on the basis of the type of feldspar. On O'Conner's (1965) diagram (Figure 5.13), the Tati Greenstone Belt granitoids fall within the tonalite-trondhjemite-granodiorite-granite fields. On a K-Na-Ca ternary diagram (Figure 5.14), these rocks show both sodic (Na-enrichment) and potassic (K-enrichment) trends of Hunter (1979). These two trends, suggest the possible presence of different petrogenetic suites.

Granitoids with a sodic trend (AR 60, 63, 128, 150, 188, 234 and 245) generally have high normative Ab (32-42 wt%), and wide range of normative Or, from zero to 19 wt%. These granitoids also have alumina values of 14.1-17.3 wt% with silica ranges of 52.4-71.1 wt%. The K_2O/Na_2O ratios of these rocks are low, < 0.75 . A subgroup of these alumina-rich granitoids (AR 234 and 245) have moderately high Mg-numbers (60-73), relatively low silica contents (53.1-55.5 wt%), and alumina values greater than both Na_2O+K_2O and $CaO+Na_2O+K_2O$ values. These granitoids have virtually no normative Or, comparatively low Ab (21-22 wt%), low normative Q, and high modal mafic mineral contents. Although the main mafic minerals are biotite and hornblende in these rocks, hypersthene is also present in small amounts.

The second group of granitoids follow the potassic trend on the K-Na-Ca diagram (Figure 5.14) (samples AR 55, 65, 81, 142, 143, 145, 181, 232 and 246). They have relatively low alumina values (10.8-14.1 wt%), with silica contents ranging between 69.9 to 76.5 wt%. Although these granitoids have widely variable K_2O/Na_2O



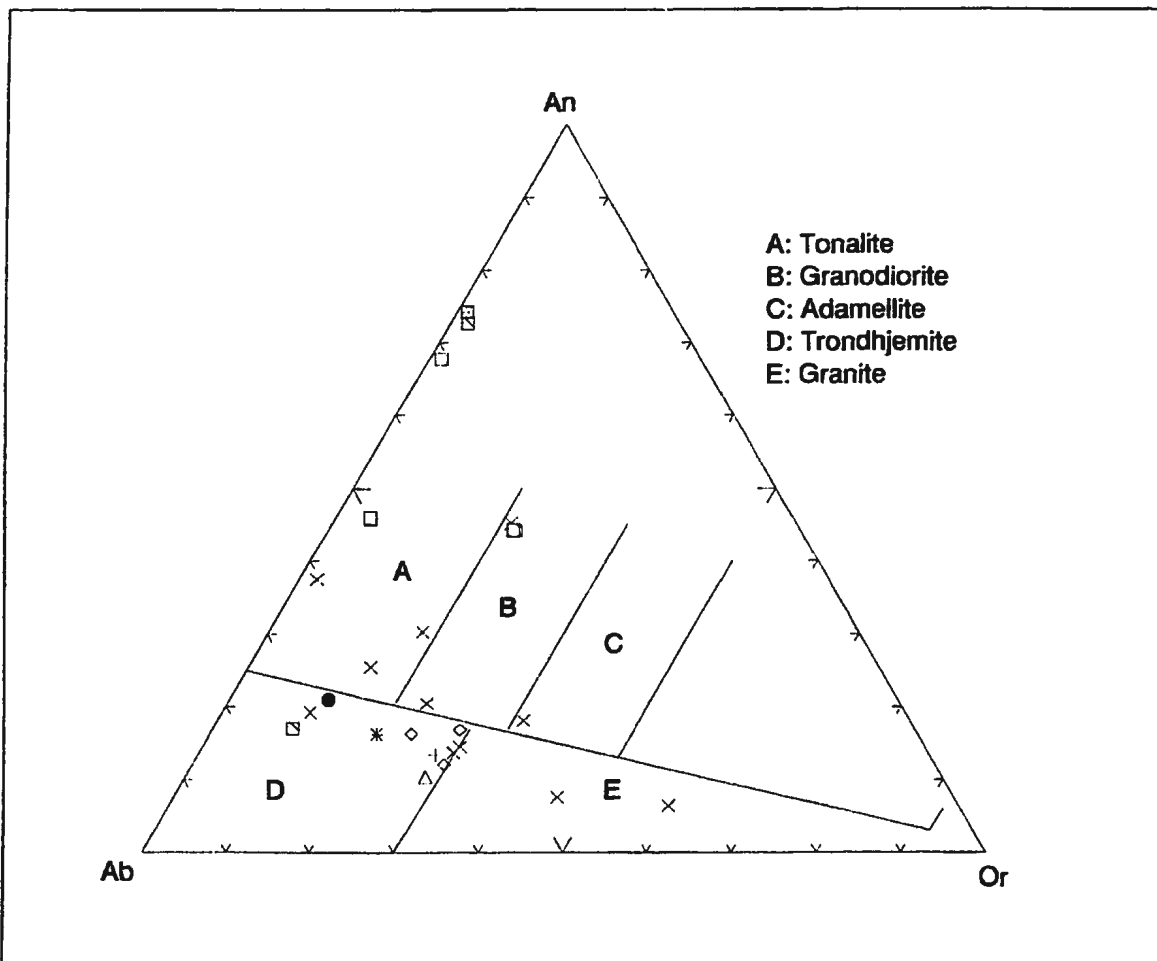


Figure 5-13: O'Conner's (1965) Ab-Or-An norm ternary plot for Tati Greenstone Belt granitoids. Most of the rocks plot near the field boundaries of tonalite-trondhjemite-granodiorite (TTG) and and trondhjemite-granite. Symbols are Tati Batholith (crosses), Airport pluton (open circles), northern part of the belt (open diamond), Selkirk Igneous Complex (filled squares), Mphoeng Pluton Complex (open squares), Matsiloje Batholith (open triangles), Hillview Pluton (*), Trondhjemite dyke (solid circle) and Southern Tati Pluton (+).

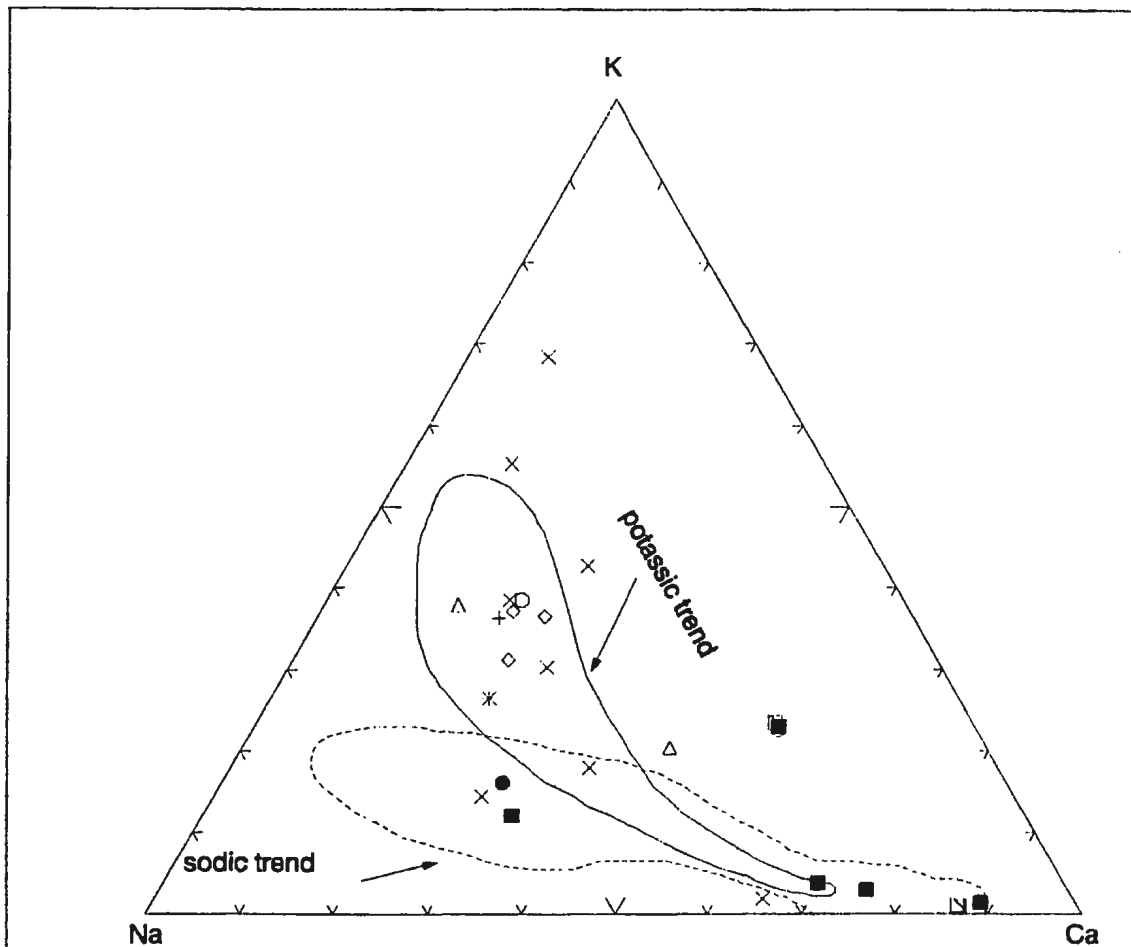


Figure 5.14: K-Na-Ca ternary plot (after Nockolds and Allan, 1953) of Tati Greenstone Belt granitoids. These rocks define two trends towards either the Na or K corners. The solid and dashed outlines define the potassic and sodic trends of the Ancient gneisses of Swaziland and within greenstone belt granitoids of the Zimbabwe Craton, respectively, as defined by Hunter (1979).

Symbols are Tati Batholith (x), Airport Pluton (o), Selkirk Igneous Complex (solid squares), Granitoids north of the belt (open diamond), Mphoeng Plutonic Complex (open squares), Hillview Pluton (*), Southern Tati Pluton (+) trondhjemite dyke (solid circle) and Matsiloje Batholith (open triangle).

ratios, most of the samples have generally high ratios (>0.75). Normative Or is also quite variable (10-29 wt%), whereas normative Ab and Q are relatively very high at 22-38 wt% and 30-43 wt%, respectively. These are two feldspar granitoids and they plot within the granodiorite-monzogranite fields (Figure 5.12).

A subgroup of these granitoids have silica contents between 71.4 and 72.6 wt%. These are the only granitoids (Samples AR 55, AR 142 and AR 145) in the belt with K_2O contents higher than Na_2O contents. They also have very low Mg-numbers (22.5-31.2) and the lowest alumina contents (12.3 to 13.1 wt%) of all granitoids of the Tati Greenstone Belt.

All of the Tati Greenstone Belt granitoids contain average molecular $Al_2O_3/(CaO+Na_2O+K_2O)$ ratios of 1.09 ± 0.33 and have $Al_2O_3/(Na_2O+K_2O)$ ratios >1 . The molecular ratios $K_2O/(K_2O+Na_2O)$ are less than 0.35, with an overall average ratio of 0.26 ± 0.15 . According to the classification scheme of Debon and Le Fort (1988), such a ratio indicates that these rocks are sodic granitoids. The chemistry of these rocks is therefore, consistent with the observations of Hunter (1979) that greenstone-related granitoids are generally sodic.

The two main groups of Tati Greenstone Belt granitoids are similar to Arth's (1979) high and low alumina-type granitoids. High alumina-type granitoids contain $Al_2O_3 > 15$ wt% at 70 wt% SiO_2 . The low alumina-type group, on the other hand, has Al_2O_3 less than 14 wt% at 75 wt% SiO_2 . Using this concept, Barker (1979) subdivided Archean granitoid complexes into high and low alumina-types trondhjemites. The Tati Greenstone Belt granitoids with strong Na-enrichment (including high-Mg plutons)

would be collectively grouped under the high alumina-type granitoid class, and fall within the tonalite-trondhjemite field (Figure 5.12). Granodiorites of this group are relatively Or-poor. Gabbros and diorite plutons typical of the Tati Greenstone Belt that are associated with the more silicic granitoids, generally contain high CaO, Na₂O and Al₂O₃ contents and are, therefore, part of the high alumina-type granitoid group. The features of the high and low alumina-type granitoids of Tati Greenstone Belt are summarized on the Al₂O₃ versus Yb diagram (Figure 5.15).

5.4.4 Trace Element Geochemistry

Tati Greenstone Belt granitoids, although divided into high and low alumina-types, are generally sodic granitoids with the dominant feldspar being plagioclase. Trace element contents, such as Sr, Ba and Rb, in these rocks vary little between the main groups; the variations in the granitoids are summarised on plots of K-Rb, Ba-Rb, Rb-Sr and Sr-Ba (Figures 5.16a-d).

The K-Rb plot (Figure 5.16a) illustrates the covariation of the two elements, from lower abundances in mafic rocks (gabbros, diorites and mafic tonalites) to high contents in the monzogranites. The majority of the rocks, especially tonalites, trondhjemites, granodiorites and monzogranites, cluster around the high K and high Rb area on the K-Rb plot, irrespective of the geographic location. In general, K/Rb ratios for all granitoids fall between 100 and 500. The mafic tonalite unit of the Tati batholith (sample 128), however, has a much higher K/Rb ratio than the highest limit for the rest of the granitoid rocks (ca 1000). Although, the K/Rb ratio of this sample

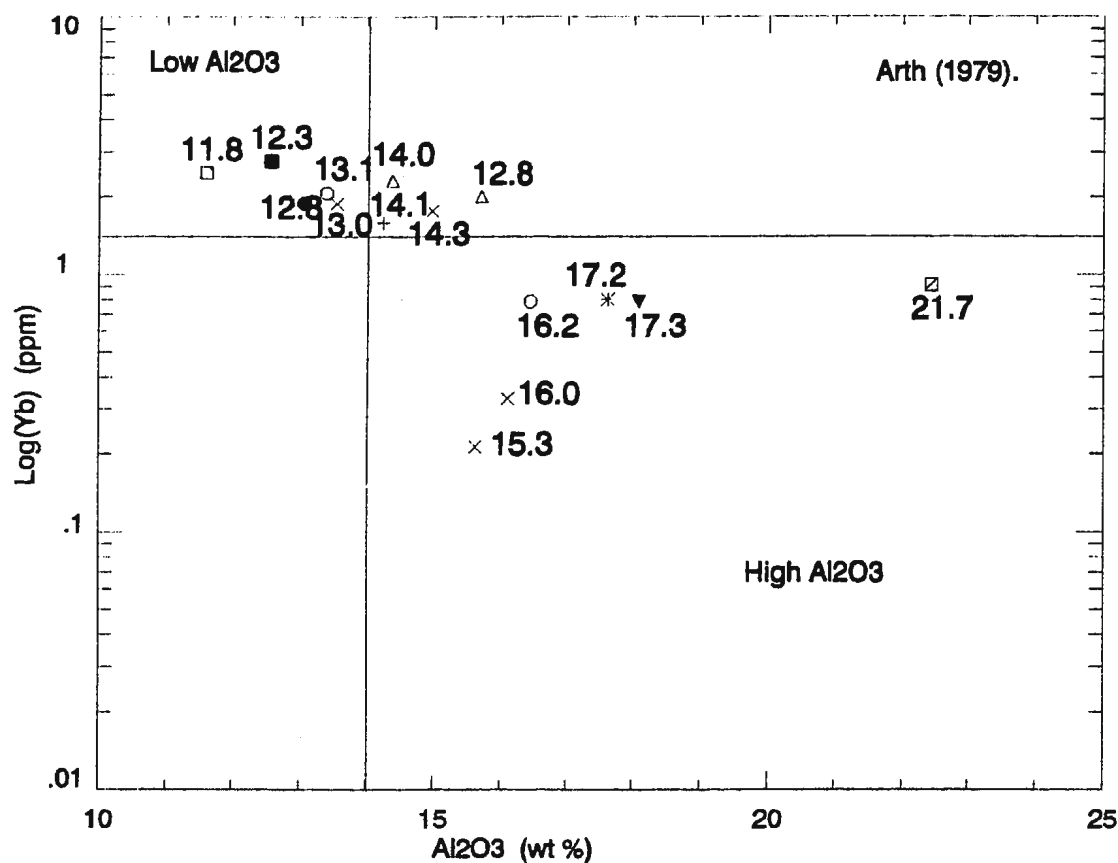
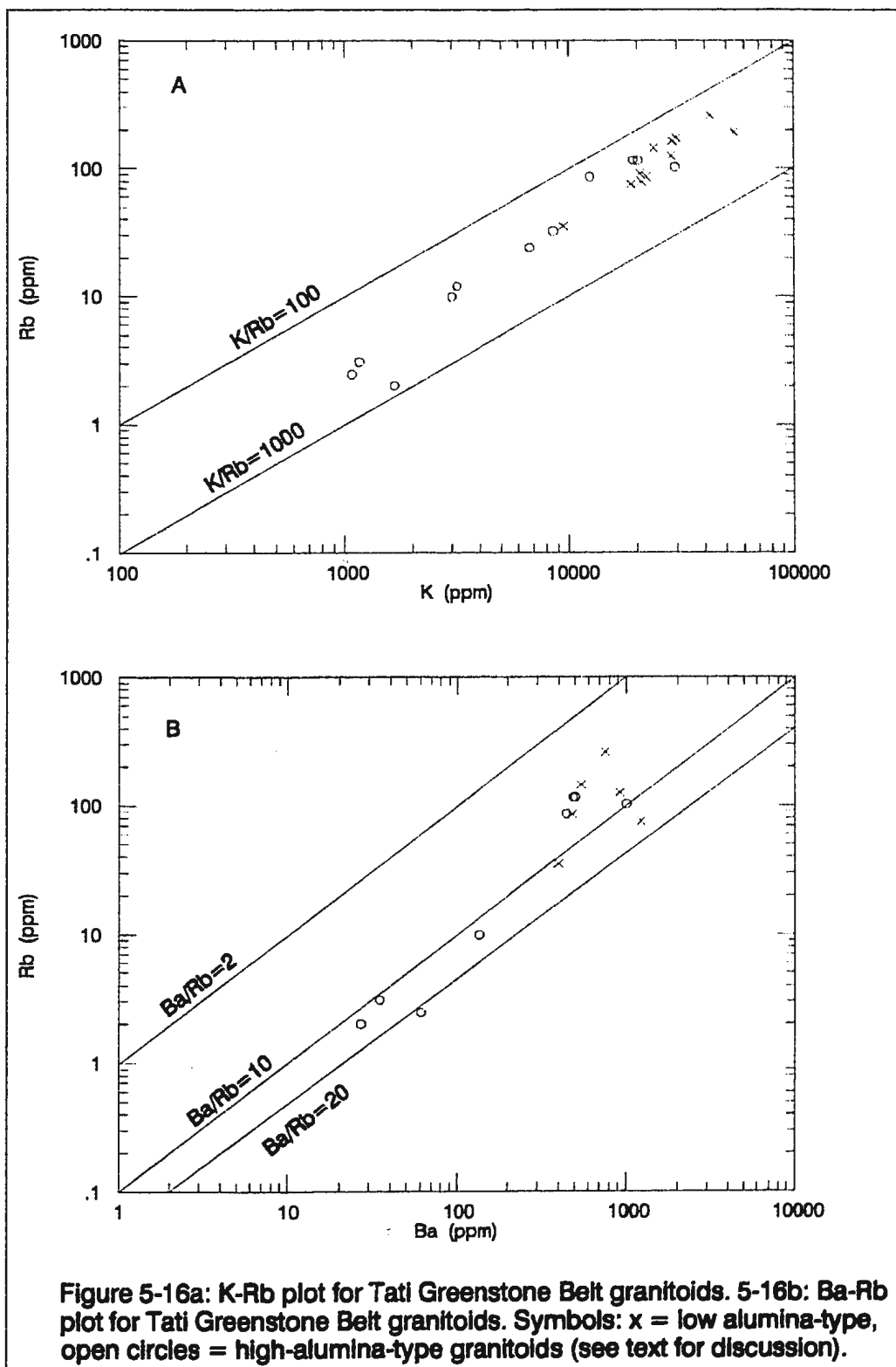
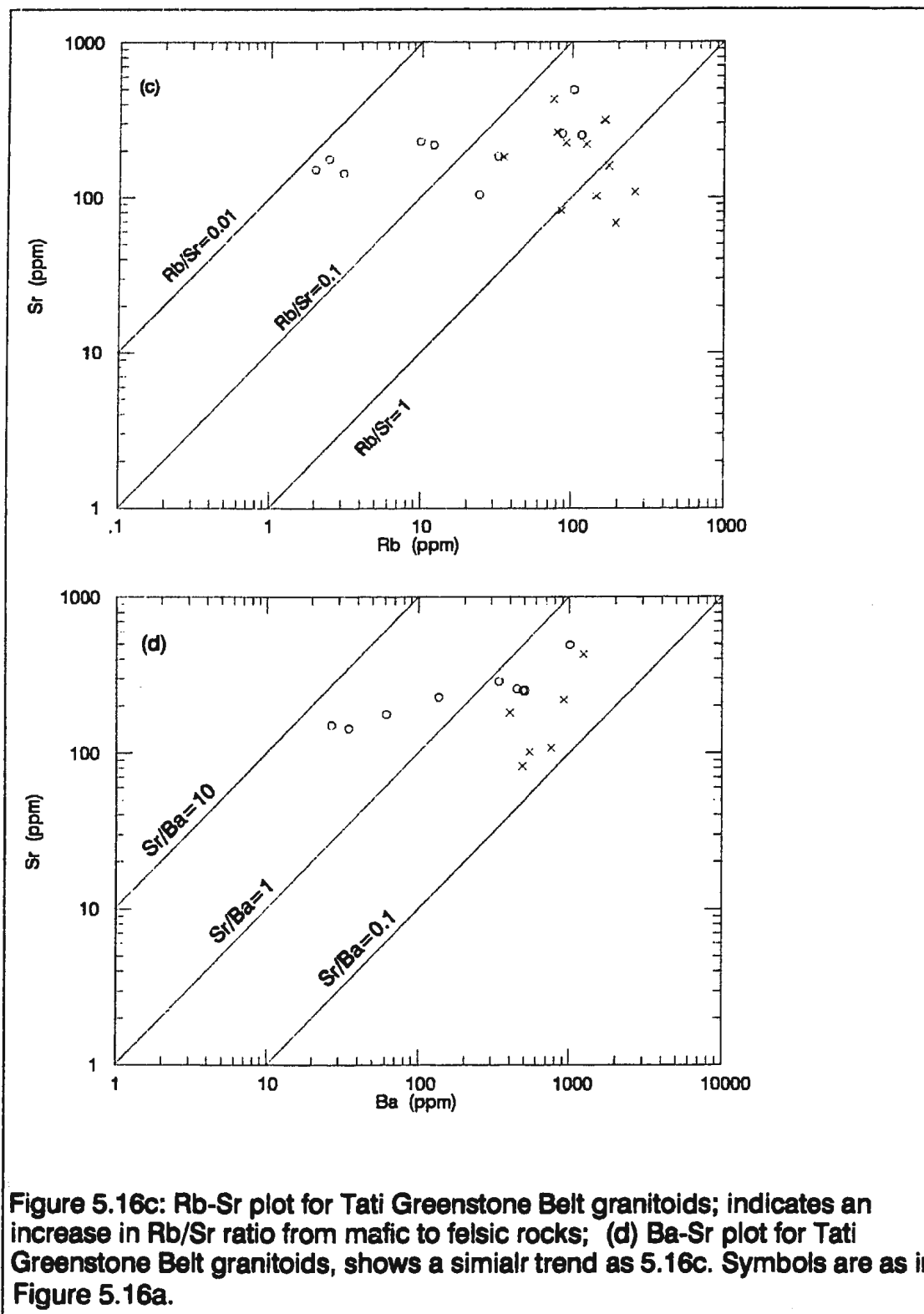


Figure 5.15: Yb vs Al₂O₃ diagram showing the subdivision of Tati Greenstone Belt granitoids into low and high alumina types. The dotted vertical line is the original field boundary at 14.5 wt% Al₂O₃ defined by Arth (1979). The field boundary is shifted to 14 wt% for the Tati rocks, so that it encloses only those rocks that have true low alumina-type characteristics as indicated by other geochemical features. Alumina values (in wt %) are plotted next to plot symbols; symbols as on Figure 5.12.





is very high, its K content is low and, hence, the high ratio is a result of extremely low Rb content. Except for the mafic and potassic units of the Tati granitoids, the increase in the K-Rb contents does not show any systematic relationship to the increase in SiO_2 contents.

The Ba-Rb diagram (Figure 5.16b) also demonstrates the covariation of the two elements from mafic granitoids to the sodic and potassic varieties. The Ba/Rb ratios of Tati granitoids fall between 2 and 20. The Rb-Sr and Ba-Sr diagrams (Figure 5.16c and 5.16d) are the only alkali and alkali earth element diagrams that reveal any correspondence to the granitoid subdivisions. In general, the Sr/Ba ratios (Figure 5.16d) decrease from about 10 in the mafic varieties to between 1 and 0.1 in the sodic and potassic units. The high-Mg sodic granitoids of the high alumina-type contain very low Rb/Sr, whereas this ratio is relatively high in the potassic units of the low-alumina type granitoids. Low alumina-type granitoids have the highest contents of Ba, Rb, Zr, Nb and Pb. They also have comparatively enriched contents of Sr, U and Y. The transition metals Ni and Cr are relatively low. High alumina-type granitoids, on the other hand, generally, contain high values of Ba and Sr. They also contain moderately high values of Ni, Cr, Zr and V and very low values of Th, U, Y, and Rb. The high-Mg subgroup contain the highest Ni and Cr values of all granitoids in the Tati Greenstone Belt (Table 5.3). Sr, Ba, Zr and Rb contents are also comparatively high in this subgroup.

5.4.5 Rare Earth Element Geochemistry

Most of the high alumina-type granitoids of the Tati Greenstone Belt contain relatively low contents of the total REE (sum of total REE < 130); only sample AR 60 has higher total REE at 187. Chondrite-normalized REE diagrams for the Tati Greenstone Belt granitoids are presented in Figure 5.17(a-b). The REE patterns indicate that the granitoids can be divided into two main groups, which correspond to the high and low-alumina types described above. High alumina-type granitoids have highly fractionated REE patterns with $(La/Yb)_n$ ratios ranging from 22 to 38 (Figure 5.17a) and relatively low total REE contents. La_n ranges from about 45 to 110x and Yb_n from 1.2 to 5x chondrite abundance. These granitoids are highly depleted in HREE and contain a recognizable positive Eu anomaly.

Low alumina-type granitoids have higher total REE contents, ranging from La_n of about 60x to as much as 600x, and $(Yb)_n$ between about 10x and 15x chondritic abundance. They also have relatively fractionated REE patterns on chondrite-normalized plots. $(La/Yb)_n$ ratios for these granitoids vary between 6 and 34 (Figure 5.17b). These granitoids also contain pronounced negative Eu anomalies (Eu/Eu^* between 0.2 and 0.4).

The low alumina-type granitoids generally intrude high alumina-type granitoids. These latter granitoids are in contact with mafic volcanic rocks. Such relationships are well illustrated by the composite Tati Batholith. REE patterns for samples from the Tati batholith indicate a progressive change in total REE contents as REE slopes (Figure 5.18) increase with silica content, from flat patterns in mafic tonalites (e.g.

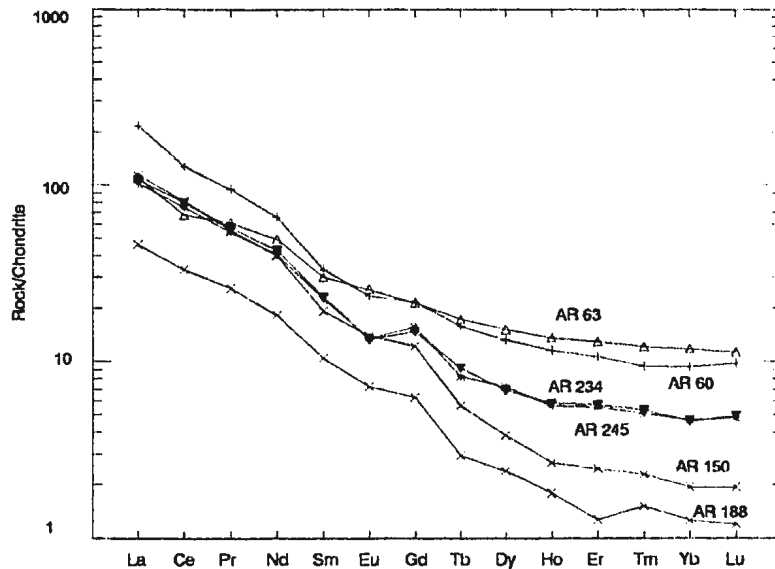


Figure 5.17a: Chondrite-normalized REE diagram for the high alumina-type granitoids of Tati Greenstone Belt (normalizing values from Sun and McDonough (1989)).

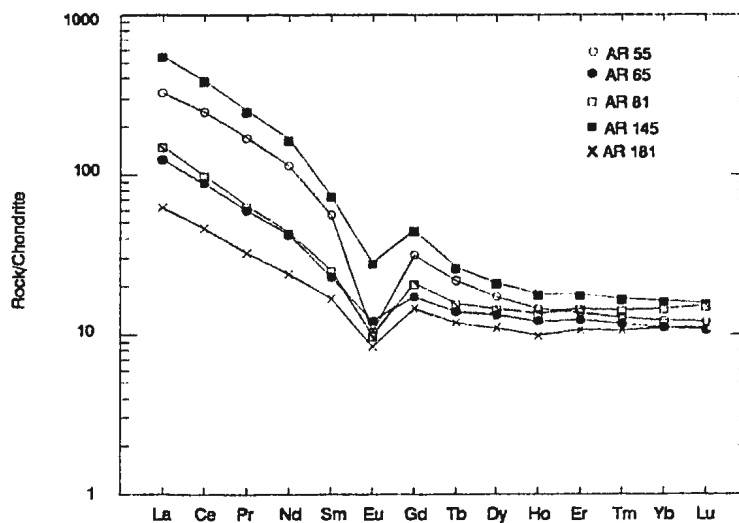
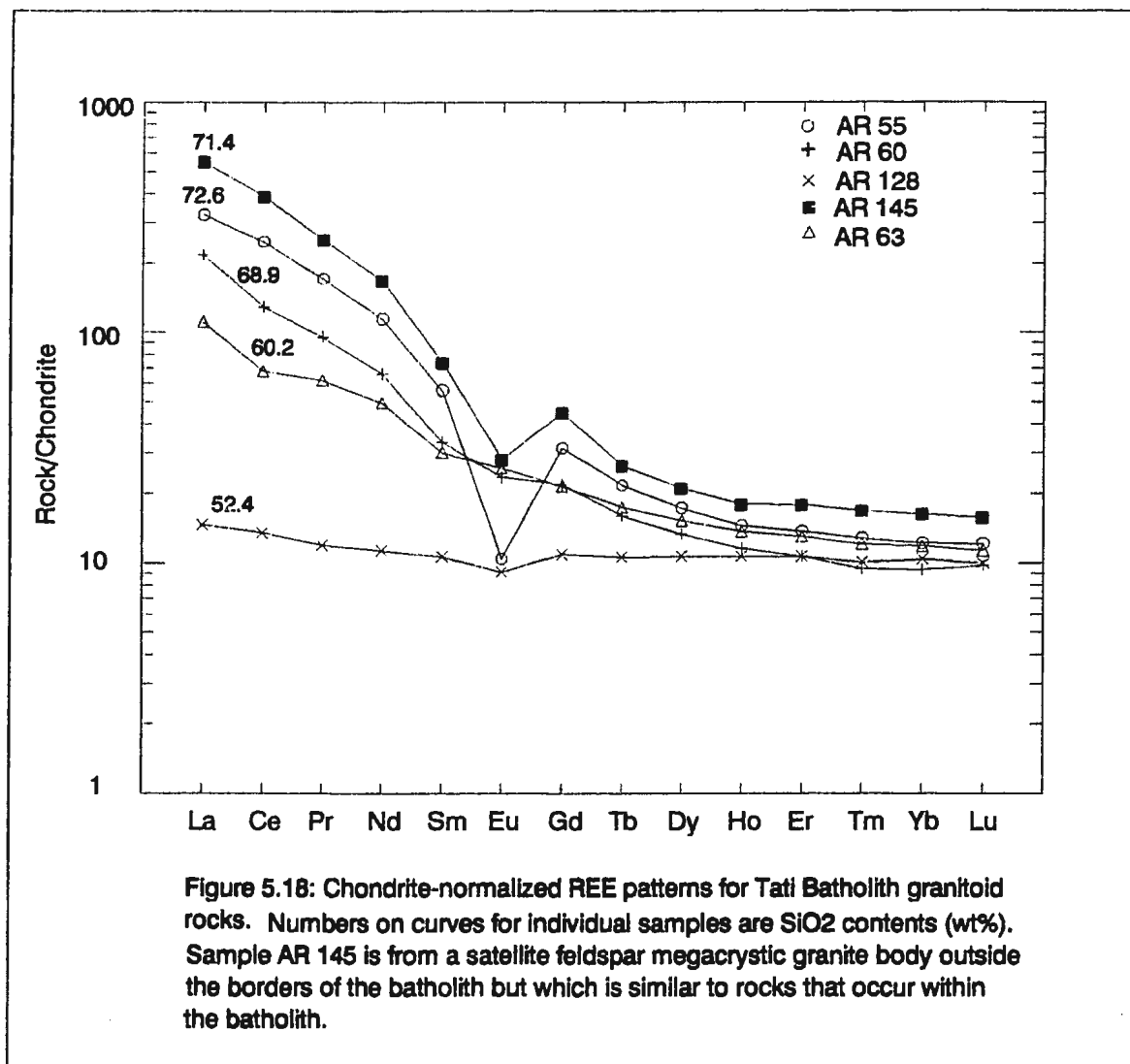


Figure 5.17b: Chondrite-normalized REE diagram for low alumina-type Tati Greenstone Belt granitoids (normalizing values from Sun and MacDonough (1988)). Samples AR 55 and AR 145 have K/Na ratios of 1.5 and 1.3, respectively, and compared to the other samples, they have the largest negative Eu anomalies. While samples with the greatest negative Eu anomalies generally have higher SiO₂ contents, there is no positive correlation between SiO₂ and Eu/Eu*.



AR 128); Eu anomalies also increase with silica in this batholith. In detail, sodic granitoids (samples AR 60 and 63; high alumina-type) form the margins of the batholith and K-rich granites, the core and southern part of the batholith (samples AR 55 and 145; low alumina-type).

5.4.6 Primitive Mantle-normalized Extended Trace Element Diagrams

Element patterns of the high alumina-type granitoids (Figure 5.19a) are not as uniform as those of the low alumina-type. The high alumina-type granitoids contain variable trace element patterns that subdivide these granitoids into; (i) high HREE-bearing samples AR 60 and 63, (ii) low HREE samples AR 150 and 188, and (iii) high-Mg subgroup (samples AR 234 and 245) which have HREE patterns between the two other subgroups. The high-Mg granitoids have pronounced negative Ta-Nb anomalies and smaller negative Sr and Ti anomalies. The high HREE subgroup also has strong Ta-Nb negative anomalies and small negative Sr and Ti anomalies. The HREE enrichments in this group are the greatest of any in the high alumina-type granitoids of the Tati Greenstone Belt. The low HREE group (samples AR 150 and 188) are highly depleted in Y and HREE and contain strong Ta-Nb negative anomalies and positive Sr and Ti anomalies.

Low alumina-type granitoid rocks have trace element patterns which are distinctly different from those of high alumina-type granitoids on normalized extended trace element diagrams (Figure 5.19). The patterns for this group all show pronounced negative anomalies in the Ta-Nb pair, Sr and Ti. HREE are relatively

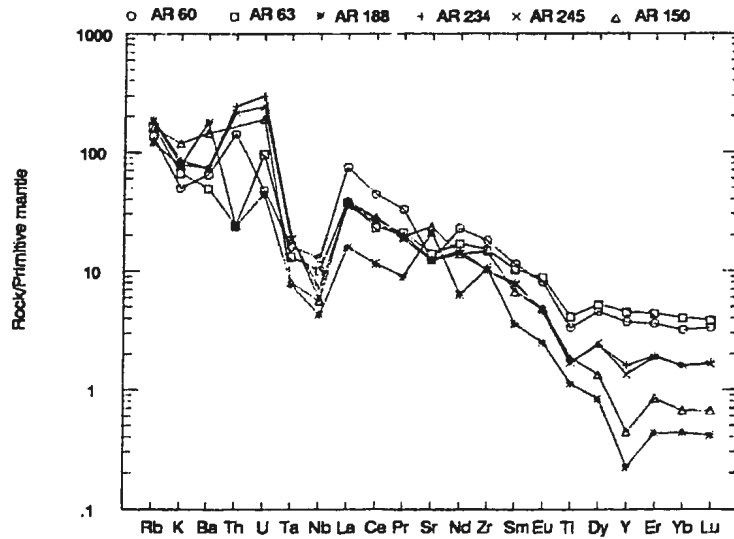


Figure 5.19a: Primitive mantle normalized extended trace element diagram for the high alumina-type granitoids of the Tati Greenstone Belt. Samples AR 60 and AR 63 are tonalites from the Tati Batholith and, although, they do not plot in the high alumina-type granitoid field in Figure 5.18, they have characteristics of the latter but are slightly HREE-enriched (normalizing factors as in Figure 5.19a).

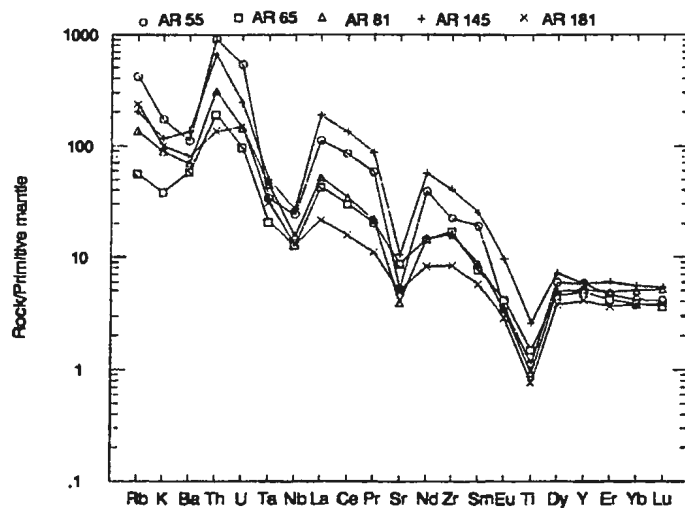


Figure 5.19b: Primitive mantle normalized extended trace element diagram for the low alumina-type Tati Greenstone Belt granitoids. The diagram documents the elevated contents of HYG elements and negative anomalies in TNT elements (Ta, Nb & Ti) in these rocks. Normalizing factors as in Fig. 5.19a.

uniform and undifferentiated (Figure 5.19b). Despite the overall similarities in trace element patterns within this group, however, potassic granitoids (samples AR 55 and 145) have higher element abundances relative to primitive mantle.

5.4.7 Discussion

General geochemical characteristics of the Tati Greenstone Belt granitoids are summarized in Table 5.4.

Hunter (1979) divided the Archean granitoids of Swaziland and Eastern Transvaal into; (1) grey gneisses or ancient gneisses of tonalitic and trondhjemitic composition, (2) a granodiorite suite intrusive into the grey gneisses, and (3) diapiric tonalites within greenstone belts. Hunter (1979) also suggested that K_2O/Na_2O ratios increase from the older granitoids to the younger varieties. Granitoids within greenstone belts, on the other hand, showed a general trondhjemitic trend and as such follow the sodic trend on a K-Na-Ca ternary diagram. Therefore, in Hunter's formulation, the differences in the K_2O/Na_2O ratios are process and source-related, rather than just time related, as suggested by other researchers. Tati Greenstone Belt granitoids follow both the sodic and potassic trends on a K-Na-Ca ternary diagram (Figure 5.14) and also plot along the trends of Zimbabwe Craton greenstone-related granitoids (after Hunter, 1979). These trends are similar to the calc-alkaline and trondhjemitic trends described by Barker and Arth (1976) for Archean granitoids in general. The sodic and potassic trends in granitoids of the Tati Greenstone Belt are also similar to the characteristics of Baker's (1979) high and low alumina-type

TABLE 5.4

Geochemical characteristic of Tati Greenstone Belt Granitoids.

Granitoid type	Chemical characteristics	Granitoid groups	Compositional type	Comparable tectonic setting	Possible mineral deposit type	
Low Alumina-type	High total REE (REE> 130), (La) _n =60 to 600x and (Yb) _n =10 to 15x chondritic. Relatively unfractionated REE patterns (La/Yb) _n =6 to 34.	Lower total REE and negative Eu anomalies. Na ₂ O > K ₂ O.	Samples AR 81, 181 and 65	Tonalites and granodiorites	VAG (volcanic arc granitoids)	Cu-Mo±Au
	Negative Eu anomalies (Eu/Eu* =0.2 to 0.4). Al ₂ O ₃ values of 10.8 to 14.1 wt% at SiO ₂ 69.9 to 76.5 wt%. High K ₂ O/Na ₂ O ratios (>0.75). High normative Ab (22-38 wt%) and Q (30-43wt %)	High Ba, Rb, Zr, Nb and Rb. Moderately high Sr, U and Y. Al ₂ O ₃ between 12.3 and 13.1 wt%. Enhanced negative Eu anomalies and low Cr and Ni. K ₂ O>Na ₂ O	Samples AR 55, 145 and 142	alkalic granites and megacrystic feldspar granites	Collisional granites; e.g. Thailand.	Sn, Mo, W ±Ag.

TABLE 5.4

Geochemical characteristics of Tati Greenstone Belt Granitoids.

Granitoid type	Chemical characteristics		Granitoid group	Compositional type	Comparable tectonic setting	Possible mineral deposit type
High Alumina	Low total REE (REE<130). (La) _n =45 to 110x and (Yb) _n =1.2 to 5x chondritic.	Great depletion in HREE; negative Ta-Nb and positive Ti and Sr anomalies.	Samples AR 150 and 188.	Trondhjemites	VAG (volcanic arc granitoids)	Cu-Au±Mo.
	Highly fractionated REE (La/Yb) _n =22 to 38. Depleted in HREE.	Highest HREE; negative Ta, Nb, Ti and Sr anomalies	Samples AR 60 and 63	Tonalites	VAG	Cu-Au±Mo
	No Eu anomaly Al ₂ O ₃ values 14.1-17.3 wt%, SiO ₂ ranges from 52.4-71.1 wt%. Low K ₂ O/Na ₂ O ratios (<0.75). High normative Ab (32-42 wt%).	High-Mg (60-73); high Cr, Ni and modal mafic minerals. K ₂ O=Na ₂ O	Samples AR 234 and 244	High-Mg granodiorites or sanukitoids.	VAG	Cu-Au±Mo

granitoids.

High alumina-type granitoids of the Tati Greenstone Belt have similar characteristics to the first magmatic cycle granitoids of the Barberton Mountainland Greenstone Belt (Robb and Anhaeusser, 1983). According to Robb and Anhaeusser (1983), the first magmatic cycle varied in composition from tonalite to trondhjemite with low total REE, low Rb/Sr ratios and high Sr contents. The high alumina-type granitoids of the Tati Greenstone Belt are also similar to the grey gneisses of Finland (Martin et al., 1983) and group B granitoids of O'Nions and Pankhurst (1978).

The high-Mg subgroup of the high alumina-type granitoids (samples AR 234 and 245; Table 5.4) are similar to sanukitoids (Stern et al., 1989). Sanukitoids have Mg# >60, 55-60 wt% SiO₂, Ni and Cr >100 ppm and strong enrichment of some large-ion-lithophile elements (LILE) such as the REE and also high Sr and Ba contents (ca >500 ppm) (Shirey and Hanson, 1984; Stern et al., 1989). Sanukitoids are common in the Setouchi orogenic volcanic belt of Japan (Tatsumi and Maruyama, 1989).

Low alumina-type granitoids of the Tati Greenstone Belt are similar to those of the second magmatic cycle in the Barberton Mountainland Greenstone Belt (Robb and Anhaeusser, 1983). The second cycle plutons have higher total REE, low Sr contents and high Rb/Sr ratios. The Tati belt low alumina-type granitoids are also similar to the K-feldspar augen gneisses of Finland (Martin et al., 1983) and Group A granitoids of O'Nions and Pankhurst (1978).

There is a general consensus in the literature that high alumina-type

granitoids, such as the first magmatic cycle of Robb and Anhaeusser (1983), the grey gneisses of Martin et al. (1983), or the group B granitoids of O'Nions and Pankhurst (1978)), were derived from sources in which hornblende and/or garnet were residual after partial melting and formation of the granitoid magmas. Hornblende in the residue will lead to HREE retention, more especially of the middle HREE, resulting in an upwards concavity in HREE patterns in the magma (Hanson, 1978). Garnet in the residue also leads to the depletion of the HREE in the magma (O'Nions and Pankhurst, 1978; Barker and Arth, 1976; Arth et al., 1978; Simmons and Hanson, 1978; Hanson, 1978; Wyllie, 1984; Whitney, 1988; Atherton and Sanderson, 1987; Martin et al., 1983; Robb and Anhaeusser, 1983; Sheraton et al., 1985).

Granitoids of the second magmatic cycle in the Barberton Mountainland Greenstone Belt are similar to the low alumina-type Tati granitoids. Petrogenetic models for these former rocks indicate the influence of plagioclase in the residue, as evidenced by the negative Eu anomalies and Sr depletions in the derived partial melts. The comparatively higher SiO₂ contents of these rocks also suggest a plagioclase feldspar-bearing source. Although petrogenetic models for the Tati Greenstone Belt granitoids are not presented, similar processes to those discussed above could have operated during their formation.

It is interesting to observe that negative Ta-Nb anomalies exist in both the high and low-alumina type granitoids of the Tati Greenstone Belt. Whatever petrogenetic processes might be used to explain the depletion of these elements, the Ta-Nb anomalies may reflect a very fundamental property, perhaps related to

tectonic setting. For example, modern island arc volcanic rocks generally contain negative Ta-Nb anomalies (e.g. Wood et al., 1979). Tati Greenstone Belt granitoids plot in Pearce et al.'s (1984) volcanic arc granitoid field (VAG) on a Rb vs. Nb+Y diagram (Figure 5.20). Some of these granitoids, especially the potash monzogranite, plot on the tie line between volcanic arc and syn-collisional granitoids (Figure 5.16). In addition, the Tati granitoids overlap with the fields defined for Archean granitoids from the Kaapvaal Craton (Harris et al., 1987). They also overlap with the fields of "association 1 and 2" granitoids from the Norseman-Wiluna Greenstone Belt of Australia (Cassidy et al., 1991). Association 1 granitoids are calc-alkaline plutons that are said to be both syn-volcanic and syn-tectonic. Association 2 granitoids, on the other hand, are syn to post-tectonic plutons.

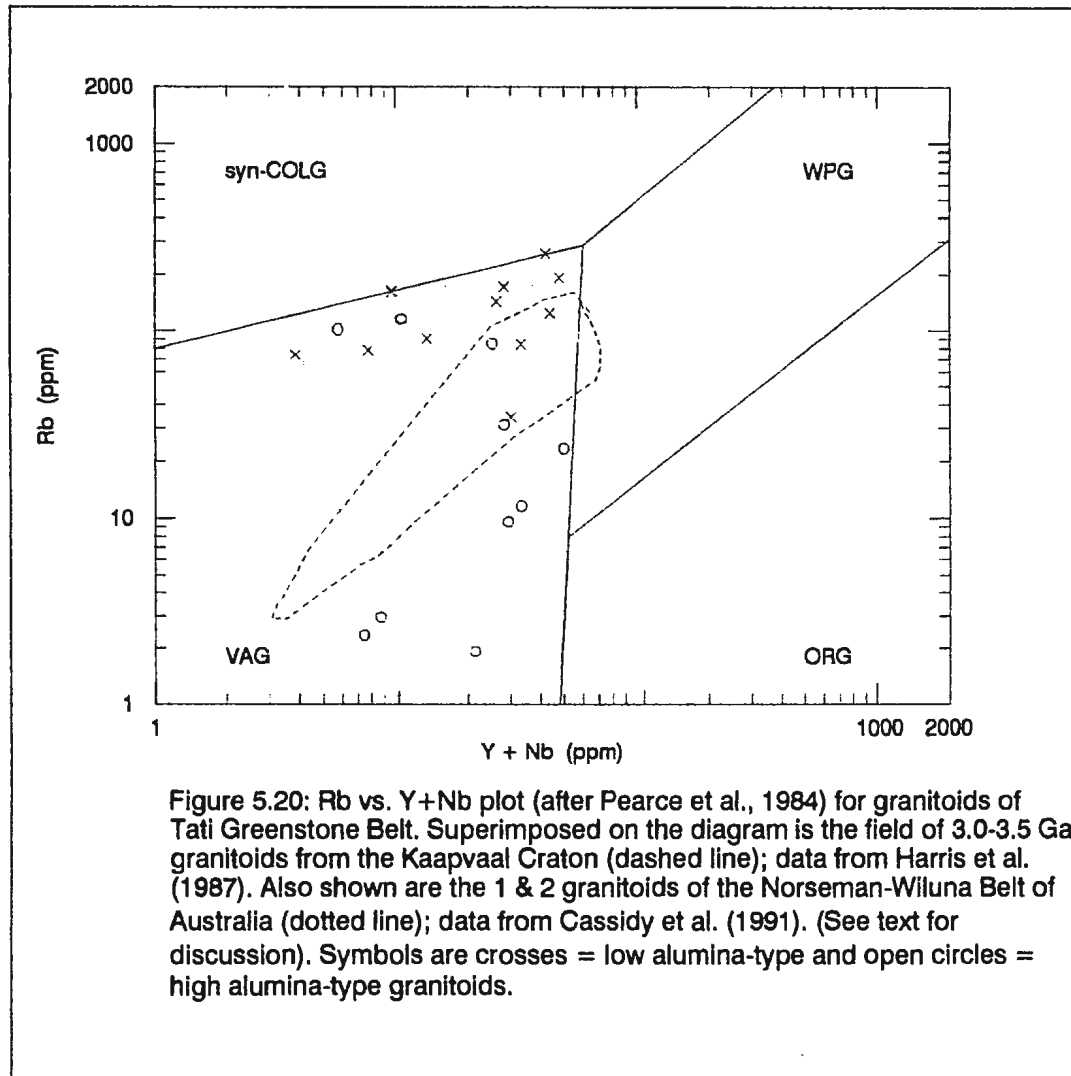


Figure 5.20: Rb vs. Y+Nb plot (after Pearce et al., 1984) for granitoids of Tati Greenstone Belt. Superimposed on the diagram is the field of 3.0-3.5 Ga granitoids from the Kaapvaal Craton (dashed line); data from Harris et al. (1987). Also shown are the 1 & 2 Ga granitoids of the Norseman-Wiluna Belt of Australia (dotted line); data from Cassidy et al. (1991). (See text for discussion). Symbols are crosses = low alumina-type and open circles = high alumina-type granitoids.

CHAPTER SIX

6. GEOLOGICAL SYNTHESIS OF THE TATI GREENSTONE BELT

6.1 Summary of the Stratigraphy of the Tati Greenstone Belt

Since the only published geological map for the Tati Greenstone Belt was produced 18 years ago (Key, 1976), the geological data base on the belt has improved appreciably. Large scale geological mapping of isolated areas during mineral exploration and regional geophysical surveys (aeromagnetism and gravity) have contributed to the understanding of the Tati Greenstone Belt geology. In this present work, data from regional and local geophysical surveys, satellite imagery and photogeological interpretations, large scale mapping by mineral exploration companies and Department of Geological Survey staff and research workers, and current fielding mapping have been combined to interpret the structure and the geological evolution of the Tati Greenstone Belt.

6.2 Geochronology

Due to the lack of precise radiometric age dating, geochronological control on the deformational events is the weakest link in Southern African geology. Even in the Republic of South Africa, where a considerable number of age dates have been derived, the ages of some units have changed back and forth. For example, until Barton's (1983) Rb/Sr age of 3.8 Ga was derived for the Sand River Gneisses of the Limpopo Belt, the Limpopo Belt was considered to have been Proterozoic and,

therefore, younger than the surrounding Archean cratonic areas (e.g. Mason, 1973). U/Pb zircon ages of between 3.2 and 3.29 Ga and a Sm/Nd age of 3.2 Ga have recently been obtained for the Sand River Gneisses (McCourt and Vearncombe, 1992). In the Zimbabwe Craton, where Rb/Sr dates form the bulk of the geochronological data base, the confusion is even greater. For example, the Mushandike tonalite gneisses were considered to be about 3.5 Ga old, but are now believed to be 2.9 Ga on the basis of Pb/Pb dating (Moorbath et al., 1987; Taylor et al., 1991).

Against this background of problematic ages, areas where very little dating has been done, such as the Tati Greenstone Belt, present serious problems for the understanding of geological events. The most significant date from the Tati Greenstone Belt is a U/Pb zircon age of 2715 ± 5 Ma for the Nyambabwe Tonalite (Key, 1976). The Nyambabwe Tonalite is part of an igneous complex which is intrusive into volcano-sedimentary rocks of the Tati Greenstone Belt. The complex is a very important tectonic marker because it was emplaced in a tectonic zone, probably a paleo-suture, that separates volcano-sedimentary rocks of the Tati Greenstone Belt to the south, from a granitoid area to the north. This is a post-volcanic age and, therefore, sets a lower age limit on the rocks within the Tati Greenstone Belt.

Key (1977) reported that a three point Rb/Sr isochron date of 2570 ± 70 Ma had been derived by Van Breeman and Dodson (1972) for a felsic volcanic rock from the Selkirk Group. This 2570 ± 70 Ma age for siliceous volcanic rocks is much

younger than the 2715 ± 5 Ma minimum age described above. It may, however, be a metamorphic age not related to the actual age of volcanism. A similar date has been reported for the paragneisses from the Northern Marginal Zone of the Limpopo Belt, south of the Tati Greenstone Belt (Key, 1977).

A ca. 2600 Ma metamorphic event is also reported to be widespread in rocks along the Southern and Northern Marginal Zones of the Limpopo Belt (Van Breeman and Dodson, 1972). Paragneisses at the northern margin of Limpopo Belt, just south of the main Tati Greenstone Belt, have yielded an Rb/Sr isochron age of 2640 ± 40 Ma (Hickman and Wakefield, 1975). A post-kinematic granitoid north of Francistown, the Timbale granite in the Vumba Greenstone Belt, has been dated by Rb/Sr techniques at 2540 ± 29 Ma (Key, 1977). K-Ar mineral dates (on biotite, biotite-plagioclase pairs and plagioclase-potassic feldspar pairs) of 1800 to 2000 Ma have been reported for some granitoids in the belt (Key, 1977). These ages have also been recorded in gneisses from the Limpopo Belt and were interpreted by Key (1977) to date the final metamorphic cooling stages for the Limpopo Belt.

The 2.7 Ga age of the Nyambabwe Tonalite is similar to the ca. 2.7 Ga ages of the Limpopo tectono-metamorphic event (Van Reenen et al., 1987). Kröner (1977a), on the other hand, indicated that the 2.7 Ga event was not confined to the Limpopo Belt, but was actually a much more widespread African tectonic event, which he termed the Limpopo-Liberian Orogeny. A 2.7 Ga event is by no means confined to high metamorphic grade areas such as the Limpopo Belt of Southern Africa. The Upper Greenstones of the Zimbabwe Craton formed in this age range

(Wilson, 1979). The Chengezi and Chilimanzi granitoids of the Zimbabwe Craton have this same age range and are more widely distributed in the craton than the areas adjacent to the Limpopo Belt (Wilson et al., 1978). Most greenstone belts in Canada (e.g. Card, 1990) and in the Yilgarn Craton of western Australia (Barley and Groves, 1990) are also of this general age range. It is therefore concluded that the 2.7 Ga event is a major crustal forming tectonic event which was not confined to the Limpopo Belt.

6.3 Tectonic Evolution of the Tati Greenstone Belt

6.3.1 Paleotectonic Setting

Three fault-bounded volcano-plutonic sequences, capped by thin horizons of sedimentary rocks and a younger overlying feldspathic sedimentary sequence, constitute the overall supracrustal rock stratigraphy of the Tati Greenstone Belt (Figure 6.1). These volcano-plutonic sequences are:

- (1) the komatiite-tholeiite sequence of the Lady Mary Group,
- (2) the calc-alkaline sequence of the Phenalonga Group,
- (3) the calc-alkaline sequence of the Selkirk Group.

The younger feldspathic sedimentary sequence, the Last Hope Group, was deposited in a fault-bound basin that occupies most of the southeastern part of the belt. The volcano-plutonic sequences are separated from each other by major lineaments or faults, such as the Sekukwe-Long Gossan Lineament (SLGL), which are coincident with thin horizons of sedimentary rock units including banded iron formations (Figure

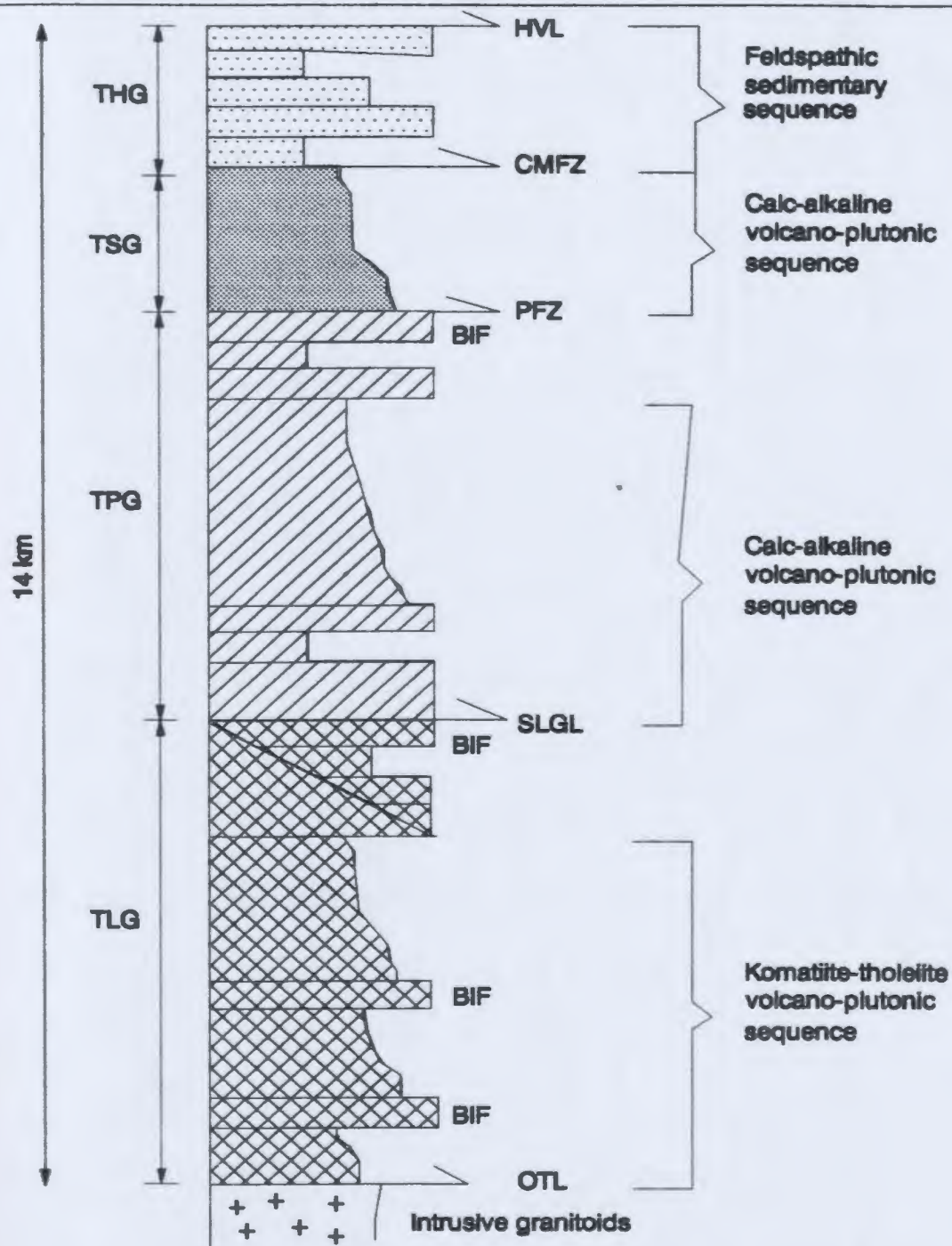


Figure 6.1: Interpretative stratigraphic column of Tati Greenstone Belt rocks with major lithological boundary parallel fault/shear zones marked. THG=Last Hope Group; TSG=Selkirk Group; TPG=Phenalonga Group; TLG=Lady Mary Group; OTL=Old Tati Lineament; SLGL=Sekukwe-Long Gossan Lineament; PFZ=Phenalonga Fault Zone; CMFZ= Charlie Mine Fault Zone; HVL=Hillview Lineament; BIF = banded iron formation.

6.1). Since these lineaments separate major lithotectonic units or volcano-plutonic sequences, they constitute terrane boundary faults. Each lithotectonic unit, for example the Lady Mary Group, represents a distinct tectonostratigraphic terrane that characterizes a particular geotectonic setting.

The Lady Mary Group consists mainly of ultramafic to mafic volcano-plutonic rocks with minor interflow argillites (including black shales) and banded iron formation intercalations. In general, the bulk of the volcanic flows succeed each other conformably with minor interflow sediments. The whole succession is capped by a unit consisting of banded iron formation, clastic sediments and limestones (Figure 3.9). Furthermore, vesicles and amygdules in volcanic rocks are more abundant towards the sedimentary cap. Lithological compositions of the Lady Mary Group suggest that the volcano-plutonic rocks were emplaced in a deepwater environment (cf. Dimroth et al., 1985). As volcanism increased, the environment progressively changed from deep to shallow water. The sedimentary cap was deposited in a shallow environment on top of an emergent basaltic volcanic basement (cf. Carlisle and Susuki, 1973).

It has previously been suggested (Barley and Groves, 1990) that Archean komatiite-tholeiite sequences, associated with calc-alkaline volcano-plutonic and feldspathic sedimentary sequences along fault contacts, were deposited in back-arc basins. Geochemical data present an important constraint on the paleotectonic setting for the volcano-sedimentary rocks of the Tati Greenstone Belt. Major and trace element data for ultramafic-mafic rocks from the Lady Mary Group indicate the

presence of three magmatic suites including; LREE-depleted rocks, LREE-enriched rocks and komatiites. It is postulated that the LREE-enriched rocks form the margins of a basinal structure which encloses the LREE-depleted and komatiite rocks at the core of the basin. The komatiites may have formed from plume-type magmas generated in the deeper parts of the Archean mantle. This suggests a paleotectonic setting that is similar to modern back arc basins, like the Lau Basin (Hawkins et al., 1985; Price et al., 1990). In such basins, the earliest magmas are low-K island arc tholeiitic basalts, while later magmas are similar to depleted MORB (Figure 6.2).

Detailed geochemical studies have not been carried out on rocks from the Phenalonga and Selkirk Groups. Major element and petrographic studies by others (e.g. Key, 1976; Mason, 1970) suggest that the volcano-plutonic rocks of the Phenalonga Group are calc-alkaline. On the basis of field distribution and nature of the rocks, the Selkirk Group may also be the remnant of a calc-alkaline suite. It can be speculated on the basis of the proximity to, and relationships with, the Lady Mary Group, which has back arc basin characteristics, that the Phenalonga and Selkirk Groups are remnants of an island arc, or perhaps two arcs.

In the Phanerozoic, fault-bound sequences (or tectonostratigraphic terranes) are defined as zones with internally consistent stratigraphy, structure and tectonic history different from those of adjacent terranes (e.g. Crowell, 1985; Crowell et al., 1985; Thakur, 1987; Edelman, 1991; Paterson et al., 1989). Such terranes can either be composite, formed by the amalgamation (or accretion) of more than one horizontally displaced crustal slices or fault-bound sequences derived from

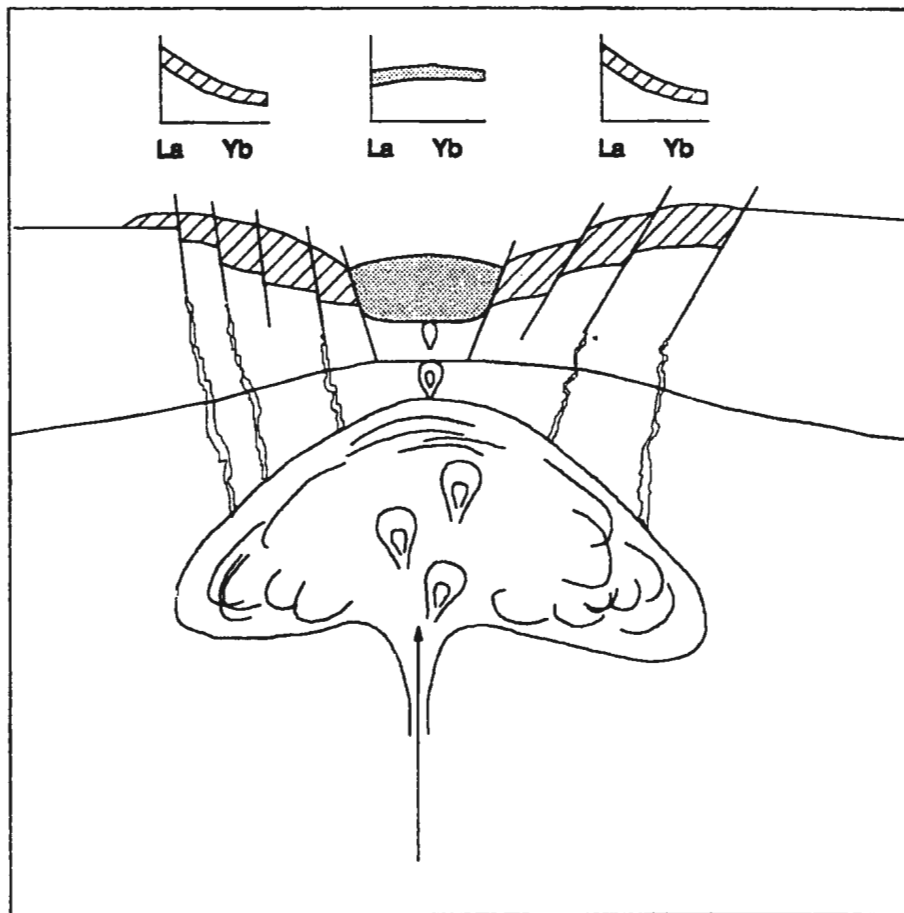


Figure 6.2: Schematic diagram showing the distribution of magmatic suites of the Lady Mary Group volcano-plutonic sequence in a back-arc basin tectonic setting. The LREE-enriched rocks occur at the flanks of a back-arc basin whose centre is occupied by flat to LREE-depleted rocks.

dismembered plate margins, or they can be single terranes consisting of one crustal block.

Current research suggests that Archean greenstone belts consist of fault-bound volcano-plutonic sequences (e.g. Hubert and Marquis, 1989; De Wit, 1991; Barley and Groves, 1990). In the Abitibi Greenstone Belt, Hubert and Marquis (1989) defined three types of fault-bounded terranes (lozenge-shaped crustal blocks) each enclosing several volcano-plutonic sequences. These are simple, composite, and orthogneissic-granitic terranes. In the Wiluna-Norseman Greenstone Belt, a major lineament, the Keith-Kilkenny Lineament, separates a komatiite-tholeiite sequence from a calc-alkaline-feldspathic sedimentary sequence (Barley and Groves, 1990). De Wit (1991) describes the Saddleback Fault System as separating a komatiitic ophiolite sequence from an island arc terrane comprising the Upper Onverwacht Group.

Apart from fault-bound sequences within greenstone belts, Archean cratons generally consist of crustal blocks separated by major terrane boundary faults or shear zones. The Anton, Contwoyto, Sleepy Dragon and Hackett River terranes of the Slave Province (Kusky, 1990) and the subprovinces of the Superior Province (Card, 1990) are examples of major fault-bound crustal blocks. In these cratons and belts, terrane boundaries are commonly zones of structural and metamorphic transitions with appreciable widths in which faulting and igneous activity have masked any primary lithological transitions (Card, 1990). In modern tectonic environments, terrane boundary faults are commonly characterized by belts of melange, crushed rocks, blueschist facies metamorphism and ophiolite slivers (Howell, 1989). Howell

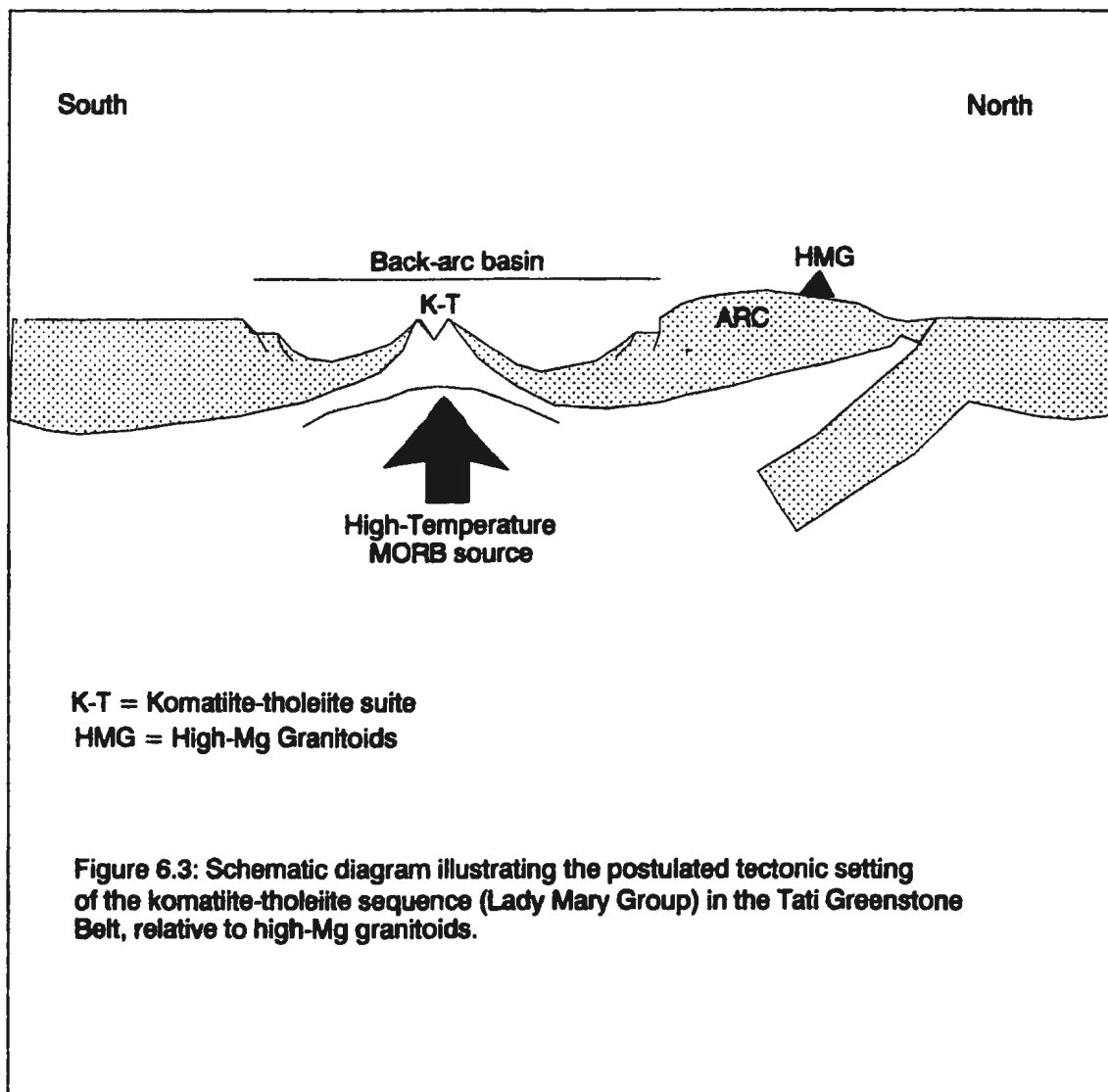
(1989) further states that these boundary faults can appear as cryptic, inconspicuous and unimpressive fault zones. Therefore, it would be difficult to distinguish them from the thrust faults that bound duplex slices within the same terrane. Without question, the SLGL between the Lady Mary and Phenalonga Groups and other lithological boundary faults in the Tati Greenstone Belt are of this type (i.e. fault zones without any distinctive boundary fault characteristics).

Several lines of evidence suggest that the Tati Greenstone Belt rocks were emplaced in a tectonic setting where the komatiite-tholeiite sequence represents a back-arc basin and the calc-alkaline volcanic and feldspathic sedimentary rock sequences indicate the existence of an arc environment. This evidence includes:

- (1) the association of a komatiite-tholeiite sequence (Lady Mary Group) with calc-alkaline volcanic sequences (Phenalonga and Selkirk Groups) and a feldspathic sedimentary sequence (the Last Hope Group),
- (2) the separation of these volcano-plutonic sequences from each other by major lineaments,
- (3) geochemical characteristics of the komatiite-tholeiite sequence,
- (4) the occurrence of high-Mg granodiorites (Figure 6.3) which are generally regarded as derivatives from high-Mg andesites generated in subduction zones at anomalously high temperature (Tatsumi and Maruyama, 1989).

6.3.2 Tectonics and Geodynamics

In modern tectonic environments it has been observed that structures in fault-



bound sequences generally form in two similar, but unrelated, deformational events (Crowell et al., 1985). Early deformational events are related to the amalgamation of separate terranes to form composite terranes. This amalgamation generally forms prior to accretion of the composite terrane to the continental margin. The second, and younger, deformation event is related to the accretion (or collision) and welding of the amalgamated terrane to the continent. The accretion/collision constitutes a major tectonic event in the tectonic evolution of a craton. This deformational event usually produces intense folding, penetrative deformation fabrics and metamorphism. The tectonic fabric may be regionally distributed or localized in narrow tectonized zones (Crowell et al., 1985).

Structures in the Western Structural Zone of the Tati Greenstone Belt have a dominant NW-SE trend but with a progressively changing direction to NNW-SSE or N-S as the Shashe Belt is approached (Figure 6.4). The disruption and re-orientation of NW-SE structure in the Western Structural Zone by the deformational event which formed the Shashe Belt, suggests that two major tectonic events affected rocks of the Tati Greenstone Belt. In summary, two main tectonic events, informally named the Tati and Shashe Orogenic Events, are interpreted as having been responsible for the tectonic evolution of the Tati Greenstone Belt.

The first tectonic event, the Tati Orogeny, led to the formation of the Francistown crustal block. NE verging overturned, inclined or recumbent folds and thrusting along lithological boundary-parallel faults were the major structures formed during this deformation. Also related to this tectonic event are two major trans-belt

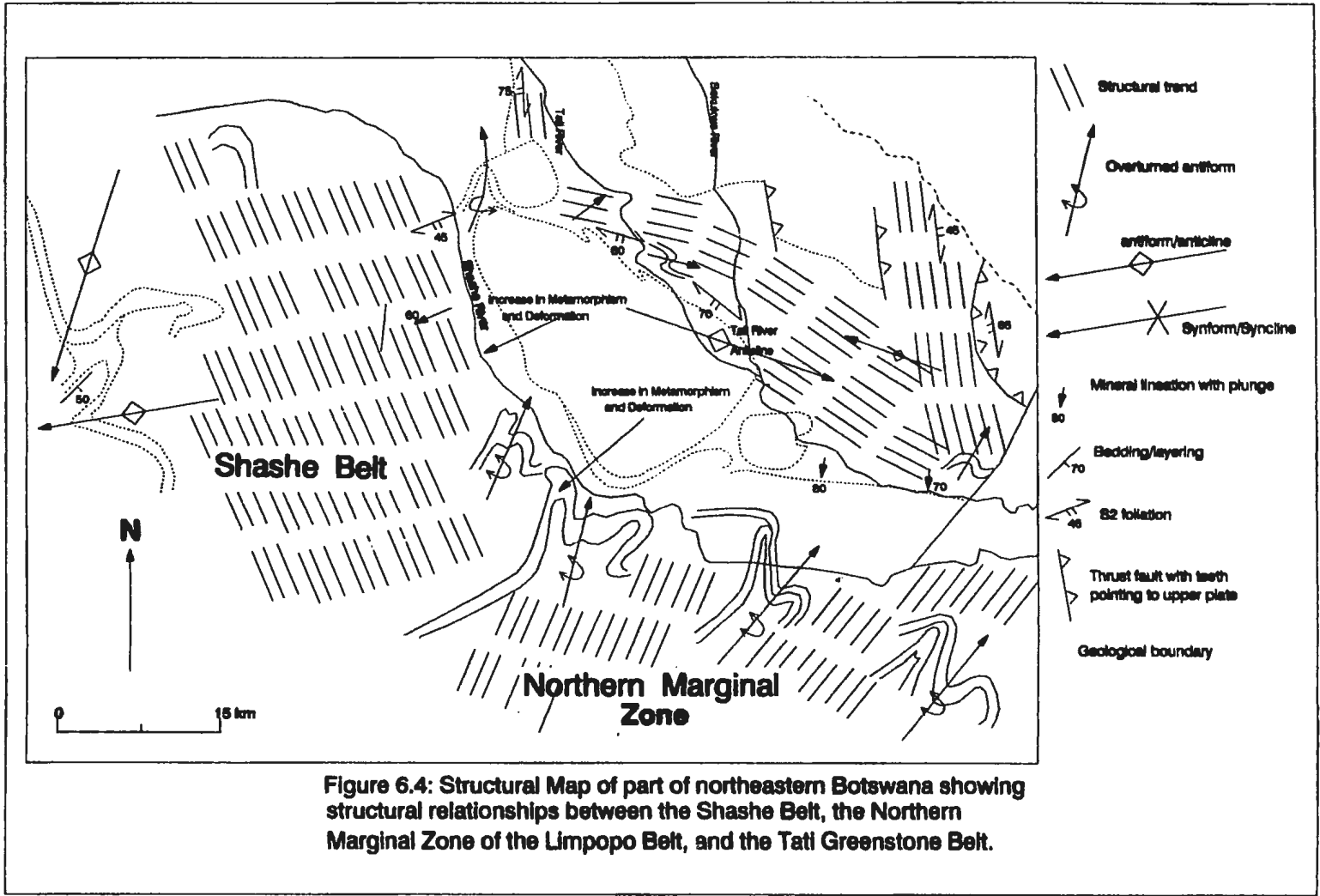


Figure 6.4: Structural Map of part of northeastern Botswana showing structural relationships between the Shashe Belt, the Northern Marginal Zone of the Limpopo Belt, and the Tati Greenstone Belt.

lineaments marked by narrow linear magnetic anomalies with a NW-SE trend, the Matsiloje-Francistown Lineament (MFL) and Ramokgwebana-Tsamaya Lineament (RTL). These two lineaments bound a narrow tectonic discontinuity that separates the main volcano-plutonic rock sequences of the Tati Greenstone Belt to the south, from a dominantly plutonic terrane to the north (Figure 3.6). This discontinuity is intruded and disrupted by the linear, NW-trending, Selkirk Igneous Complex plutonic belt. The Mphoeng Plutonic Complex and Ramokgwebana megacrystic feldspar granite also intruded into this tectonic zone (Figure 3.6). This event may have been related to a N-directed subduction process. This subduction would have led to the collision of arc rocks from the south with continental crust to the north (Figure 6.5). This collisional deformation produced a large weak crustal zone, the Matsiloje-Francistown Tectonic Zone, marked at the southern end by the MFL. The MFL may form a paleo-suture along which arc rocks were accreted to the continental crust. To the SE, a fault-bounded sedimentary basin, the Last Hope Basin, formed during this thrusting and collisional event. Calcareous and turbiditic sedimentary rocks occur at the northern part of the basin, whereas continental type sediments, conglomerates and sandstones occur in the south. This suggests that the southern part of the basin was on the side of the advancing orogen, whereas the northern part was in a deeper portion of the basin.

The second tectonic event, the Shashe Orogeny, followed the formation of the micro-craton, the Francistown Block, and is related to SW-directed movements leading to collision of the craton with the Limpopo Protocraton. The Northern

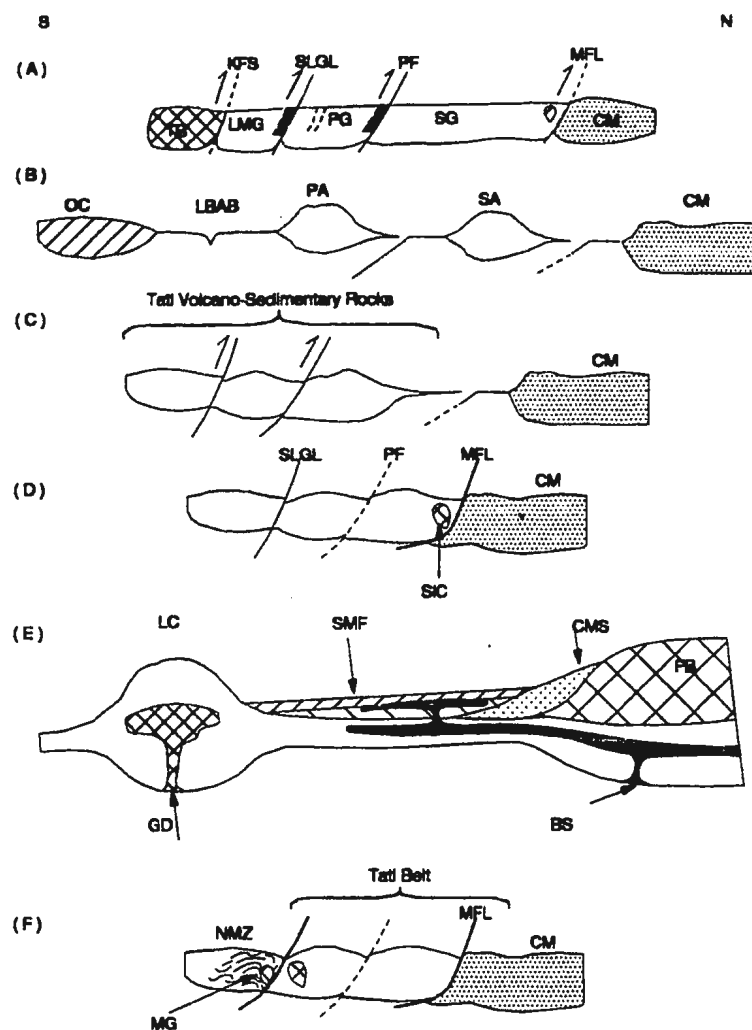


Figure 6.5: Schematic diagram showing tectonic elements and tectonic evolution of the Tati Greenstone Belt (TGB). Stage (A) to (D) relates to the evolution of the belt, whereas stages (E) to (F) relate to the accretion of the composite belt to the continental margin (CM). (A) shows present configuration of TGB; (B) shows tectonic elements of the TGB; (C) indicates that formation of the composite belt through accretion of the volcano-sedimentary rocks, occurred prior to the accretion of belt rocks to the continental margin (CM); (D) shows collision of the volcano-sedimentary rocks with CM; (E) shows the rifted continental crust between the Limpopo Craton (LC) and TGB; (F) shows configuration after collision of LC and TGB. KFS, SLGL, PFZ and MFL are major shear zones (see Figure 4.6 for details); LMG, PG and SG are Lady Mary, Phenalonga and Selkirk Groups; OC=oceanic crust; LBAB=Lady Mary back-arc basin PA=Phenalonga arc; SA=Selkirk arc; SIC=Selkirk Igneous Complex; FB=Francistown Block of the Zimbabwe Craton; CMS=Continental margin sediments; SMF= Shashe and Monstahane Formations; BS=basaltic sills; GDF=granitoids; NMZ=Northern Marginal Zone and MG=megacrystic feldspar granites.

Marginal Zone of the Limpopo Belt and its off-shoot, the Shashe Belt, were formed during this process. The emplacement of the allochthonous Eastern Structural Zone may have either occurred at this time, or prior to this event.

Data derived in this study suggest that Tati Greenstone Belt rocks were emplaced into both island arc and back-arc environments, and that they also represent an amalgamation of different terranes (Figure 6.6). The amalgamation of the Selkirk arc (Terrane A), the Phenalonga arc (Terrane B), and the Lady Mary back-arc basin (Terrane C) may have occurred before the accretion of the Tati volcano-sedimentary assemblages to the northern craton (Figure 6.6). The Selkirk Igneous Complex stitches the volcano-plutonic sequences to the northern craton. The accretion of the volcano-plutonic sequences to the craton resulted in the formation of the Francistown crustal block and occurred before the emplacement of the Eastern Structural Zone. Evidence for the formation of the Francistown block before the emplacement of the Eastern Structural Zone is derived from the fact that the MFL structures do not displace the Matsiloje ranges.

The N-S trending Mphoeng Plutonic Complex welds the Eastern Structural Zone to the Francistown crustal block. Formation of the Tati Greenstone Belt superterrane preceded formation of the Northern Marginal Zone Orogen, Limpopo Belt. Megacrystic and charnockite granites of the Northern Marginal Zone, therefore, weld the Tati Belt to the Limpopo Belt. The other interesting observation is that banded iron formations (BIF) are confined to the top of major tectonostratigraphic units such as the Lady Mary Group. The BIF's are confined to major crustal

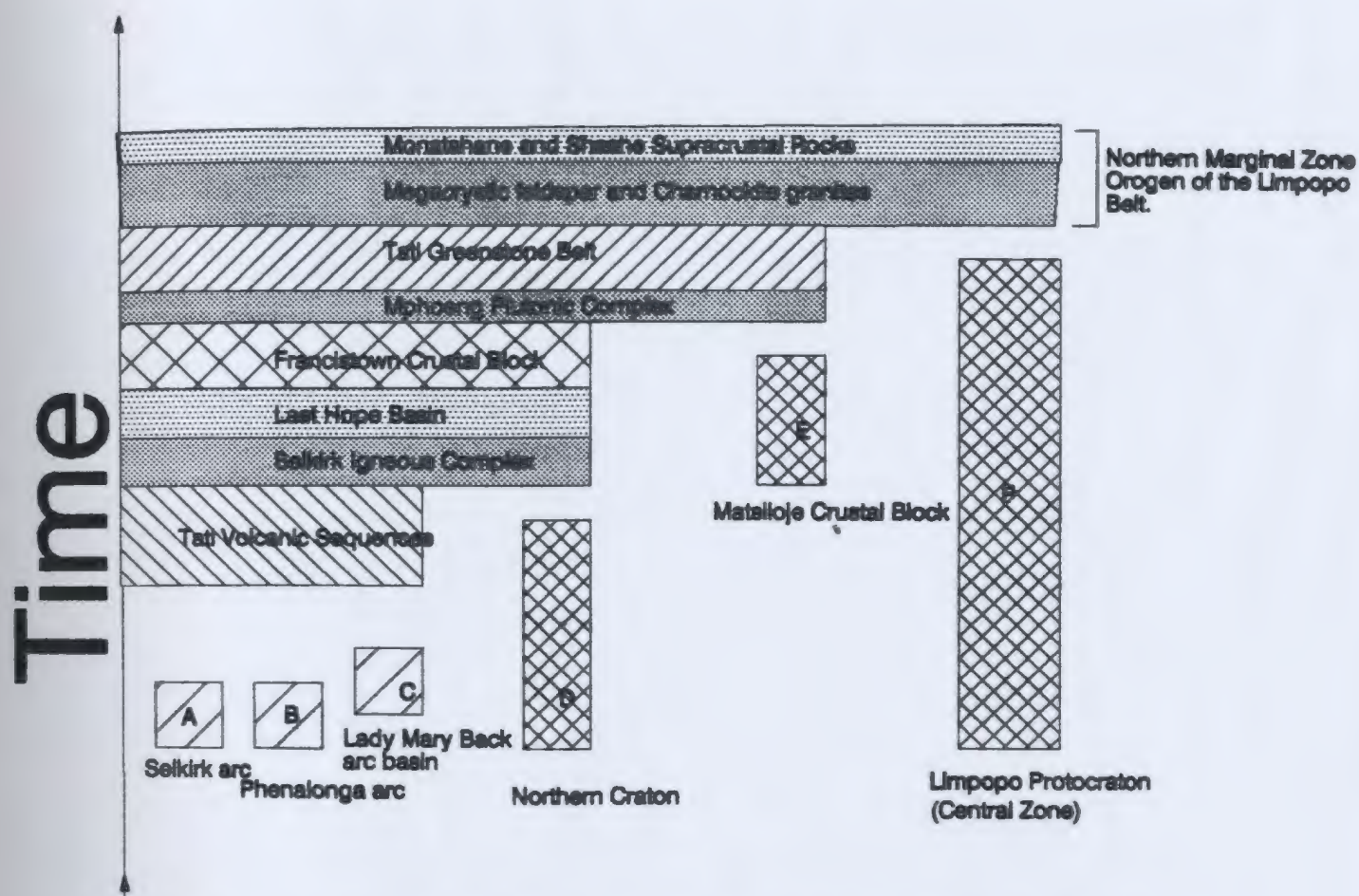


Figure 6.6: Schematic chronological diagram depicting the tectonic evolution of the Archean Tati Greenstone Belt (TGB) and formation of the Archean crust of NE Botswana. The vertical axis represents the length of time for tectonic processes and formation of crustal blocks. The formation of the Tati Greenstone Belt started with the amalgamation of the arcs, A and B and the back-arc basin (C) to form a composite crustal block consisting of Tati volcanic sequences. The second process involved collision of the crustal block made up of Tati volcanic sequences, and the northern craton (D) to form the Francistown crustal block, followed by the formation of the Last Hope Basin. The crustal blocks were stitched together by the Selkirk Igneous Complex. The Matsiloje crustal block was accreted to the Francistown block through NW-directed thrusting, resulting in the formation of the TGB. The two were stitched together by the Mphoeng Plutonic Complex. The final stage in accretion involved collision of the TGB with the Limpopo Belt leading to deposition of the Monatshane and Shashe supracrustal rocks, including the intrusion of megacrystic feldspar granites and charnockites in the Northern Marginal Zone of the Limpopo Belt.

lineaments that form tectonic boundaries/breaks between these major volcanic sequences. They, therefore, may have formed as chemical precipitates of hydrothermal fluids that accompanied volcanism.

CHAPTER SEVEN

7. METALLOGENY OF THE TATI GREENSTONE BELT

7.1 Introduction

The concept of metallogeny is based on understanding the relationship of mineral deposits to the overall tectonic setting of their host rocks (e.g. Strong, 1987; Laznicka, 1985). Mineral deposits are generally small compared to the spatial extents of their host lithotectonic units which can cover several hundreds of square kilometres. This raises the question as to what influences host rock compositions have on mineral deposits. In porphyry systems, where the relationships of mineral deposits to their subduction-related tectonic setting has been successfully demonstrated (e.g. Sillitoe and Hart, 1984), there are internal differences in mineral deposit compositions. For example, Cu-Au porphyry mineralization is associated with diorite-granodiorite plutonic suites as opposed to the Cu-Mo association with granodiorite-granite plutonic suites (Kesler et al., 1977). Thus, a class of deposits can be related to a specific tectonic setting, whereas individual mineral deposit composition may be related to the specific host rock composition.

The influence of host rock composition on mineral deposit composition is a very intrinsic, yet diffuse, feature. For example, the chemical compositions of metalliferous sediments in oceanic basins reflect the chemical compositions of their metal source, MORB (Bonatti and Joensuu, 1966; Bonatti, 1983). The same is true for sulphide deposits that form at spreading environments (Rona, 1988; Hekinian et al.,

1980).

Modern tectonic environments are very complex and are often composed of different magmatic suites. The question thus arises as to what specific effects individual magma compositions have on the nature of mineral deposits in a given environment? For example, would the occurrence of different magmatic suites, such as MORB-like vs. low potash magmas in some back-arc basins, have an effect on the mineral deposits that might form in that particular environment?

Fouquet et al. (1991) suggest that hydrothermal sulphides in back-arc basins (e.g. the Lau Basin) are different from those that form in oceanic spreading ridge environments, as sulphide assemblages from back-arc basins contain higher concentrations of Ba, Pb and As, compared to those from spreading centres. Other important aspects in defining the compositions of mineral deposits are the physico-chemical parameters of the mineralizing fluids. Fluid compositions are controlled by water/rock interactions during fluid generation, mineralization and/or alteration related to mineralization. At high water/rock ratios, the major cation composition of hydrothermal fluids is not fundamentally changed by interaction with host rocks. At low water/rock ratios, fluid compositions will evolve towards equilibrium with the rocks through which they flow. Fluids that form mesothermal gold deposits are considered to have evolved differently from those that generate other types of mineral deposits (eg. massive sulphide deposits). As a function of their overall low Cl/S ratios, these auriferous fluids have low base metal contents due to their inability to transport these metals (e.g. Kerrich, 1989; Burrows et al., 1986; Nesbitt et al.,

1987; Colvine, 1989; Groves and Phillips, 1987).

Current research on geothermal systems (e.g. Krupp and Seward, 1990) and massive sulphide deposits from oceanic spreading environments (Hannington et al., 1986) indicates that there is a progressive change in fluid composition as result of boiling at depth. Boiling produces metal separation through immiscibility of gaseous and fluid phases as these two phases contain different concentrations of specific metals and other elements. The metal separation leads to zonation of Cu-Zn, Zn-Pb and Au-As-Sb-Ag±Pb±Zn±Hg in massive sulphide deposits with decreasing temperature.

In the Hoydal Deposit of the central Norwegian Caledonides, a volcanogenic massive sulphide deposit hosted by ophiolites, there is a pronounced metal zonation from high temperature, Cu-dominated, massive base metal deposits, to low temperature Au-related metals (Zn, Pb, Ag, As and Sb) (Grenne and Vokes, 1990). This suggests that fluids responsible for the deposition of volcanogenic sulphides can evolve to Au-bearing fluids.

In this chapter the distribution of mineral deposits in the Tati Greenstone Belt will be related to the tectonic evolution of the belt. The first section of the chapter will deal with the regional distribution of the mineral deposits in the Tati Belt (summarised in the form of the metallogenic map). The second part will concentrate on two examples of mineral deposits from this belt which exhibit two different styles of mineralization and two contrasting compositions. Finally, a metallogenic model for gold deposits of the Tati Greenstone Belt will be presented and discussed.

7.2 Regional Distribution of Mineral Deposits of the Tati Greenstone Belt

7.2.1 Historical Background

Archean greenstone belts of southern Africa are essentially gold-producing belts with very few known massive sulphide deposits (Johnston and Griffiths, 1982). It is estimated that during the period from 1866 to 1964, between 400,000 and 500,000 ounces of gold were produced from at least 70 shear-hosted lode gold quartz veins in the Tati Greenstone Belt (Key, 1976). Currently, the Shashe mine, located four kilometres south of Francistown, is the only significant gold producer in the Tati belt. Several small scale operations scattered across the belt are also in production. The pre-1866 gold production by local tribesmen also constituted a significant amount of the total production from the Tati Greenstone Belt. Other mineral production in the belt has been restricted to 27,000 ounces of silver and 10,000 tonnes of kyanite during the same period. Current exploration has also delineated three small nickel-copper massive sulphide deposits. Two other small scale nickel-copper deposits were mined in the southeastern part of the belt in the Kgarimacheng area.

7.2.2 Elements of Metallogenic Mapping

Maps showing the nature and distribution of mineral deposits can vary from simple mineral deposit spot maps to complex interpretative maps. Mineral deposit spot maps show only the distribution of deposits. Interpretative, or metallogenic, maps usually group deposits with common geological and genetic characteristics

under one symbol (Bowman and Stevens, 1978). The essential component of the metallogenic map is that symbolized information, which groups deposits with similar genetic aspects, should be clear and concise. The format of the metallogenic map of Tati Greenstone Belt produced for this study was based on Bowman and Stevens' (1978) approach for the metallogenic map of New South Wales in Australia and Chatterjee's (1983) metallogenic map of Nova Scotia. The main constraint on the construction of the Tati belt map was the quality of the available data. For example, whereas mining production data are available from the beginning of the mining period to the present, the records were not kept properly or consistently and as a result some are missing. It was, therefore, not possible to show the relative sizes of individual deposits, and it was decided that the best method would be to disregard grade/tonnage differences between individual deposits and represent deposits with similar sized symbols (even though this may distort the true picture).

The second problem was the relative distribution of commodities within a mineral deposit. This aspect also depends on the availability and quality of production data. A deposit is designated Cu-Au if production data report relative tonnages of the two metals. It was recognised, however, that this parameter can be distorted by production preferences. It is possible that records may show gold as the only commodity produced for a particular deposit, although other commodities may have been present, but not reported. To circumvent this problem it was decided to include, as part of the symbol, metallic associations based on the mineralogy of the deposit. Metallic associations based on the mineralogy are also problematical,

especially with regard to missing data, and thus, in such cases a "polymetallic" deposit may be represented by a gold symbol only.

Because of the problems in deciding what actually constitutes the primary control for the gold deposits, it was decided that both structure and host rock compositions should be incorporated in the mineral deposit symbol. Where gold occurs in several forms, such as in sulphides or as the native metal, the map symbol is repeated as many times as there are forms of occurrence. Modifiers are, however, added to the symbol to denote each form. For example, Au represents gold in sulphides, whereas (Au) represents native gold. It must also be noted that the symbol of gold in sulphides does not distinguish between gold as inclusions, gold in colloidal form along sulphide grain boundaries, or gold in solid solution.

7.2.3 Descriptions of Mineral Deposit Groups

The regional distribution of the mineral deposits in the Tati greenstone belt is summarized on the attached metallogenic map in the pocket. The most significant detail emphasized by the map is that shear-hosted lode gold deposits are controlled by structures that are confined within the belt. These deposits occur in discrete groups or clusters. In particular, lode gold deposits are hosted by second generation shear zones and structures related to them, such as folds and minor fracture systems. The mineral deposit groups or clusters are:

7.2.3.1 Shashe Group

Deposits in this group are associated with a linear ridge of silicified basaltic rocks which extends for about ten kilometres from the abandoned New Prospect Mine to the Lady Mary Mine (Figure 7.1). This group of deposits is hosted by lithological units from the upper part of the Lady Mary Group, submarine basalts of the Map-Nora Formation. At the Shashe Mine (Figure 7.1), steeply south-dipping, mineralized shear zones are localized at the contact between a feldspathic basalt and syn-volcanic gabbroic sill. Gold at the Shashe Mine occurs both as the native metal and within sulphide minerals, especially arsenopyrite (Blaine, 1986a). Sulphide mineralization consists mainly of pyrite, pyrrhotite and arsenopyrite, with minor amounts of marcasite, chalcopyrite, sphalerite and the antimony minerals, berthierite and gudmundite. The mineralized shear zones are layer parallel. Mineralized veins are generally enveloped by a diagnostic alteration zone consisting of brown to pinkish-red biotite (Figure 7.2). At the Lady Mary Mine, feldspathic basalts similar to those at the Shashe Deposit form the host rock. The shear zones which host these deposits are controlled by D_2 related hydro-fracture veins. The deposits also occur adjacent to the northern edge of the contact between the Tati batholith and supracrustal rocks.

7.2.3.2 Golden Eagle Group

Deposits in this group are hosted by folded meta-sedimentary rocks of the Golden Eagle Formation at the top of Lady Mary Group (Figure 7.1). The host rocks

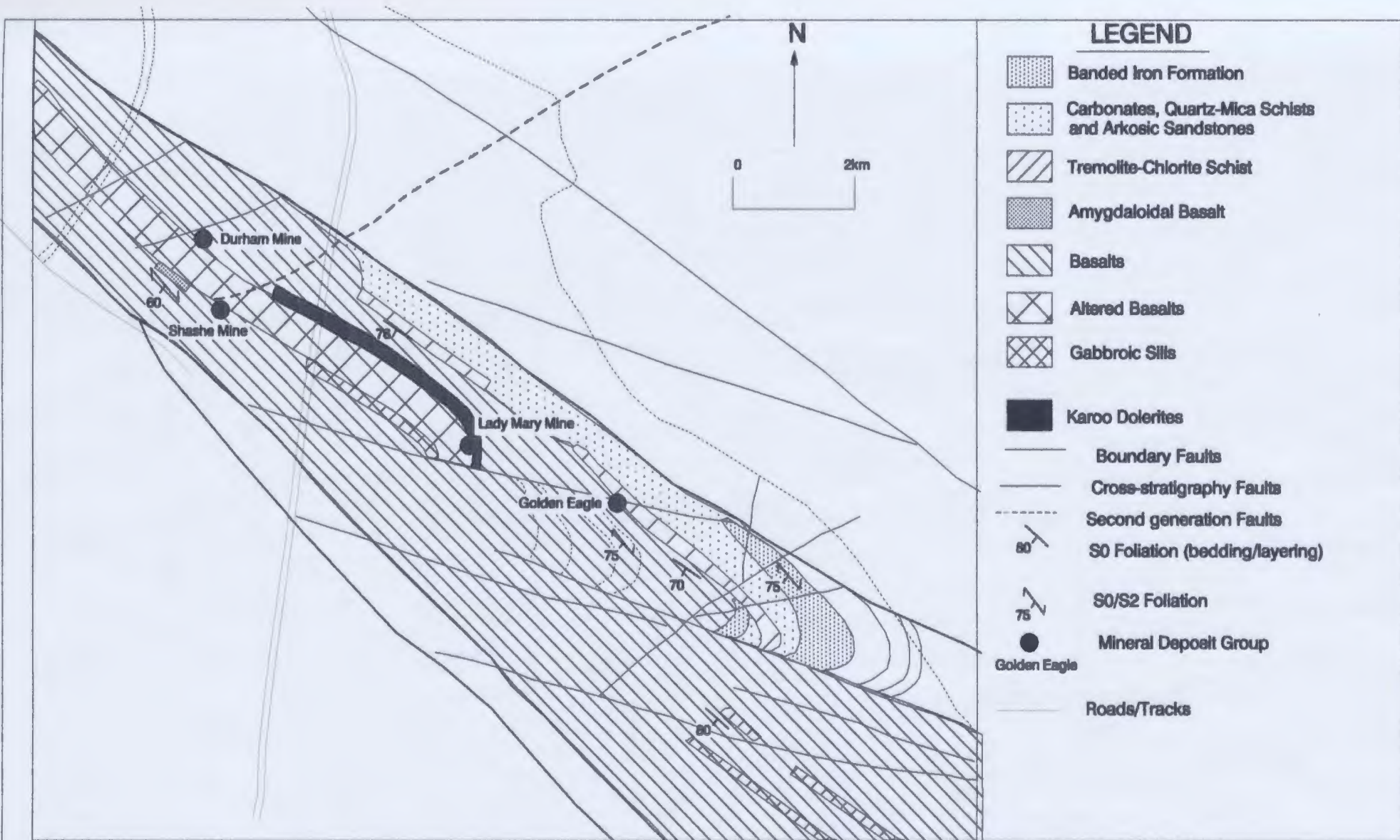


Figure 7.1: Geological map of part of the Tati River Subzone showing distribution of the Shashe Group of Deposits.

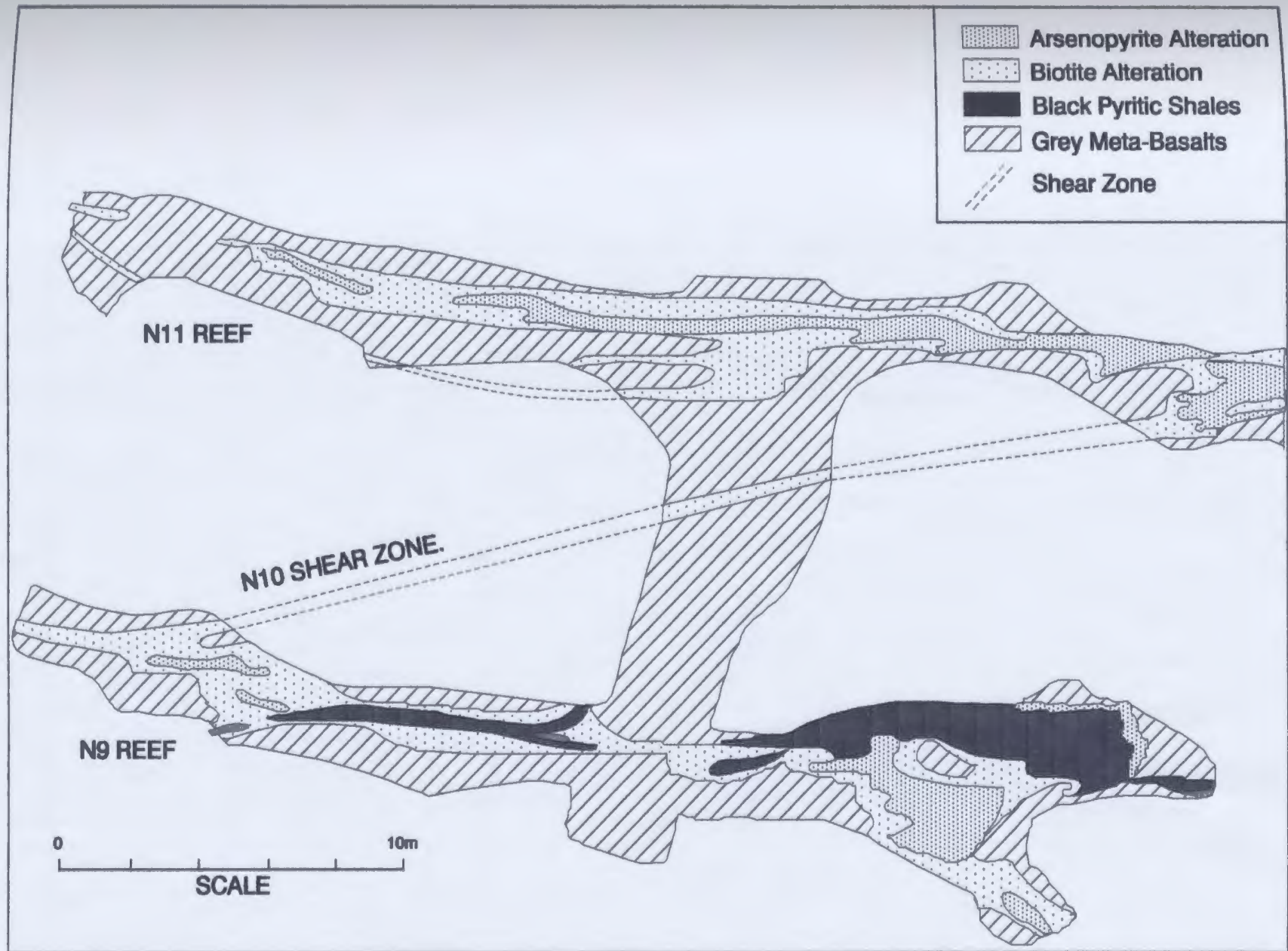


Figure 7.2: Geology of the underground third level lateral development at the Shashe Mine. (after Falconbridge Exploration Company mine plans, 1982).

are highly fissile greenish-grey phyllites which, in most cases, are red stained due to the presence of ferric iron. Mineralized zones also appear rusty brown or red due to the presence of hematite. Mineralization occurs in steeply dipping shears (ca 65° SW). Gold is present as both native metal and in sulphides and the main sulphide minerals are pyrrhotite, pyrite, and arsenopyrite. Chalcopyrite, scheelite and unnamed silver minerals occur in minor amounts (Molyneux, 1971). Ankerite and stilpnomelane form the main alteration assemblage.

7.2.3.3 Charlie Group

This group of deposits is located 32 kilometres southeast of Francistown. They are hosted by basaltic rocks in a folded structure that consists of interlayered basalts and gabbroic sills (Figure 4.13) in the Map-Nora Formation, Lady Mary Group. There are no production data available from this group of gold deposits. Examination of tailings, however, indicates that the mineralization is sulphide-controlled. Pyrrhotite, pyrite and minor chalcopyrite are common sulphides in the mine dumps. Carbonate-quartz veins, in pinkish-red or brown biotite alteration zones, carry the sulphides. These deposits have similar characteristics to those of the Shashe Group.

7.2.3.4 New Zealand Group

These gold deposits are hosted by banded iron formations of the Lady Mary Group at the southern limb of the south-vergent isoclinal fold (OTA; Figure 4.3), and are located in the Old Tati Subzone. The mineralization occurs in south steeply-

dipping quartz veins controlled by structures (shear zones) near contacts between supracrustal rocks and the New Zealand pluton. A WNW-ESE trending major fault/shear zone (OTL; Figure 4.6) occurs south of the New Zealand deposit. It is reported that some of the richest ore in the area, 5 to 90 g/t, was produced from the New Zealand Mine in the early 1960's (Molyneux, 1971).

7.2.3.5 Blue Jacket Group

These occurrences are hosted by steeply south-dipping E-W trending shear zones, in highly altered basaltic rocks of the Lady Mary Group in the Old Tati Subzone (Figure 4.2). The alteration visible in mine dumps consists mainly of numerous quartz-carbonate veins. Gold is carried by sulphide minerals such as pyrrhotite and arsenopyrite.

7.2.3.6 Flora Group

This group of deposits occurs in the eastern extension of the Lady Mary Group. They seem to have been very small workings located on relatively long quartz or quartz-carbonate veins. In areas where these deposits are located, only fine dispersed dumps are found. Because of the poor state of the dumps and lack of proper records, it is therefore, not possible to confidently identify host rocks or the mineralogy of the deposits. These deposits, however, cluster around small granitoid intrusions considered to be similar to the Hillview trondhjemite of the Last Hope basin.

7.2.3.7 Monarch Group

Several abandoned mines are located west of Francistown (Figure 4.5). These deposits occur in a N-S to SSE-NNW-trending shear zone at the contact between Selkirk Group volcanic rocks and the Nyambabwe Tonalite. The deposits are spread over a distance of 1.5 kilometres along the shear zone. The host rocks are hornblende schists, interlayered with mica-schists, graphitic-talc schists and calcareous units. The mineralized shear is conformable with the S_0/S_2 foliation which dips steeply to the west (ca. 85°). The mineralization is sulphide dominated, and the dominant sulphides are arsenopyrite, pyrrhotite, pyrite and minor chalcopyrite. Au and Ag are the main commodities. Bi is also reported to be present (Molyneux, 1971).

Monarch Mine was the first gold mine to be opened in southern Africa when it started production in 1869. Production is recorded as having taken place in two stages. The early mining stage lasted until 1910, when refractory sulphide ore presented complications to the milling process. Up to this time it is reported that about 136,000 tonnes of ore grading at 17 g/t gold was extracted. The second mining stage covers the period between 1934 and 1952. During this period about 514,020 tonnes of ore produced approximately 3,357,330 g of Au at an average recovery of 6.53 g/t and 260,240g Ag at 3.87 g/t (Molyneux, 1971).

7.2.3.8 Francistown Group

These deposits are localised in shear zones along contacts between the Nyambabwe Tonalite and Selkirk Group volcanic rocks. They may form a continuation of the Monarch Group and their trend is approximately east-west (Figure 7.1). No data are available on the mineralogy and nature of the deposits.

7.2.3.9 Bonanza Group

Deposits of this group are hosted by en echelon tension quartz veins localised in shear zones within massive andesitic volcanic rocks of the Phenalonga Group (Figure 3.10). These mineralized shear zones are layer parallel and dip at angles between 60° and 80° to the WNW. The mineralized zones occur near the base of the group just above the contact of the Phenalonga and Lady Mary Groups.

The mineralization consists of gold-bearing sulphides (Molyneux, 1971). The main sulphides are pyrrhotite and pyrite with minor chalcopyrite. Silver has also been reported (Molyneux, 1971), although the form in which it occurs has not been documented. Pyrrhotite occurs as massive bodies and as disseminated sulphides in altered andesitic hosts. The main alteration consists of chlorite and carbonate minerals.

7.2.3.10 Cherished Hope Group

These occurrences are hosted by shear zones within and at the contacts of granitoids, between the intruding Nyambabwe Tonalite and Francistown Diorite. The

diorite and tonalite are part of the Selkirk Igneous Complex which intrudes the Selkirk Group volcano-plutonic rocks. These gold deposits are generally hosted by thin SE-NW quartz veins enveloped by thin advanced argillic alteration zones. The main shaft around the Cherished Hope mine has been poorly kept, and therefore, it was difficult to assess the nature of the deposit from this shaft. Only fine dumps are available from this mine, which made sampling to determine nature of the mineralization and type mineralogy very difficult. Production records required to help with the interpretations are also not available. These gold occurrences are similar to that of the Francistown Group (Section 7.2.3.10).

7.2.3.11 Phenalonga Group

These deposits are hosted by Dinuku Formation carbonates at the top of Phenalonga Group (Figure 3.10) and are located at the intersection of shear zones. The Phenalonga Group contains appreciable concentrations of base metals, Pb, Cu and Zn, compared to other lode gold deposits in the Tati Greenstone Belt. Tungsten is also reported (Molyneux, 1971).

7.2.3.12 Vermaark Group

This group of gold deposits is hosted by ENE-WSW and NNE-SSW trending shear zones localized in silicious volcanic rocks of the Selkirk Group. The mineralized shear zones occur near contacts between Phenalonga and Selkirk Groups, and also near the intrusive Selkirk Igneous Complex. No proper records

were kept and dumps are not in a suitable state to confidently determine the nature of the mineralization and the mineralogy. It is not known whether these deposits are related to the main mineralization event prevalent in the Western Structural Zone of the belt, or to a later event related to emplacement of the Selkirk Igneous Complex.

7.2.3.13 Signal Hill Group

These deposits are shear hosted Sb-Au-bearing quartz veins in meta-sedimentary rocks of the Last Hope Group (Figure 4.2). They are hosted by quartz-mica schists at the contact of a matrix-supported conglomeratic unit and gritty arkosic sandstones. Three mineralized zones (Figure 7.3) have been delineated (Blaine, 1986b). The mineralized zones, however, reflect the pattern of outcrops rather than the different styles of mineralization. The most prominent feature of these deposits is that they contain elevated concentrations of Sb compared to other lode gold deposits in the Tati belt.

The mineralization consists mainly of the Sb sulphide minerals, stibnite, gudmundite and berthierite. Arsenopyrite, pyrrhotite, pyrite and marcasite are also present. Gold is carried by sulphides, such as arsenopyrite, and also occurs as the native metal.

7.2.3.14 Rainbow Group

These gold deposits occur in shear zones localised along contacts between

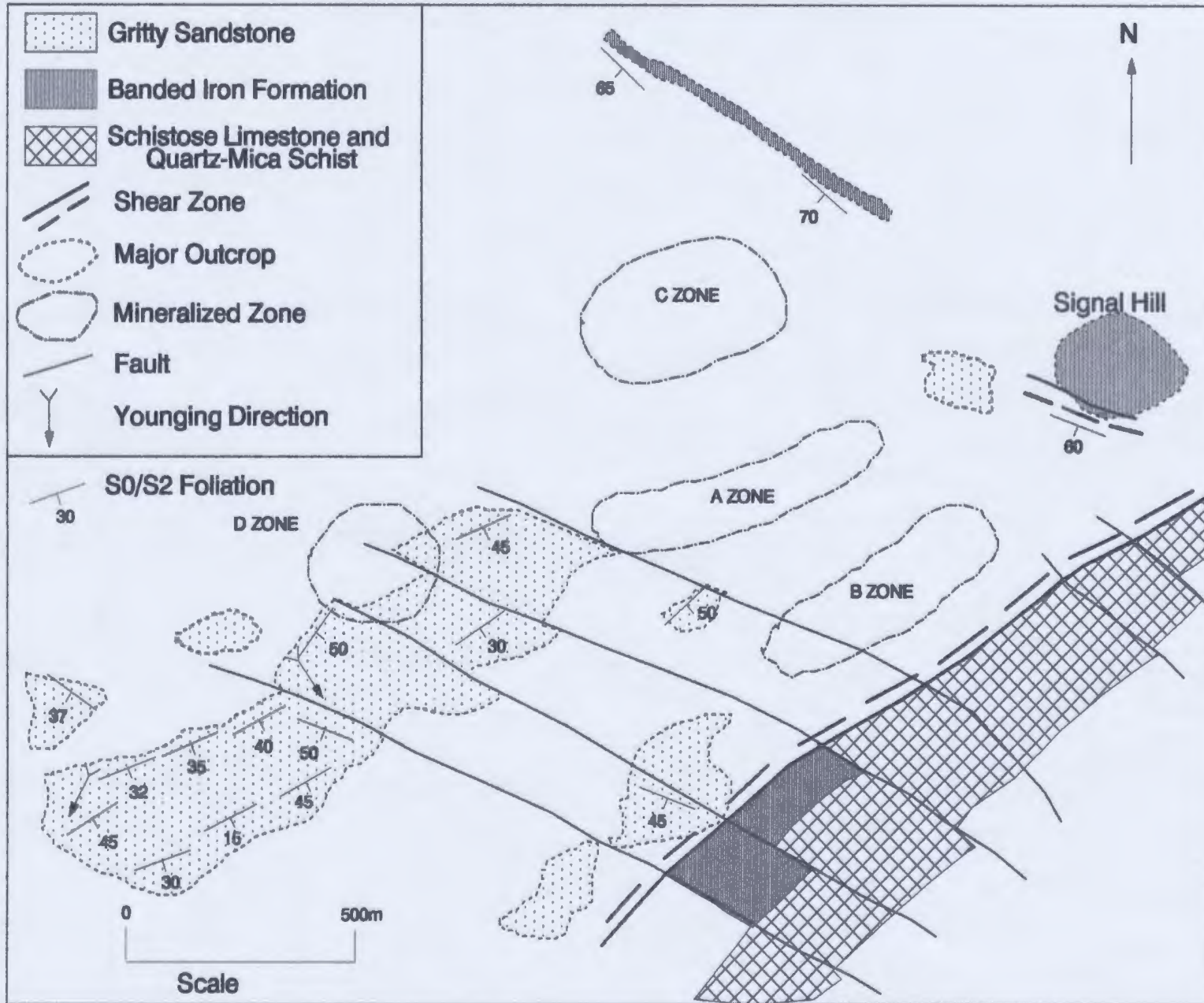


Figure 7.3: Geological map of the Signal Hill area showing the distribution of Sb-Au mineralized zones (geological map modified from Falconbridge Explorations Company plans).

phyllites and banded iron formations (e.g. Rainbow) and in shear zones within banded iron formations (Jim's Luck) in the Matsiloje Ridge area. Tennarite, chalcocite, and chalcopyrite are the common copper sulphides in these deposits. Other sulphides, especially those associated with gold mineralization, include pyrite and arsenopyrite. These deposits follow the northeast trend of the Eastern Structural Zone (Figure 4.2), however, their time of emplacement relative to the other groups in the area is uncertain.

7.2.3.15 Massive Sulphide Deposits

These massive sulphide deposits occur in the northern part of the main outcrop area of the Tekwani Troctolite (Figure 3.12). A series of circular structures, or domes, are visible on aerial photographs, and two of these are related to the Phoenix and Selkirk massive sulphide deposits (Figure 7.4). The third massive sulphide prospect, Tekwani, seems to be off-axis from this linear array of domal structures. The Phoenix deposit is localised in two intersecting shear zones with N-S and E-W trends, and the mineralization is hosted by amphibolites that were intruded by numerous trondhjemitic stocks. The mineralization consists of nickeliferous pyrrhotite, pentlandite, and chalcopyrite, with minor pyrite. About 4.5 million tonnes of ore, grading 2.1 percent Ni and 0.8 percent Cu, have been delineated (Baldock et al., 1977). The Phoenix deposit has relatively high Ni/Cu ratios compared to the other massive sulphide deposits.

The massive sulphide deposit at Selkirk is hosted by a coarse-grained gabbroic

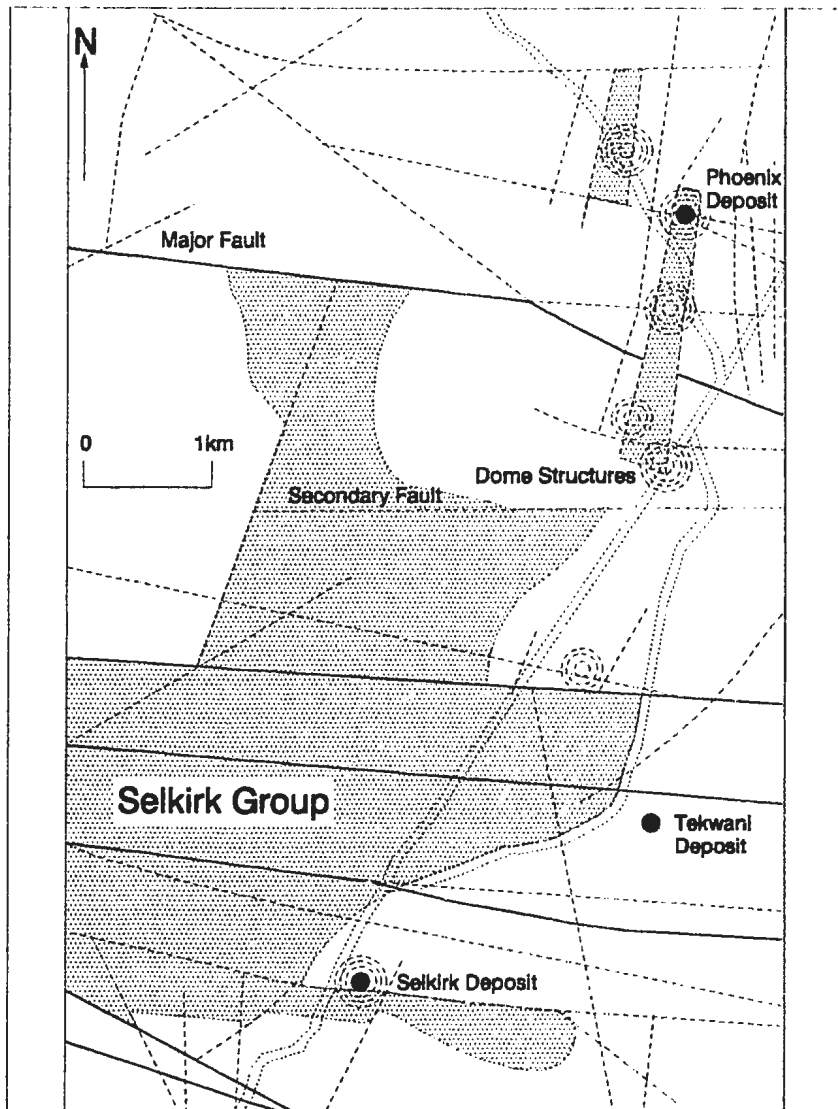


Figure 7.4: Geological Map showing the distribution of Massive Sulfide Deposits in the Tati Greenstone Belt. Broken and full lines are faults and lineaments.

body that intrudes the Selkirk Group feldspar-porphyry. The deposit comprises a zone of massive sulphide bodies with disseminated sulphides at the top and stringer sulphide veins below the massive sulphide zone. The sulphides consist of pyrrhotite, pentlandite, chalcopyrite, and minor pyrite. The deposit contains ~ 3 million tonnes of ore, grading 0.9 percent Ni and 0.8 percent Cu. The average Ni/Cu ratio is about one, but varies widely in the deposit (Baldock et al., 1977).

Minor platinum group element concentrations have been reported from this deposit (Robinson, 1990, personal communication). The Phoenix massive sulphide deposit has not been evaluated to the same extent as the Selkirk Deposit, and, therefore, it is not known whether it contains any similarly enriched concentrations of platinum group elements. The high Ni/Cu ratio of the Phoenix Deposit, however, suggests that elevated values of platinum group elements may exist.

7.2.4 Regional Distribution of Mineral Deposits

Gold deposits occur in all lithological groups of the Tati Greenstone Belt. For example, basalts host the Shashe and Charlie Groups, whereas the Golden Eagle, Rainbow-Matsiloje, and Phenaloga Groups are hosted by metasedimentary units at the top of volcanic sequences. The Bonanza, Vermaak, and Monarch Groups are hosted by intermediate volcanic rocks at contacts with granitoids. The Cherished Hope deposit is hosted by shear zones within granitoid rocks and at the contact between granitoids and diorites. The Jim's Luck and New Zealand deposits are hosted by banded iron formations.

In all these areas, however, mineralization is controlled by shear zones. In general, the mineralized bodies are parallel to the S_0/S_2 foliation but occur at the intersections of lithological boundary-parallel shear/fault zones and secondary cross-stratigraphy shear/fault shear zones (Figure 7.5). The other important observation is that the boundary faults, or thrusts, coincide with the distributions of banded iron formation-bearing sedimentary rocks at the tops of major volcanic sequences. Current research suggests that Archean banded iron formations may have been deposited from hydrothermal fluids not unlike those that form metalliferous sediments in modern oceanic basins (e.g. Sugitani, 1992). The Tati Greenstone Belt banded iron formations consist of both oxide and sulphide facies. The Long Gossan body, a few kilometres east of the Golden Eagle Mine, is a major sulphide banded iron formation body which is reported to contain barite (Johnston and Griffiths, 1983).

Figure 7.6 shows the distribution of the banded iron formations with respect to major structures or lineaments, and illustrates that the distribution of banded iron formation is controlled by major boundary parallel lineaments. The relative distributions of the Tati Greenstone Belt gold deposits with respect to the distribution of banded iron formations are also shown on Figure 7.6. There is close correspondence between the distributions of banded iron formation and gold mineral deposits.

It has also been observed that mineral deposits such as the Shashe Group, hosted by basaltic rocks, occur at contacts between gabbroic sills and basalts. The presence of pillow and amygdaloidal textures in the basalts indicates that these rocks

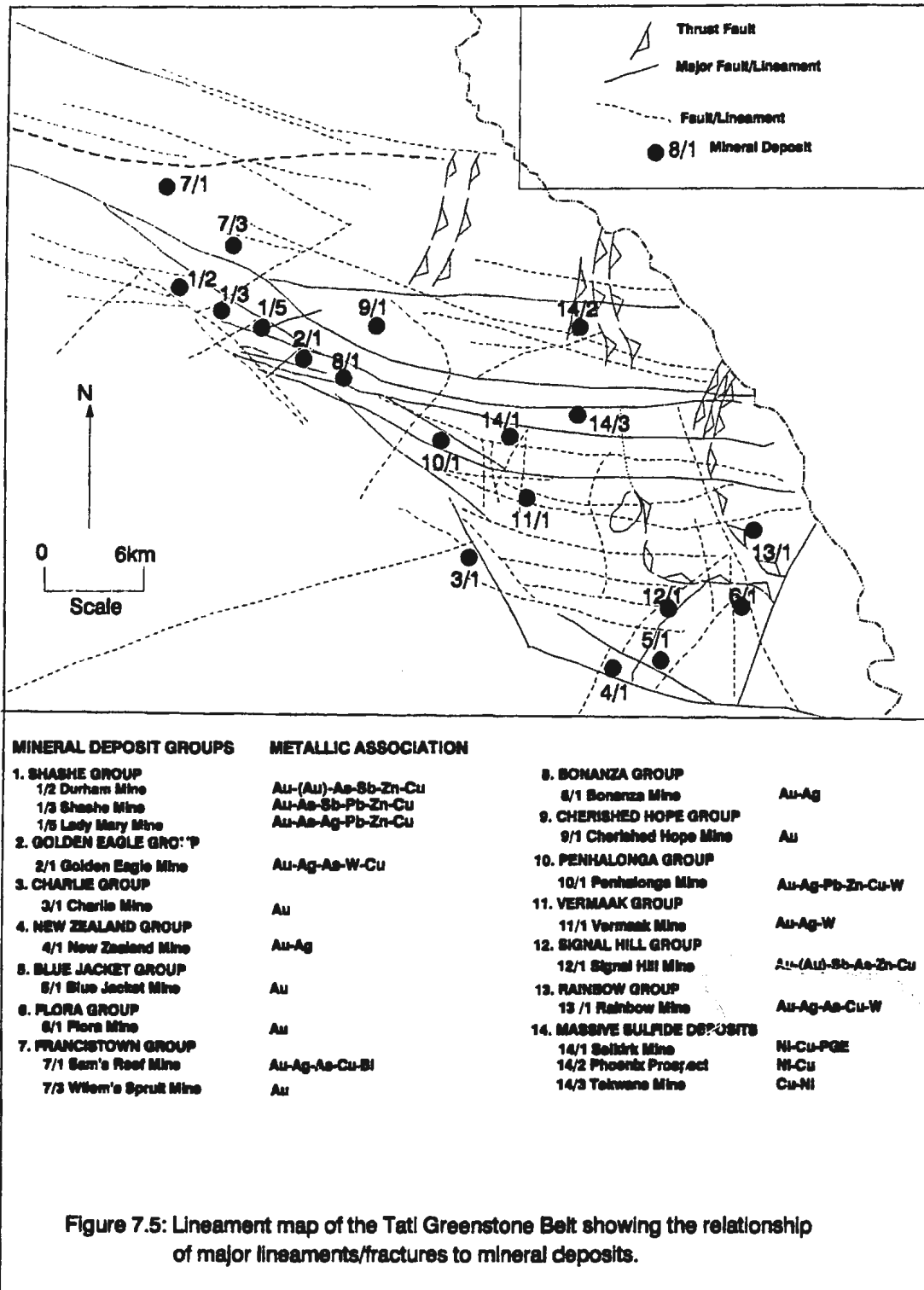
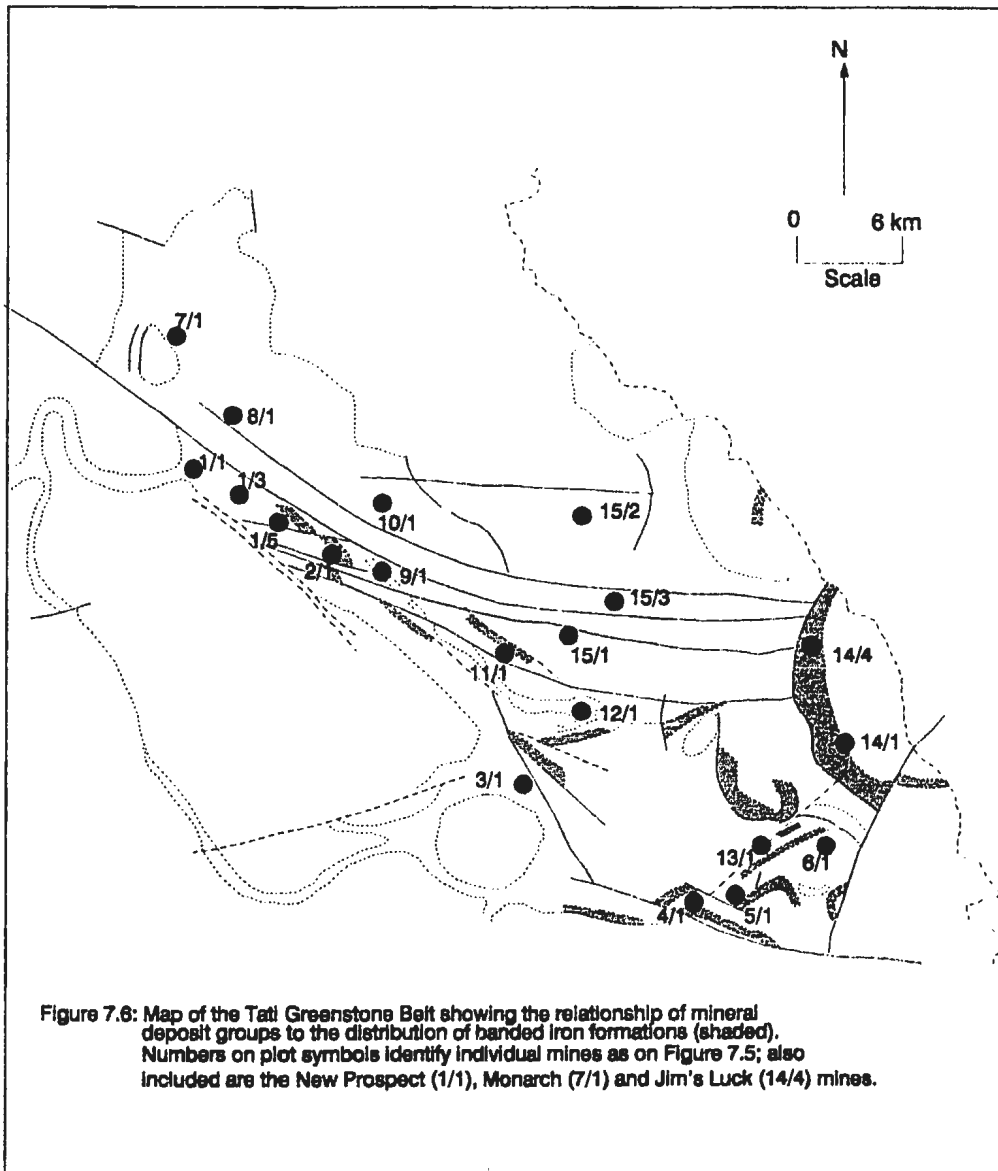


Figure 7.5: Lineament map of the Tati Greenstone Belt showing the relationship of major lineaments/fractures to mineral deposits.



were deposited in a submarine environment. In such tectonic settings there is some considerable potential for the development of large hydrothermal systems. Fluids from such systems could have migrated down through regional scale fault zones to the hotter and deeper parts of the volcanic pile and leached metals, before being driven upwards to be discharged as geothermal systems. The banded iron formations would have been deposited at this stage.

7.3 Metallogenic Analysis

7.3.1 Introduction

The Tati Greenstone Belt is comparatively small (60 x 30 km) compared to the world's largest Archean greenstone belts. The belt is smaller than other belts such as the Bulawayo Greenstone Belt in Zimbabwe, the Barberton Mountain Land Greenstone Belt in South Africa and the Abitibi Greenstone Belt in Canada, among others. Although it is smaller in size, the Tati Greenstone Belt has a wide range of lode gold mineralization styles, comparable to those found in the larger belts.

Two of these deposits, the Signal Hill deposit, hosted by metasedimentary rocks of the Last Hope Group, and the Shashe deposit, hosted by basaltic rocks of the Lady Mary Group, will be described in detail in this section. These two deposits were chosen for examination because of their differences in both host rock lithology, structure, alteration and mineralogy. Since these two deposits are emplaced in widely different lithologies (volcanic and sedimentary rocks respectively), they provide an opportunity to carry out a comparative metallogenic analysis of lode gold deposits

within the Tati Greenstone Belt. The main emphasis of this section is to define the role played by structure during the mineralization events, especially with regard to fluid transportation, distribution of alteration and control of mineralization. The latter part of the section will present geochemical data in order to assess fluid/rock interaction during mineralization and alteration.

7.3.2 Signal Hill Deposit

The Signal Hill deposit occurs at the southeastern margin of the Last Hope Sedimentary Basin (Figure 3.7), about 45 kilometres southeast of Francistown. The deposit was mined during two periods, the ancient mining period (pre-1866) and the period between 1930 and 1940 (Byron, 1983). Several excavations scattered around the Signal Hill area expose mainly stibnite-rich areas, suggesting that the ore was probably mined for antimony. Quartz veins and dumps from three shallow shafts, estimated to be about 15 to 20 metres deep, indicate that gold may also have been targeted. Processing of the ore was probably carried out at the Rainbow mine site, about 7 kilometres to the east (Byron, 1983).

7.3.2.1 Local Geology

Lithologic units in the vicinity of the deposit crop out on small ridges that form the southeastern boundary of the Last Hope sedimentary basin (Figure 7.3). These units vary from pale red, fine-grained quartz-mica schist (or arkosic sandstone) to pale grey gritty sandstone. The quartz-mica schist contains interbedded pebble

conglomerate units of variable thicknesses. The pebbles and clasts are mostly siliceous materials, vein quartz and granitic clasts, and bluish green clasts from altered mafic rocks. The conglomerate is matrix supported with the quartz-mica schist forming the matrix. A dark brown ferruginous conglomerate unit with banded iron formation and quartz-mica schist clasts caps the sedimentary succession (Figure 7.7). The most important unit in this area, especially with regard to mineralization, is the pale-red, quartz-mica schist which varies from finer grained varieties to relatively thick conglomeratic zones.

The rocks in this area have a general southwest trend with a well-defined bedding-parallel secondary foliation. This foliation is marked by mica flakes, alignment of detrital quartz grains and rock fragments. The foliation and bedding all dip at moderate to high angles to the southeast (45° - 70°). The dip steepens from north to south as the edge of the basin is approached. The finer-grained varieties contain microscopic crenulation folds. The surface expression of this deformation is shown by boudin structures in more competent layers (especially quartz veins).

North and east of these meta-sedimentary rocks are banded iron formation ridges, the most prominent of which is Signal Hill (Figure 3.7). These ridges comprise mainly banded iron formations composed of alternating bands of milky white chert and fine reddish brown hematite bands. Variants of this unit consist of jasperoid cherty quartzite. A small hill of highly brecciated banded iron formation, situated several metres east of the main Signal Hill, overlies schistose reddish-brown limestones and phyllites. These schistose calcareous sedimentary rocks are

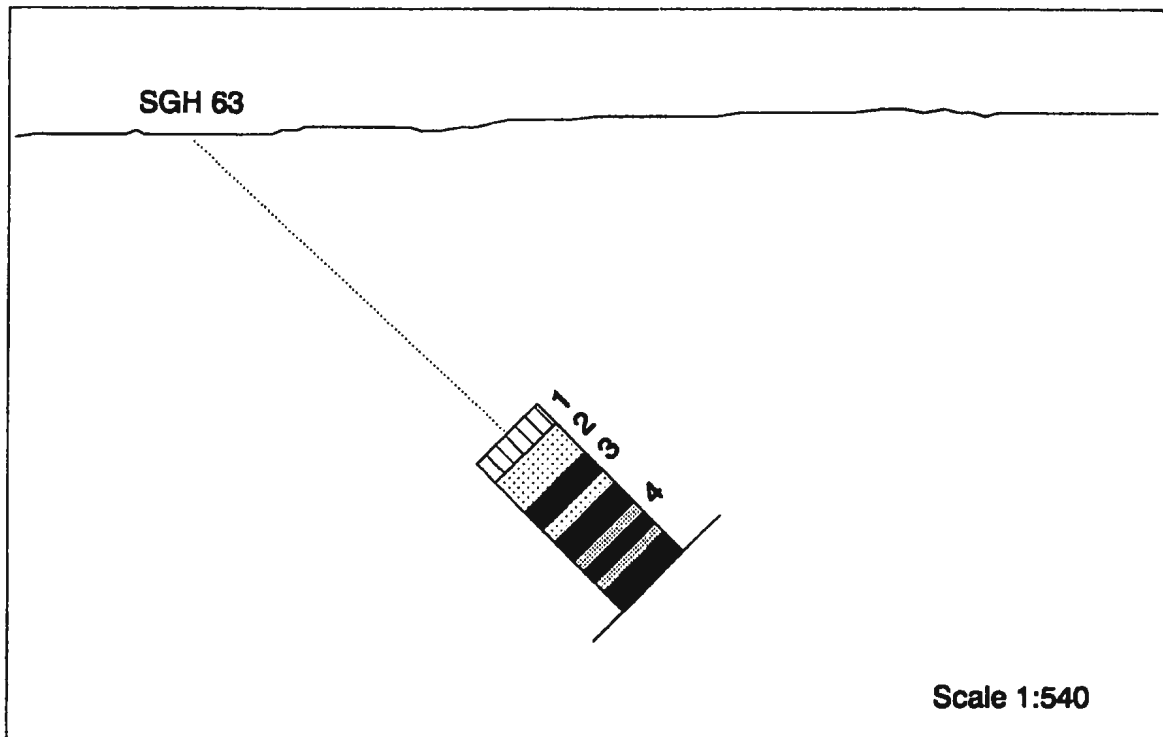


Figure 7.7: Host sediments to the Signal Hill mineralization in borehole SGH 63 . The package consists of dark conglomerate (regolith) with banded iron formation and mica schist clasts (1); pinkish brown conglomerate with mica schists interbeds (2); whitish grey gritty sandstone (3); and pinkish brown mica schists (4).

interpreted (see Chapter 4) to form the sole to the thrust block consisting of brecciated banded iron formations.

A conglomerate containing clasts of quartz-mica schist, chert, and fragments of other rock types in a dark brown ferruginous cement, forms part of this thrust surface. The trends of the banded iron formation ridges, including Signal Hill, are all at right angles to the main trend of the host sedimentary rocks. They also dip at high angles into the sedimentary basin (i.e. SW and W). They are, therefore, interpreted as having been thrust over the sedimentary rocks of the Last Hope Basin. The regional structure of this area was described in Chapter 4.

7.3.2.2 Method of Study

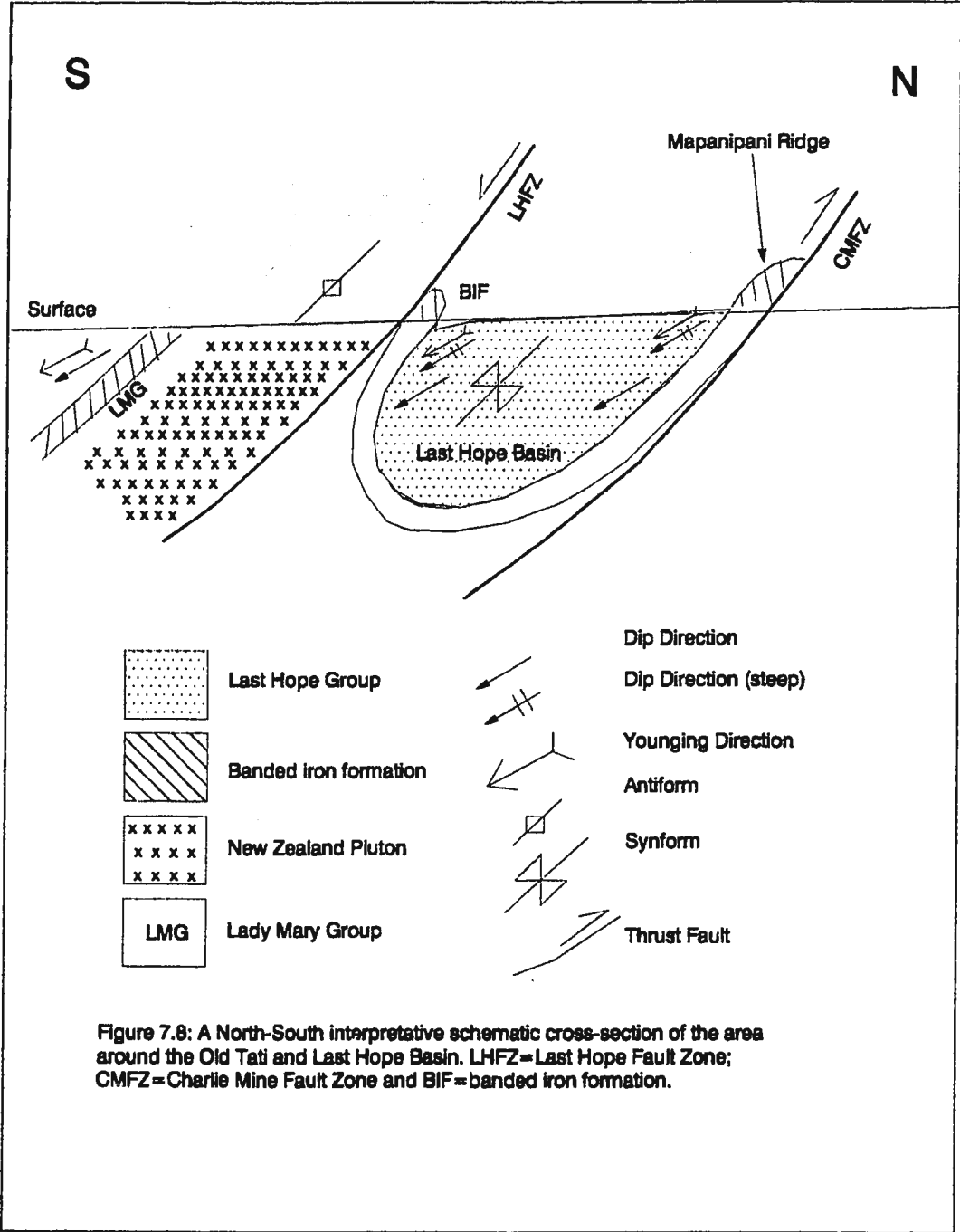
One hundred and ten quartered borehole core samples were collected from the five most representative boreholes at the Signal Hill deposit (Chiepe, 1989, per. comm.). Ninety thin sections were prepared from these samples to investigate the structural control of mineralization and distribution of alteration.

7.3.2.3 Structure of the Signal Hill Area

The structural evolution of the Last Hope Sedimentary Basin was presented in Chapter 4 as part of the overall regional structure of Tati Greenstone Belt. The data and interpretations will not be repeated here, except to highlight essential points that have a bearing on mineralization. In Chapter 4 it was pointed out that the deposition of sedimentary rocks in the Last Hope Basin may have been controlled

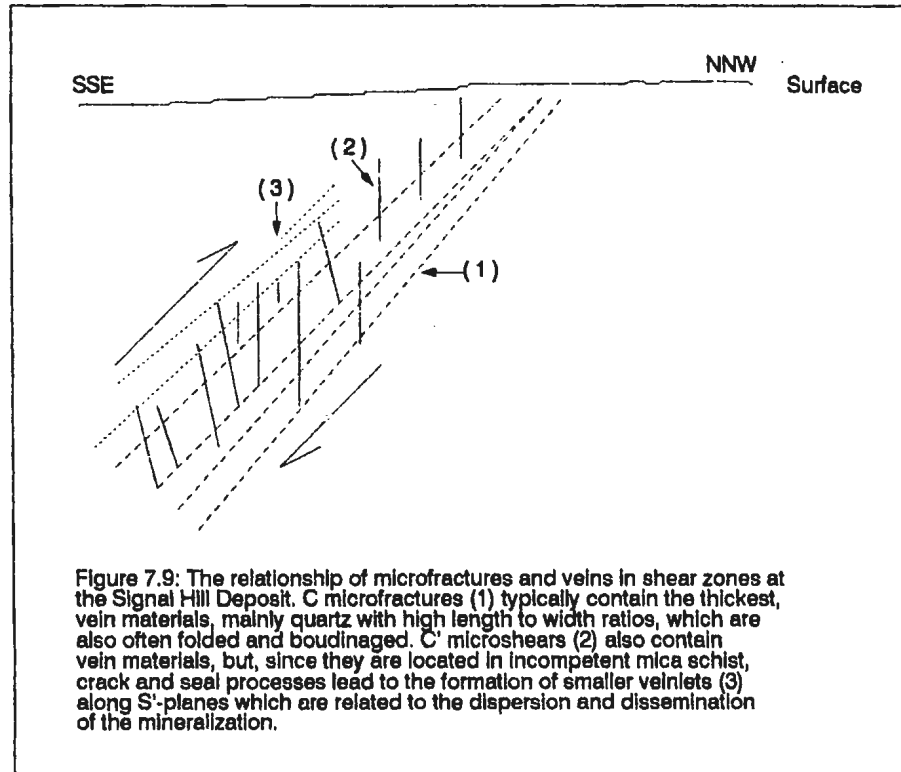
by normal faults related to transpressional movements on a strike-slip couple consisting SLGL-CMFZ-OTL to the south and HVL to the north (Figure 4.6 & 4.7). The southern margin of the basin, separating rocks of the Lady Mary Group in the Old Tati area to the south from the sediments of the Last Hope Basin to the north, is marked by SW-trending, SE-dipping high-angle reverse or thrust fault (Figure 7.8 and LHFZ in Figure 4.6). The LHFZ is interpreted to have been a re-activated normal fault formed as part of the strike-slip shear couple. The re-activation of this fault was part of the NW-directed thrust movement (D_4). This thrusting resulted in the duplication of the Last Hope Group quartzitic rocks around the Signal Hill area (Figure 7.3) through faulting and folding. Thrusting occurred along the boundary between the Lady Mary Group rocks around the Old Tati area and the Last Hope Basin sediments. Therefore, the LHFZ forms a lithological boundary-parallel fault/shear zone.

The LHFZ controls the distribution of the Signal Hill Sb-Au mineralization. This mineralization, although not directly hosted by this structure, is controlled by structures (folds and secondary faults) related to movements on this fault/shear zone. Mineralized secondary shear zones are parallel to lithological boundaries which are parallel to the main fault/shear zone. At the surface, highly bleached, pale-grey kaolinite-chlorite-mica schists mark the sites of these mineralized high-angle secondary shear zones. These alteration/shear zones are mainly localized at lithological transitions between the conglomeratic and fine-grained mica-schist units. These transition zones seem to have been areas of major fluid transport as they



contain quartz and quartz-carbonate shear veins parallel to the main shear zone and foliation. Petrographic and XRD analyses indicate that the white clay mineral which occurs along these lithological boundaries is hydrothermal kaolinite derived from the breakdown of mica (muscovite) and detrital potassic feldspar. These kaolinite-bearing alteration pipes, although not widely developed, are interpreted as evidence for major fluid circulation along these transition zones.

The distribution of veins, and the structure of the mineralization, in the Signal Hill deposit (Figure 7.9) are controlled by NW-directed thrust movements along the LHFZ. The re-activated LHFZ acted as a SE-dipping WSW-ENE trending high-angle detachment fault. In general, displacements on detachment zones are accompanied by the formation of two classes of fractures; tensional, and shear or extensional fractures (Reynolds and Lister, 1987). Reynolds and Lister (1987) interpreted tension fractures as planar structures occurring in parallel sets. Shear fractures, on the other hand, occur as sets that intersect at acute angles. Sibson et al. (1988) and Sibson (1989) described similar fractures and veins in high-angle reverse faults as "steep fault veins" subparallel to the main shear zone, and subhorizontal veins "flats". The distribution and formation of such veins were described as being related to the interplay between fluid pressure (P_f) and deviatoric stress (Sibson et al., 1988; Reynolds and Lister, 1987). Subhorizontal veins, or "flats", were interpreted (Sibson et al., 1988) as having formed in hydraulic tension fractures, perpendicular to the least principal compressive stress (σ_3), that were held open during vein-filling by fluid pressures in excess of the lithostatic load ($P_f > \sigma_3$).



In the Signal Hill deposits, during progressive simple shear deformation in the main shear zone (LHFZ thrust), the pre-existing S_2 foliation, marked by alignment of phyllosilicates in the quartz-mica schist, was crenulated (Plate 7.1). This resulted in the formation of asymmetrical crenulation folds that can be used in assessing the direction of flow (eg. Knipe, 1989; Gray, 1977; and Barker, 1990). The initial stages of the deformation were dominated by microfolding of the phyllosilicate minerals. With further deformation, crystallization of new phyllosilicates parallel to the axial surfaces of crenulation folds dominated over the mechanical rotation of grains, leading to the formation of zonal crenulation cleavage (Plate 4.13) (eg. Barker, 1990). Further progressive deformation led to the formation of microfractures at variable angles to the main shear zone boundaries (Teisseyre, 1970; Barker, 1990; and Platt, 1984) (Plate 4.13, Figure 7.10).

The nature of displacements along these microfractures can be illustrated by microfractures adjacent to folded quartz veins (Plate 4.13 and Figure 7.10). The folded quartz vein was initially oriented parallel to the main shear zone. These quartz veins are, therefore, hosted by shear zone parallel "fault veins" (Sibson et al., 1988) or extensional shear veins (Reynolds and Lister, 1987). The microfractures which formed at variable angles to the main shear zones are similar to extensional crenulation cleavage (Platt, 1979; Platt and Vissers, 1980; Platt, 1984) or C'-S' shear bands (Ponce de Leon and Choukroune, 1980) (Figure 7.11). Similar microfractures also formed in areas between detrital quartz grains and/or rock fragments in conglomeratic units (Figure 4.13). Microfractures at high-angles to the main shear

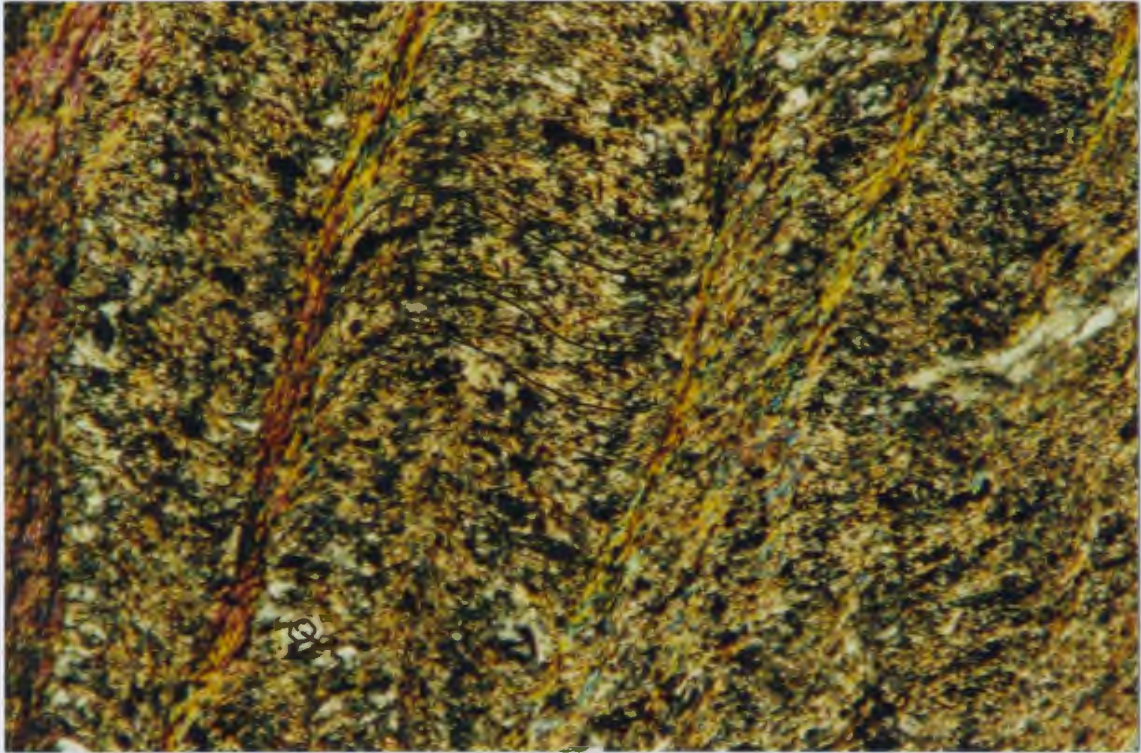
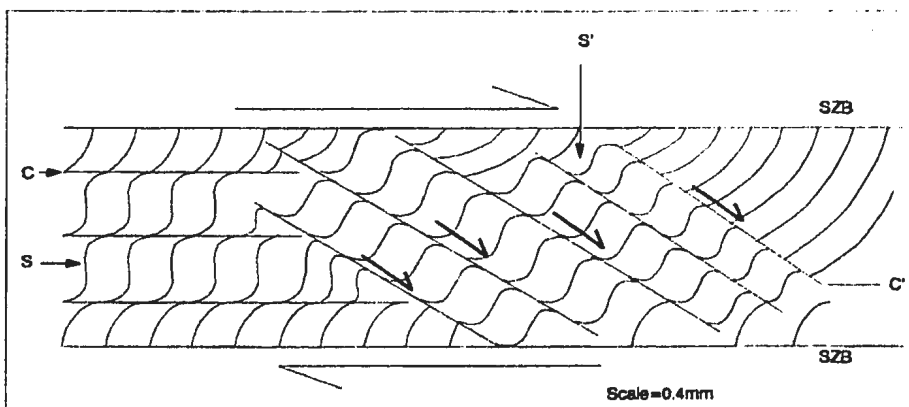
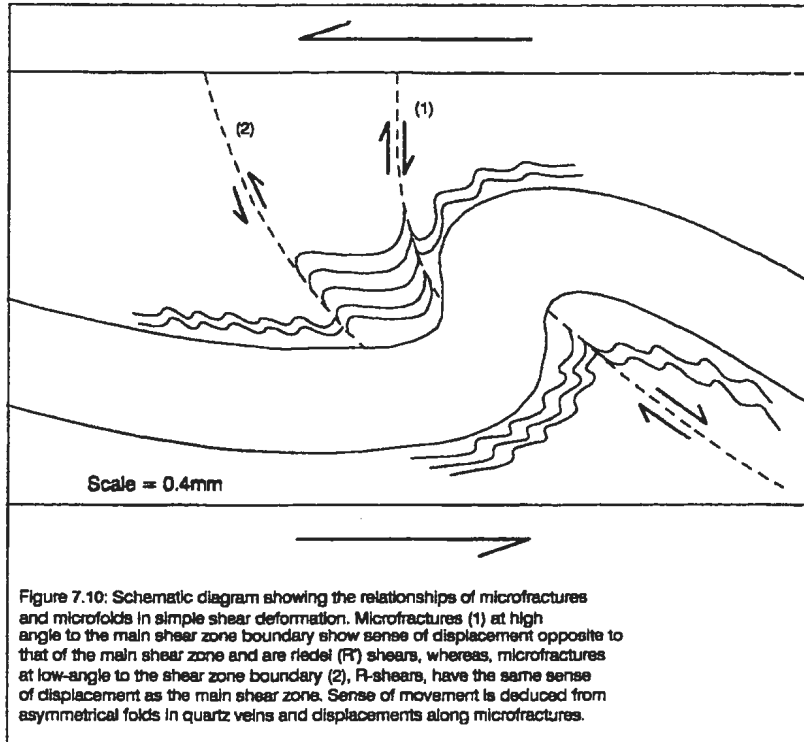


Plate 7.1: Photomicrograph illustrating crenulation folds (H) and crenulation cleavage (L). Phyllosilicate minerals (P) are deposited in the fracture cleavage which cut limbs of the crenulation folds. (Q=Quartz; scale = 0.5mm PL).



zone (Plate 4.13) show reverse displacements relative to the main shear zone direction, whereas displacement directions in low-angle microfractures are the same as those in the main shear zone (Figure 7.10). Therefore, high-angle microfractures may be interpreted as antithetic riedel shears (R') and the low-angle microfractures as synthetic riedel shears (R) (Tchalenko, 1968).

Fluids derived from either within, and/or external to, the host rocks were pumped along the main S_0/S_2 foliation-parallel secondary shear zones forming alteration pipes at lithological transition zones. Areas between grains and rock fragments in the conglomeratic units and at crests of folded quartz veins also formed sites where fluids could accumulate. Accumulation of fluids in such areas lead to the deposition of ribbon quartz along the margins of detrital quartz grains and production of pressure shadow features (Plate 4.14). Further evidence that the main shear zone was the site of major fluid flow is suggested by the presence of fluid inclusion trails in tension microfractures within detrital quartz grains (Plate 7.2). These fluid inclusion trails are contained in microfractures formed at high angles to the main shear zone (Plate 7.2).

In some instances the fluid inclusion-bearing micro-fractures were the sites of phyllosilicate deposition (Plate 7.3). Sibson et al.'s (1988) subhorizontal tension veins formed in hydraulic fractures perpendicular to the least compressive principal stress (σ_3). These microfractures were kept open during vein-filling by a build-up of fluid pressure (P_f) in excess of lithostatic pressure (P_l). Microfractures in the quartz-mica schists of the Signal Hill deposit would seal off through the precipitation of either

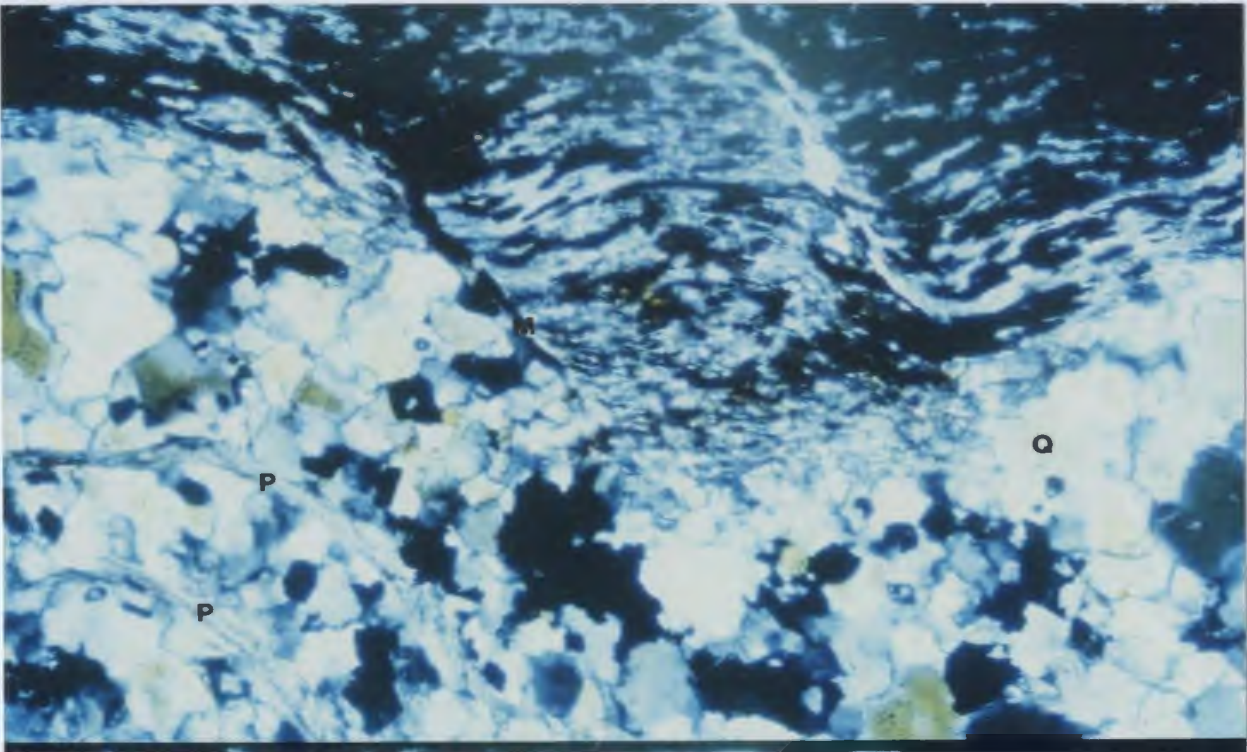
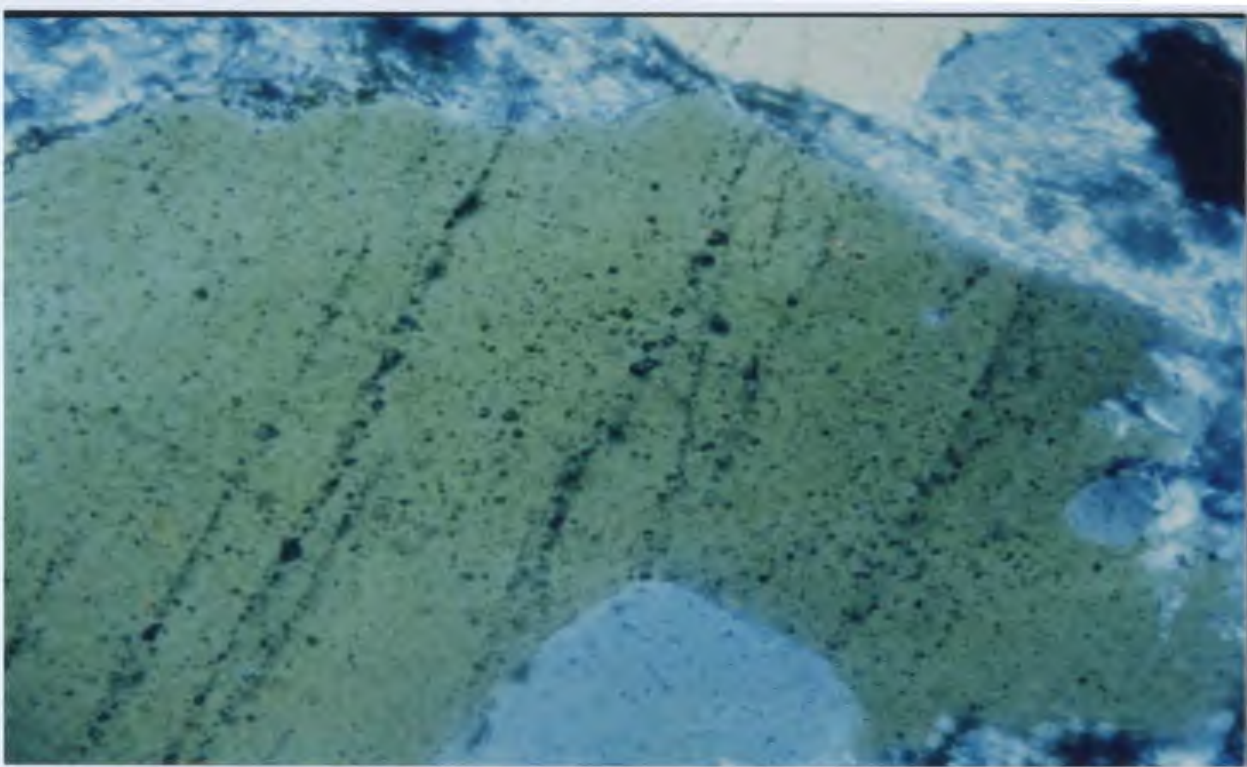


Plate 7.2: Fluid inclusion trails in tension microfractures. The microfractures generally occur at relatively high angles to the main shear zone boundaries. Fluids that are pumped along the direction of the main shear movement diffuse into these fractures (scale = 0.4 mm PL).

Plate 7.3: Folded quartz vein (Q) containing microfractures in which late phyllosilicate minerals (P) were deposited. Although the quartz is extensively recrystallized it clearly pre-dates the shearing event that accompanied deposition of phyllosilicates in microfractures. Examples of such microfractures are marked (M) on the photomicrograph (scale = 0.4 mm PL).

quartz or phyllosilicates. Therefore, repeated opening and sealing led to precipitation of different and/or the same materials at different stages in the crack and seal propagation (Plate 7.4). In some cases fluid pressure was not sufficient to re-open these fractures. In those circumstances, the fluids would flow laterally along the S' planes depositing their materials as stringer quartz veins. These microfractures were also sites along which dissolution of early precipitated materials, such as quartz, took place (Plate 7.5). Some of these micro-shear bands are now relatively large discontinuities (Plate 7.6) that could have also acted as conduits for the downward percolating surface fluids that later oxidized the mineral deposit.

7.3.2.4 Alteration at Signal Hill Deposit

The Signal Hill deposit contains minimal hydrothermal alteration, as suggested by the controversial identification of mineralized quartz veins as chert bands (Byron, 1983). The most intense alteration is mainly silicification, as epitomised by large scale quartz precipitation. White mica (muscovite) is very common in the fine-grained sandstone varieties (quartz-mica schist). The micas are prograde metamorphic products from detrital potassic feldspar within the arkosic sandstone. Minor phyllosilicates (white mica and chlorites), however, also crystallized from hydrothermal fluids within micro-fractures. Kaolinite formed from the alteration of phyllosilicates and detrital potassic feldspar along the main shear zone, as indicated by the bleaching of the quartz-mica schist to a white colour. These areas of massive kaolinite thus define fluid transport zones. Overall this type of alteration should be

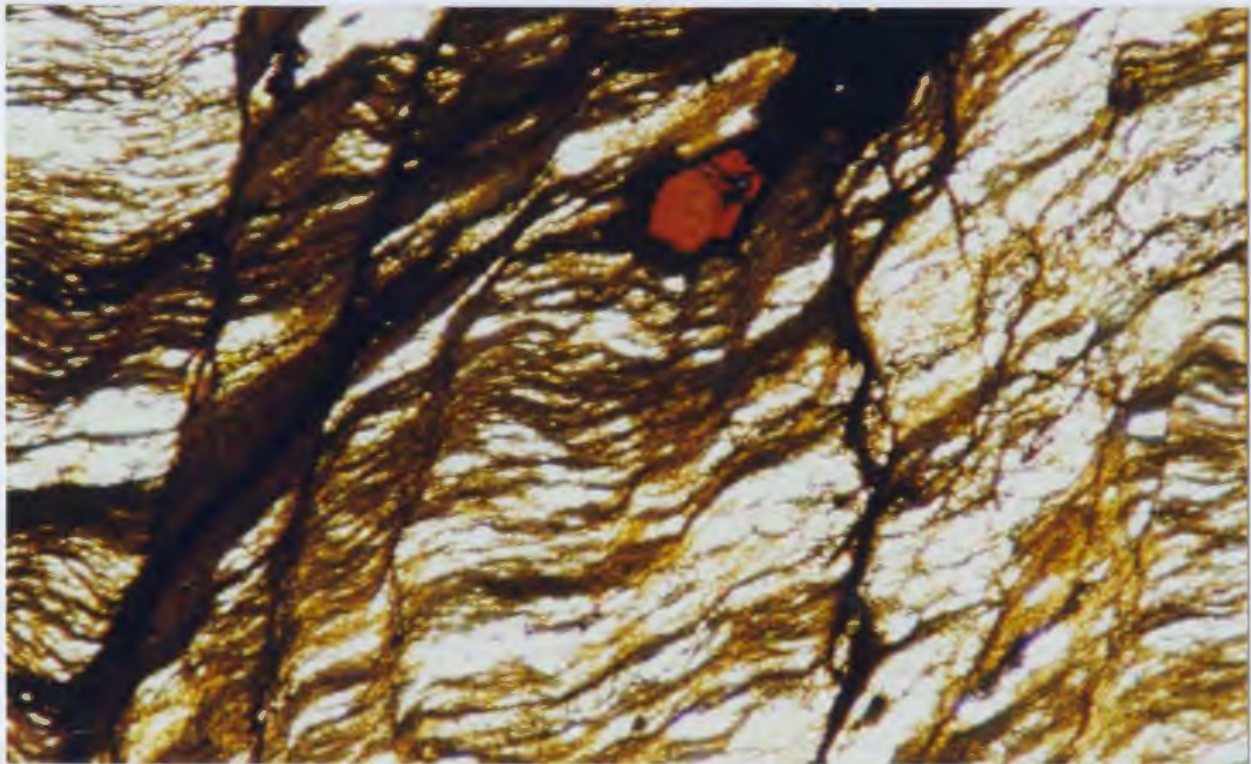
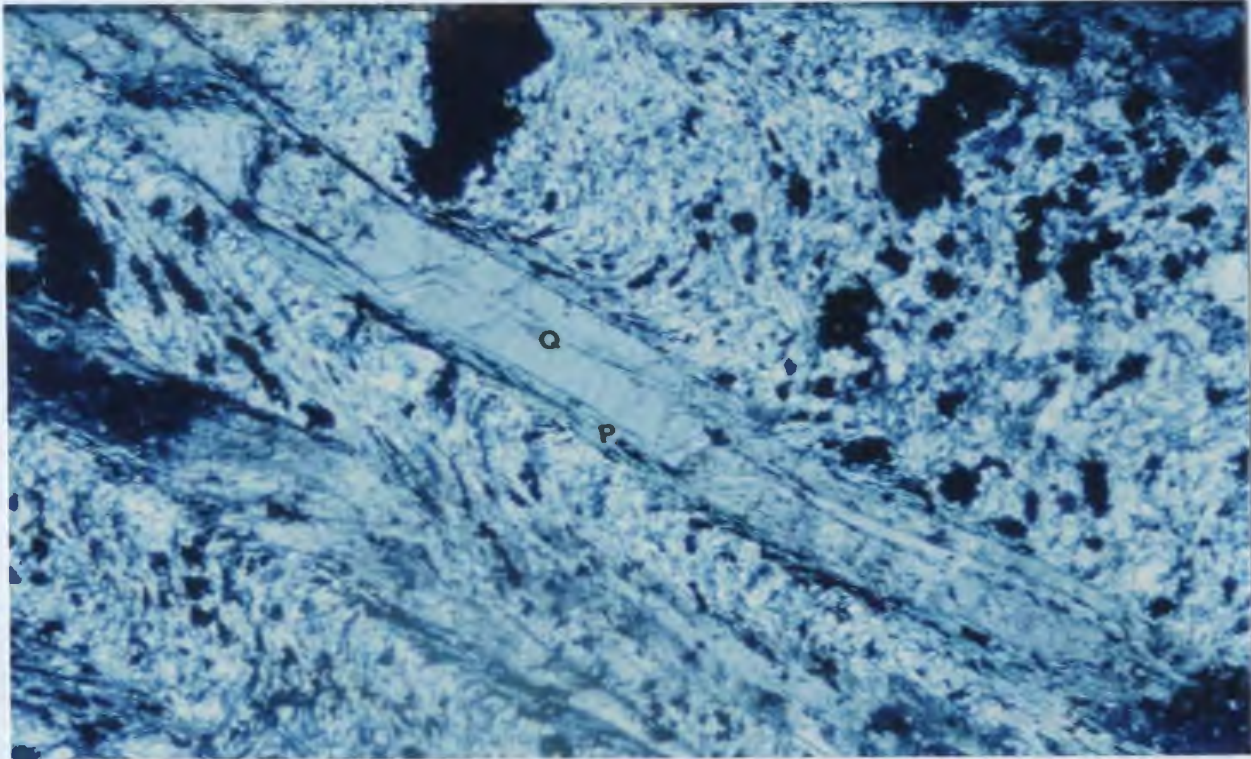


Plate 7.4: Photomicrograph showing multiple vein materials in C' microshears, demonstrating the crack and seal deposition vein materials in fractures. The deposition includes superimposition of late quartz veins (Q) on early phyllosilicates (P), through crack and seal processes (scale = 0.4 mm PL).

Plate 7.5: These C' microshears also form sites along which materials were dissolved, thus enlarging the discontinuities and creating paths for late fluids to remobilize ore-minerals (scale = 0.4 mm PL).

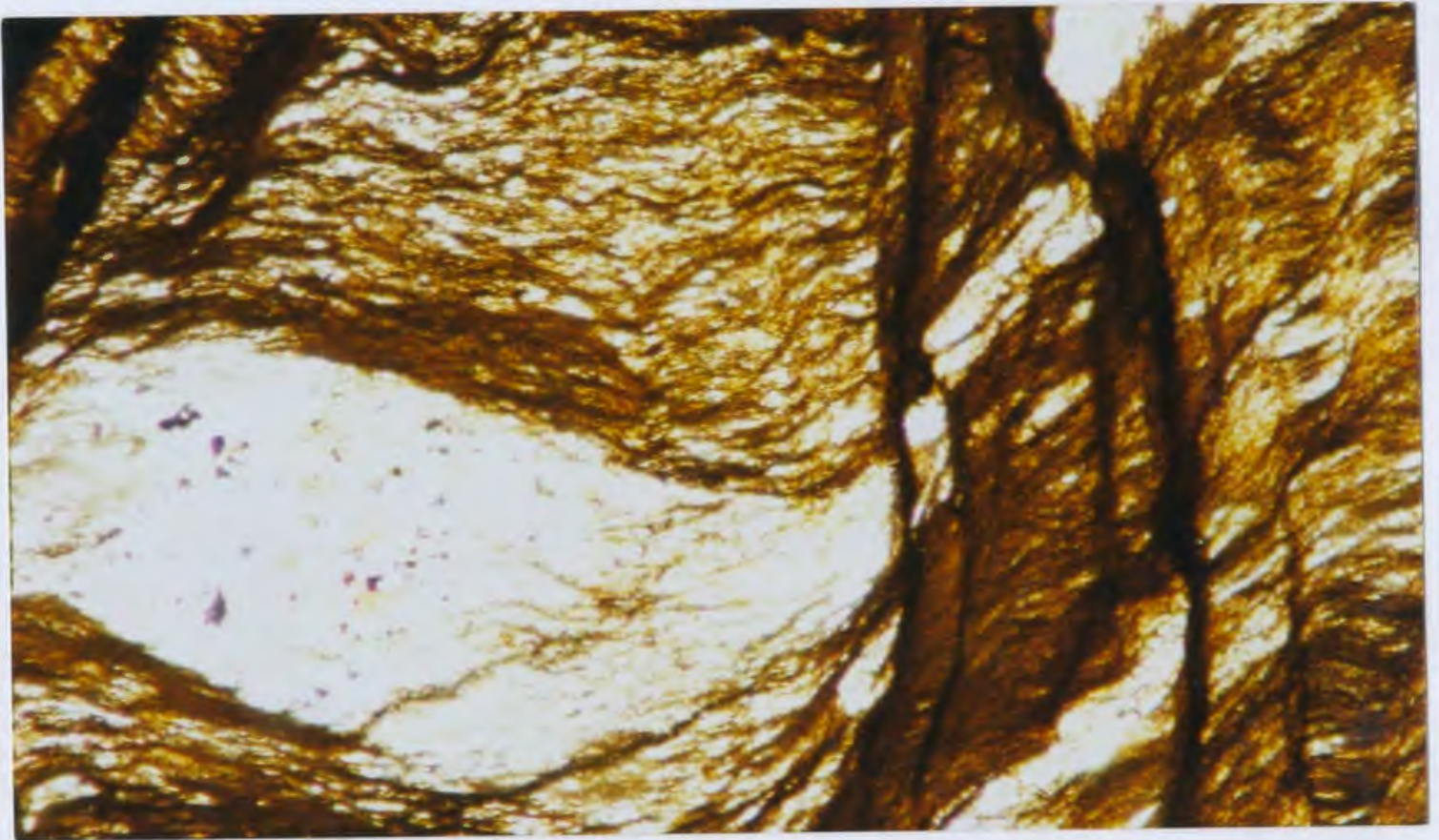


Plate 7.6: Photomicrograph illustrating microfractures that developed into larger discontinuities along which late fluids were transported to oxidize mineralization. These C° microshears are also sites along which materials were dissolved, thus enlarging the discontinuities (scale = 0.5 mm PL).

described as argillic.

7.3.2.5 Nature of Mineralization

There is confusion among geologists working in the area as to what is the nature of the mineralization and what actually constitutes the host rock to the mineralization (Molyneux, 1971; Byron, 1983; Blaine, 1986b; and M. Chiepe, 1989, per. comm.). Molyneux (1971) suggested that mineralization occurs in quartz veins parallel to the (S_0/S_2) bedding/foliation within quartz-sericite schists near a limestone unit. He envisaged the limestone unit as having had a genetic influence upon the mineralization. A slightly different, yet similar, view was presented by Blaine (1986b). He thought that sulphide mineralization occurs as both massive and bleb textures within boudinaged quartz veins, as well as in a stockwork vein system hosted by sericitized and kaolinitized arkosic sandstone (quartz-mica schist). Harwood (1986) suggested that the mineralization consists of disseminated sulphides and replacement bodies following the foliation of a silicate rock.

Byron (1983), on the other hand, considered the boudinaged quartz veins of Molyneux (1971) and Blaine (1986b) to be syn-sedimentary chert bands deposited during siliceous volcanism and that these chert bands were later boudinaged. Mineralization occurs as blebs, stringers, lenses and finely disseminated stibnite in these chert bands (Byron, 1983). He also noted the association of the "cherty" bands with kaolinite-bearing alteration zones in quartz-mica schists. This alteration was interpreted to be syn-sedimentary hydrothermal alteration.

The sulphide mineralization at Signal Hill deposit generally consists of pyrrhotite, pyrite and arsenopyrite, and the antimony minerals, stibnite and gudmundite. Berthierite was also described in samples from one of the boreholes as being replaced by stibnite (Harwood, 1986). Minor chalcopyrite and sphalerite also are present. Gold is commonly associated with, and generally carried by, arsenopyrite and, to a lesser extent, pyrrhotite. Harwood (1986) also reported minute flecks of native gold associated with the antimony minerals gudmundite (FeSbS) and stibnite (Sb_2S_3). Minute gold specks were also observed where stibnite replaces berthierite (FeSb_2S_4). The main carriers of gold are therefore arsenopyrite and pyrrhotite with gudmundite and berthierite as secondary carriers. Sulphide mineralization generally occurs as blebs, disseminations and stringers within the sub-horizontal to horizontal quartz veins (eg Harwood, 1986; Byron, 1983; Blaine, 1986b) and in the discontinuous quartz veins in S'-planes. Because of the variable sizes of these quartz veins, the mineralization is generally dispersed and erratic. The best sites for mineralization are clusters of C'-S' shear bands.

7.3.3 Shashe Deposit

7.3.3.1 Introduction

The Shashe deposit is one of the Shashe Group of deposits (Figure 7.1) hosted by the Map-Nora Formation basalts of the Lady Mary Group. These deposits occur along an elongated ridge of silicified metabasalt which extends from the abandoned New Prospect mine, south of Francistown, for about 10 kilometres to the abandoned

Lady Mary mine (Figure 7.1). The Shashe mine itself is located about 8 kilometres south of Francistown. The deposit is intersected by a series of old shafts that mark the location of four small mines, the Map, Nora, Durham, and St. Kilda. Mining operations were carried out between 1869 and 1945. It has been suggested (Jackson and Griffiths, 1981) that the ancient mining period (pre-1869) exploited the oxidized zones of these deposits.

7.3.3.2 Local Geology

The Shashe deposit occurs within a steeply southwest-dipping shear zone that cuts fine-grained, dark green basalt. The shear zone is localized near the contact between the basalt and syn-volcanic, coarse-grained, metagabbro sills. There are, however, no surface exposures of these shear zones; their existence was proven from underground workings and boreholes. Apart from the presence of the silicified ridge which marks the location of highly altered rocks in the shear zone, some indirect shear indications have been observed, such as deformed amygdaloidal basalt (Plate 4.5) at the base of the silicified ridge. The zone of silicic alteration which forms the ore, or reef, zone consists of brown to red jasperoid or cherty rocks, with variable thicknesses ranging from a few millimetres to several metres.

7.3.3.3 Method of Study

Fifty-five quartered borehole core samples were collected from two of the most representative boreholes at the Shashe Deposit. In addition, thirty-three chip

samples were collected underground along the N9 reef (part of the old Nora workings). Thin sections were prepared from 50 of the 55 core samples.

7.3.3.4 Structure and Alteration at the Shashe Deposit

The structure around Shashe mine was described in Chapter 4 as part the regional structure synthesis of the Tati Greenstone Belt. In this section the interrelations of the microstructures within the shear zones and the distribution of both mineralization and alteration are investigated. Perhaps the most important difference between the Shashe Deposit and the Signal Hill Deposit is the pervasive hydrothermal alteration in the former (Figure 7.12). Three main alteration zones can be recognized; (a) a carbonate zone which constitutes the most widespread and pervasive alteration, (b) a silicified (or reef) zone which is also widespread, but which occurs as discrete zones of variable thicknesses enveloped by the carbonate alteration, and (c) biotite-sulphide veinlets that occur almost exclusively as bands in microfractures within the silicified zone (Figure 7.13).

Secondary silicification zones consist of quartz veins, with variable thicknesses, composed of blue-tinted quartz crystals. These zones are also sulphide-bearing. Another alteration assemblage is the coarse-grained hornblende-biotite zone in which the biotite consists of dark green coarse-grained crystals. The green biotite of this zone is different from the distinctive pink biotite in the main alteration zone.

The carbonate zone is the most pervasive and widespread alteration in the Shashe Deposit. The alteration occurs as single veins, or groups of veins, of variable

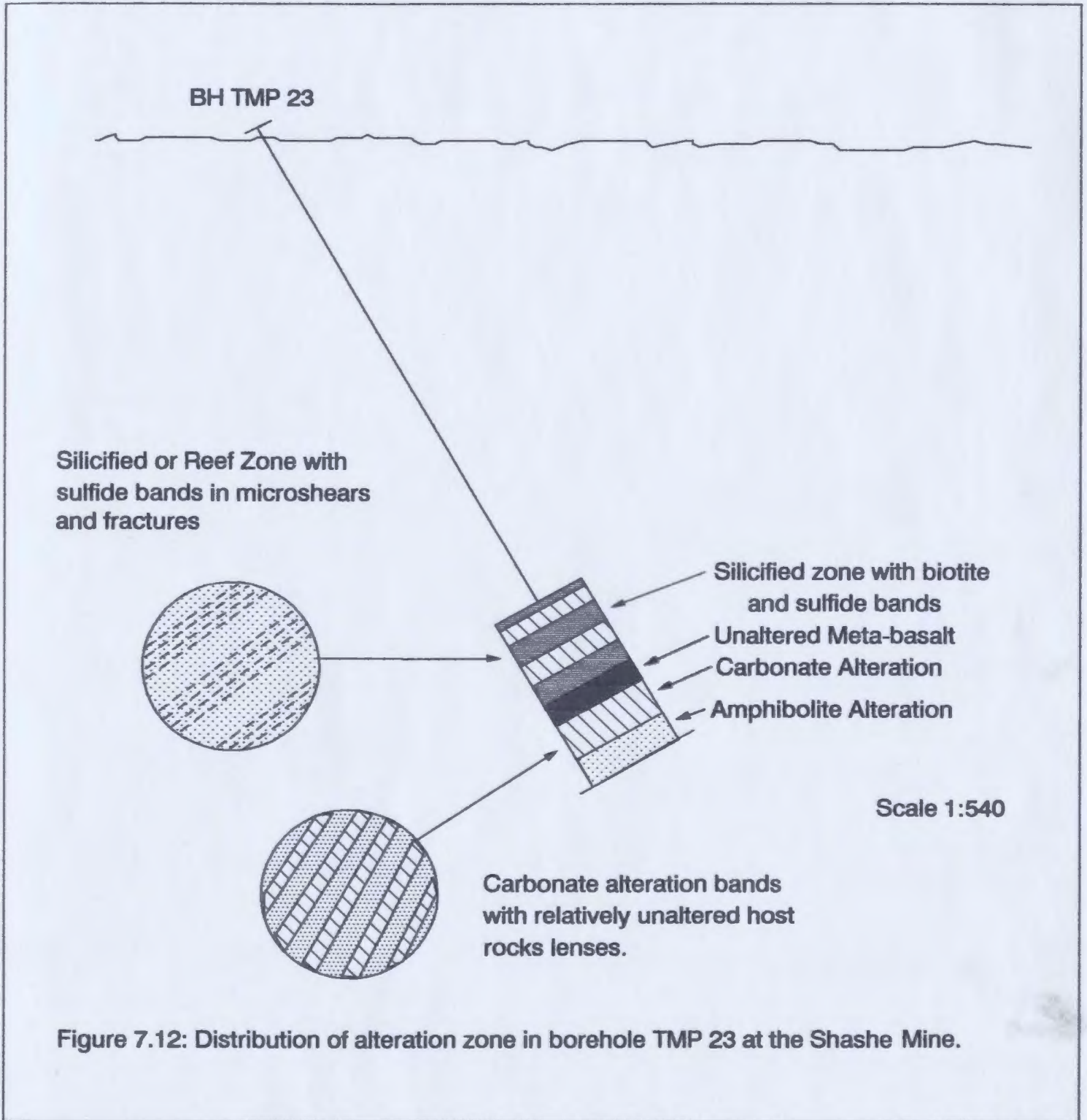


Figure 7.12: Distribution of alteration zone in borehole TMP 23 at the Shashe Mine.

ALTERATION ZONATION AT THE SHASHE MINE

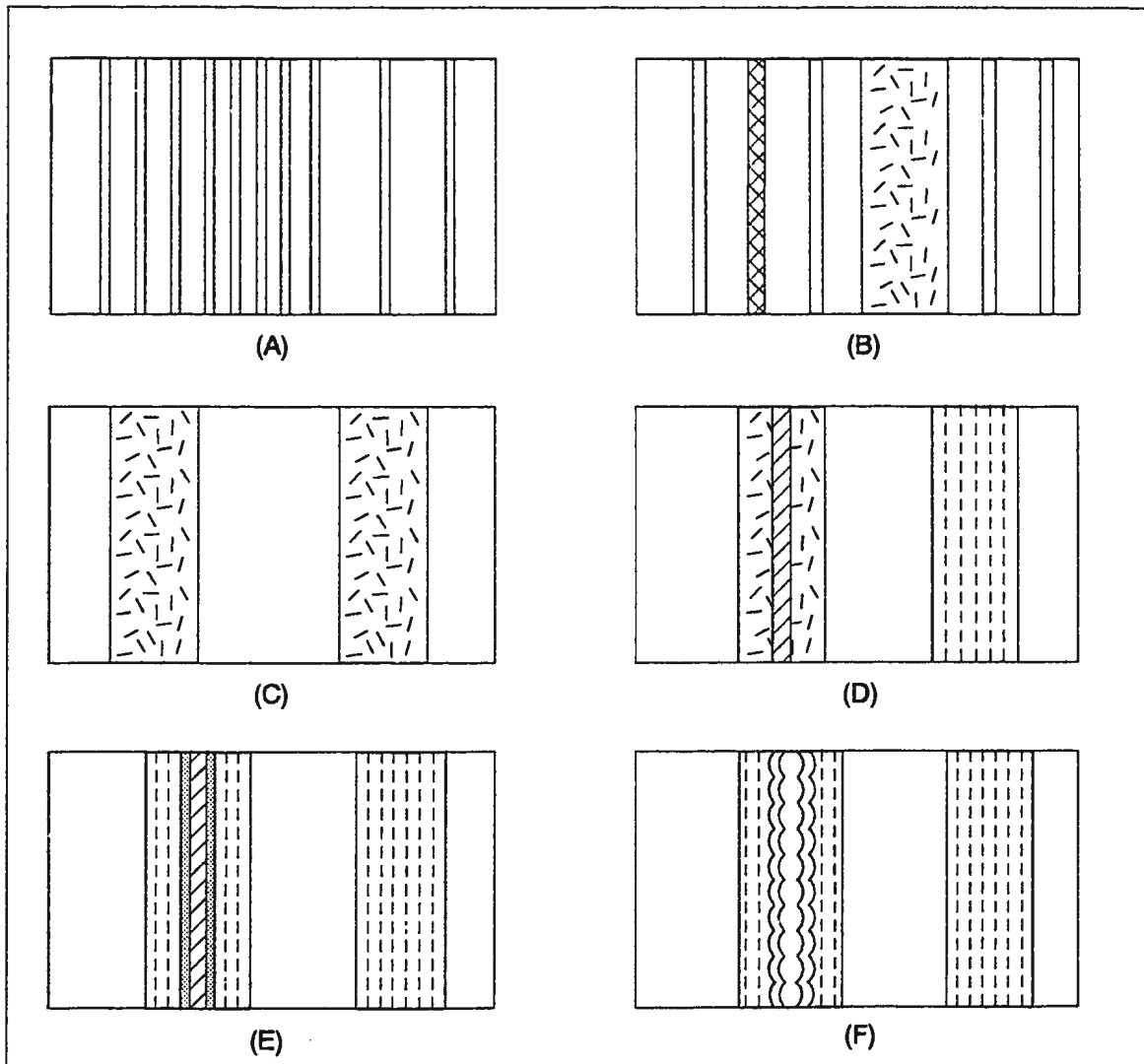


Figure 7.13: The progressive development of hydrothermal alteration and mineralization at the Shashe deposit. (A) Banded carbonate alteration (Zebra rock); (B) replacement of carbonate alteration by silicification and development of reef zones, the sizes of the silicified zones are controlled by the sizes of carbonate alteration zone; (C) sulfide bands on silicified zones, (D) superimposition of late silicified zone or late quartz veining; (E) brown biotite envelope on the quartz veins and (F) boundinaged late quartz veins.

thicknesses ranging from several metres to a few centimetres or millimetres. The multiple nature of these veins gives the altered rock a characteristic banded appearance, or zebra pattern. The carbonate veins consist of euhedral calcite crystals, minor dolomite and siderite (Plate 7.7). The veins are usually surrounded by highly altered host rock. The alteration at the margins of these veins consists mainly of sericite, chlorite, quartz and minor albite (Plate 7.8). The size and abundance of the white carbonate bands decrease from the mineralized zones outwards to relatively unaltered rocks, where only a few, thin bands occur. In most cases, the margins of the carbonate crystals show corroded edges indicating some interaction with acidic fluids (Plate 7.9). The interconnected spaces at crystal boundaries (Plate 7.9) may have acted as channelways along which fluids could infiltrate these zones producing the alteration minerals present at these boundaries (Plate 7.10). In other words, these acidic fluids caused precipitation of silica and/or phyllosilicates (Plate 7.10).

Since the interaction of acidic fluids with carbonate minerals increases the fluid pH, silica solubility in the fluids is reduced leading to deposition of sulphides and brown biotite. Fe-rich sulphides and Fe-rich biotite (i.e. brown biotite) would form since iron is less soluble in high-pH (alkaline) fluids. In hand specimen, these rocks are strongly banded.

Silicification of the zones increased their relative competencies. Subsequent shearing resulted in microfracturing of the silicified zones and these microfractures were exploited by later fluids, leading to the deposition of sulphides, and in some places minor carbonate. These sulphides occur as bands in the silicified zone often

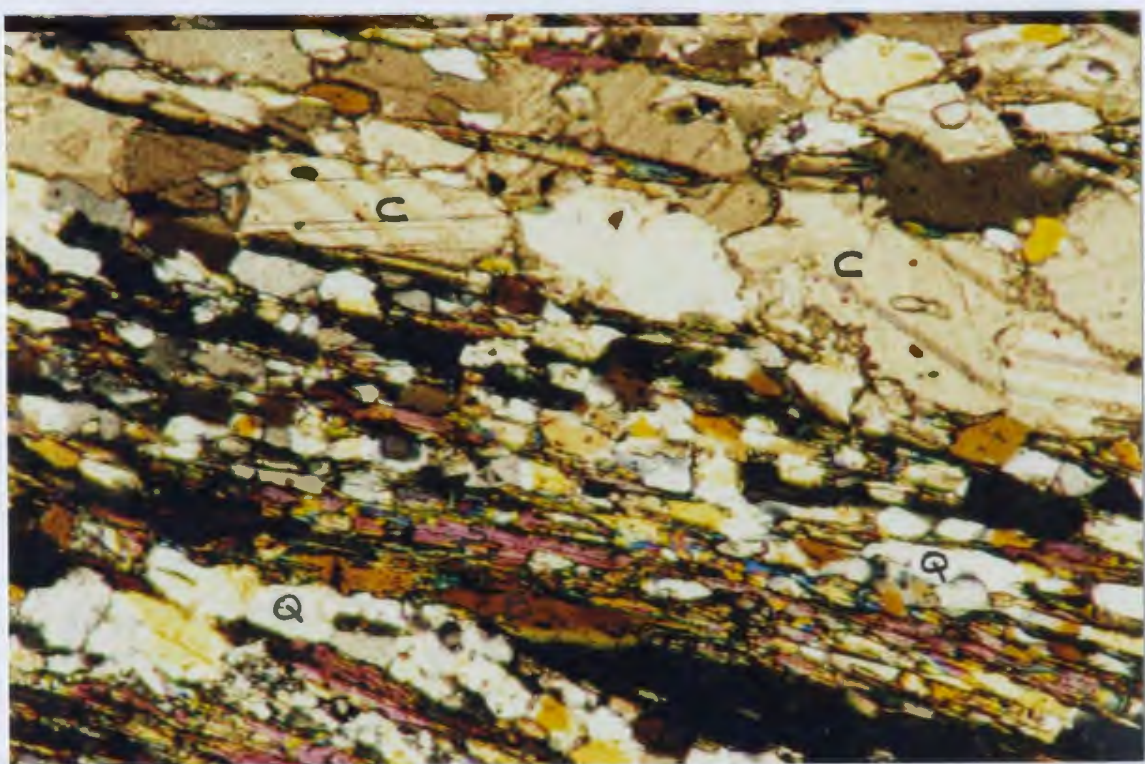
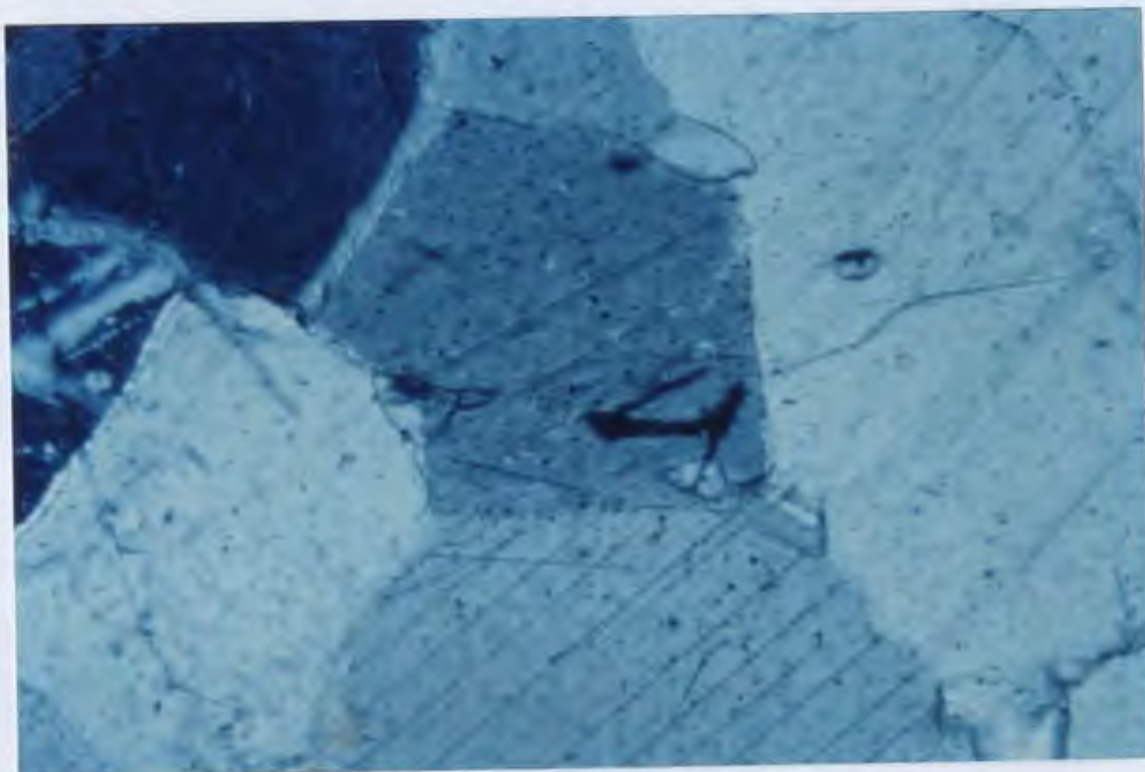


Plate 7.7: Photomicrograph of euhedral carbonate crystals (C) in the carbonate alteration zone. (Scale = 0.4 mm PL).

Plate 7.8: Photomicrograph of highly strained, altered host rocks at the margins of the carbonate alteration veins (C). This texture indicates that, although cores of these veins are undeformed (e.g. Plate 7.7), alteration occurred in wall rocks to the shear zone (Q = quartz; B = biotite and S = sericite - scale = 0.5 mm XPL).

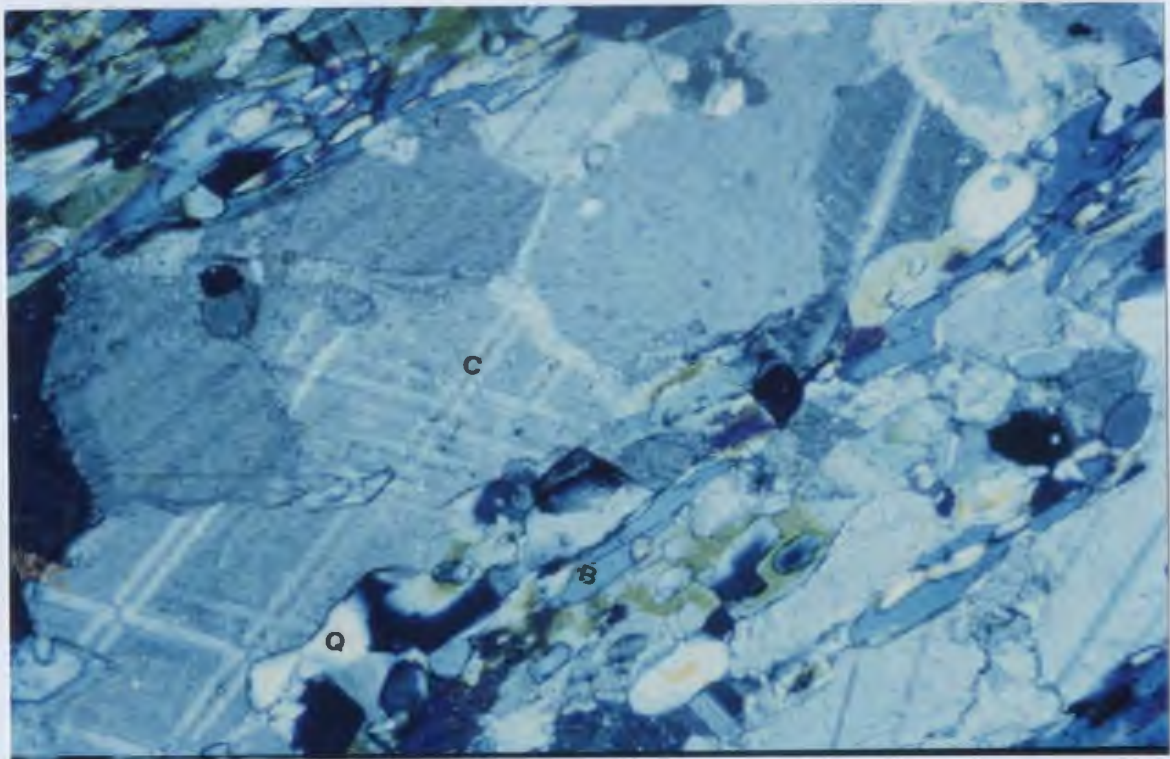
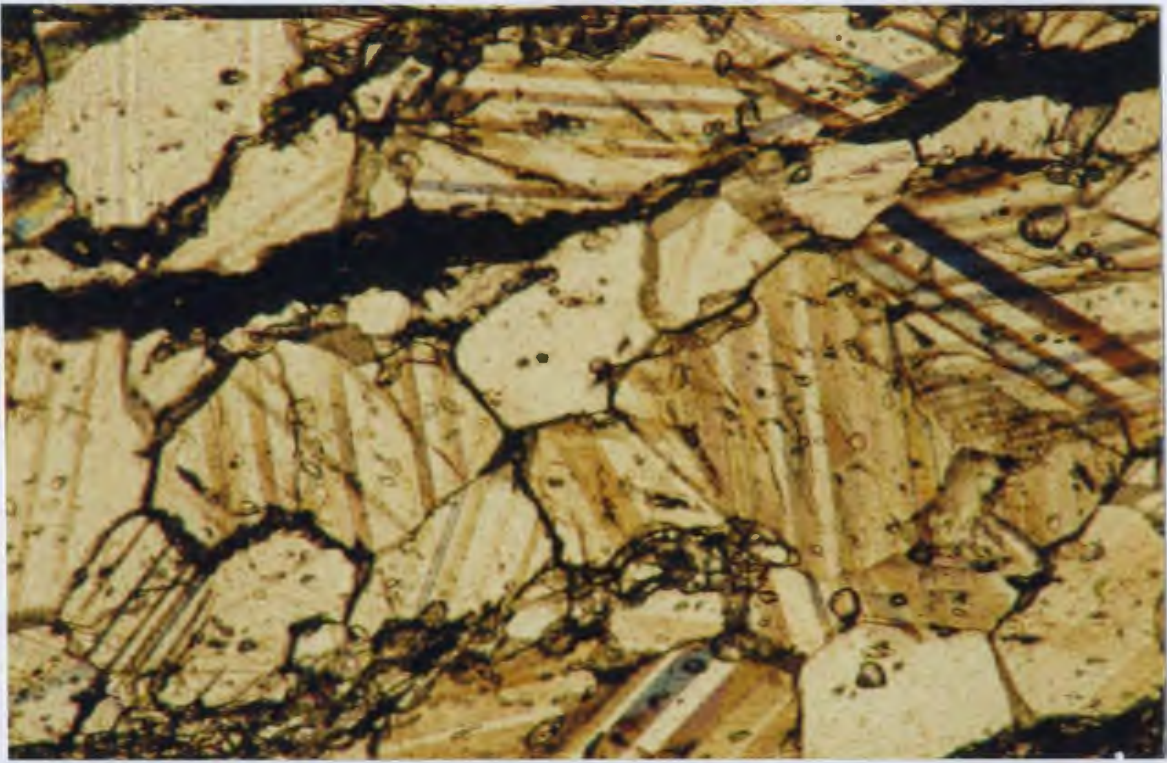


Plate 7.9: Photomicrograph of interconnected microfractures formed by the interaction of fluids which infiltrated along crystal edges and margins with carbonate minerals in carbonate alteration zone. The fluid reactions with carbonate minerals resulted in the deposition of vein materials in these microfractures (mainly quartz) leading to the silicification of the carbonate alteration zone (scale = 0.5 mm PL).

Plate 7.10: Photomicrograph indicating the progressive replacement of carbonate alteration through the deposition of silica minerals (Q = quartz) and minor phyllosilicates (B = biotite). Fluids penetrated through the margins of the carbonate crystals (C) (scale = 0.4 mm PL).

enveloped by distinctive pink coloured, fine-grained biotite (Plate 7.11 and Figures 7.12 and 7.13).

Late quartz veiniron (Plate 7.12) is widespread. These late quartz veins were emplaced in the silicified zones, and in most cases, replace the sulphide-biotite micro-bands. This silicification event is very distinctive in that the secondary quartz ranges in colour from clear (rare), to blue tinted, relatively coarse-grained quartz (common).

7.3.3.5 Nature of Mineralization

Gold mineralization at the Shashe Mine is associated with sulphides as solid solutions and as native gold. Gold is carried by arsenopyrite, and to a lesser extent, by berthierite and pyrrhotite. The sulphide mineralization consists of pyrrhotite and pyrite as the main sulphides, with minor occurrences of arsenopyrite, marcasite, chalcopyrite and sphalerite. The Sb minerals, berthierite and gudmundite, are more common here than at Signal Hill where stibnite is the most common.

The gold-bearing sulphides occur as bands of multiple stringers in micro-fractures hosted by the silicified zone. Brown biotite envelopes these bands. Thin carbonate and quartz veinlets also occur in this zone (Figure 7.13). The sulphide micro-bands constitute an early episode of mineralization. Locally, second-generation quartz and carbonate veins are superimposed on these early micro-bands, and commonly also carry sulphide mineralization. The second-generation veins, especially quartz, are up to 0.5m thick. The smaller veins consist of blue tinted quartz, whereas,

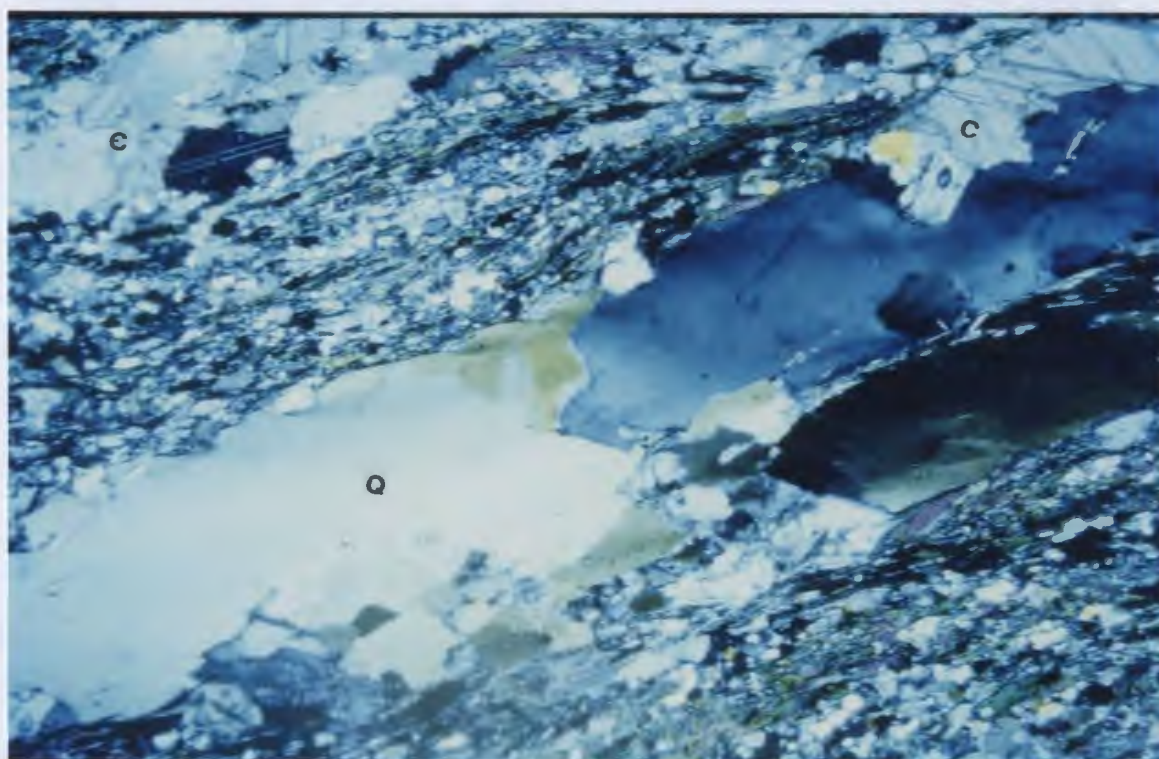
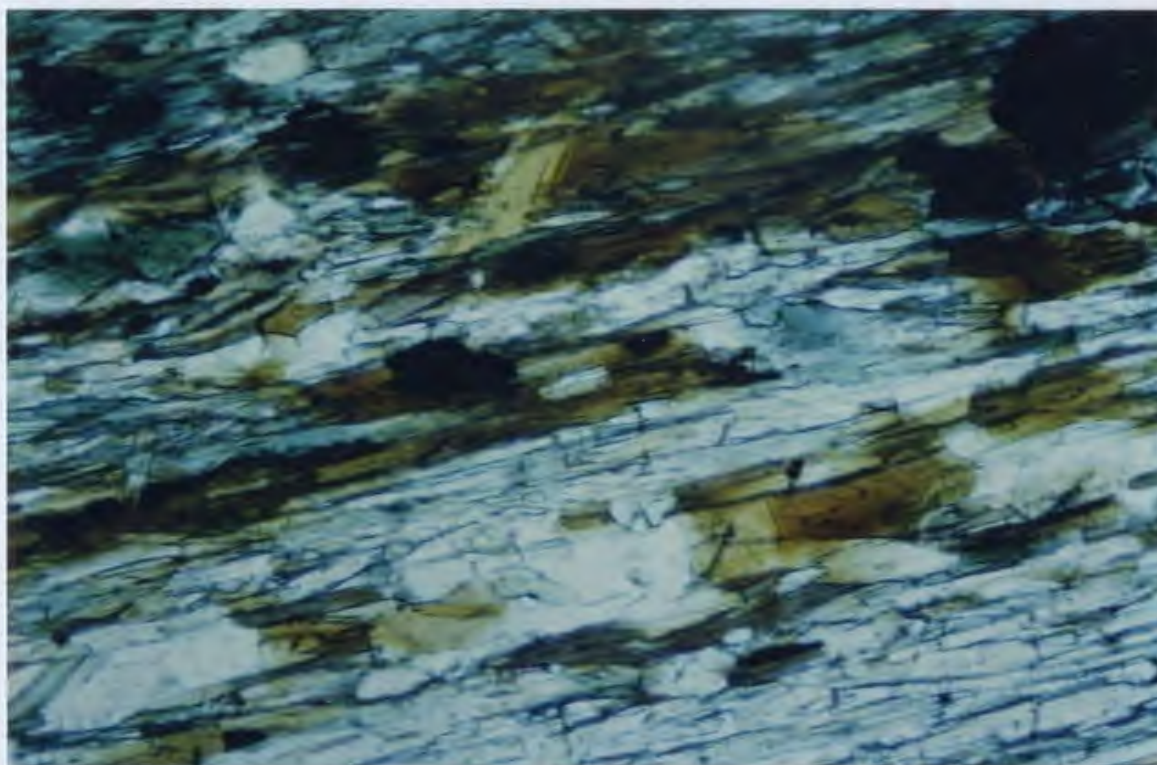


Plate 7.11: Photomicrograph showing brown biotite which is the most common mineral in alteration zones that envelope gold-bearing sulphide mineralization (scale = 0.4 mm PL).

Plate 7.12: Photomicrograph showing late silicification (Q = quartz veins) superimposed on early carbonate alteration (C). The early carbonate veins are highly altered with late silicification veins deposited in alteration zones (scale = 0.4 mm PL).

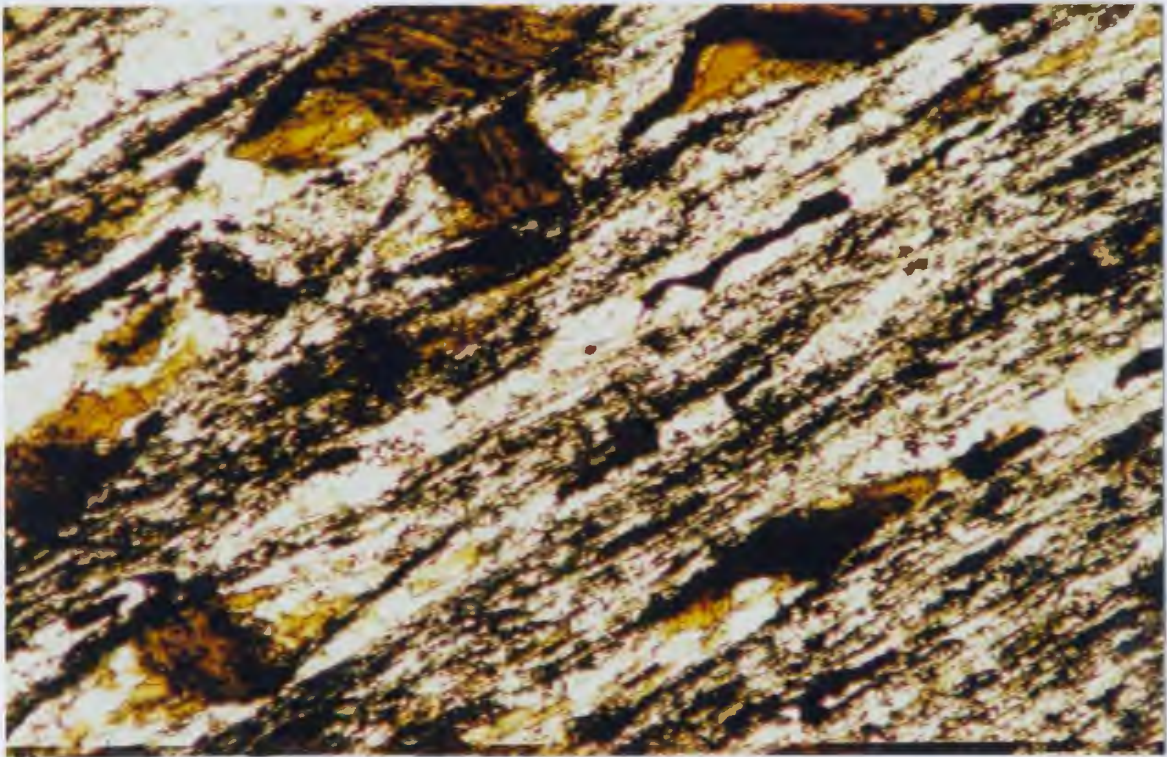
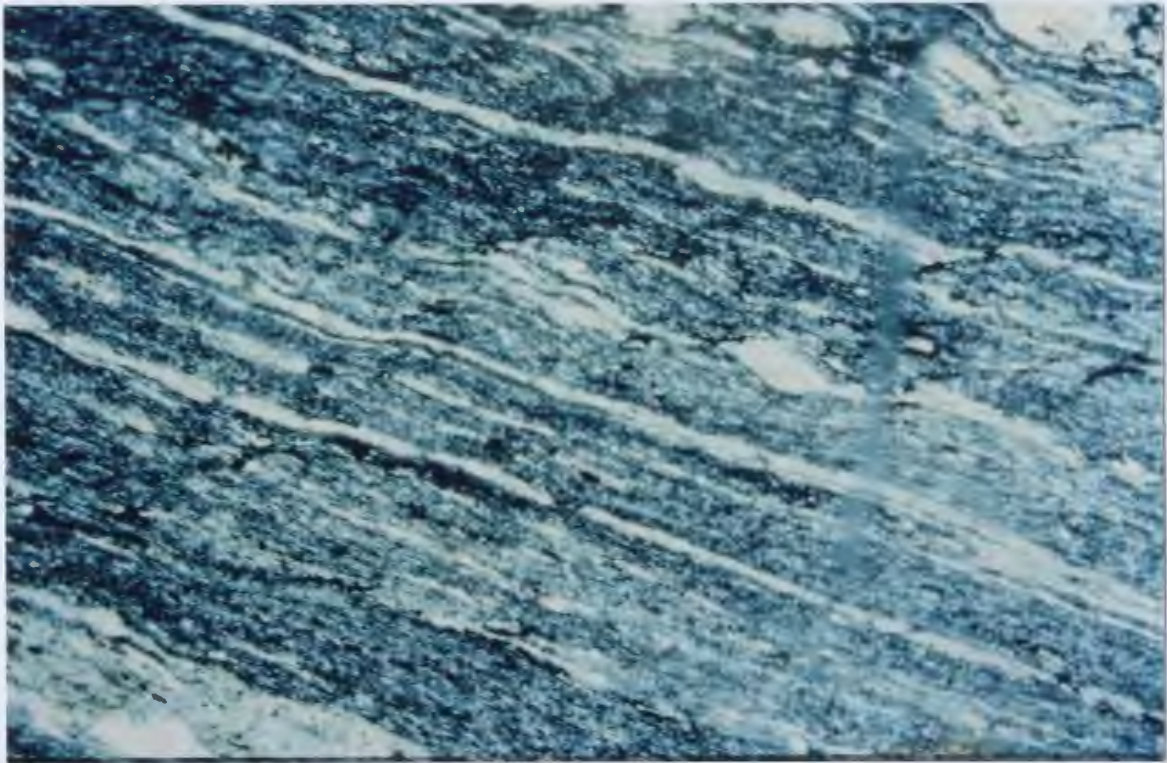


Plate 7.13: Photomicrograph of deformed and boundinaged quartz veins in mineralized shear zones at the Shashe Mine (scale = 0.4 mm PL).

Plate 7.14: Photomicrograph illustrating a trail of lozenge-shaped mica-fish microstructures in shear zones at the Shashe Deposit. The mica-fish structures were formed by tectonic shearing (scale 0.4mm PL).

the larger ones, such as in the N9 reef, are milky-white. Blaine (1986a) argued that gold is generally associated with the small veins rather than the larger ones. A small (7 cm thick) massive galena vein was found in a carbonate alteration zone within borehole TMP 23, below a thicker section (40m) of alternating bands of carbonate and silicified alteration zones.

The nature and form of the mineralization is controlled by the nature and size of the hosting shear zone. Geologists working in the area have described the silicified zones as representing shear zones (e.g. Molyneux, 1971; Jackson and Griffiths, 1981). Microstructural investigations in this study clearly indicate that the silicified zones accommodated most of the deformation, as evidenced by the sulphide-bearing brittle microfractures (Figure 7.13). They are, therefore, early alteration zones on which secondary shear zones were localized. Rock lenses between sulphide bands and quartz veins (Plate 7.13) are commonly boudinaged.

The confines of these shear zones are much wider than the silicified zones and approximate the full extent of the carbonate alteration. Plate 7.14 shows that mica fish structures and C-micro-shear bands are present outside silicified zones, indicating that the shear zone is much larger than the silicified zones. Thinner quartz veins that replace carbonate alteration in the main host rock are boudinaged, further indicating the wider extent of the shear zone (Figure 7.12).

The chronology of mineralization processes at the Shashe Deposit can be summarized as follows:

1. The process started with large scale pervasive carbonate alteration of the

host rocks, the carbonate alteration was controlled by fractures in the altered host rocks. Spacing between fractures resulted in the formation of bands in this alteration zone and its overall zebra rock texture.

2. Subsequently, acidic fluids (as evidenced by corrosion of carbonate crystal boundaries) percolated through fractures and crystal edges, leading to large scale replacement of the carbonate alteration and formation of multiple silicified zones. The thicknesses of the silicified zones were controlled by the width of the replaced carbonate veins.

3. During subsequent deformation movements, the silicified zones were comparatively more competent than both altered and unaltered host rocks, consequently accommodating most of the strain through brittle failure and the formation of micro-fractures.

4. The brittle shear micro-fractures became the sites for deposition of gold-bearing sulphide mineralization. The most distinctive feature of this mineralization is the brown biotite enveloping the micro-sulphide bands.

5. Late fluids were focused along these early sulphide-bearing micro-fractures and deposited secondary blue-tinted quartz veins and gold-bearing sulphides (mainly arsenopyrite and minor berthierite). The margins of these veins have reaction rims suggesting re-mobilization of the sulphides.

6. At the margins of these late quartz and some carbonate veins, the early silicified zone has reddish-brown staining, probably due to the breakdown of iron-rich sulphides and biotite.

Secondary shear zones are widespread throughout the belt, but not all are mineralized. It seems that only those fluids which were focused along carbonate alteration-bearing shear zones have the potential for mineralization. The nature of the alteration (especially the presence of jasperoid bodies formed by silicification) and the metallic association (Au-Ag-Sb-Pb-Zn-Cu) suggest that the Shashe Deposit is somewhat similar to disseminated epithermal (Romberger, 1985) and hot-spring precious metal deposits (e.g. Berger, 1982; Panteleyev, 1985).

7.4 Geochemistry of the Mineral Deposits

7.4.1 Introduction

In this section the geochemical characteristics of the metallotect features related to gold mineralization are reviewed. Metallotect refers to specific tectonic, geological, mineralogical or geochemical features of the host rocks to mineral deposits that controlled ore formation (Strong, 1987). This section combines alteration geochemistry, geochemistry of banded iron formations, fluid inclusion data from mineralized areas, and stable isotope data to develop a genetic model for gold mineralization in the Tati Greenstone Belt.

7.4.2. Geochemistry of Alteration Zones

7.4.2.1 Signal Hill Deposit

Hydrothermal alteration at the Signal Hill Deposit is very weak, as

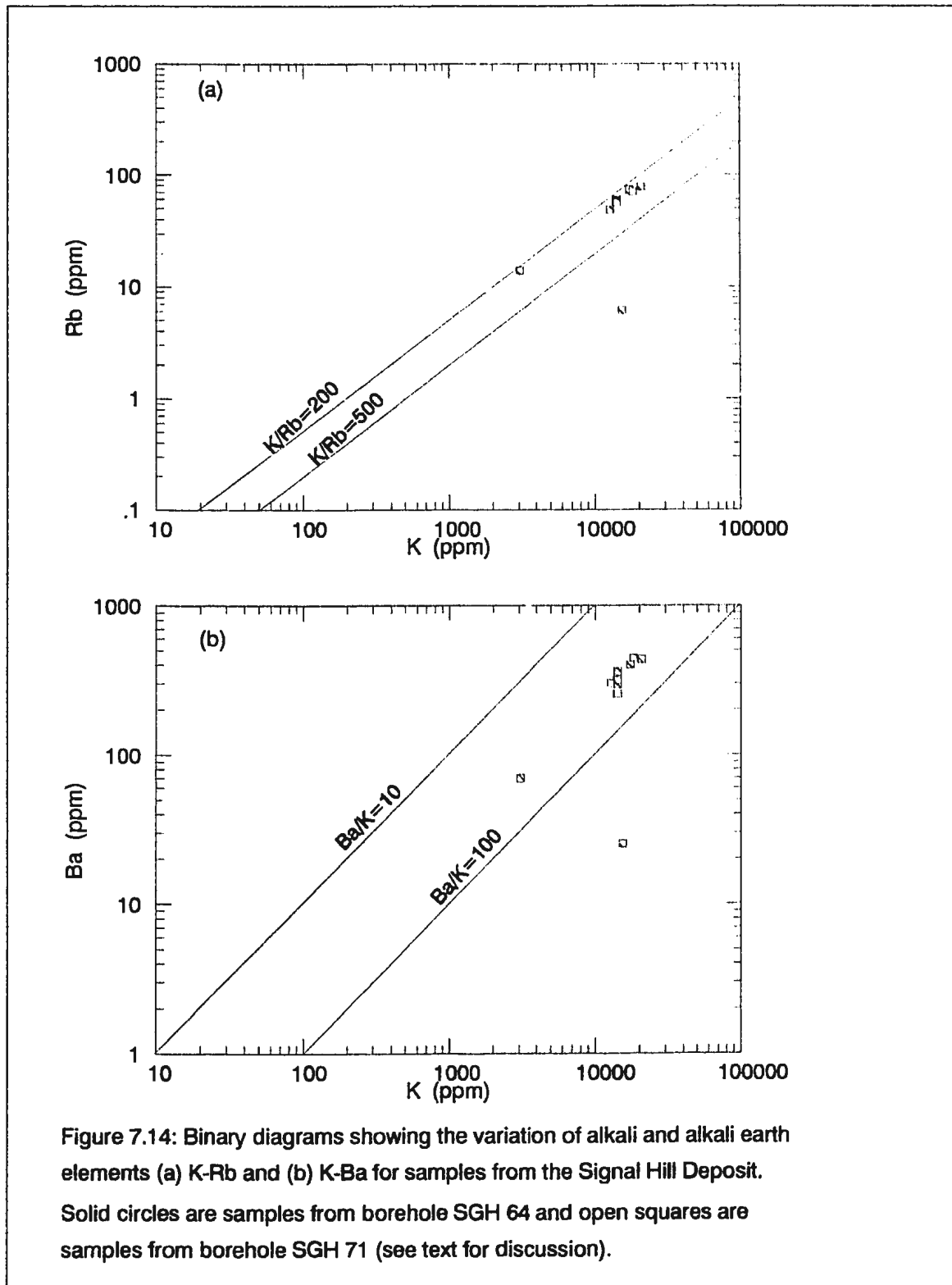
demonstrated by the absence of significant geochemical changes between the alteration zones and the host sedimentary rocks. Geochemical data for samples from two boreholes, SGH 64 and SGH 71, at the Signal Hill Deposit are summarized in Table 7.1. Borehole SGH 64 is sited over the pinkish brown conglomeratic unit interbedded with mica schists. Core samples from borehole SGH 71 are mainly of mature gritty sandstone. Geochemical data (Table 7.1) indicate that most of the samples from borehole SGH 71 have high silica (>85 wt%) contents. Potash in samples from this borehole although not very high, (ca. 1.5- 2.5 wt%) but are generally higher than those from most samples in borehole SGH 64 (< 1 wt%). Iron in samples from borehole SGH 71 has relatively low concentrations (ca 1 wt%). SGH 71 samples also have low concentrations of Ti, V, Mo and Sr, and elevated concentrations of Ba, Rb, and Pb.

Samples from borehole SGH 64 have very low silica contents (38-53 wt%) compared to those from borehole SGH 71. Potash is also comparatively very low, whereas other major element oxides, especially FeO, Na₂O and CaO are higher.

Alkali and alkali earth element plots, K-Rb (Figure 7.14a), K-Ba (Figure 7.14b), and Sr-K (Figure 7.14c), indicate positive correlations for all samples, irrespective of borehole site and alteration zone. The ratios of these elements vary between 200 and 500 for K/Rb, 10 and 1000 for K/Sr and 10 and 100 for the K/Ba. The K-Sr diagram (Figure 7.14c) indicates that although there is scatter in Sr contents, samples from borehole SGH 64 generally contain higher Sr contents compared to those from SGH 71. The K/Sr ratios of samples from borehole SGH

Table 7.1: Geochemical data for rocks from boreholes, SGH 64 & 71 at the Signal Hill Deposit.

	SGH 64/1	SGH 64/3	SGH 64/4	SGH 64/6	SGH 64/8	SGH 64/9	SGH 64/10	SGH 64/11	SGH 64/14	SGH 64/15	SGH 64/17	SGH 71/6	SGH 71/8	SGH 71/11	SGH 71/15	SGH 71/16	SGH 71/21	SGH 71/24	SGH 71/25	SGH 71/27	SGH 71/31	SGH 71/33	SGH 71/34
SiO2	38.80	49.40	48.40	74.50	45.40	31.20	46.20	44.50	65.90	47.90	53.20	---	85.70	84.50	87.00	85.30	86.00	84.80	81.20	87.20	80.70	85.00	85.90
TiO2	0.20	0.22	0.24	0.14	0.22	---	0.20	0.30	0.24	0.12	0.12	---	0.04	0.04	0.04	0.08	0.06	0.06	0.04	0.02	0.06	0.08	0.06
Al2O3	10.50	13.40	11.80	11.00	12.70	5.21	12.90	14.20	15.30	13.60	14.40	---	7.89	8.47	8.21	7.02	1.62	9.47	11.40	7.89	11.90	9.16	8.00
FeO*	18.52	10.59	13.48	8.08	8.37	10.02	6.64	11.29	2.11	7.51	8.28	---	1.40	0.80	0.77	0.13	0.25	0.17	0.31	0.66	0.75	1.08	1.09
MnO	0.24	0.22	0.18	0.11	0.17	0.23	0.16	0.24	0.23	0.20	0.16	---	0.21	---	0.01	---	---	---	---	0.02	0.01	0.01	---
MgO	1.31	2.46	5.48	0.90	5.34	5.47	5.35	5.60	1.33	6.44	4.60	---	0.09	0.56	0.40	0.06	0.02	0.07	0.07	0.21	0.51	0.83	0.60
CaO	18.80	8.80	6.18	1.38	9.36	18.80	8.78	6.82	4.46	6.48	8.34	---	0.08	0.10	0.06	0.46	0.02	0.04	---	0.02	0.02	0.02	0.04
Na2O	1.25	1.73	1.52	0.37	1.69	0.30	1.52	1.09	2.43	3.03	4.37	---	0.48	0.48	0.41	0.38	0.09	0.53	0.66	0.48	0.78	0.44	0.31
K2O	0.99	0.58	0.22	0.79	0.48	0.61	0.64	0.74	3.11	0.41	0.04	---	1.71	1.99	1.85	1.72	0.37	2.09	2.50	1.71	2.20	1.72	1.54
P2O5	0.09	0.08	0.04	0.10	0.09	0.08	0.08	0.07	0.20	0.06	0.08	---	0.09	0.08	0.04	0.03	0.08	0.04	0.02	0.08	0.05	0.01	0.02
LOI	18.38	11.77	14.98	3.05	15.98	24.83	15.34	13.36	5.02	11.83	7.69	---	1.63	1.84	1.37	1.58	0.48	1.50	2.61	1.35	1.80	1.56	1.48
Sc	22.97	29.85	27.97	14.23	26.44	18.34	27.87	33.29	4.78	32.80	26.86	27.32	2.16	---	0.24	2.15	0.63	4.45	3.78	3.58	4.52	3.58	2.68
V	130	181	157	102	155	76	164	190	39	190	180	176	15	---	14	4	63	4.45	3.78	3.58	4.52	3.58	2.68
Pb	18	10	9	27	8	7	7	8	13	11	8	82	43	---	---	68	24	45	41	11	10	7	8
Bi	0.15	0.15	0.17	0.12	0.09	0.11	0.12	0.05	0.11	0.10	0.08	0.03	0.23	---	---	0.18	0.15	0.29	0.13	0.03	0.17	0.16	0.20
Mo	3.81	3.56	3.52	4.87	2.73	3.26	3.14	3.23	3.12	4.15	0.63	5.92	1.58	0.65	0.65	0.45	0.65	0.44	0.43	0.47	0.27	0.49	0.88
K	8218	4649	1828	6558	3619	5064	5313	6143	25817	3404	332	0	14195	16520	15357	14278	3071	17350	20753	14195	18263	14278	12784
Rb	31	17	5	28	15	23	23	27	111	15	4	78	60	---	---	8	58	14	73	78	57	71	57
Cs	3.54	1.17	0.30	2.65	1.12	2.28	1.66	2.61	11.67	1.83	0.21	7.21	5.45	0.53	5.13	1.05	6.72	6.65	4.95	5.20	3.98	2.79	2.79
Ba	201	166	64	128	98	163	238	261	825	128	20	372	256	---	25	295	70	400	437	318	445	361	302
Sr	138	171	172	29	138	107	144	114	184	165	72	183	114	---	4	48	12	67	74	54	63	43	40
Tl	0.74	0.38	0.14	0.39	0.14	0.17	0.25	0.19	0.88	---	---	0.02	0.85	0.64	---	0.05	0.48	0.08	0.56	0.54	0.36	0.48	0.28
Li	17.50	27.17	34.35	11.26	22.80	12.53	30.96	52.09	8.17	37.31	30.20	9.47	11.72	---	0.78	3.07	0.42	2.65	3.88	5.26	8.85	7.86	5.85
Ta	0.50	0.40	0.37	0.79	0.74	0.31	0.29	0.24	0.81	0.28	0.20	0.10	0.82	---	0.04	0.31	0.38	0.28	0.23	0.47	0.35	0.33	0.47
Nb	1.58	1.50	1.58	1.79	1.18	0.56	1.54	1.18	1.71	1.81	0.32	0.10	0.27	---	0.01	0.18	0.28	0.33	0.17	0.07	0.09	0.15	0.12
Hf	1.65	1.81	1.82	2.19	1.74	0.44	1.65	1.78	3.17	1.69	1.54	1.26	1.66	---	0.18	1.61	0.38	2.14	2.02	1.73	2.29	1.83	1.69
Zr	50	86	63	78	57	20	57	64	120	64	52	39	52	---	5	51	12	63	60	56	63	61	54
Tl	1199	1319	1439	839	1319	---	1199	1799	1439	719	719	---	240	240	240	360	360	360	240	120	360	480	360
Y	5	8	5	7	4	7	5	6	5	8	8	5	5	---	1	5	1	5	5	5	6	4	4
Th	2.14	2.64	2.74	4.84	2.90	0.77	2.04	2.88	10.66	2.34	---	---	---	---	---	---	---	---	---	---	---	---	---
U	0.77	1.83	1.13	1.78	0.84	0.84	0.66	0.81	3.31	0.64	---	---	---	---	---	---	---	---	---	---	---	---	---
La	8.13	9.29	8.78	12.38	8.14	3.70	7.55	11.52	38.09	8.44	7.48	9.17	9.75	---	1.42	15.49	3.55	7.49	7.66	13.79	14.56	10.27	10.27
Ce	18.22	19.04	17.72	23.45	18.80	7.81	15.13	23.03	71.63	16.89	15.73	18.37	18.48	---	2.66	22.80	5.27	16.64	12.89	25.28	27.00	19.24	19.13
Pr	1.99	2.32	2.17	2.64	2.05	0.87	1.84	2.86	7.85	2.07	1.94	1.96	2.04	---	0.28	2.50	0.52	1.89	1.50	2.72	2.85	2.10	2.08
Nd	7.81	9.59	8.85	8.27	8.14	4.16	7.48	11.29	27.84	8.64	7.90	7.75	7.22	---	1.00	8.73	1.87	6.57	5.48	9.29	10.18	7.08	6.82
Sm	1.69	2.15	1.85	1.78	1.83	1.45	1.78	2.53	3.64	2.05	1.92	1.88	1.39	---	1.82	1.58	0.29	1.32	1.15	1.77	1.98	1.34	1.36
Eu	0.80	0.58	0.50	0.48	0.54	1.05	0.48	0.68	0.97	0.64	0.63	0.51	0.32	---	0.04	0.29	0.08	0.35	0.29	0.33	0.49	0.30	0.28
Gd	1.55	1.81	1.79	1.59	1.50	1.83	1.70	2.33	2.82	2.23	2.10	1.49	1.20	---	0.14	1.22	0.22	1.05	0.85	1.45	1.76	1.24	1.09
Tb	0.19	0.21	0.18	0.22	0.17	0.25	0.17	0.26	0.23	0.28	0.30	0.20	0.17	---	0.02	0.15	0.03	0.17	0.14	0.18	0.21	0.15	0.13
Dy	1.02	1.23	1.08	1.39	0.87	1.32	0.98	1.35	1.13	1.47	1.83	1.09	0.84	---	0.10	0.86	0.18	1.08	0.92	1.01	1.25	0.83	0.74
Ho	0.20	0.24	0.21	0.28	0.16	0.28	0.19	0.24	0.18	0.25	0.34	0.21	0.19	---	0.02	0.17	0.04	0.21	0.18	0.20	0.24	0.17	0.15
Er	0.61	0.77	0.68	0.86	0.58	0.72	0.56	0.70	0.47	0.71	0.98	0.63	0.59	---	0.06	0.60	0.11	0.80	0.68	0.67	0.70	0.56	0.51
Tm	0.10	0.14	0.11	0.12	0.09	0.10	0.09	0.12	0.06	0.10	0.16	0.10	0.10	---	0.01	0.12	0.01	0.11	0.12	0.11	0.12	0.09	0.09
Yb	0.74	0.80	0.81	0.85	0.66	0.87	0.74	0.93	0.32	0.88	1.02	0.84	0.57	---	0.06	0.53	0.10	0.73	0.61	0.62	0.73	0.51	0.44
Lu	0.14	0.16	0.14	0.13	0.13	0.10	0.14	0.17	0.06	0.12	0.18	0.11	0.08	---	0.01	0.08	0.02	0.12	0.09	0.09	0.13	0.07	0.07



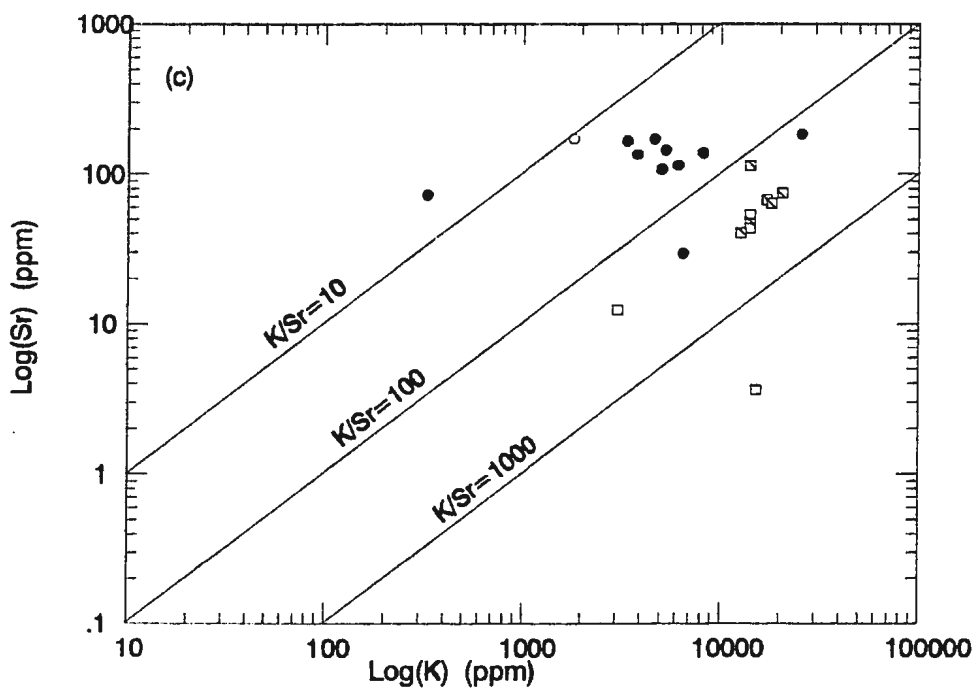


Figure 7.14(c) K-Sr plot which indicates that arkosic metasedimentary rocks at Signal Hill Deposit from borehole SGH 64, contain high Sr (K/Sr ratios between 10 and 100) compared to mature coarse-grained sandstones (borehole SGH 71) with ratios between 100 and 1000.

64 (mica-chlorite schists and iron-rich conglomerates) vary between 10 and 100, while those from borehole SGH 71 (mature gritty quartzite) have K/Sr ratios of 100 and 500. Such features are probably due to the fact the quartz-mica schists were derived from shales which are generally metal-rich, whereas the quartzites of borehole SGH 71 are comparatively metal-poor.

7.4.2.2 Shashe Deposit

The main alteration zones at the Shashe Mine show considerable overlap as seen from the formation of late quartz veins on the carbonate alteration (Figure 7.11). The overlap makes it very difficult to compare geochemical analyses between the different zones. Despite this problem, distinct geochemical characteristics for some alteration zones can be observed and these are outlined below. Geochemical data for two types of samples from the Shashe Deposit are presented in Tables 7.2a and 7.2b. Table 7.2a summarizes the geochemical data for underground chip samples from the N9 reef. The data, consisting only of major and trace elements, are from the mineralized zone, highly altered, and less altered wall rocks. The distinction between highly altered and less altered was based on analyses similar to those carried in Chapter 5 (i.e. microscopic and geochemical evidence and LOI < 2.5 in unaltered rocks). Table 7.2b contains geochemical data from borehole UKD 31 which penetrated about 60 metres of mineralized rock at the Shashe Mine. N9 data represent the geochemical characteristics of one zone, whereas borehole UKD 31 traverses different mineralized zones.

Table 7.2a: Geochemical data for rocks from the N9 reef zone at the Shashe Mine.

	SH 02	SH 03	SH 05	SH 09	SH 10	SH 11	SH 12	SH 13	SH 15	SH 16b	SH 17	SH 19	SH 20	SH 21	SH 22	SH 25	SH 26	SH 27	SH 18	SH 28	SH 29	AR 179	AR 190	AR 196
SiO2	50.80	48.80	49.80	48.20	52.90	48.40	50.80	48.70	48.50	43.80	48.70	48.70	50.40	52.90	51.40	48.90	47.90	57.00	48.60	50.00	48.20	89.50	86.50	75.60
TiO2	0.96	0.84	1.00	0.96	0.84	0.88	1.00	0.88	0.96	0.64	0.76	0.84	1.04	0.88	1.04	0.92	0.76	0.36	0.88	0.84	0.84	0.12	---	---
Al2O3	13.70	13.70	14.10	14.10	13.50	13.60	14.10	13.60	14.20	10.20	13.70	13.80	14.30	13.30	14.30	13.80	13.90	13.60	13.60	13.40	14.20	0.23	0.31	0.31
FeO*	11.00	10.21	11.04	11.10	10.93	10.80	10.29	11.64	11.24	12.17	10.90	10.39	11.43	10.73	10.33	11.60	10.20	8.46	10.99	11.93	11.40	8.27	8.74	21.65
MnO	0.22	0.19	0.22	0.18	0.21	0.24	0.20	0.23	0.18	0.29	0.24	0.20	0.20	0.21	0.21	0.23	0.20	0.04	0.23	0.21	0.18	0.12	0.02	0.14
MgO	6.56	4.99	5.35	7.04	3.09	5.64	5.66	4.87	7.02	4.18	5.64	4.89	5.58	3.03	5.67	4.79	4.92	0.87	5.69	4.82	7.09	0.16	0.03	0.07
CaO	9.84	10.82	10.56	8.56	5.46	12.50	10.16	10.66	8.62	10.44	12.50	10.68	10.32	5.44	9.96	10.60	10.72	2.12	12.52	10.66	8.60	0.20	---	0.08
Na2O	2.59	2.42	2.72	2.59	3.18	1.82	3.00	1.86	2.68	1.74	1.80	2.24	1.62	3.17	3.00	1.86	2.25	3.78	1.83	1.88	2.60	0.02	0.01	---
K2O	0.30	0.94	0.30	0.27	1.96	0.23	0.29	0.63	0.26	2.30	0.23	0.93	0.47	1.94	0.29	0.62	0.94	1.43	0.23	0.65	0.26	0.01	0.04	0.01
P2O5	0.09	0.17	0.09	0.10	0.08	0.09	0.08	0.10	0.10	0.07	0.08	0.07	0.10	0.06	0.08	0.08	0.09	0.08	0.08	0.10	0.12	0.06	0.29	0.04
LOI	1.46	2.64	2.43	3.91	3.07	3.53	2.18	2.07	3.74	4.12	3.68	2.68	2.18	3.07	2.13	2.17	2.73	5.98	3.86	2.38	4.31	1.13	1.88	0.28
Cr	305	261	221	309	296	316	272	314	260	278	305	229	340	289	281	309	218	454	302	326	261	229	219	553
Ni	129	125	94	137	99	142	125	122	126	100	140	96	137	99	128	121	94	150	140	125	127	7	6	5
V	282	280	229	288	323	263	271	273	277	227	258	229	294	321	270	275	227	322	262	278	279	2	7	14
Cu	89	81	151	129	228	95	82	145	81	185	92	155	92	233	85	148	151	105	94	150	78	17	64	7
Pb	5	---	13	1	4	---	1	6	1	---	1	12	6	5	---	6	14	31	1	6	---	---	4	---
Zn	104	108	122	91	107	99	95	121	109	106	108	91	95	107	96	120	120	111	91	113	108	69	39	31
K	2490	7803	2490	2241	16271	1909	2407	5230	2158	19093	1909	7720	3902	16105	2407	5147	7803	11871	1909	---	---	83	332	83
Rb	9	7	30	10	67	4	16	26	8	---	4	30	17	67	19	27	30	64	4	---	---	---	---	---
Sr	58	71	75	70	54	88	65	83	71	---	89	74	74	54	64	83	74	64	88	---	---	7	4	5
Ga	15	15	18	16	17	16	15	15	14	15	16	18	16	17	14	16	18	24	16	16	16	---	2	---
Nb	5	4	4	3	4	5	5	5	5	---	5	4	5	4	4	5	4	4	4	---	---	---	---	---
Zr	59	71	79	59	58	58	63	59	71	---	57	80	62	59	60	60	79	62	58	---	---	1	6	1
Ti	5755	5036	5995	5755	5036	5276	5995	5276	5755	3837	4556	5036	6235	5278	6235	5515	4556	2158	5276	---	---	719	---	---
Y	23	23	24	24	19	26	24	26	24	---	23	24	25	19	23	24	23	20	25	---	---	1	2	4

Table 7.2b: Geochemical data for rocks from borehole UKD 31 at the Shashe Mine.

	UKD 31/1	UKD 31/3	UKD 31/5	UKD 31/6	UKD 31/7	UKD 31/12	UKD 31/14	UKD 31/16	UKD 31/17	UKD 31/19	UKD 31/21	UKD 31/22	UKD 31/23	UKD 31/24	UKD 31/25
SiO ₂	46.20	44.20	41.00	46.60	46.00	44.90	47.40	50.80	50.80	55.90	48.40	68.60	58.80	51.00	50.20
TiO ₂	1.28	1.18	0.74	0.74	0.88	0.78	0.82	0.88	0.88	0.96	1.02	0.42	0.56	1.66	1.70
Al ₂ O ₃	13.50	12.10	11.50	13.60	16.10	11.70	13.00	14.90	13.70	14.20	15.30	14.40	19.10	13.10	12.80
FeO*	13.13	11.25	11.31	9.21	13.53	11.47	10.73	12.35	12.07	9.48	11.27	3.39	5.02	14.95	14.08
MnO	0.23	0.23	0.26	0.22	0.19	0.21	0.20	0.16	0.19	0.14	0.16	0.03	0.04	0.23	0.22
MgO	5.16	4.48	5.45	4.16	8.07	6.65	6.07	7.11	7.06	4.34	7.52	1.42	3.57	6.55	6.05
CaO	12.06	15.26	16.84	13.56	7.62	13.96	12.76	6.68	9.68	7.54	9.96	5.04	2.32	7.38	8.28
Na ₂ O	2.44	1.79	1.71	2.03	2.35	1.24	2.01	3.18	2.39	2.20	2.15	2.54	2.76	1.88	2.53
K ₂ O	0.31	0.51	0.23	0.96	0.26	0.39	0.21	0.14	0.13	0.68	0.58	1.97	3.72	0.26	0.12
P ₂ O ₅	0.17	0.13	0.06	0.09	0.08	0.06	0.11	0.07	0.07	0.13	0.07	0.12	0.14	0.10	0.14
LOI	2.10	6.72	8.17	6.94	2.62	5.73	4.04	1.19	0.62	1.53	1.81	2.14	3.13	0.57	1.15
Sc	38.18	32.83	29.68	32.79	43.06	33.20	35.80	27.00	35.70	25.77	39.60	4.70	8.45	28.00	31.59
V	352	297	224	263	252	264	277	312	288	231	298	37	55	423	395
Pb	2.78	2.49	2.08	7.34	8.41	4.00	5.00	3.70	1.77	5.86	8.60	8.00	3.70	3.00	3.80
Bi	0.09	0.06	0.05	0.08	0.07	0.06	0.07	0.03	0.04	0.09	0.08	0.17	0.03	0.07	0.05
Mo	0.64	0.51	0.51	1.23	0.43	0.55	0.28	0.75	1.29	0.78	0.26	0.55	0.57	0.41	0.31
K	2573	4234	1909	7969	2158	3238	1743	1162	1079	5645	4815	16354	30881	2158	996
Rb	5	28	7	35	9	16	6	3	1	28	14	51	72	7	1
Cs	0.27	3.63	0.40	3.74	0.83	1.25	0.90	0.32	0.12	2.95	1.59	7.08	8.40	0.61	0.03
Ba	61	187	28	290	36	33	31	37	26	236	82	211	709	31	16
Sr	162	118	72	96	131	74	133	110	138	95	124	152	123	123	169
Ti	0.10	0.51	0.11	0.62	0.14	0.25	0.16	0.11	0.11	0.39	0.17	0.57	0.58	0.10	0.01
Li	15.76	22.99	16.50	24.39	31.65	21.54	17.04	23.83	13.82	16.38	19.16	20.58	73.55	22.03	15.81
Ta	1.01	0.51	0.64	5.82	1.78	2.42	0.45	0.95	4.59	1.74	0.73	1.13	0.95	0.93	1.33
Nb	4.90	4.22	2.21	2.62	2.99	2.39	2.57	2.59	2.40	5.49	3.53	4.39	4.63	4.70	0.00
Hf	0.87	0.86	0.65	0.41	0.38	0.16	0.36	0.59	0.36	2.36	0.91	2.07	2.99	0.61	0.67
Zr	34	32	23	14	16	4	12	21	11	90	30	75	104	17	22
Ti	7674	7074	4436	4436	5276	4676	4916	5276	5276	5755	6115	2518	3357	9952	10192
Y	26	22	16	18	21	17	19	18	19	21	19	5	7	29	30
Th	1.23	1.04	0.44	0.50	0.59	0.53	0.55	0.62	0.56	3.87	0.37	0.52	7.10	0.51	0.51
U	0.35	0.28	0.13	0.15	0.17	0.14	0.14	0.15	0.16	1.11	0.10	1.42	1.89	0.10	0.11
La	7.69	6.64	3.57	3.49	4.07	3.73	3.63	3.92	3.87	16.71	3.57	20.03	22.00	5.49	5.61
Ce	18.59	15.82	8.28	8.82	10.64	9.45	9.31	10.23	9.92	32.50	9.57	34.73	41.65	14.54	15.55
Pr	2.63	2.26	1.18	1.36	1.58	1.38	1.39	1.52	1.46	3.83	1.50	3.55	4.48	2.25	2.37
Nd	13	11	6	7	8	7	7	8	7	15	7	21	16	12	12
Sm	3.63	3.00	1.91	2.31	2.61	2.19	2.18	2.41	2.22	3.61	2.44	1.99	2.82	3.70	3.84
Eu	1.30	1.03	0.91	0.69	0.19	0.93	0.88	0.98	0.86	1.08	0.82	0.77	0.98	1.26	1.37
Gd	4.75	3.83	2.54	3.12	3.80	2.90	3.08	3.26	3.27	4.29	3.35	2.00	2.82	5.14	5.17
Tb	0.77	0.60	0.42	0.50	0.64	0.48	0.52	0.54	0.53	0.62	0.57	0.21	0.30	0.83	0.86
Dy	4.88	4.14	2.92	3.59	4.11	3.16	3.41	3.54	3.60	3.88	3.74	1.07	1.50	5.57	5.75
Ho	1.01	0.89	0.59	0.75	0.85	0.68	0.73	0.73	0.75	0.81	0.79	0.19	0.26	1.17	1.19
Er	2.97	2.53	1.80	2.19	2.29	2.00	2.18	2.15	2.23	2.38	2.15	0.54	0.69	3.44	3.42
Tm	0.42	0.37	0.26	0.32	0.30	0.29	0.31	0.29	0.32	0.35	0.32	0.08	0.09	0.49	0.49
Yb	2.76	2.44	1.81	1.99	1.72	1.95	2.05	1.85	2.01	2.29	2.08	0.43	0.60	3.13	3.10
Lu	0.38	0.32	0.26	0.34	0.22	0.27	0.29	0.28	0.30	0.35	0.33	0.07	0.09	0.47	0.45

For the purposes of geochemical analysis, samples from both the N9 reef zone and borehole UKD 31 are divided into three main groups. These groups are the wall rock zone, the carbonate alteration zone, and the silicified zone with sulphide veins and biotite alteration zones. Samples SH 10, 16b, 21 and 27 (Table 7.2a) and samples UKD 31/22 and 31/23 (Table 7.2b) are all from silicified alteration zones, whereas samples SH 05 (Table 7.2a), UKD 31/1, 31/3, 31/5, 31/24 and 31/25 (Table 7.2b) are from the main carbonate alteration zone. Sample SH 16b carries both sulphides and late carbonate veins, whereas samples UKD 31/24 and 31/25 contain wider carbonate veins. The remainder of the samples in Tables 7.2a and 7.2b have variable degrees of carbonate alteration.

Major element data (Tables 7.2a and 7.2b) indicate that samples from the silicified zones, as expected contain the highest silica contents, between 52 and 69 weight percent. Because samples from the silicified zones contain both sulphides and the biotite alteration, their K_2O and total FeO contents are relatively high. CaO is low, 2 to 6 wt%, for most samples except sample SH 16b which contains late carbonate veins leading to higher values of CaO. Rb, Zr, Li, Ba, Ni, Cu, Zn and Pb concentrations are relatively high in silicified zones compared to other zones, whereas Ti and Y are comparatively low. The most diagnostic geochemical feature of the carbonate alteration zones, as expected, are the high CaO contents (>12 wt%). The samples with the highest CaO contents also have the lowest silica contents. Rb, Ba, and Zr are comparatively low, whereas Ti and Y are comparatively higher. Sr is approximately equivalent in both the silicified and carbonate zones.

When samples from the Shashe Mine are plotted on a $\text{Na}_2\text{O}-\text{CaO}-\text{K}_2\text{O}$ ternary diagram (Figure 7.15), most of the samples plot near the $\text{Na}_2\text{O}-\text{CaO}$ side of the diagram and towards the CaO corner. Some samples plot within Condie and Allen's (1980) tholeiitic field (Figure 7.15). Samples from the silicified zone are displaced away from the main cluster towards the K_2O corner.

The silicified zones contain mineralized microfractures which occur as microbands of sulphide veinlets enveloped by distinctive brown biotite. The presence of biotite in the silicification zone increases the potash or alkali element content of the silicified alteration zone. Samples collected from carbonate alteration zones are slightly displaced from Condie and Allen's (1980) amphibolite field (Figure 7.15). They plot towards the $\text{CaO}-\text{Na}_2\text{O}$ join (i.e. they have very low K_2O), due to the fact, that in some instances carbonate alteration zones contain relatively pure carbonate minerals with very minimal extraneous material.

Base metals Cu , Zn and Pb from the N9 reef zone cluster along the $\text{Cu}-\text{Zn}$ side of a $\text{Pb}-\text{Cu}-\text{Zn}$ ternary diagram (Figure 7.16). This indicates that these alteration zones have relatively low Pb contents in comparison to Cu and Zn (Figure 7.16) irrespective of the type of alteration zone. On the basis of absolute values, however, Pb is comparatively enriched in the silicified zone compared to the carbonate alteration zone. Therefore, both host rocks and the mineralizing fluids that interacted with them contained too little Pb to make any significant changes in the Pb contents of the resulting alteration and mineralization zones. The banded iron formation sample (AR 190) plots in the same field as the alteration and mineralization zones

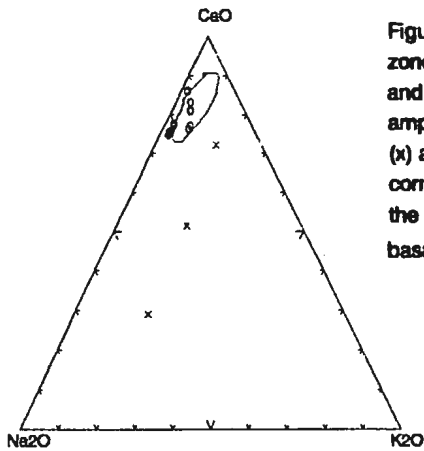


Figure 7.15: Na₂O-CaO-K₂O ternary diagram of mineralized and alteration zone samples from the N9 reef at the Shashe mine. Most of the altered and unaltered rock samples plot in Condie and Allen's (1960) Archean amphibolite field marked by the field on the diagram. Samples marked by (x) are from the silicified zone (reef) and are displaced away from the CaO corner in accordance with the formation of this zone by silica replacement of the carbonate zone. Circles are samples from variably altered to unaltered basaltic rocks.

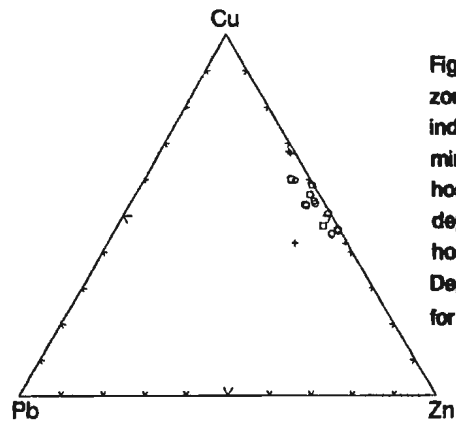


Figure 7.16: Pb-Cu-Zn ternary diagram of mineralized and alteration zone samples from the N9 reef at the Shashe mine. These samples indicate that host basaltic rocks control the composition of the mineralization and alteration zones, in the same way that basaltic hosted volcanogenic massive sulfides are enriched in Cu and Zn and depleted in Pb compared to Koroko VMS type deposits (felsic volcanic hosted). BIF sample AR 190 (open diamond) as plotted in the Shashe Deposit field. Other symbols are (+) for the silicified zone; open circles for variously altered and unaltered basaltic rocks.

at the Shashe deposit. The significance of this will be discussed later.

Figure 7.17 illustrates the distribution of the alkali and alkali earth elements in samples from borehole UKD 31. Figures 7.17a, 7.17b and 7.17c indicate that K-Rb, K-Ba and Ba-Rb are positively correlated. They also vary within the ratio limits of 100 to 1000 for K/Rb, 10 to 100 for K/Ba and 2 and 10 for Ba/Rb. The variation is not distinct for individual alteration zones. Figure 7.17a shows that, in general, the mineralization zones have higher K and Rb contents than other alteration zones, including the unaltered host rock (UKD 31/17). Secondly, most altered samples contain lower K/Rb ratios than the unaltered rocks, suggesting that alteration displaces the K/Rb ratios to lower values. This is a function of the preferential partitioning of Rb relative to K into hydrothermal fluids. Therefore, the interaction of rocks with fluids containing comparatively lower K/Rb ratios would lead to an increase of Rb in altered rocks, and hence, lower K/Rb ratios. The K-Sr diagram (Figure 7.17d) indicates that Sr contents are relatively constant in all these zones. The similarities of the alkali and alkali earth element ratios within the mineralization and alteration zones at the Shashe Deposit indicate uniformity in the fluid composition. The constancy of Sr suggests that the mineralizing and alteration fluids did not significantly alter the Sr contents of plagioclase-rich host rock (basalt).

Very few studies have been carried out on the distribution of Rare Earth Element (REE) in the alteration zones of mineral deposits, especially Archean mesothermal gold deposits. One of the pioneering studies in this field was that of Kerrich and Fryer (1979) at the Dome mine in the Abitibi Belt which suggested that REE

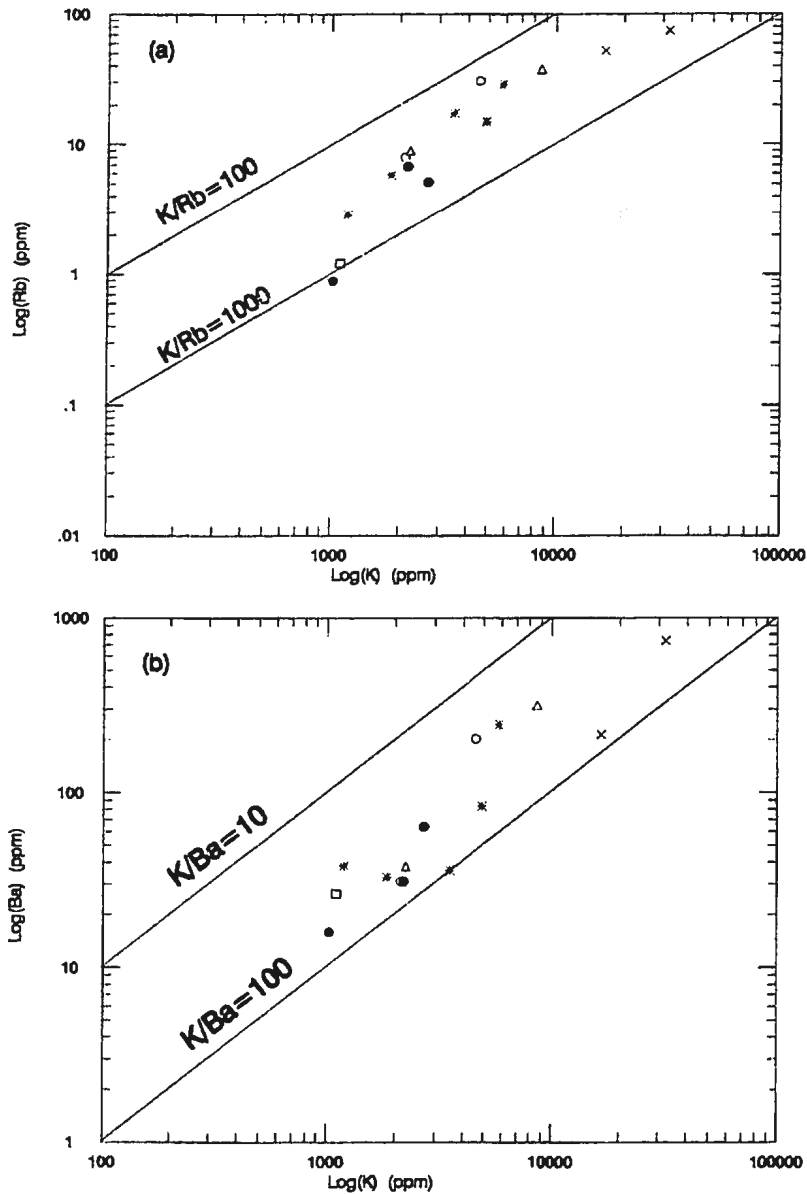
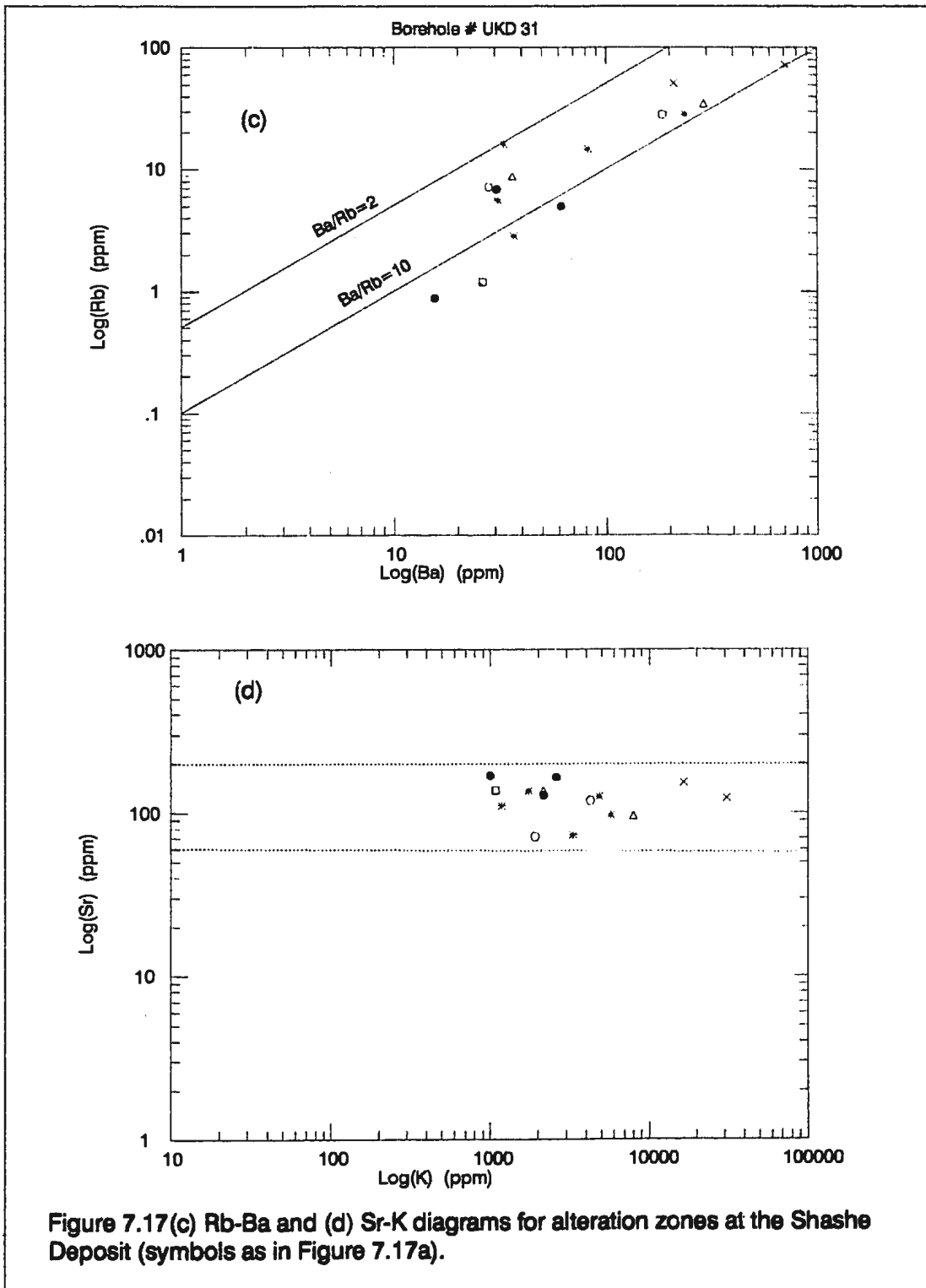


Figure 7-17: Log-log diagrams indicating the variation of alkali elements in alteration zones of Shashe Mine; (a) K-Rb, (b) K-Ba, Samples are from borehole UKD 31. Symbols are as follows: crosses (silicified zone or mineralization); open circles are carbonate alteration zones with visible sulfides; solid circles are carbonate zones of variable intensity, asterisks are altered rocks that could not be separated into individual zones; open triangles are amphibole zones; square = relatively fresh rock.



mobility is controlled by the relative stabilities of their carbonate, fluoride or sulphate complexes in alkaline solutions. They further indicated that HREE complexes are more stable than those of the LREE in alkaline solutions. This suggests the potential to fractionate the REE where, in the case of the Tati Belt deposits, HREE will be deposited in late forming alteration zones.

There are several recent studies on the distribution of REE in hydrothermal systems from oceanic environments (Olivarez et al., 1989; Campbell et al., 1988), in geothermal waters (Michard, 1989; Sanjuan et al., 1988), in hydrothermal minerals (Morgan and Wandless, 1980), and in hydrothermal fluids (Wood, 1990; Lottermoser, 1992; Millero, 1992). The majority of these studies deal with REE distributions in hydrothermal fluids rather than REE distribution in alteration zones. However, because these fluids are responsible for alteration, and possibly mineralization, these studies are relevant to investigations of hydrothermally altered rocks. Most studies indicate that the fluid chemistry of REE in geological environments is very complex. Many of the ideas on REE fractionation and general distribution are based on extrapolations from studies at lower temperatures (Sverjensky, 1984; Wood, 1990; Millero, 1992).

REE were determined in samples from borehole UKD 31 (Table 7.2b) at the Shashe Mine to investigate the distribution of these elements in different alteration zones. Table 7.2b indicates that samples from the silicified and mineralized zones (UKD 31/22 and 31/23) have higher concentrations of LREE (La-Nd) relative to the HREE (Sm-Lu). Figure 7.18a summarizes REE distribution in the carbonate

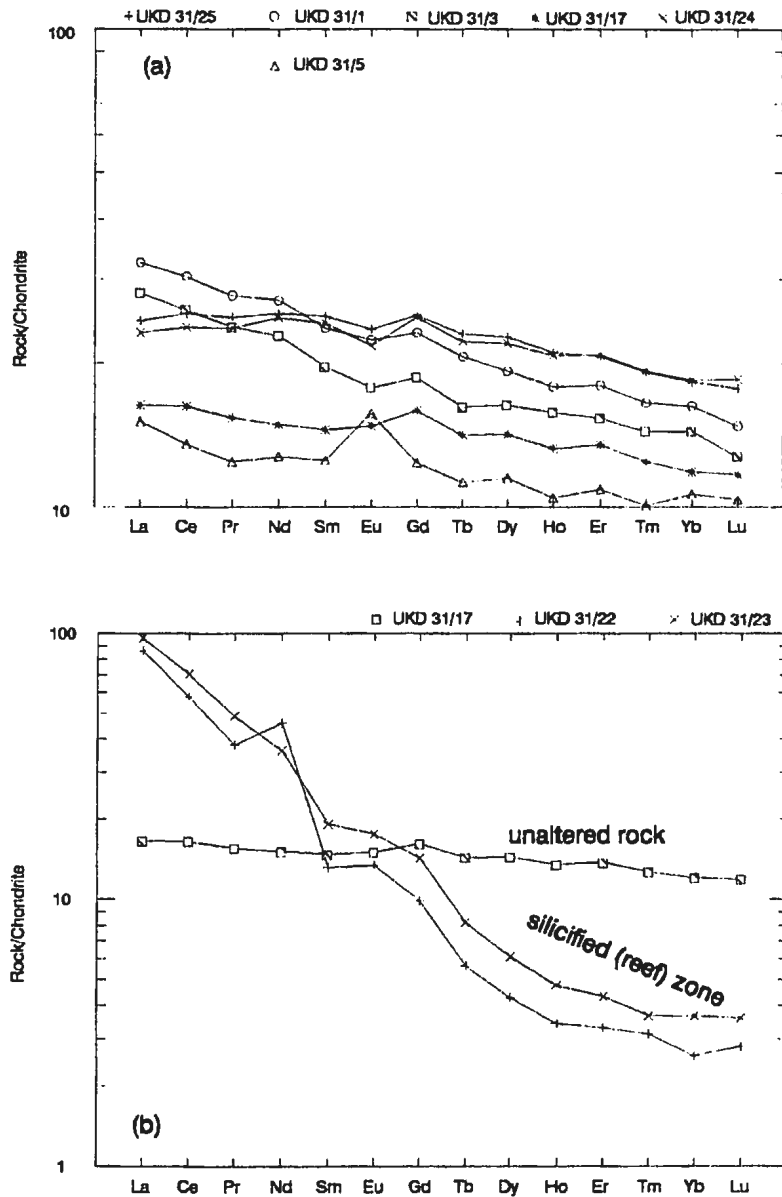


Figure 7-18: Chondrite-normalized REE diagrams - (a) Carbonate alteration; (b) comparison of silicified zones and unaltered rock (UKD 31/17). Normalization factors from Sun and McDonough (1989).

alteration zone, it also compares the chondrite-normalized REE pattern of this zone, with that of unaltered basaltic rock (sample UKD 31/17). The carbonate alteration zone was sampled in such a way as to illustrate the progressive chemical changes from the less altered rocks to the most advanced alteration.

Samples UKD 31/1 and UKD 31/3 represent different stages of carbonate alteration. UKD 31/1 contains thin carbonate veinlets, whereas in UKD 31/3 the number and sizes of the carbonate veins are greater. These samples exhibit similar REE patterns with slight enrichments in total REE, especially in the LREE, compared to the host rock (UKD 31/17). They also contain small negative Eu anomalies.

Samples UKD 31/24 and UKD 31/25 represent another variation in the carbonate alteration zone. In these samples the carbonate alteration bands are comparatively wider (≥ 5 cm to <1 cm) than those in UKD 31/1 and UKD 31/3. The samples contain elevated chondrite-normalized total REE contents (as do the other two) relative to the unaltered basalt, and they also contain small negative Eu anomalies. Compared to UKD 31/1 and 31/3, these samples have lower LREE/HREE ratios.

Sample UKD 31/5 (Figure 7.18a) is from the most advanced carbonate alteration zone and contains sulphide veinlets. This sample represents the transition from carbonate to silicified alteration zones (which are replacements of the carbonate alteration). This sample has the lowest total REE contents compared to the other four samples. The HREE are the most depleted when compared to the

unaltered basalt (UKD 31/17). The sample exhibits a positive Eu anomaly and contains the lowest Sr content (Table 7.2b).

The REE patterns of the two samples from the silicified and mineralized zone are shown on Figure 7.18b. In comparison to the carbonate alteration, samples UKD 31/22 and UKD 31/23 contain very high LREE (>100x chondritic abundance).

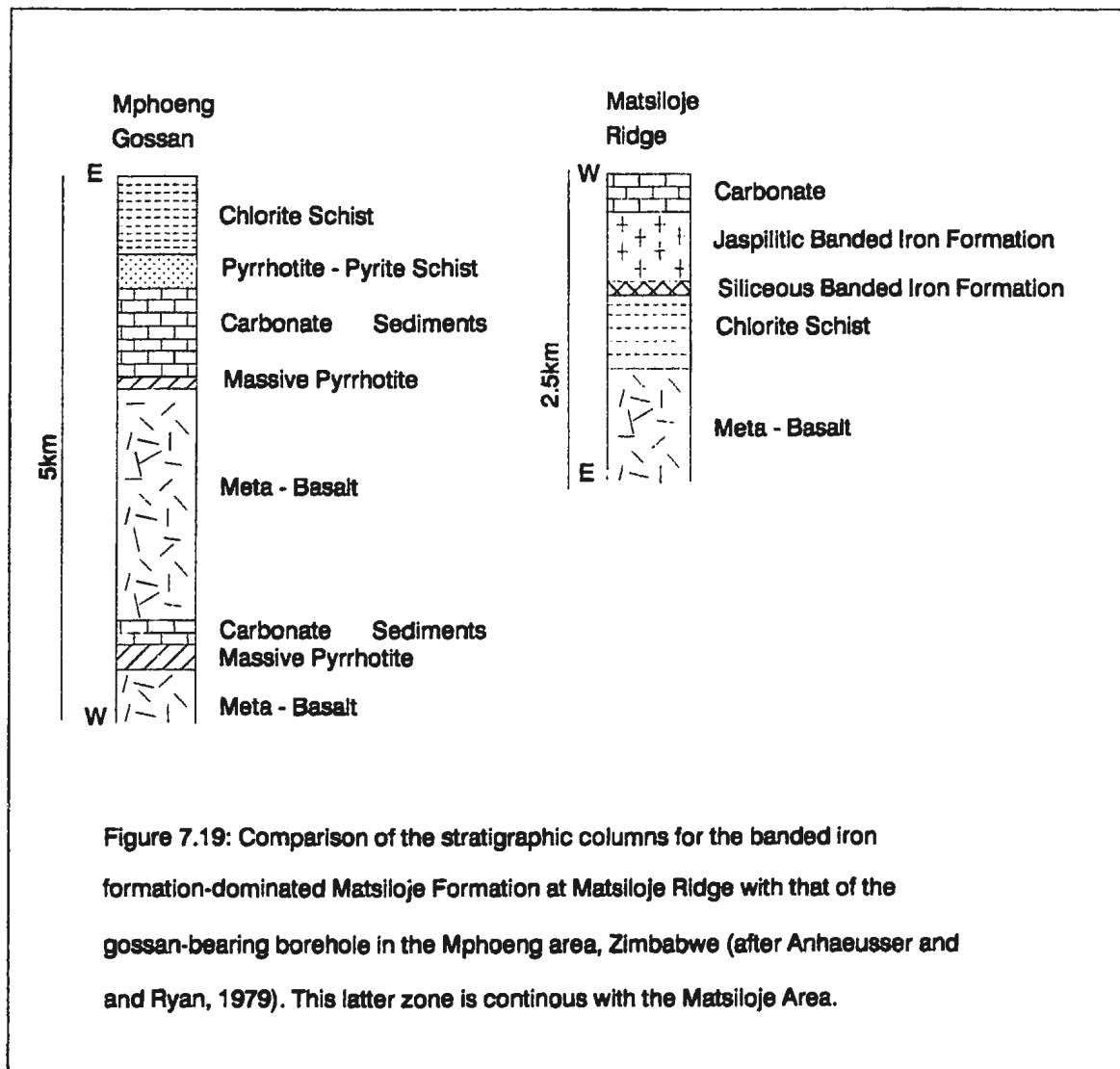
In summary, silicified/mineralized alteration zones have comparatively more fractionated REE patterns than the carbonate alteration zones. They are generally LREE-enriched and HREE-depleted (Figure 7.18b). The carbonate alteration zones, on the other hand, are more complex. Sample UKD 31/5 is depleted in all REE and has a small positive Eu anomaly. The other four samples (UKD 31/1, 31/3, 31/24 and 31/25) all contain relatively elevated chondrite-normalized REE abundances and small negative Eu anomalies, compared to the unaltered basalt (sample UKD 31/17).

7.4.4 Geochemistry of Banded Iron Formations

Banded iron formations in the Tati Greenstone Belt have not received much geological attention and no modern data existed previous to this study for these rocks (especially geochemical data). Sulphide facies banded iron formations at Long Gossan, however, have been investigated for their massive sulphide potential (Johnston and Griffiths, 1983). This investigation revealed that although these rocks are barren, they contain pyrrhotitic and pyritic massive sulphide bands at depth, with minor disseminations and blebs of galena and sphalerite \pm magnetite. Barite is also present, especially towards the top of the lithological package. Follow-up trenching

revealed pockets of metal concentrations (Zn, Pb, and Ag), which Johnston and Griffiths (1983) related to secondary re-mobilization and concentration. A similar exploration program was conducted in the Mphoeng area of Zimbabwe by Anhaeusser and Ryan (1979). This area is the extension of the Tati Greenstone Belt into Zimbabwe. The Mphoeng gossans are continuous with the Matsiloje banded iron formation ridge of Botswana, and probably represent the sulphide facies of the former. Figure 7.19 indicates that the stratigraphic columns for the banded iron formations of the Matsiloje Ridge and gossans of the Mphoeng area are comparable and both are overlain by carbonates.

An extensive geochemical study of Archean banded iron formations in Southern Africa was undertaken by Oberthur et al. (1990). They suggested that banded iron formations from various parts of southern Africa have similar geochemical patterns, with flat chondrite-normalized REE patterns, distinct positive Eu anomalies and depletion in total REE. Figures 7.20a, 7.20b and 7.20c illustrate the REE patterns of the banded iron formations from the Tati Greenstone Belt. In Figure 7.20a REE contents of banded iron formations are normalized to chondrite values from Sun and McDonough (1989). In the other two diagrams, banded iron formation REE contents are normalized to host basalt rock (UKD 31/17) at the Shashe Deposit (Figure 7.20b) and to LREE-enriched basalts of the Tati belt (AR 152). The reason for normalising REE contents in banded iron formations to basaltic rocks associated with the banded iron formations is to compare REE patterns in both rock types in order to assess if they are genetically related. If banded iron formations



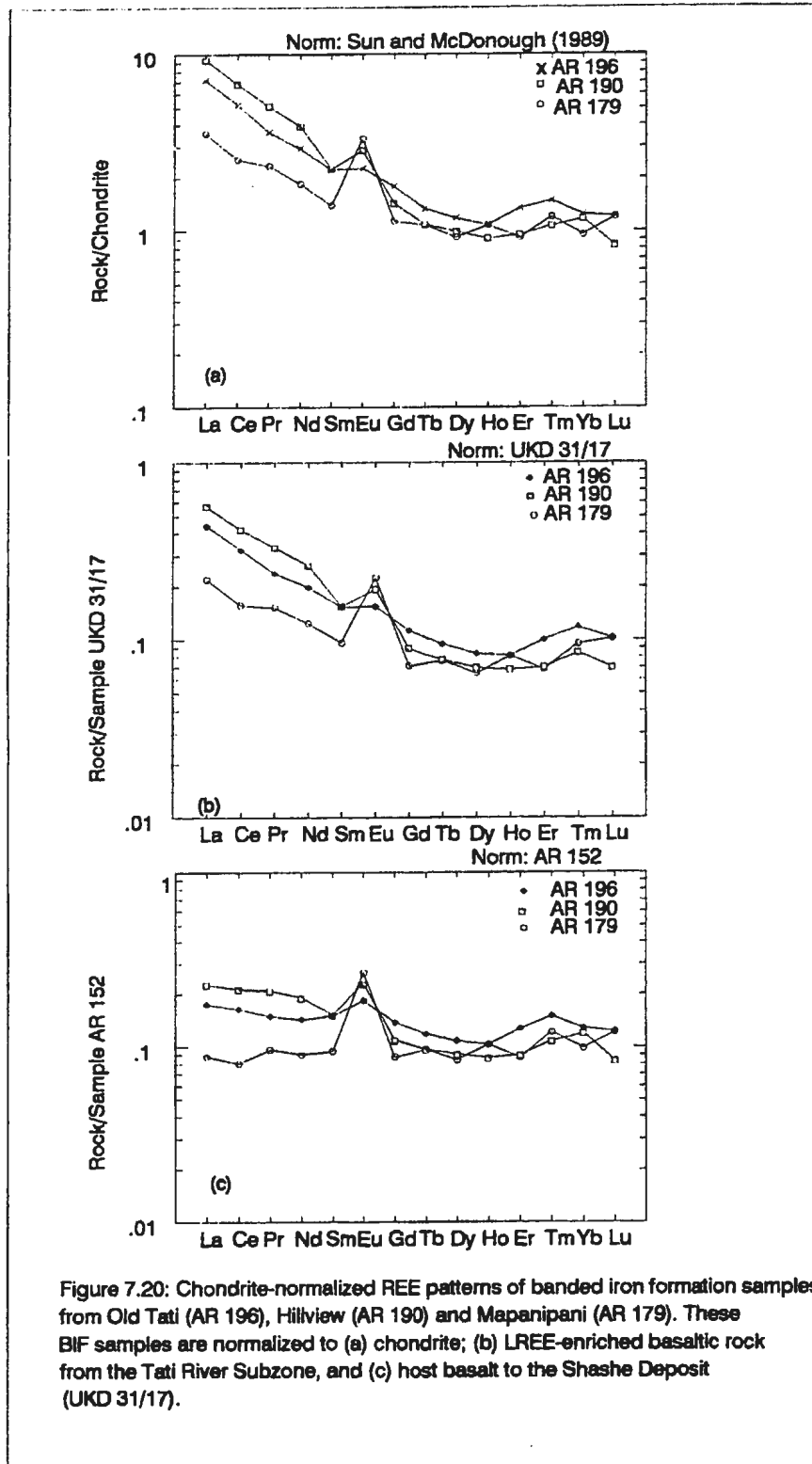


Figure 7.20: Chondrite-normalized REE patterns of banded iron formation samples from Old Tati (AR 196), Hillview (AR 190) and Mapanipani (AR 179). These BIF samples are normalized to (a) chondrite; (b) LREE-enriched basaltic rock from the Tati River Subzone, and (c) host basalt to the Shashe Deposit (UKD 31/17).

were derived by alteration of basaltic rocks in rock-dominated reactions, then the REE patterns of the banded iron formations should reflect those of the source rocks (Graff, 1977). In general, these diagrams indicate a depletion in total REE relative to the normalizing basalts and well developed positive Eu anomalies. Relative to chondrite (Figure 7.20a) and host basalt (Figure 7.20b), banded iron formation samples are LREE-enriched and HREE-depleted. Compared to the LREE-enriched mafic rocks (sample AR 152, Figure 7.20c), the depletion is basically uniform for both HREE and LREE (i.e. they contain flat REE patterns). The flat REE patterns of the banded iron formations when normalized to LREE-enriched basalt are consistent with their slightly LREE-enriched nature. Oberthur et al. (1990) suggested that the banded iron formation REE patterns may be related to their derivation from the leaching of seafloor basalts.

Graf (1977) argued that massive sulphide bodies are commonly overlain by two types of iron-oxide sediments. The first type consists of a reddish sediment containing variable amounts of hematite and/or iron-oxyhydroxides. The second type consists of a magnetite-rich iron formation with iron carbonates, hematite, quartz and iron silicates. He further pointed out that these sulphide bodies are localized along the upper surfaces of volcanic flows and, therefore, form contacts between the underlying volcanic rocks and the overlying detrital sedimentary rocks or volcanic rocks. Hannington et al. (1986) observed that sulphide deposits forming in oceanic basins with high sedimentation rates, such as the active Guaymas Basin in the central Gulf of California, are very small. In these areas, sulphides are not commonly

associated with sulphide mounds but are deposited directly on the ocean floor. They observed that pyrrhotite is the earliest and most abundant sulphide mineral.

Gossans at the Mphoeng area of Zimbabwe (Anhaeusser and Ryan, 1979) and the Long Gossan of Tati Greenstone Belt of Botswana contain massive iron sulphides, mainly pyrrhotite and pyrite (i.e. similar to the massive sulphides at the Guaymas Basin). It is suggested that the similarities in REE patterns of banded iron formations of the Tati Greenstone Belt with those from other parts of Southern Africa (Figure 7.21a-7.21d) (Oberthur et al., 1990) indicate that these rocks may have been deposited from hydrothermal systems in similar environments.

7.4.5 Fluid Inclusion Studies

7.4.5.1 Introduction

Fluid inclusions in vein material, especially quartz and quartz-carbonate, represent a medium in which the physico-chemical characteristics of the fluids can be measured. In most cases, however, the regional quartz-carbonate veins are so small that the probability of finding any measurable fluid inclusions is minimal. The majority of samples investigated in this study, therefore, were collected from the Signal Hill and Shashe mines. Prior to this research, there has been only one fluid inclusion study carried out on all the gold deposits in the Tati Greenstone Belt and that was on the Signal Hill Deposit (Harwood, 1986).

Two vein quartz samples were also collected from barren quartz outside the mining areas. Although numerous fluid inclusions of different types were found in

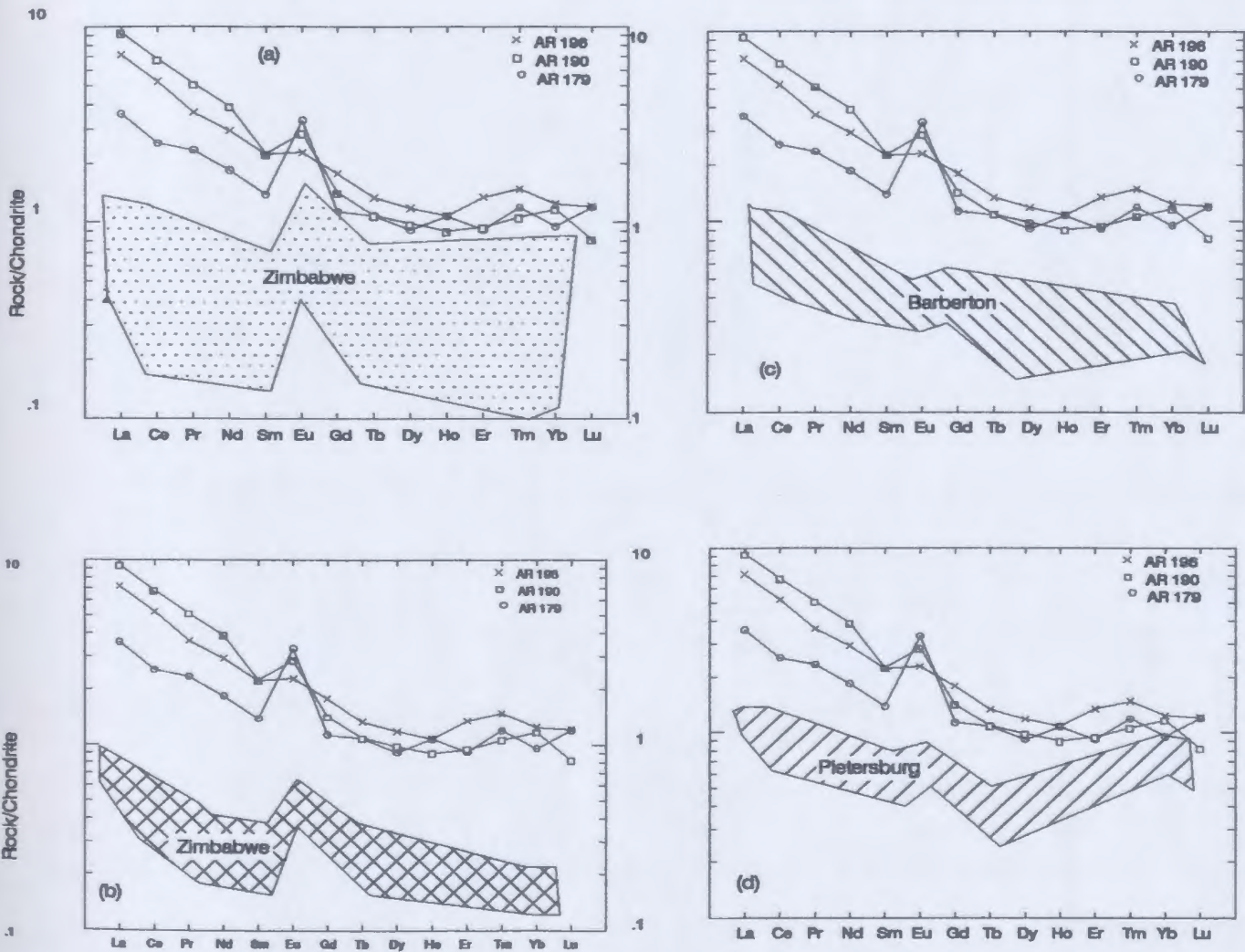


Figure 7.21: Comparison of REE patterns for banded iron formations from the Tati Greenstone Belt with those from other parts of Southern Africa (shaded). (a) data from western Zimbabwe (e.g. Vumbachikwe); (b) data from central Zimbabwe (e.g. Que Que); (c) Barberton, South Africa; and (d) Pietersburg, South Africa. The REE data for these other Southern African banded iron formations from Orbertur et al. (1990). Normalizing factors from Sun and McDonough (1979).

these two samples, the majority were too small to be studied. Only five fluid inclusions were found in one barren quartz sample from which thermometry data could be determined. The purpose of the fluid inclusion study was to evaluate, compare and contrast the nature of the fluids related to gold mineralization in the two mine case studies and the barren veins. The fluid inclusion data are summarized in Table 7.3.

7.4.5.2 Method of Study

Microthermometry data on the fluid inclusions were collected using a Fluid Inc. heating/freezing stage mounted on a Leitz petrographic microscope. Measurements were carried out on doubly polished sample wafers. Freezing data were collected prior to heating to avoid destroying inclusions through decrepitation.

Fluid inclusions can be classified as primary, secondary and pseudosecondary. Primary fluid inclusions represent samples of the fluid from which the host mineral crystallized. Primary fluids are trapped at time of the host mineral growth and during the crystal nucleation process. They are, therefore, completely enclosed within host minerals. Their chemistry should reflect the chemistry of the mineralizing fluid. Measurement of their chemical parameters indicates the chemical composition of the mineralizing fluid and the physico-chemical conditions at the time of mineralization.

Secondary fluids, on the other hand, are those fluids that traversed through crystals in the mineralized zones at some time after they had formed. They are generally contained within healed fractures which traverse the lengths of host crystals.

TABLE 7.3
Fluid Inclusion Data

Sample Number	Type of Fluid Inclusion	T _h °C	T _m °C	T _a °C	T _b CO ₂ (g)	T _a Clat hrate	Salinity NaCl Equivalent wt%
	Aqueous	182 (6)	---	250 (5)	----	----	35
SGH 64/5	3-phase H ₂ O-CO ₂	272 (7)	---	---	23 (7)	7.6 (7)	4
	2-phase H ₂ O-CO ₂	310 (2)	---	---	----	4.9	----
SGH 71/12	3-phase H ₂ O-CO ₂	256 (8)	---	---	26.4 (8)	9.9 (9)	2
SGH 71/32	3-phase H ₂ O-CO ₂	276 (4)	---	---	----	6.0 (4)	8
	2-phase H ₂ O-CO ₂	210 (4)	-0.3 (5)	---	----	----	0.5
SGH 71/22	3-phase H ₂ O-CO ₂	219 (7)	-2.9 (2)	---	29.8 (7)	9.8 (7)	5
TMP 23/19	CO ₂ Dominated	386 to 340	----	---	----	----	----
TMP 23/45	Aqueous	218 (3)	-21 (3)	---	----	----	----
	H ₂ O-CO ₂	235 (3)	----	---	----	----	----
	Aqueous	170 (2)	-1.5 (2)	---	----	----	----
SH 07	H ₂ O-CO ₂	232 (5)	----	---	25.4 (5)	9.7 (5)	3
UKD 31/18	Aqueous 2 phases	185 (4)	-16 (4)	---	----	----	19.6
AR 90	Aqueous 2 phases	158 (5)	-6.5 (6)	---	----	----	10

(note: the numbers in brackets represent number of measurements)

Hence, chemical parameters measured from secondary fluids do not give information on mineralizing fluids or on the mineralization event. Where different generations of secondary fluids are present, however, chemical data can yield some information on the deformational history of the host. For example, pressure and salinity measurements from such fluids might provide data on different episodes of uplift.

Pseudosecondary fluids refer to late fluids that were trapped when the host crystals were completely nucleated. They are commonly contained within healed fractures that are completely enclosed by the host crystal. Such fractures do not cross different crystals. These fluids are not primary in the sense that they do not represent samples of fluids from which the host crystals grew, but they represent late fluids which may have evolved from primary fluids. Pseudosecondary fluids may yield information about the evolutionary path of the mineralizing fluids.

A total of 15 samples were prepared for fluid inclusion work. Of the 15 samples, only 9 contained measurable inclusions. The majority of the fluid inclusions are very small ($< 20\mu\text{m}$) and are contained in fractures, suggesting that they are secondary inclusions. However, primary and pseudosecondary inclusions were also observed, from which the measurements were made.

7.4.5.3 Nature and Occurrence of Fluid inclusions

Mineralization and related hydrothermal alteration zones at the Shashe Mine can be subdivided into three stages. The first stage is responsible for the formation of the widely distributed pervasive carbonate alteration which was accompanied by

early quartz veining. The second stage was related to the formation of the silicified (reef) zone through the widespread replacement of the carbonate alteration. The third stage involved a series of small substages. It started with early fracturing of the silicified zone and emplacement of the gold-bearing sulphide-biotite zone. Late quartz veining (with higher gold grades) followed the formation of sulphide-biotite alteration zone.

Sampling was designed to assess and compare fluids from each stage. Although numerous fluid inclusions were observed in carbonate minerals of the carbonate zone, it was not possible to collect any useful data from them and so the attempt was abandoned. This is because most of the carbonate minerals are fine-grained, and therefore, they contain numerous fluid inclusions of very small sizes, which are too difficult to measure. Similar problems were experienced with the silicified zone. Data summarized in Table 7.3 from the Shashe Mine were, therefore, collected from late quartz veins only (late silicification).

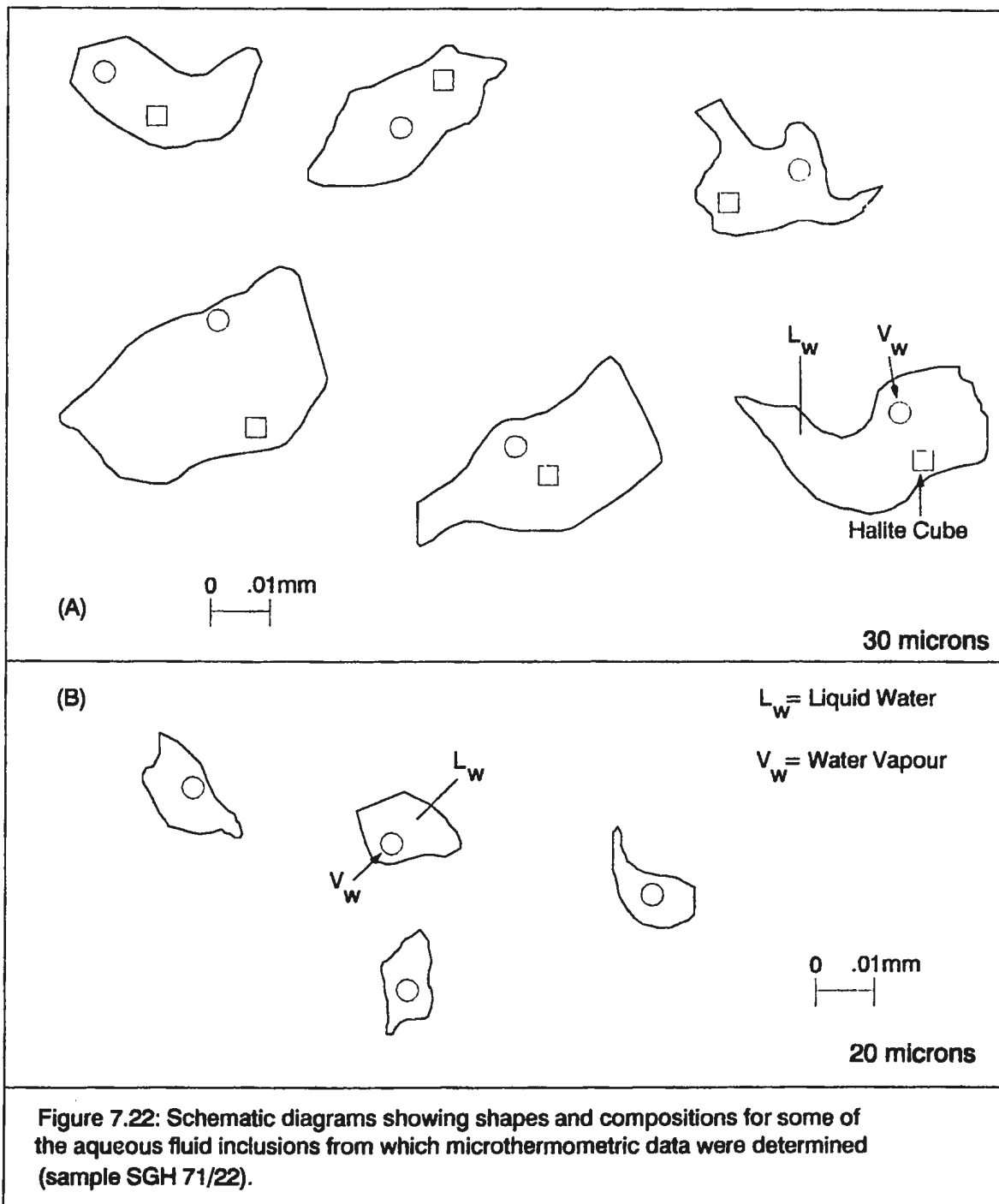
At Signal Hill only one hydrothermal system is interpreted to have been responsible for mineralization. Two fluid inclusion sites were identified and sampled. The materials studied were quartz veins related to mineralization and barren quartz veins within tension microfractures or shears. These microfractures accumulated fluids during the main fluid transport along the main shear zones (e.g. Plate 7.2). Since fluid inclusions in the barren quartz veins were very small in size and difficult to measure, fluid inclusion data from the Signal Hill Deposit (Table 7.3) were derived from mineralized quartz veins only.

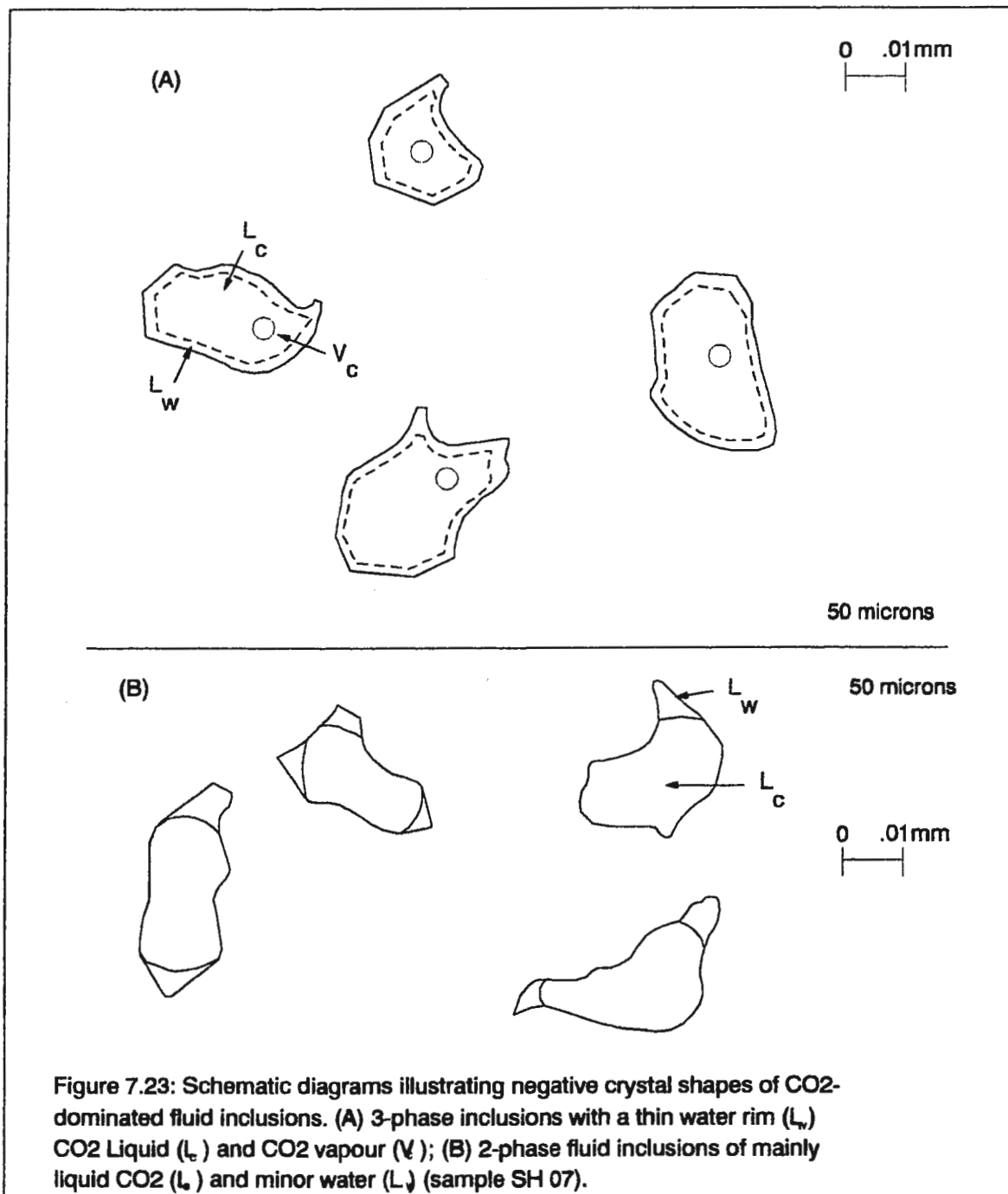
The classification scheme used in this study is slightly different from Harwood's (1986) classification of fluid inclusion data from the Signal Hill Deposit. Harwood (1986)'s classification scheme was as follows:

1. Type A - CO₂-rich fluid inclusions, commonly with liquid and gaseous CO₂. Type A fluid inclusions are mainly primary.
2. Type B - aqueous fluid inclusions, with a bubble. Type B inclusions are primary and pseudosecondary fluid inclusions.
3. Type C - aqueous fluid inclusions without a bubble. Type C are mainly secondary.

In general, fluid inclusions from late mineralized quartz veins at the Shashe Mine and mineralized quartz veins at Signal Hill Deposit have similar compositions. They can be divided into three main types; A, B and C. Type A are mainly aqueous fluid inclusions with a vapour phase (Figure 7.22). Type B fluid inclusions consist mainly of CO₂ liquid and some have liquid and gas CO₂ (Figure 7.23). Type C are H₂O-CO₂ fluid inclusions (Figure 7.24). Harwood's (1986) classification scheme was taken into consideration in deriving the classification used in this study.

1. Aqueous fluid inclusions (Type A) consist of two phases with consistent proportions; a liquid H₂O-rich phase and a very small vapour phase that may be either CO₂ or H₂O (Figure 7.22b). These fluid inclusions are the most widely distributed in all the samples. They also are the smallest which makes their study very difficult. A small number of these inclusions contain daughter minerals (Figure 7.22a).





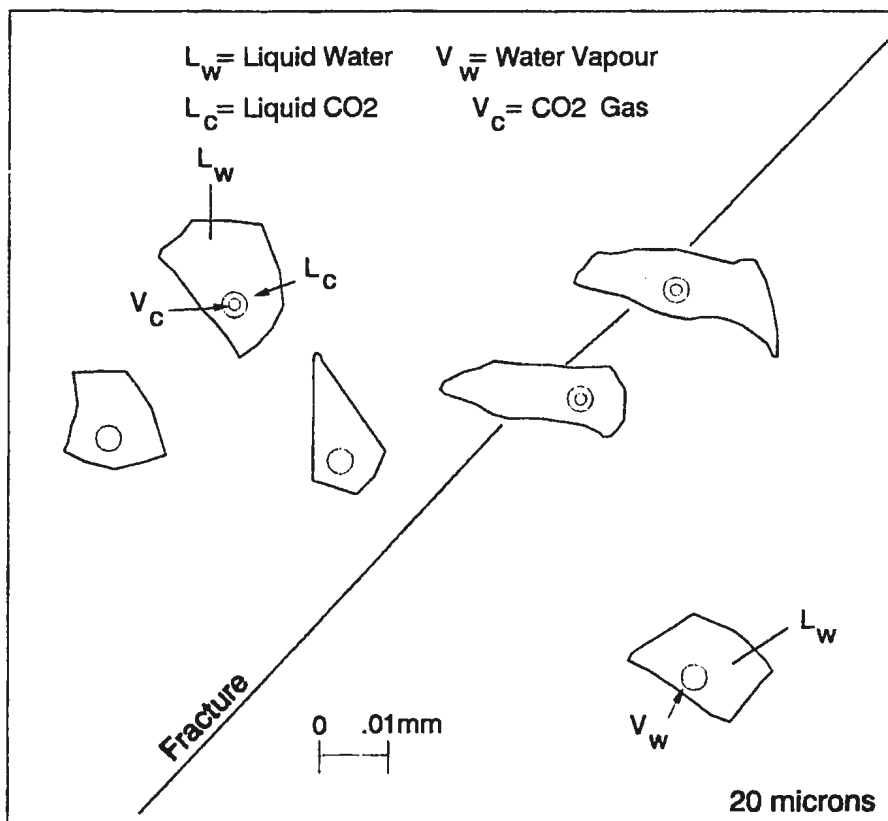


Figure 7.24: Schematic diagram showing the distribution of the 3-phase H₂O-CO₂ inclusions that are associated with higher salinity 2-phase aqueous inclusions (sample TMP 23/45).

2. CO₂-rich Fluid Inclusions (Type B) consist of CO₂-dominated fluid inclusions. They contain three phases which are difficult to recognize.

These phases are: a CO₂ fluid, aqueous fluid and H₂O-gas. Type B fluid inclusions are the largest.

3. H₂O-CO₂ Fluid Inclusions (Type C), although variable in size, constitute the largest occurrences in all the samples. The largest ones in the group are up to about 50 μ m. They vary in composition from two to three phase fluid inclusions. The three phase inclusions contain liquid H₂O, which is the dominant phase, liquid CO₂ and CO₂ gas.

Two-phase fluid inclusions contain about equal proportions of liquid H₂O and liquid CO₂ (Figure 7.24). There is a general overlap between types B and C fluid inclusions due to variable CO₂/H₂O ratios. Type B fluid inclusions consist of all those inclusions in which the volumetric proportions of the CO₂ phase is greater than 90%.

7.4.5.4 Microthermometric Analysis

In his study of the Signal Hill Deposit, Harwood (1986) carried out microthermometric studies on his type B fluid inclusions (i.e. two phase aqueous fluid inclusions). They were found to have variable salinities from 8 to 13 wt% NaCl equivalent. The average homogenization temperatures were about 230°C. In this study over one hundred heating and freezing experiments were carried out on about 30 plates from the 15 fluid inclusions sample wafers. The majority of the data are from the Signal Hill and Shashe deposits.

Freezing temperatures for the aqueous fluid inclusions (type A) range from -25°C to -6.5°C . The highest temperatures (-6.5°C) were recorded in a barren quartz sample (AR 90; Table 7.3). These temperatures correspond to salinity ranges of between 10 and 21 wt% NaCl equivalent. Those fluid inclusions containing daughter minerals suggest salt concentrations of 35 wt% NaCl equivalent (Collins, 1979; Shepherd et al., 1985).

Homogenization temperatures range from about 160°C to 208°C . Daughter mineral salt crystals dissolve at temperatures around 250°C .

$\text{H}_2\text{O}-\text{CO}_2$ fluid inclusions (type C) are the most numerous in terms of inclusions of measurable size ($> 20\mu\text{m}$) and are perhaps the most complicated. Freezing experiments show that melting starts at about -56°C corresponding to the melting of solid CO_2 . The melting continues to temperatures of about -1.5°C when the last ice disappears. The final measurable melting temperatures are those of a clathrate solid which fall between 4.5° and about 10.5°C . Salinity calculations indicate that these are very low salinity solutions. Salinity ranges from 0.5 to about 8 wt%, with an average of about 5 wt% NaCl equivalent.

Most of the type C fluid inclusions contain small CO_2 vapour bubbles that homogenize into liquid CO_2 at about 30.2°C (Figure 7.25c). Homogenization temperatures range from 235°C to 260°C (Figure 7.25a) for the majority of the three phase H_2O -rich fluid inclusions. CO_2 dominated type C fluid inclusions generally, have higher temperatures, between 285 and 310°C (Figure 7.26).

The CO_2 -rich fluid inclusions (type B), despite the fact that they are generally

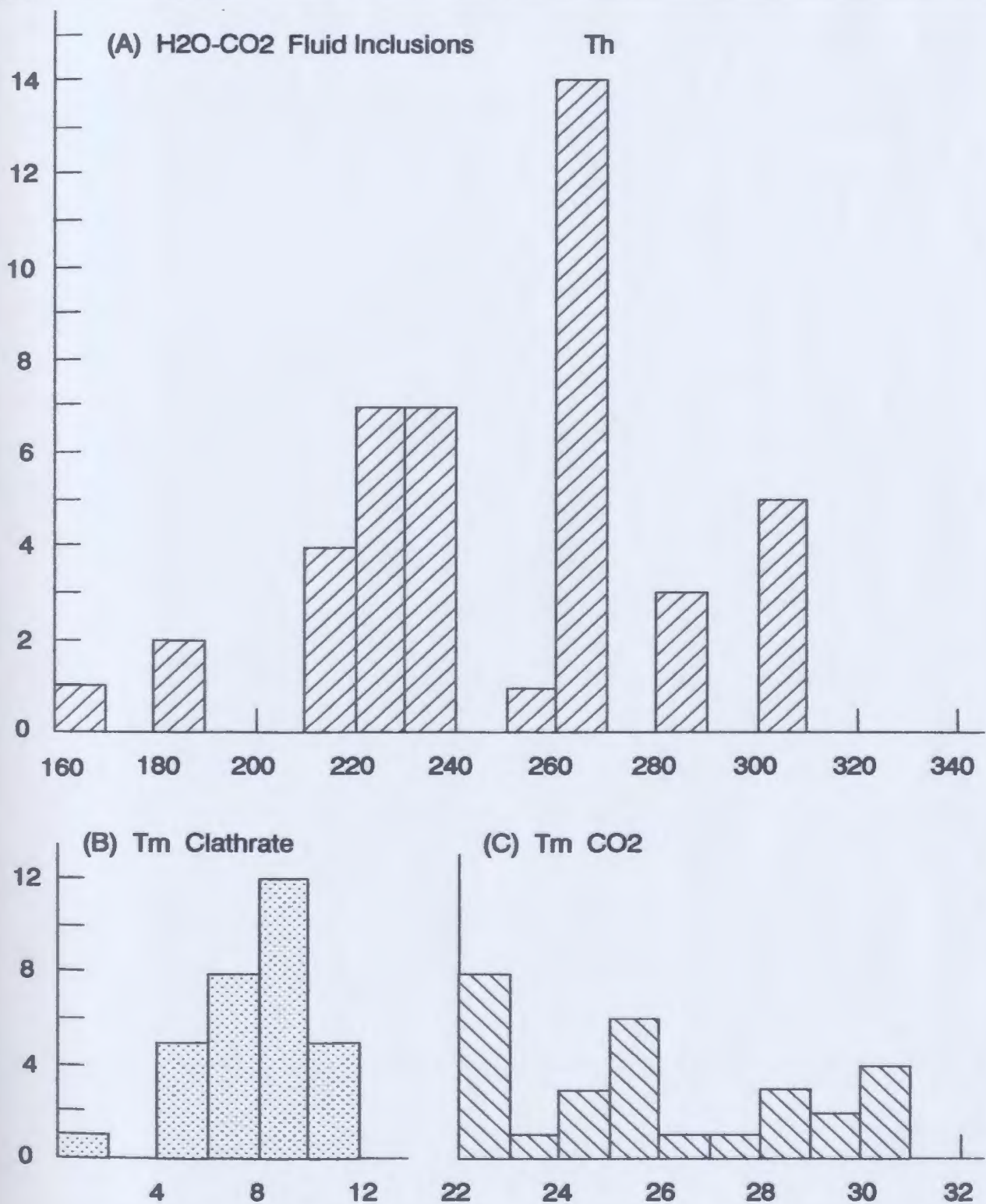


Figure 7.25: Histograms showing homogenization temperatures of various type C fluid inclusions; (A) CO₂ homogenizing into aqueous liquid (B) dissolution of clathrate solid, and (C) CO₂-gas dissolving in CO₂-liquid.

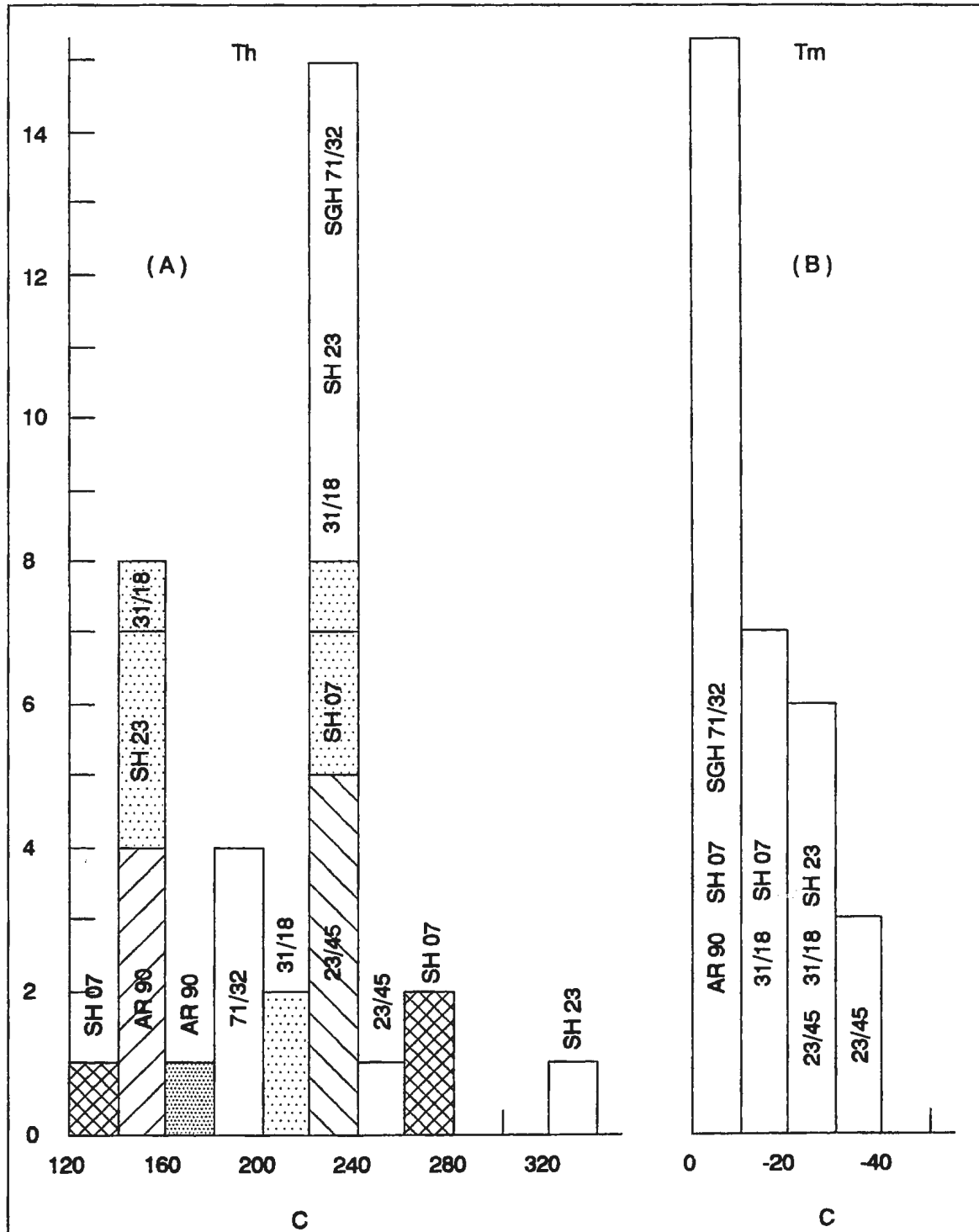


Figure 7.26: Homogenization (Th) and Freezing (Tm) temperatures for Type A fluid inclusions (aqueous). Labels on graph bars are sample numbers (see Table 7.3).

the largest in size, are the most difficult to study. This is especially true for freezing experiments. Homogenization temperatures for type B fluid inclusions range from 386 to 430°C.

7.4.6 Oxygen and Carbon Isotope Geochemistry

7.4.6.1 Introduction

Oxygen and carbon isotope compositions of carbonate in mineralized quartz veins from mesothermal gold mineral deposits fall within restricted compositional ranges of 12.5 to 15 per mil and -11 to 0.5 per mil, respectively (Kerrick, 1989). Oxygen and carbon isotope compositions are homogeneous irrespective of the host rock type. The uniformity in both oxygen and carbon isotope compositions in mesothermal gold deposits has been interpreted to indicate that the carbonate precipitated from a water dominated hydrothermal system. Oxygen and carbon isotopic compositions of mesothermal gold deposits overlap with the isotopic compositions of major fluid reservoirs such magmatic fluids, metamorphic fluids, meteoric fluids and juvenile fluids. This overlap has led to a debate regarding the sources of mineralizing fluids (Kerrick, 1989; Burrows et al., 1986; Colvine et al., 1984; Cameroon, 1988; Nisbett et al., 1987). No attempt in this study is made to use oxygen and carbon isotopic composition to assess the nature of the source of the mineralizing fluids; the isotope compositions derived in this study are only used to compare the isotopic compositions of gold deposits of the Tati Greenstone Belt to Archean mesothermal gold deposits elsewhere. On this basis only six samples from

the carbonate alteration zones were analyzed for carbon and oxygen isotopes and the results are summarised in Table 7.4. Four of the samples (TMP 23/10, TMP 23/25, TMP 23/26 and UKD 31/10) are core samples of quartz-carbonate alteration veins from the two boreholes at the Shashe Mine. One sample (SGH 64/17) is from a borehole at the Signal Hill Deposit. The sixth sample (AR 218) is a sedimentary carbonate rock associated with banded iron formation in the Golden Eagle Formation of the Lady Mary Group.

7.4.6.2 Oxygen Isotopes

Although the sample base is small, two distinct oxygen isotopic compositions can be recognised in carbonate alteration zones at the Shashe Deposit. The first is defined by samples from the main part of the mineralization zone (UKD 31/10 from borehole UKD 31, and TMP 23/10 and TMP 23/25 from borehole TMP 23). The $\delta^{18}\text{O}$ values of these samples vary from +11.9 to +16 per mil (Table 7.4). The $\delta^{18}\text{O}$ values of these three samples show a crude correlation with stratigraphic position. Isotopically enriched samples were collected at higher stratigraphic positions (i.e. shallower depth). A similar covariance of oxygen isotopic composition with stratigraphic positions were recognised in gold deposits from the Archean Timmins District (Fyon et al., 1983). This phenomena has been suggested to be related to decreasing precipitation temperatures with increasing stratigraphic level.

The second isotopic composition in carbonate minerals of the Shashe Mine is defined by only sample (TMP 23/26). This sample is from a small, massive

TABLE 7.4

Carbon and Oxygen Isotopic Composition of carbonate separates from the Tati Greenstone Belt.

Sample Number	Location	Mineral (Rock) Type	$^{18}\text{O}_{\text{cc}}$	$^{13}\text{C}_{\text{cc}}$	$^{18}\text{O}_{\text{w}}$
TMP 23/10	Shashe Mine	Calcite-Quartz Veins	+13.1	-0.9	+6.6
TMP 23/25	Shashe Mine	Calcite-Quartz Veins	+11.9	-5.7	+5.4
TMP 23/26	Shashe Mine	Calcite Veins	+ 7.4	-7.0	
UKD 31/10	Shashe Mine	Calcite-Quartz Veins	+16.0	-4.6	+6.7
SGH 64/17	Signal Deposit	Calcite-Quartz Veins	+13.7	-1.2	+4.4
AR 218	Golden Eagle	Limestone	+16.7	+0.5	n/a

cc = Calcite

w = Water

The oxygen isotopic composition of hydrothermal fluids from which the carbonate minerals in carbonate-quartz veins were deposited, were calculated using the following equation: $1000 \ln \alpha_{12} = \delta_1 - \delta_2 = A(10^6 T^{-2}) + B$ where T = Absolute Temperature. 1 and 2 are phases with isotopic composition δ_1 and δ_2 respectively and A and B are temperature dependent constants (A = 2.78 and B = -2.89 for temperatures between 0 and 500°C from data compiled by Faure, 1986). The temperature used in the calculations was approximated from fluid inclusion homogenization temperatures (273°C). n/a = not applicable.

galena-sphalerite bearing carbonate vein (ca 7 cm thick). The vein has the $\delta^{18}\text{O}$ value of +7.4 per mil. The galena-sphalerite-bearing carbonate vein is fracture-controlled, and has been suggested to be a product of the secondary mineralization event (M. Chiepe, 1990, per. comm.). The sample (TMP 23/26) is from the deeper part of borehole TMP 23 compared to samples TMP 23/25 and TMP 23/10. The $\delta^{18}\text{O}$ value of sample TMP 23/26 is very much different from the other two. No significant conclusion can be reached on the basis of these three samples, nevertheless the galena-sphalerite vein appears to have been formed from a fluid of different composition than that which formed the other two samples. The $\delta^{18}\text{O}$ value of +7 per mil for this vein, although lower than that of the main system, still falls within the general limits of Archean gold deposits (Figure 7.27). The $\delta^{18}\text{O}$ values from such deposits generally overlap the fields of magmatic and metamorphic hydrothermal fluids (e.g. Kerrich, 1989; Golding et al., 1989). The sample from the Signal Hill Deposit (SGH 64/17) with a $\delta^{18}\text{O}$ value of +13.7 per mil falls within the trend of the main carbonate alteration zone at the Shashe Deposit.

It has been suggested in the literature that mesothermal gold deposits formed at average temperatures of around 250°C (e.g. Nisbett et al., 1987). In the Tati Greenstone Belt, Harwood (1986) argued that the main mineralization at Signal Hill was deposited at around 250°C. Fluid inclusion data derived in this study suggest that mineralization may have occurred at an average temperature of 273°C. Therefore, isotope compositions of the mineralizing fluids were calculated based on a fluid inclusion homogenization temperature of 273°C (Table 7.3). Calculated $\delta^{18}\text{O}$ values

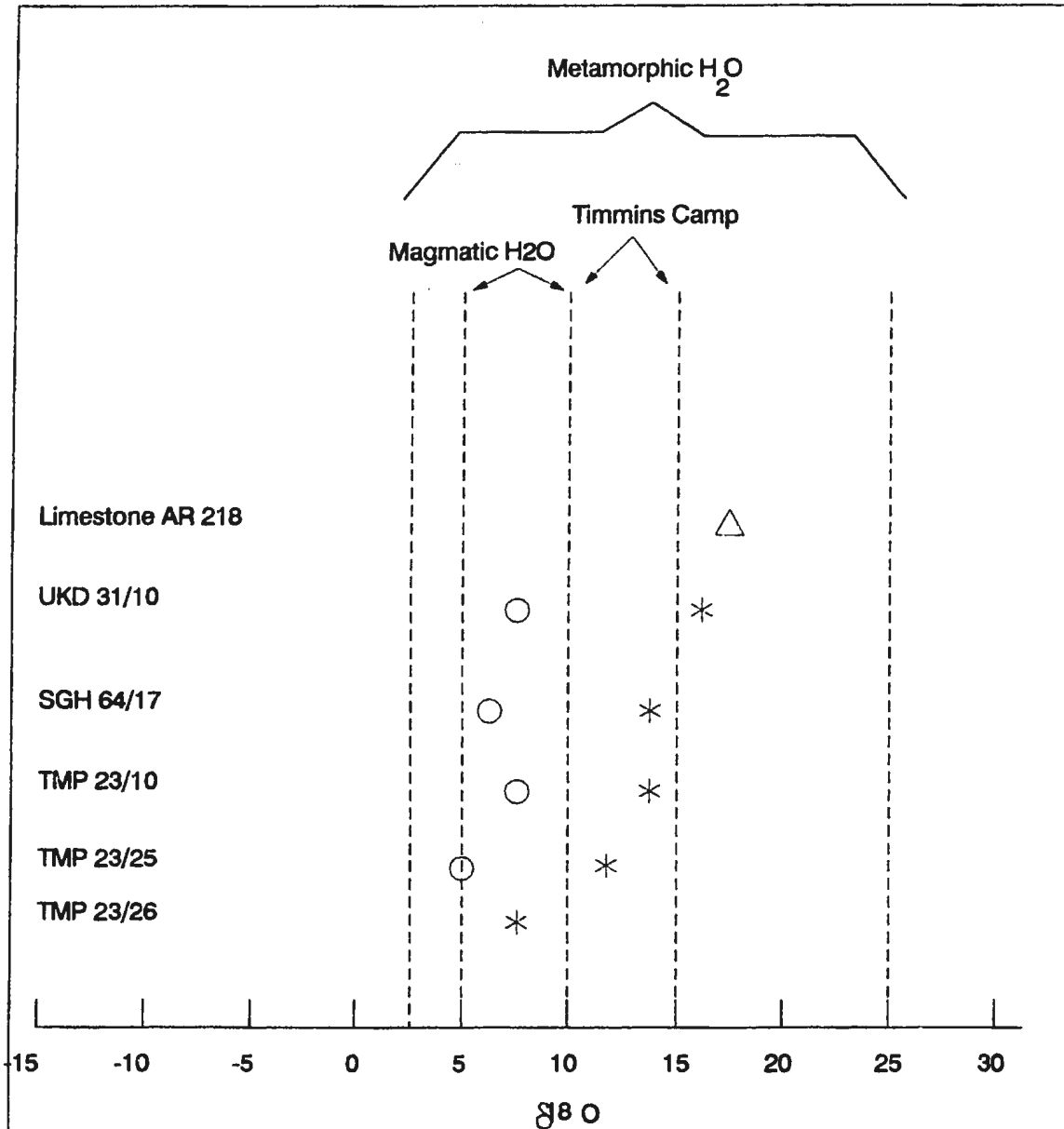


Figure 7.27: Oxygen isotopic composition of carbonate alteration at both Signal Hill and Shashe Deposits (*). The open circles are calculated fluid compositions at 273°C (from fluid inclusions). Also shown are fields for magmatic fluids, metamorphic fluids and the range of vein quartz and carbonates from the Timmins Camp, Abitibi Greenstone (Kerrich, 1989). Also plotted is the limestone sample AR 218 from the Golden Eagle Formation (△).

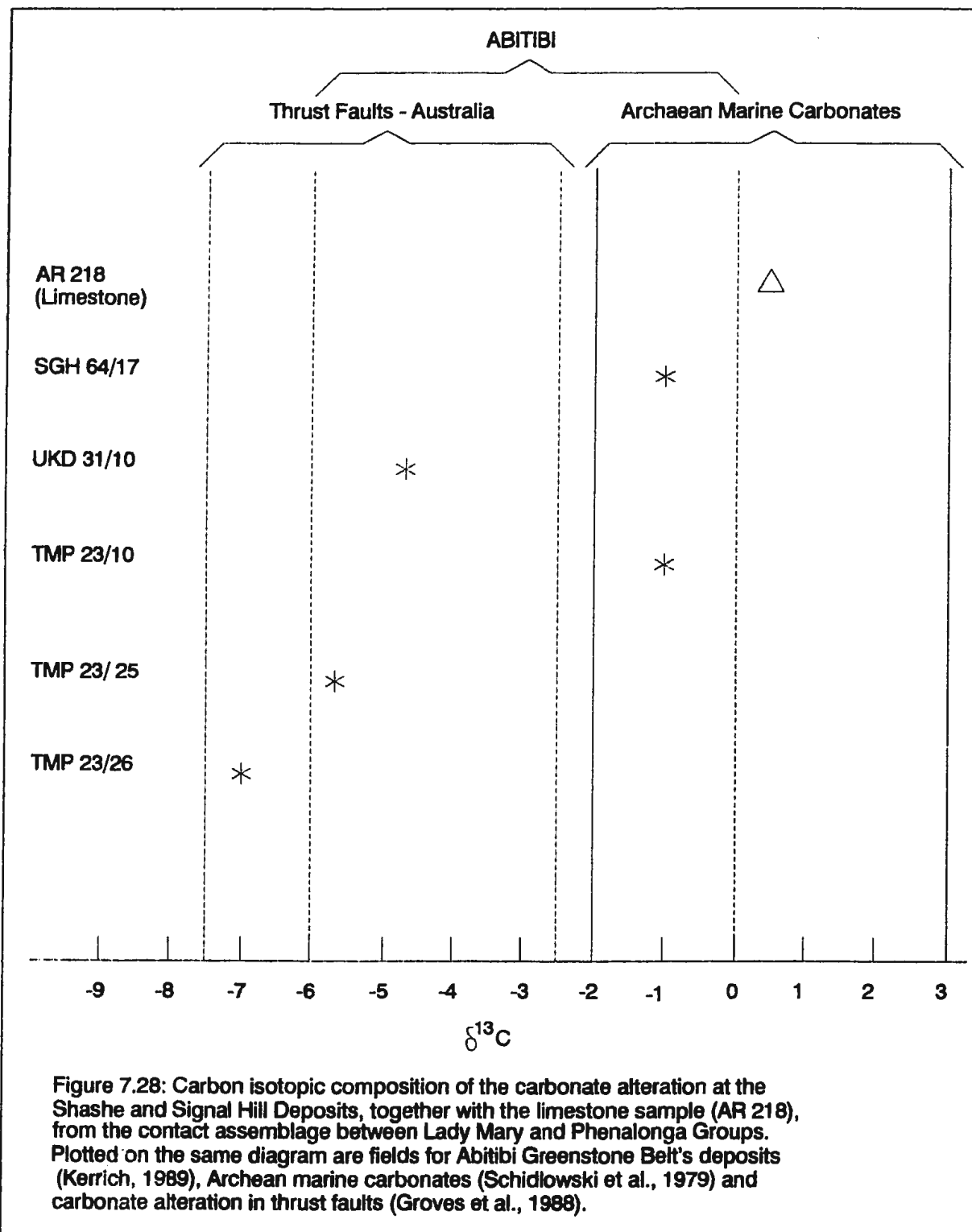
for the main mineralizing fluid at the Shashe Mine range between +4 and +7 per mil. The $\delta^{18}\text{O}$ value of +16.7 per mil for the limestone (sample AR 218) from Golden Eagle Formation is at the higher end of the gold deposit values (Figure 7.27).

7.4.6.3 Carbon Isotopes

Carbon isotopic compositions of the carbonate separates are summarized in Table 7.4. In general, $\delta^{13}\text{C}$ values show compositional variations similar to those of the oxygen isotopes with an enrichment of $\delta^{13}\text{C}$ values with an increasing stratigraphic level (i.e. decreasing with depth in borehole TMP 23). The lowest $\delta^{13}\text{C}$ value is also found in the Pb-Zn vein, similar to the oxygen isotopic composition (Figure 7.28). The $\delta^{13}\text{C}$ value of the limestone sample is 0.5 per mil. This value is similar to that of Archean carbonates deposited in a marine environment (Longstaffe, 1983, Kerrich, 1989).

7.4.6.4 Summary on Oxygen and Carbon Isotopic Data

The main conclusion to be derived from this small database of oxygen and carbon isotopic compositions is that the isotopic compositions of the Archean Tati Greenstone Belt gold deposits fall within the fields of mesothermal gold deposits from elsewhere (i.e. 12.5 to 15 per mil and -11 to 0.5 per mil for oxygen and carbon, respectively). It is also concluded that the galena-sphalerite vein in borehole TMP 23 at the Shashe Mine was deposited from a fluid that had a different composition



compared to that which deposited the major gold mineralization.

7.5 Occurrences of Banded Iron Formations and Gold Mineralization

Banded iron formations of the Tati Greenstone Belt crop out at different stratigraphic positions throughout the entire belt. The best occurrences, however, are found at contacts between different volcanic rock units. The most prominent of these occurrences are in the Golden Eagle Formation which marks the contact between the Lady Mary and Phenalonga groups, and the Dinuku Formation which separates the Phenalonga and Selkirk groups. Several other occurrences have been mapped elsewhere in the belt such as the Matsiloje Ridge. Most of the banded iron formations occur as laterally discontinuous low lying hills and have variable thicknesses. The banded iron formations are generally either overlain by, or interbedded with, limestones and minor clastic sediments.

Three compositional facies may be recognized in the Archean banded iron formations, i.e. siliceous oxide, carbonate, and sulphide facies. The siliceous oxide facies consist of thin alternating bands of iron oxides (mostly magnetite or hematite) and chert. In most cases this variety is brecciated and consists of angular chert fragments in a reddish-brown jaspilitic matrix. The sulphide facies consist of yellow to black, crudely banded gossaniferous varieties and usually contain massive bands of mainly pyrrhotite and pyrite (Anhaeusser and Ryan, 1979; Johnston and Griffiths, 1983). Carbonate facies banded iron formations generally occur as crudely banded massive lenses of maroon coloured carbonate units (mainly siderite).

In section 7.4.4, banded iron formations of the Tati Greenstone Belt were suggested to have similar characteristics to those of ancient massive sulphides and modern oceanic massive sulphides on the basis of the nature of constituent iron sulphide minerals and their relationship with sedimentary rocks at the top of major volcanic sequences. Massive sulphide deposits in modern oceanic environments are known to contain gold and related metals as pockets in low temperature areas of the depositing hydrothermal system (e.g. Hannington et al., 1986). Although it cannot be proven at this stage that banded iron formations contained sufficient quantities of gold to lead to the formation of the gold deposits in the Tati Greenstone Belt, it is speculated that the distribution of the gold deposits and banded iron formations indicates that they are genetically related. Foster and Wilson (1984) and Kramers and Foster (1984) have also noted the importance of banded iron formations to Archean gold deposits in Zimbabwe, particularly those related to the 3.5 Ga greenstone belts.

7.6 Discussion

This section presents a synthesis of geological, geochemical and isotopic characteristics of gold mineral deposits from the Tati Greenstone Belt. The synthesis draws on all of the data presented in this chapter, especially data from both the Signal Hill and Shashe Deposits. Reconnaissance and past production data have also been taken into consideration.

7.6.1 Summary of Geochemical Data of Mineral Deposits

A recent trend in metallogenic research has been to compare Archean mesothermal gold deposits with Mesozoic mesothermal gold deposits (e.g. Nesbitt et al., 1986; Kerrich, 1989; Kerrich and Feng, 1992). One of the most important characteristics of mesothermal gold deposits from both periods is that they contain low abundances of base metals. There has, however, never been any study carried out to investigate whether there are variations in base metal contents between Archean mesothermal gold deposits. In this section, an attempt is made to document the metallic variations between gold deposits of the Tati Greenstone Belt. This is done by making comparisons similar to those of Shikazono and Shimuzu (1992) in a study of vein mineral deposits hosted by Cretaceous to Quaternary island arc volcanic rocks in the Japanese Islands.

The Japanese vein-type mineral deposits were subdivided into two main types on the basis of metallic associations; (i) Au-Ag and, (ii) base metal types. The main metals produced from the Au-Ag type deposits are Au, Ag, Te, Se, and Cu (Shikazono, 1985; Shikazono and Shimuzu, 1992). This type of deposit also contains accessory metals Hg, Tl, Sb, As, and Cd. The Au/Ag ratios (by weight) estimated from past production data in these Japanese vein-type deposits vary between 1 and 100. Other characteristics of the Au-Ag type include abundant pyrite and hematite. Depositional temperatures range between 170° and 250°C, and fluid inclusion salinities vary from 0 to 3 wt% NaCl-equivalent. Common gangue minerals are quartz, chalcedonic quartz, adularia, calcite, smectite, interstratified mica-smectite,

interstratified chlorite-smectite, sericite, zeolites and kaolinite.

Metallic associations for the base metal type are Cu, Zn, Pb, Mn and Ag. In, Ga, Bi, As, Sb, W and Sn are accessory metals. Base metal type deposits contain chlorite, quartz, sericite, carbonates (calcite, rhodochrosite and siderite), and magnetite as gangue minerals. Salinities range from 3 to 10 weight percent NaCl equivalent in fluid inclusions, and temperatures of deposition vary from 200° to 300°C. In general, Shikazono and Shimizu (1992) conclude that base metal type deposits form at greater depths than the Au-Ag type.

Table 7.5a summarizes the metallic associations of the gold deposits in the Tati Greenstone Belt. The gangue minerals in these deposits, where data are available, are listed in Table 7.5b. The data do not enable subdivision of the Tati Greenstone Belt gold mineral deposits into Au-Ag and base metal types. There are, however, several comparisons that can be made. Metallic associations and gangue minerals (Table 7.5a and 7.5b) suggest, for example, that the Signal Hill deposit has some similarities to Shikazono and Shimizu's (1992) Au-Ag type. Most of the other deposits, although containing various metallic associations, approximate Shikazono and Shimizu's (1992) base metal vein-type deposits.

Fluid inclusions in samples collected from the Shashe and Signal deposits were found to have different composition types in any one sample. Different types of fluid inclusions commonly dominate in any one fluid inclusion trail, cluster or fracture (cf. Robert and Kelly, 1987). In general, the H₂O-CO₂ fluid inclusions (type C) appear in minute quantities in regions dominated by either CO₂-rich (type B) or aqueous

TABLE 7.5a

Metallic associations in gold deposits of the Tati Greenstone Belt. Metals listed in the table occur together with Au and/or Ag.

Mineral Deposit Group	Metallic Association							
	Cu	Pb	Zn	Sb	As	W	Sn	Bi
Shashe	x	x	x	x	x	-	-	-
Golden Eagle	-	x	x	-	x	x	x	-
Charlie	-	-	-	-	x	-	-	-
New Zealand	-	-	-	-	x	-	-	-
Blue Jacket	-	-	-	-	x	-	x	-
Flora	-	-	-	-	x	-	-	-
Signal Hill	x	-	x	x	x	-	-	x
Rainbow	x	-	-	x	x	x	-	-
Vermaak	-	-	-	-	x	x	-	-
Phenalonga	x	x	x	-	x	-	-	-
Bonanza	x	-	-	-	x	-	-	-
Cherished Hope	-	-	-	-	x	-	-	-
Francistown	-	-	-	-	x	-	-	x
Monarch	x	-	-	-	x	-	-	x

x=present based on mineralogy of hand specimens; Bi reported as >1000 ppm; - = absent and/or not reported

TABLE 7.5b

Gangue Minerals in gold deposits of the Tati Greenstone Belt. Minerals listed are in addition to quartz which is ubiquitous in all deposits.

Mineral Deposit Groups	Gangue Minerals												
	py	p	c	l	m	b	a	h	k	s	v	w	d
Shashe	x	x	x	x	i	x	i	-	-	x	x	-	x
Golden Eagle	x	x	-	x	-	x	x	x	-	x	-	-	x
Charlie	x	i	x	i	-	x	-	-	-	i	-	-	x
New Zealand	x	x	-	-	-	-	x	x	-	-	-	-	-
Blue Jacket	x	x	i	-	-	-	i	-	-	-	-	-	x
Flora	x	x	i	-	-	-	-	-	-	-	i	-	-
Signal Hill	x	i	-	i	i	-	-	i	x	x	-	i	-
Rainbow	x	x	-	x	-	i	x	i	-	x	-	-	i
Vermaak	x	i	-	-	-	-	-	-	-	-	i	-	-
Phenalonga	x	x	-	-	-	-	x	x	-	-	i	-	-
Bonanza	x	x	-	x	-	x	-	-	-	x	i	-	x
Cherished Hope	i	x	-	-	-	-	-	-	i	x	i	-	-
Francistown	i	x	-	x	-	-	-	-	-	i	-	-	-
Monarch	x	x	-	x	-	x	-	-	i	x	i	-	i

py=pyrite; p=pyrrhotite; c=calcite/dolomite; l=chlorite; m=marcasite; b=biotite; a=ankerite/siderite; h=hematite; k=kaolinite; s=sericite; v=muscovite; w=mackinawite; and d=amphibole (hornblende/actinolite/tremolite); i=minor occurrence and x=abundant.

inclusions (type A). The other two types rarely occur together and this is common for both deposits examined, i.e. Signal Hill and Shashe.

Homogenization temperatures tend to be highest in the CO₂-rich inclusions (386-430°C). It was not possible to calculate salinities for this type of fluid inclusion. The aqueous fluid inclusions (type A) have the lowest homogenization temperatures (170-185°C) and highest salinities (19.6-35 wt% NaCl equivalent). Homogenization temperatures for the type C H₂O-CO₂ fluid inclusions fall into two ranges. The lower temperatures (210-240°C) were measured on two phase type C fluid inclusions. Higher temperatures (272-310°C) for this group are from the three phase fluid inclusions. Salinities for type C fluid inclusions range from 0.8-8 and 10-23 weight percent NaCl equivalent, respectively.

According to Shikazono and Shimizu (1992) and Shikazono (1985), fluid inclusion temperatures are 150-250°C for the Au-Ag type and 200-350°C for the base metal type in Mesozoic vein deposits of Japan. Fluid inclusion filling temperatures of gold deposits from the Tati Greenstone Belt are comparable to these.

The carbon and oxygen isotopes of carbonate separates from the two deposits in the Tati Greenstone Belt fall within the isotopic compositional limits of Archean and other mesothermal gold deposits (Kerrick, 1989; Golding et al., 1989; Nesbitt et al., 1986;1989).

7.6.2 Relationship of Banded Iron Formations to Gold Mineralization

The resemblance of banded iron formations to barren massive sulphides from

oceanic spreading axes is a very interesting point. Scott (1990) described the mode of emplacement of massive sulphide deposits in sediment-covered spreading ridges. He suggested that hydrothermal fluids are discharged under a sedimentary rock cover. The dissolved metallic loads are, therefore, dumped in the sediments through chemical interaction. Hannington et al. (1986) also compared barren massive sulphides at sediment covered ridges (e.g. Guaymas Basin) with those from sediment-starved ridges, such as the Explorer ridge in the Pacific. They concluded that sulphides from sediment-starved ridges are generally better mineralized than those from sedimentary covered ridges.

The mineralization at ridge settings is zoned from high temperature Cu-rich deposits to Zn-Pb dominated, and finally to lower temperature Pb-Zn deposits with high concentrations of Au-Ag-Sb-As-Ba and SiO₂. It is interesting to note that the metallic associations at the Long Gossan and the Shashe Group of deposits, all from the Tati Greenstone Belt, are similar to metallic associations of the low temperature mineralization components of massive sulphides at oceanic spreading ridges (Table 7.5).

Oberthur et al. (1990) observed that Au in banded iron formations correlates with As and S, and banded iron formations contain elevated abundances of these elements. The metallogenic importance of sulphide facies banded iron formations is that they were deposited by large scale hydrothermal systems, whose waning stages may have been related to gold enrichment.

CHAPTER EIGHT

8. METALLOGENIC MODEL FOR THE TATI GREENSTONE BELT GOLD DEPOSITS

8.1 Introduction

There are several unifying characteristics that tie the mesothermal gold deposits within the Tati Greenstone Belt together. These deposits may, therefore, be explained by a single genetic model in which different deposits represent separate parts of the same hydrothermal system. Regional distributions of gold deposits in the Tati Greenstone Belt and their relationships with major structures and stratigraphy of the belt are combined to develop a metallogenic model for these deposits. The model proposed is, however, largely speculative, as some of the ideas used in developing the model cannot be substantiated with the present data. For example, the role played by banded iron formations in gold mineralization in the Tati Greenstone Belt is inferred from the general associations of gold deposits with banded iron formations in the belt (Figure 7.6). It is also inferred from the general association of banded iron formations with massive sulphides at modern oceanic environments (Scott, 1990; Hannington et al., 1986) and ancient massive sulphide deposits (Graf, 1977). It is not possible at this stage to show any systematic variation of gold and related metals in different facies of the banded iron formations and how this might relate to the distribution of the mineral deposits. It is, however, hoped that the proposed model will act as a building block or foundation for future research. As

more data become available, these ideas can be tested and evaluated.

8.2 Gold Deposits in Archean Greenstone Belts of Zimbabwe

This section will present a brief review of gold deposits in greenstone belts from Zimbabwe in order to compare and contrast them with those of the Tati Greenstone Belt. Several reviews concerning gold deposits in Zimbabwe have been carried out by a number of authors (e.g. Robertson, 1973; Kramers and Foster, 1984; Foster and Wilson, 1984; Porter and Foster, 1990). Robertson (1973) carried out an extensive study of the lead isotope systematics in Archean gold deposits from Zimbabwe and found that the deposits could be subdivided into two broad groups on a Pb-Pb plot (Figure 8.1a). These groups were: (i) Que Que-type lead, and (ii) Bulawayo-type lead, named after the major Zimbabwean greenstone belts in which they occur.

The Que Que-type lead isotopic composition has comparatively higher $^{207}\text{Pb}/^{204}\text{Pb}$ ratios and, thus, is more radiogenic than the Bulawayo-type. In general, Que Que-type lead isotope compositions are found in areas east of the Bulawayo-type lead isotope signatures such as Mashaba, Fort Victoria and Que Que, whereas deposits with the Bulawayo-type lead isotopes occur around Bulawayo, Filabusi, and Gwanda (Figure 2.4).

As pointed out in Chapter 2, areas east of the Great Dyke contain relatively K-rich granitoids and granite gneisses, whereas areas to the west are dominated by volcano-sedimentary rocks and tonalites. The older granitoid gneisses are more

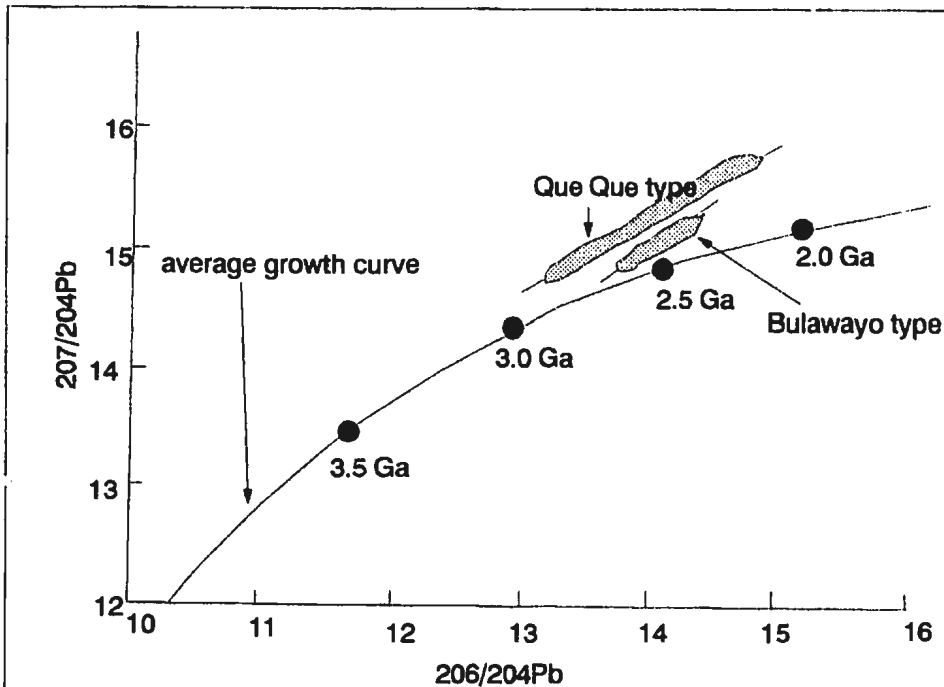


Figure 8.1a: $^{207}/^{204}\text{Pb}$ vs. $^{206}/^{204}\text{Pb}$ plot showing Pb-isotopic signatures for Archean gold mineral deposits in Zimbabwe, designated Que Que and Bulawayo types as distinguished by Robertson (1973). Deposits plot above Stacey and Kramers's (1975) growth curve (see text for discussion).

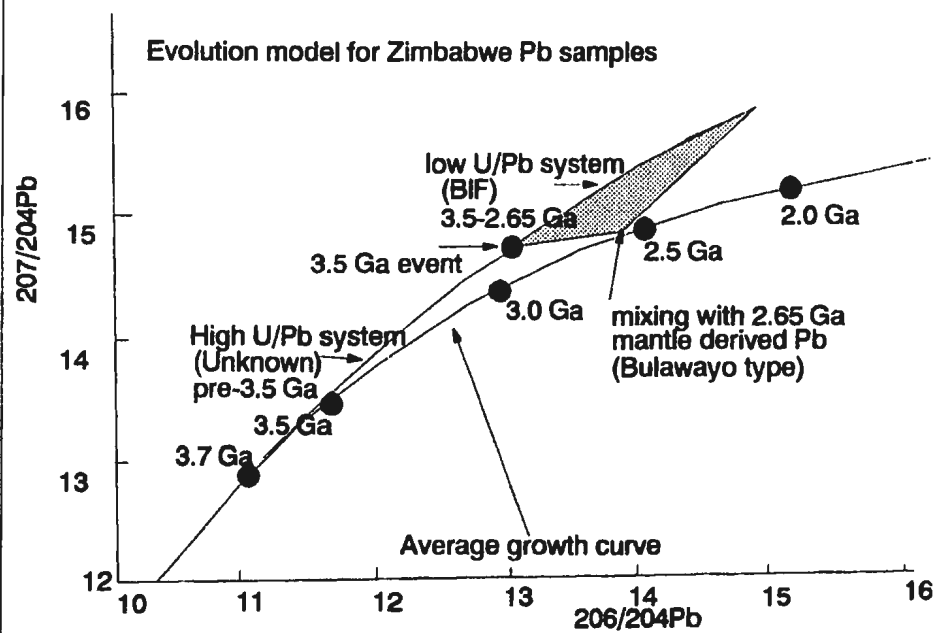


Figure 8.1b: $^{207}/^{204}\text{Pb}$ vs. $^{206}/^{204}\text{Pb}$ plot showing the evolution model for Zimbabwe Archean gold deposits developed by Kramers and Foster (1984), based on Robertson ' (1973) data. Deposits form a triangular field (shaded) above Stacey and Kramers (1975) growth curve (see text for discussion).

common to the east of the Great Dyke than in the west. The Que Que-type deposits also form a linear array on a Pb-Pb diagram whose regression line can be interpreted as a "secondary isochron" (Figure 8.1a). The secondary isochron should indicate two distinct ages; t_0 , the age of the mineralization, and t_1 , the age of the lead source. Robertson (1973) calculated that if the age of the mineralization is fixed at 2.7 Ga on the basis of regional geochronological controls, the source age would be ca. 3.5 Ga.

Robertson's data were reviewed by Kramers and Foster (1984) and the data were re-interpreted on the basis of both Stacey and Kramers's (1975) growth curve and Doe and Zartman's (1979) plumbotectonic model. All of the data (both Que Que and Bulawayo-types) plotted (Figure 8.1b) above Stacey and Kramers' (1975) average growth curve, which is equivalent to the "Orogen" curve in Doe and Zartman's (1979) plumbotectonic model. The complete data set also formed an inverted triangle above the growth curve (Figure 8.1b). Kramers and Foster (1984) suggested that the data actually defined a spectrum of Pb isotopic compositions of which the Que Que and Bulawayo types are the extremes (Figure 8.1b). The data also indicated that, although there was continuous variation from one end of the field to the other, regional variations in the isotopic compositions of the deposits were apparent. For example, deposits from central Zimbabwe and east of the Great Dyke tended to plot towards the right side of the triangular field (Figure 8.1b), whereas those from the west plotted at the top left of the triangular field. Kramers and Foster (1984) interpreted the lead isotopic compositions as indicating the mixing of Pb

isotopic compositions from sources of different compositions, a low U/Pb source and high U/Pb source. It was suggested that lead isotopic compositions to the west (Bulawayo-type) were derived primarily from the mantle during greenstone volcanism, and subsequently mixed with crustal lead to produce variable signatures. The Que Que-type lead isotopic compositions on the other hand, were believed to have formed in two stages. The first involved derivation of lead and other metals from a high U/Pb ratio source (old granitic gneisses) and deposition in a low U/Pb ratio source at about 3.5 billion years. The low U/Pb ratio lead sink is believed to have been banded iron formations (BIF) of the 3.5 Ga Sebakwian Greenstone Belts. The lead deposited in the low U/Pb source (BIF) retained its original composition (i.e. high U/Pb) until it was remobilized at around 2.65 Ga to form deposits with Que Que-type lead isotopic compositions. Therefore, the more radiogenic nature of the Que Que-type deposits is a reflection of their occurrence in the eastern areas dominated by older gneisses and granitoids and with fewer volcanic rocks.

No Pb-isotopic data for gold deposits of the Tati Greenstone Belt are available to compare with those of the Zimbabwe side of the Zimbabwe Craton. It should be noted, however, that since the Bulawayo-type Pb isotopic signatures in gold deposits occur in greenstone belts in western Zimbabwe, the western part of the craton to which the Tati Greenstone Belt belongs, it is probable these signatures could also be found in the Tati Greenstone Belt.

In addition to the work on lead isotopes in gold deposits, Foster and Wilson (1984) carried out a comprehensive review of the gold deposits in Zimbabwe. These

authors classified the gold deposits of Zimbabwe into two main groups:

(1) Stratabound gold deposits hosted by banded iron formations, banded sulphides, volcanoclastic and clastic sediments.

(2) Non-stratabound gold deposits hosted by veins and shear zones.

Some of the features of gold deposits in Zimbabwe summarized by Foster and Wilson (1984) and Porter and Foster (1990) are similar to those in the Tati Greenstone Belt. For example, Porter and Foster (1990) argue that "carbonatisation (sic) was an important precursor event, rendering ultramafic rocks susceptible to brittle failure and subsequent vein emplacement." It was argued in Chapter 7 that carbonate alteration at the Shashe Deposit was pre-mineralization. The point raised by Foster and Wilson (1984) that gold mineralization in banded iron formations may have been deposited syngenetically with the host and then re-mobilized during deformation and metamorphism, is also similar to the conclusions in this thesis, though derived from a different perspective.

Foster and Wilson (1984) argue that some gold deposits in greenstone belts of Zimbabwe are confined to a particular strata (e.g. banded iron formations), and on this basis they subdivided gold deposits in Zimbabwe into stratabound and non-stratabound. The observation presented in this thesis is that all deposits studied in the Tati Greenstone Belt occur at a particular stratigraphic position (especially towards the tops of major stratigraphic units). Secondly, these deposits occur in shear zones that are generally parallel to the stratigraphy and are therefore confined to particular strata, even though some occur at lithological boundaries between different

rock units. In this respect gold deposits of the Tati Greenstone Belt cannot be classified into stratabound and non-stratabound.

8.3 Characteristics of Gold Deposits of the Tati Greenstone Belt

Even though gold deposits of the Tati Greenstone Belt are hosted by all lithological units within the belt, stratigraphic control on mineral deposit distribution seems to have been an important factor. For example, the Shashe Group (Figure 7.1), the Golden Eagle Group (Figure 7.1) and the Phenalonga Group (Figure 3.10) occurrences are located at the tops of major stratigraphic units. Figure 7.6 illustrates the distribution of gold deposits in the Tati Greenstone Belt with respect to the distribution of banded iron formations and the distribution of banded iron formations is controlled by major boundary faults (Figure 7.6). Major structures, therefore, also play a very important role in the distribution of the gold deposits. The most important mineral deposit localization sites are areas where D_3 shears cut the stratigraphy and D_1 fault/shear zones.

8.3.1 Summary of metallogenic features of gold mineralization in the Tati Greenstone Belt

There is a fair degree of consensus among researchers on a number of features found in mesothermal gold deposits, especially those in Archean greenstone belts. Such features may be summarised as follows:

1. Compositions of the mineralizing fluids in Archean lode gold

deposits as deduced from fluid inclusions, light stable isotopes and geochemistry of alteration zones are generally uniform. They are low salinity and low density CO₂-H₂O fluids (Kerrick and Fryer, 1979; Perring et al., 1987; Colvine et al., 1984; Ho et al., 1985).

2. Mineralization temperatures are estimated to have been between 200 and 400°C at low confining pressures of about 1 to 2 kb, as deduced from light stable isotopes and fluid inclusions (Kerrick and Fryer, 1979; Perring et al., 1987; Colvine et al., 1984).

3. Mineralization is structurally controlled and not confined to any particular lithology in the greenstone belt lithological assemblage (Colvine et al., 1984; Roberts, 1987).

4. The mineral deposits are epigenetic (Browning et al., 1987; Colvine et al., 1984; Roberts, 1987).

5. The ore metal association in Archean lode deposits is Au-Ag-As-W-Sb-Te (Groves and Phillips, 1987; Sang and Ho, 1987).

6. Mineralization occurs after major periods of deformation and metamorphism.

Where data are available, gold deposits from the Tati Greenstone Belt have similar characteristics to those from other Archean Greenstone Belts as summarised above. There are, however, certain characteristics observed in the Tati Greenstone Belt deposits that have not been interpreted as common characteristics of mesothermal deposits, although some have been observed by different researchers

in different parts of the world. In particular:

1. Gold deposits in the Tati Greenstone Belt generally occur in clusters or groups towards the tops of major lithological sequences.
2. The distribution of these mineral deposit clusters or groups are controlled by structures, and are also associated with banded iron formations which themselves are structurally controlled.
3. Gold deposits postdate the main foliation-forming deformation event, and are also localized at intersections of secondary shear zones and other related structures, such folds.
4. Minor differences are observed between and within deposit groups/clusters, in terms mineralogy and metallic association (e.g. Sb-Au at Signal Hill and Au-Ag-Pb at Phenalonga). The differences are related to different host rocks and, therefore, variable rock/water interactions.
5. Mineral deposits are more abundant in the komatiite-tholeiite sequence and also at the contact between Selkirk Group (calc-alkaline sequence) and the intrusive Selkirk Igneous Complex.
6. The Phenalonga Group (calc-alkaline sequence) is comparatively poorly mineralized.

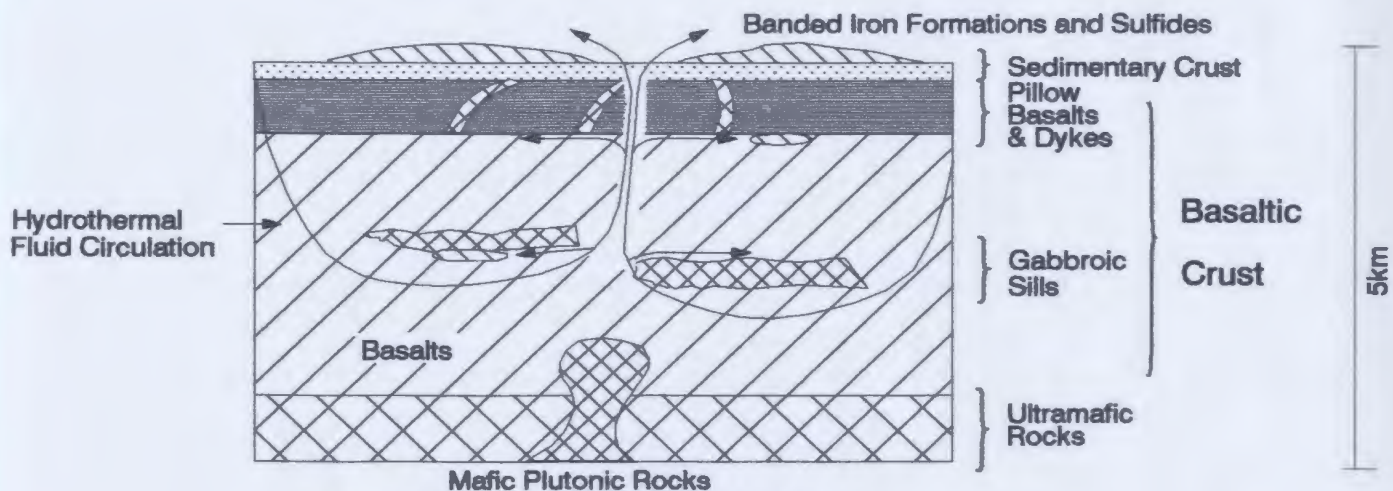
8.4 Metallogenic Model

A schematic metallogenic model for the Tati Greenstone Belt is provided in

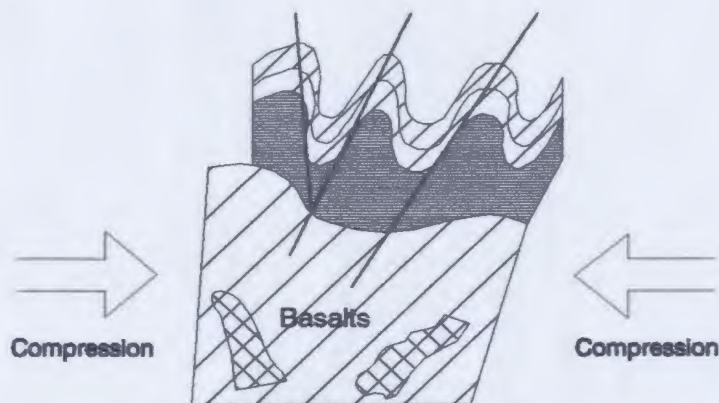
Figure 8.2. Mesothermal gold mineralization in the Archean Tati Greenstone Belt can be summarized as having formed in three main stages. The first stage succeeded formation of the ultramafic-mafic rocks in a back-arc basin. Geochemical data for the ultramafic-mafic rocks of the Lady Mary Group (see Chapter 5) suggest that they were formed in a back-arc-like basin similar to modern ones. During this stage, circulation and leaching of metals from within the young basaltic crust by major hydrothermal fluids (Figure 8.2a) occurred. The metal-bearing hydrothermal fluids flowed along and were discharged through large terrane boundary faults, such as the Selukwe-Long Gossan Lineament (SLGL; on Figure 4.6), and dissolved metals were deposited as massive sulphides and/or ferruginous metalliferous sediments.

The association of carbonate sedimentary rocks with the banded iron formations suggests that the banded iron formations were deposited on the seafloor, possibly under a cover of sedimentary rocks made up of carbonates and clastic sediments shed from nearby island arcs. These banded iron formations may have formed in a similar environment as massive sulphides of modern oceanic environments (Scott, 1990; Hannington et al., 1986; Richardson et al., 1987; Reed, 1983).

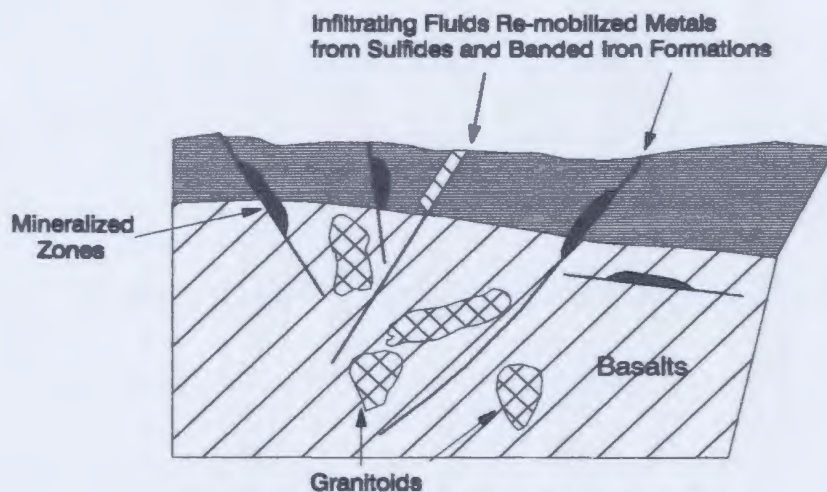
Large amounts of fluids, from which the massive sulphides, metalliferous sediments, or banded iron formations precipitated, flowed along terrane boundary faults. Residual fluids from such massive sulphide-depositing fluids deposit low temperature metal sulphides (Au-Ag-Sb-As-Pb-Zn±Hg±Ba) in pockets at sites distal to the main massive sulphide deposits (Hannington et al., 1986). Some of these



(a) METAL LEACHING STAGE



(b) THE DEFORMATION STAGE



(c) RE-MOBILIZATION STAGE

Figure 8.2: Metallogenic model for gold mineralization in the Tati Greenstone Belt - (a) Metal leaching during the formation of the basaltic crust; (b) Processes of cratonization wherein favourable structural sites formed; (c) Re-mobilization of metals from a deformed but relatively stable crust.

metals were also deposited in the cover sediment horizons. The metal leaching and deposition processes would have been accompanied by large scale alteration and it would appear that carbonate and quartz-carbonate veining of the greenstone belt rocks took place at this stage.

In mineral deposits where carbonatization and silicification formed the main alteration processes, these alteration zones are more widespread than the mineralization. Data presented in Chapter 7 from the Shashe Deposit suggest that the auriferous mineralization was superimposed on the alteration zones. The best mineralized zones in the Shashe Deposit are brittle microshears superimposed on the extensive silicified zones. Early alteration processes induced competency and lithological heterogeneity in otherwise ductile supracrustal rocks.

The second stage of mineralization resulted from the main deformation and metamorphism of the supracrustal rocks in the belt (Figure 8.2b). The first deformational (D_1) event was related to N to NE-directed folding and thrusting, which led to the N to NE overturning of the stratigraphy. The second deformation event (D_2) was the main foliation forming event. Metamorphic dewatering (Groves and Phillips, 1987) would lead to regional veining of supracrustal rocks and the formation of layer-parallel quartz and quartz-feldspar veins (Sawyer and Robin, 1986). This regional veining was a very important step in gold mineralization as it created favourable mineralization sites. These veins range in composition from quartz-feldspar near contacts between granitoid and host supracrustal rocks, to quartz and quartz-carbonate away from such contacts.

Subsequent D_3/D_4 deformation events, or the later stages of the D_2 movements, resulted in the formation of secondary shear zones cross-cutting the stratigraphy (Figure 4.6). In addition, these layer/bedding parallel veins and early carbonatized and silicified zones became zones along which brittle failure was localised. This brittle failure resulted from their higher competency compared to the surrounding rocks and created favourable sites for gold mineralization.

The third stage was related to the leaching and reconcentration of Au and related metals from earlier sites by secondary fluids. These late fluids were focused into earlier formed structures, remobilizing metals from metalliferous sediments (banded iron formations), sediments associated with banded iron formation (see Golden Eagle Formation) and/or any other alteration zones of the first stage. The third stage also coincided with a period of major granitoid magmatism. Granitoids, especially tonalites and trondhjemites (high alumina-type) at the margins of the belt, were intruded post- D_2 and pre- D_3 . This is shown by deflection and disruption of the D_2 foliation by granitoid intrusions and the shearing and faulting of quartz-feldspar veins near granitoid margins and quartz, quartz-carbonate veins away from such margins by D_3 deformation. D_2/D_3 deformation processes and granitoid magmatism, therefore, provided the thermal energy needed to initiate the circulation of the secondary fluids.

The heated metal-rich hydrothermal fluids were driven upwards along all the different forms of fractures causing extensive alteration. Only those shear zones localized on early quartz-carbonate veins formed favourable sites for mineralization.

These early alteration zones, therefore, constitute an important control for mesothermal gold mineralization. The hydrothermal fluids reacted with early carbonate alteration minerals in quartz-carbonate veins to produce second generation silicification zones (see Shashe Deposits; Chapter 7). These silicification zones are similar to jasperoids described by Romberger (1985) from epithermal gold mineralization. Local small differences may exist between deposits in different rock types and these differences result from the interactions of fluids with host rocks. Even within the same deposit, minor differences may occur as a result of fluid/rock ratio variation during the formation of these deposits. Differences may also be related to the depth of emplacement of individual systems leading to overlap between epithermal and mesothermal characteristics.

CHAPTER NINE

9. SUMMARY AND CONCLUSIONS

9.1 Summary of Geological Characteristics

The Archean has been defined as a period during which the Earth was unstable and the crust not rigid enough to sustain cratonic sedimentary basins (e.g. Windley, 1981). The change from the mobile stage (Archean) to a period during which cratons were stable (Proterozoic) is generally fixed at about 2.5 Ga (Plumb and James, 1986). Some geologists, however, (e.g. Cloud, 1987; Nisbet, 1982) feel that the choice of a single isotopic date, 2.5 Ga, to define the Archean/Proterozoic boundary is incorrect. They contend that the boundary should reflect either major geological events during the period in question (Nisbet, 1982), or stratigraphy (Cloud, 1987). In other words, the boundary should reflect change in geological conditions, rather than be tied to isotopic age data. An example of the disagreement between ca. 2.5 Ga age and geology is seen in the Kaapvaal Craton of southern Africa. Some large cratonic sedimentary basins (e.g. the Pongola in Kaapvaal Craton) appeared much earlier than 2.5 Ga (between 2.8 and 2.9 Ga) and led Ohtani (1990) to suggest that there were early stabilized cratons (e.g. the Kaapvaal Craton) with ages between 3.5 and 3.1 Ga, and younger cratons (e.g. the Superior and Zimbabwe Cratons) which stabilized between 2.9 and 2.5 Ga.

In addition to the development of early cratonic basins, older cratons were supposed to contain Al-depleted komatiites in contrast to Al-enriched komatiites of

the younger cratons (e.g. Ohtani, 1990). On the basis of experimental data, Ohtani (1990) suggested that Al-depleted komatiites can be generated by any degree of partial melting at the transition zone between the upper and lower mantle (450 to 650 km), or by low degrees of partial melting between 180 and 450 km. The Al-saturated komatiites on the hand were derived from partial melting of residues after the separation of Al-depleted komatiites. The Zimbabwe Craton contains both Al-depleted komatiites, described in this study, and Al-saturated komatiites described by Nesbitt et al. (1987). In general, Al-depleted komatiites, as seen in the Tati Greenstone Belt, occur near contacts of supracrustal rocks with major granitoid bodies suggesting that they form the bases to komatiite-tholeiite sequences intruded by granitoid bodies.

There are several factors that point to the similarities in tectonism between Archean and Mesozoic environments. These include, for example, similarities in the geochemistry of Archean mafic rocks and those from modern tectonic environments. The presence of horizontal deformation structures within Archean terranes has also been used as evidence of the similarities (e.g Kusky, 1990). Stratigraphic associations further indicate similarities between Archean and Mesozoic tectonic environments. For example, the relationships of komatiite-tholeiite volcanic rock sequences with the calc-alkaline volcanic-feldspathic sedimentary rock sequences as seen in some Archean greenstone belts (e.g. Norseman-Wiluna; Barley and Groves, 1990) and in the Tati Greenstone Belt, are comparable to those of modern back-arc tectonic environments, where ultramafic-mafic volcanic rock sequences are associated with

calc-alkaline volcanic-feldspathic sedimentary rock sequences (Barley and Groves, 1990).

In the Tati Greenstone Belt, geochemical and regional structural studies of volcanic rocks indicate that these rocks can be divided into three main lithotectonic units. The first unit is the komatiite-tholeiite sequence, Lady Mary Group, which is similar to modern back-arc basin ultramafic-mafic sequences. The calc-alkaline volcano-plutonic sequence, Phenalonga Group, constitutes the second lithotectonic unit. The Selkirk Group constitutes the second calc-alkaline volcano-plutonic sequence. The youngest unit in the Tati Greenstone Belt, the Last Hope Group (feldspathic sedimentary rocks), overlies the eastern end of Phenalonga Group volcano-plutonic sequence. The relationship of the Phenalonga and Last Hope groups is similar to a sequence of calc-alkaline volcano-plutonic rocks associated with feldspathic sedimentary rocks described in the Wiluna-Leonara Greenstone in Australia suggested to be an Archean island arc sequence (Barley and Groves, 1990). The Tati Greenstone belt rocks may have also formed in a similar tectonic setting. In some modern back-arc environments, especially those characterised by high thermal energy, high-Mg andesites and basalts (HMA) occur (Tatsumi and Maruyama, 1989). These high-Mg rocks are often associated with high-Mg granitoids. In the Tati Greenstone Belt, high-Mg granitoids (or sanukitoids after Stern et al., 1989) occur in the western part of the Francistown Subzone (Airport Pluton) and are part of the Mphoeng Plutonic Complex in the Eastern Structural Zone. Sanukitoids were so named (Shirey and Hanson, 1984) because they contain the same

characteristics as the high-Mg andesitic volcanic rocks of the Japanese Islands. Sanukitoids generally occur in subduction environments (Stern et al., 1989).

9.2 Summary of Characteristics of Mineral Deposits

Perhaps one of the more interesting observations from this study is that banded iron formations within the belt coincide with boundary faults that separate major litho-tectonic units of the belt. The compositions of the banded iron formations indicate that these rocks may have formed in environments similar to the massive sulphide horizons deposited in modern oceanic environments (Scott, 1990; Hannington et al., 1986; Richardson et al., 1987; Reed, 1983). Some of the massive sulphide deposits in oceanic environments are deposited under a sediment cover at contacts between major litho-tectonic units marked by large discontinuities, similar to the boundary faults of the Tati Greenstone Belt. It has been suggested that the banded iron formations are related to the mineralization.

A pyroxene isograd has been described as separating the Zimbabwe Craton from the high metamorphic grade Northern Marginal Zone (NMZ) of the Limpopo Belt (e.g. Mason, 1973; Key and Hutton, 1976; Coward et al., 1976; Watkeys, 1983; Tankard et al., 1982; Treloar et al., 1992; McCourt and Vearncombe, 1992; Wilson, 1990). The pyroxene isograd gneisses were derived from porphyritic (megacrystic feldspar) granites and charnockites (Tankard et al., 1982; Ridley, 1992). These granitoids, especially the megacrystic feldspar granites, are known to extend westwards into Botswana (Tankard et al., 1982) and are believed to be an intrinsic

feature of the NMZ (Ridley, 1992).

It has been pointed out in this study that megacrystic feldspar granites form part of the southern end of the Tati batholith. These megacrystic feldspar granites intrude both the Tati Greenstone Belt and the high metamorphic grade area of the NMZ. These rocks crop out as elliptical bodies whose long axes are orientated NW-SE. The megacrystic granites change, north to south, from slightly deformed granites with brittle structures to ductilely deformed bodies. The brittle structures are microfractures in large feldspar crystals and re-alignments of the mafic minerals, biotite and hornblende, a weak foliation. The ductile structures include upright isoclinal folds, presence of leucocratic veins, and in some cases, pegmatites. Microshear zones are also present. The transition from the slightly deformed megacrystic feldspar granites to the highly deformed and metamorphosed varieties, occurs over a very short distance. These megacrystic feldspar granites are, therefore, believed to have been intruded syn-tectonically within and around a large discontinuity that constitutes the boundary between the NMZ and the Tati Greenstone Belt. The change from brittle to ductile structures in megacrystic feldspar granites from the craton to the NMZ indicates structural change as the boundary between NMZ and the craton (Tati Greenstone Belt) is approached.

9.3 Recommendations for Future Studies

1. Geochronological data are needed to constrain the relative timing of lithologic units and deformation events in the Tati Greenstone Belt. With

geochronological data it will be possible to subdivide the Tati Greenstone Belt into micro-terrane or cratonic blocks. Isotopic ages for plutonic rocks, such as Selkirk Igneous and the Mphoeng Plutonic Complexes, must be derived to constrain the accretion of the Tati Greenstone Belt.

2. A reconnaissance study of the sulphide deposits in the Tati Greenstone Belt (e.g. Phoenix and Selkirk) indicates that these deposits may not be magmatic, as currently proposed, and therefore a study of these deposits is needed in order to determine their actual nature.

3. The structural control of gold deposits in the Tati Greenstone Belt has been demonstrated in this study. It is hoped that this work will help to direct future exploration to the most favourable targets and also lead to a better understanding of the control and nature of gold deposits.

4. Further geochemical studies are needed to more completely understand the petrogenesis and tectonic setting of the volcanic and plutonic rocks of the Tati Greenstone Belt.

REFERENCES

- ABBOTT, D.H., and HOFFMAN, S.E. 1984. Archean Plate tectonics revisited 1: Heat flow, spreading rate and the age of the subducting oceanic lithosphere and their effects on the origin and evolution of continents. Tectonics, **3**(4), pp.429-444.
- ALLEN, P.A., HOMEWOOD, P., and WILLIAMS, D.D. 1986. Foreland basins: an Introduction. In Special Publication of the International of the Association of Sedimentologists, **8**, 3-12. P.A. Allen and P. Homewood, (eds.). Blackwell Scientific Publications.
- ANHAEUSSER, C.R. 1973. The Evolution of the Early Precambrian crust of southern Africa. Philosophical Transactions of the Royal Society of London, **A273**, pp.359-388.
- ANHAEUSSER, C.R. 1975. Precambrian tectonic environments. Annual Reviews of Earth and Planetary Sciences, **3**, pp.31-53.
- ANHAEUSSER, C. R. 1976. The nature and distribution of Archean gold mineralization in southern Africa. Minerals Science Engineering, **8**, pp.46-84.
- ANHAEUSSER, C.R., AND RYAN, P.J. 1979. "Barren" massive sulphide deposits in the Mphoengs Schist Belt, Rhodesia: a case history. Special Publication of the Geological Society of South Africa, **5**, pp.181-203.
- ANHAEUSSER, C.R. 1983. Structural elements of Archean granite-greenstone terranes as exemplified by the Barberton Mountain Land, Southern Africa. Economic Geology Research Unit Information Circular, **162**, pp.21-34.
- ARCULUS, R.J. 1987. The Significance of Source versus process in tectonic controls of magma genesis. Journal of Volcanology and Geothermal Research, **32**, pp.1-12.
- ARTH, J.G., BARKER, F., PETERMAN Z.E., and FRIEDMAN, I. 1978. Geochemistry of the gabbro-diorite-tonalite-trondhjemitic suite os SW Finland and its implications for the origin of tonalitic and trondhjemitic magmas. Journal Petrology, **19**, pp.289-316.
- ARTH, J.G. 1979. Some trace elements in trondhjemitites-their implications to magma genesis and paleotectonic setting. In "Trondhjemitites, Dacites, and Related Rocks". F. Barker (ed.) Developments in Petrology, **6**, pp.123-132.

AYRES, L.D., and THURSTON, P.C. 1985. Archean Supracrustal Sequences in the Canadian Shield: an Overview. in Evolution of Archean Supracrustal Sequences, Geological Association of Canada Special Paper, 28, pp. 343-380. Edited by L.D. Ayres, P.C. Thurston, K.D. Card, and W. Weber.

ATHERTON, M.P., and SANDERSON, L.M. 1987. The Cordillera Blanca Batholith: a study of granite intrusion and the relation of crustal thickening to peraluminosity. Geologische Rundschau, 76(1), pp.213-232.

BALDOCK, J.W., HEPWORTH, J.V., and MARENGWA, B.S. 1976. Gold, Base metals and Diamonds in Botswana. Economic Geology, 71, pp.139-156.

BALDOCK, J.W., HEPWORTH, J.V., and MARENGWA, B.S. 1977. Resources Inventory of Botswana: Metallic Minerals, Mineral Fuels and Diamonds. Botswana Geological Survey, Mineral Resources Report, 4, 69p.

BARKER, A.J. 1990. Introduction to Metamorphic Textures and Microstructures. Chapman and Hall, New York, 162pp.

BARKER, F., and ARTH, J.G. 1976. Generation of trondhjemitic-tonalitic liquids and bimodal trondhjemite-basalt suites. Geology, 4, pp.596-600.

BARKER, F. 1979. Trondhjemite: definition, environment and hypotheses of origin. In "Trondhjemites, Dacites, and Related Rocks." F. Barker (ed.) Developments in Petrology, 6, pp.1-12.

BARLEY, M.E. 1986. Incompatible-element enrichment in Archean basalts: A consequence of contamination by older sialic crust rather than mantle heterogeneity. Geology, 14, pp.947-950.

BARLEY, M.E. 1987. The Archean Whim Creek Belt, an ensialic fault-bounded basin in the Pilbara Block, Australia. Precambrian Research, 37(3), pp.199-215.

BARLEY, M.E., EISENLOHR, B.N., GROVES, D.I., PERRING, C.S., and VEARNCOMBE, J.R. 1989. Late Archean convergent margin tectonics and gold mineralization: A new look at the Norseman-Wiluna Belt, Western Australia. Geology, 17(9), pp.826-829.

BARLEY, M.E., and GROVES, D.I. 1990. Mesothermal gold mineralization in the Yilgarn Craton, Western Australia. Chron. Rech. Min. 498, pp.3-13.

BARLEY, M.E. 1992. A Review of Archean Volcanic-Hosted Massive Sulfide and Sulfate Mineralization in Western Australia. Economic Geology, 87, pp.855-872.

BARTON, J.M. Jr. 1981. The Pattern of Archean Crustal Evolution in Southern Africa, as deduced from the Evolution of the Limpopo Mobile Belt and the Barberton Granite-Greenstone Terrain. Special Publication of the Geological Society of Australia, 7, pp. 21-31.

BARTON, J.M. Jr. 1983. Isotopic Constraints on Possible Tectonic Models for Crustal Evolution in the Barberton Granite-Greenstone Terrane, southern Africa. Special Publication of the Geological Society of South Africa, 9, pp. 73-79.

BENDER, J.F., LANGMUR, C.H., and HANSON, G.N. 1984. Petrogenesis of basalt glasses from the Gamago region, East Pacific Rise. Journal of Petrology, 25, pp.213-254.

BENNETT, J.D. 1971. Tectono - metamorphic map of eastern Botswana Botswana Government Printer, Publishers.

BERGER, B.R. 1982. Geologic-Geochemical features of Hot-Spring precious-metal deposits. United States of Geological Survey, monograph

BESWICK, A.E., and SOUCIE, G. 1978. A correction procedure for metasomatism in Archean Greenstone Belt. Precambrian Research, 6, pp.235-248.

BICKLE, M.J. 1978. Heat Loss from the earth: a constraint on Archean tectonics from the relation between geothermal gradients and the rate of plate production. Earth and Planetary Science Letters, 40, pp.310-315.

BICKLE, M.J. 1986. Implications of melting for stabilization of the lithosphere and heat loss in the Archean. Earth and Planetary Science Letters, 80, 314-324.

BIENVENU, P., BOUGAULT, H., JORON, J.L., TREUIL, M., and DMITRIEV, L. 1990. MORB alteration: rare-element/non-rare-earth hydromagmaphile element fractionation. Chemical Geology, 82, pp.1-14.

BLAINE, J.L. 1986a. Prospecting licence 23/84- Map Nora Quarterly progress report for the period 1/7/85-30/9/85. Unpubl.

BLAINE, J.L. 1986b. Progress report on the Signal Hill project, prospecting licence 24/84, for the period August 1984 to June 1986. Falconbridge Explorations (Botswana) (PTY) LTD Bull. B219A unpubl.

BONATTI, E., and JOENSU, O. 1966. Deep sea iron deposits from the South Pacific. Science, 154, pp.643-645.

BONATTI, E., 1983. Hydrothermal Metal Deposits from the Oceanic Rifts; a Classification. in Hydrothermal Processes at seafloor spreading centers; pp. 491-502. Edited by P.A. Rona, K. Boström, L. Laubier, and K.L. Smith Jr. Plenum Press Publishers.

BONNERMAISON, M. and MARCOUX, E. 1990. Auriferous mineralization in some shear-zones: a three-stage model of metallogenesis. Mineralium Deposita, 25, pp.96-104.

BOOCOCK, C. 1951. Geological notes on the northwest portion of the southern schist belt - Tati Concession. Botswana Geological Survey, unpublished report CB/4/51.

BOWMAN, H.N. and STEVENS, B.P.J. 1978. The philosophy, design and applications of the New South Wales Geological Survey's metallogenic mapping programs. Journal of Geological Society of Australia, 25(3), pp.121-140.

BRIQUEU, L., BOUGAULT, H., and JORON, J.L. 1984. Quantification of Nb, Ta, Ti and V anomalies in magmas associated with subduction zones: Petrogenetic implications. Earth and Planetary Science Letters, 68, pp.297-308.

BROWN, G.C. 1982. Calc-alkaline intrusive rocks: their diversity, evolution, and relation to volcanic arcs. In "Andesites: Orogenic Andesites and Related Rocks." pp.437-461. R.S. Thorpe (ed.). John Wiley and Sons. Publishers.

BROWNING, P., GROVES, D.I., BLOCKLEY, J.G. and ROSMAN, K.R.J. 1987. Lead isotopes constraints on the age and source of gold mineralization in the Archean Yilgarn Block, western Australia. Economic Geology, 82, pp.971-986.

BURKE, K., DEWEY, J.F. and KIDD, W.S.F. 1976. Dominance of horizontal movements, arc and microcontinental collisions during the later permobile regime. In The History of the Earth. B.F. Windley, (ed.), pp.113-129. John Wiley and Sons, Publishers.

BURROWS, D.R., WOOD, P.C. and SPOONER, E.T.C. 1986. Carbon isotope evidence for a magmatic origin for Archean gold - quartz vein ore deposits. Nature, 321, pp.851-854.

BURROWS, D.R., and SPOONER, E.T.C. 1989. Relationships between Archean gold quartz vein-shear zone mineralization and igneous intrusions in the Val d'Or and Timmins areas, Abitibi Subprovince, Canada. In "The Geology of Gold Deposits: the Perspective in 1988." Economic Geology Monograph, 6, pp.424-444.

- BYRON, C.L. 1983. Progress report on the Last Hope Antimony/Gold Deposit. Prospecting licence 1/78 (Tati)- Botswana. Falconbridge Explorations (Botswana) (PTY) LTD, Bulletin, B194 (Unpubl.)
- CAMEROON, W.E., NISBET, E.G. and DIETRICH, V.J. 1979. Boninites, Komatiites and Philitic Basalts. Nature (London), 280, pp.550-553.
- CAMEROON, W.E. and NISBET, E.G. 1982. Phanerozoic Analogues of Komatiitic Basalts. In Komatiite, N.T. Arndt and E.G. Nisbet eds., George Allen and Unwin, Publishers, pp.29 - 50.
- CAMEROON, E.M. 1988. Archean gold: Relation to granulite formation and redox zoning in the crust. Geology, 16, pp. 109 - 112.
- CAMPBELL, A.C., PALMER, M.R., KLINKHAMMER, G.P., BOWERS, T.S., EDMOND, J.M., LAWRENCE, J.R., CASEY, J.F., THOMPSON, G., HUMPHRIS, S., RONA, P., and KARSON, J.A. 1988. Chemistry of hot springs on the Mid-Atlantic Ridge. Nature, 335, pp.514-518.
- CARD, K.D. and CIESIELSKI, A. 1985. DNAG #1. Subdivisions of the Superior Province of the Canadian Shield. Geoscience Canada, 13, pp.5-13.
- CARD, K.D. 1990. A review of the Superior Province of the Canadian Shield: a product of Archean accretion. Precambrian Research, 48, pp.99-156.
- CARLISLE, D. and SUSUKI, T. 1974. Emergent basalt and submergent carbonate-clastic sequences including the Upper Triassic Dilleri and Welleri Zones on the Vancouver Island. Canadian Journal of Earth Sciences, 11, pp. 254-279.
- CASSIDY, K.F., BARLEY, M.E., GROVES, D.I., PERRING, C.S., and HALLBERG, J.A. 1991. An overview of the nature, distribution and inferred tectonic setting of granitoids in the late-Archean Norseman-Wiluna Belt. Precambrian Research, 51, pp.51-83.
- CASTRO, A., MORENO-VENTAS, I., and De La Rosa, J.D. 1991. H-type granitoids: a proposed revision of the granite-type classification and nomenclature. Earth Science Reviews, 31, pp.237-253.
- CATTELL, A. 1987. Enriched komatiitic basalts from Newton Township, Ontario: Their genesis by crustal contamination of depleted komatiite magma. Geological Magazine, 124, pp. 303-309.

CATTELL, A. and ARNDT, N. 1987. Low and high-alumina komatiites from a late Archean sequence, Newtown Township, Ontario. Contributions to Mineralogy and Petrology, **97**, pp. 218-227.

CATTELL, A. and TAYLOR, R.N. 1990. Archean basic magmas. In "Early Precambrian basic magmatism", edited by R.P. Hall and D.J. Hughes, pp. 11-39.

CHAPPELL, B.W., and WHITE, A.J.R. 1974. Two contrasting granite types. Pacific Geology, **8**, pp.173-174.

CHAPPELL, B.W., and WHITE, A.J.R. 1982. I and S-type granites in the Lachlan Fold Belt, S.E. Australia. In "The Geology of Granites and their Metallogenic Relations". Proceedings of the International Symposium, held at Nanjing University, Nanjing, China, October,26-30 1982, pp.87-101.

CHATTERJEE, A.K. 1983. Metallogenic map of the province of Nova Scotia. Published by Depart. of Mines and Energy, of Nova Scotia.

CHRISTENSEN, U.R. 1985. Thermal Evolution Models for the Earth. Journal Geophysical Research, **90**,B4, pp.2995-3007.

CLIFFORD, T.N. 1968. Radiometric dating and the pre-Silurian geology of Africa. In "Radiometric Dating for Geologists." E.L. Hamilton and R.M. Farquhar (eds.), John Wiley and Sons, Publishers, pp.299-416.

CLOUD, P. 1987. Trends, transitions and events in Cryptozoic history and their calibration: a propos recommendations by the Subcommittee on Precambrian Stratigraphy. Precambrian Research, **37**, pp.257-264.

COLLINS, P.L.F. 1979. Gas hydrates in CO₂-bearing fluid inclusions and the use of freezing data for estimation of salinity. Economic Geology, **74**, pp.1435-1444.

COLLINS, W.J. 1989. Polydiapirism of the Archean Mount Edgar Batholith, Pilbara Block, Western Australia. Precambrian Research, **43**, pp.41-62.

COLVINE, A.C. et al.,1984. An integrated model for the origin of Archean lode gold deposits. Ontario Geological Survey Open File Report 5524, 98p.

COLVINE, A.C. 1989. An empirical model for the formation of Archean gold deposits: products of final cratonization of the Superior Province, Canada. In "The Geology of Gold Deposits: the Perspective in 1988." Economic Geology Monograph, **6**, pp.37-53.

COMPSTON, W., WILLIAMS, I.S., CAMPBELL, I.H., and GRESHAM, J.J. 1986. Zircon xenocrysts from the Kambalda volcanics: age constraints and direct evidence for older continental crust below the Kambalda-Norseman Greenstones. Earth and Planetary Science Letters, **76**, pp.299-311.

CONDIE, K.C. 1976. Trace-element geochemistry of Archean greenstone belts. Earth Science Reviews, **12**, pp.393-417.

CONDIE, K.C., and ALLEN, P. 1980. Origin of Archean migmatites from the Gweno Dam area, Zimbabwe-Rhodesia. Contributions to Mineralogy and Petrology, **74**, pp.35-43.

CONDIE, K.C. 1982. Early and middle Proterozoic supracrustal successions and their tectonic setting. American Journal of Science, **282**, pp.341-357.

CONDIE, K.C., and SHADEL, C.A. 1984. An early Proterozoic volcanic arc succession in southeastern Wyoming. Canadian Journal of Earth Sciences, **21**, pp.415-427.

CONDIE, K.C. 1985. Secular Variation in the composition of Basalts: an Index to Mantle evolution. Journal of Petrology, **26(3)**, pp.545-463.

CONDIE, K.C. 1986. Geochemistry and Tectonic setting of early Proterozoic supracrustal rocks in the Southwestern United States. Journal of Geology, **94**, pp.845-864.

CONDIE, K.C. 1989. Geochemical changes in basalts and andesites across the Archean-Proterozoic boundary: Identification and significance. Lithos, **23**, pp.1-18.

COWARD, M.P., GRAHAM, R.H., JAMES, P.R., and WAKEFIELD, J. 1973. A structural interpretation of the northern margin of the Limpopo Orogenic belt, southern Africa. Transactions of the Royal Philosophical Society of London, **A273**, pp.487-492.

COWARD, M.P., and JAMES, P.R. 1974. The deformation patterns of two Archean greenstone belts in Rhodesia and Botswana. Precambrian Research, **1**, pp.235-258.

COWARD, M.P. 1976. Archean deformation patterns in southern Africa. Transactions of the Royal Philosophical Society of London, **A280**, pp.313-331.

COWARD, M.P., JAMES, P.R., and WRIGHT, L. 1976. Northern margin of the Limpopo belt, southern Africa. Geological Society of America Bulletin, **87**, pp.601-611.

COWARD, M.P. 1980. Shear zones in the Precambrian crust of southern Africa. Journal of Structural Geology, **2**, pp.19-27.

COWARD, M.P. 1984. Major shear zones in the Precambrian crust; examples from NW Scotland and southern Africa and their significance. In Precambrian Tectonics Illustrated. A. Kroner and R. Greiling (eds.), pp.207-235.

COX, S.F., ETHERIDGE, M.A. and WALL, V.J. 1986. The Role of Fluids in Syntectonic Mass Transport, and the Localization of Metamorphic Vein-type Ore Deposits. Ore Geology Reviews, **2**, pp. 65-86.

CRAWFORD, M.L., and HOLLISTER, L.S. 1986. Metamorphic fluids: The evidence from fluid inclusions. in "Fluid-Rock Interactions during metamorphism" J.V. Walther and B.J. Wood (eds.) Advances in Physical Geochemistry **5**, pp.1-35.

CROCKETT, R.N. 1968. The Geology of the Shashe Area (Quarter Degree Sheet 2127A. Botswana Government Printer, Publishers.

CROCKETT, R.N., GERRARD, I., KEY, R.M., and LITHERLAND, M. 1974. The map of The Precambrian Geology of North-East Botswana. Botswana Government Printer, Publishers.

CROWELL, J.C. 1985. The Recognition of Transform Terrane Dispersion within Mobile Belts. "in Principles and Applications of Terrane Analysis, pp.51-61.

DEBON, F., and LE FORT, P. 1988. A Cationic classification of common plutonic rocks and their magmatic associations: principles, method, applications. Bull. Mineral. **111**, pp.493- 510.

DE WIT, M.J. 1991. Archean greenstone belt tectonism and basin development: some insights from the Barberton and Pietersburg greenstone belts, Kaapvaal Craton, South Africa. Journal of African Earth Sciences, **13**, pp.45-63.

DE Wit, M.J., JONES, M.G., and BUCHANAN, D.L. 1992. The geology and tectonic evolution of the Pietersburg Greenstone Belt, South Africa. Precambrian Research, **55**, pp.123-153.

DIMROTH, E., IMREH, L., COUSINEAU, P., LEDUC, M. and SANSCHAGRIN, Y. 1985. Paleogeographic analysis of mafic submarine flows and its use in the exploration for massive sulphide deposits. in Evolution of Archean Supracrustal Sequences. Geological Association of Canada Special Paper, 28, pp. 203-222. Edited by L.D. Ayres, P.C. Thurston, K.D. Card, and W. Weber.

DIMROTH, E., MUELLER, W., DAIGEALT, R., BRISSON, H., POITRAS, A. and ROCHELEAU, M. 1986. Diapirism during regional compression: The structural pattern in the Chibogamau region of the Abitibi belt, Québec. Geologische Rundschau, 75(3), pp.715-736.

DOE, B. R. and ZARTMAN, R. E. 1979. Plumbotectonics I, the Phanerozoic. In Geochemistry of Hydrothermal Ore Deposits, H. L. Barnes (ed). J. Wiley and Sons Publ., New York, pp. 22-70.

DRUGOVA, G.M., TURCHENKO, S.I. and SHUSTOVA, L.E. 1990. Junction Zones of Precambrian Gneiss-Granulite and Granite-Greenstone Regions in the Baltic and Aldan Shields. Geotectonics, 24, pp.293-298.

DUNCAN, A.R. 1987. The Karoo igneous Province-A problem area for inferring tectonic setting from basalt chemistry. Journal of Volcanology and Geothermal Research, 32, pp.13-34.

EDELMAN, S.H. 1991. Relationships between kinematics of arc-continent collision and kinematics of thrust faults, folds, shear zones and foliations in the Nevadan orogen, northern Sierra Nevada, California. Tectonophysics, 191, pp. 223-236.

EISENLOR, B.N. 1989. Structural geology of the Kathleen Valley-Lawlers region, western Australia, and some implications for Archean gold mineralization. In "The Recent advances in understanding Precambrian Gold Deposits" Geology Department & University of Western Australia . Publication No. 11, pp.85-95.

EISENLOR, B.N., GROVES, D.I. and PARTINGTON, G.A. 1989. Crustal-scale shear zones and their significance to Archean gold mineralization in western Australia. Mineralium Deposita, 24, pp. 1-8.

ERMANOVICS, I.F. 1977. Post-tectonic re-mobilization along the Southern Marginal Zone of the Limpopo Belt. In "The Proceedings of a Seminar Pertaining to the Limpopo Mobile Belt." Botswana Geological Survey, Bulletin, 12, pp.129-139. I.F. Ermanovics, R.M. Key and G. McEwen (eds.), Botswana Government Printers, Publishers.

FODOR, R.V., and VETTER, S.K. 1984. Rift zone magmatism: petrology of basaltic rocks transitional from CFB to MORB, Southeastern Brazil margin. Contributions to Mineralogy and Petrology, 88(4), pp.307-

FOSTER, R.P. and WILSON, J.F. 1984. Geological setting of Archean gold deposits in Zimbabwe. in Gold'82: The Geology, Geochemistry and Genesis of Gold Deposits, R.P. Foster ed., pp.522-551.

FOSTER, R.P. 1985. Major Controls of Archean Gold Mineralization in Zimbabwe. Transactions of the Geological Society of South Africa, 88, pp.109-133.

FOUQUET, Y., VON STACKELBERG, U., CHARLOU, J.L., DONVAL, J.P., FOUCHER, J.P., ERZINGER, J., HERZIG, P., MUHE, R., WIEDICKE, M., SOAKAI, S., and WHITECHURCH, H. 1991. Hydrothermal activity in the Lau back-arc basin: sulfides and water chemistry. Geology, 19, pp.303-306.

FRIPP, R.E.P. 1983. The Precambrian Geology of the Area around the Sand River, Near Messina, Central Zone, Limpopo Mobile Belt. Special Publication of the Geological Society of South Africa, 8, pp.89-102.

GERRARD, I. 1960. A petrographic note on the granitic gneiss contact - metamorphosed by dolerite in the Francistown area. Report of the Geological Survey of Bechuanaland. IG7 unpublished.

GILL, R.C.O. 1979. Comparative petrogenesis of Archean and modern tholeiites: a critical view of some geochemical aspects. in Origin and Distribution of the Elements; 11, pp.431-447. Physics and Chemistry of the Earth. Edited by L.H. Ahrens.

GLASSON, M.G., and KEAYS, R.R. 1978. Gold mobilization during cleavage development in sedimentary rocks from the auriferous alate belt of Central Victoria, Australia: some important boundary conditions. Economic Geology, 73, pp.496-511.

GOLDING, S.D., MCNAUGHTON, N.J., BARLEY, M.E., GROVES, D.I., HO, S.E., ROCK, N.M.S., and TURNER, J.V. 1989. Archean carbon and oxygen reservoirs: their significance for fluid sources and circulation paths for Archean mesothermal gold deposits of the Norseman-Wiluna Belt, Western Australia. In The Geology of Gold Deposits: the Perspective in 1988. Economic Geology Monograph, 6, pp.376-388.

GOLDING, S.D. and WILSON, A.F. 1987. Oxygen and hydrogen isotope relationships in Archean gold deposits of the eastern Goldfields Province, Western Australia: constraints on the source of Archean Gold-bearing fluids. In "The Recent advances in understanding Precambrian Gold Deposits" Geology Department & University of Western Australia . Publication No. 11. pp.203-213.

GOODWIN, A.M. 1981. Archean plates and greenstone belts. In "Precambrian Plate Tectonics." A. Kroner (ed.) pp.105-135.

GORMAN, B.E., PEARCE, T.H., and BIRKETT, T.C. 1978. On the structure of Archean Greenstone Belts. Precambrian Research. 6. pp.23-41.

GRAF, J.L. 1977. Rare earth elements as hydrothermal tracers during the formation of massive sulfide deposits in volcanic rocks. Economic Geology. 72. pp.527-548.

GRAY, D.R. 1977. Morphologic classification of crenulation cleavage. Journal of Geology. 85. pp.229-235.

GRENNE, T., and VOKES, F.M. 1990. Sea-floor sulfides at the Hoydal volcanogenic deposit, Central Norwegian Caledonides. Economic Geology. 85. pp.344-359.

GROVES, D.I., and PHILLIPS, N. 1987. The genesis and tectonic control on Archean gold deposits of the western Australia shield- a metamorphic replacement model. Ore Geology Reviews. 2. pp.287-322.

HANNINGTON, M.D., PETER, J.M., and SCOTT, S. 1986. Gold in sea-floor polymetallic sulfide deposits. Economic Geology. 81. pp.1867-1883.

HANSON, G.N. 1978. The application of trace elements to the petrogenesis of igneous rocks of granitic composition. Earth and Planetary Science Letters. 38. pp.26-43.

HANSON, G.N. 1980. Rare earth elements in petrogenetic studies of igneous systems. Annual Review of Earth and Planetary Sciences. 8. pp.371-406.

HARRIS, N.B.W., HAWKESWORTH, C.J., VAN CALSTEREN, P., and McDERMOTT, F. 1987. Evolution of continental crust in southern Africa. Earth and Planetary Science Letters. 83. pp.85-93.

HARRIS, L.B. 1987. A Tectonic Framework for the Western Australian Shield and its Significance to Gold Mineralization: A Personal View. In "The Recent advances in understanding Precambrian Gold Deposits" Geology Department & University of Western Australia . Publication No. 11. pp.97-107.

HARWOOD, A.H. 1986. A mineralogical and fluid inclusion investigation of a Falconbridge exploration prospect, Botswana. Falconbridge Explorations (Botswana) Bulletin, 219 (Unpubl.)

HAWKESWORTH, C.J. and O'NIONS, R.K. 1977. The petrogenesis of some Archean volcanic rocks from southern Africa. Journal of Petrology, 18(3), pp.487-520.

HAWKINS, J.W., and MEKHIOR, J.T. 1985. Petrology of Mariana trough and Lau Basin basalts. Journal of Geophysical Research, 90, 11431-11468.

HAYNES, L. 1982. The distribution of Archean nickel mineralization in Zimbabwe and the development of new exploration concepts. Unpublished Report c279, Institute of Mining Research, University of Zimbabwe.

HEKINIAN, R., FEVRIER, M., BISCHOFF, J.L., PICOT, P., and SHANKS, W.C. 1980. Sulfide Deposits from the East Pacific Rise near 21N. Science, 207, pp.1433-1444.

HELMSTAEDT, H., PADGHAM, W.A., AND BROPHY, J. 1986. Multiple dikes in the lower Kam Group, Yellowknife greenstone belt: evidence for Archean sea floor spreading? Geology, 14, pp.562-566

HELMSTAEDT, H. and SCHULZE, D.J. 1989. Southern African Kimberlites and their Mantle sample: implications for Archean Tectonics and Lithosphere Evolution. In Kimberlites and Related Rocks: their Composition, Occurrence, Origin and Emplacement. Geological Society of Australia Special Publication, 14 (V.1) pp.358-368. Blackwell Scientific Publications.

HICKMAN, M.H., and WAKEFIELD, J. 1975. Tectonic implications of new geochronologic data from the Limpopo belt at Phikwe, Botswana, southern Africa. Geological Society of America bulletin, 86, pp.1468-1472.

HO, S.E., GROVES, D.I. and PHILLIPS, G.N. 1985. Fluid inclusions as indicators of the nature and source of ore fluids and ore depositional conditions for Archean gold deposits of the Yilgarn Block, Western Australia. Transactions of the Geological Society of South Africa, 88, pp.149-158.

HODGSON, C.J. 1989. The Structure of Shear-related, Vein-type Gold Deposits: A Review. Ore Geology Reviews, 4, pp.231-273.

HOFFMANN, A.W., and WHITE, W.M. 1982. Mantle plumes from ancient oceanic crust. Earth and Planetary Science Letters, 57, pp.431-436.

- HOFFMANN, A.W., JOCHUM, K.P., SEUFERT, M., and WHITE, W.M. 1986. Nb and Pb in oceanic basalts: new constraints on mantle evolution. Earth and Planetary Science Letters, **79**, pp.33-45.
- HOWELL, D.G., JONES, D.L. and SCHERMER, E.R. 1985. Tectonostratigraphic Terranes of the Circum-Pacific Region. In "In Tectonostratigraphic Terranes of the Circum-Pacific Region, pp.3-30. Edited by D.G. Howell.
- HOWELL, D.G. 1989. Tectonics of Suspect Terranes: mountain building and continental growth. Topics in the Earth Sciences **3**, 232p. Chapman and Hall, Publishers.
- HUBERT, C. and MARQUIS, P. 1989. Structural Framework of the Abitibi Greenstone Belt of Quebec and its Implications for Mineral Exploration. In "Mineralization and Shear Zones", Special Publication of the Geological Association of Canada, short course notes, **6**, pp.219-238.
- HUGHES, C.J., and HUSSEY, E.M. 1979. Standardized procedure for presenting corrected Fe₂O₃/FeO ratios in analyses of fine grained mafic rocks. Neues Jahrbuch Fur Mineralogie Monatshefte, **12**, pp.570-572.
- HUNTER, D.R. 1974. Crustal development of the Kaapvaal Craton I: The Archean. Precambrian Research, **1**, pp.259-294.
- HUNTER, D.R. 1979. The role of tonalitic and trondhjemitic rocks in the crustal development of Swaziland and the Eastern Transvaal, South Africa. In "Trondhjemitic, Dacitic, and Related Rocks", F. Barker (ed.) Developments in Petrology, **6**, pp.301-322.
- HUNTER, D.R. 1991. Crustal Processes during Archean Evolution of the Southeastern Kaapvaal Province. Journal of African Earth Sciences, **13**, pp.13-25.
- HUPPERT, H.E., and SPARKS, R.S.J. 1988. The Generation of Granitic Magmas by Intrusion of Basalt in Continental Crust. Journal of Petrology, **29**(3), pp.599-624.
- HUTCHINSON, R.W. and BURLINGTON, J.L. 1984. Some broad characteristics of greenstone belt gold lodes. In "Gold '82: The Geology, Geochemistry and Genesis of Gold Deposits, pp.339-372. Special Publication of the Geological Society of Zimbabwe. R.P. Foster eds.
- IKEDA, Y., and YUASA, M. 1989. Volcanism in nascent back-arc basins behind the Shichito Ridge and adjacent areas in the Izu-Ogasawara arc, Northwest Pacific: evidence for mixing between E-type MORB and Island arc magmas at the initiation of back-arc rifting. Contributions to Mineralogy and Petrology, **101**, pp.377-393.

INTERNATIONAL SUBCOMMISSION ON STRATIGRAPHIC CLASSIFICATION (ISSC). 1976. A Guide to Stratigraphic Classification, Terminology, and Procedure. 200p. edited by H.D. HEDBERG. John Wiley and Sons, Publishers.

JACKSON, A.R.N. 1981. Geology of part of the Tati Schist Belt-N.E. Botswana. Falconbridge Explorations (Botswana) (PTY) LTD. Prospecting Licence 1/78. Tati project 92 (1:50 000 Geological Map).

JACKSON, A.R.N., and GRIFFITHS, D.H.C. 1981. Report on work done at the Map-Nora gold prospect, N.E. Botswana, to November, 1981. Falconbridge Explorations (Botswana) (PTY) LTD. Prospecting Licence 1/78. Project 92. Unpublished Bulletin. B154 (1260).

JAHN, B.M., and SUN, S.S. 1979. Trace element distribution and isotopic composition of Archean Greenstones. in Origin and Distribution of the Elements: 11. pp.597-618. Physics and Chemistry of the Earth. Edited by L.H. Ahrens.

JAHN, B.J., GRUAU, G., and GLIKSON, A.Y. 1982. Komatiites of the Onverwacht Group, South Africa: REE Geochemistry, Sm/Nd age and mantle Evolution. Contributions to Mineralogy and Petrology. 80. pp.25-40.

JENNER, G.A., LONGERICH, H.P., JACKSON, S.E., and FRYER, B.J. 1990. ICP-MS-A powerful tool for high-precision trace-element analysis in Earth Sciences: Evidence from analysis of selected U.S.G.S. reference samples. Chemical Geology. 83(1/2). pp.133-148.

JENSEN, L.S. 1976. A new cation plot for classifying subalkalic volcanic rocks. Ontario Division of Mines Miscellaneous paper 66. pp.1-22.

JOHNSON, M.R. and RUST, I.C. 1988, Terranes, tectonostratigraphy and unconformity-bounded units:a review of current nomenclature. South African Journal of Geology. 91. pp.522-526.

JOHNSTON, D., and GRIFFITHS, D.H.C. 1982. Regional mapping of the Tati Schist Belt, northeast Botswana, prospecting licence 1/78. Falconbridge Exploration (Botswana) Bulletin B155 unpublished.

JOHNSTON, D., AND GRIFFITHS, D.H.C. 1983. Lead-Zinc exploration at the "Long Gossan" prospect near Francistown, N.E. Botswana 1979-1982 prospecting licence 1/78, project 92. Falconbridge Explorations (Botswana) (PTY) LTD. Bulletin. B188.

- JONES, M.T. 1962. Report on the road gravel surveys undertaken from Francistown to Ramaquabane and from Palapye to Serowe, March, 1962. Report of the Geological Survey of Bechuanaland, MTJ/39. Unpublished.
- JORON, J.L., and TREUIL, M. 1989. Hydromagmaphile element distributions in oceanic basalts as fingerprints of partial melting and mantle heterogeneities: a specific approach and proposal of an identification and modelling method. Geological Society of London Special Publication, 42, pp.277-299.
- KAY, R.W. 1984. Elemental abundances relevant to identification of magmas sources. Philosophical Transactions of the Royal Society of London, A310, pp.535-547.
- KEAYS, R.R. 1987. Principles of mobilization (dissolution) of metals in mafic and ultramafic rocks - the role of immiscible magmatic sulphides in the generation of hydrothermal gold and volcanogenic massive sulphides deposits. Ore Geology Reviews, 2, pp.47-63.
- KERRICH, R., and FRYER, B.J. 1979. Archean precious metal hydrothermal systems, Dome mine, Abitibi Greenstone belt 11. REE and oxygen isotope relations. Canadian Journal of Earth Sciences, 6, pp.440-458.
- KERRICH, R. 1989. Geochemical evidence on the sources of fluids and solutes for shear zone hosted mesothermal Au deposits. In "Mineralization and Shear Zones", Special Publication of the Geological Association of Canada, short course notes, 6, pp.129-197.
- KERRICH, R. and FENG, R. 1992. Archean geodynamics and the Abitibi-Pontiac collision: implications for advection of fluids at transpressive collisional boundaries and the origin of giant quartz vein systems. Earth Science Reviews, 32, pp.33-60.
- KESTLER, S.E., SUTTER, J.F., ISSIGONIS, M.J., JONES, L.M., and WALKER, R.L. 1977. Evolution of Porphyry Copper mineralization in an oceanic island arc: Panama. Economic Geology, 72, pp.1142-1153.
- KEY, R.M. 1976. The geology of the area around Francistown and Phikwe, Northeast and Central Districts, Botswana. Geological Survey of Botswana District Memoir 3, 121p. Botswana Government Printer, publishers.
- KEY, R.M., LITHERLAND, M., and HEPWORTH, J.V. 1976. The evolution of the Archean crust of northeast Botswana. Precambrian Research, 3, pp.375-413.

KEY, R.M. 1977. The Geochronology of Botswana. Transactions of the Geological Society of South Africa, **80**, pp.31-42.

KEY, R.M. and HUTTON, S.M. 1976. The Tectonic Generation of the Limpopo Belt, and a Definition of its Western Extremity. Precambrian Research, **3**, pp.79-90.

KINNY, P.D., COMPSTON, W., BRISTOW, J.W., and WILLIAMS, I.S. 1989. Archean mantle xenocrysts in a Permian kimberlite: Two generations of kimberlitic zircon in Jwaneng DK2, southern Botswana. In Kimberlites and Related Rocks: their Composition, Occurrence, Origin and Emplacement. Geological Society of Australia Special Publication, **14 (V.2)** pp.833-842. Blackwell Scientific Publications

KIRKLEY, M.B., GURNEY, J.J., and LEVINSON, A.A. 1992. Age, origin and emplacement of diamonds: a review of scientific advances in the last decade. Canadian Mining and Metallurgical Bulletin, **85(956)**, pp.48-57.

KNIPE, R.J. 1989. Deformation mechanisms-recognition from natural tectonites. Journal of Structural Geology, **11**, pp.127-146.

KRAMERS, J.D., and FOSTER, R.P. 1984. A reappraisal of lead isotope investigations of gold deposits in Zimbabwe. in Gold'82: The Geology, Geochemistry and Genesis of Gold Deposits, R.P. Foster ed., pp.569 - 582.

KRÖNER, A. 1977a. The Precambrian Geotectonic Evolution of Africa: Plate Accretion versus Plate Destruction. Precambrian Research, **4**, pp.163-213.

KRÖNER, A. 1977b. Problems of correlation in Precambrian Mobile Belts. In "The Proceedings of a Seminar Pertaining to the Limpopo Mobile Belt." Botswana Geological Survey, Bulletin, **12**, pp.9-27. I.F. Ermanovics, R.M. Key and G. McEwen (eds.), Botswana Government Printers, Publishers.

KRÖNER, A. and COMPSTON, W. 1988. Ion-probe ages from early Archean granite pebbles and greywacke, Barberton Greenstone Belt, South Africa. Precambrian Research, **38**, pp.367-380.

KRUPP, R.E., and SEWARD, T.M. 1990. Transport and deposition of metals in the Rotokawa geothermal system, New Zealand. Mineral. Deposita, **25**, pp.73-81.

KUSKY, T.M. 1990. Evidence for Archean ocean opening and closing in the Southern Slave Province. Tectonics, **9**, pp.1533-1563.

KUSKY, T.M. and KIDD, W.S.F. 1992. Remnants of an Archean oceanic plateau, Belingwe Greenstone Belt, Zimbabwe. Geology, **20**, pp.43-46.

LAJTAI, E.Z. 1969. Mechanics of second order faults and tension gashes. Geological Society of America Bulletin, **80**, pp.2253-2272.

LAMONT, G.T. 1950a. Report on the Halfway Kop kyanite prospect Report of the Geological Survey of Bechunaland. GLT/2. Unpublished.

LAMONT, G.T. 1950b. Preliminary report on the Tati Schist Belt. Report of Geological Survey of Bechunaland. GLT/3. Unpublished.

LAWTON, T.F. 1986. Compositional trends within a clastic wedge adjacent to a fold-thrust belt: Indianola Group, Central Utah, U.S.A. In Special Publication of the International Association of Sedimentologists, **8**, pp.411-423. P.A. Allen and Homewood, P. (eds.). Blackwell Scientific publications.

LAZNICKA, P. 1985. Empirical metallogeny: depositional environments, lithologic associations and metallic ores. "Developments in Economic Geology, no.19.

LEAKE, B.E. 1990. Granite Magmas: their Sources, Initiation and Consequences of Emplacement. Journal of the Geological Society, London, **147**, pp.579-589.

LE MAITRE, R.W. 1989 (eds.). A Classification of Igneous Rocks and Glossary of Terms. Blackwell Publishers, Oxford, 193p.

LE ROEX, A.P., ERLANK, A.J., and NEEDHAM, H.D. 1981. Geochemical and mineralogical evidence for the occurrence of at least three distinct magma types in the "FAMOUS" region. Contributions to Mineralogy and Petrology, **77**, pp.24-37.

LE ROEX, A.P., ERLANK, A.J., REID, A.M., FREY, F.A., and HART, S.R. 1983. Geochemistry, mineralogy and petrogenesis of lavas erupted along the Southwest Indian Ridge between the Bouvet triple junction and 11 degrees east. Journal Petrology, **24**, pp.267-318.

LE ROEX, A.P., DICK, H.J.B., REID, A.M., FREY, F.A., ERLANK, A.J., and HART, S.R. 1985. Petrology and geochemistry of basalts from the American-Antarctic Ridge, southern ocean: implications for the westward influence of the Bouvet mantle plume. Contributions to Mineralogy and Petrology, **90**, pp.367-380.

LE ROEX, A.P., DICK, H.J.B., GULEN, L., REID, A.M., and ERLAND, A.J. 1987. Local and regional heterogeneity in MORB from the mid-Atlantic Ridge between 54.5 S and 51 S; evidence for geochemical enrichment. Geochimica et Cosmochimica Acta, **51**, pp.541-555.

- LE ROEX, A.P., DICK, H.J.B., and FISHER, R.L. 1989. Petrology and Geochemistry of MORB from 25E to 46E along the Southwest Indian Ridge: Evidence for contrasting styles of Mantle Enrichment. Journal of Petrology, **30(4)**, pp.947-986.
- LIGHT, M.P.R. 1982. The Limpopo Mobile Belt: A result of Continental Collision. Tectonics, **1**, pp.325-342.
- LITHERLAND, M. 1973. Uniformitarian approach to Archean schist relics. Nature (Physical Science), **242**, pp. 125-127.
- LONGSTAFFE, F.J. 1983. Diagenesis 4. Stable isotope studies of diagenesis in clastic rocks. Geoscience Canada, **10(2)**, pp.43-58.
- LOTTERMOSER, B.G. 1992. Rare earth elements and hydrothermal ore formation processes. Ore Geology Reviews, **7**, pp.25-41.
- LUDDEN, J., and HUBERT, C. 1986. Geologic evolution of the late Archean Abitibi Greenstone Belt. Geology, **14**, pp.707-711.
- MADU, B.E., NESBITT, B.E., and MUEHLENBACHS, K. 1990. A mesothermal gold-stibnite-quartz vein occurrence in the Canadian Cordillera. Economic Geology, **85**, pp.1260-1268.
- MARTIN, A. 1975. The Geology of the Shabani area. Annals of the Rhodesian Geological Survey, **1**, pp.35-48.
- MARTIN, H., CHAUVEL, C., and JAHN, B.M. 1983. Major and Trace element geochemistry and crustal evolution of Archean granodioritic rocks from Eastern Finland. Precambrian Research, **21**, pp.159-180.
- MASON, R. 1968. The geology of the Southern Tati. Botswana Geological Survey, unpublished report, RM3/68.
- MASON, R. 1970. The geology of the country between Francistown and Mmadinare, eastern Botswana. Unpublished Ph.D thesis (University of Witwatersrand).
- MASON, R. 1973. The Limpopo Mobile Belt-South Africa. Philosophical Transactions of the Royal Society of London, **A273**, pp.463-485.
- MAWER, C.K. 1986. The bedding concordant gold-quartz veins of the Meguma Group, Nova Scotia. Geological Association of Canada Special paper **32**, pp.135-148.

McCOURT, S., and VEARNCOMBE, J.R. 1987. Shear zones bounding the Central Zone of the Limpopo Belt, southern Africa. Journal of Structural Geology, **9(2)**, pp.127-137.

McCOURT, S., and VEARNCOMBE, J.R. 1992. Shear zones of the Limpopo Belt and adjacent granitoid-greenstone terranes: implications for late Archean collision tectonics in southern Africa. Precambrian Research, **55**, pp.553-570.

McCOURT, S., and VAN REENEN, D. 1992. Structural geology and tectonic setting of the Sutherland Greenstone Belt, Kaapvaal Craton, South Africa. Precambrian Research, **55**, pp.93-110.

MEYER, M., and SAAGER, R. 1985. The origin of gold in Archean epigenetic gold deposits. Economic Geology Research Unit of the University of Witwatersrand, information circular, **172**, pp.11

MICHARD, A., BEAUCAIRE, C., and MICHARD, G. 1987. Uranium and rare earth in CO₂-rich waters from Vals-les-Bains (France). Geochimica et Cosmochimica Acta, **51**, pp.901-909.

MILCHARD, A. 1989. Rare earth element systematics in hydrothermal fluids. Geochimica et Cosmochimica Acta, **53(3)**, pp.745-750.

MILLER, C.F., WATSON, E.B., and HARRISON, T.M. 1988. Perspectives on the source, segregation and transport of granitoid magmas. Transactions of the Royal Society of Edinburgh: Earth Sciences, **79**, pp.135-156.

MILLERO, F.J. 1992. Stability constants for the formation of rare earth inorganic complexes as a function of ionic strength. Geochimica et Cosmochimica Acta, **56**, pp.3123-3132.

MOLYNEUX, T.G. 1971. Prospecting Tati Concession. Report of gold section of Sedge (Botswana): a subsidy of Anglo American Corporation. Unpublished.

MOORBATH, S., TAYLOR, P.N., ORPEN, J.L., TRELOAR, P., and WILSON, J.F. 1987. First direct radiometric dating of Archean stromatolitic limestone. Nature, **326**, pp.865-867.

MOREL, S.W. 1968. The mineral potential of the Tati District. Report of Geological Survey of Botswana, **SWM/3/68**. Unpublished

MORGAN, J.W., and WANDLESS, G.A. 1980. Rare earth element distribution in some hydrothermal minerals: evidence for crystallographic control. Geochimica et Cosmochimica Acta, **44**, pp.973-980.

MOSIGI, M.B. 1991. Tati Nickel Project: Final Report (Old Tati Project Grids CBG East, CBG West and NZ-BJ). Falconbridge, Unpublished Bulletin, **B263**, 20p.

MULLER, A.G. and HARRIS, L.B. 1987. An Application of Wrench Tectonics Models to Mineralized Structures in the Golden Mile District, Kalgoolie, Western Australia. In "The Recent advances in understanding Precambrian Gold Deposits" Geology Department & University of Western Australia, Publication No. **11**, pp.97-107.

MYERS, R.E., and BREITKOPF, J.H. 1989. Basalt Geochemistry and tectonic setting: A new approach to relate tectonic and magmatic processes. Lithos, **23**, pp.53-62.

MYERS, J.S. 1990. Western Gneiss Terrane. In "The Geology and Mineral Resources of western Australia, pp.13-32. Geological Survey of western Australia, memoir #3.

NATLAND, J.H. 1989. Partial melting of a lithologically heterogeneous mantle: inferences from crystallization histories of magnesian abyssal tholeiites from Siqueiros Fracture Zone. in "magmatism in the Oceanic Basin" Geological Society of London Special Publication, **42**, pp.41-70. Sanders et al. (eds).

NISBET, E.G. 1982. Definition of "Archean"-comment and proposal on the recommendations of the International Subcommittee on Precambrian Stratigraphy. Precambrian Research, **19**, pp.111-118.

NISBET, E.G., BICKLE, M.J., MARTIN, A., ORPEN, J.L., and WILSON, J.F. 1982. Komatiites in Zimbabwe. In "Komatiites", N.T.A. Arndt and E.G. Nisbet (eds.), George Allen and Unwin, pp.97-104.

NISBET, E.G., ARNDT, N.T., BICKLE, M.J., CAMERON, W.E., CHAUVEL, C., CHEADLE, M., HEGNER, E., KYSER, T.K., MARTIN, A., RENNER, R., and ROEDDER, E. 1987. Uniquely fresh 2.7 Ga komatiite from the belingwe greenstone belt, Zimbabwe. Geology, **15**, pp.1147-1150.

NESBIT, R.W., and SUN, S.-S. 1976. Geochemistry of Archean spinifex-textured peridotites and magnesian and low magnesian tholeiites. Earth and Planetary Science Letters, **31**, pp.433-

- NESBITT, B.E., MUROWCHICK, J.B., and MUEHLENBACHS, K. 1986. Dual Origin of Lode Gold Deposits in the Canadian Cordillera. Geology, **14**, pp.506-509.
- NESBITT, B.E., MUEHLENBACHS, K., and MUROWCHICK, J.B. 1989. Genetic implications of stable isotopes characteristics of mesothermal Au deposits and related Sb and Hg deposits in the Canadian Cordillera. Economic Geology, **84**, pp.1489-1506.
- NEWSOM, H.E., WHITE, W.M., JOCHUM, K.P. and HOFFMANN, A.W. 1986. Siderophile and chalcophile element abundances in oceanic basalts, Pb-isotope evolution and growth of the Earth's core. Earth and Planetary Science Letters, **80**, pp.229-313.
- NOCKLODS, S.R., and ALLEN, R. 1953. The Geochemistry of some igneous rock series. Geochimica et Cosmochimica Acta, **4**, pp.105-142.
- OBERTHUR, T., SAAGER, R., and TOMSCHI, H.-P. 1990. Geological, mineralogical and geochemical aspects of Archean banded iron-formation-hosted gold deposits: some examples from Southern Africa. Mineral. Deposita, **25**, pp.125-135.
- O'CONNOR, J.T. 1965. A classification for quartz-rich igneous rocks based on feldspar ratios. United States of America Geological Survey Professional paper 525-B, pp.1379-1384.
- O'DRISCOLL, E.S.T. 1985. The application of lineament tectonics in the discovery of the Olympic Dam Cu - Au - U deposit at Roxby Downs, south Australia. Global Tectonics and Metallogeny, **3**, pp.43-57.
- OHTANI, E. 1990. Majorite fractionation and genesis of komatiites in the deep mantle. Precambrian Research, **48(3)**, pp.195-202.
- OLIVAREZ, A.M., and OWEN, R.M. 1989. REE/Fe variations in hydrothermal sediments: implications for the REE content of seawater. Geochimica et Cosmochimica Acta, **53(3)**, p.757-
- O'NIONS, R.K., HAMILTON, P.J., and EVENSEN, N.M. 1977. Variation in $^{143}\text{Nd}/^{144}\text{Nd}$ and $^{87}\text{Sr}/^{86}\text{Sr}$ ratios in oceanic basalts. Earth and Planetary Science Letters, **34**, pp.13-22.
- O'NIONS, R.K., and PANKHURST, 1978. Early Archean rocks and geochemical evolution of the earth's crust. Earth and Planetary Science Letters, **38**, pp.211-236.

ORI, G.G. Sedimentary Basins formed and carried piggyback on active thrust sheets. Geology, **12**, pp.475-478.

ORPEN, J.L. and WILSON, J.F. 1981. Stromatolites at ≈ 3500 Myr and a greenstone-granite unconformity in the Zimbabwean Archean. Nature, **291**, pp.218-220.

PANTELEYEV, A. 1985. Ore deposits #10. A Canadian Cordilleran Model for epithermal Gold-Silver deposits. Geoscience Canada, **13(2)**, pp.101-111.

PATERSON, S.R., VERNON, R.H. and TOBISCH, O.T. 1989. A review of criteria for the identification of magmatic and tectonic foliations in granitoids. Journal of Structural Geology, **11(3)**, pp.349-363.

PEARCE, J.A., and CANN, J.R. 1973. Tectonic setting of basic volcanic rocks determined using trace elements analysis. Earth and Planetary Science Letters, **19**, pp.290-300.

PEARCE, J.A., and NORRY, M.J. 1979. Petrogenetic implications of Ti, Zr, Y and Nb variations in volcanic rocks. Contributions to Mineralogy and Petrology, **69**, pp.33-47.

PEARCE, J.A. 1982. Trace-element characteristics of lavas from distinctive plate boundaries. In "Andesites", Thorpe, E.S.(ed.), pp.525-548.

PEARCE, J.A., HARRIS, N.B.W., and TINDLE, A.G. 1984. Trace element discrimination diagrams for the tectonic interpretation of granitic rocks. Journal of Petrology, **25(4)**, pp.956-983.

PEARCE, J.A., LIPPARD, S.J., and ROBERTS, S. 1984. Characteristics and tectonic significance of supra-subduction zone (s.s.z.) ophiolites. In "Marginal Basin Geology." Geological Society of London Special Publication, **16**, pp.77-94.

PERRING, C.S., GROVES, D.I., and HO, S.E. 1987. Constraints on the source of auriferous fluids for Archean gold deposits. in Recent Advances in Understanding Precambrian Gold Deposits, publication no.1. S.E. Ho and D.I. Groves eds, pp.287 - 305.

PHILLIPS, G.N. and GROVES, D.I. 1984. An Epigenetic origin for Archean banded iron-formation-hosted gold deposits. Economic Geology, **79**, pp. 162-171.

PIRC, S. and ROSE, A.W. 1990. The Abundance and distribution of antimony in the red-beds of the Devonian Catskill Formation, eastern Pennsylvania, U.S.A. Chemical Geology, **85**, pp. 321-328.

- PITCHER, W.S. 1987. Granites and yet more granites forty on. Geologische Rundschau, **76(1)**, pp.51-79.
- PLATT, J.P. 1979. Extensional crenulation cleavage. Journal of Structural Geology, **1**, pp.95.
- PLATT, J.P., and VISSERS, R.L.M. 1980. Extensional structures in anisotropic rocks. Journal of Structural Geology, **2**, pp.397-410.
- PLATT, J.P. 1984. Secondary cleavages in ductile shear zones. Journal Structural Geology, **6**, pp.439-442.
- PLUMB, K.A. 1985. Subdivision of late Precambrian sequences in Australia. Precambrian Research, **29**, pp.303-329.
- PLUMB, K.A., and JAMES, H.L. 1986. Subdivision of the Precambrian time: recommendations and suggestions by the Subcommittee on Precambrian Stratigraphy. Precambrian Research, **32**, pp.65-92.
- POLDERVAART, A. 1950. Suggested mining development in the Tati Concession area. Report of Geological Survey of Bechuanaland, **AP/10**. Unpublished.
- PONCE DE LEON, M.J., and CHOUKROUNE, P. 1980. Shear zones in the Iberian arc. Journal Structural Geology, **2**, pp.63-68.
- PORTER, C.W. and FORSTER, R.P. 1990. Multi-phase ductile-brittle deformation and the role of Archean thrust tectonics in the evolution of the Globe and Phoenix Gold Deposit, Zimbabwe. Economic Geology, pp.34-38.
- POTTER 11, R.W. 1977. pressure corrections for fluid-inclusion homogenization temperatures based on the volumetric properties of the system NaCl-H₂O. Journal Research of United States Geological Survey, **5**, pp.603-607.
- POULSEN, K.H. and ROBERT, F. 1989. Shear Zones and Gold: Practical Examples from the southern Canadian Shield. In "Mineralization and Shear Zones". Special Publication of the Geological Association of Canada, short course notes, **6**, pp.239-266.
- PRICE, R.C., JOHNSON, L.E., and CRAWFORD, A.J. 1990. Basalts of the North Fiji Basin: the generation of back arc basin magmas by mixing of depleted and enriched mantle sources. Contributions to Mineralogy and Petrology, **105**, pp.106-121.

- REED, M.H. 1983. Seawater-Basalt Reaction and the Origin of Greenstones and Related Ore deposits. Economic Geology, **78**, pp.466-485.
- REEVES, C.V., and HUTCHINS, D.G. 1976. The national gravity survey of Botswana, 1972 - 1973. Botswana Geological Survey Bulletin, **5**. Botswana Government Printer, publishers.
- REEVES, C.V. 1978. Reconnaissance aeromagnetic survey of Botswana 1975-1977, final report. Botswana Geological Survey.
- REEVES, C.V. and HUTCHINS, D.G. 1978. A failed Gondwana spreading axis in Southern Africa. Nature, **273**, pp.222.
- REYNOLDS, S.J. and LISTER, G.S. 1987. Structural aspects of fluid-rock interactions in detachment zones. Geology, **15**, pp.362-366.
- RICHARDSON, C.J., CANN, J.R., RICHARDS, H.G., and COWAN, J.G. 1987. Metal-depleted root zones of the Troodos ore-forming hydrothermal systems, Cyprus. Earth and Planetary Science Letters, **84**, pp.243-253.
- RIDLEY, J. 1992. On the Origins and Tectonic Significance of the Charnockite Suite of the Archean Limpopo Belt, Northern Marginal Zone, Zimbabwe. Precambrian Research, **55**, pp.407-427.
- RINGWOOD, A.E., SEIFERT, S., and WANKE, H. 1986. A komatiite component in Apollo 16 highland breccias: implications for the nickel-cobalt systems and bulk composition of the moon. Earth and Planetary Science Letters, **81**, pp.105-117.
- RIVALENTI, G. 1976. Geochemistry of meta-volcanic amphibolites from SW Greenland. in "The Early History of the Earth" B.F. Windley (ed.), pp.213-224
- ROBB, L.J., and ANHAEUSSER, C.R. 1983. Chemical and petrogenetic characteristics of Archean tonalite-trondhjemite gneiss plutons in the Barberton Mountain Land. Special Publication of the Geological Society of South Africa, **9**, pp.103-116.
- ROBERT, F., and KELLY, W.C. 1987. Ore-forming Fluids in Archean Gold-Bearing Quartz Veins at the Sigma Mine, Abitibi Greenstone Belt, Quebec, Canada. Economic Geology, **82**, pp.1464-1482.
- ROBERTS, R.G. 1987. Archean lode gold deposits: Ore Deposits Models no.11, Geoscience Canada, **14**, pp.37-52.

ROBERT, S., FOSTER, R.P. and NESBITT, R.W. 1990. Mineralization associated with early Precambrian basic magmatism. In "Early Precambrian basic magmatism", edited by R.P. Hall and D.J. Hughes, pp. 157-188.

ROBERTSON, I.D.M. 1973. A Model for discussing the early history of the earth based on a study of lead isotope ratios from veins in some Archean cratons of Africa. Geochimica et Cosmochimica Acta, 37, pp.2099-2124.

ROBERTSON, I.D.M. 1977. Some granulite facies metasediments of the Rhodesian part of the Northern Marginal Zone of the Limpopo Mobile Belt. In "The Proceedings of a Seminar Pertaining to the Limpopo Mobile Belt." Botswana Geological Survey, Bulletin, 12, pp.157-176. I.F. Ermanovics, R.M. Key and G. McEwen (eds.), Botswana Government Printers, Publishers.

ROERING, C., VAN REENEN, D.D., SMIT, C.A., BARTON, J.M. Jr., De BEER, J.H., DE WIT, M.J., STETTLER, E.H., VAN SCHALKWYK, J.F., STEVENS, G., and PRETORIUS, S. 1992. Tectonic model for the evolution of the Limpopo Belt. Precambrian Research, 55, pp.539-552.

ROLLINSON, H.R., and ROBERTS, C.R. 1987. Ratio corrections and major element mobility in altered basalts and komatiites. Contributions to Mineralogy and Petrology, 93, pp.89-97.

ROMBERGER, S.B. 1985. Ore Deposits #.9. Disseminated gold deposits. Geoscience Canada, 13(1), pp.23-31.

RONA, P.A. 1984. Hydrothermal mineralization at seafloor spreading centres. Earth Science Reviews, 20, pp.1-104.

RONA, P.A. 1988. Hydrothermal mineralization at oceanic ridges. Canadian Mineralogist, 26, pp.431-465.

SANG, J. and HO, S.E. 1987. A review of gold deposits in China. in Recent Advances in Understanding Precambrian Gold Deposits, publication no.1, S.E. Ho and D.L. Groves eds, pp.307 - 320.

SANJUAN, B., MICHARD, N., and MICHARD, G. 1988. Influence of the temperature of CO₂-rich springs on their aluminum and rare-earth element contents. Chemical Geology, 68, pp.57-67.

SAUNDERS, A.D., TARNEY, J., and WEAVER, S.D. 1980. Transverse Geochemical Variations across the Antarctic Peninsular: Implications for the genesis of Calc-alkaline magmas. Earth and Planetary Science Letters, 46, pp.344-360.

SAWYER, E.W., and ROBIN, P.-Y.F. 1986. The Subsolidus Segregation of Layer-parallel Quartz-Feldspar Veins in Greenschist to upper Amphibolite facies Metasediments. Journal of Metamorphic Geology, **4**, pp.237-260.

SCHUTZ, W., EBNETH, J., and MEYER, K.D. 1987. Trondhjemites, tonalites and diorites in the South Portuguese Zone and their relation to the vulcanites and mineral deposits. Iberian Pyrite Belt. Geologische Rundschau, **76(1)**, pp.201-212.

SCHWAB, F.L. 1986. Sedimentary 'Signatures' of Foreland Basin Assemblages: Real or Counterfeit? Special Publication of International Association of Sedimentologists, **8**, pp. 395-410.

SCOTT, S.D. 1990. Massive sulphide deposits of the modern oceanic floor. In "Frontier in Ore Deposit and Exploration studies." In R.L. Stanton Symposium (10th Australian Geological Convention). pp.29-30.

SEARLE, M.P., WINDLEY, B.F., COWARD, M.P., COOPER, D.J.W., REX, A.J., REX, D., TINGDONG, LI., XUCHANG, X., JAN, M.Q., THAKUR, V.C., and KUMAR, S. 1987. The Closing of Tethys and the Tectonics of the Himalaya. Geological Society of America Bulletin, **98**, pp.678-701.

SERDYUCHENKO, D.P. 1968. Metamorphosed Weathering Crusts of the Precambrian, their Metallogenic and Petrographic Features. The XXIII International Geological Congress, **4**, pp.37-42.

SHEERAN, D.A. 1986. Eastern Botswana gold investigation: Tati Greenstone Belt, geological reconnaissance. Goldfields (Botswana). GFB/64/5/1/2. unpublished.

SHEPHERD, T.J., RANKIN, A.H., and ALDERTON, D.H.M. 1985. A practical guide to fluid inclusions studies.

SHERATON, J.W., ELLIS, D.J., and KUEHNER, S.M. 1985. Rare-earth element geochemistry of Archean orthogneisses and evolution of the East Antarctic shield. BMR Jour. Austr. Geology and Geophysics, **9**, pp.207-218.

SHIKAZONO, N. 1985. Gangue Minerals from Neogene Vein-type Deposits in Japan and an Estimate of their CO² Fugacity. Economic Geology, **80**, pp.754-768.

SHIKAZONO, N., and SHIMUZU, M. 1992. Associated Metals in Vein-type Deposits in Japan: Interpretation using HSAB Principle. Canadian Mineralogist, **30**, pp.137-143.

SHIREY, S.B., and HANSON, G.N. 1984. Mantle-derived Archean monzodiorites and trachyandesites. Nature, **310**, pp.222-224.

SIBSON, R.H., ROBERT, F. and POULSEN, K.H. 1988. High-angle reverse faults, fluid-pressure cycling, and mesothermal gold-quartz deposits. Geology, **16**, pp.551-555.

SIBSON, R.H. 1989. High-angle reverse faulting in northern New Brunswick, Canada, and its implications for fluid pressure levels Journal of Structural Geology, **11**, pp.873-877.

SILLITOE, R.H., and HART, S.R. 1984. Lead-isotopic signatures of porphyry copper deposits in oceanic and continental settings, Colombian Andes. Geochimica et Cosmochimica Acta, **48**, pp.2135- 2142.

SIMMONS, E.C., and HANSON, G.N. 1978. Geochemistry and origin of massif-type anorthosites. Contributions to Mineralogy and Petrology **66**, pp.119-135.

SPARKS, R.S.J. 1986. The role of crustal contamination in magma evolution through geological time. Earth and Planetary Science Letters, **78(2/3)**, 211-223.

SPOONER, E.T.C. 1989. Mineralization and shear zones. Geological Association of Canada, Short Course Notes, **6**.

STACEY, J.S. and KRAMERS, J.D. 1975. Approximation of terrestrial lead isotope evolution by a two-stage model. Earth and Planetary Science Letters, **26**, pp.207-221.

STAGMAN, J.G. 1978. An Outline of the Geology of Rhodesia. Rhodesia Geological Survey Bulletin, **80**, 126p. Government Printer, Salisbury.

STERN, R.A., HANSON, G.N., and SHIREY, S.B. 1989. Petrogenesis of Mantle-derived, LILE-enriched Archean Monzodiorites and Trachyandesites (Sanukitoids) in Southwest Superior Province. Canadian Journal of Earth Sciences, **26**, pp.1688-1712.

STERN, R.A., and HANSON, G.N. 1991. Archean high-Mg granodiorite: A derivative of light rare element-enriched monzodiorite of mantle origin. Journal of Petrology, **32(1)**, pp.201-238.

STONE, W.E. 1990. Archean Volcanism and sedimentation in the Bousquet gold district, Abitibi Greenstone Belt, Quebec: Implications for stratigraphy and gold mineralization. Geological Society of America Bulletin, **102**, pp.147-158.

STOREY, M., MAHONEY, J.J., KROENKE, L.W. and SAUNDERS, A.D. 1991. Are Oceanic plateaus sites of Komatiite Formation? Geology, **19**, pp.376-379.

STOWE, C.W. 1980. Wrench tectonics in the Archean Rhodesian Craton. Transactions of the Geological Society of South Africa, **83**, pp.193-205.

STRONG, D.F. 1987. Metallogeny. Encyclopedia of Physical Science and Technology, **8**, pp.147-163.

SUGITANI, K. 1992. Geochemical characteristics of Archean cherts and other sedimentary rocks in the Pilbara Block, Western Australia: evidence for Archean seawater enriched in hydrothermally derived iron and silica. Precambrian Research, **57**, pp.21-47.

SUN, S.-S., and NESBITT, R.W. 1977. Chemical heterogeneity of the Archean mantle, composition of the earth and mantle evolution. Earth and Planetary Science Letters, **35**, pp.429-448.

SUN, S.-S., NESBITT, R.W., and SHARASKIN, A-Y. 1979. Geochemical characteristics of mid-ocean ridge basalts. Earth and Planetary Science Letters, **44**, pp.119-138.

SUN, S.-S. 1980. Lead isotopic study of young volcanic rocks from mid oceanic ridges, oceanic islands and island arcs. Transactions of the Royal Philosophical Society of London, **A297**, pp.409-445.

SUN, S.-S., 1982. Chemical composition and origin of the earth's primitive mantle. Geochimica et Cosmochimica Acta, **46**, pp.179-192.

SUN, S.-S., 1984. Geochemical characteristics of Archean ultramafic and mafic volcanic rocks: Implications for mantle composition and evolution.

SUN, S.-S. 1987. Chemical composition of Archean komatiites: implications for early history of the earth and mantle evolution. Journal Volcanology and Geothermal Research, **32**, pp.67-82.

SUN, S.-S., and MCDONOUGH, W.F. 1989. Chemical and isotopic systematics of oceanic basalts: implications for mantle composition and processes. In "Magmatism in the oceanic Basins" Special Geological Society of London Publication, **42**, pp.313-345.

SVERJENSKY, D.A. 1984. Europium Redox Equilibria in Aqueous Solution. Earth and Planetary Science Letters, **67**, pp.70-78.

SYLVESTER, A.G. 1988. Strike-slip Faults. Geological Society of America Bulletin, **100**, pp. 1666-1703.

TANKARD, A. J., JACKSON, M. P. A., ERICKSSON, K. A., HOBDAI, D. K., HUNTER, D. R., and MINTER, W. E. L. 1982. Granulite-Gneiss Terrane: Limpopo Province. In "Crustal Evolution of Southern Africa: 3.8 Ga of earth history." Springer-Verlag, Publishers., pp.87-111.

TARNEY, J. 1976. Geochemistry of Archean high grade gneisses, with implications as to the origin and evolution of the Precambrian Crust. In "The Early History of the Earth." B.F. Windley (ed.), pp.405-417.

TARNEY, J., DALZIEL, I.W.D. and DE WIT, M.J. 1976. Marginal Basin "Rocas Verdes" Complex from southern Chile: A Model for Archean Greenstone Belt Formation. In "The Early History of the Earth". Edited by B.F. Windley. J. Wiley & Sons, Publishers.

TARNEY, J., SAUNDERS, A.D., and WEAVER, S.D. 1977. Geochemistry of volcanic rocks from the island arcs and marginal basins of the Scotia Arc region. In "Island Arcs, Deep Sea Trenches and Back Arc Basins." American Geophysical Union, Maurice Ewing Series, **1**, pp.367-377. M. Talwani and W.C. Pitman (eds.).

TARNEY, J., and SAUNDERS, A.D. 1979. Trace element constraints on the origin of Cordilleran Batholiths. In "Origin of Granite Batholiths: Geochemical Evidence". M.P. Atherton and J. Tarney (ed.), 90-105

TARNEY, J., WEAVER, B., and DRURY, S.A. 1979. Geochemistry of Archean Trondjemitic and tonalitic gneisses from Scotland and East Greenland. In "Trondjemites, Dacites, and Related Rocks." F. Barker (ed.), Developments in Petrology, **6**, pp.275-299.

TATSUMI, Y., and ISHIZAKA, K. 1982. Origin of high-magnesian andesites in the Setouchi volcanic belt, southwest Japan, 1. Petrological and chemical characteristics. Earth and Planetary Science Letters, **60**, pp.293-304.

TATSUMI, Y., and MARUYAMA, S. 1989. Boninites and high-Mg andesites: tectonics and petrogenesis. In "Boninites and Related Rocks" pp. 50-71. Edited by A.J. Crawford. Unwin Hyman Publishers.

TAYLOR, P.N., KRAMERS, J.D., MOORBATH, S., WILSON, J.F. ORPEN, J.L., and MARTIN, A. 1991. Pb/Pb, Sm/Nd and Rb/Sr geochronology in the Archean Craton of Zimbabwe. Precambrian Research, **87**, 175-196.

- TAYLOR, S.R., and MCLENNAN, S.M. 1985. The continental crust: its composition and evolution. Blackwell, Oxford, 312p.
- TCHALENKO, J.S. 1968. The evolution of kink-bands and the development of compression textures in sheared clays. Tectonophysics, **6**, pp.159-174.
- TEISSEYRE, R. 1970. Crack formation and energy release caused by the concentration of dislocations along fault planes. Tectonophysics, **9**, pp.547-557.
- THAKUR, V.C. 1987. Development of margin structures across the northwestern Himalaya, India. Tectonophysics, **133**, pp.1-13.
- THOMPSON, R.N., MORRISON, M.A., HENDRY, G.L., and PARRY, S.J. 1984. An assessment of the relative roles of crust and mantle in magma genesis: an elemental approach. Philosophical Transactions of the Royal Society London, **A310**, pp.549-590.
- THURSTON, P.C., and CHIVERS, K.M. 1990. Secular variation in greenstone sequence development emphasizing Superior Province, Canada. Precambrian Research **46**, pp.21-58.
- TRELOAR, P.J., COWARD, M.P., and HARRIS, N.B.W. 1992. Himilaya-Tibetan Analogies for the Evolution of the Zimbabwe Craton and Limpopo Belt. Precambrian Research, **55**, pp.571-587.
- TULLOCH, 1929. Geological map the Tat area. Unpublished
- TURNER, F.J. 1980. Metamorphic Petrology: mineralogical, field, and tectonic aspects. 2nd Edition. Hemisphere Publishing Corporation, 524p.
- VAN BREEMEN, O., and DODSON, M.H. 1972. Metamorphic chronology of the Limpopo Belt, southern Africa. Geological Society of America Bulletin, **83**, pp.2005-2018.
- VAN REENEN, D.D., BARTON, J.M. Jr., ROERING, C., SMITH, C.A., and VAN SCHALKWYK, J.F. 1987. Deep crustal response to the continental collision: the Limpopo belt of southern Africa. Geology, **15**, pp.11-14.
- VAN REENEN, D.D., ROERING, C., ASHWAL, L.D., and De WIT, M.J. 1992. Regional geological setting of the Limpopo Belt. Precambrian Research, **55**, pp.1-5.
- VAN STRATEN, O.J. 1954. Samples of the lepidolite - bearing pegmatite. Report of Geological Survey of Bechuanaland, **OJVS/36**, unpublished.

VEIZER, J., HOFFS, J., RIDLER, R.H., JENSEN, L.S., and LOWE, D.R. 1989a. Geochemistry of Precambrian carbonates: 1. Archean hydrothermal systems. Geochimica et Cosmochimica Acta, **53(4)**, pp.845-857.

VEIZER, J., HOEFS, J., LOWE, D.R., and THURSTON, P.C. 1989b. Geochemistry of Precambrian carbonates II. Archean greenstone belts and Archean sea water. Geochimica et Cosmochimica Acta, **53(4)**, pp.859-

VIERECK, L.G., FLOWER, M.F.J., HERTOGEN, J., SCHMINCKE, H.-U., and JENNER, G.A. 1989. The genesis and significance of N-MORB sub-types. Contributions to Mineralogy and Petrology, **102**, pp.112-126.

VILJOEN, M.A., VILJOEN, R.P., SMITH, H.S. and ERLANK, A.J. 1983. Geological, Textural and Geochemical Features of Komatiitic Flows from the Komati Formation. Special Publication of the Geological Society of South Africa, **9**, pp. 1-20.

VILJOEN, M.J. and VILJOEN, R.P. 1969. The Geology and Geochemistry of the lower Ultramafic unit of the Onverwacht Group and a proposed new class of igneous rocks. Special Publication of the Geological Society of South Africa, **2**, pp.55-86.

VLAAR, N.J. 1986. Archean global dynamics. Geologische Mijnb., **65**, 91-101.

WATKEYS, M.K. 1983. Brief Explanatory Notes on the Provisional Geological Map of the Limpopo Belt and Environs. Special Publication of the Geological Society of South Africa., **8**, pp.89-102.

WATKEYS, M.K., LIGHT, M.P.R., and BRODERICK, T.J. 1983. A retrospective view of the Central Zone of the Limpopo Belt, Zimbabwe. Special Publication of the Geological Society of South Africa., **8**, pp.65-80.

WELLS, P.R.A. 1979. Chemical and thermal evolution of Archean sialic crust, Southwest Greenland. Journal of Petrology, **20**, pp.187-226.

WHALEN, J.B., CURRIE, K.L. and CHAPPELL, B.W. 1987. A-type granites: geochemical characteristics, discrimination and petrogenesis. Contributions to Mineralogy and Petrology, **95**, pp.407-419.

WHITNEY, J.A. 1988. The origin of granite: the role and source of water in the evolution of granitic magmas. Geological Society of America Bulletin, **100**, pp.1886-1897.

WICKHAM, S.M. 1987. The segregation and emplacement of granitic magmas. Journal of the Geological Society of London, **144**, pp.281-297.

WILLIAMS, P.R., NISBET, B.W. and ETHERIDGE, M.A. 1989. Shear zones, gold mineralization and structural history in the Leonora district, Eastern Goldfields province, western Australia. Australian Journal of Earth Sciences, **36**, pp.383-404.

WILSON, J.F., BICKLE, M.J., HAWKESWORTH, C.J., MARTIN, A., NISBET, E.G., and ORPEN, J.L. 1978. Granite-greenstone terrains of the Rhodesian Archean Craton. Nature, **271**, pp.23-27.

WILSON, J.F. 1979. A preliminary reappraisal of the Rhodesian basement complex. Geological Society of South Africa, special publication, **5**, pp. 1 - 23.

WILSON, J.F. 1982. The Geology of the Great "Dyke", Zimbabwe: the ultramafic rocks. Journal of Petrology, **32(2)**, pp. 240-292.

WILSON, J.F. 1990. A Craton and its cracks: some of the behaviour of the Zimbabwe block from the Late Archean to the Mesozoic in response to horizontal movements, and the significance of some of its mafic dyke fracture patterns. Journal of African Earth Sciences, **10**, pp.483-501.

WINCHESTER, J.A., and FLOYD, P.A. 1977. Geochemical discrimination of different magma series and their differentiation products using immobile elements. Chemical Geology, **20**, pp.325-343.

WINDLEY, B.F. 1973. Crustal development in the Precambrian. Philosophical transactions of the Royal Society of London, **A273**, 321-341.

WINDLEY, B.F. 1981. Precambrian rocks in the light of the plate-tectonic concept. in "Precambrian Plate Tectonics" A. Kroner (ed.), pp.1-20

WINDLEY, B.F. 1991. Early Proterozoic collision tectonics, and rapakivi granites as intrusions in an extensional thrust-thickened crust: the Ketilidian orogen, South Greenland. Tectonophysics, **195**, pp.1-10.

WOOD, D.A., JORON, J.L., and TREUIL, M. 1979. A re - appraisal of the use of trace elements to classify and discriminate between magma series erupted in different tectonic settings. Earth and Planetary Science Letters, **45**, pp.326-336.

WOOD, B.J., and WALTHER, J.V. 1986. Fluid flow during metamorphism and its implications for fluid-rock ratios. in "Fluid-Rock Interactions during metamorphism" J.V. walther and B.J. Wood (eds.) advances in Physical Geochemistry **5**, pp.89-108.

WOOD, S.A. 1990. The aqueous geochemistry of the rare-earth elements and yttrium. Chemical Geology, **82**, pp.159-186.

WYLLIE, P.J. 1984. Constraints imposed by experimental petrology on possible and impossible sources and products. Philosophical Transactions of the Royal Society London, **A310**, pp.439-456.

APPENDIX: GEOCHEMICAL METHODS

Sample Preparation

Tati Greenstone Belt mafic rocks are extremely fissile in places and therefore present very difficult problems for sampling. In addition, these rocks contain carbonate alteration veins, which are locally invisible to the naked eye, and brown stained surfaces due to oxidation. Sampling was therefore designed in such way that only representative and relatively fresh samples were collected. Before crushing for geochemical analysis, petrographic investigation was undertaken to screen altered samples.

Mainly chip samples were collected underground along the N9 reef, at the Shashe Mine. However, it was locally possible to collect larger samples. Samples were also collected from cored boreholes. It was only possible to collect part of a core. This is because companies always analyze part of the their core leaving half of the sample for further analysis when necessary. The samples collected were adequate. Up to five centimetre long samples were taken. The same procedure was also followed at Signal Hill.

Samples for geochemical analysis were prepared at both the Botswana Geological Survey and Department of Earth Sciences Geochemical Laboratories. Samples were crushed with a hammer on steel. Crushed rock chips were pulverized for up to two minutes in a tungsten-carbide mill, to powder of at least -100 mesh. The tungsten-carbide rings and the bearing were inspected after each sample, for possible

contamination of the sample powder, by the tungsten-carbide. Where contamination was suspected the sample was noted for special attention.

Major Element Analyses

Loss of ignition (LOI), (volatiles) was determined by weighing the sample powder accurately to 4-10 gms into porcelain crucible, for heating to a temperature of about 1050°C, for at least two hours; after which the sample was cooled in a dessicator and then reweighed to determine LOI. P₂O₅ was colourimetrically analyzed with a Bausch and Lomb Spectronic colorimeter, whereas other major elements were determined by atomic absorption spectroscopy. Analysis were carried out on the Perkin-Elmer Model 370 atomic absorption spectrometer. Precision of this method is indicated in Table I.

TABLE 1a:

Accuracy and precision of Major Element Analyses (based on published values of a standard rock sample). (MA-N GRANITE).

Oxide	P	N	M	M-P	σ	R
SiO ₂	66.6	6	65.61	-0.99	0.08	65.58-65.80
Al ₂ O ₃	17.2	6	17.39	-0.23	0.24	17.13-17.89
Fe ₂ O _{3t}	0.47	6	0.45	-0.02	0.01	0.44-0.45
MgO	0.04	6	0.05	+0.01	0.01	0.04-0.05
CaO	0.59	6	0.58	-0.01	0.01	0.56-0.58
Na ₂ O	5.84	6	5.84	0.00	0.02	5.82-5.87
K ₂ O	3.18	6	3.23	+0.05	0.04	3.18-3.29
TiO ₂	0.01	6	0.00	-0.01	0.00	—
MnO	0.04	6	0.04	0.00	0.00	0.04-0.04

P= published analysed value for the standard sample in weight percent, and are taken from Flanagan (1970); N= number of analysis; M= mean value for the analyses; M-P= mean difference from published values; σ = standard deviation of the analyses and R= range of analyses.

TABLE 1b

Accuracy and precision of Major Element Analyses based on published values of the standard rock sample BE-N BASALT.

Oxide	P	N	M	M-P	σ	R
SiO ₂	38.20	6	38.50	+0.30	0.18	38.21-38.67
Al ₂ O ₃	10.07	6	10.02	-0.05	0.09	9.85-10.00
Fe ₂ O ₃	12.84	6	12.84	0.00	0.11	12.89-12.96
MgO	13.15	6	13.14	-0.01	0.07	13.04-13.27
CaO	13.87	6	13.91	+0.04	0.05	13.84-13.96
Na ₂ O	3.18	6	3.25	+0.07	0.02	3.22-3.28
K ₂ O	1.39	6	1.46	+0.07	0.01	1.45-1.47
TiO ₂	2.61	6	2.59	-0.02	0.04	2.56-2.64
MnO	0.20	6	0.19	-0.01	—	0.19-0.19

Symbols as in Table 1a, and published values are from Flanagan (1970).

Minor Element Analysis

Minor elements (Rb, Sr, Ga, Zr, Y, Nb, Th, U, Pb, Cu, Zn, V, Cr, and Ni), were determined by X-Ray Fluorescence techniques on pressed whole rock pellets, using a Phillips 1450 automatic X-Ray Spectrometer with a rhodium tube. The pellets were made from a mixed powder containing 10 gm sample and 1.5gm binding material (Union Carbide Phenolic Resin). The powder was pressed at 30 tons per square inch for a minute, after which the mixture was baked for 10 minutes at 200°C. Data reduction was done with a Hewlett-Packard 9845B computer.

Accuracy and precisions for minor elements are summarized in Table II, and means are compared with data published by Flanagan, (1973) for the standard W-1.

TABLE II

Precision and accuracy of minor elements analyses in Sample W-1.

E	P(ppm)	N	M(ppm)	M-P	σ
V	260	8	263	+3.00	3.02
Cr	120	8	118	-2.00	4.57
Ni	75	8	76	+1.00	1.69
Cu	110	10	104	-6.00	3.26
Zn	86	6	90	+4.00	1.79
Ga	16	6	18	+2.00	0.89
Pb	8	6	8	0.00	1.27
Rb	21	6	22	+1.00	0.63
Sr	190	6	189	-1.00	2.24
Zr	105	6	98	-7.00	1.55
Y	25	6	22	-3.00	0.89
Nb	9.5	6	8	-1.50	0.45

E=element

REE and Other Trace Elements

A total of thirty-three elements were determined on the ICP-MS using the method outlined by Jenner et al. (1990). The precision and accuracy of the method are illustrated in Table III below, for the REE.

TABLE III

Precision and Accuracy for RRE Analyses for standard rock sample SY-2, compared to published values from Govindaraju (1989).

E	P(ppm)	N	M(ppm)	M-P	σ
La	75.00	8	69.67	-5.33	1.07
Ce	175.00	8	162.57	-12.43	2.11
Pr	18.80	8	20.02	+1.22	0.30
Nd	73.00	8	75.99	+2.99	1.40
Sm	16.10	8	15.94	-0.16	0.26
Eu	2.42	8	2.43	+0.01	0.05
Gd	17.00	8	17.31	+0.31	0.80
Tb	2.50	8	2.89	+0.39	0.44
Dy	18.00	8	19.97	+1.97	0.12
Ho	3.80	8	4.58	+0.78	0.36
Er	12.40	8	15.05	+2.65	0.10
Tm	2.10	8	2.47	+0.37	0.39
Yb	17.00	8	17.67	+0.67	0.06

Lu	2.70	8	2.95	+0.25	
----	------	---	------	-------	--



Xg

Xg

APPENDIX A

GEOLOGICAL MAP OF TATI GREENSTONE BELT

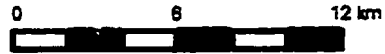
BY

A.R. TOMBALE

1982

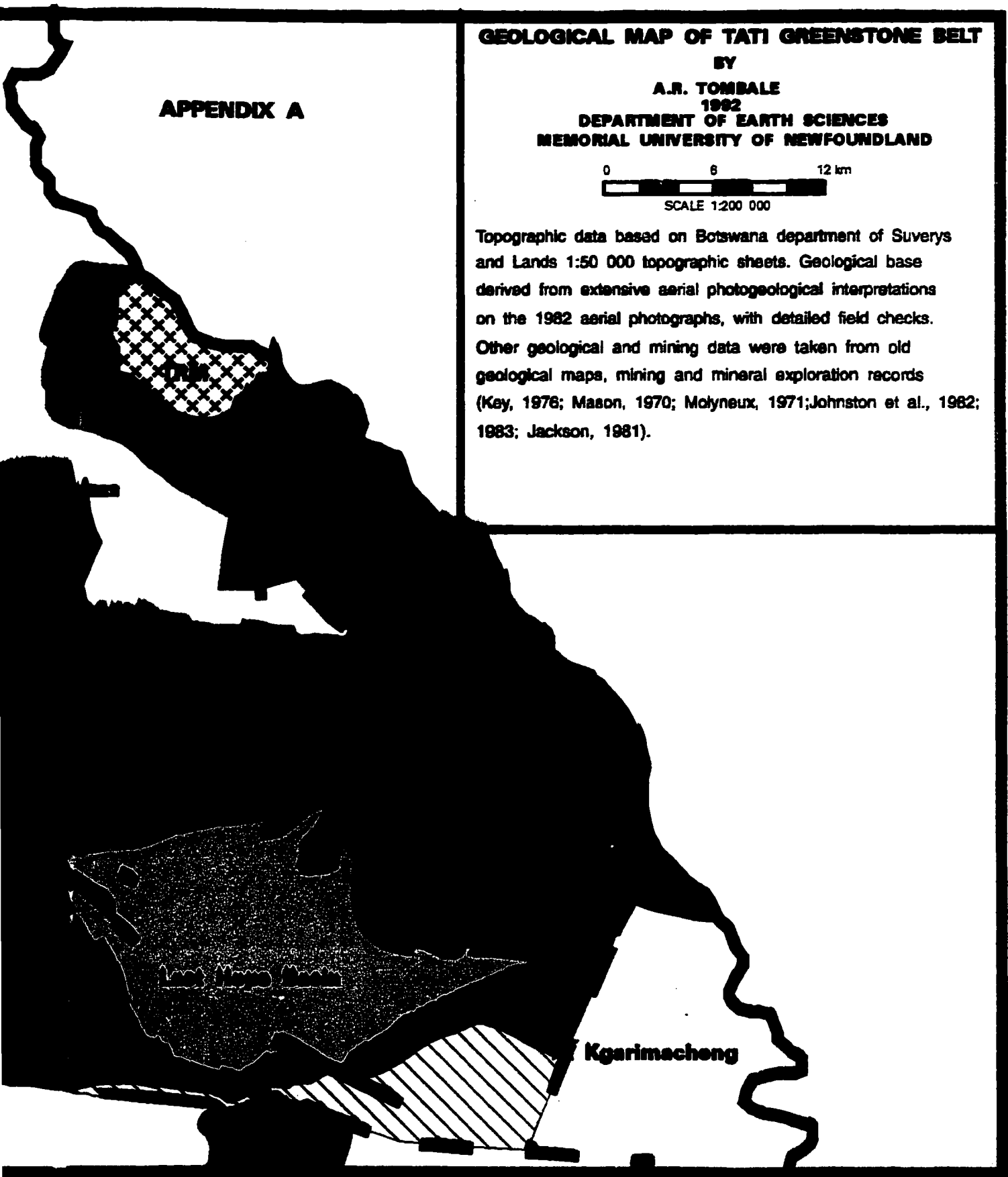
DEPARTMENT OF EARTH SCIENCES

MEMORIAL UNIVERSITY OF NEWFOUNDLAND



SCALE 1:200 000

Topographic data based on Botswana department of Suverys and Lands 1:50 000 topographic sheets. Geological base derived from extensive aerial photogeological interpretations on the 1982 aerial photographs, with detailed field checks. Other geological and mining data were taken from old geological maps, mining and mineral exploration records (Key, 1976; Mason, 1970; Molyneux, 1971; Johnston et al., 1982; 1983; Jackson, 1981).



GEOLOGICAL MAP LEGEND (APPENDIX B)

(a) SUPRACRUSTAL ROCKS



Arkose/grits/sandstones/conglomerates and calcareous sediments

LAST HOPE GROUP



Basalts/Andesites/Rhyolites and minor sediments.

SELKIRK GROUP



Banded iron formatins/limestones and quartz-mica schists.

DINUKU FORMATION

PHENALONGA GROUP



Basaltic andesites/andesites/dacites/rholites agglomerates and minor sediments.
Aluminous Schists (HALFWAY KOP FORMATION)

SEKUKWE SUBGROUP



Basalts/Andesites/Rhyolites and minor sediments.

GOLDEN EAGLE FORMATION



Basalts/Andesites/Rhyolites and minor sediments.

MATSILOJE FORMATION

LADY MARY GROUP



Basalts and gabbroic sills

MAP-NORA FORMATION



Ultramafic schists/serpentinites komatiites and minor sediments

OLD TATI FORMATION

(b) GRANITOID ROCKS



Troctolites/gabbros/serpentinites diorites and tonalites

Selkirk Igneous Complex



Leucogabbro/gabbros/high-Mg tonalites and granodiorites

Mphoeng Plutonic Complex



Ramokgwebana

 Troctolites/gabbros/serpentinites
diorites and tonalites

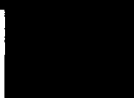
 Leucogabbro/gabbros/high-Mg
tonalites and granodiorites

 Megacrystic Feldspar Granite

Selkirk Igneous
Complex

Mphoeng Plutonic
Complex

Ramokgwebana
Granite

 Basaltic andesites/andesites/dacites/rholites
agglomerates and minor sediments.
Aluminous Schists (HALFWAY KOP FORMATION)

SEKORWE
SUBGROUP

 Basalts/Andesites/Rhyolites
and minor sediments.

GOLDEN EAGLE
FORMATION

 Basalts/Andesites/Rhyolites
and minor sediments.

MATSILOJE
FORMATION

 Basalts and gabbroic sills

MAP-NORA
FORMATION

 Ultramafic schists/serpentinites
komatiites and minor sediments

OLD TATI
FORMATION

LADY MARY
GROUP

(b) GRANITOID ROCKS

 Troctolites/gabbros/serpentinites
diorites and tonalites

 Leucogabbro/gabbros/high-Mg
tonalites and granodiorites

 Megacrystic Feldspar Granite

 Trondhjemites

 High-Mg granodiorites and granites

 Trondhjemites

 Biotite-hornblende tonalites

 Granodiorites

 Trondhjemites/tonalites/granodiorites
megacrystic feldspar granites and
granites.

Selkirk Igneous
Complex

Mphoeng Plutonic
Complex

Ramokgwebana
Granite

Hillview Pluton

Airport Pluton

South Tati
Pluton

Matsiloje
Batholith

New Zealand
Pluton

Tati Batholith

APPENDIX C



METALLOGENIC MAP OF TATI GREENSTONE BELT NORTHEAST BOTSWANA

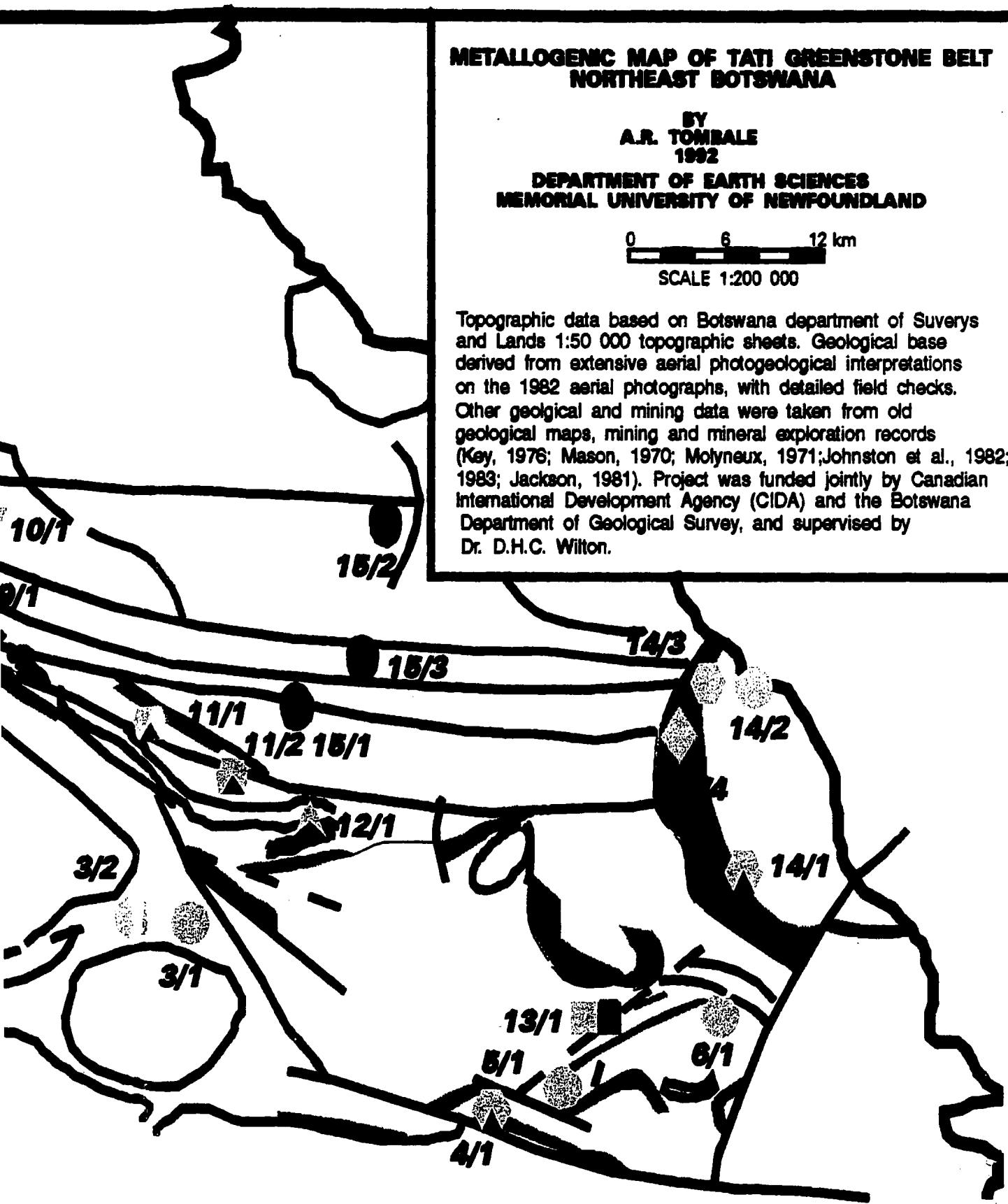
BY
A.R. TOMBALE
1982

DEPARTMENT OF EARTH SCIENCES
MEMORIAL UNIVERSITY OF NEWFOUNDLAND



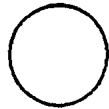
SCALE 1:200 000

Topographic data based on Botswana department of Suverys and Lands 1:50 000 topographic sheets. Geological base derived from extensive aerial photogeological interpretations on the 1982 aerial photographs, with detailed field checks. Other geological and mining data were taken from old geological maps, mining and mineral exploration records (Key, 1976; Mason, 1970; Molyneux, 1971; Johnston et al., 1982; 1983; Jackson, 1981). Project was funded jointly by Canadian International Development Agency (CIDA) and the Botswana Department of Geological Survey, and supervised by Dr. D.H.C. Wilton.



METALLOGENIC MAP

RELATIONSHIP OF MINERAL DEPOSIT TYPES TO HOST ROCKS



Lode gold deposits hosted by shear zones in ultramafic rocks of the Lady Mary Formation



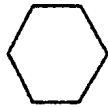
Lode gold deposits hosted by shear zones in calcareous rocks of the Penhalonga Formation



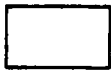
Lode gold deposits hosted by shear zones in siliceous rocks of the Selkirk Formation



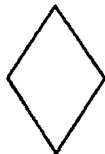
Lode gold deposits hosted by shear zones at contact between granitoids and supracrustal rocks



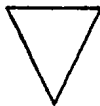
Lode gold deposits hosted by shear zones at contact between banded iron formation and schistose rocks



Lode gold deposits hosted by shear zones in metasedimentary rocks of the Last Hope Formation



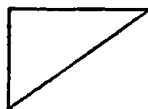
Lode gold deposits hosted by shear zones in barren rocks



Lode gold deposits hosted by shear zones in granitoid rocks



Massive sulfide deposits



Kyanite mineralization

LEGEND (APPENDIX D1).

T TO GEOLOGY

c-mafic

ine

rocks

between

between

imentary

ron formations

3

COMMODITIES



Gold (Au)



Silver (Ag)



Antimony (Sb)



Nickel (Ni)



Copper (Cu)



Platinum Group Elements (PGE)



Lead (Pb)



Zinc (Zn)



Kyanite

RELATIVE IMPORTANCE OF COMMODITIES



One major commodity



Two major commodities



Three major commodities



One major and two minor commodities

COMMODITIES

RELA



Gold (Au)



Silver (Ag)



Antimony (Sb)



Nickel (Ni)



Copper (Cu)



Platinum Group Elements (PGE)



Lead (Pb)



Zinc (Zn)



Kyanite

RELATIVE IMPORTANCE OF COMMODITIES



One major commodity



Two major commodities



Three major commodities



One major and two minor commodities

E)

METALLOGENIC MAP LEGI

MINERAL DEPOSIT GROUPS

METALLIC ASSOCIATION

1. SHASHE GROUP

1/1 New Prospect Mine

Au-Sb-W-Li-Be

1/2 Durham Mine

Au-(Au)-As-Sb-Zn-Cu

1/3 Shashe Mine

Au-As-Sb-Pb-Zn-Cu

1/4 Todd's Creek Mine

Au-As-Sb-Pb-Zn-Cu

1/5 Lady Mary Mine

Au-As-Ag-Pb-Zn-Cu

1/6 Phoenix Mine

Au-As-Ag-Pb-Zn-Cu

2. GOLDEN EAGLE GROUP

2/1 Golden Eagle Mine

Au-Ag-As-W-Cu

3. CHARLIE GROUP

3/1 Charlie Mine

Au

3/2 Phoenician Mine

Au

4. NEW ZEALAND GROUP

4/1 New Zealand Mine

Au-Ag

5. BLUE JACKET GROUP

5/1 Blue Jacket Mine

Au

6. FLORA GROUP

6/1 Flora Mine

Au

7. MONARCH GROUP

7/1 Monarch Mine

Au-Ag-As-Cu-Bi

7/2 Amelia Mine

Au-Ag-As-Cu-Bi

8. FRANCISTOWN GROUP

8/1 Sam's Reef Mine

Au-Ag-As-Cu-Bi

8/2 Baron Rothchild's Mine

Au

GENIC MAP LEGEND (APPENDIX D3).

SOCIATION

9. BONANZA GROUP

9/1 Bonanza Mine Au-Ag

10. CHERISHED HOPE GROUP

10/2 Cherished Hope Mine Au

11. PENHALONGA GROUP

11/1 Penhalonga Mine Au-Ag-Pb-Zn-Cu-W

11/2 Helstone Mine Au

12. VERMAAK GROUP

12/1 Vermaak Mine Au-Ag-W

13. SIGNAL HILL GROUP

13/1 Signal Hill Mine Au-(Au)-Sb-As-Zn-Cu

14. RAINBOW GROUP

14/1 Rainbow Mine Au-Ag-As-Cu-W

14/2 Falcon Mine Au

14/3 Matsiloje Mine Au-W

14/4 Jim's Luck Mine Au-W

15. MASSIVE SULFIDE DEPOSITS

15/1 Selkirk Mine Ni-Cu-PGE

15/2 Phoenix Prospect Ni-Cu

15/3 Tekwane Mine Cu-Ni

(Geological base for the metallogenic map is shown on APPENDIX A whereas structural base is summarised on Chapter 4).

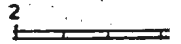
27°30'
21° 00'

27° 40'

21°10'

1.5 3A U P I 3





- 16 Dolerit
- 15 Syenit
- 14 Granod
- 13 Diorite
- 12 Granit
- 11 Granod
- 10 Trocto
- 9 Serper

- 8 Porphy
Undiffe

- 7 Amphit
Quartz
Marble
Undiffe

- bi
s
lm 6 Chlorite
Schist, s
limestor

- bi
lm 5 Actinoli
Schists,
minor

- bi
lm 4 Graphit
limesto
Quartz

- lm
bi 3 Graphi
Undiffe
limesto

- lm 2 Limesto
chlorit

- lm
bi 1 Kyanite
Meta-a
sericite

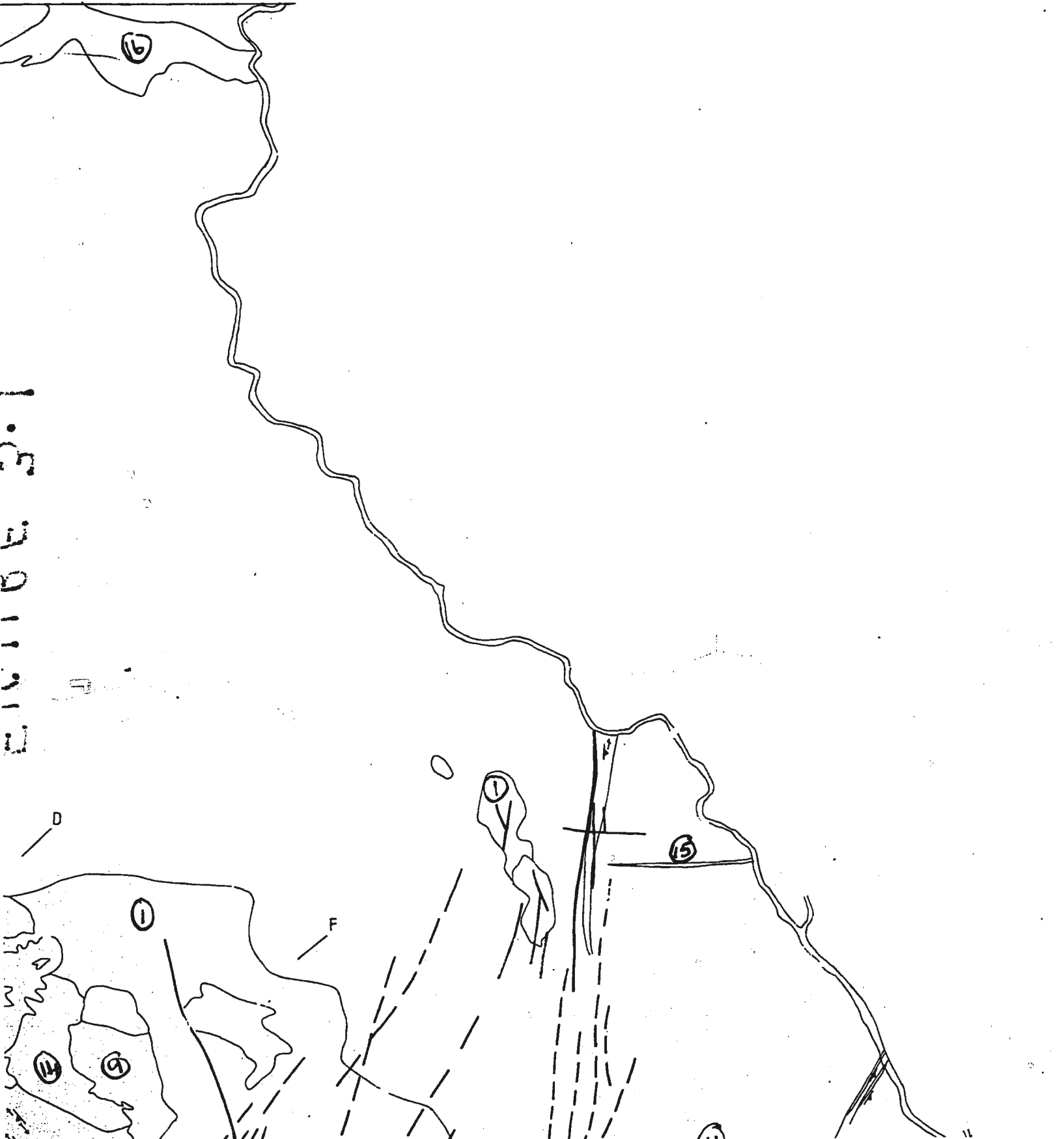
- lm
bi
lm 0 Undiffe

- lm
bi
lm 1 Phyllite

- 1 Porphy



27° 40'

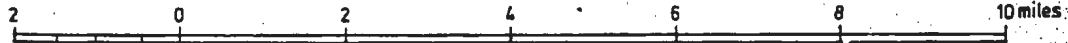


1:30
110
111
112
113
114
115
116
117
118
119
120

GOLD FIELDS BOTSWANA (PTY) LTD

SOUTHERN TATI AREA By R. Mason 1965-1966

Scale 1:125,000



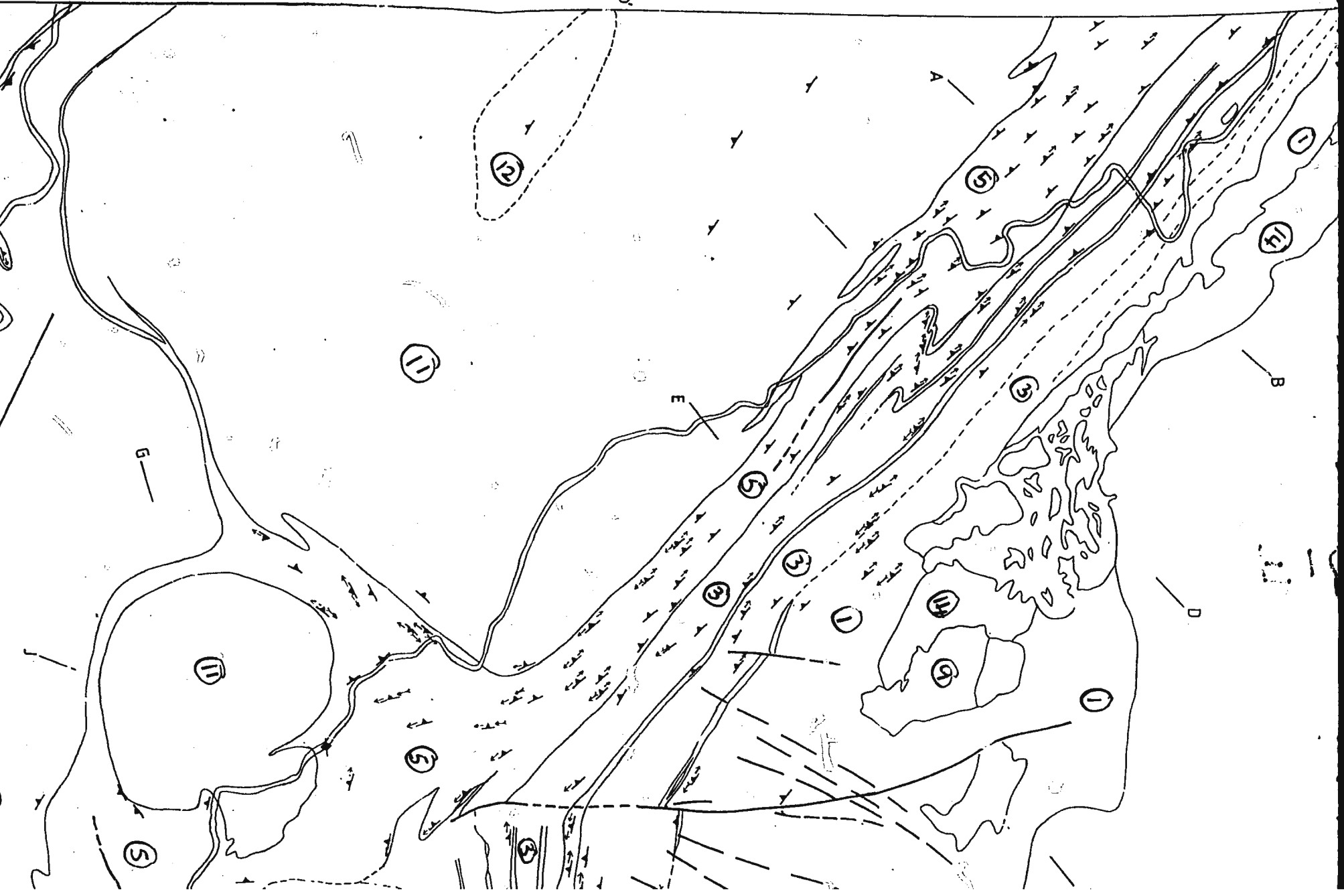
LEGEND

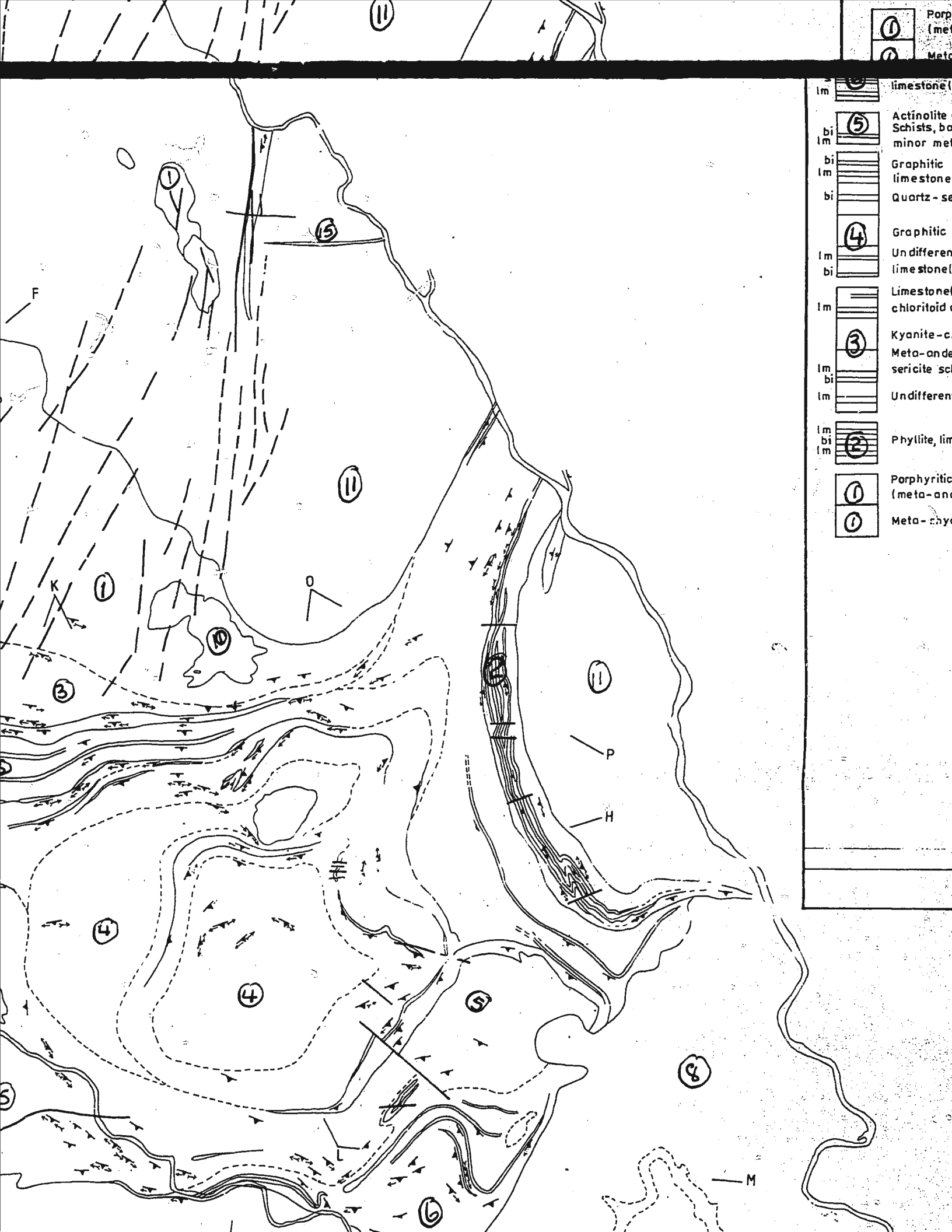
(16)	Dolerite	INTRUSIVE ROCKS
(15)	Syenite	
(14)	Granodiorite	
(13)	Diorite	
(12)	Granite	
(11)	Granodiorite	
(10)	Tractolitic Gabbro	
(9)	Serpentinite	
(8)	Porphyroblastic gneiss Undifferentiated paragneiss	GNEISSIC FORMATION
(7)	Amphibolite Quartzite Marble Undifferentiated	BAINES DRIFT FORMATION
bi s lm (6)	Chlorite, tremolite-chlorite and talc-antigorite Schist, serpentinite(s), banded ironstone (bi), limestone (lm) minor meta-sedimentary rocks	OLD TATI SERIES
bi lm (5)	Actinolite chlorite-tremolite and chlorite-talc Schists, banded ironstone (bi) limestone (lm), minor meta-sedimentary rocks	
bi lm (4)	Graphitic phyllite, banded ironstone (bi), limestone (lm)	LADY MARY SERIES
bi lm (3)	Quartz-sericite schist, banded ironstone (bi)	
lm bi (2)	Graphitic phyllite Undifferentiated meta-sedimentary rocks, limestone (lm) banded ironstone (bi)	LAST HOPE SERIES
lm bi (1)	Limestone (lm) tremolite-quartz biotite, kyanite - chloritoid and quartz-chlorite-muscovite schists	
lm bi lm (3)	Kyanite-chloritoid schist. Meta-andesite, actinolite schist, minor quartz sericite schist, limestone (lm), banded ironstone (bi)	PENHALONGA SERIES
lm bi lm (2)	Undifferentiated Penhalonga Series..	
lm bi lm (2)	Phyllite, limestone (lm), banded ironstone (bi)	MATSILOJE SERIES
(1)	Porphyritic meta-volcanic rocks	

BULAWAYAN

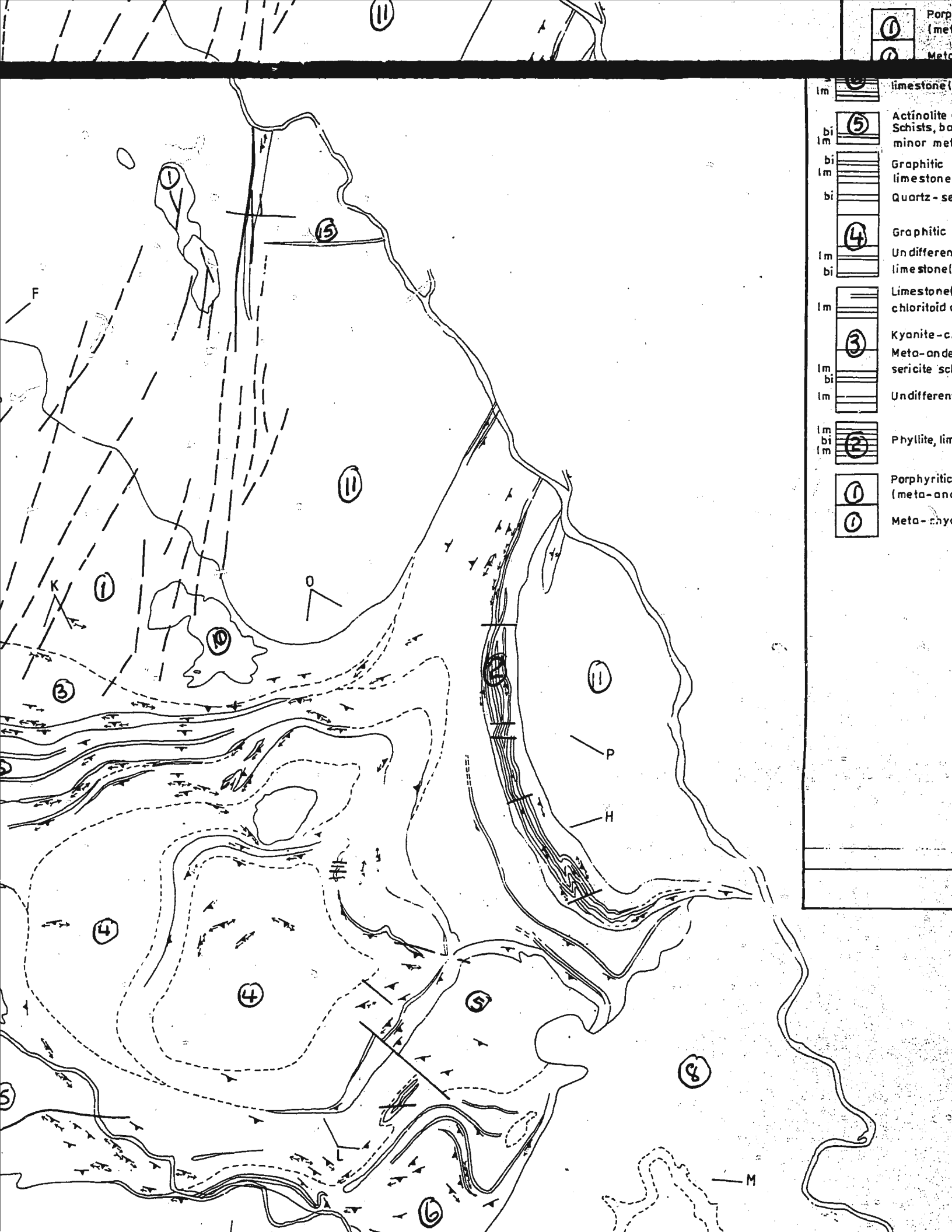
SYSTEM

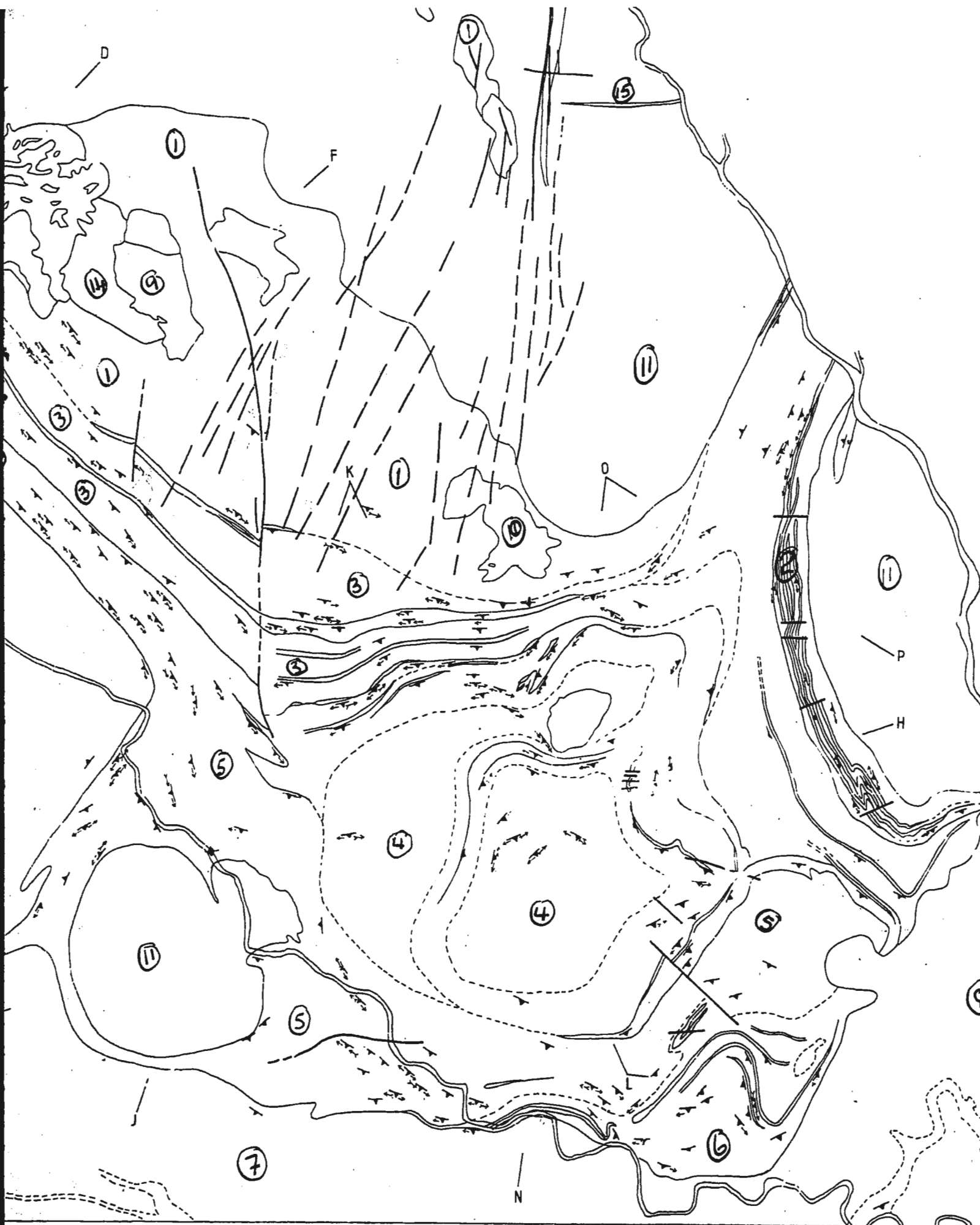
21° 20'





①	Porphyritic (meta- and)
②	Meta-phyllite
③	Undifferentiated limestone
④	Undifferentiated limestone
⑤	Graphitic limestone
⑥	Quartz-schist
⑦	Graphitic limestone
⑧	Actinolite schists, basic
⑨	Minor metachert
⑩	limestone
⑪	limestone





bi	Graphitic phyllite, banded ironstone (bi), limestone (lm)	} LAST HOPE SERIES	} BULAWAYAN		
lm					
bi	Quartz-sericite schist, banded ironstone (bi)				
④	Graphitic phyllite				
lm	Undifferentiated meta-sedimentary rocks, limestone (lm) banded ironstone (bi)				
bi					
lm	Limestone (lm) tremolite-quartz biotite, kyanite-chloritoid and quartz-chlorite-muscovite schists			} PENHALONGA SERIES	} SYSTEM
③					
lm	Meta-andesite, actinolite schist, minor quartz sericite schist, limestone (lm), banded ironstone (bi)				
bi					
lm	Undifferentiated Penhalonga Series.				
lm	Phyllite, limestone (lm), banded ironstone (bi)	} MATSILOJE SERIES			
bi					
lm	Porphyritic meta-volcanic rocks (meta-andesite, meta-dacite)	} SELKIRK SERIES			
①					
①	Meta-rhyolite				



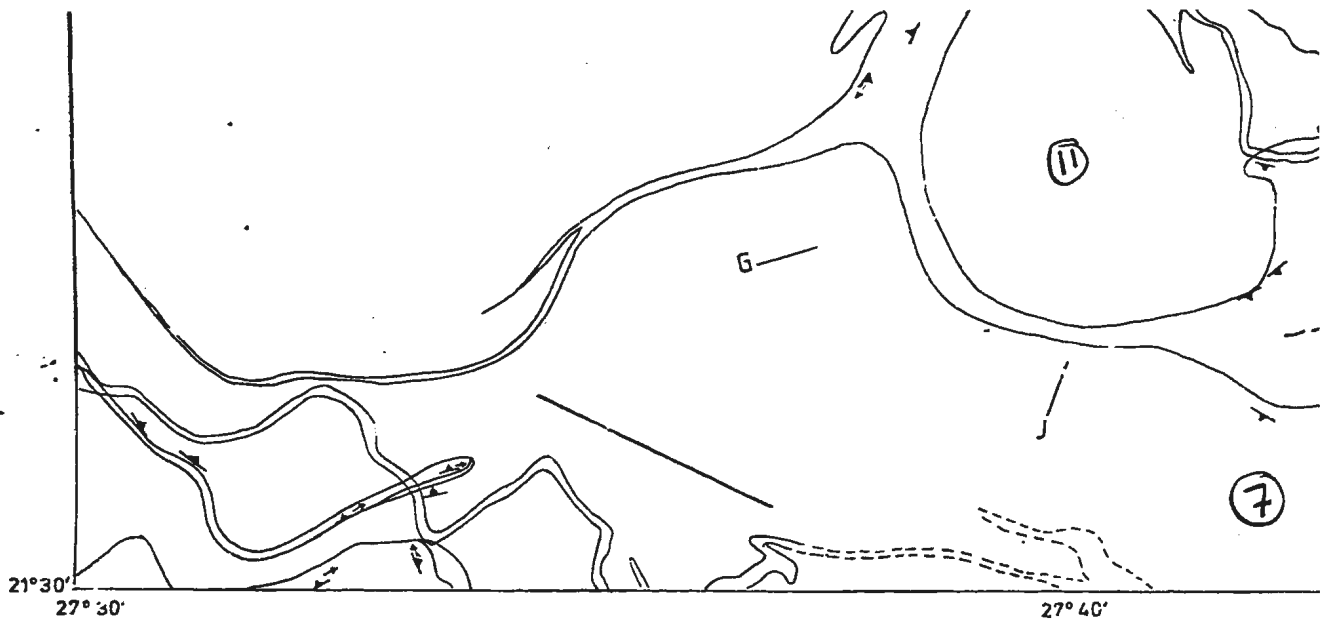
Date 18 / 11 / 85

Drawn by J. Chikwe

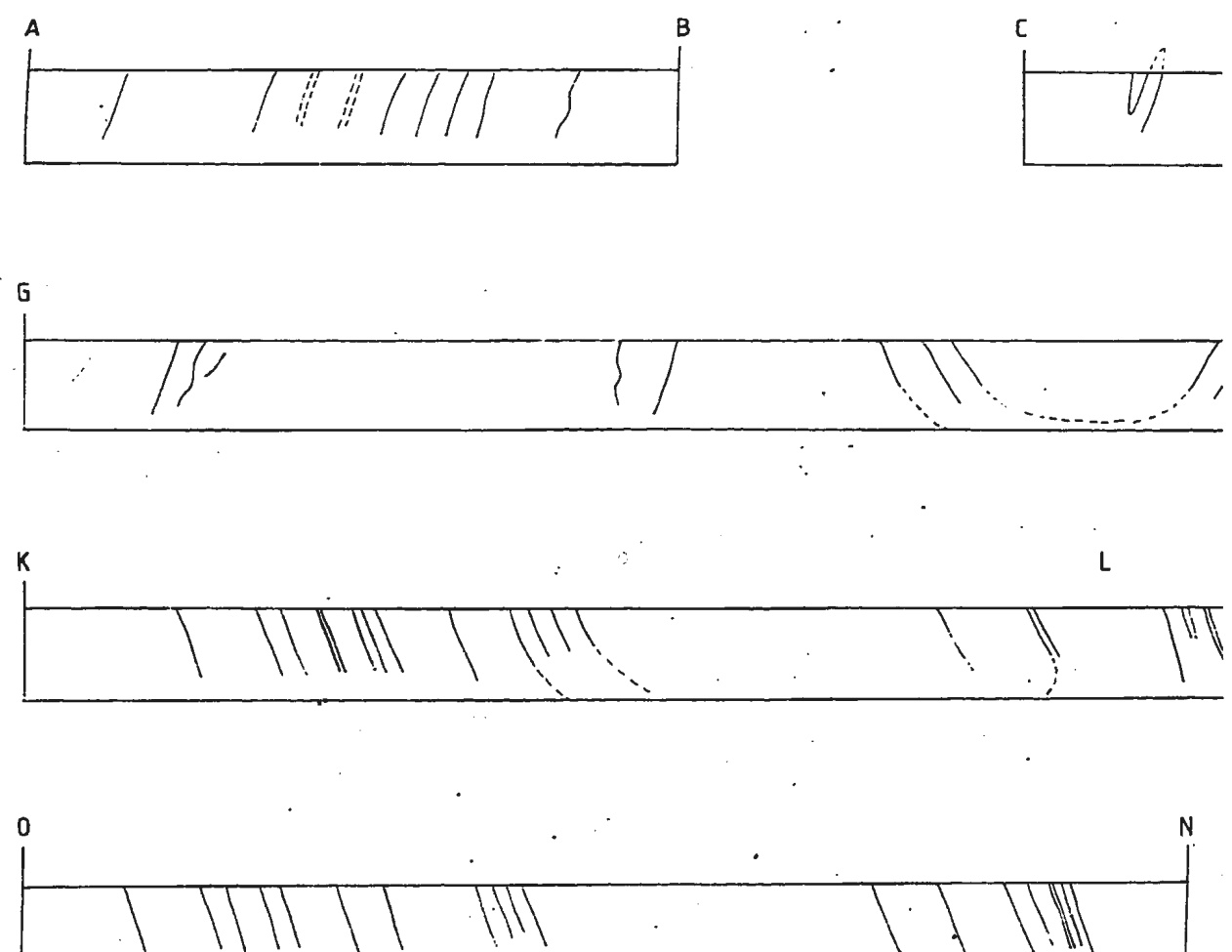
- ↖ Strike and Dip of schistosity
- ↖ Vertical schistosity
- ↖ Plunge of mineral lineation on schistosity surfaces
- ↖ Plunge of crenulate lineation on schistosity surfaces
- Faults and shears
- ~ Geological boundary
- - - Inferred geological boundary

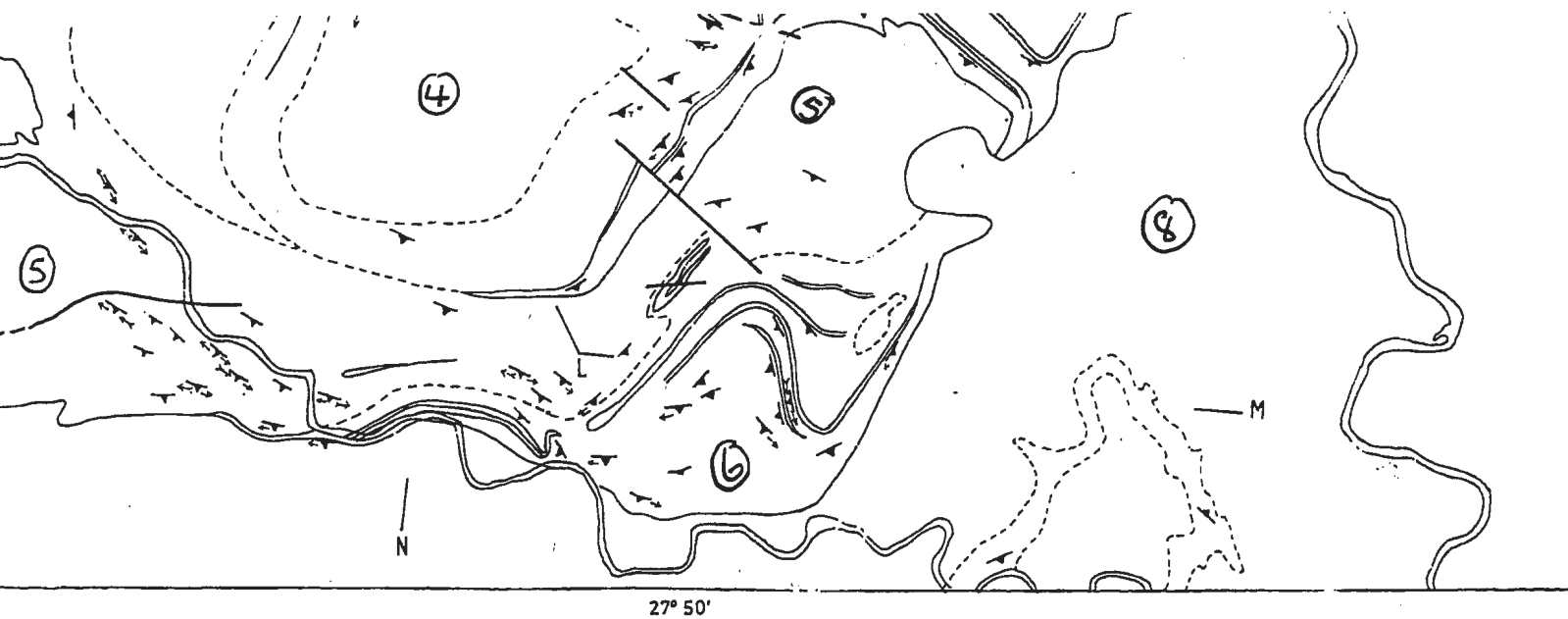
A — B Line of section

||| Rivers

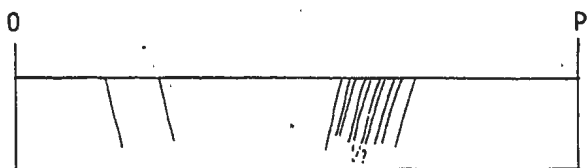
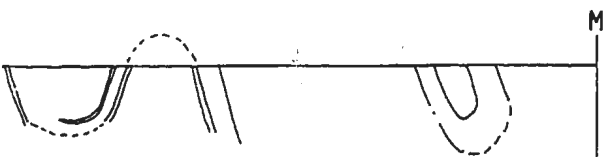
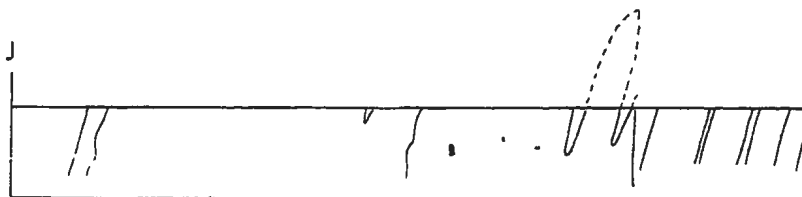
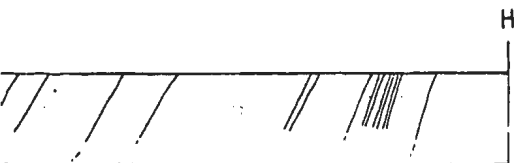
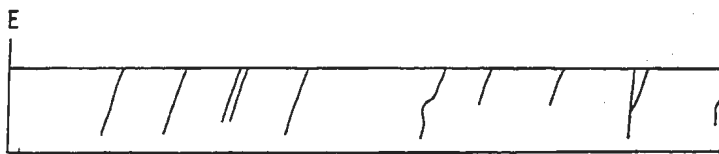
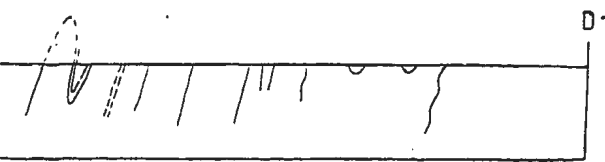


SECTIONS

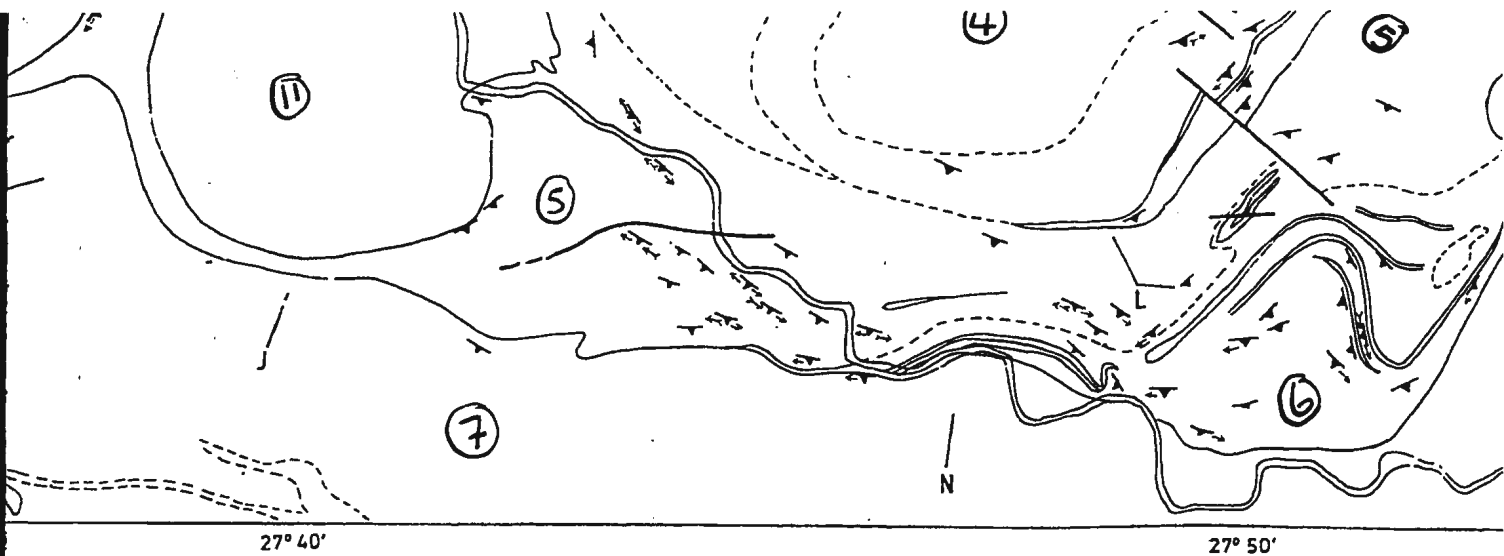




ACROSS THE SCHIST BELT



GEOLOGICAL M
 BELT (FROM M
 BY GOLDFIELD



SECTIONS ACROSS THE SCHIST BELT

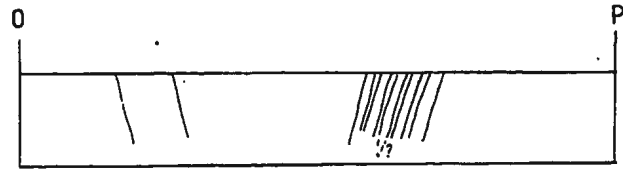
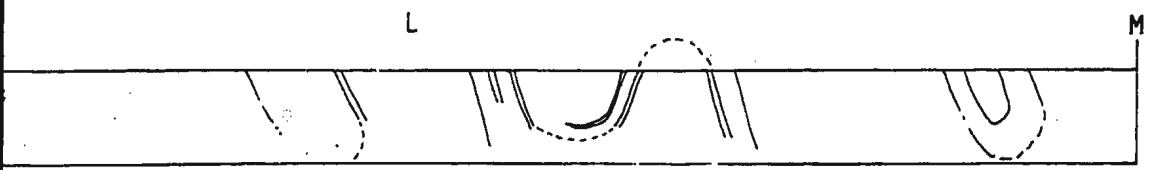
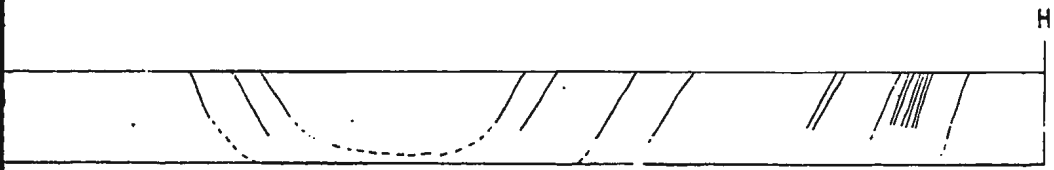
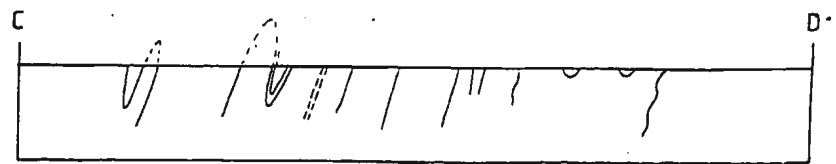


FIG
MAP
MAS
DS

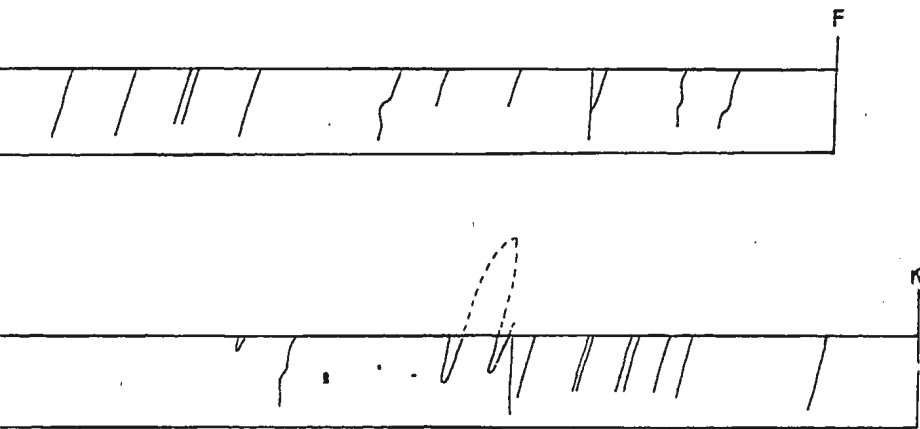
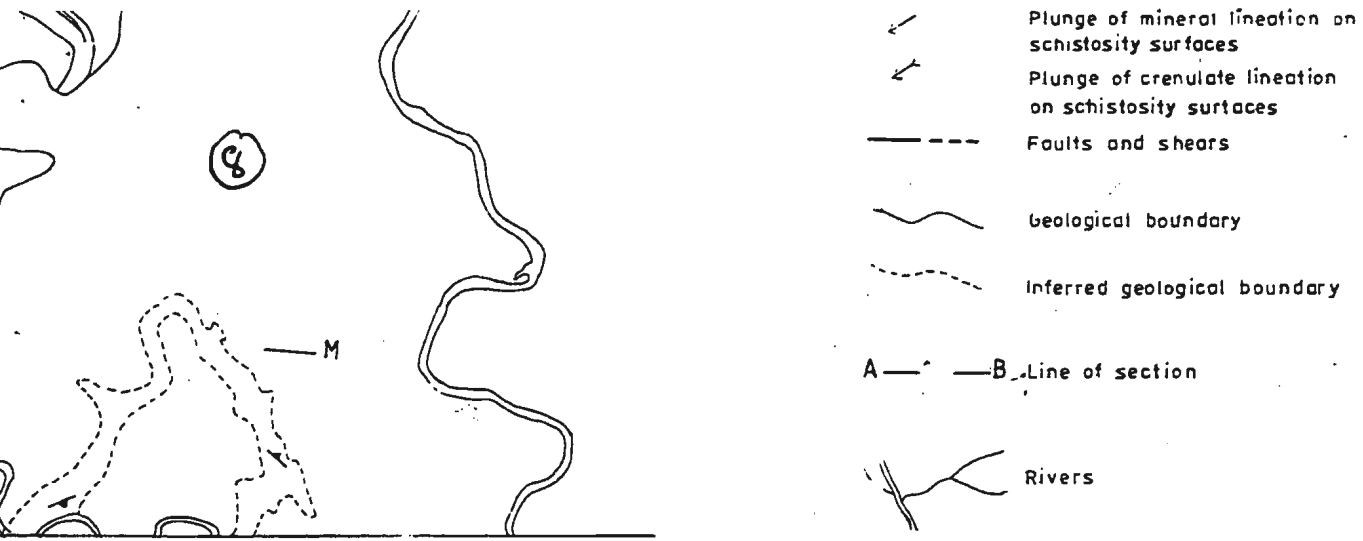


FIGURE 3.1

GEOLOGICAL MAP OF THE TATI GREENSTONE BELT (FROM MASON, 1970; AND REDRAWN BY GOLDFIELDS DOTSWANA (PTY) LTD, 1985).

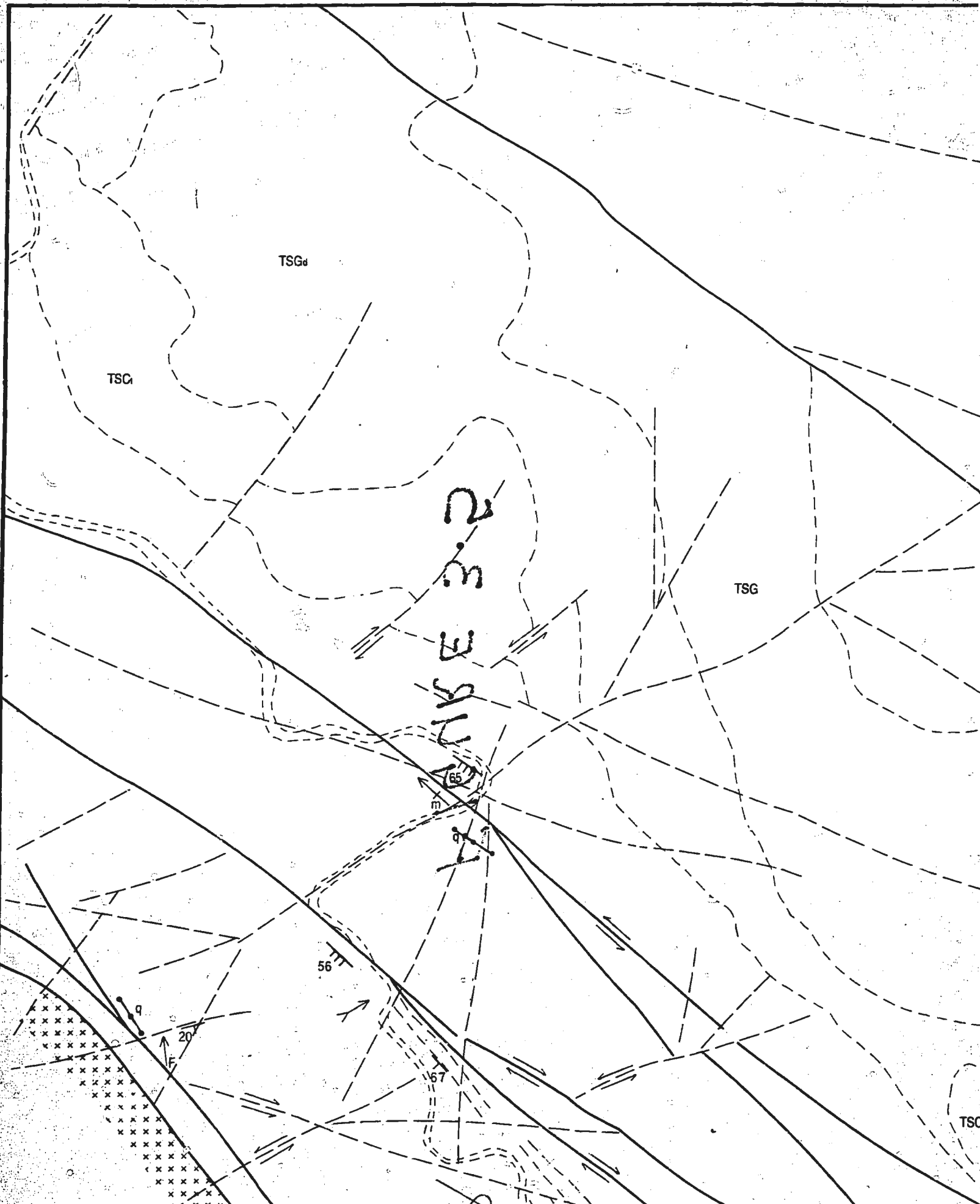
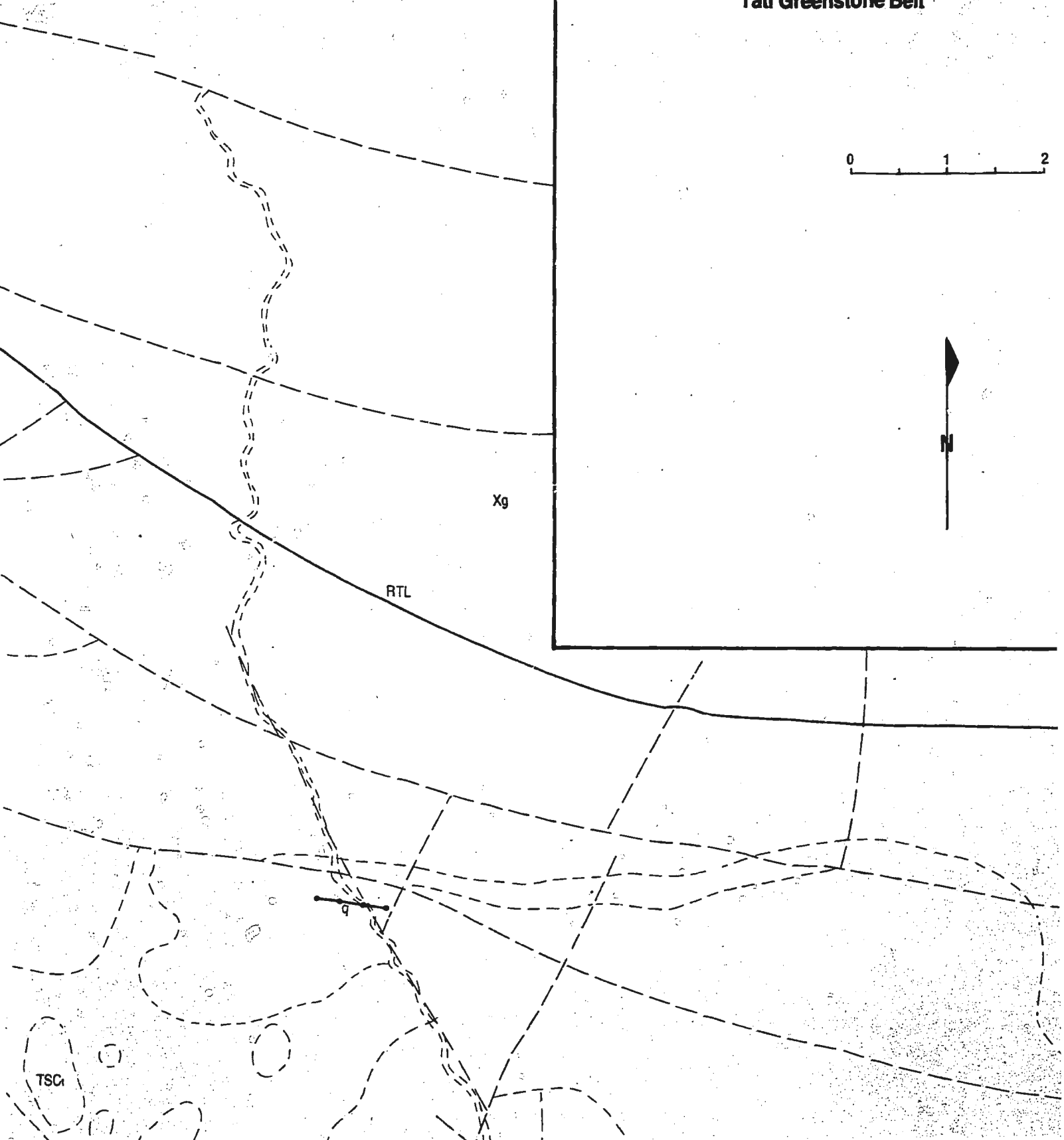


Figure 3.5: Simplified Geological Map of the V Tati Greenstone Belt



em Z

TSGd

2
m
E
S
I
L
E

TSG

65

56

20

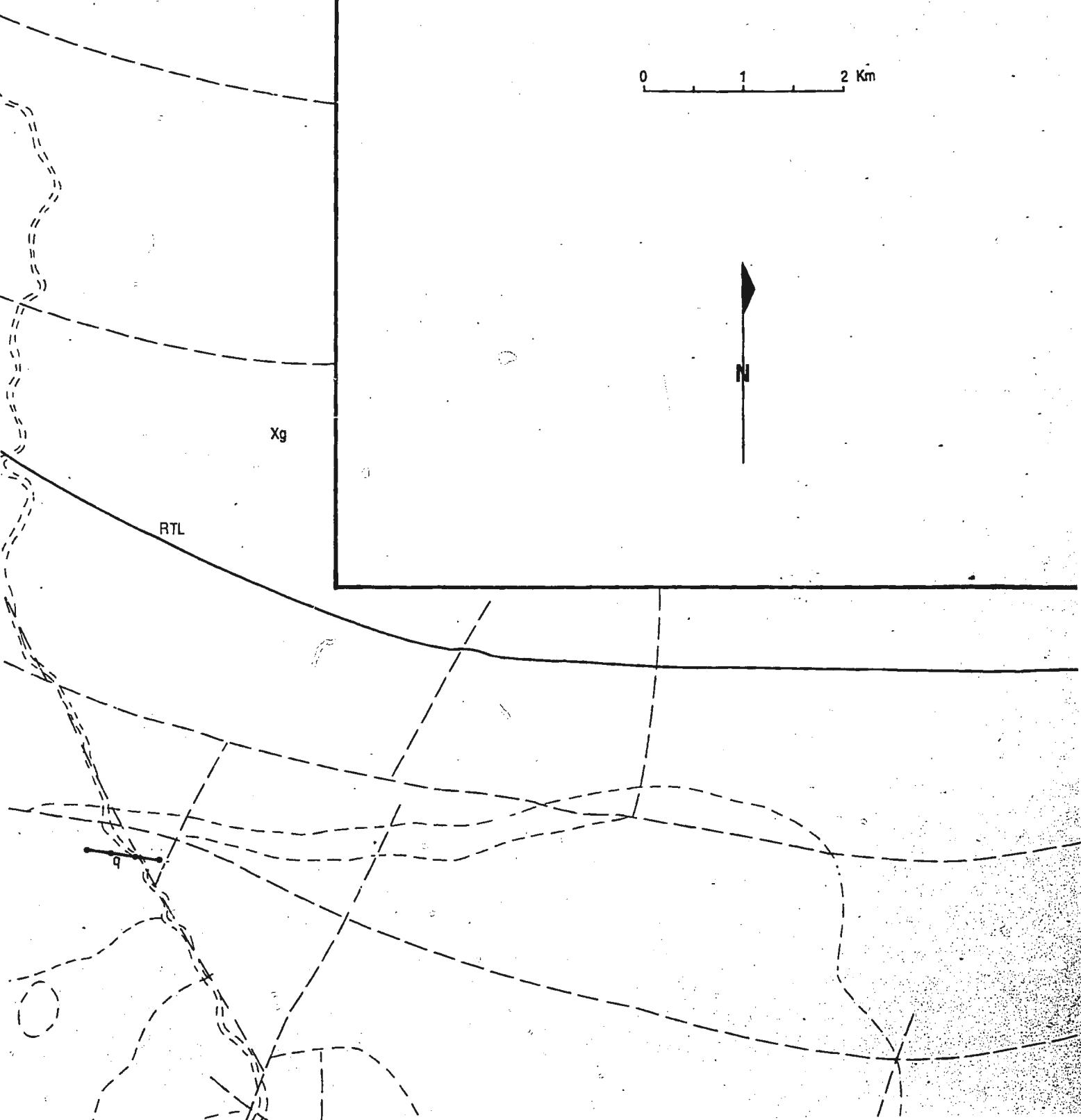
67

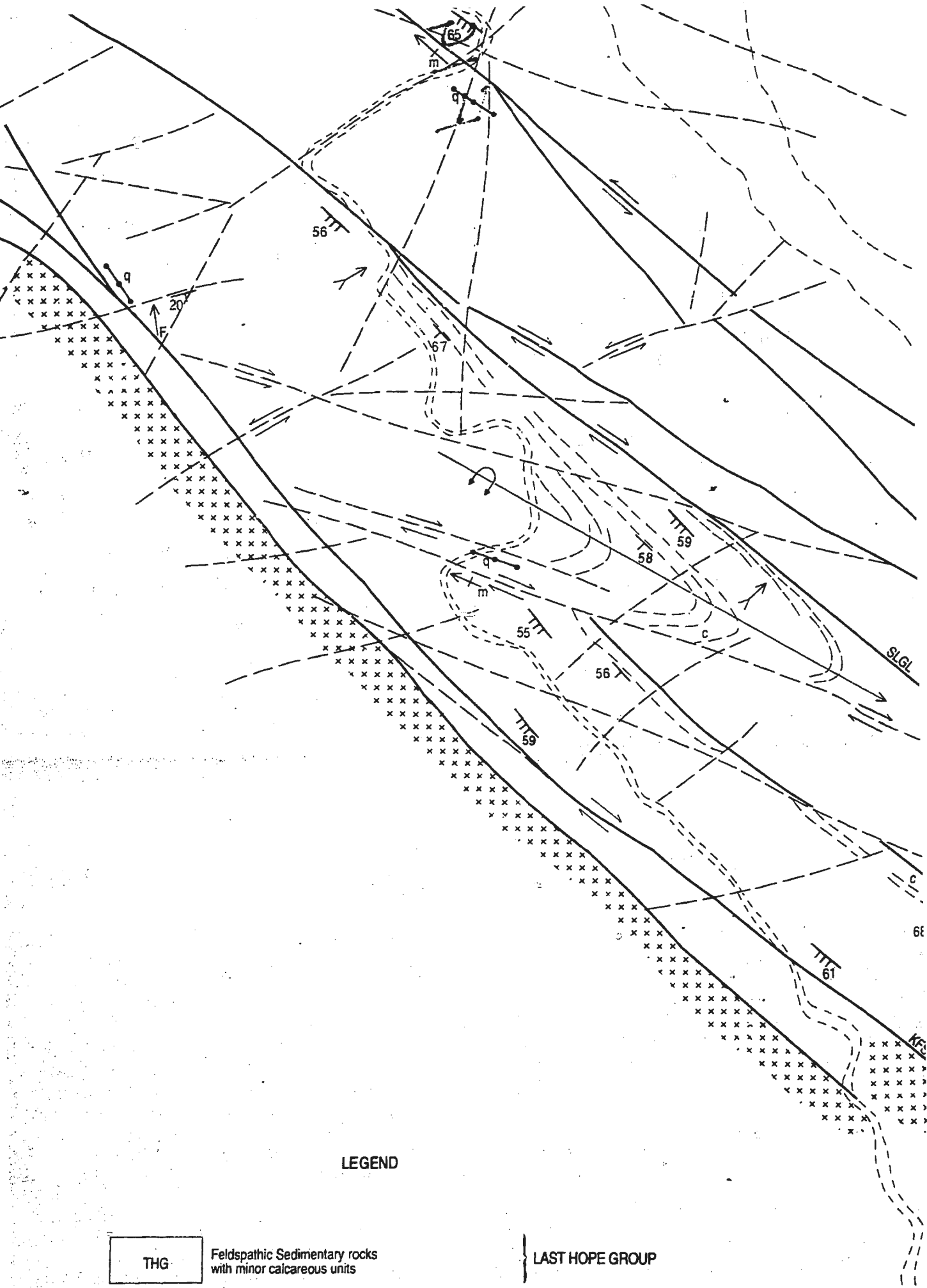
TSC



62

Figure 3.5: Simplified Geological Map of the Western Zone of the Tati Greenstone Belt



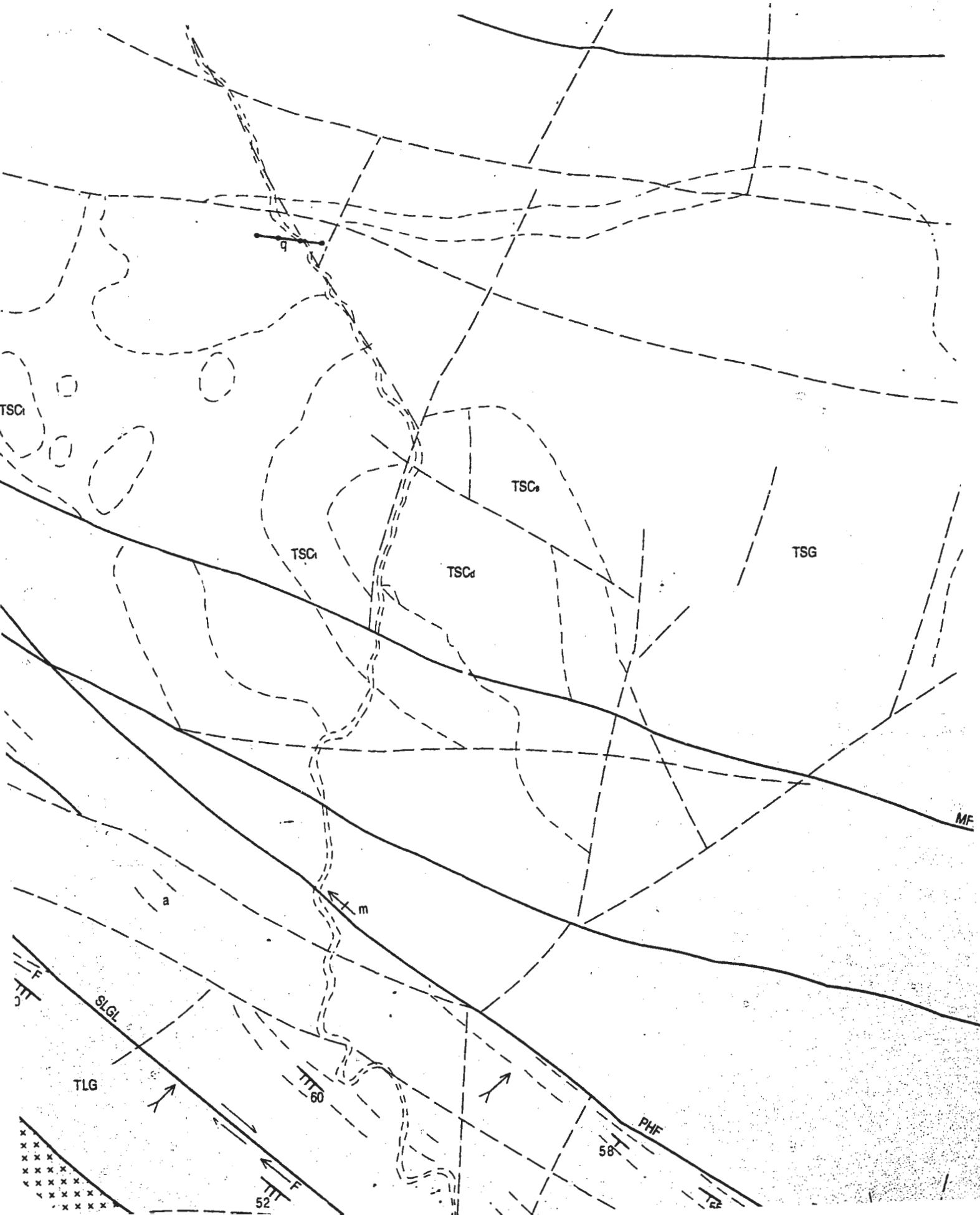


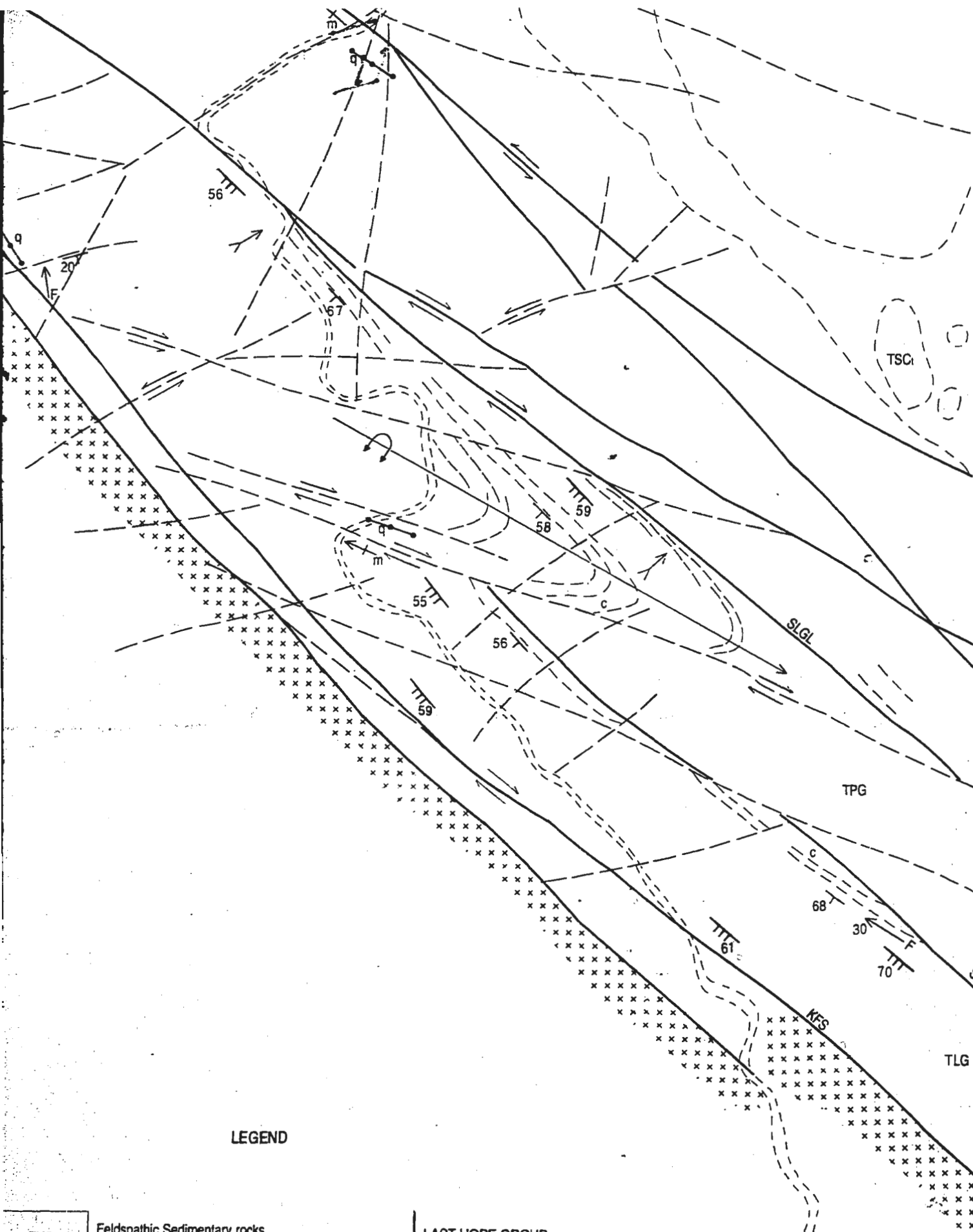
LEGEND

THG

Feldspathic Sedimentary rocks
with minor calcareous units

LAST HOPE GROUP

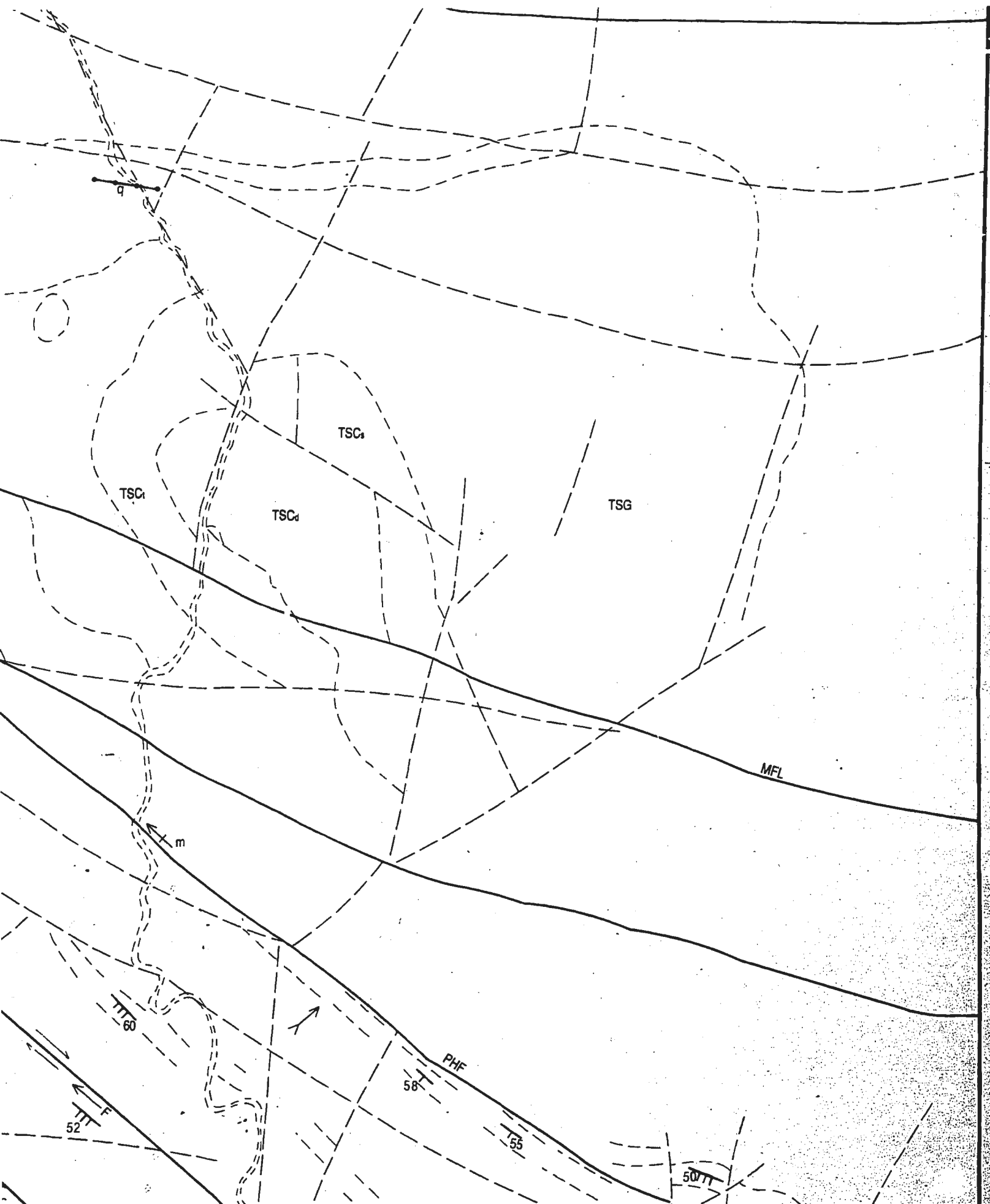




LEGEND

- THG
 Feldspathic Sedimentary rocks with minor calcareous units
- TSG
 Calc-alkaline volcano-Plutonic rocks with

- LAST HOPE GROUP
- SELKIRK GROUP



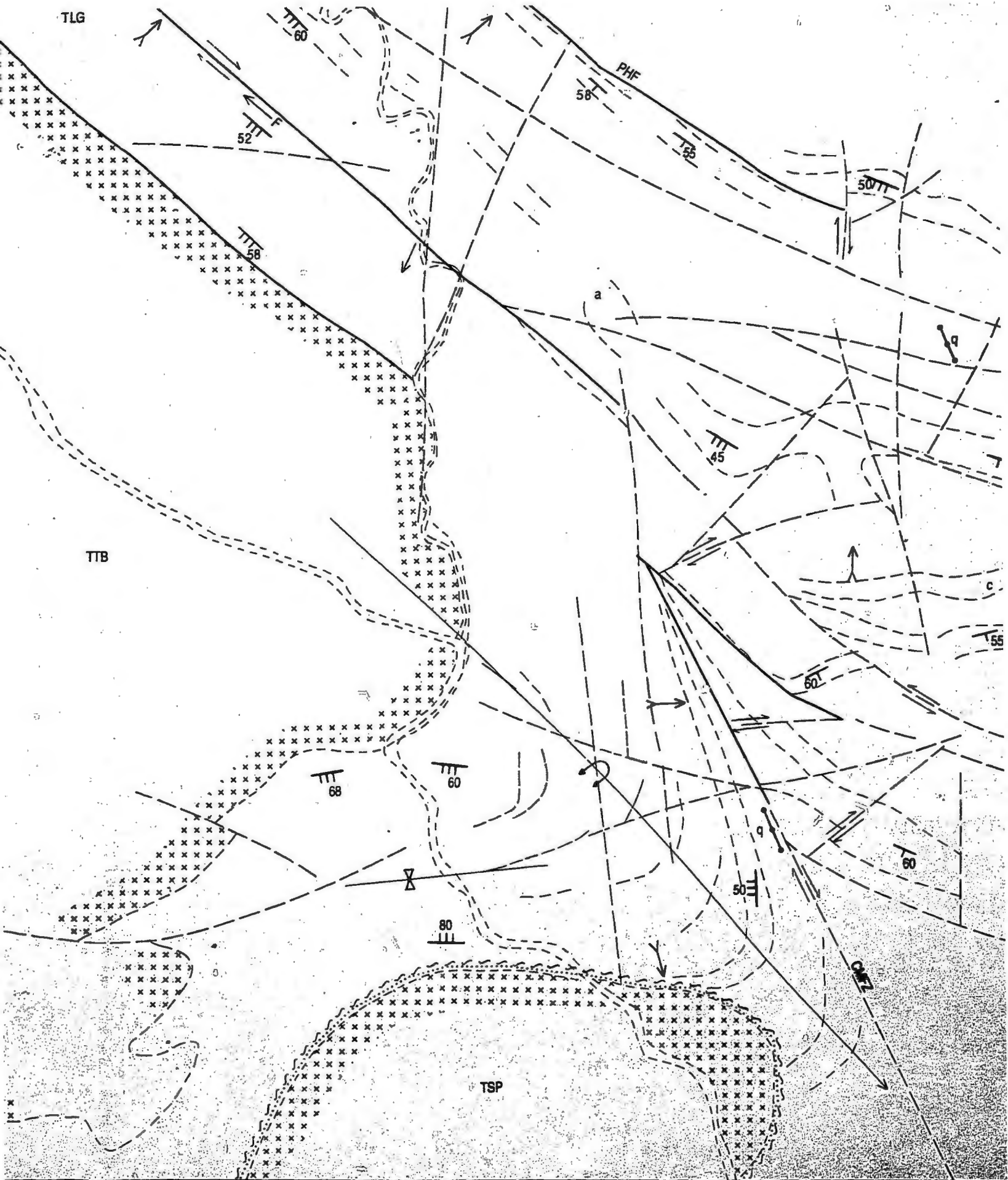


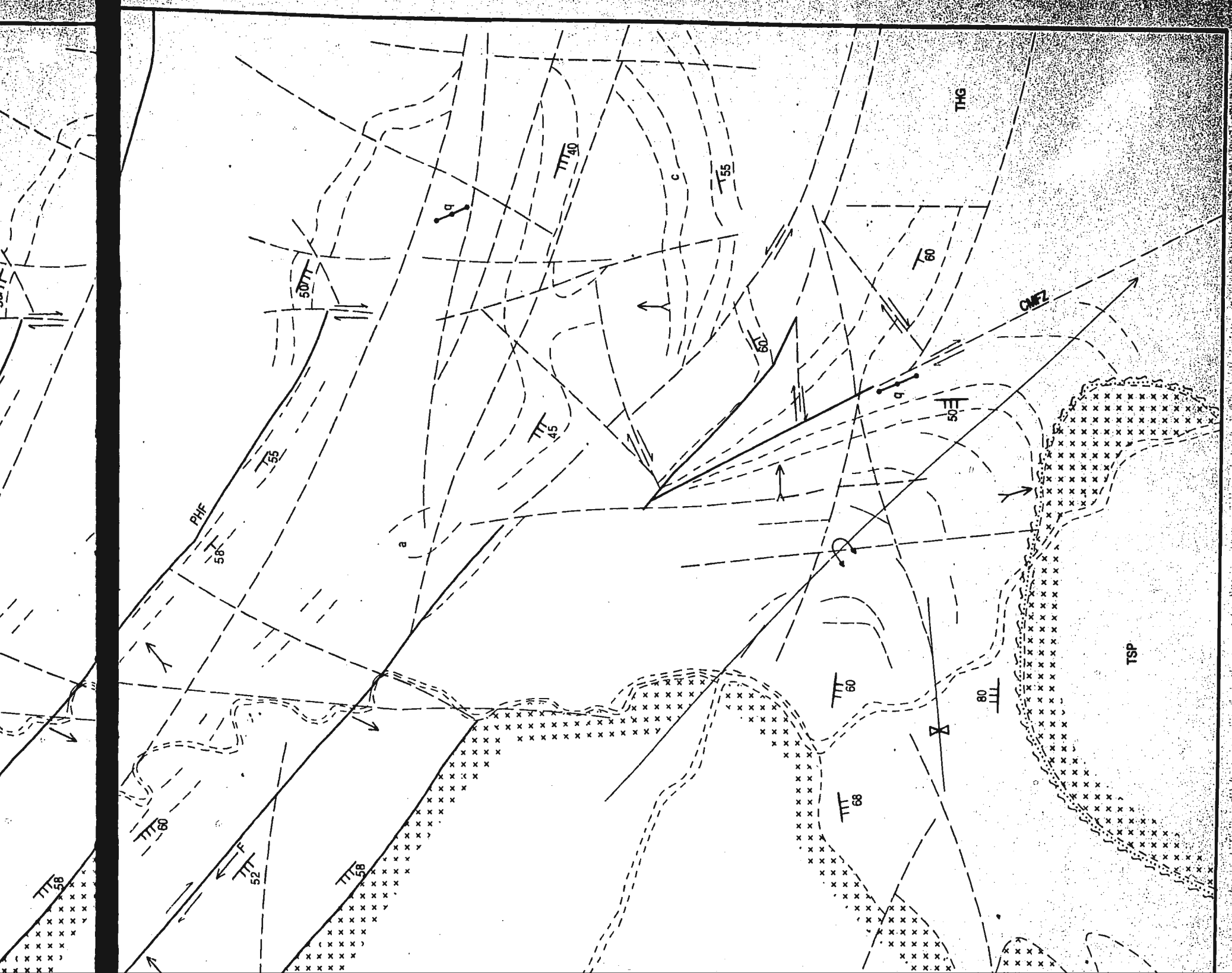
LEGEND

THG	Feldspathic Sedimentary rocks with minor calcareous units	} LAST HOPE GROUP																																																																																																				
TSG	Calc-alkaline volcano-Plutonic rocks with minor sediments both at the top and base	} SELKIRK GROUP																																																																																																				
<table style="width: 100%; border-collapse: collapse;"> <tr><td style="width: 30px; text-align: center;">c</td><td>—</td></tr> <tr><td style="text-align: center;">i</td><td>—</td></tr> <tr><td style="text-align: center;">TPG</td><td>—</td></tr> <tr><td style="text-align: center;">a</td><td>—</td></tr> </table>	c	—	i	—	TPG	—	a	—	Calc-alkaline Volcano-Plutonic rocks with aluminous Schists (a) and band iron formation(i) and Calcareous sediments at the top.	} PHENALONGA GROUP																																																																																												
c	—																																																																																																					
i	—																																																																																																					
TPG	—																																																																																																					
a	—																																																																																																					
<table style="width: 100%; border-collapse: collapse;"> <tr><td style="width: 30px; text-align: center;">a</td><td>—</td></tr> <tr><td style="text-align: center;">i</td><td>—</td></tr> <tr><td style="text-align: center;">TLG</td><td>—</td></tr> </table>	a	—	i	—	TLG	—	Komatiite-tholeiite Volcano-Plutonic rocks with banded iron formation (i) and calcareous sediments at the top.	} LADY MARY GROUP																																																																																														
a	—																																																																																																					
i	—																																																																																																					
TLG	—																																																																																																					
TSC_i	Nyambabwe Tonalite	} SEIKIRK IGNEOUS COMPLEX																																																																																																				
TSC_d	Francistown Diorite.																																																																																																					
TSC_s	Sekukwe Kop Layered Body																																																																																																					
<table style="width: 100%; border-collapse: collapse;"> <tr><td style="width: 30px; text-align: center;">x</td><td>x</td><td>x</td><td>x</td><td>x</td><td>x</td><td>x</td><td>x</td><td>x</td><td>x</td></tr> <tr><td style="text-align: center;">x</td><td>x</td><td>x</td><td>x</td><td>x</td><td>x</td><td>x</td><td>x</td><td>x</td><td>x</td></tr> </table>	x	x	x	x	x	x	x	x	x	x	x	x	x	x	x	x	x	x	x	x	x	x	x	x	x	x	x	x	x	x	x	x	x	x	x	x	x	x	x	x	x	x	x	x	x	x	x	x	x	x	x	x	x	x	x	x	x	x	x	x	x	x	x	x	x	x	x	x	x	x	x	x	x	x	x	x	x	x	x	x	x	x	x	x	x	x	x	x	x	x	x	x	x	x	x	x	x	x	x	x	Trondhjemites	} SOUTHERN TATI PLUTON
x	x	x	x	x	x	x	x	x	x																																																																																													
x	x	x	x	x	x	x	x	x	x																																																																																													
x	x	x	x	x	x	x	x	x	x																																																																																													
x	x	x	x	x	x	x	x	x	x																																																																																													
x	x	x	x	x	x	x	x	x	x																																																																																													
x	x	x	x	x	x	x	x	x	x																																																																																													
x	x	x	x	x	x	x	x	x	x																																																																																													
x	x	x	x	x	x	x	x	x	x																																																																																													
x	x	x	x	x	x	x	x	x	x																																																																																													
x	x	x	x	x	x	x	x	x	x																																																																																													
<table style="width: 100%; border-collapse: collapse;"> <tr><td style="width: 30px; text-align: center;">x</td><td>x</td><td>x</td><td>x</td><td>x</td><td>x</td><td>x</td><td>x</td><td>x</td><td>x</td></tr> <tr><td style="text-align: center;">x</td><td>x</td><td>x</td><td>x</td><td>x</td><td>x</td><td>x</td><td>x</td><td>x</td><td>x</td></tr> </table>	x	x	x	x	x	x	x	x	x	x	x	x	x	x	x	x	x	x	x	x	x	x	x	x	x	x	x	x	x	x	x	x	x	x	x	x	x	x	x	x	x	x	x	x	x	x	x	x	x	x	x	x	x	x	x	x	x	x	x	x	x	x	x	x	x	x	x	x	x	x	x	x	x	x	x	x	x	x	x	x	x	x	x	x	x	x	x	x	x	x	x	x	x	x	x	x	x	x	x	x	Tonalite-trondjemite-granodiorite-granite	} TATI BATHOLITH
x	x	x	x	x	x	x	x	x	x																																																																																													
x	x	x	x	x	x	x	x	x	x																																																																																													
x	x	x	x	x	x	x	x	x	x																																																																																													
x	x	x	x	x	x	x	x	x	x																																																																																													
x	x	x	x	x	x	x	x	x	x																																																																																													
x	x	x	x	x	x	x	x	x	x																																																																																													
x	x	x	x	x	x	x	x	x	x																																																																																													
x	x	x	x	x	x	x	x	x	x																																																																																													
x	x	x	x	x	x	x	x	x	x																																																																																													
x	x	x	x	x	x	x	x	x	x																																																																																													
Xg	High metamorphic grade Gneiss Terrane																																																																																																					

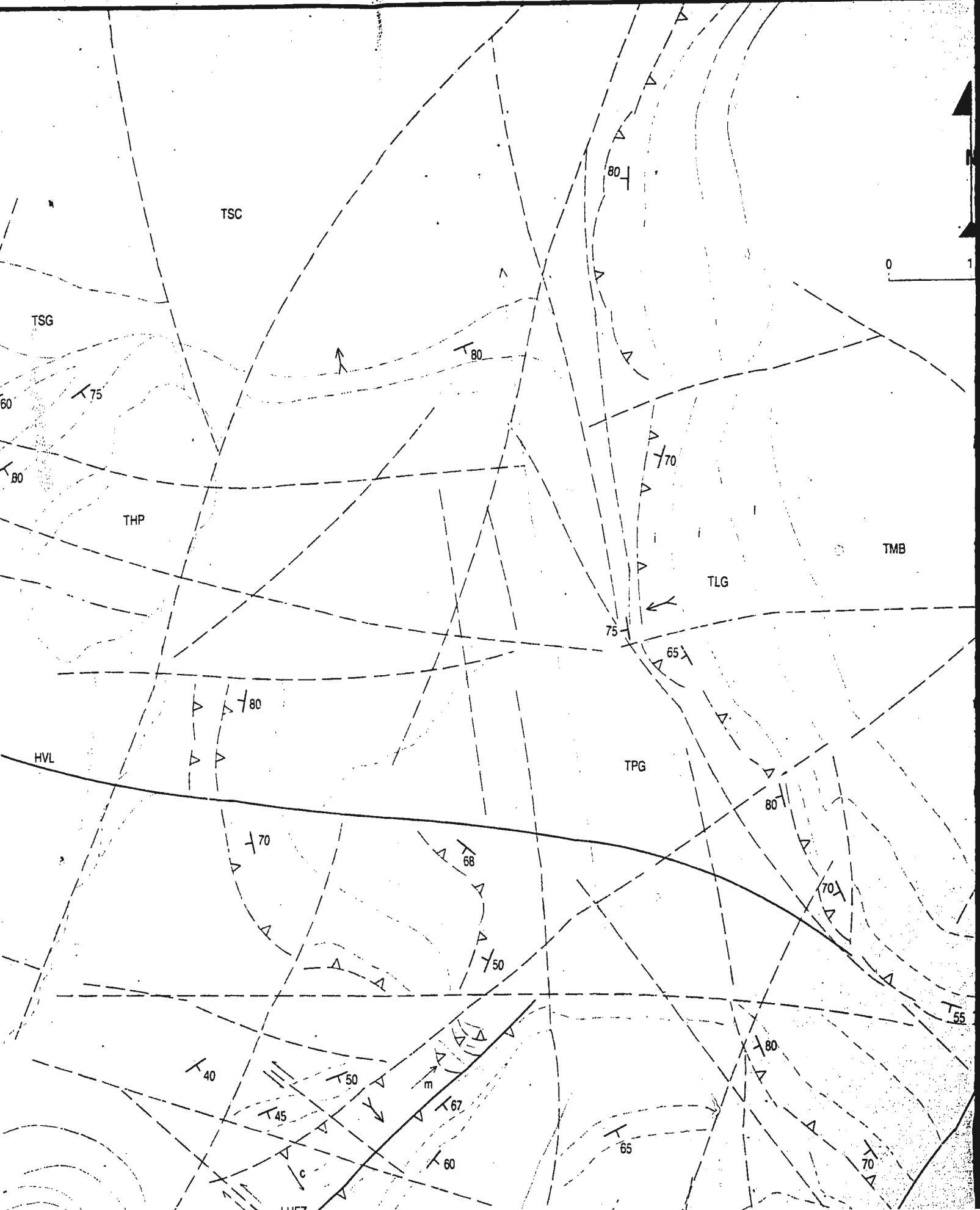
- Lithological boundary (certain)
- - - Lithological boundary (uncertain)
- · - · - Lithological boundary (inferred)
- MFL — Major Fault / Lineament
- - - Fault / Lineament
- Bedding / igneous Layering (So)
- ⁵⁰ S₂ foliation
- ⁶⁰ TTT₆₀ Mineral Lineation(L₂) on S₂ - Surface
- Younging direction
- Overtured anticline
- Overtured Syncline
- F₂₀ Minor fold with plunge
- q — Quartz Vein
- Strike-Slip / wrench fault
- ≡≡≡≡≡ Photogeological / structural trends

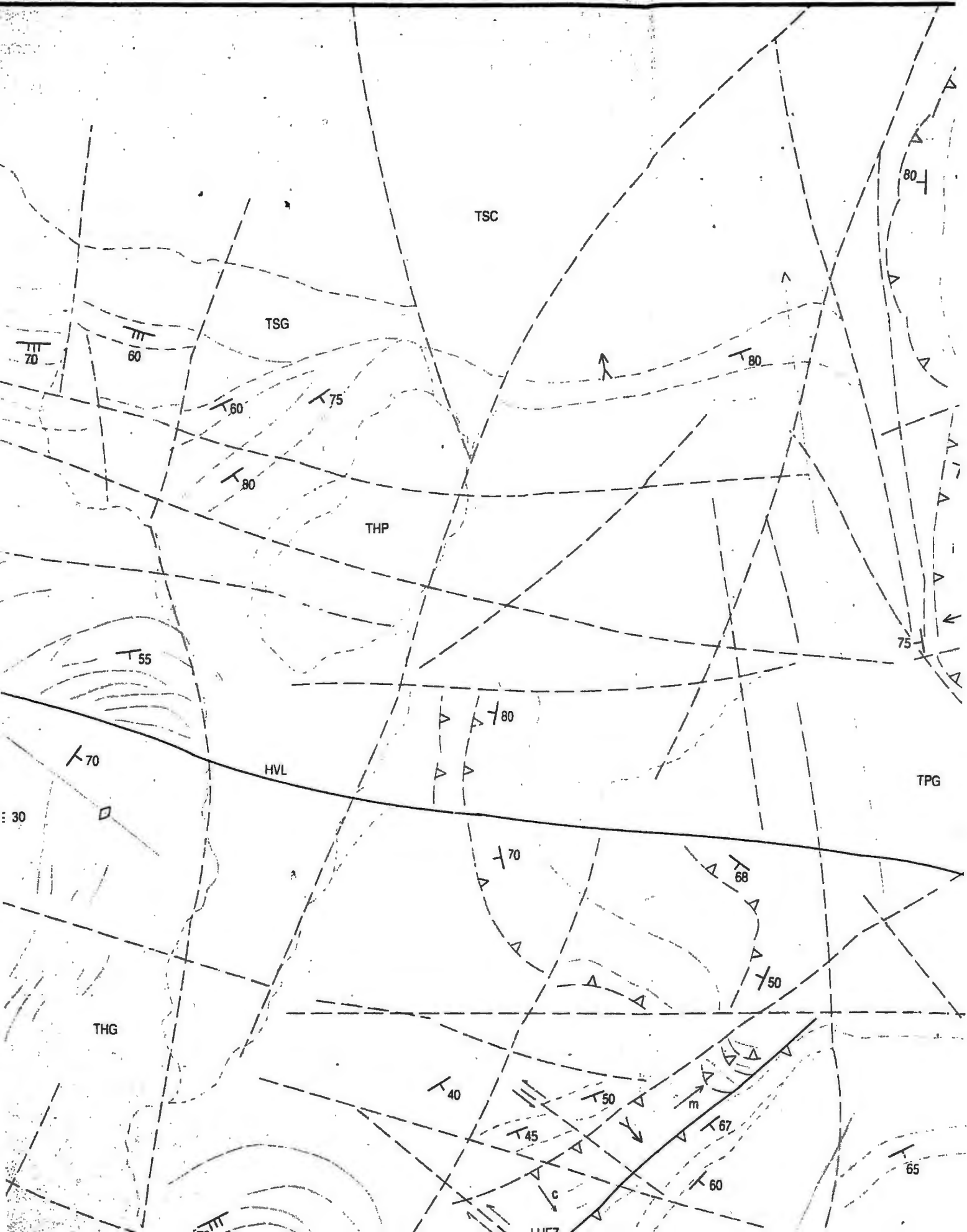
x x
x x











TSC

TSG

THP

HVL

TPG

THG

70

60

60

75

80

55

70

80

75

80

80

30

70

68

50

40

50

45

67

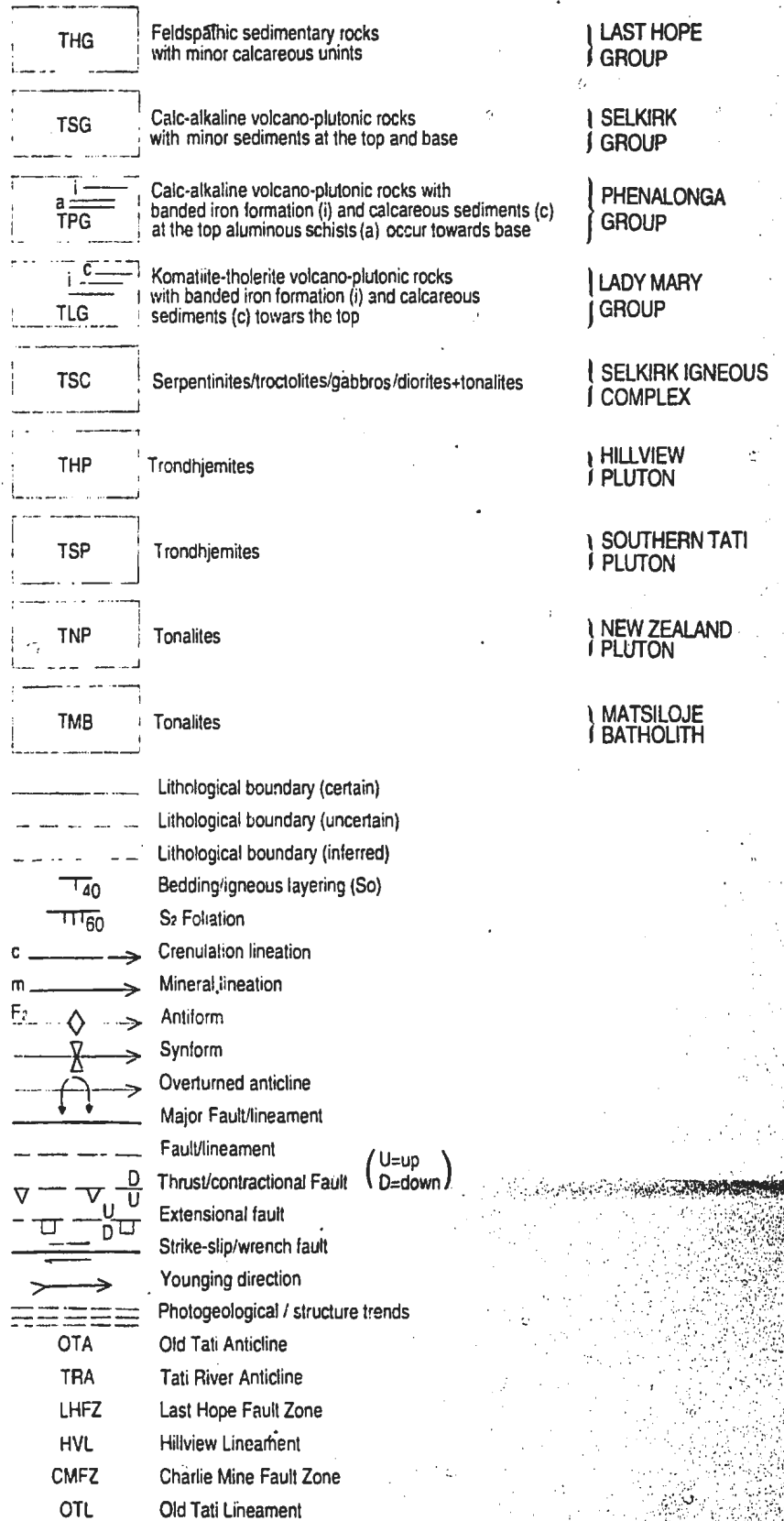
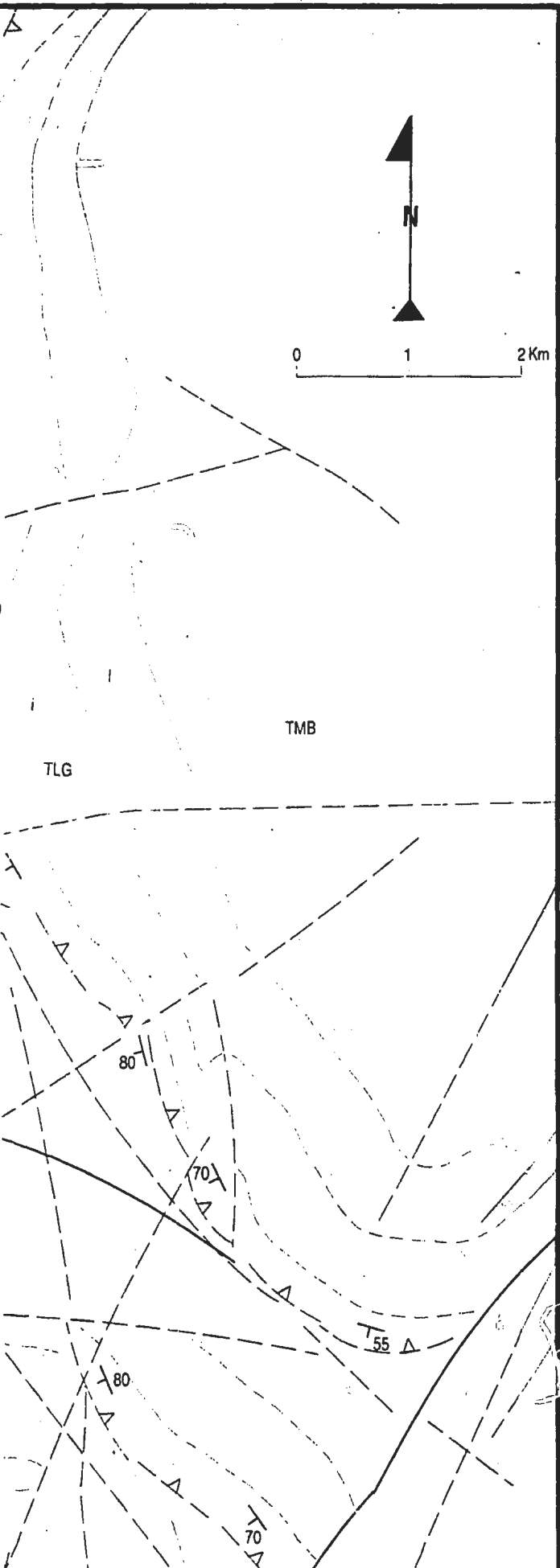
60

65

m

c

Figure 3.7: Geological Map of the area around Old Tati, Last Hope basin and Matsiloje Ridge



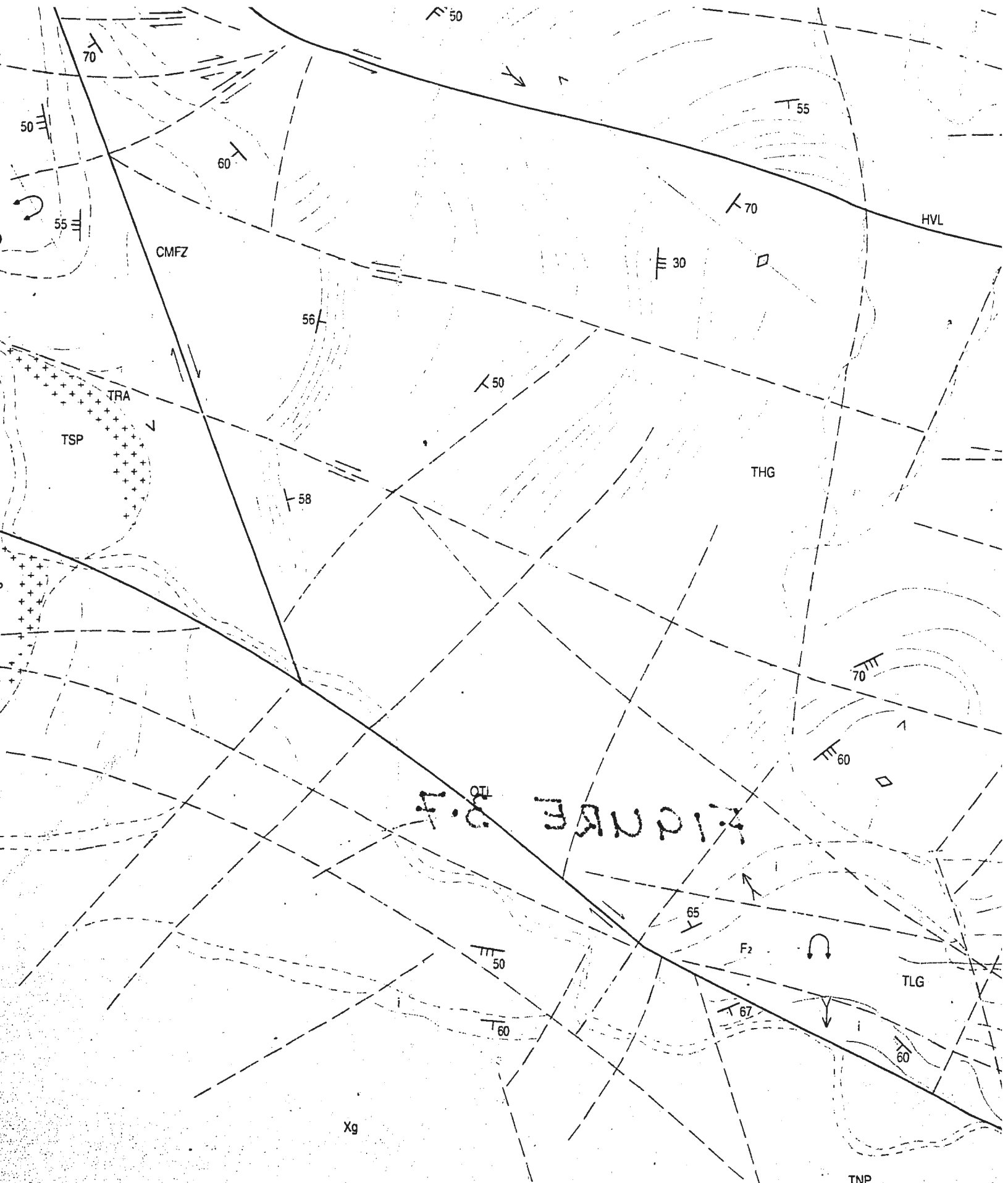
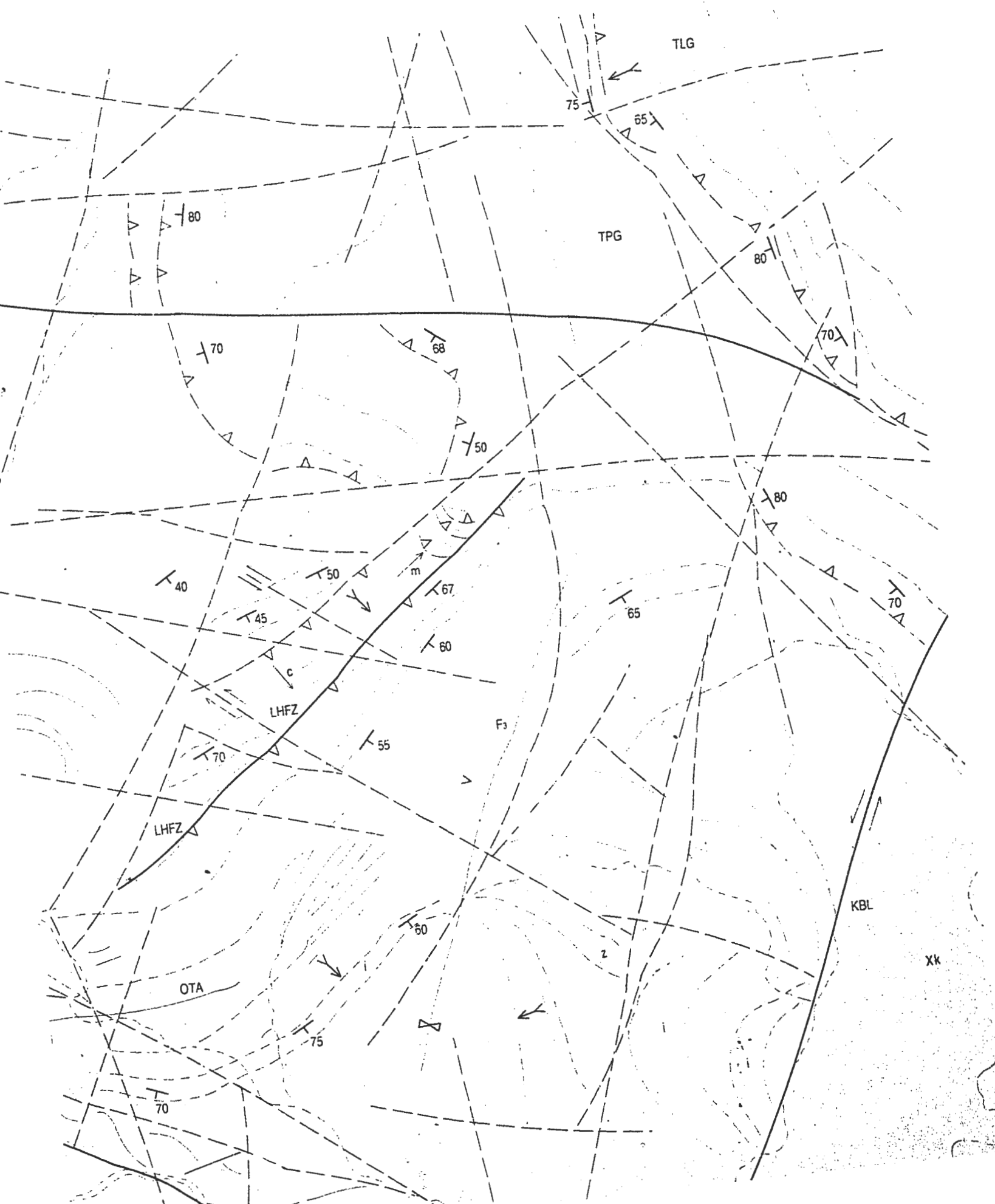
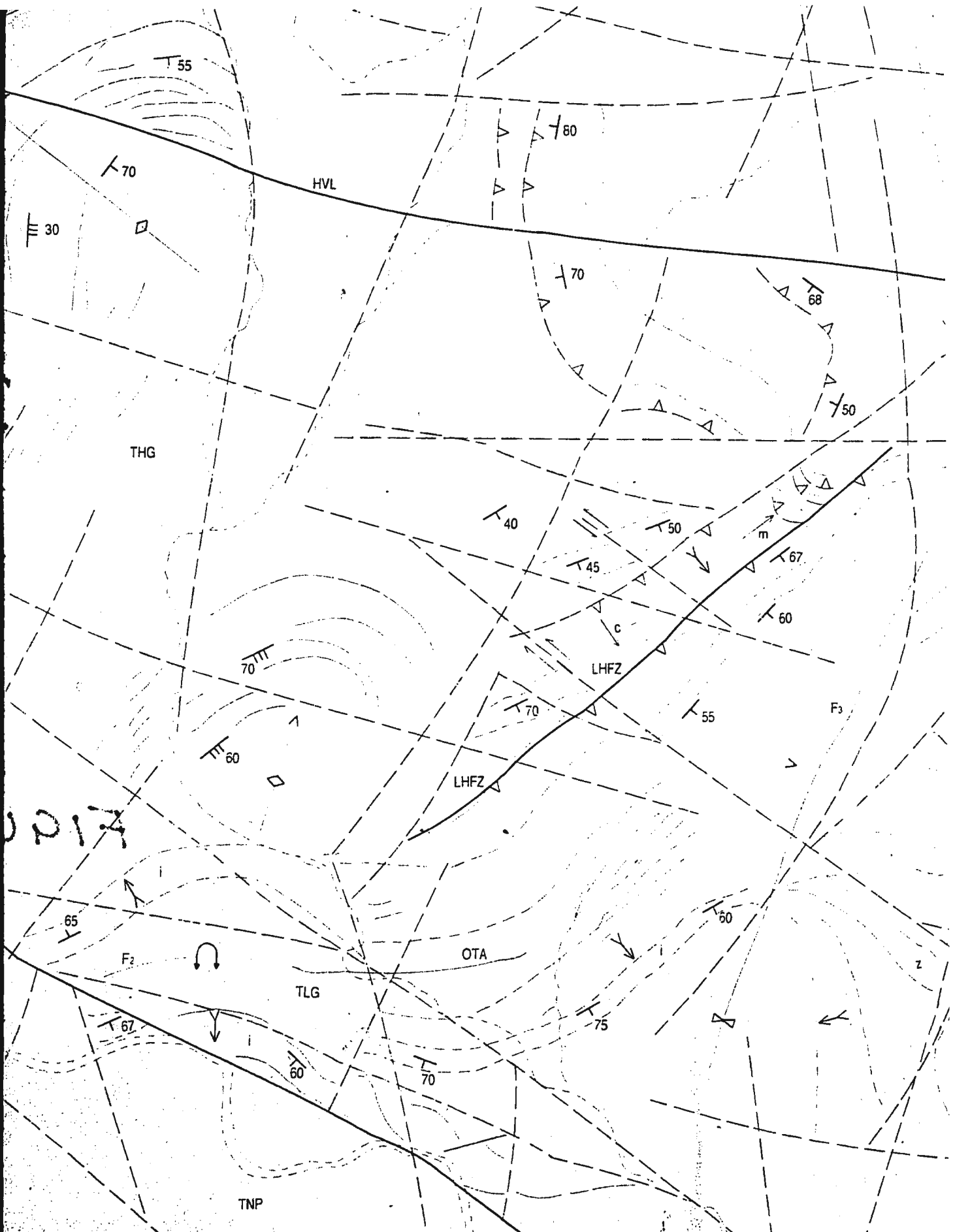
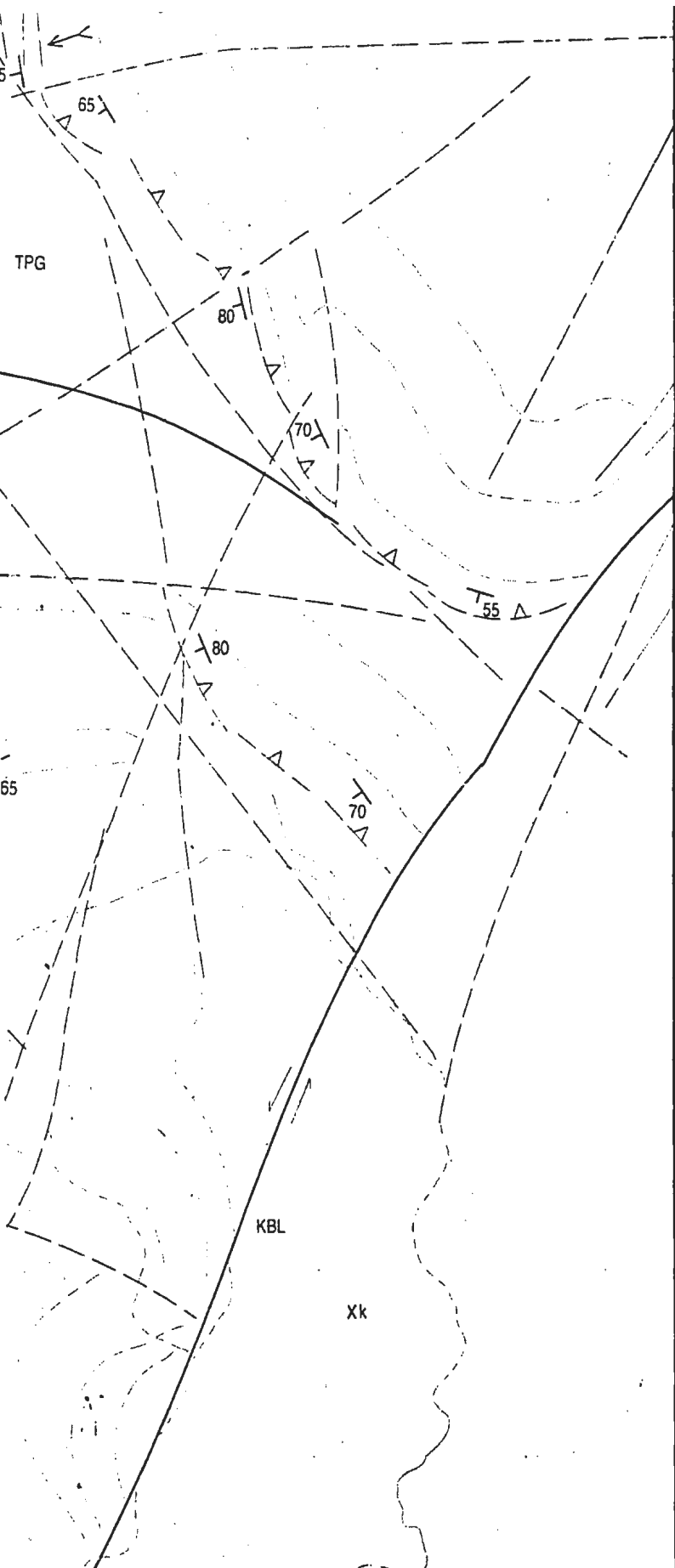


FIGURE 3.1







- Lithological boundary (certain)
- Lithological boundary (uncertain)
- Lithological boundary (inferred)
- Bedding/igneous layering (So)
- S₂ Foliation
- Crenulation lineation
- Mineral lineation
- Antiform
- Synform
- Overtured anticline
- Major Fault/lineament
- Fault/lineament
- Thrust/contractional Fault (U=up, D=down)
- Extensional fault
- Strike-slip/wrench fault
- Younging direction
- Photogeological / structure trends
- OTA Old Tati Anticline
- TRA Tati River Anticline
- LHFZ Last Hope Fault Zone
- HVL Hillview Lineament
- CMFZ Charlie Mine Fault Zone
- OTL Old Tati Lineament

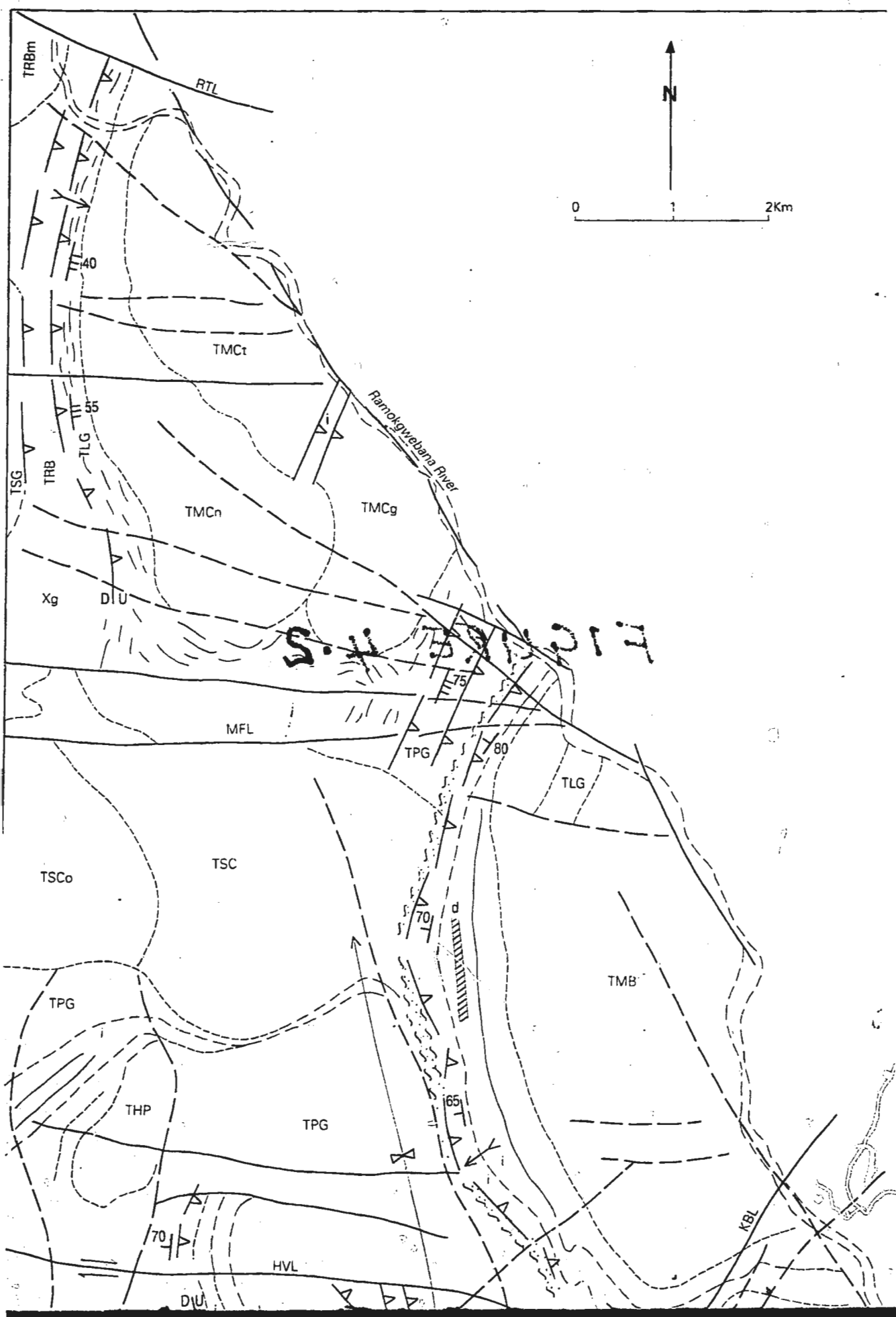
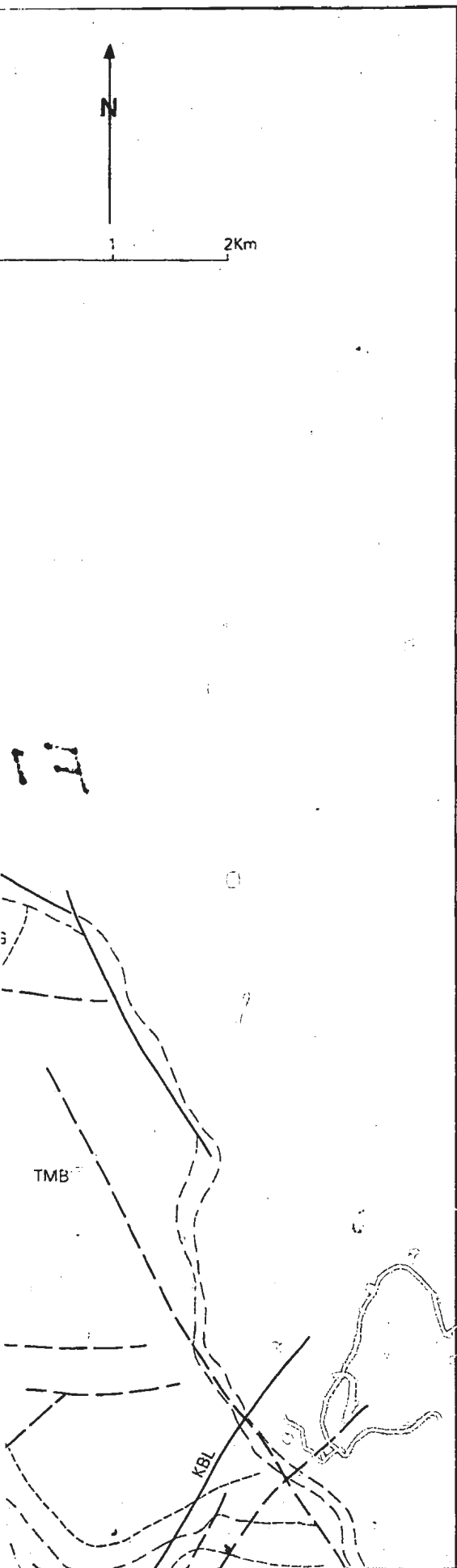


Figure 4.2: Simplified Geological Map of the Eastern Structural Zone of the Tati Greenstone Belt.



SUPRACRUSTAL ROCKS

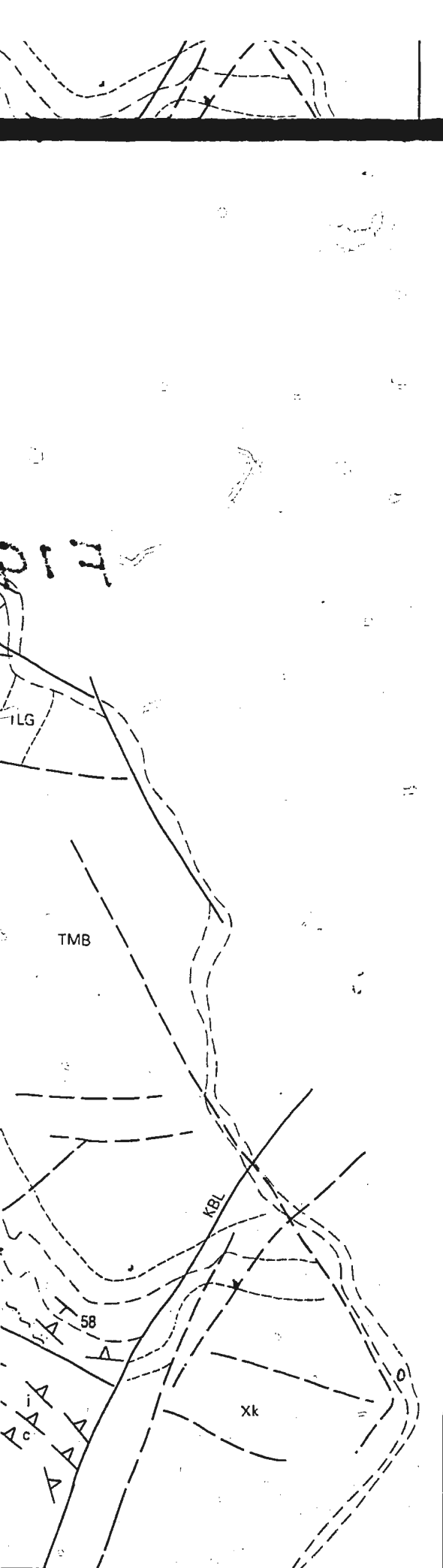
THG	Feldspathic sedimentary rocks with minor calcareous units	LAST HOPE GROUP
TSG	Calc-alkaline volcano - plutonic rocks with minor sediments at base and top	SELKIRK GROUP
TPG	Calc - alkaline volcano - plutonic rocks with banded iron formation (i) and calcareous sediments (c) towards the top	PHENALONGA GROUP
TLG	Komatiite - tholeiite volcano - plutonic rocks with banded iron formation (i) and calcareous sediments (c) at the top	LADY MARY GROUP
Xk	Ultramafic - mafic volcano - plutonic rocks with younger intrusions	KGARIMACHENG FORMATION
Xg	Gneisses (granitoid, paragneiss and amphibolite)	GRANITOID TERRANE

INTRUSIVE ROCKS

TSCo TSC	Gabbros (TSCo), diorites tonalites with troctolite (TSC.)	SELKIRK IGNEOUS COMPLEX
THP	Trondhjemites	HILLVIEW PLUTON
TMCt	Grey tonalites	MPHOENG PLUTONIC COMPLEX
TMCn	Granodiorite	
TMCg	Coarse-grained gabbros	
TRBm TRB	Undivided granodiorite with megacrystic feldspar granite (TRBm)	RAMOKGWEBANA BATHOLITH
TMB	Grey tonalite	MATSILOJE BATHOLITH

—————	Lithological boundary (Certain)
- - - - -	Lithological boundary (Uncertain)
- · - · -	Lithological boundary (Inferred)
T50	Bedding / Igneous layering (So)
T160	S1 Foliation
T165	S2 Foliation
→	Younging direction
↘	Synform
▨	Dolerite Dyke (karoo ?)
~	Shear Zone
— —	Strike - slip / Wrench Fault
— — U D	Thrust / Contractional Fault { D = Down plate } { U = up plate }
— — U D	Extensional Fault
— —	Major Fault /Lineament
- - - - -	Fault /Lineament
~~~~~	River
MEI	Mafic - Ultramafic Intrusions





--- Fault /Lineament  
 - - - - - River

$\frac{c}{i}$   
 TLG

Komatite- tholeiite volcano - plutonic rocks with banded iron formation (i) and calcareous sediments (c) at the top

LADY MARY GROUP

Xk

Ultramafic - mafic volcano - plutonic rocks with younger intrusions

KGARIMACHENG FORMATION

Xg

Gneisses ( granitoid, paragneiss and amphibolite )

GRANITOID TERRANE

INTRUSIVE ROCKS

$\frac{TSCo}{TSC}$

Gabbros (TSCo), diorites tonalites with troctolite ( TSC )

SELKIRK IGNEOUS COMPLEX

THP

Trondhjemites

HILLVIEW PLUTON

TMCt

Grey tonalites

TMCn

Granodiorite

TMCg

Coarse-grained gabbros

MPHOENG PLUTONIC COMPLEX

$\frac{TRBm}{TRB}$

Undivided granodiorite with megacrystic feldspar granite ( TRBm )

RAMOKGWEBANA BATHOLITH

TMB

Grey tonalite

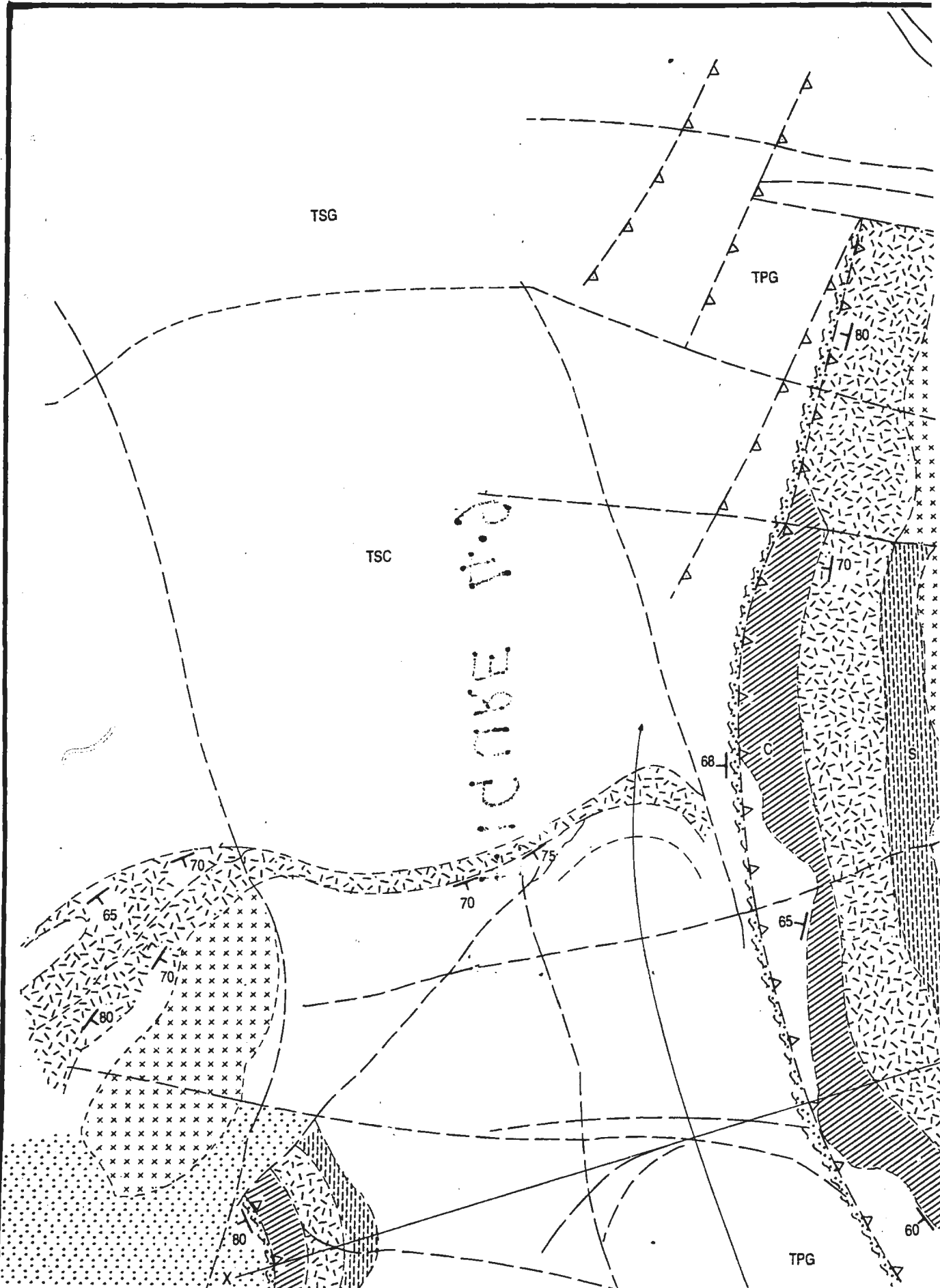
MATSILOJE BATHOLITH

— Lithological boundary ( Certain )  
 - - - Lithological boundary ( Uncertain )  
 - - - - - Lithological boundary ( Inferred )  
 T50 Bedding / Igneous layering ( So )  
 T160 S1 Foliation  
 T165 S2 Foliation

→ Younging direction  
 ↘ Synform  
 // Dolerite Dyke ( karoo ? )  
 ~ Shear Zone  
 ⇄ Strike - slip / Wrench Fault  
 ⇄ Thrust / Contractonal Fault { D = Down plate }  
 ⇄ Extensional Fault { U = up plate }

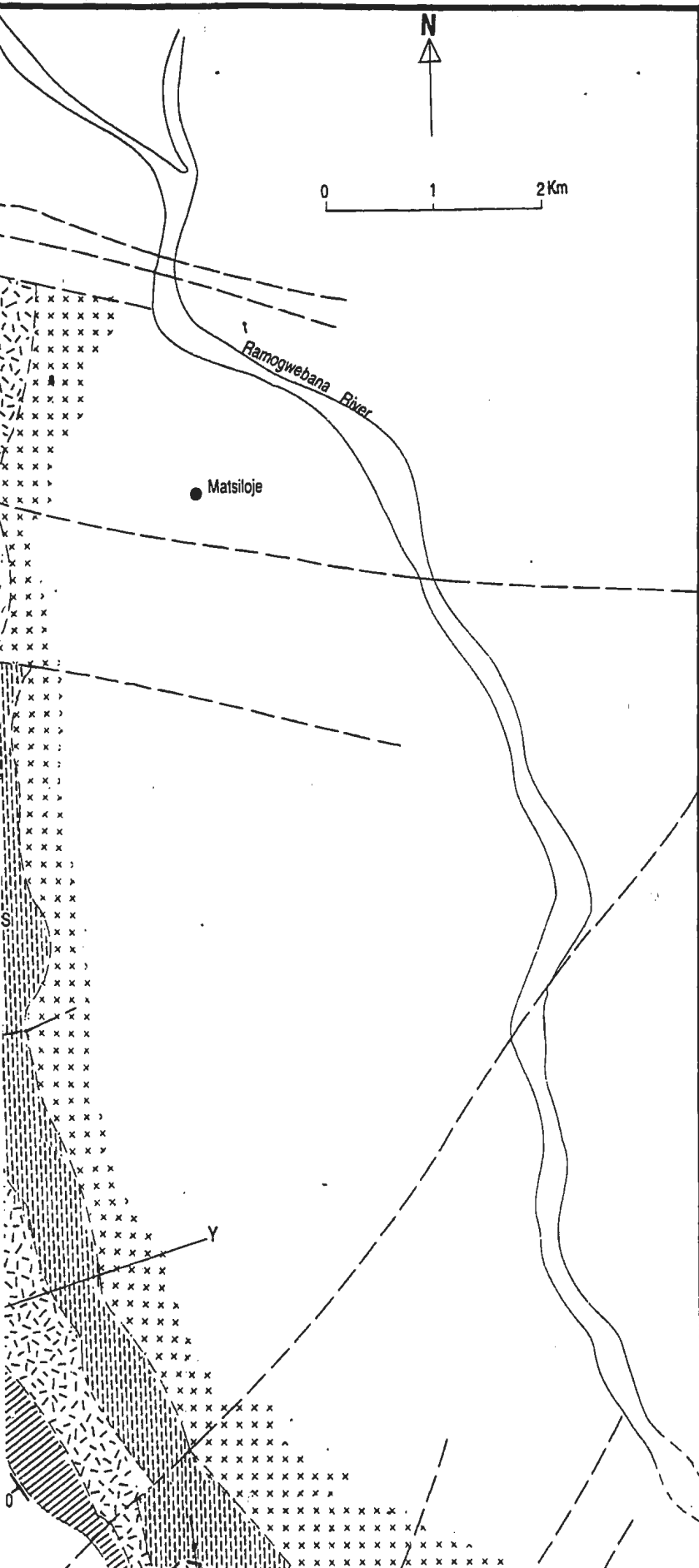
— Major Fault /Lineament  
 - - - Fault /Lineament  
 - - - - - River

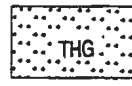
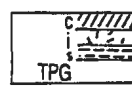
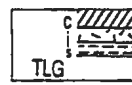
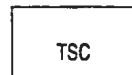
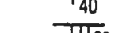
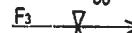
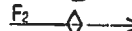
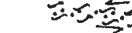
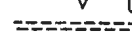
MFL Matsiloje - Francistown Lineament  
 RTL Ramokgwebana - Tsamaya Lineament  
 HVL Hillview Lineament  
 LHFZ Last Hope Fault Zone  
 KBL Kgarimacheng boundary lineament



0.11 EQUID

Figure 4.9 ; Simplified Geological Map of the area between Matsiloje and SignalHills



- 
Feldspathic Sedimentary rocks with minor calcareous units.
} LAST HOPE GROUP
- 
Calc-alkaline volcano-Plutonic rocks with minor sediments both at the base and top
} SELKIRK GROUP
- 
Calc-alkaline Volcano-Plutonic rocks with clastic(s) banded iron formation(i) and calcareous sediments (c) at the top.
} PHENALONGA GROUP
- 
Komatiite-tholeiite Volcano-plutonic rocks with clastic sediments(c), banded iron formation(i) and calcareous sediments (c) at the top.
} LADY MARY GROUP
- 
Selkirk Igneous Complex
- 
Granitoids
- 
Lithological boundary (certain)
- 
Lithological boundary (uncertain)
- 
Lithological boundary (inferred)
- 
Bedding/igneous Layering(S₀)
- 
D2 foliation (S₂)
- 
F₃ → Synform,
- 
F₂ → Antiform
- 
→ Overturned anticline
- 
→ Shear zone
- 
Major Fault/Lineament
- 
Fault/Lineament
- 
Thrust fault (D=lower plate;U=up-plate)
- 
Photo lineament trends
- 
River

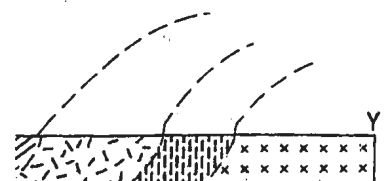
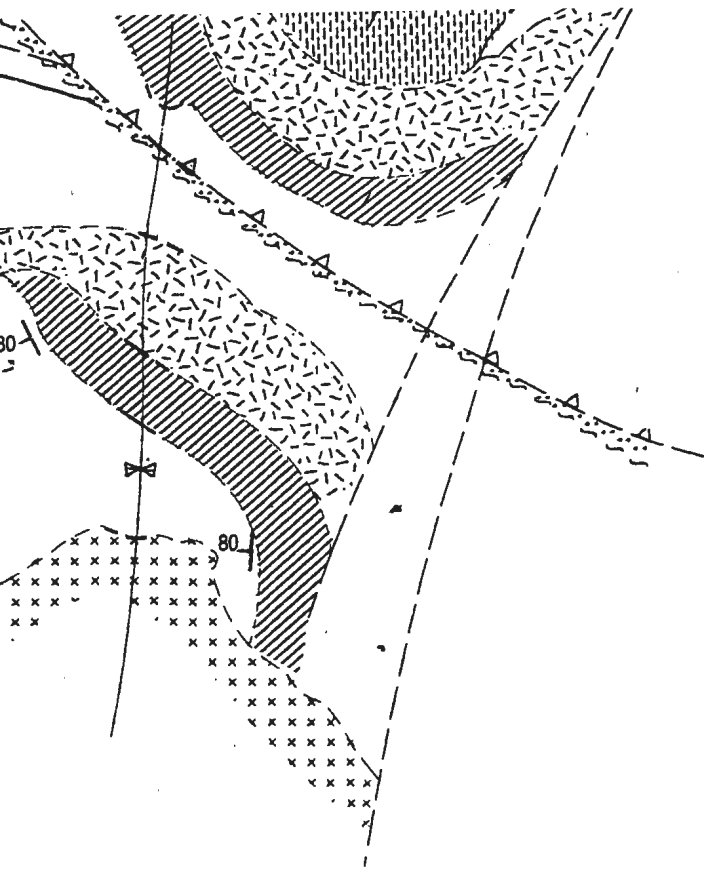




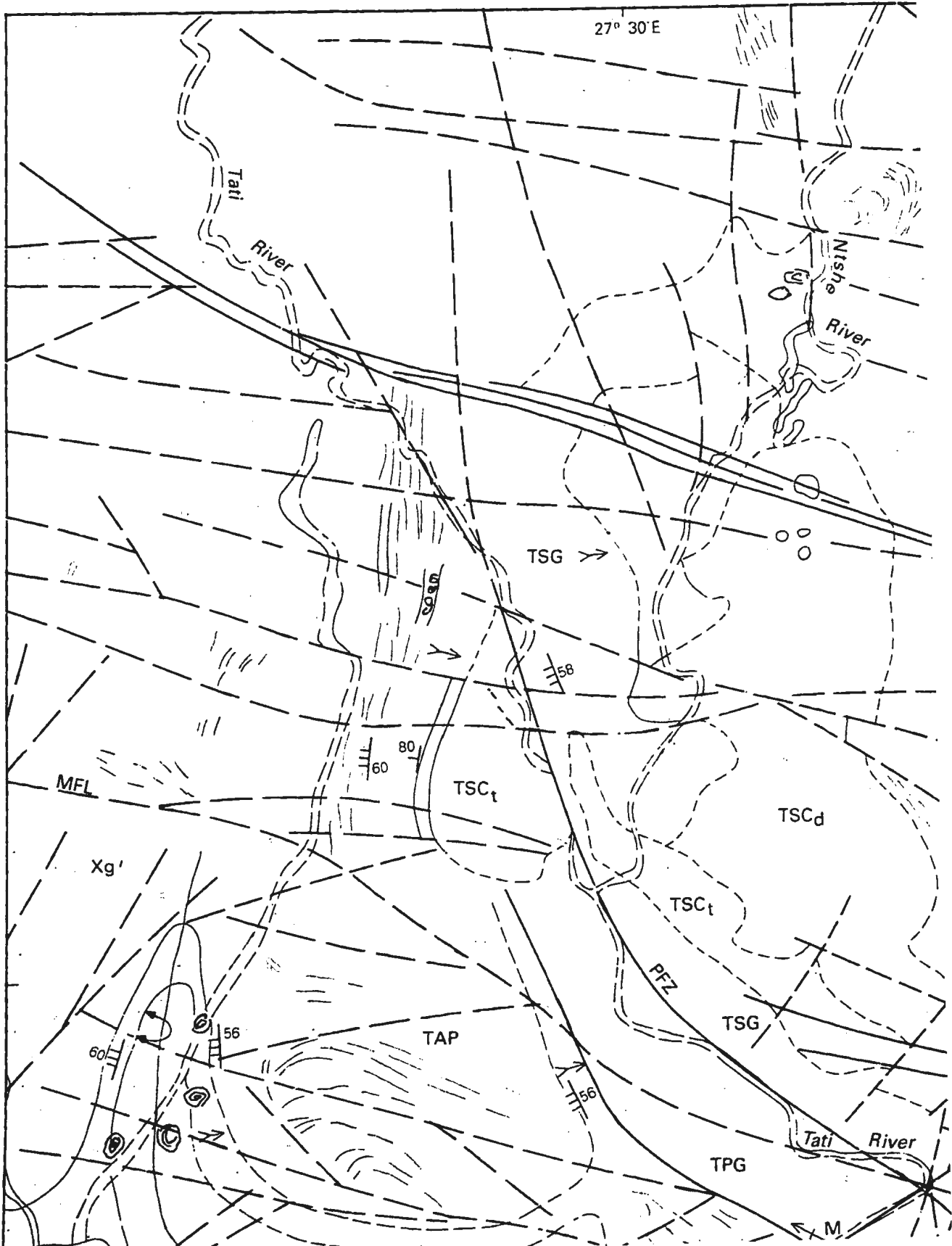
- .....bu UZ rotation (S2)
- F₃ Synform.
- F₂ Antiform
- Overturned anticline
- Shear zone
- Major Fault/Lineament
- Fault/Lineament
- Thrust fault (D=lower plate; U=up-plate)
- Photo lineament trends
- River



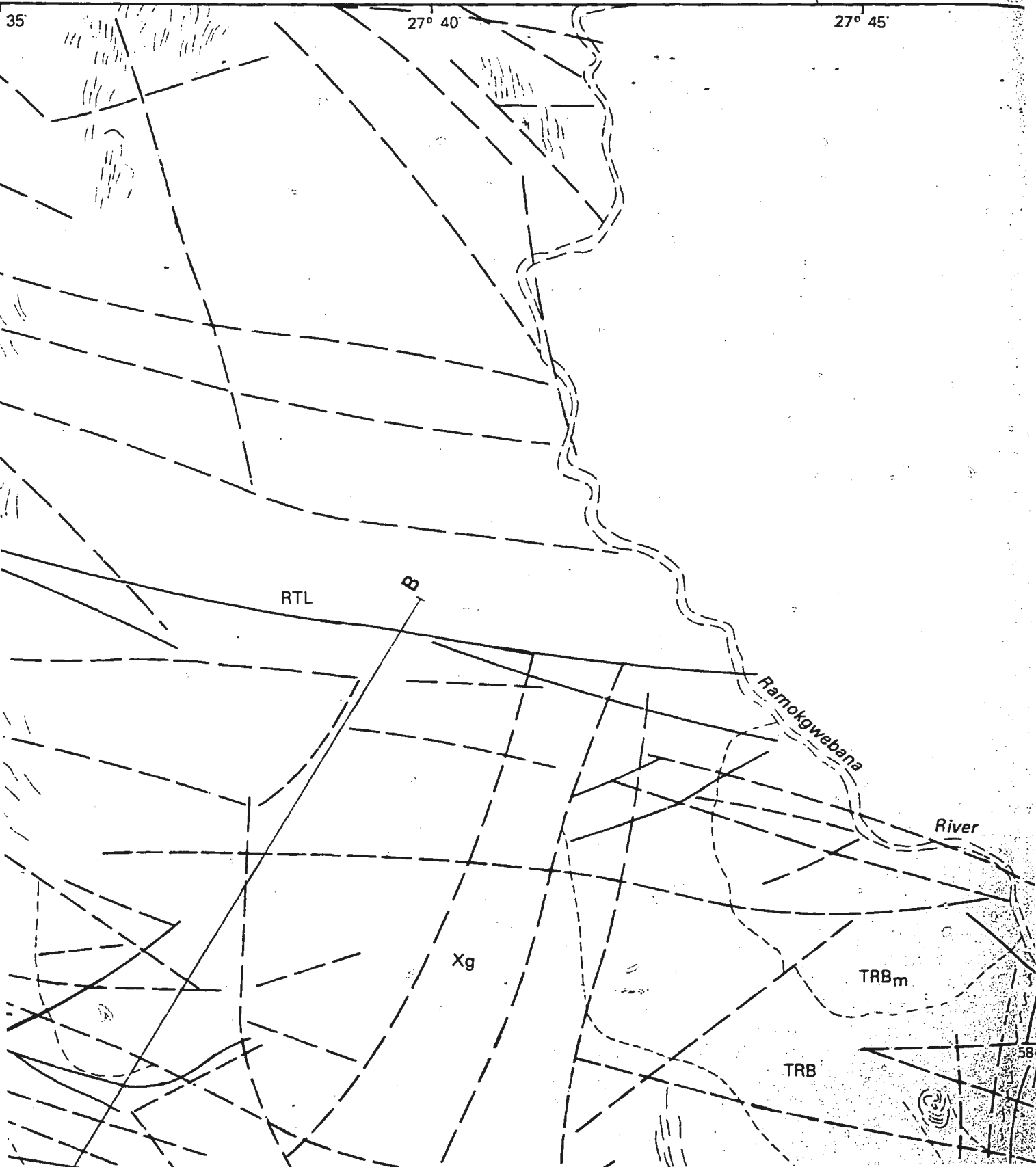
X F F F



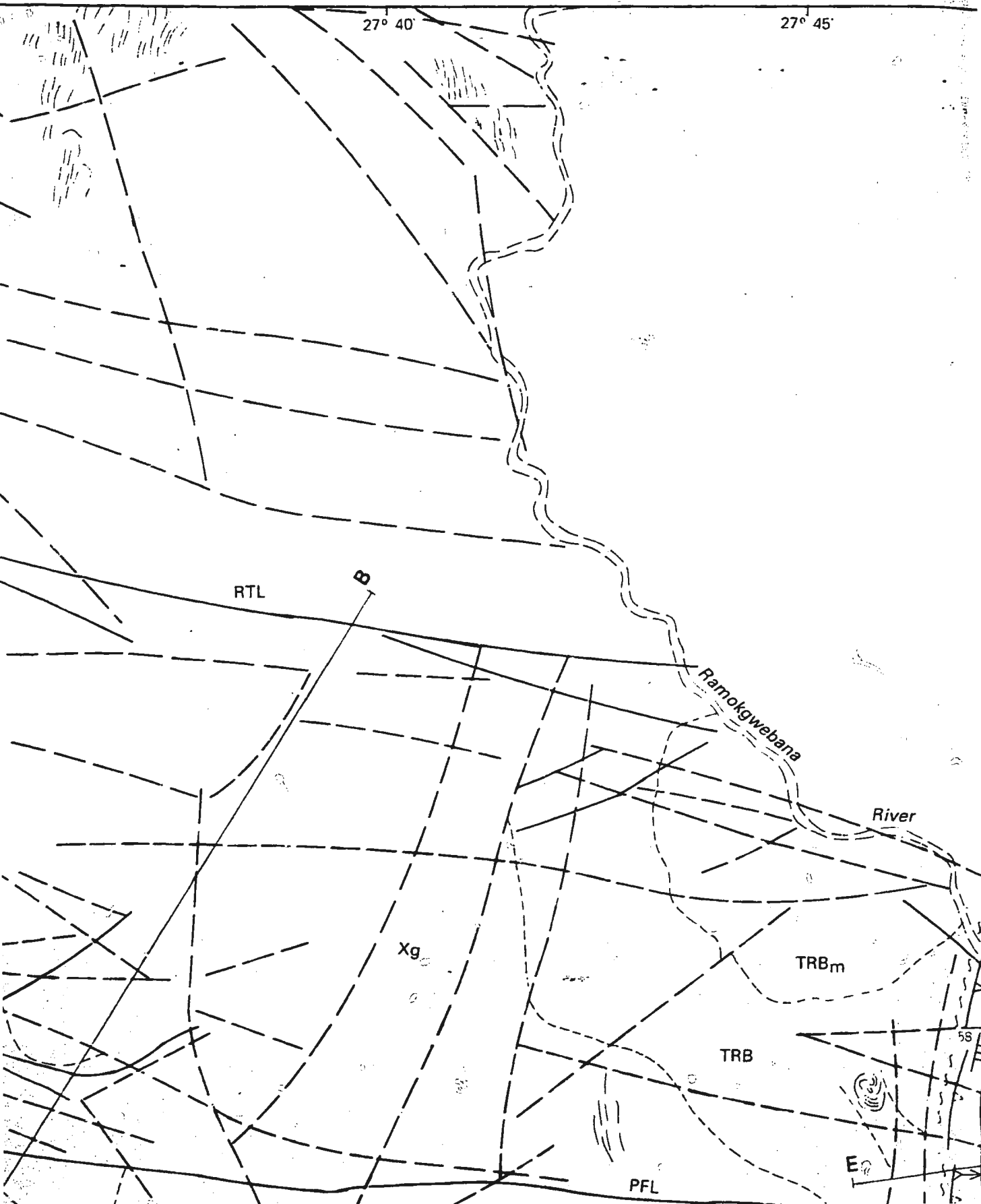
# SUMMARY OF THE GEOI



# AND STRUCTURE OF THE TATI GREI



# AND STRUCTURE OF THE TATI GREE

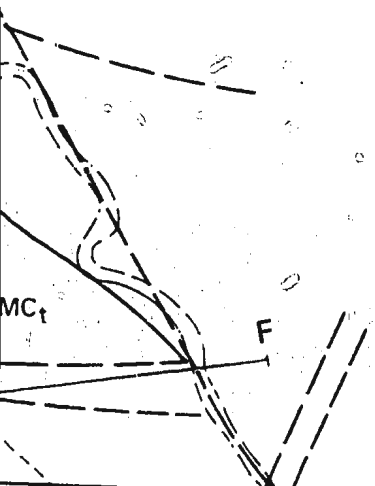
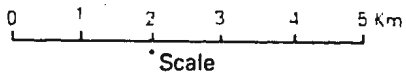


# STONE BELT, NE BOTSWANA.

27° 50'

27° 55'

## Appendix E



21° 10'S

THG

TSG

TPG

TLG

TSC

TSC

TSC

TSC

TSC

TMC

TMC

TMC

THP

TSP

TAP

TNP

TRB

TRB

TMB

TTB

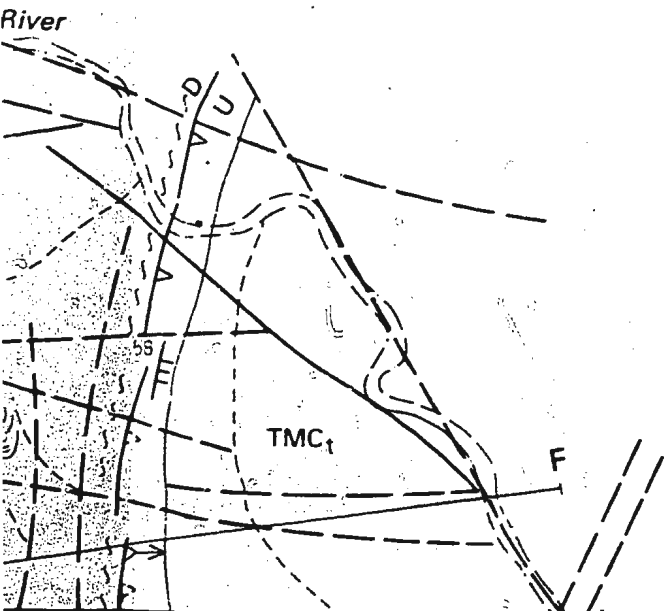
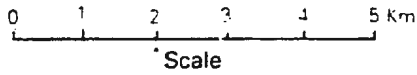
TTB

# GREENSTONE BELT, NE BOTSWANA.

27° 50'

27° 55'

*Appendix*



E

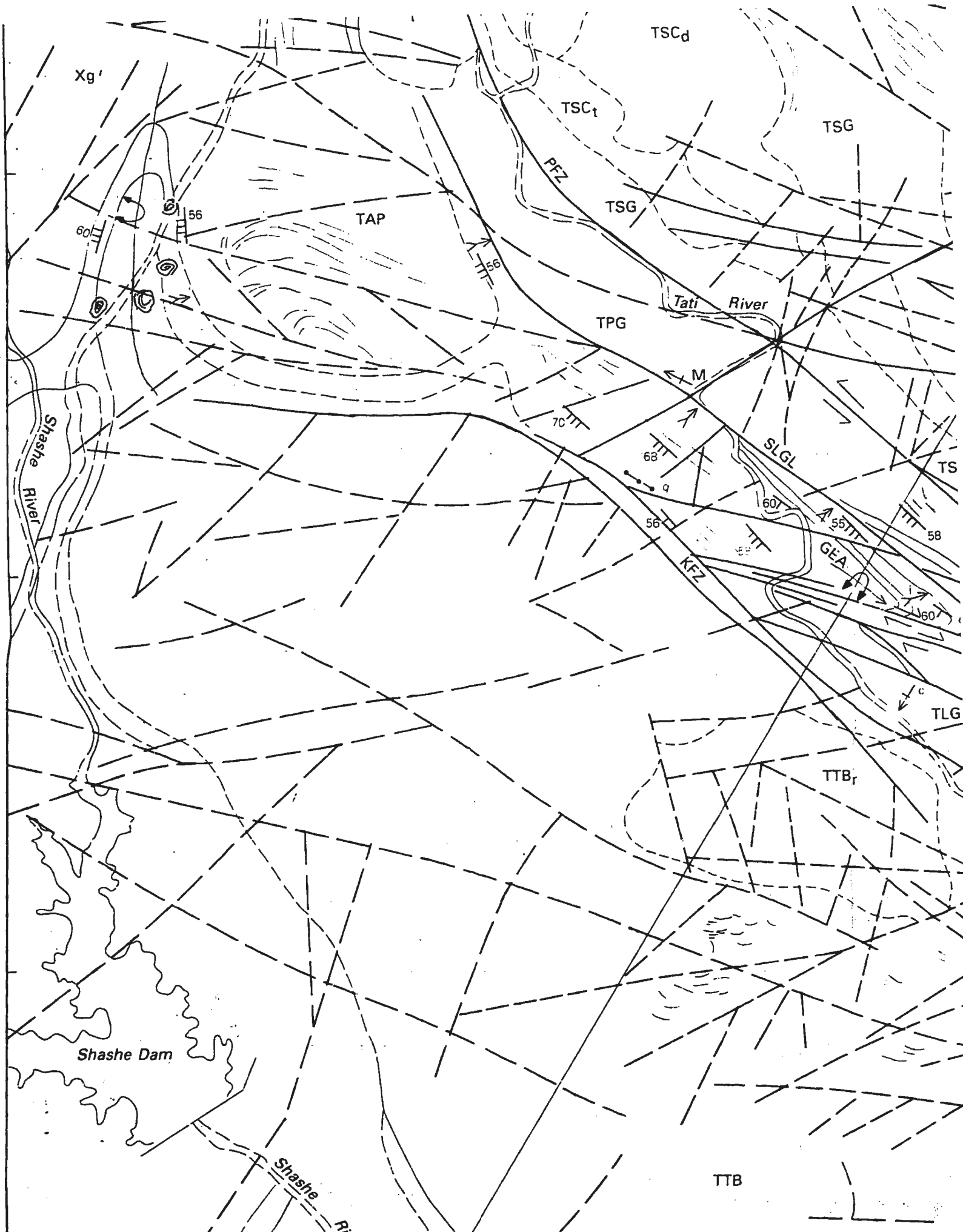
1. SUPRACRUSTAL ROCKS

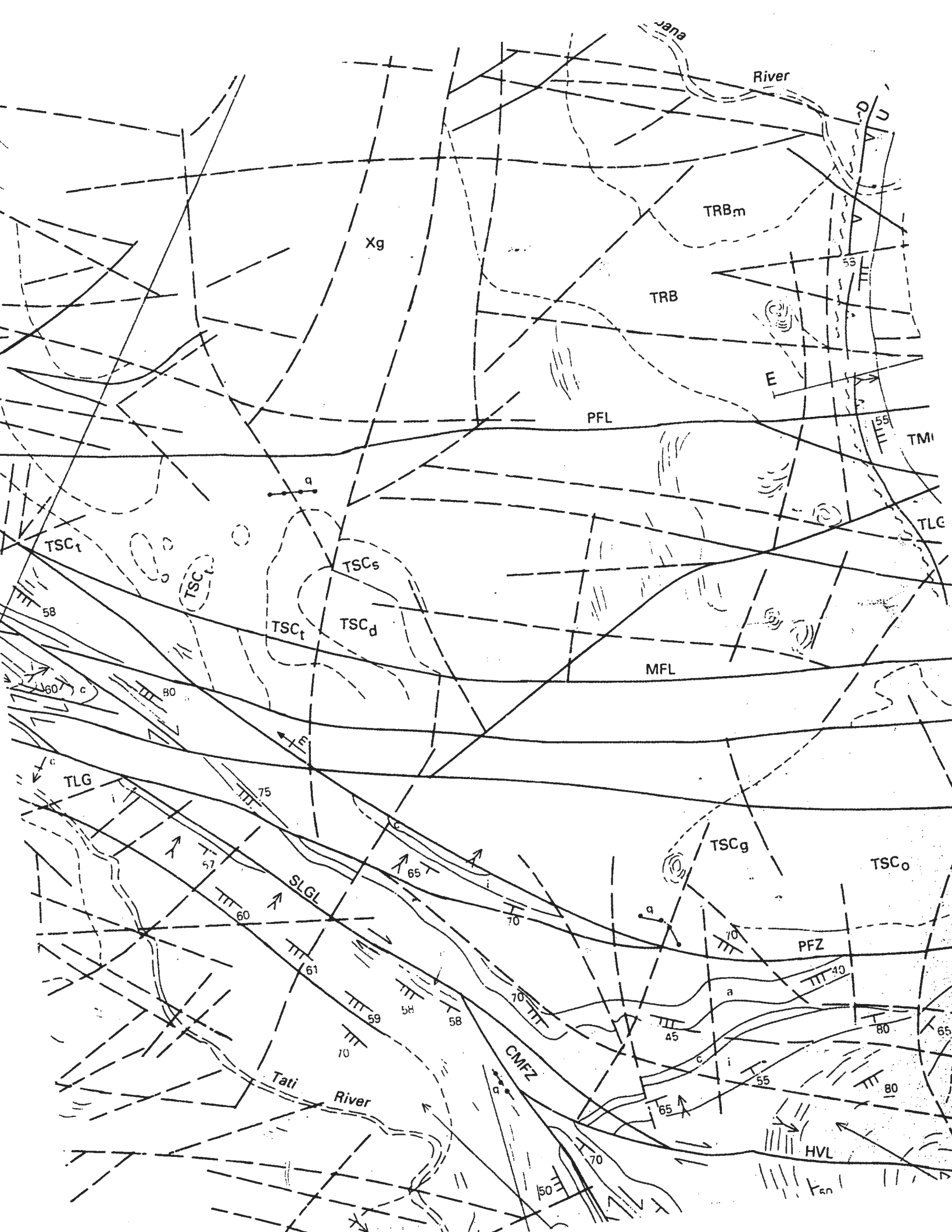
THG	Feldspathic sedimentary rocks with minor calcareous units	LAST HOPE GROUP
TSG	Calc. alkaline volcano-plutonic rocks with minor sediments at the top and base	SELKIRK GROUP
TPG	Calc. alkaline volcano-plutonic rocks with banded iron formation (i) and calcareous sediments (c) at the top, aluminous schists (a) occur towards base.	PHENALONGA GROUP
TLG	Komatiite-tholeiite volcano-plutonic rocks with banded iron formations (i) and calcareous sediments (c) towards the top	LADY MARY GROUP

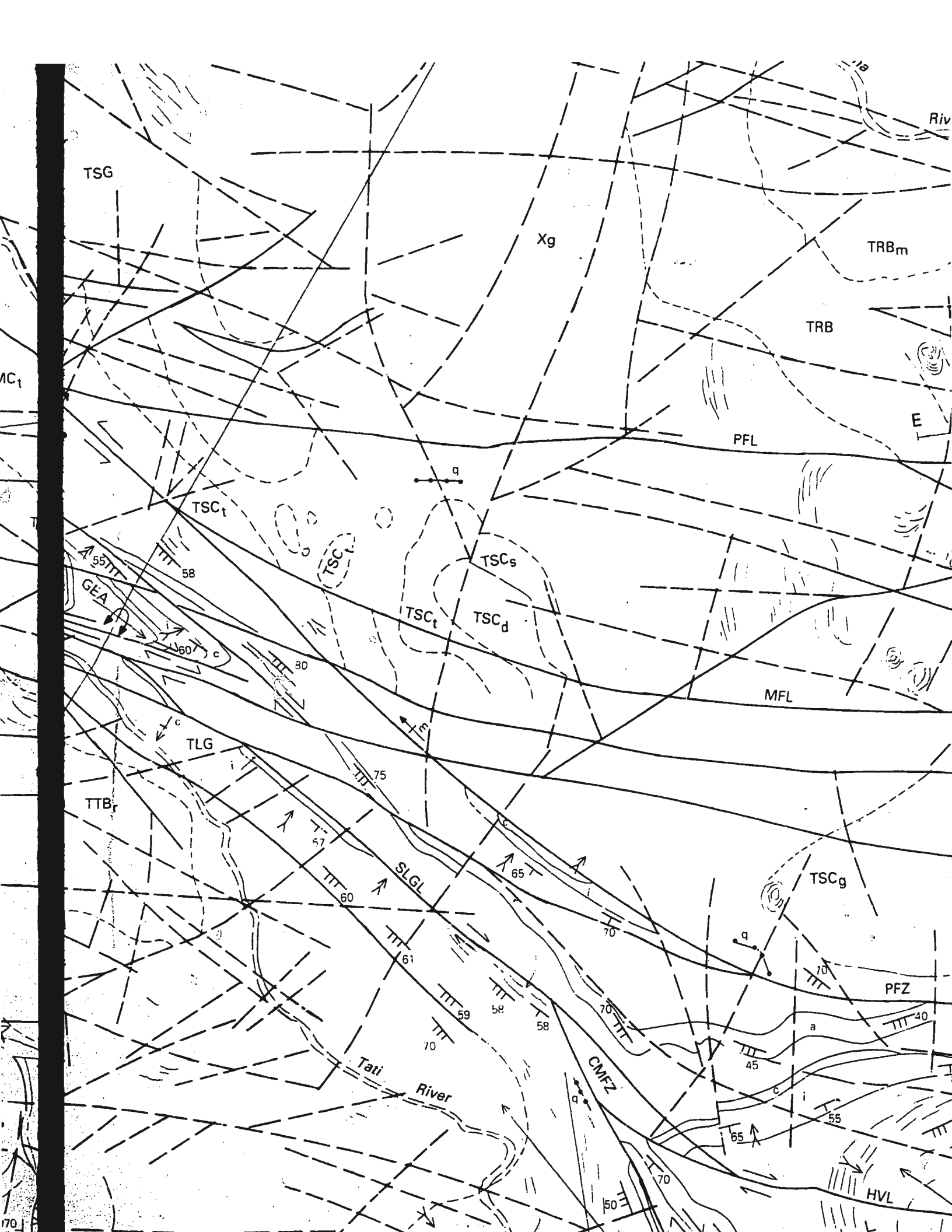
2. INTRUSIVE ROCKS

TSC _t	Nyambabwe Tonalite	SELKIRK IGNEOUS COMPLEX
TSC _d	Francistown Diorite	
TSC _s	Sekukwe kop layered body	
TSC _g	Selkirk Gabbro	
TSC _o	Tekwani Troctolite	
TMC _t	Grey High mg tonalite (TMC _t )	MPHOENG PLUTONIC COMPLEX
TMC _n	Coarse-grained granodiorite (TMC _n )	
TMC _g	Gabbroic rocks (TMC _g )	
THP	Trondhemite	HILLVIEW PLUTON
TSP	Trondhemite	SOUTHERN TATI PLUTON
TAP	Grey High-mg granodiorite with granites	AIRPORT PLUTON
TNP	Tonalite	NEW ZEALAND PLUTON
TRB _m TRB	Granodiorites with megacrystic feldspar granite (TRB _m )	RAMOKGWEBANA BATHOLITH
TMB	Tonalites	MATSILOJE BATHOLITH
TTBr TTB	Tonalite-granodiorite-trondhemite suites with younger megacrystic feldspar granites and homogenous granites (TTBr)	

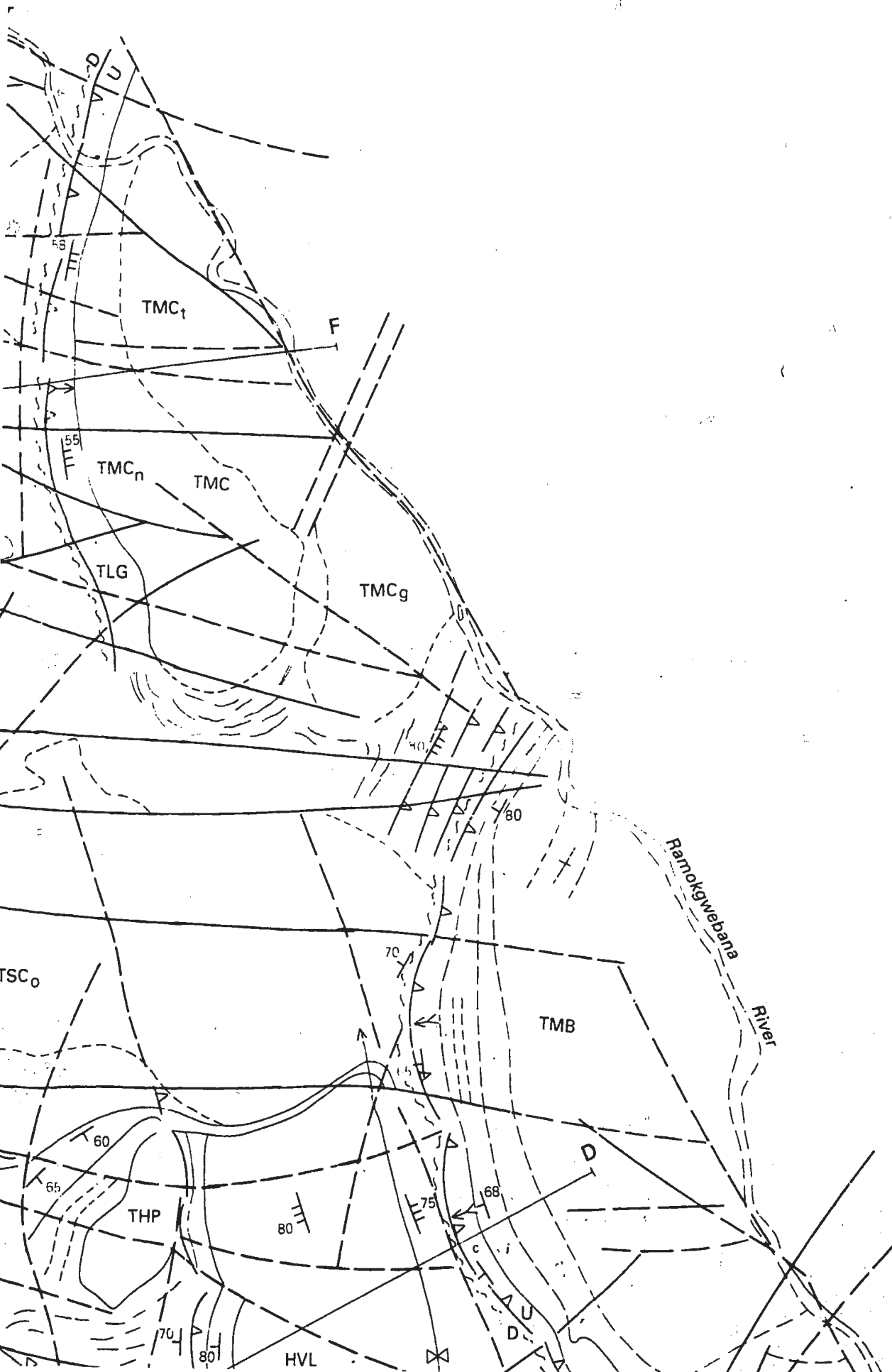
21° 10'S





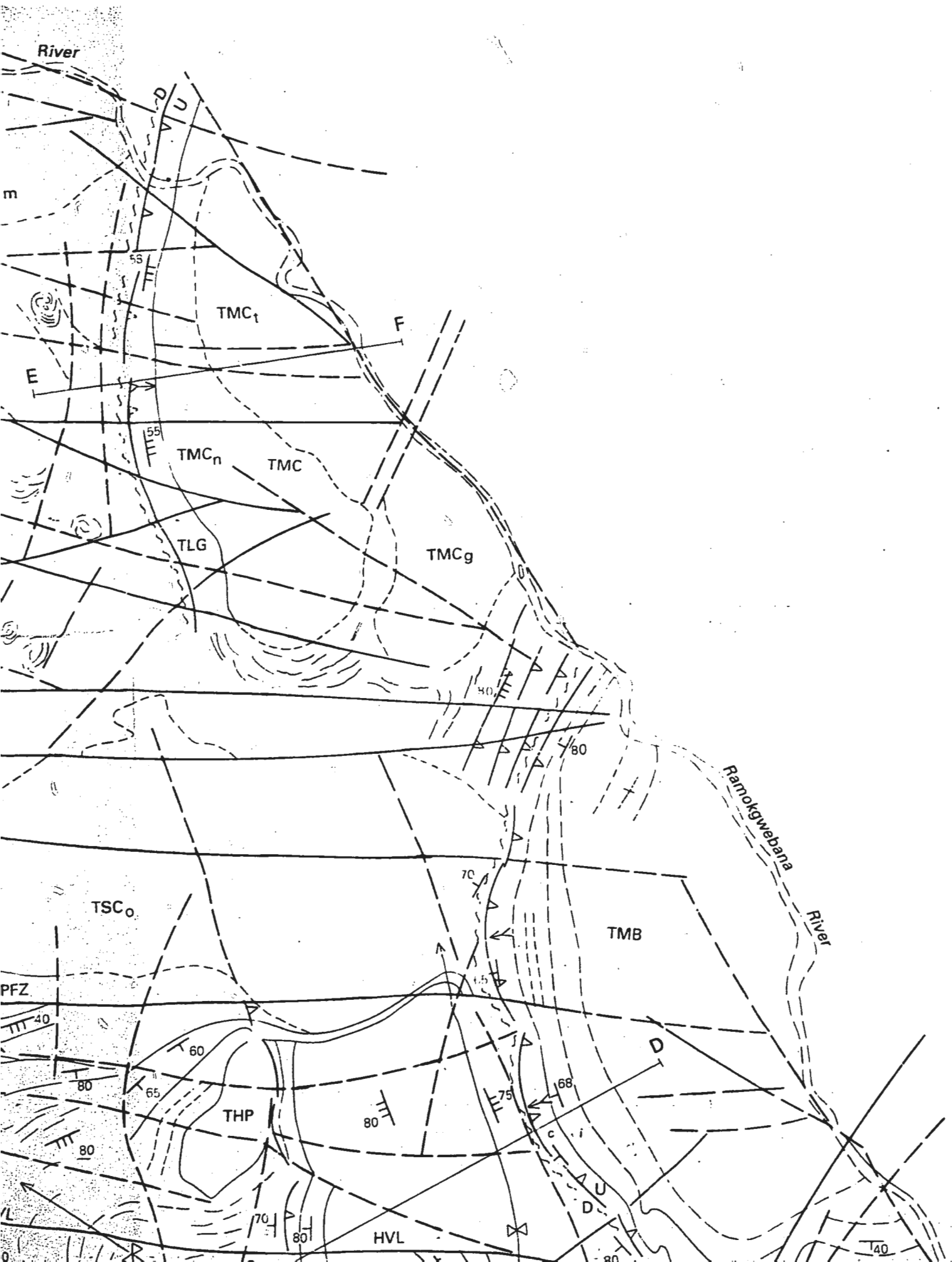


21° 10'S



21° 15'

21° 20'



21° 10'S

THP

Trondhemite

PLUTON

TSP

Trondhemite

SOUTHERN TATI PLUTON

TAP

Grey High - mg granodiorite with granites

AIRPORT PLUTON

TNP

Tonalite

NEW ZEALAND PLUTON

TRBm  
TRB

Granodiorites with megacrystic feldspar granite (TRBm)

RAMOKGWEBANA BATHOLITH

TMB

Tonalites

MATSILOJE BATHOLITH

TBr  
TTB

Tonalite - granodiorite - trondhemite suites with younger megacrystic feldspar granites and homogenous granites (TBr)

3. ROCKS OUTSIDE THE TATI GREENSTONE BELT

21° 15'

Xk

Ultramafic - mafic volcano - plutonic rocks with granitoid plutons.

KGARIMACHENG FORMATION

Xg

Gneisses (granitoid and paragneisses) with younger granitoid intrusions.

NORTHERN TATI GRANITOID TERRANE

Xg'

High metamorphic grade gneisses (amphibolitic, granitic, and paragneisses) with limestones, banded iron formations and clastic sediments.

SHASHE GNEISS FORMATION

Xg''

High metamorphic grade gneisses including granite, amphibolitic and paragneisses

SHASHE BELT

— Lithological boundary (certain)  
- - - Lithological boundary (uncertain)  
- · - · - Lithological boundary (inferred)

RTL Ramokgwebana - Tsamaya Lineament

 Bedding/igneous layering (overturned)

PFL Phoenix - Francistown Lineament

 Bedding/Layering (30)

MFL Matsiloje - Francistown Lineament

 Foliation (S₁)

PFZ Phenalunga Fault zone

 Foliation (S₂)

SLGL Sekukwe - Long Gossan Lineament

 Mineral lineation on S₂ surface

KFZ Kororo Fault Zone

 Crenulation cleavage

CMFZ Charlie Mine Fault Zone

 Minor fold with plunge (2nd phase)

OTL Old Tati Lineament

 Minor fold with plunge (1st phase)

HVL Hillview Lineament

 Younging direction

LHFZ Last hope Fault Zone

 Quartz vein

KBL Kgarimacheng Boundary Lineament

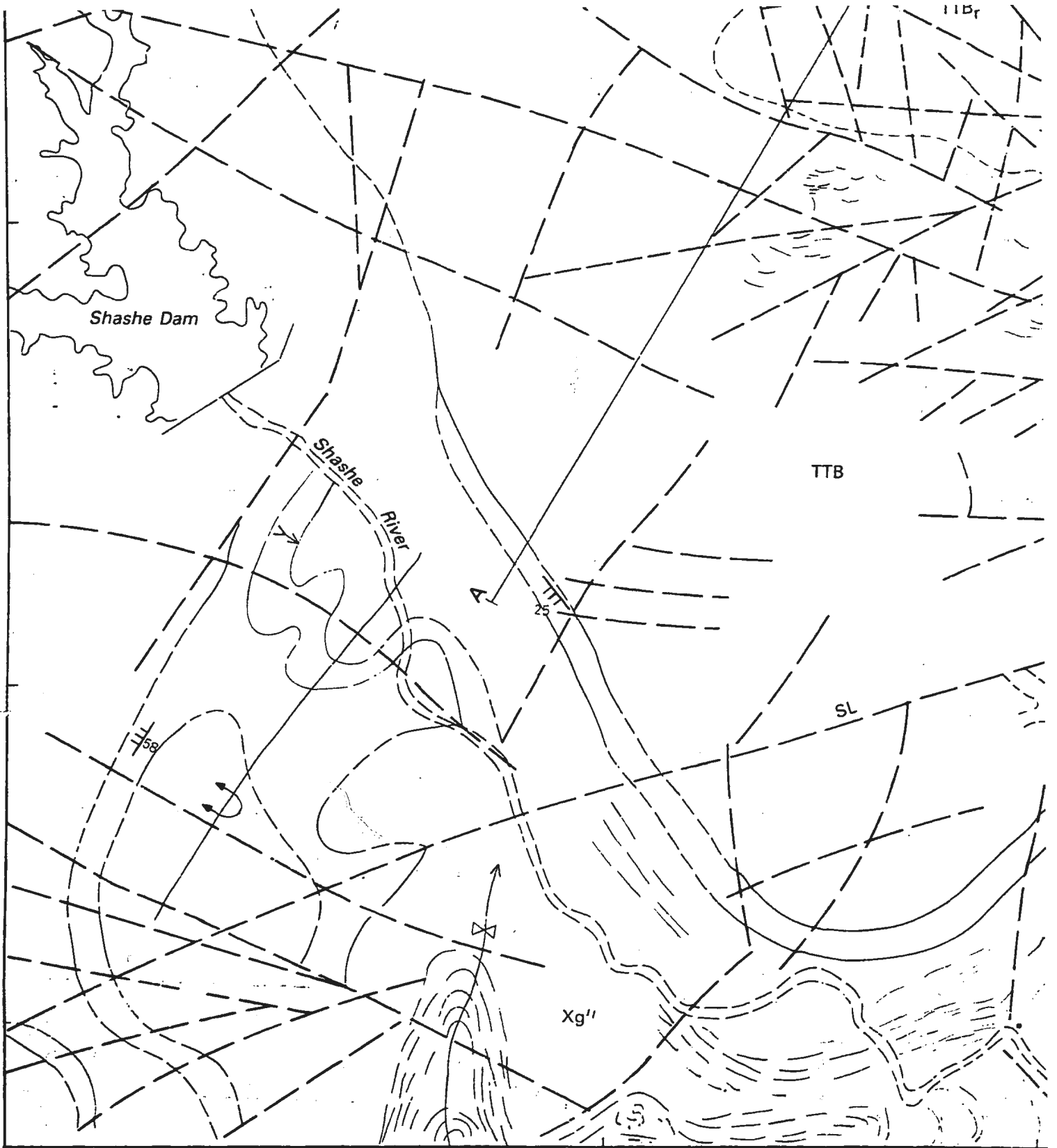
 Antiform

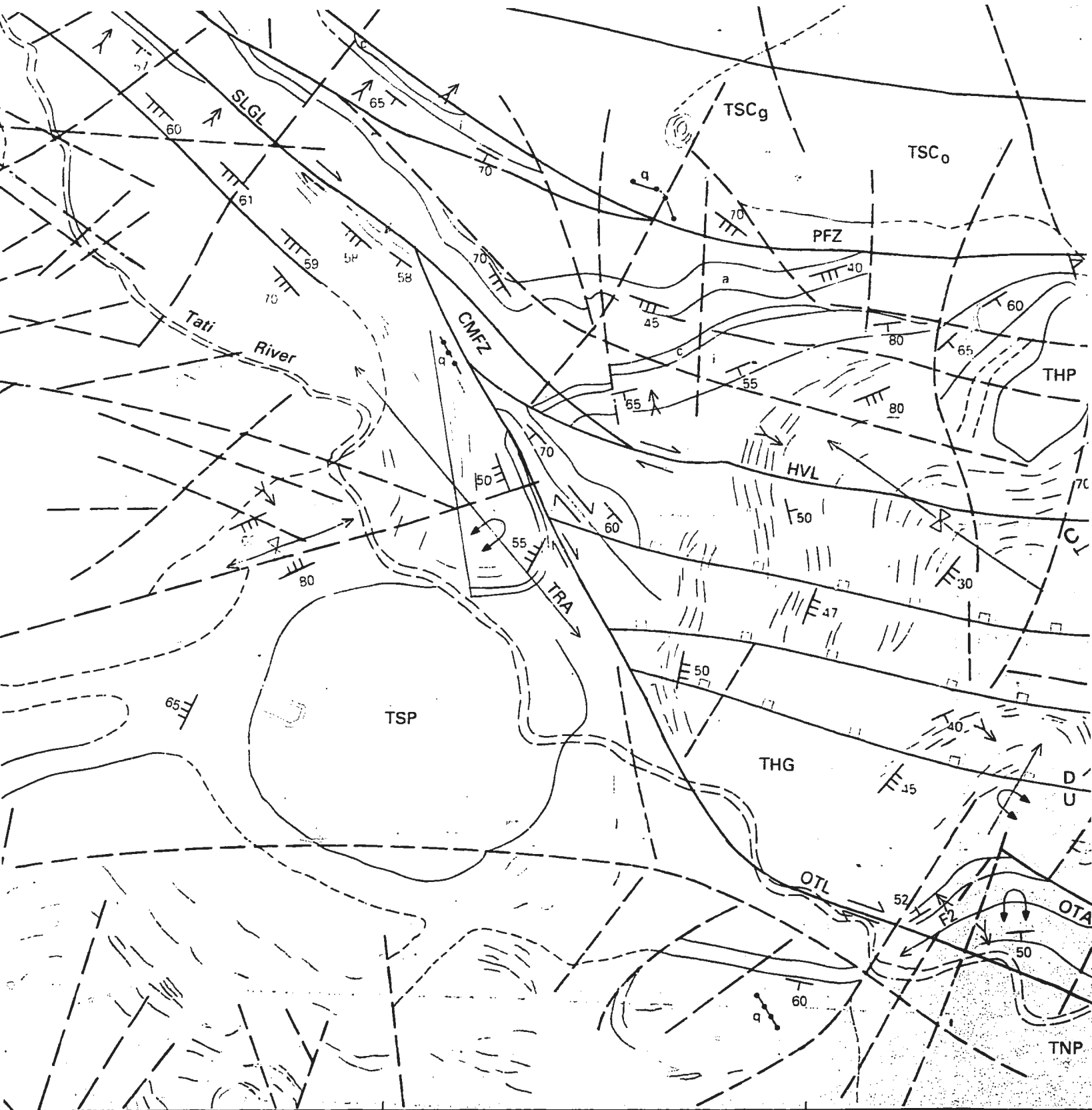
SL Shashe Lineament

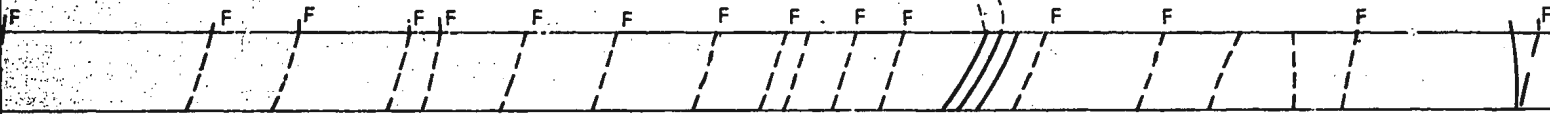
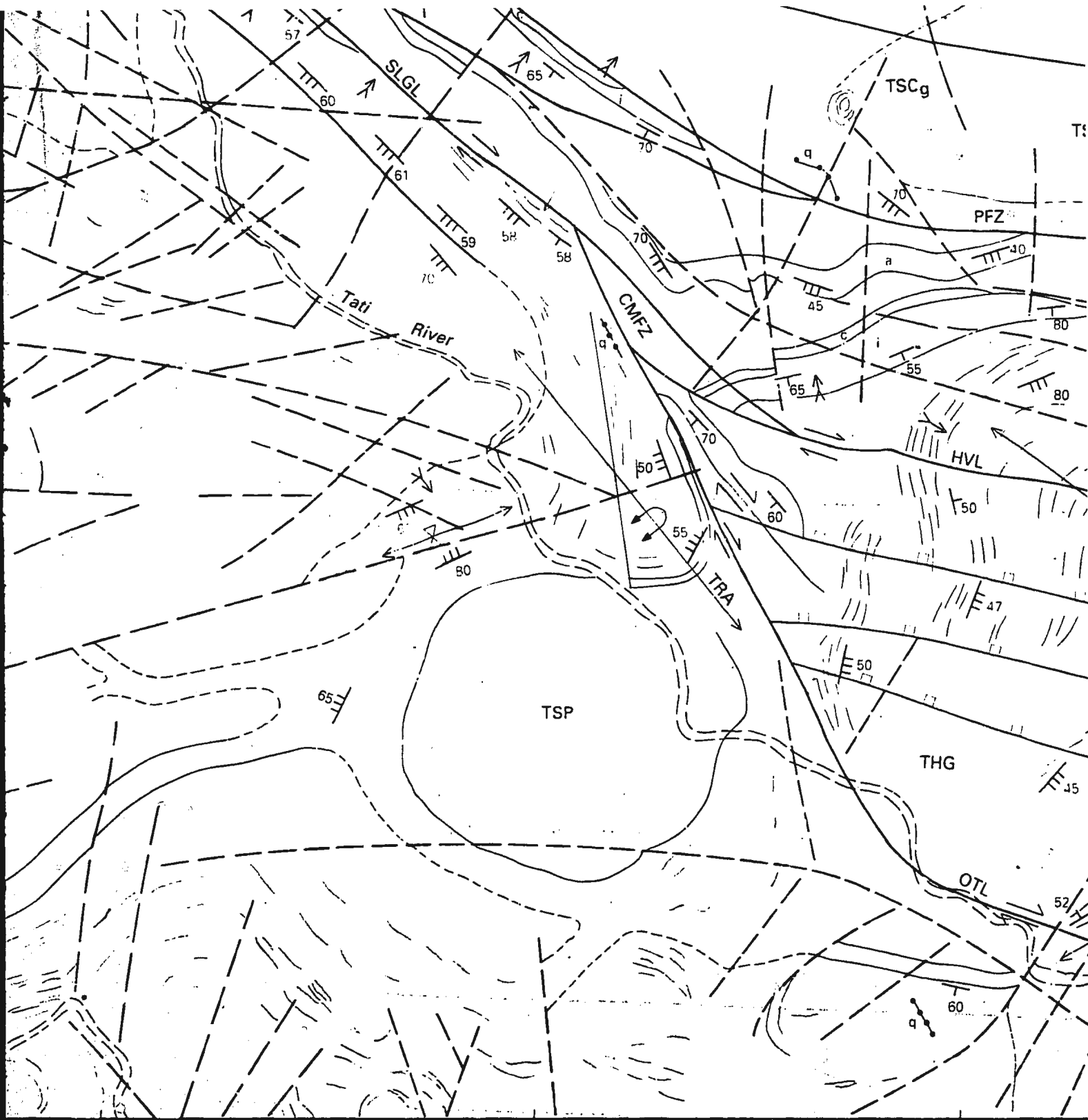
 Synform

OTA Old Tati Anticline

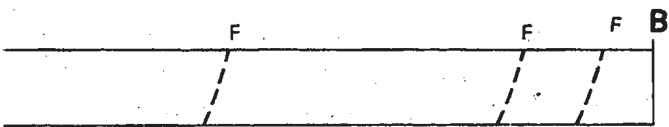
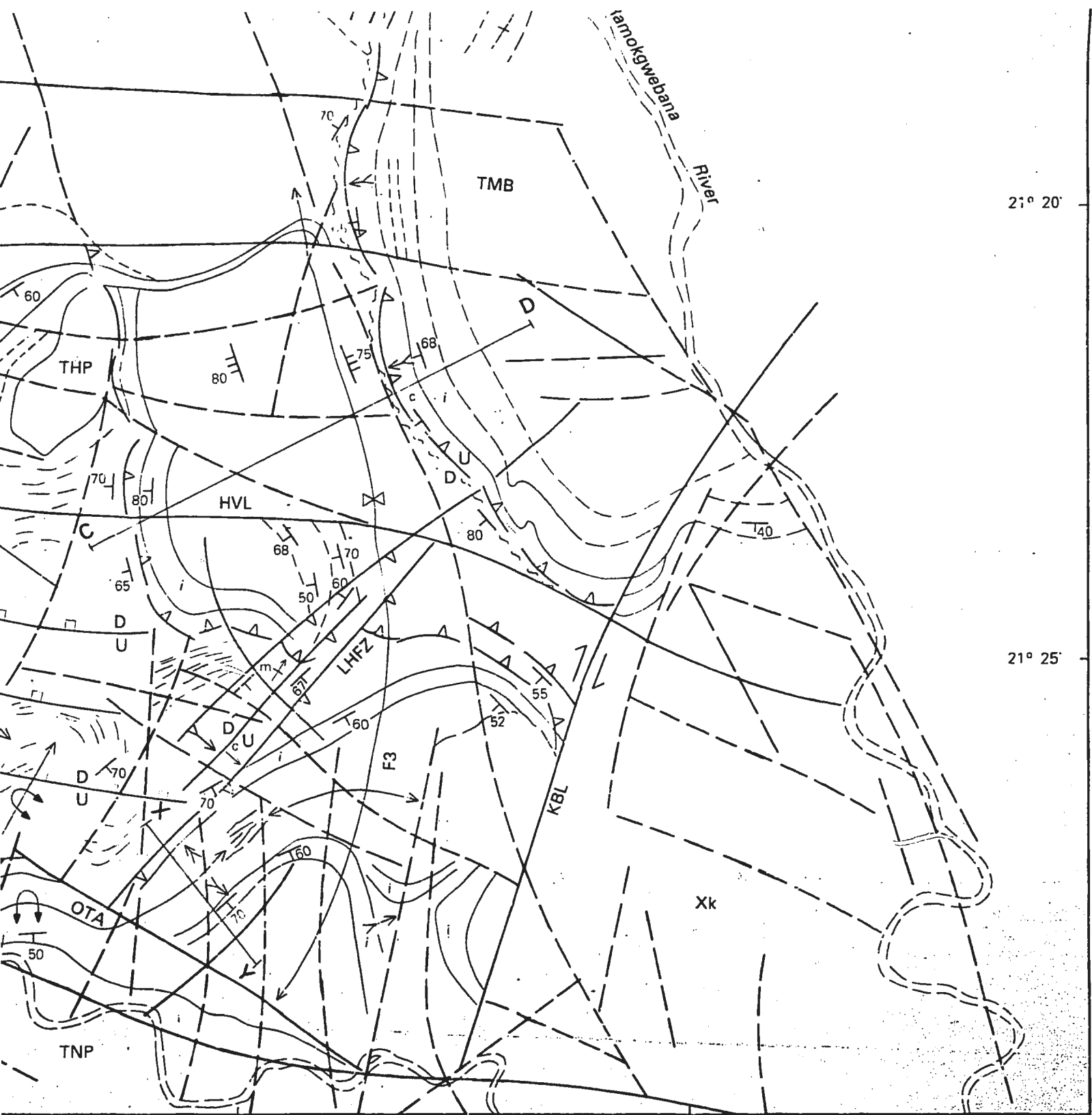
21° 20'

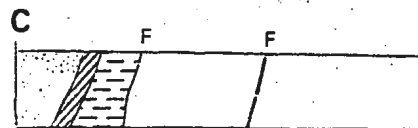
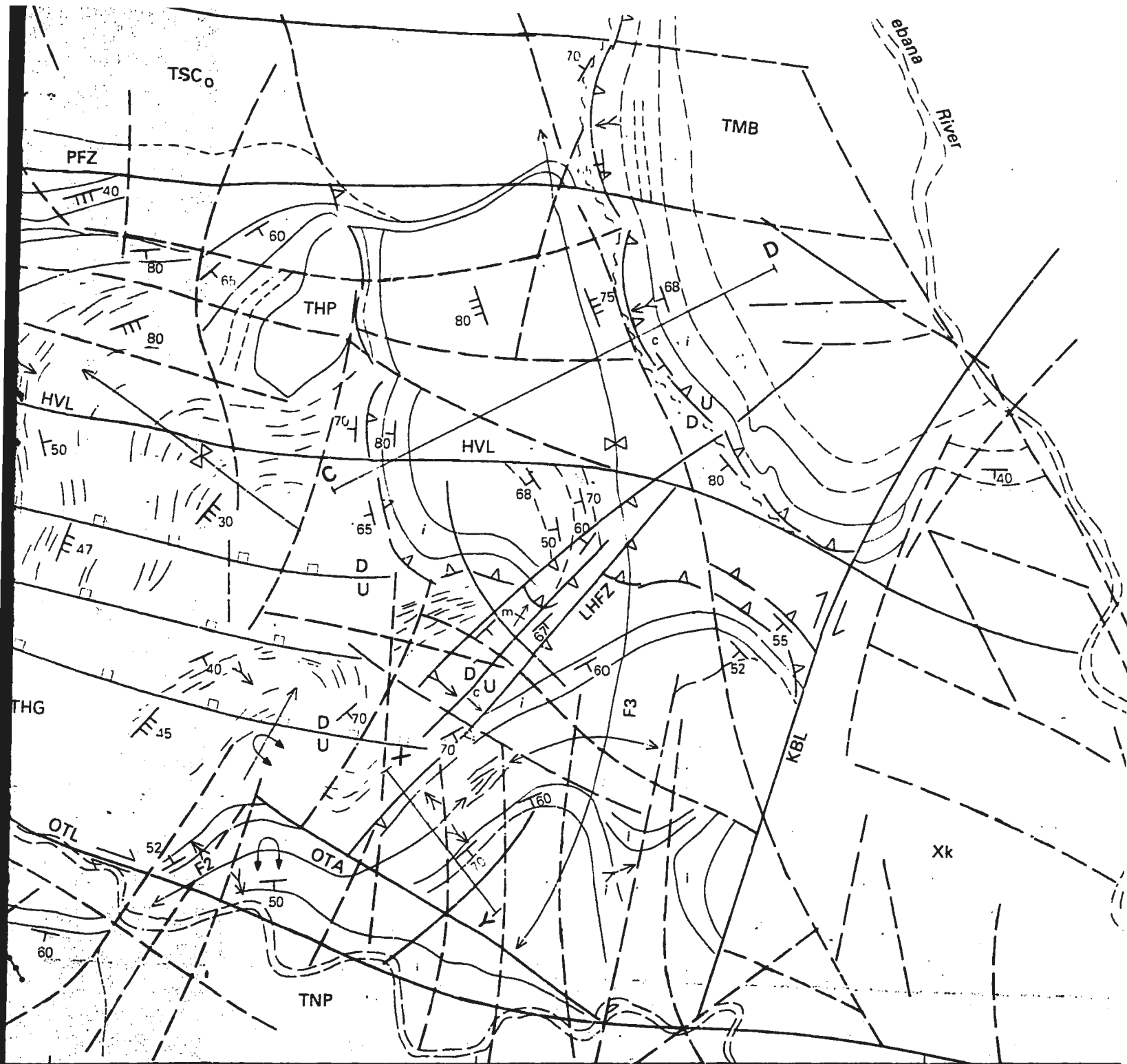






Scale Vertical = Horizontal



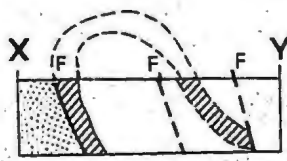


21° 20'

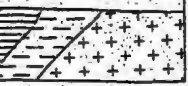
21° 25'

-  Bedding/Layering ( $S_0$ )
-  Foliation ( $S_1$ )
-  Foliation ( $S_2$ )
-  Mineral lineation on  $S_2$  surface
-  Crenulation cleavage
-  Minor fold with plunge (2nd phase)
-  Minor fold with plunge (1st phase)
-  Younging direction
-  Quartz vein
-  Antiform
-  Synform
-  Strike-slip (wrench) fault
-  Shear zone
-  High-angle extensional fault } U = up plate  
D' = down plate
-  Thrust/contractional fault
-  Overturned anticline
-  Overturned syncline
-  Major fault/lineament or shear zone
-  Fault/lineament
-  Photogeological trends/structural trends

- MFL Matsiloje - Francistown Lineament
- PFZ Phenalunga Fault zone
- SLGL Sekukwe - Long Gossan Lineament
- KFZ Kororo Fault Zone
- CMFZ Charlie Mine Fault Zone
- OTL Old Tati Lineament
- HVL Hillview Lineament
- LHFZ Last hope Fault Zone
- KBL Kgarimacheng Boundary Lineament
- SL Shashe Lineament
- OTA Old Tati Anticline
- TRA Tati River Anticline
- GEA Golden Eagle Anticline



D



100

101

102

103

104

105

106

107

108

109

110

111

112

113

114

115

116

